BEHAVIOUR OF CONCRETE SHEAR WALLS REINFORCED WITH HIGH-STRENGTH REINFORCEMENT UNDER REVERSED CYCLIC LOADING

Nima Aghniaey

Thesis submitted to the University of Ottawa
in partial Fulfillment of the requirements for the
Doctor of Philosophy

Civil Engineering Department

Faculty of Engineering

University of Ottawa

To my mother, Farah, my strength, my happiness, my world.

Acknowledgements

I would like to express my deepest appreciation to the University of Ottawa's administrative staff whose patience, support, and professionalism made this accomplishment possible.

I owe a very special thanks to the technical officers of the Structures Laboratory who shared their vast experience and expertise and assisted me throughout my experimental works. I would also like to thank my fellow students and researchers specially Mr. Sasan Ghanea without whom I could not have reached this milestone.

Thanks to my co-supervisor, Dr. Hassan Aoude for his relentless support, his encouragements, for being a wonderful supervisor and for being my friend throughout the last 10 years of my graduate studies.

Lastly, I offer my most sincere gratitude to my supervisor, Dr. Murat Saatcioglu, my role model, my inspiration and my source of wisdom. It was a privilege to learn from him and will always be an honor to have been his student.

Abstract

Shear walls are ordinarily reinforced with conventional steel reinforcement with a maximum specified yield strength of 400 MPa. The use of higher strength reinforcement in such walls may be advantageous to reduce reinforcement congestion and improve constructability. However, data on the seismic behavior of structural walls built with higher strength steel reinforcement is limited. To help provide much needed data, two large-scale concrete shear walls with barbell-shaped and rectangular cross-sections and reinforced with Grade 690 MPa (ASTM A1035) reinforcement were constructed and tested under constant axial compression and cyclic load reversals. The walls were ¼ -scale representations of a 6-storey shear wall with height-to-length aspect ratios of 3.0 and 2.0. Test results show that the walls with aspect ratios of 3.0 and 2.0 failed at lateral drift capacities (Δ/H) of 1.8% and 1.9%. Both walls failed due to the rupture of boundary element longitudinal reinforcement. In addition, the wall with aspect ratio of 2.0 exhibited anchorage slip which contributed to the overall top displacement. VecTor2 Finite Element Modelling software was used to model the walls and conduct an analytical parametric study that investigated the impact of selected design parameters on the seismic behaviour of the wall with aspect ratio of 3.0. The effects of wall aspect ratio, steel type, as well as concrete strength on the response of the walls were investigated. Analytical results show that increasing aspect ratio increases the drift capacity and ductility of the walls. Reinforcement type was found to have a significant impact on ductility of the wall. Concrete strength was shown to shave a small impact on drift capacity.

Table of Contents

List of Figures

List of Tables

Chapter 1

1 Introduction

Regular-strength reinforcement has been the basis for developing guidelines for concrete structures throughout the world and have therefore been established as the standard reinforcement material in construction of reinforced concrete structures. High-Strength Steel (HSS) reinforcements with yield strength of 550 MPa and higher are now commercially available. Technological advancements in the recent decades have allowed for reduced production costs of such reinforcement material while a considerable amount of research has contributed to the increase in popularity of high-strength reinforcement in concrete construction; however, current concrete design guidelines allow only for a very limited use of high-strength reinforcement in concrete construction. On the other hand, the existing research database does not substantiate sufficient basis for incorporating high-strength reinforcement into the design guidelines.

In the 2014 versions of the ACI 318 and the CSA A23.3, the use of high-strength reinforcement is limited to non-seismic applications due to their potential impact on ductility of structural concrete members. High-strength steel reinforcement often have a different stress-strain behaviour compared to conventional Grade 400 MPa steel reinforcement. For example, Grade 690 MPa steel that conforms to ASTM A1035 is not as ductile as the conventional reinforcement and does not exhibit a defined yield point or a yield plateau. Experimental data from previous investigations show that structural members constructed with such reinforcement material may experience reduced ductility. Other steel types, such as those conforming ASTM A706, may have a defined yield point but have a much shorter yield plateau and slightly more ductility as compared to ASTM A1035 steel.

High-strength reinforcement have several potential benefits. They reduce congestion of reinforcement in critical areas of a structure resulting in reduced construction costs and reduced project management and labour time. The US National Institute of Standards and Technology (NIST GCR 14-917-30, 2014) conducted case studies of two high-rise buildings with shear wall and moment frame Seismic Force Resisting Systems. The results indicated that despite a 5% premium for the higher-grade reinforcement, replacing conventional 400 MPa steel with 500 MPa

steel results in 3.4% and 3.8% reduction in costs of the structures for the shear wall and moment frame buildings respectively. Less quantity of steel could also reduce the adverse environmental effects of steel production. These effects include air emissions (CO, SOx, NOx, PM2), water emissions, and waste material, all of which contribute significantly to climate change and global warming. In an era of global concerns over such environmental impacts, minimizing the amount of steel used in the construction industry can benefit all.

Research on the use of high-strength reinforcement started in the early 1900s. Studies by Richart & Brown, (1934), Pfister & Mattock, (1963) and Todeschini et al. (1964) examined the response of columns constructed with high-strength bars under concentric and eccentric axial loads. Research on girders (Gaston and Hognestad, 1962) and beams (Thomas and Sozen, 1965; Kaar, 1966) reinforced with high-strength bars were also conducted by several researchers in the 1960s.

Several researchers have investigated the seismic performance of reinforced concrete members built with HSR. Japanese researchers conducted extensive experimental research in the 1980s and 1990s that included cyclic tests on beams, columns and walls reinforced with HSR under a research program known as the "New RC Project" to study the use of high-strength reinforcement in concrete structures (Otani et al, 1996). In North America, several research projects have been conducted on the behaviour of beams and columns reinforced with Grades 550 MPa [80 ksi], 690 MPa [100 ksi] and 830 MPa [120 ksi] steel bars under cyclic loading (Shahrooz et al, 2014; Yotakhong, 2003; Restrepo et al, 2006; Reutenberg, 2011; Tavallali, 2011; Pfund, 2012; Cheng and Giduqui, 2014). Several studies in North America, Europe and Japan, have also been conducted on the use of high-strength reinforcement in shear walls. Dazio et al. (2009) tested shear walls reinforced with HSR and observed that the high-strength longitudinal reinforcement ruptured prematurely during early drift stages (i.e., 1.5%). On the other hand, tests conducted on shear walls reinforced with high-strength reinforcement by Park et al (2015) and Cheng et al (2016) indicate that HSR may be safely used in squat concrete shear walls without a significant impact on ductility. Several important questions remain on the subject of seismic performance of HSR in shear walls. Specifically, the contribution of high-strength reinforcement to member strength, stiffness, ductility and stability, as well as the susceptibility of high-strength bars to premature rupture, requires further study. A survey of the existing literature shows that there has been limited experimental studies particularly on slender shear walls ($h_w/l_w > 2.0$). Furthermore, there are no

previous studies on shear walls reinforced with Grade 690 MPa [100 ksi] conforming to ASTM A1035.

This study aims at increasing the understanding of the seismic behavior of concrete walls built with Grade 690 MPa ASTM A1035 steel reinforcement that lack a defined yield point or a yield plateau. As part of the study presented herein, two ¼-scale concrete shear walls with aspect ratios of 2.0 and 3.0 and reinforced with Grade 690 MPa steel were constructed and tested under cyclic load reversals and constant axial load to investigate the effect of high-strength reinforcement with limited ductility on strength, ductility and energy dissipation capacity of walls. An analytical study was also conducted using VecTor2 Finite Element Modelling software. As part of this study, the tested walls were modelled and the analytical predictions were compared to the experimental results. An analytical parametric study was also conducted to investigate the effects of wall aspect-ratio, concrete strength and steel type on the reverse cyclic behaviour of the tested walls.

1.1 Objectives

The objectives of this research are as follows:

1) Study the effect of Grade 690 MPa (ASTM A1035) reinforcement on reverse cyclic behaviour, strength, ductility, energy dissipation capacity, failure mechanism, and plastic hinging behaviour of reinforced concrete shear walls with different aspect ratios and cross-sectional shapes.
2) Evaluate accuracy of available Finite Element Modelling tools for predicting reverse cyclic behaviour of walls reinforced with high-strength reinforcement.
3) Further investigate the effects of selected parameters on reverse cyclic behaviour of concrete shear walls reinforced with Grade 690 MPa (ASTM A1035) by conducting analytical parametric investigation.
4) Formulate design recommendations for concrete shear walls reinforced with Grade 690 MPa (ASTM A1035) reinforcement for use in seismically active regions.

1.2 Scope

The scope of the research project includes experimental and analytical investigations on the effects of Grade 690 MPa reinforcement without a defined yield point or a yield plateau on the seismic behaviour of reinforced concrete shear walls designed according to the ACI 318-14. The

experimental investigation consisted of two ¼-scale reinforced concrete shear walls with barbell-shaped and rectangular cross-sections, having aspect ratios of 3.0 and 2.0, labeled W1HS and W2HS, respectively. The walls were tested under constant axial compression and reversed cyclic loading. It was instrumented with cable transducers along the wall height within the critical wall region to measure flexural rotations. Strain gauges were installed at locations of interest, including the flexural reinforcement within the boundary elements as well as the web transverse and vertical reinforcement to record reinforcing steel strains during the tests. The strain data were later analyzed to investigate the performance of HSS reinforcement at different stages of loading.

The analytical investigation consisted of Finite Element Models (FEM) of the walls using VecTor2 software. The software was first validated by modelling walls previously tested by other researchers (Dazio, 2009; Tran & Wallace, 2014; Teng & Chandra, 2016; Navidpour, 2018). The walls in the current study were modelled using VecTor2 and the results were compared to the experimental data. A parametric study was then conducted on the effects of selected design parameters on reverse cyclic behaviour of walls using the analytical model for W1HS. These parameters included the steel type (ASTM A615, ASTM A706, ASTM A955, ASTM A1035, AS/NZ 500E, and USD685), wall aspect ratio (H/L= 1.0, 2.0, 3.0, and 4.0), and concrete strength (f'_c=30 MPa, 60 MPa, 80 MPa, 120 MPa, and 150 MPa).

Chapter 2

2 Literature Review

This section provides background on high-strength steel reinforcement, current design standards, high-strength steel grades available worldwide, and summarizes existing literature related to experimental and analytical investigations on concrete shear walls reinforced with conventional and high-strength steel. It should be noted that there is limited experimental data on slender walls ($H/L \geq 2.0$) reinforced with high-strength reinforcement, with no previous studies on shear walls reinforced with Grade 690 MPa [100 ksi] reinforcement conforming to ASTM A1035 reinforcement.

2.1 High-Strength Steel Reinforcement

There is no universally established definition for high-strength steel reinforcement (HSR). The term often refers to a type of reinforcing steel used in concrete structures that, due to metallurgical alteration of its composition and other factors during the manufacturing process, exhibits enhanced strength and durability compared to the conventional Grade 400 MPa steel reinforcement. The National Cooperative Highway Research Program (NCHRP) Report 679 (NCHRP Report 679, 2011) defines HSR as steel reinforcement having a yield strength greater than 500 MPa [72 ksi]. ACI 318-14 and CSA A23.3-14 design standards limit the yield strength of main steel reinforcement used in seismic design of structural members to 400 MPa. Hence, any steel reinforcement with grades higher than 400 MPa can be regarded as high-strength from a seismic design perspective. Some high-strength reinforcement types may have a different stress-strain response compared to conventional Grade 400 MPa steel while others may also have enhanced corrosion resistance (i.e., stainless steel, MMFX®).

In this study, HSR refers to Grade 690 MPa reinforcement conforming to ASTM A1035 which lacks a defined yield point or plateau and has reduced ductility compared to conventional ASTM A615 reinforcing steel.

2.1.1 North American Reinforcing Steel Standards

2.1.1.1 Canadian Standards

Canadian Standards Association (CSA) G30.18 specifies the requirements for two types of hot rolled carbon steel used as conventional concrete reinforcement. CSA A23.1/A23.2- *Concrete materials and methods of concrete construction/Test methods and standard practices for concrete* requires reinforcement steel used in concrete to conform to the requirements of CSA G30.18 standard.

2.1.1.2 American Standards

American Society for Testing and Materials (ASTM) specifies the minimum requirements for various types of reinforcement steel listed below:

ASTM A-615/A-616M: Deformed and plain carbon-steel bars for concrete reinforcement;

ASTM A-616/A-616M: Deformed and plain rail-steel bars for concrete reinforcement;

ASTM A-617/A-617M: Deformed and plain axle-steel bars for concrete reinforcement;

ASTM A-706/A-706M: Deformed and plain low-allow steel bars for concrete reinforcement;

ASTM A767/A767M: Zinc-Coated (Galvanized) Steel Bars for Concrete Reinforcement;

ASTM A775/A775M: Epoxy-Coated Reinforcing Steel Bars;

ASTM A934/A934M: Epoxy-Coated Prefabricated Steel Reinforcing Bars;

ASTM A-1055: Zinc and Epoxy Dual-Coated Steel Reinforcing Bars;

ASTM A955: Deformed and plain stainless-steel bars for concrete reinforcement;

ASTM A1035A/1035M: Deformed and Plain, Low-carbon, Chromium, Steel Bars for Concrete Reinforcement;

In the United States (US), a wider variety of steel is commercially manufactured and marketed including Grades 40, 60, 75, 80, 100 and 120 steel where the Grade number indicates yield strength in ksi [1 ksi = 6.9 MPa].

2.1.2 High-Strength Steel Grades

2.1.2.1 Canada

The only high-strength reinforcement type manufactured according to a Canadian standard is Grade 500 MPa which is referenced in CSA G30.18. Grade 500 is manufactured in two types of 500R and 500W which are the 'Regular' and 'Weldable' types. They have a specified minimum yield strength of 500 MPa. Grade 500R and 500W have minimum tensile (ultimate) strengths of 625 MPa and 675 MPa respectively.

2.1.2.2 United States of America

Grades 520 MPa [75 ksi], 550 MPa [80 ksi], 690 MPa [100 ksi] and 830 MPa [120 ksi] reinforcement steel bars are commercially available in the US. Each Grade may be produced in accordance with different standards depending on the desired mechanical properties of the bars. The following sections summarize the different grades and their corresponding manufacturing standards:

Grade 520 MPa: Produced as high-strength carbon steel under ASTM A615. This grade has a defined yield plateau and minimum specified yield and tensile strengths of 520 MPa and 690 MPa as per ASTM A615 respectively.

Grade 550 MPa [80 ksi]: Referenced in both ASTM A615 and ASTM A706-09b. Grade 550 MPa steel must have minimum yield and tensile strengths of 550 MPa and 725 MPa respectively according to ASTM A615. ASTM A706 however, specifies an upper limit of 675 MPa for the yield strength and a minimum tensile (ultimate) strength of 690 MPa for Grade 550 MPa bars. Figure *2.1* shows typical stress-stress behaviour for Grade 550 MPa reinforcement confirming to ASTM A706.

Grade 690 MPa [100 ksi] and 830 MPa [120 ksi]: Referenced in ASTM A1035 standard. They usually lack a well-defined yield plateau and reach ultimate tensile strength at smaller strains compared to Grade 400 steel. Figure 2.2 presents typical stress-strain diagrams for Grade 690 MPa and Grade 830 MPa reinforcing steel conforming to ASTM A1035. Grade 690 MPa is used in the current experimental program. In 2015, Grade 690 MPa reinforcing bars were introduced in ASTM A615.

Another type of high-strength steel reinforcement available in the US is the German-manufactured SAS 670/800 threaded bars that have yield strengths of 670 MPa and 800 MPa. The International Code Council (ICC) Evaluation Services (ES) has published an evaluation of this type of steel for use in US in 2011, which has been revised annually. It was last updated in February 2019 (ICC-ES Evaluation Report ESR 1163, 2019).

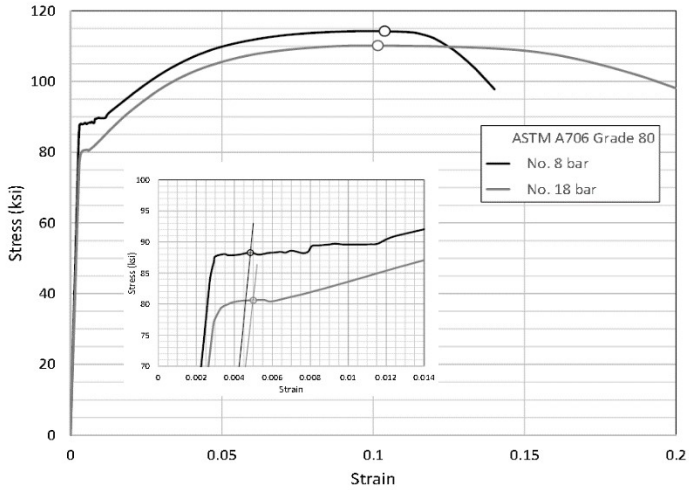

Figure 2.1 - Example stress-strain curves for ASTM A706 Grade 550 MPa [80 ksi] bars.

[Adapted from NIST GCR 14-917-30, 2014]

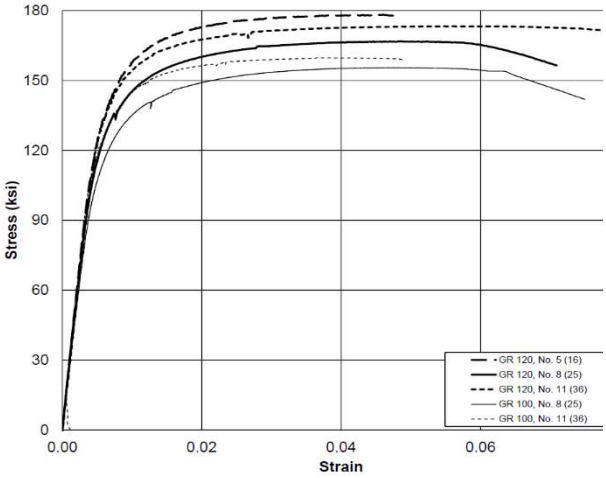

Figure 2.2 - Example Stress-strain curves for ASTM A1035 Grade 690 MPa [100 ksi] and Grade 830 MPa [120 ksi] Reinforcement

[Adapted from NIST GCR 14-917-30, 2014]

2.1.2.3 Japan

In Japan, steel reinforcing bars are manufactured under Japanese Industrial Standards (JIS) G 3112, G 3536 and G 3109. Grades USD685 and USD980, commonly used for longitudinal or transverse reinforcement, conforming to the requirements of JIS G 3112 and have yield strengths of 685-785 MPa and 980 MPa, respectively. Other Japanese Grades include USD785 and USD1275 with minimum yield strengths of 785 MPa and 1275 MPa that conform to JIS G 3536 and G 3109. JIS Standards also specify minimum tensile strengths of 930 MPa and 1420 MPa for Grades USD 785 and USD 1275 which can only be used as transverse reinforcement in structural concrete members.

2.1.2.4 Austria

High-Strength Reinforcing Steel Grades in Austria conform to ONORM B 4200/7 standard and include Grade B500, B550 and B600 with minimum yield strengths of 485 MPa, 533 MPa and 582 MPa.

2.1.2.5 China

Available high-strength steel grades in China include HRB500, HRB500E, GR75, GR460 (BS4449) and GR500 (BS4449). All grades conform to GB1499.2-2007 standard as well as BS4449 and ASTM A615. Grades HRB500 and HRB500E have minimum yield and tensile strengths of 500 MPa and 630 MPa. Grade HRB500E also has a specified maximum tensile strength of 820 MPa. Grade GR75 has minimum yield and tensile strengths of 520 MPa and 690 MPa. GR460 and GR500 have minimum yield strengths of 460 MPa and 500 MPa.

2.1.2.6 Taiwan

Steel Grade SD685 was developed in Taiwan for structural concrete applications. The properties of this steel grade are very similar to those of Japanese Grade USD685.

2.1.2.7 Australia / New Zealand

Australian/New Zealand Standard 4671 specifies the requirements for reinforcing steels bars. Steel Grades AS/NZS Grade 500 and 500E both have specified minimum yield strength of 500 MPa. Grade 500E has adequate ductility to be used in earthquake-resisting structures.

Table 2.1 - Summary of common steel grades worldwide

Grade	Standard	Yield, Minimum MPa [ksi]	Yield, Maximum MPa [ksi]	Tensile, Minimum MPa [ksi]	Tensile, Maximum MPa [ksi]	Specified Elongation %
USA						
520 MPa	ASTM A615	520 [75]	-	690 [100]	-	7
550 MPa	ASTM A615	550 [80]	-	725 [105]	-	7
	ASTM A706	550 [80]	675 [98]	690 [100]	-	12
670 MPa	SAS670	669 [97]	-	800 [116]	-	10
690 MPa	ASTM A615	690 [100]	-	790 [115]	-	7
	ASTM A1035	690 [100]	-	1030 [150]	-	7
Grade 830 MPa	ASTM A1035	830 [120]	-	1030 [150]	-	7
Canada						
500R	CSA G30.18	500 [73]	-	675 [98]	-	6-9
500W	CSA G30.18	500 [73]	625	625 [91]	-	10-12
Japan						
USD685	JIS G 3112	685-785 [99-114]	-	860 [125]	-	10
USD980	JIS G 3112	980 [142]	-	1030 [150]		7
USD785	JIS G 3536	785 [115]	-	930 [135]	-	8
USD1275	JIS G 3109	1275 [185]	-	1420 [205]	-	7
China						
HRB500	BGB1499.2	500 [73]	-	630 [91]	-	7.5
HRB500E	BGB1499.2	500 [73]	-	630 [91]	820 [119]	11-12
GR75	BGB1499.2	520 [75]	-	690 [100]	-	6-7
GR460	BS4449	460 [67]	-	-	-	-
GR500	BS4449	500 [73]	-	-	-	-
Taiwan						
SD685	N/A	685 [99]	-	860 [125]	-	10
Australia / New Zealand						
500L	AS/NZS 4671	500		750		1.5
500N	AS/NZS 4671	500		600		5
500E	AS/NZS 4671	500		650	910	10

2.1.3 Stress-Strain Models for High-Strength (ASTM A1035) Steel Reinforcement

American Concrete Institute (ACI) Innovative Task Group (ITG) 6R-10 guide (ACI Innovation Task Group 6, 2010) recommends a numerical approach to predict the stress-strain characteristics of ASTM A1035 steel (ACI ITG 6R-10, 2010). Equation 2.1 presents the model recommended by this guide and Figure 2.3 compares it to experimental results:

$$f_s = \begin{cases} 200{,}000\varepsilon_s & \varepsilon_s \le 0.0024 \\ 1170 - \dfrac{2.96}{\varepsilon_s + 0.0019} & 0.0024 < \varepsilon_s \le 0.02 \\ 1040 & 0.02 < \varepsilon_s \le 0.06 \end{cases} \qquad \text{[Eq. 2.1]}$$

Alternatively, as shown in equation [2-2], a bi-linear model proposed by Mast (2006) can be used to model the stress-strain behaviour of ASTM A1035 steel.

$$f_s = \begin{cases} 200{,}000\varepsilon_s & \varepsilon_s \le 0.00241 \\ 1172 - \dfrac{2.379}{\varepsilon_s + 0.00104} & 0.00241 < \varepsilon_s \le 0.06 \end{cases} \qquad \text{[Eq. 2.2]}$$

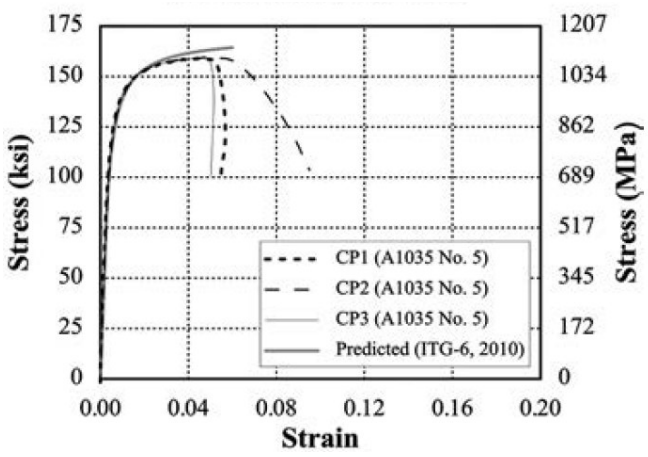

Figure 2.3 - Stress-strain curves of actual test and ACI ITG-6R model

[Adapted from Cheng & Giduquio, 2014]

Another method which can be used to model the stress-strain behaviour of high-strength steel that does not have a defined yield plateau is the Ramberg-Osgood method, which involves using a bilinear function as represented by Equation 2.3. Parameters A and B are determined based on

cross-sectional area and modulus of elasticity of steel. Parameter C is a variable and is determined by trial and error (or using experimental stress-strain data) to optimize the transition curve.

$$f_s = 200{,}000\varepsilon_s \times \left(A + \frac{1 - A}{[1 + (B\varepsilon)^C]^{\frac{1}{C}}} \right) \leq f_u \qquad \text{[Eq. 2.3]}$$

2.1.4 Design Code Restrictions (2014)

The walls in this study were designed and constructed prior to the most recent design code revisions in 2019. The following sections provide restrictions of the 2014 design codes in Canada and the US. Current (2019) provisions for the design of ductile concrete shear walls have remained generally the same with some exceptions. Some of the notable changes include new provisions in the ACI 318-19 that require the use of additional factors in the calculation of the development lengths to account for the effect of high-strength reinforcement, confinement steel, and spacing of the anchorage reinforcement.

2.1.4.1 Canadian Standards Association, CSA A23.3-14

The CSA A23.3-14 design standard limits the yield strength of deformed reinforcing bars to 500 MPa as a general provision. For compression reinforcement having a specified yield strength exceeding 400 MPa, the yield strength used in design is not permitted to exceed the stress corresponding to a strain of 0.0035. A 400 MPa limit on the yield strength of longitudinal reinforcement is specified in Clause 11.3.6.3 when the 'Simplified Method' is used for determining the shear strength of reinforced concrete members. The yield strength used in design of shells and plates is also limited to 400 MPa as specified in Clause 19.3.

A limit for design yield strength of reinforcement in members resisting earthquake forces is not explicitly specified in the CSA A23.3 standard, however, the code states that "*the design, detailing, and ductility requirements for structures designed using a reinforcement grade greater than 400 shall account for the increased strain demands*". It is also stated that "*The procedures specified in Clause 21, with the exception of Clause 21.2.8.2, were developed for Grade 400 reinforcement. The additional strains required for higher yield-strength steel will generally reduce ductility*". Hence, to be able to use higher Grades of steel reinforcement in the design of seismic structural members, design procedures should account for the added strains and the reduced ductility of the

structure. This is however difficult to be reliably ensured by design engineers in lieu of a standardized design procedure.

2.1.4.2 American Concrete Institute, ACI 318-14

Chapter 20 of the ACI 318-14 design code specifies requirements for the steel properties used in the design of concrete structures. Tables 20.2.2.4a & b of ACI 318-14 provide the maximum yield strength values that can be used in design based on the structure's application. It limits the design yield strength value of reinforcement used in seismic systems to 400 MPa [60 ksi]. Grade 690 MPa [100 ksi] steel is currently permitted for use as lateral support of longitudinal reinforcement or confinement reinforcement in seismic applications.

Table 2.2 –Table 20.2.2.4a – Non-pre-stressed deformed reinforcement of ACI 318-14 [Adopted from ACI 318-14, 2014]

Usage	Application	Maximum value of f_y or f_{yt} permitted for design calculations, psi	Applicable ASTM specification			
			Deformed bars	Deformed wires	Welded wire reinforcement	Welded deformed bar mats
Flexure; axial force; and shrinkage and temperature	Special seismic systems	60,000	Refer to 20.2.2.5	Not permitted	Not permitted	Not permitted
	Other	80,000	A615, A706, A955, A996	A1064, A1022	A1064, A1022	A184[1]
Lateral support of longitudinal bars; or concrete confinement	Special seismic systems	100,000	A615, A706, A955, A996, A1035	A1064, A1022	A1064[2], A1022[2]	Not permitted
	Spirals	100,000	A615, A706, A955, A996, A1035	A1064, A1022	Not permitted	Not permitted
	Other	80,000	A615, A706, A955, A996	A1064, A1022	A1064, A1022	Not permitted
Shear	Special seismic systems	60,000	A615, A706, A955, A996	A1064, A1022	A1064[2], A1022[2]	Not permitted
	Spirals	60,000	A615, A706, A955, A996	A1064, A1022	Not permitted	Not permitted
	Shear friction	60,000	A615, A706, A955, A996	A1064, A1022	A1064, A1022	Not permitted
	Stirrups, ties, hoops	60,000	A615, A706, A955, A996	A1064, A1022	A1064 and A1022 welded plain wire	Not permitted
		80,000	Not permitted	Not permitted	A1064 and A1022 welded deformed wire	Not permitted
Torsion	Longitudinal and transverse	60,000	A615, A706, A955, A996	A1064, A1022	A1064, A1022	Not permitted

[1]Welded deformed bar mats shall be permitted to be assembled using A615 or A706 deformed bars.

[2] ASTM A1064 and A1022 are not permitted in special seismic systems where the weld is required to resist stresses in response to confinement, lateral support of longitudinal bars, shear, or other actions.

2.2 Concrete Shear Walls Reinforced with Conventional Reinforcement

The following sections summarize previous experimental research on the seismic behaviour of concrete shear walls reinforced with conventional Grade 400 (or similar) reinforcement. The type of reinforcing steel used in these walls have a defined yield point and have yield plateau. Section 2.3 summarizes previous experimental research on concrete wall reinforced with higher-strength

reinforcement. Appendix B provides a summary of the walls presented in this section including the deformation capacities and failure modes of the previously tested walls.

2.2.1 Tran and Wallace (2014)

In this experimental program, five large-scale cantilever reinforced concrete shear walls with aspect ratios (H/L) of 1.5 and 2.0 were tested. The walls were subjected to constant axial load and cyclic load reversals. They were designed to be flexure dominant. The objective of this study was to validate the analytical tools and the application of Performance-Based Seismic Design.

The boundary element longitudinal reinforcement ratio varied between 3.23% and 7.11%. The web transverse reinforcement ratio of the walls varied between 0.27% and 0.73% and were designed to satisfy the ACI 318-11 requirements for special boundary elements. The longitudinal reinforcement in the boundary elements consisted of a combination of No. 4, No. 5 and No. 6 bars placed in an 8-bar formation as shown in Figure 2.4.

The loading protocol consisted of three load-controlled cycles of ¼, ½, and ¾ of the calculated yield force followed by displacement-controlled cycles. LVDTs were used to measure lateral wall displacement, foundation sliding and uplift, and to collect data necessary for determination of wall average concrete strains over specified gauge lengths. Strain gauges were used to record reinforcement strains at critical locations of the boundary element and distributed web reinforcement.

Substantial loss of capacity started at around 3.0% drift for all tested walls. It was found that plastic rotation over a height of 50mm from the base of the wall, as well as the slip/extension of vertical reinforcement at the base of the wall contributed to approximately 10% to 25% of top flexural displacement for the walls with an aspect ratio of 2.0. This contribution was 10% to 40% for walls with an aspect ratio of 1.5. It was also observed that the contribution of the sliding shear to total lateral deformation at the top of the walls was very small and ranged between 1% to 4% for drift levels of 0.5% to 3.0%. The average shear deformation after the first flexural yielding ranged between 20% and 30% for walls with aspect ratio of 2.0, and between 30% and 50% for walls with an aspect ratio of 1.5.

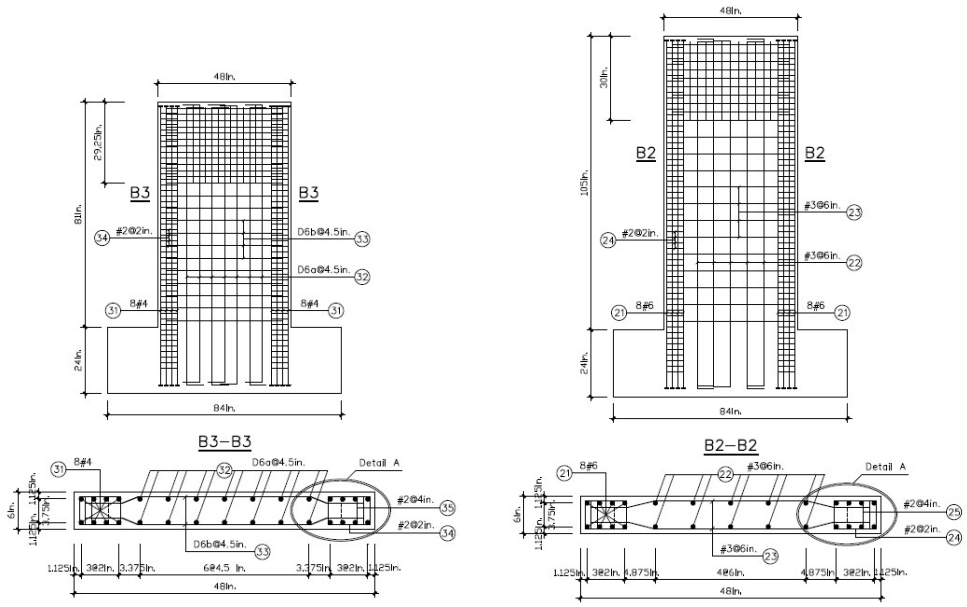

Figure 2.4 – Typical Reinforcement Details for walls tested by Tran & Wallace (2014) [Adapted from Tran, 2012]

2.2.2 Emamy et al (2008)

In this study, seven large-scale reinforced concrete shear walls were tested under constant axial load and monotonically-increased lateral displacements. The walls had an aspect ratio (H/L) of 1.25 and were constructed using concrete with compressive strengths of 80 MPa to 100 MPa. The objective of this experimental program was to investigate the behaviour of concrete shear walls constructed with high-strength concrete and to develop a rational equation for shear design of ductile structural concrete walls.

Figure 2.5 shows typical details of the tested walls. Test parameters consisted of reinforcement ratios of web transverse and vertical reinforcement, longitudinal reinforcement in the boundary elements and compressive axial load level. Horizontal reinforcement ratios of 0.47% and 0.75% were used in combination with vertical reinforcement ratios of 1.26% and 0.75%. The longitudinal reinforcement ratio in the boundary elements was 4.0% for all walls. Three axial load levels were used, which corresponded to approximately 5%, 8% and 20% of the concentric axial load capacity of the walls.

The loading protocol used was the same as that used by Gupta & Rangan (1998). Test results indicated that the capacity of walls increased with increased vertical reinforcement ratio. The effect

of the horizontal reinforcement ratio on the lateral load capacity of the walls was not as significant as that of the vertical reinforcement ratio. It was observed that the shear strength is improved very slightly with the increase of horizontal reinforcement ratio. As part of analytical investigation, results of previous wall tests (by others) were analyzed to evaluate the Australian AS 3600 and the ACI 318 design codes. It was found that the ACI 318 gives a more conservative estimate of the shear capacity of concrete shear walls with a shear strength safety factor of 1.96. This ratio was found to be 1.55 using values calculated based on the Australian AS3600 design code.

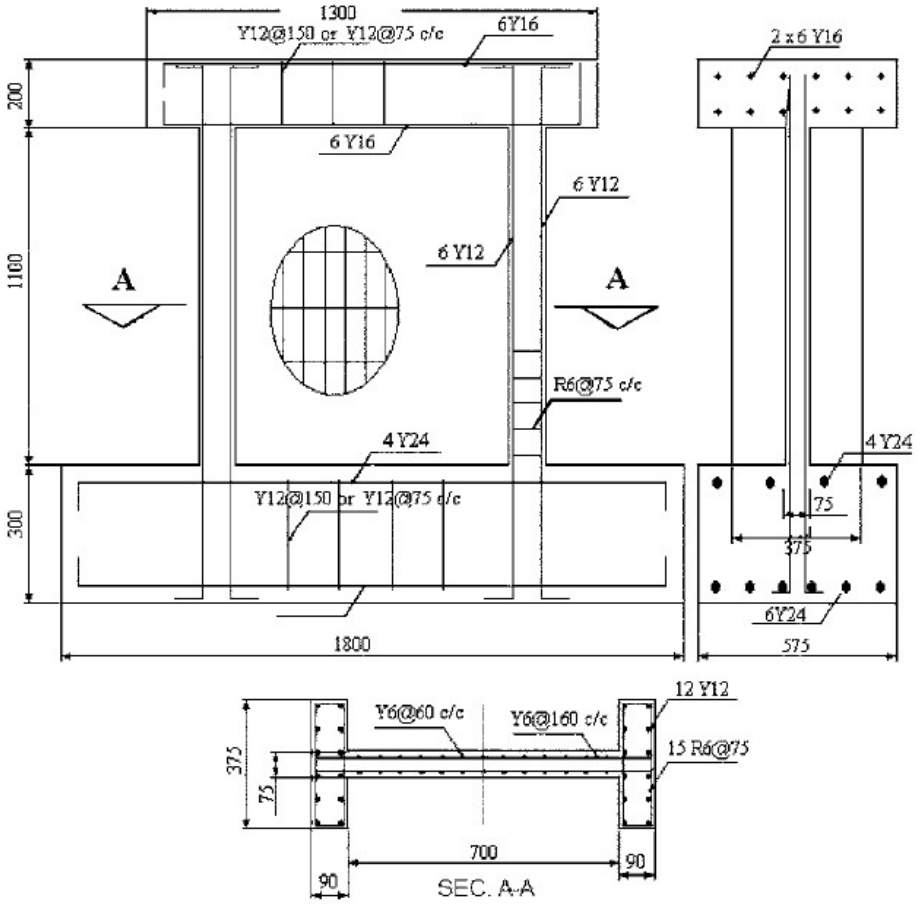

Figure 2.5 – Typical details of walls tested by Emamy et al (2008)
[Adapted from Emamy et al, 2008]

2.2.3 Thomsen and Wallace (2004)

Thomsen & Wallace presented results of four ¼-scale reinforced concrete shear walls previously tested as part of the experimental program conducted by Wallace (1994, 1995). The walls

presented in this study consisted of two walls with rectangular cross-sections and two walls with T-shaped cross-sections as shown in Figure *2.6*. The test results were used to verify a displacement-based design methodology which was incorporated into the ACI 318-99 code to evaluate detailing requirements at wall boundaries. The proposed methodology was found to produce accurate predictions of curvatures for a range of drift levels.

The geometry and reinforcement details of the tested walls were based on a typical 6-storey office building in a high seismicity area. Boundary element longitudinal reinforcement consisted of 8 No. 3 bars (d = 9.525mm). No. 2 (d=3.2mm) bars were used to for distributed web reinforcement. The reinforcement ratios were selected in proportion to the prototype walls to produce a similar neutral axis depth relative to the wall length. A design drift level of 1.5% of the wall height was selected to determine the required boundary element transverse reinforcement for the tested walls.

Instrumentation of the walls allowed for measurement of lateral displacement and rotation of the wall, shear deformations, axial displacements, concrete strains, as well as vertical and horizontal movement of the base foundation unit. Strains in the reinforcing steel were also measured at critical locations using strain gauges.

The results indicated that the drift capacities of all tested walls exceeded 2.0% which was greater than the target design drift capacity of 1.5%. Various failure modes were observed. Specimens TW-1 and TW-2 experienced significant curvature ductility when the flange section was in compression. Wall TW-1 was intentionally detailed poorly by providing larger spacing of the transverse reinforcement in the boundary elements, and as expected, failed to reach the nominal moment capacity when the lateral load capacity suddenly dropped at a drift level of 1.25%. Wall TW-2 was able to develop its peak moment capacity at a drift level of 2.5% when the web boundary compression zone started to experience out-of-plane stability failure (buckling over several hoop spacings).

Specimen RW-1 exhibited significant loss of strength at a drift level of approximately 2.5% due to the buckling of boundary element longitudinal reinforcement. This failure mode was anticipated given the relatively large spacing ($8d_b$) of boundary element transverse reinforcement compared to a spacing of $6d_b$ specified by ACI318-99 that is to prevent buckling of vertical bars. The performance of wall RW-2 was slightly better than wall RW-1 due to closely spaced hoops. Wall

RW-2 failed due to buckling of the boundary element longitudinal reinforcement (all 8 bars buckled simultaneously). It was found that analytical predications of the strain profiles were in best agreement when the length of the plastic hinge zones were assumed to be between $0.33l_w$ and $0.5l_w$. The sensitivity of the neutral axis depth to the extreme fiber strain was also examined analytically and experimentally. It was found that the code procedure based on neutral axis depth for an extreme fiber strain of 0.003 are appropriate for most cases.

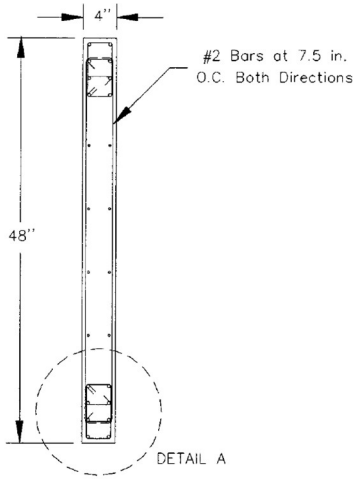

a) Walls RW1 and RW2 – Typical Cross-Section Details

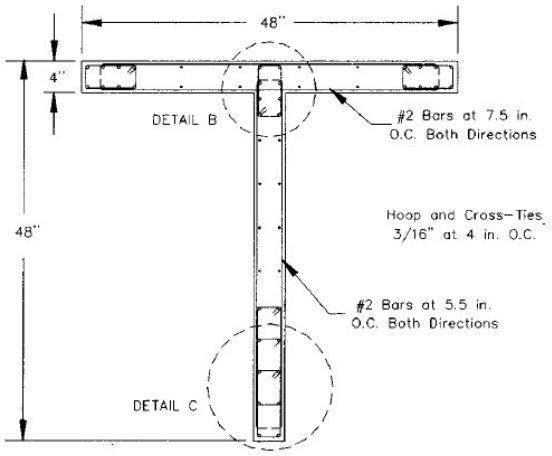

b) Walls TW1 and TW2 – Typical Cross-Section Details

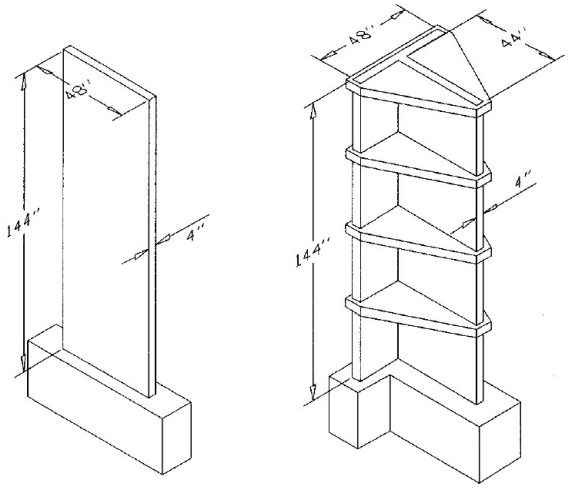

c) 3D views of the tested walls

Figure 2.6 – Details of the walls presented in the study by Thomsen & Wallace (2004) [Adapted from Thomsen & Wallace, 2004]

2.2.4 Hidalgo et al (2002)

Hidalgo et al (2002) studied the seismic behaviour of squat shear walls by testing 26 reinforced concrete shear walls with aspect ratios between 0.7 and 2.0. The walls were subjected to reverse cyclic loading with no axial compression. The authors explained that this choice was due to the fact that the axial compression on walls can change during earthquake motion. In addition, they argue that the ACI provisions neglect the contribution of axial compression to shear strength of walls. Rigid loading beams were constructed at the top and the bottom of the walls that represented full-height inter-storey shear walls. The test setup was constructed in such a way that restricted the top and the bottom of the walls from rotation and applied horizontal reverse cyclic loads at mid-height, as shown in Figure 2.7. Test parameters included the aspect ratio of the walls, vertical and horizontal reinforcement ratios, and concrete compressive strength.

The vertical and horizontal reinforcement ratios were selected to represent the minimum reinforcement ratio required by the ACI 318-1999 code, half the minimum, and no web reinforcement. Only one curtain of web distributed reinforcement was used due to the thickness of the specimens. The walls had various cross-sectional dimensions and heights. Full details of the walls are provided in Appendix B. The length of the walls varied between 1000mm and 1500mm, the height varied between 1050mm and 2000mm and the thickness ranged between 80mm and 120mm.

All walls exhibited shear failure mechanisms. The performance of the walls was evaluated based on three parameters: 1) cracking load, 2) maximum shear strength, and 3) stage at which strength dropped to 80% of the maximum shear strength. These parameters were deemed to be performance indicators for the serviceability limit state and the ultimate limit state of the walls. Pinching of the hysteresis curves was observed for all walls which was attributed to the energy used to transition between closing of the cracks in the compression side and opening of the cracks in the tension side of the walls. The effect of horizontal web reinforcement was evident as walls with higher horizontal web reinforcement ratio exhibited higher ductility; this effect was found to be more pronounced in walls with aspect ratios (H/L) of higher than 1.0. The effect of the vertical web reinforcement on strength and ductility of the walls was found to be insignificant. It was also observed that distributed reinforcement had little effect on the cracking displacement (Δ_{cr}) of the walls, whereas this effect was more significant on the displacement at ultimate strength (Δ_u), as

well as the ultimate displacement (Δ_{ult}). Walls with no distributed reinforcement showed poor performance under seismic loads, specifically after the first major diagonal cracks appeared. In addition, it was shown that walls with smaller aspect ratios exhibited smaller deformation capacities. This was deemed by the authors to be due to the increase in the lateral stiffness of the walls with smaller aspect ratios. The drift ratio of the tested walls at ultimate shear ranged between 0.21% and 0.75%. The Normalized Dissipated Energy (NDE) of the walls were also investigated. It was found that the NDE of the walls was nearly independent of the distributed reinforcement ratios and the aspect ratio of the walls. It was also observed that the strength decay was higher for walls with smaller aspect ratios and smaller ratio of distributed reinforcement.

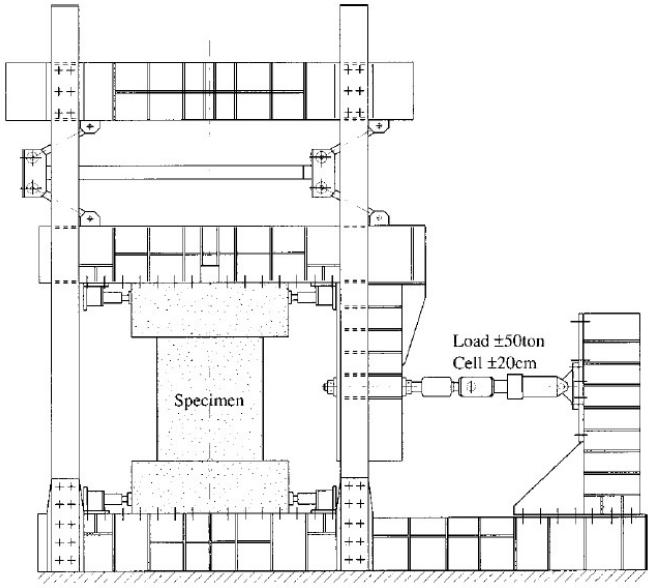

Figure 2.7- Test setup for walls tested by Hidalgo et. al (2002)
[Adapted from Hidalgo et. al, 2002]

2.2.5 Zhang and Wang (2000)

Zhang and Wang (2000) tested four reinforced concrete shear walls with aspect ratio (H/L) of 2.14 under reverse cyclic and high axial loading. The objective of this study was to investigate the failure mechanism and ductility of concrete shear walls under high axial loading. One of the four specimens was reinforced with a structural steel shape as the main flexural reinforcement, in addition to deformed steel bars. The walls were subjected to axial loads ranging from 10% to 13% of their concentric axial compressive capacity and were tested under lateral load reversals. The test parameters were axial load ratio ($\lambda_N = N/f_c A_g$) and shear compression ratio ($\lambda_V = V_{max}/f_c A_g$). Figure *2.8* show typical details of the walls tested by Zhang and Wang (2000).

The walls were designed to be flexure-dominant by ensuring that the ratio between the theoretical flexural strength and the theoretical shear strength was 1.3. The longitudinal web reinforcement was detailed in such a way that the ratio of the theoretical flexural strength to f_cA_g was equal to the pre-specified value of shear compression ratio λ_V for a particular specimen. All four walls were 1750mm high, 700mm wide and 100mm thick. The lateral reverse cyclic load was applied at a height of 1500mm above the base for all walls. For the conventionally reinforced walls, the longitudinal reinforcement in the boundary elements consisted of 12mm, 14mm and 20mm dia. bars placed in a 4-bar arrangement. One wall was reinforced with one steel channel and two 12mm diameter bars. Smooth 8mm diameter bars were used for web vertical reinforcement for all the walls. Two curtains of 8mm diameter bars were placed at a spacing of 100mm as web horizontal reinforcement for two of the walls, whereas the other two, including the wall with channel section reinforcement, were reinforced with two curtains of 6mm and 8mm dia. bars at 150mm and 75mm spacings, respectively. Tested yield strengths of the reinforcement ranged from 375 MPa to 432 MPa for the flexural bars, and 305 MPa for the web horizontal and vertical reinforcement.

The loading protocol included monotonic application of the axial load to its full magnitude before the horizontal loading started. The axial load was applied using two 600 kN hydraulic actuators. The horizontal load was applied in two phases. The first phase of the loading was divided into 10 steps consisting of fully reversed cycles up to the yield point. The second phase of the loading consisted of additional lateral displacement increments at half the yield displacement ($½\ \Delta_y$). Displacement transducers were installed along the height of the wall to record lateral displacement, curvature, base uplift, and base slip of the wall.

Test results indicated that all of the walls failed in flexure. All specimens developed plastic hinges within the lower portion of the walls approximately 0.6m from the base of the walls. It was observed that horizontal and diagonal cracks developed along the height of the walls and propagated towards the centre at higher displacements. It was observed that high axial load ratios restrained the development of major inclined cracks in the web since principal tensile stresses were smaller in the web section due to higher axial loads.

Axial load ratio was observed to have a significant effect on the failure mode, stiffness and ductility of the walls. The energy dissipation capacity of the walls decreased with higher axial load ratios. Walls subjected to higher axial load ratio exhibited higher horizontal load capacities; however,

axial load had a detrimental effect on stiffness degradation of the wall in the post-yielding stage. One wall reinforced with conventional reinforcement failed through out-of-plane buckling in the post-yielding stage. Shear-compression ratio was found to have an effect on the plastic deformation behaviour of the tested walls as well. More extensive criss-crossing cracks in the web were observed in the wall with a higher shear-compression ratio however no change was observed in the deformation capacity.

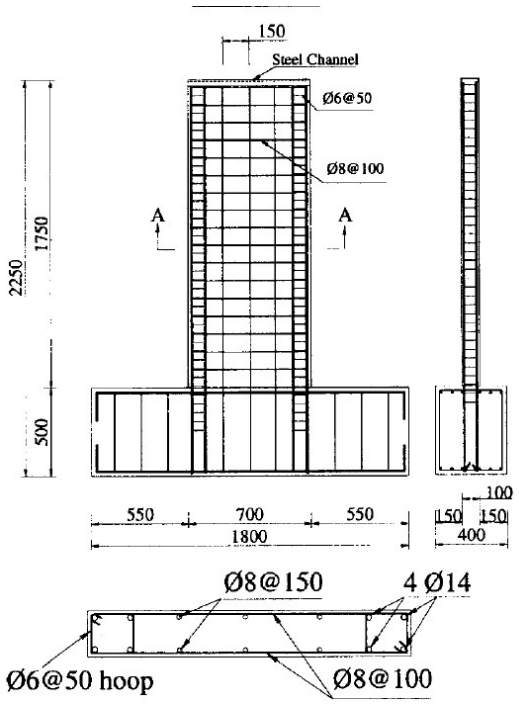

Figure 2.8 - Typical details of walls tested by Zhang & Wang (2000)
[Adapted from Zhang & Wang, 2000]

2.2.6 Salonikios et al. (1999)

Salonikios et al. tested 11 reinforced concrete shear walls with low slenderness ratios to assess the validity of Eurocode 8 design guidelines for cyclic shear in squat RC walls. The effects of axial load, boundary element reinforcement ratio, and quality of construction joints were investigated. The differences between the Eurocode 8 and ACI 318 code in shear wall design principles and guidelines were assessed. In particular, the differences of the two design codes in the use of wall aspect ratio or shear span in establishing shear design criteria was examined. Test parameters also included flexural reinforcement ratio, axial load level, and quality of reinforcement detailing at the construction joints.

The walls were designed according to Eurocode 8 and in such a way that either a diagonal tension or sliding shear mode was expected. Four walls were reinforcement with cross-inclined reinforcement as required by Eurocode 8. A series of displacement transducers were installed at various locations to measure lateral displacement of the wall at the top and 200mm from the base of the walls. The bottom measurement was to monitor sliding of the wall during testing. Diagonal transducers were installed at the lower region of the walls to measure shear deformations. In addition, transducers were installed over the height of the plastic hinge regions to measure axial deformations within this length. The horizontal force was applied at the top of the walls using a stiff beam connected to the top of each beam. Typical details of the tested walls are presented in Figure *2.9*.

All wall specimens failed in a predominantly flexural mode characterized by crushing of concrete and buckling of reinforcement within the boundary elements. Diagonal cracking of the web and sliding of the base was also observed which had little impact on failure modes. Other than the walls with aspect ratio (H/L) of 1.0, all walls except one were able to develop their expected flexural capacities and expected energy dissipation capacities. The wall reinforced with conventional reinforcement (without the cross-inclined reinforcement) exhibited significant pinching due to horizontal sliding of the walls and bond-slip of the vertical reinforcement. The cross-inclined reinforcement appeared to have significant impact on controlling the horizontal sliding of the walls; specifically, when they intersected walls within the critical regions, though this is not recommended in Eurocode 8. Walls with an aspect ratio of 1.5, despite being called squat walls in Eurocode 8, exhibited flexure-dominant behaviour. The critical parameter for design of such walls was found to be the confinement of the boundary regions. This was also observed to be the case in the walls with aspect ratio of 1.0 when the nominal shear stress did not exceed approximately $0.45\sqrt{f_c'}\ MPa$.

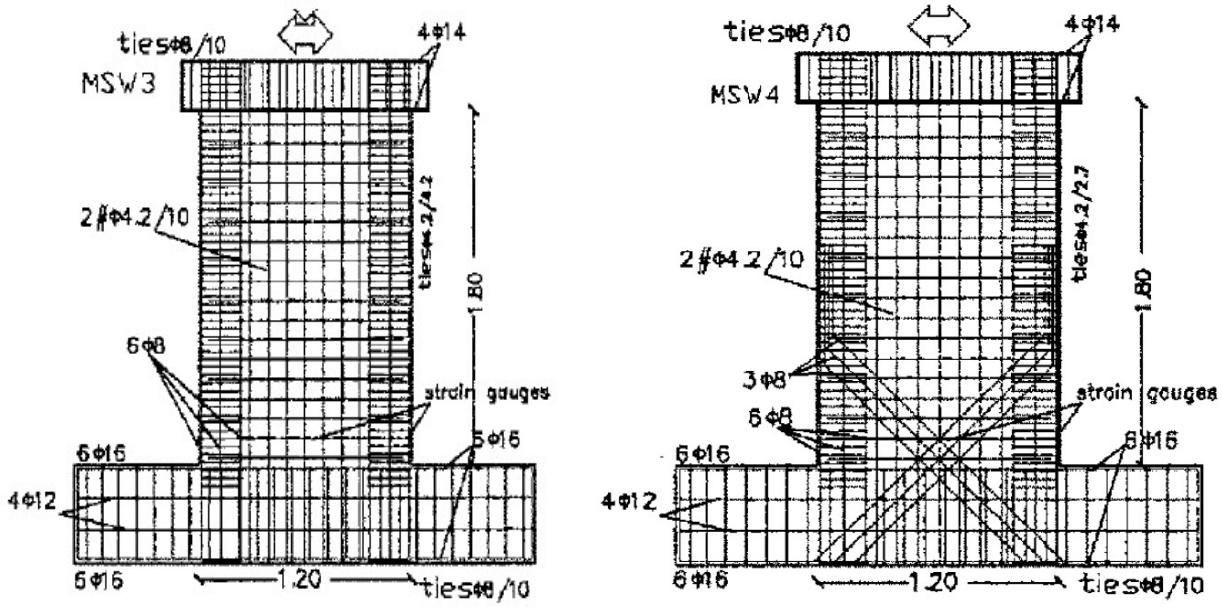

Figure 2.9 Typical details for walls tested by Salonikios et al (1999)
[Salonikios et al (1999)]

2.2.7 Gupta and Rangan (1998)

Gupta and Rangan (1998) tested eight reinforced concrete walls under constant axial compression and monotonic lateral loading to investigate the effects of longitudinal and transverse reinforcement ratios as well as axial compression on behaviour of reinforced concrete shear walls. The walls were constructed with high-strength concrete (60 MPa to 80 MPa) and were designed to exhibit both flexural and shear responses. The objectives of the tests were to develop analytical models to predict the strength of reinforced concrete structural walls under in-plane loads, and to compare results of the test with those calculated using design equations.

The horizontal load was applied monotonically using a hydraulic jack at force-controlled increments of 50KN before cracking and then at 25 KN increments after cracking. Increments of 10 KN were used near failure. The horizontal force was maintained for two minutes at every loading stage. LVDTs were used to measure top horizontal displacement at the loading point, the uplift of the foundation beam, and the horizontal movement of the base of the wall.

Figure *2.10* presents typical design details for the walls tested by Gupta and Rangan (1998). Seven of the eight walls were designed to be shear-dominant and failed in shear as expected. One specimen was designed to behave in a flexural mode, and it failed in flexure. The Compression Field Theory developed by Vecchio and Collins (1986) was modified to predict the shear strength

of the walls. A theory was developed to evaluate the shear capacity of a reinforced concrete structural wall based on the stress analysis of the central panel of the wall. The test results were used to examine the Australian Standard AS 3600 and the ACI 318 Building Code. The theoretical loads and failure modes calculated using the theory developed in this research was shown to be in good agreement with the experimental results.

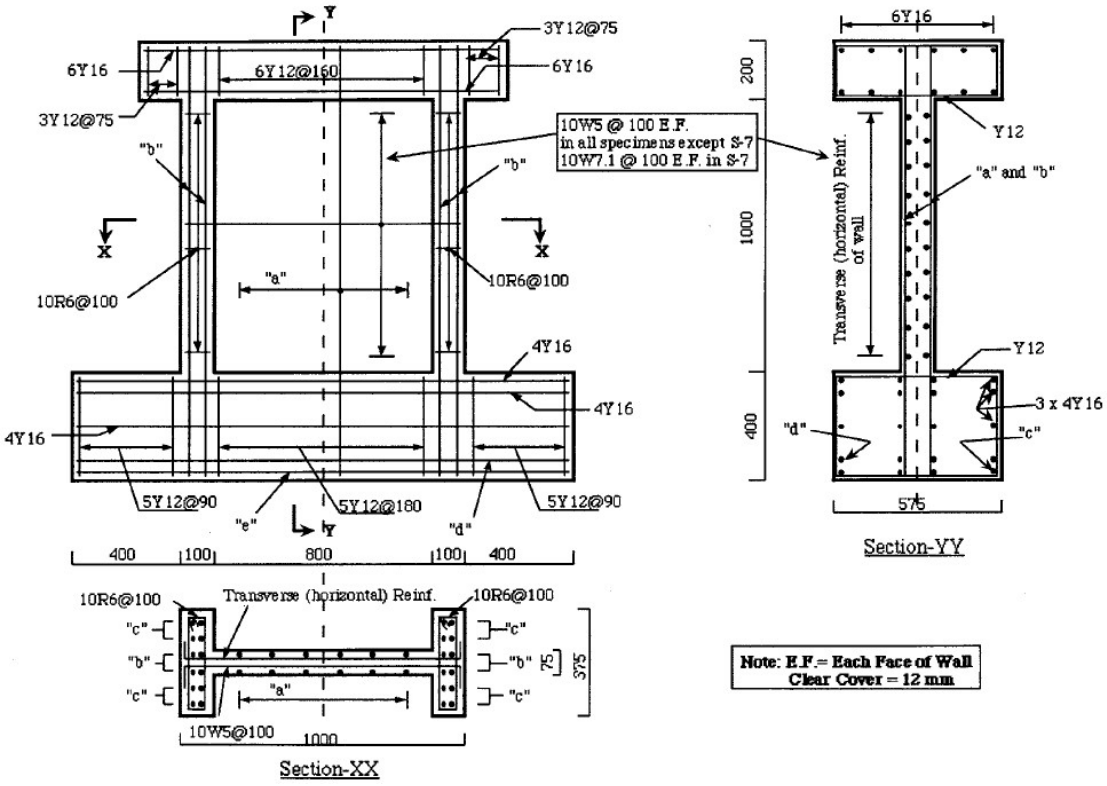

Figure 2.10 - Typical details for walls tested by Gupta and Rangan (1998)
[Gupta and Rangan, 1998]

2.2.8 Lefas et al (1990)

Lefas et al. (1990) tested 13 reinforced concrete shear walls under monotonic lateral loads to investigate 1) the mechanism through which compressive forces are transmitted to the supports, and 2) the effect of vertical force on strength, stiffness, and deformation characteristics of reinforced concrete shear walls. Two types of walls with aspect ratios (H/L) of 1.0 and 2.0 were tested in this program; Type I walls which were 750mm long, 750mm high and 70mm in thickness, and Type II walls which were 650mm long, 1300mm high, and 65mm in thickness.

The reinforcement consisted of 4mm diameter mild steel bars used as confinement reinforcement in the boundary elements; and 6.25mm diameter and 8mm diameter bars used as horizontal and vertical web reinforcement, respectively. The reinforcement details were designed according to the 1998 version of the ACI 318 Building Code (ACI 318-89) for all walls except two, which had less horizontal reinforcement. Figure 2.11 shows the geometry and reinforcement details for the two types of walls tested in this program.

The lateral load was monotonically applied using a hydraulic jack at a rate of 0.04 kN/sec which was sustained at each increment for at least 2 minutes. This was done to allow for photographing and monitoring deformations and crack patterns. LVDT sensors were used to measure in-plane, out-of-plane and axial deformations of the walls.

Test results indicated that the lateral load capacity of the walls increased with higher axial compression. This increase was more pronounced in walls with an aspect ratio of 2.0. In addition, increased axial compression resulted in reduced ultimate displacement and increased lateral stiffness. Walls with an aspect ratio of 1.0 exhibited enhanced stiffness of 65% to 100% at almost all intermediate stages of loading when axial compression increased from 10% to 20% of the concentric axial load capacity of the walls. The rate at which the lateral displacement capacity decreased with the increase in axial load was higher for walls with an aspect ratio of 2.0. Similar performance was observed in walls with higher concrete compressive strengths.

Two of the walls were constructed with reduced transverse reinforcement to allow for investigating the validity of ACI 318 shear design guidelines. The tested walls exhibited similar behaviour to walls with sufficient transverse reinforcement as per ACI 318. The authors assert that, based on this observation, horizontal reinforcement does not have a significant effect on shear capacity. They also argue that the shear capacity of the walls cannot be reliably predicted using the truss analogy method.

The authors conclude that; 1) despite the effect of axial compression in reducing vertical and horizontal displacements, increased axial compression increased the horizontal load-carrying capacity and secant stiffness; 2) the web transverse reinforcement did not appear to have significant effect on the shear capacity of the walls; 3) concrete compressive strength appeared to have negligible effect on strength and deformation capacities of the walls; 4) the walls failed in flexural

mode and at locations of inclined flexure-shear cracks; 5) shear resistance appeared to be associated with the development of tri-axial compressive stress conditions within the compressive zone near the base of the wall where the flexural moment attained its maximum value.

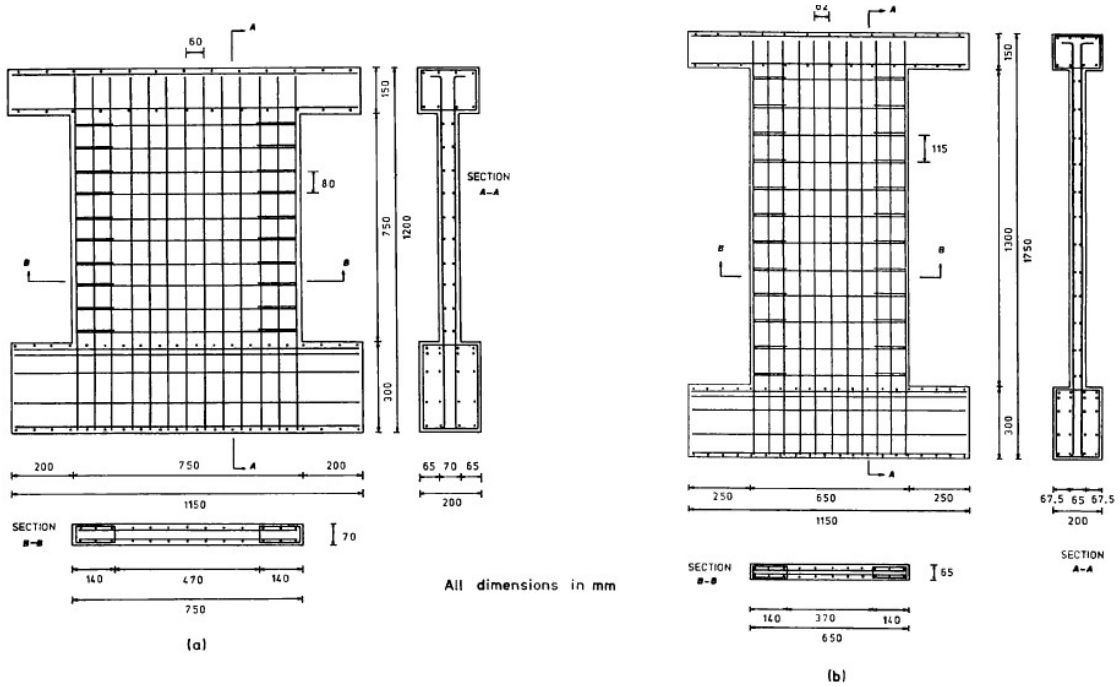

Figure 2.11 - Typical details for walls tested by Lefas et al (1990)
[Lefas, et al, 1990]

2.2.9 Oesterle et al (1976)

One of the largest experimental investigations on concrete shear walls was conducted in the 1970s at the Construction Technology Laboratories in Skokie, Illinois. In 1974 the Portland Cement Association, in collaboration with the National Science Foundation, conducted a large scale experimental and analytical investigation on the seismic performance of reinforced concrete structural walls. The objective of this investigation was to develop design criteria for earthquake-resistant shear walls.

Sixteen 1/3-scale concrete shear walls with flanged, barbell and rectangular cross-sections were tested. Typical dimensions of the walls are shown in Figure 2.12. The boundary elements of four specimens were not reinforced with transverse reinforcement. In order to investigate the behaviour of repaired walls, two specimens with damaged webs were repaired by replacing the web sections and they were then re-tested. The damaged web of the walls, which was originally 100mm thick, was replaced with a 150mm thick web before the walls were re-tested.

Three type of loadings were used in the tests: Monotonic, incrementally increasing reversed cyclic loading and modified reversed cyclic loading. The reversed cyclic loading scheme consisted of 3 cycles of force-controlled loading up to the yield point, and displacement-controlled loading following the onset of yielding. The modified reversed cyclic loading consisted of a series of large inelastic cycles separated by a cycle at the yield deformation level which was developed based on data from analytical investigations. This was to simulate seismic loads in a more realistic manner.

The tested walls were instrumented to measure displacements at six levels over the height of the walls, as well as rotations, shear deformations and anchorage slip at construction joints within the plastic hinging length (1.83m from the base of the walls).

The walls that were subjected to low nominal shear stresses exhibited a flexural behaviour and failed through rupture of longitudinal reinforcement under flexure. The author discusses that because of horizontal cracks, the shear stresses were mainly transferred through concrete interface friction and dowel action of the vertical reinforcement. Walls that were subjected to high nominal shear stresses were observed to undergo large inelastic rotations. The failure mechanism observed in these walls was web crushing which, as suggested by the authors, was caused due to the criss-crossing cracks that reduced the compressive strength of concrete. The higher shear stresses resulted in formation of inclined shear cracks that increased the interface friction, and this provided a stiffer system than that of the specimens with lower nominal shear stress.

It was observed that ductility of the walls decreased with the increase of shear stress. It was also reported that axial compressive stress decreased the ductility of the flexure-dominant walls and increased ductility in shear-dominant specimens. The lateral load capacity of walls subjected to high shear stresses was governed by web crushing. The effect of horizontal web reinforcement on rotational capacity of the walls was also investigated. It was hypothesized that the horizontal web reinforcement would decrease the rate of deterioration of compression struts and hence allow for larger rotations prior to web crushing. It was however observed that a higher horizontal reinforcement ratio did not contribute significantly to the rotational capacity of the walls.

Shear deformations (distortions) were measured and plotted against shear force for all walls. A distinct pinching behaviour was observed that indicated the loss of shear stiffness under inelastic reverse cycling. This behaviour was attributed to the fact that during the unloading cycle, shear is first resisted by dowel action and therefore the shear stiffness is small, however as the crack closes,

shear stiffness increases due to the impact of crack interface friction and truss action. Pinching increases at higher rotations and loading cycles. The results of this study suggest that shear distortion is linked to plastic hinge rotation. It was also observed that shear stiffness is directly related to the state of stress in the longitudinal reinforcement. Following the yield of the longitudinal reinforcement, both flexural and shear stiffness decreases in similar proportions.

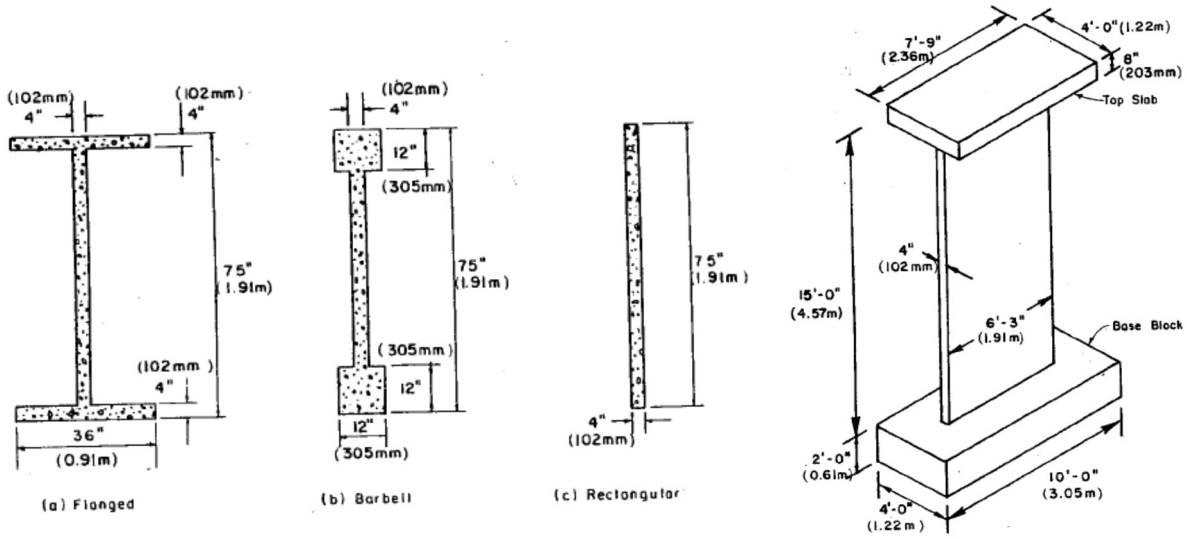

Figure 2.12 - Typical details for walls tested by Oesterle et al (1976)
[Oesterle et al, 1976]

2.3 Concrete Shear Walls Reinforced with High-Strength Reinforcement

The following section summarize existing literature on experimental studies on concrete shear walls reinforced with high-strength reinforcement. These studies include walls with different aspect ratios, steel types, geometrical dimensions and concrete properties. Appendix C provides details of the walls presented in the following sections.

2.3.1 Sajedul Hug et. al. (2018)

An experimental study sponsored by the American Concrete Institute (ACI) Foundation's Concrete Research Council was conducted by Sejadul Hug et al. (2018) that consisted of testing 4 concrete shear walls with aspect ratios of 2.9 and T-shaped cross-sections as shown in Figure *2.13*. Three of the tested walls were reinforced with Grade 690 MPa conforming to ASTM A615 standard. This type of steel has a defined yield plateau and has higher ductility compared to ASTM A1035 steel.

The walls were tested under reversed cyclic loading and zero axial compression. The lateral loading was applied as displacement-controlled load steps using two hydraulic actuators at the top of the walls. Lateral bracing was installed to prevent unwanted out-of-plane movant of the wall during the test. Instrumentation of the walls consisted of potentiometers installed at the top of the walls to measure lateral displacement of the wall. Potentiometers were also installed diagonally in the web section of the wall to measure shear deformations. The displacement of the foundation unit was also monitored using potentiometers. In addition, optical makers were applied to the surface of the walls to allow for a more accurate measure of the wall deformation during the tests. Strain gauges were installed at critical locations to measure strains in the shear and flexural reinforcement.

Figure *2.14* shows the experimental hysteresis curves for the walls tested in this study. Wall tests indicated that, based on the available data, walls with reinforcement f_t/f_y ratio of greater than 1.20 were able to reach lateral drift (Δ/H) capacity of 3%. Walls with similar f_t/f_y ratios, regardless if the reinforcement grade, has similar behaviours. Drift ratios associated with rupture of flexural reinforcement did not have a strong correlation with the uniform or fracture elongation of the reinforcement. In addition, it was found that the majority of deformation was due to flexure. Shear deformations contributed to 5% to 10% of the overall displacement up to drift ratio of 1%, and 15% to 20% of the overall displacement up to drift ratio of 3%. This was found to hold true for all tested walls regardless of the reinforcing steel type.

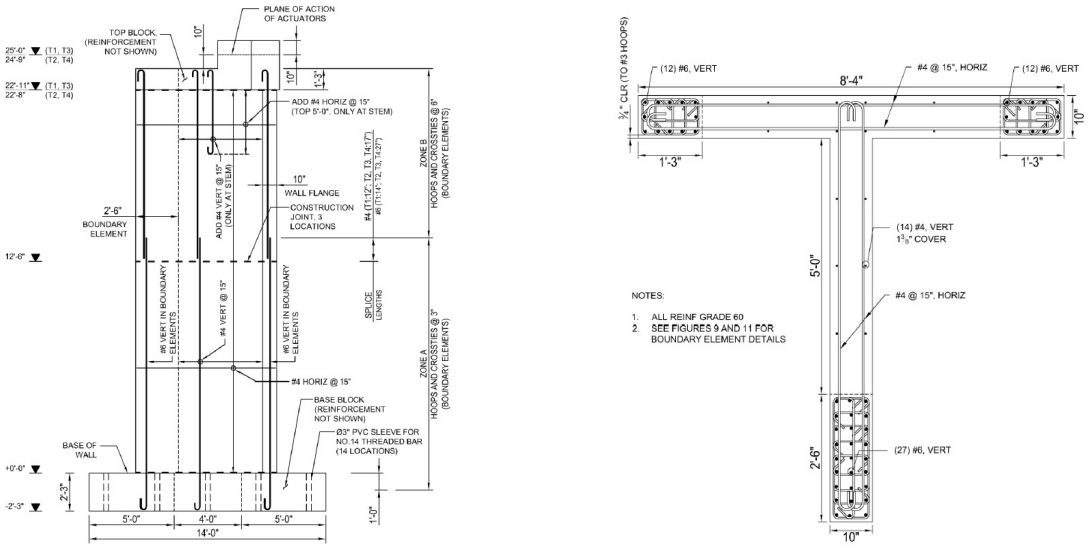

Figure 2.13 Typical details of the tested walls by Sajadul Hug (2018)
[Adapted from Sajadul Hug, 2019]

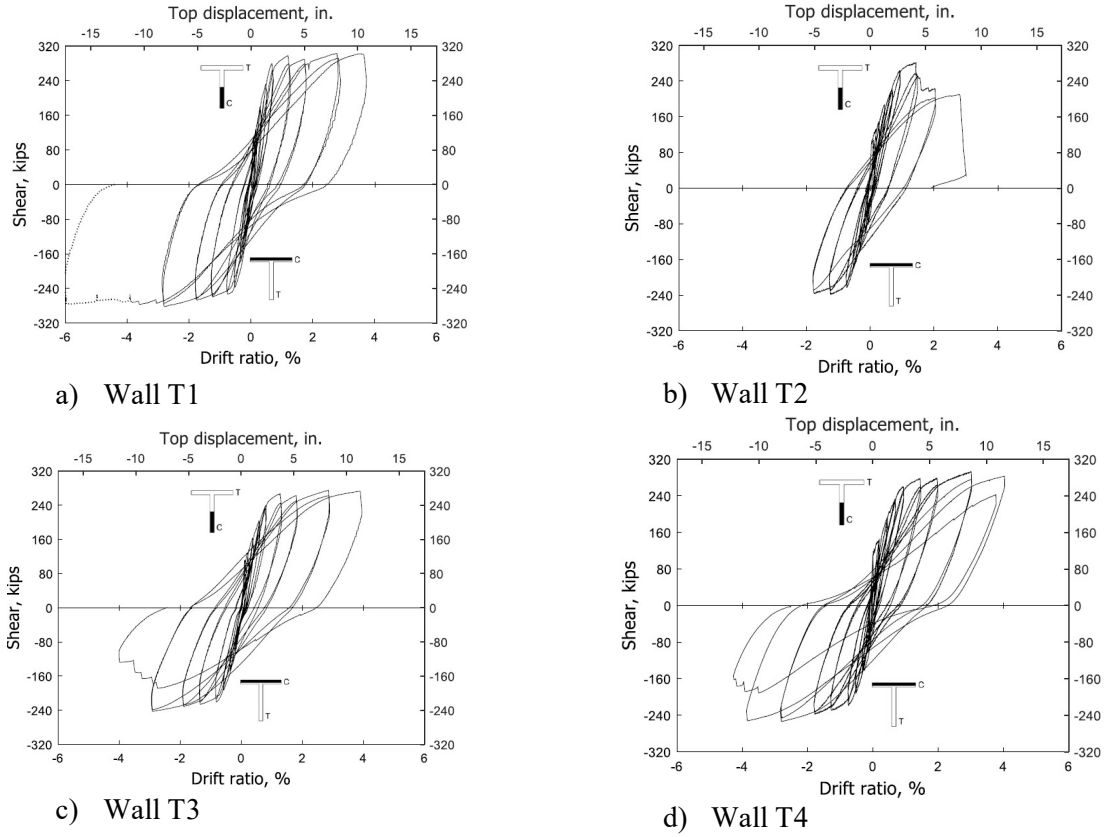

Figure 2.14 Load-deflection diagram for walls tested by Sajadul Hug (2018)
[Adapted from Sajadul Hug, 2018]

2.3.2 Chung-Chan Hung et. al. (2017)

Chung-Chan Hung et al. (2017) tested 4 reinforced concrete shear walls with aspect ratios (H/L) of 0.9 and constructed with Ultra High-Performance Concrete (UHPC). Three walls were reinforced with Grade 785 MPa steel bars conforming to the Taiwanese SD785 reinforcing steel standard. The walls consisted of pre-cast reinforced concrete sections that were 1320mm high x 1500mm wide x 160mm thick. The precast sections were attached to rigid loading blocks at the top and bottom the walls as shown in Figure 2.15. The compressive strength of the concrete used in the construction of the walls ranged between 115 and 166 MPa. Figure *2.16* presents typical reinforcement details for the walls in this study.

Loading consisted of reversed cyclic loading applied using three hydraulic actuators with a total lateral force capacity of 3000KN. The point of application of the lateral load (centerline of the

actuators) was 1700mm from the base of the wall. No axial load was applied to any of the tested walls.

Lateral deflections of the walls were recorded using Linear Variable Displacement Transducers (LVTDs) installed at the top of the walls. Additional LVDTs were installed at critical locations to measure sliding and uplift of the foundation units. Strains in the steel reinforcement were measured using strain gauges installed at strategic locations along the vertical and horizontal reinforcement. An array of Optotrack Certus optical measurement markers were installed in a 250x250 grid in the wall's web section to measure the shear deflections.

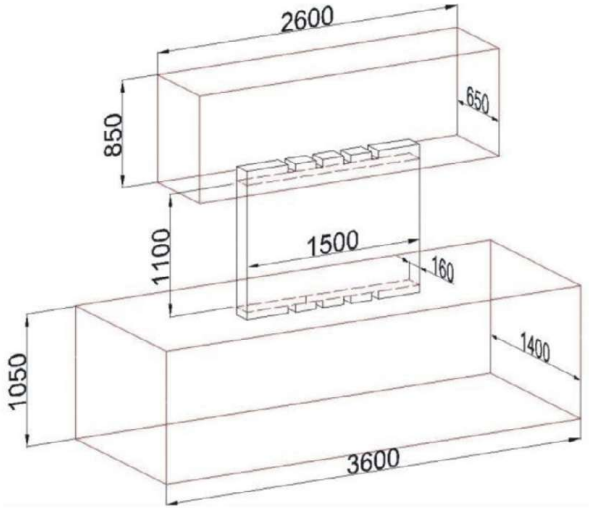

Figure 2.15 Dimensions of the tested walls

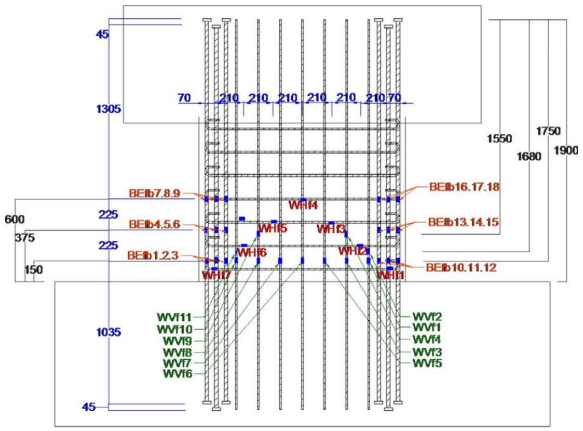

Figure 2.16 Typical reinforcement details for wall with high-strength reinforcement

The UHPC and UHPFRC shear walls reinforced with high-strength reinforcement failed in shear at 3% lateral drift (Δ/H). It was observed that despite reducing reinforcement congestion, the UHPFRC combined with the high-strength reinforcement was not able to prevent sliding shear which started at 2% drift. It was also observed that the high-strength reinforcement delays the onset of yielding.

2.3.3 Baek et. al (2017)

Baek et al (2017) 8 concrete shear walls with aspect ratio of 2.0 and reinforced with Grade 550 reinforcement conforming to ASM A615 under reversed cyclic loading and constant axial

compression. The objective of this experimental program was to investigate the effect of Grade 550 MPa reinforcement on the performance of reinforced concrete shear walls.

The walls presented in this study were 3000mm high, 1500mm wide and 200mm thick. The flexural reinforcement consisted of Grade 550 reinforcement conforming to ASTM A615. The flexural reinforcement ratio was intentionally increased in some walls to increase the shear demand and ensure a shear failure mode. Concrete compressive strength ranged between 26 and 37 MPa. Figure 2.17 provides reinforcement details of the wall presented in this study. The walls were tested under reversed cyclic loading and constant axial loads equal to 7% of the concentric axial capacity of the walls. The lateral load was applied as displacement-controlled load increments using hydraulic actuators. Two hydraulic actuators were also used at the top of the wall to apply and maintain the level of the axial compression on the walls.

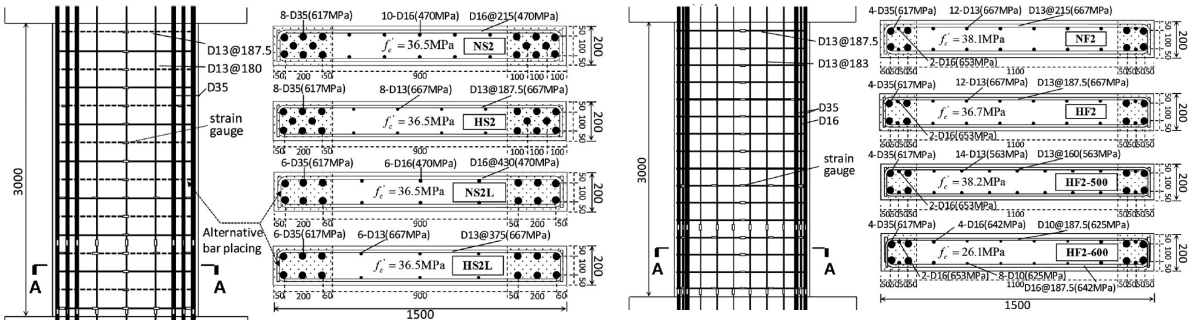

Figure 2.17 - Reinforcement details of walls tested by Baek et al. (2017)
[Adapted from Baek et al., 2017]

A finite element modelling program was used to conduct a nonlinear analysis of the tested walls. The models consisted of eight-node isoperimetric plane stress elements. The results of this analytical study were found to be in good agreement with the experimental results.

Figure *2.18* presents the experimental hysteresis curves for the walls tested in this study. All walls failed in shear or flexure as expected. It was observed that the wails reinforced with Grade 550 MPa reinforcement failed due to the rupture of the flexural bars. The shear-dominant walls were found to have shear strengths significantly greater than the predictions of the ACI 318 provisions with safety margins ranging between 1.48 and 1.83.

The lateral displacement ductility of the walls ranged between 2.3 and 2.7. The reduced ductility of the walls was attributed to the lack of confinement reinforcement in the boundary elements. In addition, it was found the majority the total wall deformation, was due to the flexural contribution,

regardless of the failure mode of the walls. In general, it was reported that the lateral displacement ductility ratios were not impacted by the use of Grade 550 MPa ASTM A615 steel.

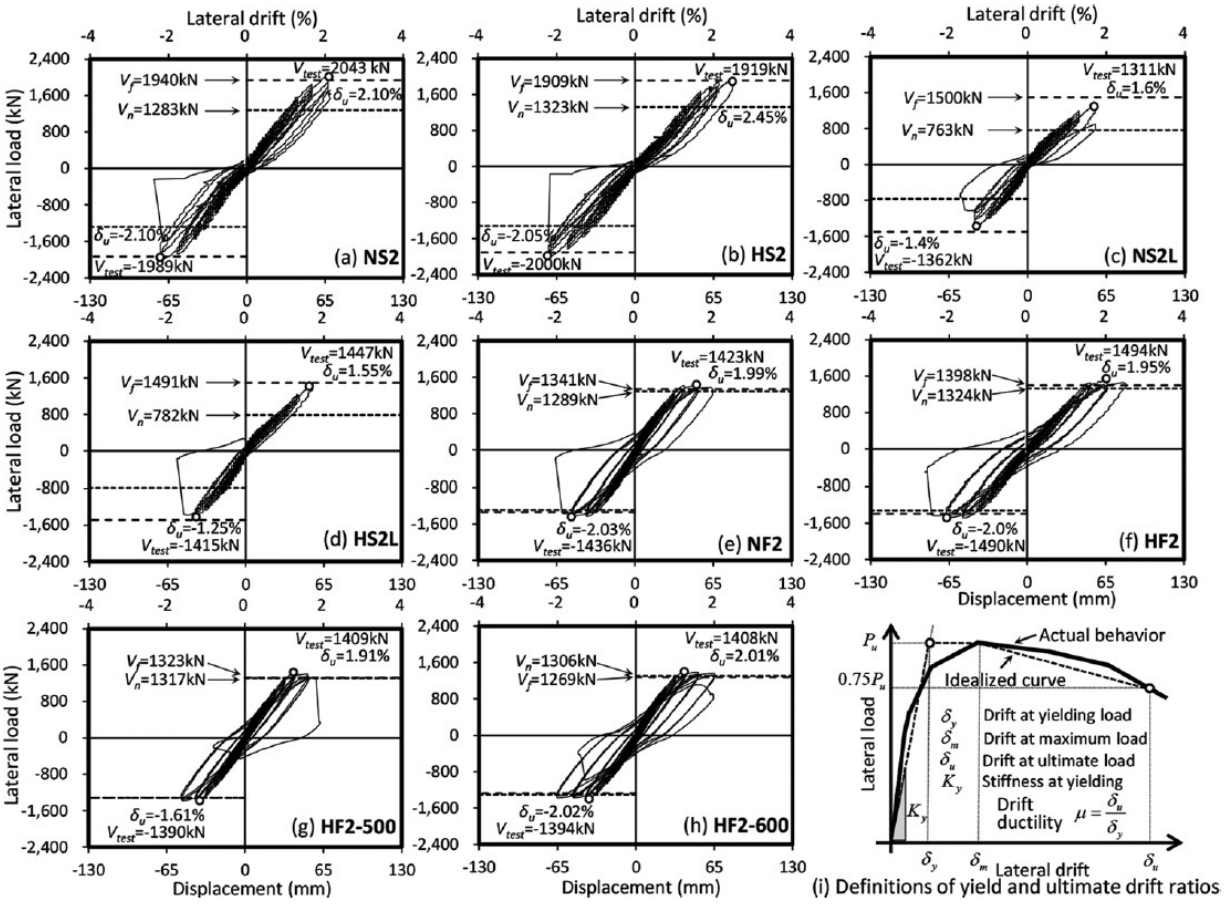

Figure 2.18 Lateral load-deformation diagrams for walls tested by Baek et al., 2017 [Adapted from Baek et al., 2017]

2.3.4 Cheng et al (2016)

In this study, five large-scale reinforced concrete shear walls with aspect ratios of 1.0 were tested under reversed cyclic loading with zero axial compression. The reinforcing steel used in the construction of the walls consisted of conventional Grade 400 MPa as well as Grade 785 MPa reinforcement that met the requirement of the Japanese USD785 reinforcing steel. The objective of this research was to investigate the effect of high-strength steel reinforcement on deformation capacity and shear resistance of reinforced concrete shear walls with low aspect ratios (squat walls). In addition, the impact of reduced boundary element confinement was investigated.

Figure 2.19 shows typical details of two tested wall specimens and their corresponding hysteresis curves. It was noted that, the Grade 785 MPa reinforcement used in the tested walls had a distinct yield plateau. The target shear strength was the shear strength corresponding to the probable moment of the wall sections.

The loading protocol consisted of displacement-controlled increments in the horizontal direction that were cycled three times at each displacement increment. LVDTs and an infrared-based non-contact monitoring system was used to record deformation history of the walls at various locations. The lateral displacement of the walls was recorded at the loading point at the top of the walls as well as their mid-height.

Walls with Grade 785 MPa [115 ksi] reinforcement exhibited a gradual loss of strength and approximately 20% greater deformation than those reinforced with conventional Grade 400 MPa [60 ksi] steel. It was shown that shear stress had a significant effect on the deformation capacity of the walls. The ultimate shear capacities of two walls that were designed to undergo high shear stresses were approximately 40% smaller compared to the other walls, regardless of their reinforcement grades. Tests of all three walls reinforced with Grade 785 MPa [115 ksi] reinforcement were terminated before reaching the target drift ratio of 3.0% due to significant loss of lateral resistance that was attributed to the formation of damage at the base of the walls. It was observed that that the ductility of the walls reinforced with Grade 785 MPa [115 ksi] reinforcement decreased with ultimate drift ratios of 1.64%, 1.9%, and 1.56% compared to the walls that were reinforced with conventional steel with ultimate drift ratios of 2.41% and 3.05%. It was also observed that strain penetration contributed approximately 50% more to the total drift in specimens reinforced with Grade 785 MPa [115 ksi] steel. The authors discuss that the reason behind this observation is the higher anchorage demand for Grade 785 MPa [115 ksi] reinforcement.

The authors conclude that the walls reinforced with Grade 785 MPa [115 ksi] steel exhibited 20% greater drift than those reinforced with Grade 400 MPa [60 ksi] steel (despite similar strength). However, drift capacity defined as drift at ‘80% of ultimate load’ was less than those of walls with conventional reinforcement. This reduction in drift capacity was deemed to be caused by severe damage to the concrete at the base of the wall. The lateral load capacities of the specimens were controlled by their flexural capacities as expected regardless of the reinforcement grade.

Conservative estimates of strength were obtained using the equation proposed by Wood (1990), and Gulec & Whittaker (2011).

It was shown that a 50% increase in the transverse reinforcement ratio in the boundary elements had no significant impact on the hysteresis curves of the tested walls. In other words, the smaller reinforcement ratio did not compromise wall behaviour. In addition, it was observed that the drift capacities of walls with higher shear stress demands were smaller. An increase in shear stress from $0.42\sqrt{f_c'}$ *to* $0.75\sqrt{f_c'}$ was associated with approximately 40% reduction in drift capacity.

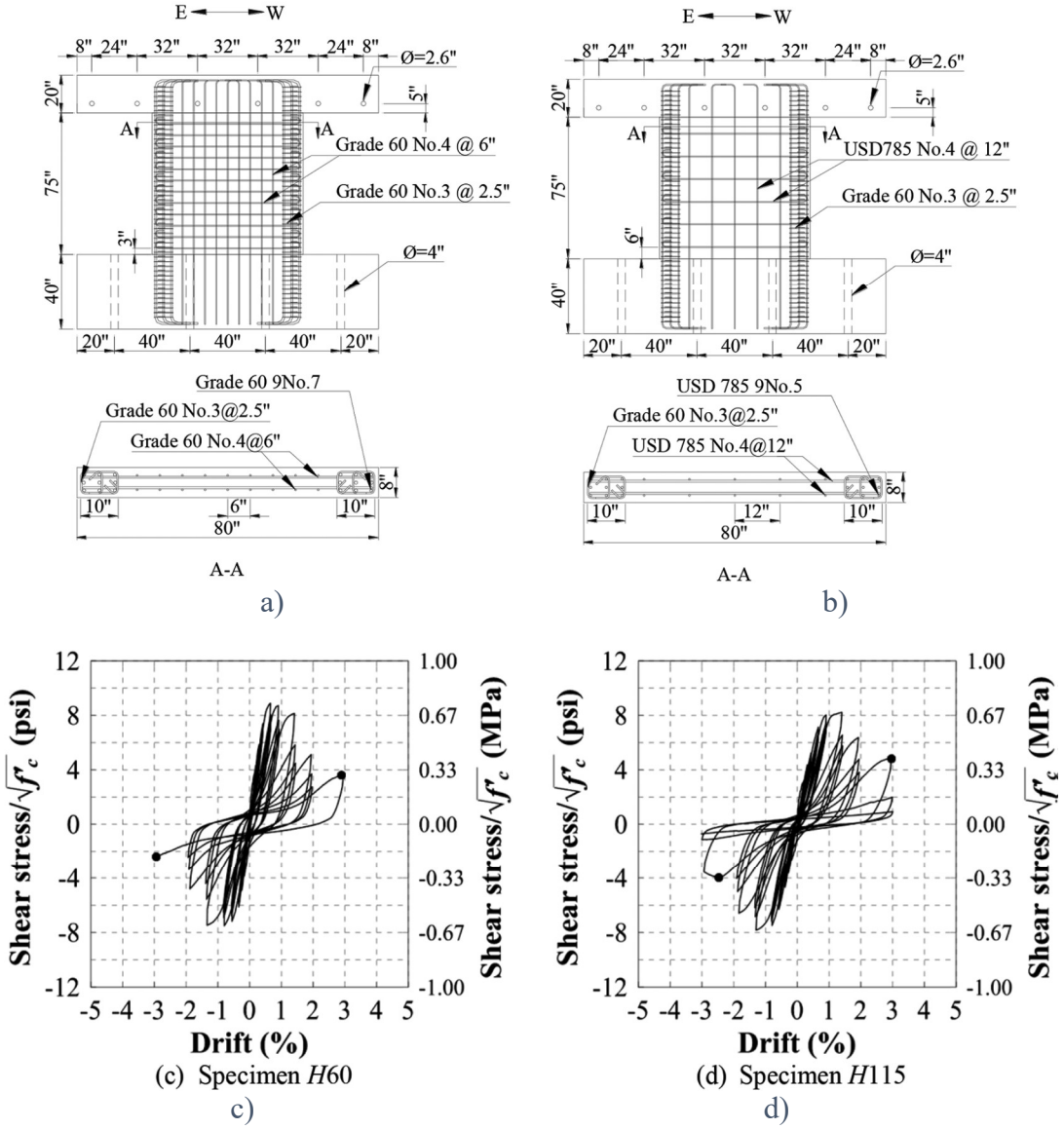

Figure 2.19 – a) & b) Reinforcement details for wall specimens H60 and H115; c) & d) hysteresis curves for specimens H60 and H115
[Adapted from Cheng et al, 2016]

2.3.5 Teng and Chandra (2016)

In this study, seven high-strength concrete (HSC) shear walls reinforced with high-strength reinforcement were tested under constant axial loading and lateral load reversals to investigate their shear behaviour. The tests were intended to provide a better understanding of the shear behaviour of HSC walls subjected to cyclic lateral loading. Test parameters were height-to-length ratio of the walls, vertical and horizontal web reinforcement ratios, and the effects of boundary elements in the form of flanges. The effect of high-strength reinforcement was not independently investigated in this research. Seismic shear provisions of ACI 318-14 and Eurocode 8 were assessed and compared to the experimental data. The parameters that were studied were the aspect ratio (h_w/l_w) of the walls, horizontal and vertical web reinforcement ratios, and the effect of the boundary elements (flanges) on the behaviour of the walls.

Figure 2.20 shows details of two types of walls that were tested. The walls had aspect ratios of 1.0 and 2.0 and were designed to fail in shear. The effect of distributed web reinforcement was investigated by varying the horizontal and vertical reinforcement ratios between 0.28% (corresponding to the minimum reinforcement ratio required by the ACI-318) and 0.75% (corresponding to the Eurocode 8 requirement).

The axial load level was maintained at 5% of the nominal axial load capacity of the walls. The lateral load was applied using two servo-controlled hydraulic actuators that applied the load through a rigid loading beam assembly at the top of the wall. LVDTs were installed at various locations of the walls to measure in-plane lateral displacements at the top and mid-height of the walls. Flexural deformations of the walls were measured using LVDTs installed along the edges and over the height of the walls. Shear deformations were measured by means of LVDTs installed diagonal on the web. Strains in the reinforcing bars were measured using strain gauges installed at critical locations. The lateral load was applied in single positive and negative drift cycles. The loading was stopped when the specimens failed abruptly, or their strength decayed to 70% of the ultimate strength.

Figure *2.21* shows the experimental hysteresis curves for the walls tested in this study. Test results showed that as the wall drift ratio increased, the contribution of flexural and shear deformations to

the total wall deformation became more dependent on the aspect ratio of the wall. For the wall with aspect ratio of 1.0, the contribution of shear deformation to total deformation was as significant as that of flexural deformations throughout the full range of applied drift ratios. For walls with an aspect ratio of 2.0, flexural deformation was the major contributor to the overall deformation of the wall at early stages of loading and prior to opening of large diagonal cracks at which point shear deformation became the major source of lateral deformation for the walls. It was observed that sliding shear was more significant in the one specimen that was constructed with flanges (wide boundary elements).

It was also observed that the walls with smaller h_w/l_w aspect ratios experienced larger shear strengths. The normalized average shear strength of walls with an aspect ratio of 1.0 was 1.6 to 2 times those of the walls with an aspect ratio of 2.0. Increasing the aspect ratio of the wall from 1.0 to 2.0 reduced the shear strength by 40% to 50%. Similar observations were made by Barda et al (1977) who found that increasing the aspect ratio of walls from 0.5 to 1.0 reduced shear strength by 20%. In addition, comparison of walls with varying amounts of horizontal and vertical reinforcement indicated that horizontal web reinforcement was more effective than vertical web reinforcement in walls with aspect ratio (h_w/l_w) of 1.0. The contribution of web reinforcement in increasing the shear strength of the tested walls was more pronounced in walls with aspect ratio of 2.0. Increasing vertical and horizontal web reinforcement individually from 0.28% to 0.75% resulted in increases in shear strength of 25% and 44% respectively.

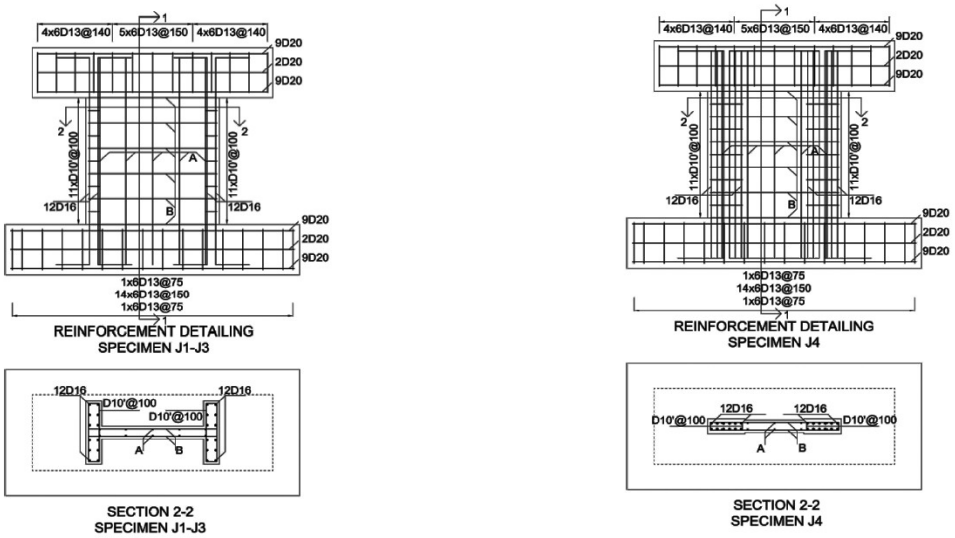

Figure 2.20 - Details of Tested Wall Specimens.
[Adapted from Teng and Chandra, 2016]

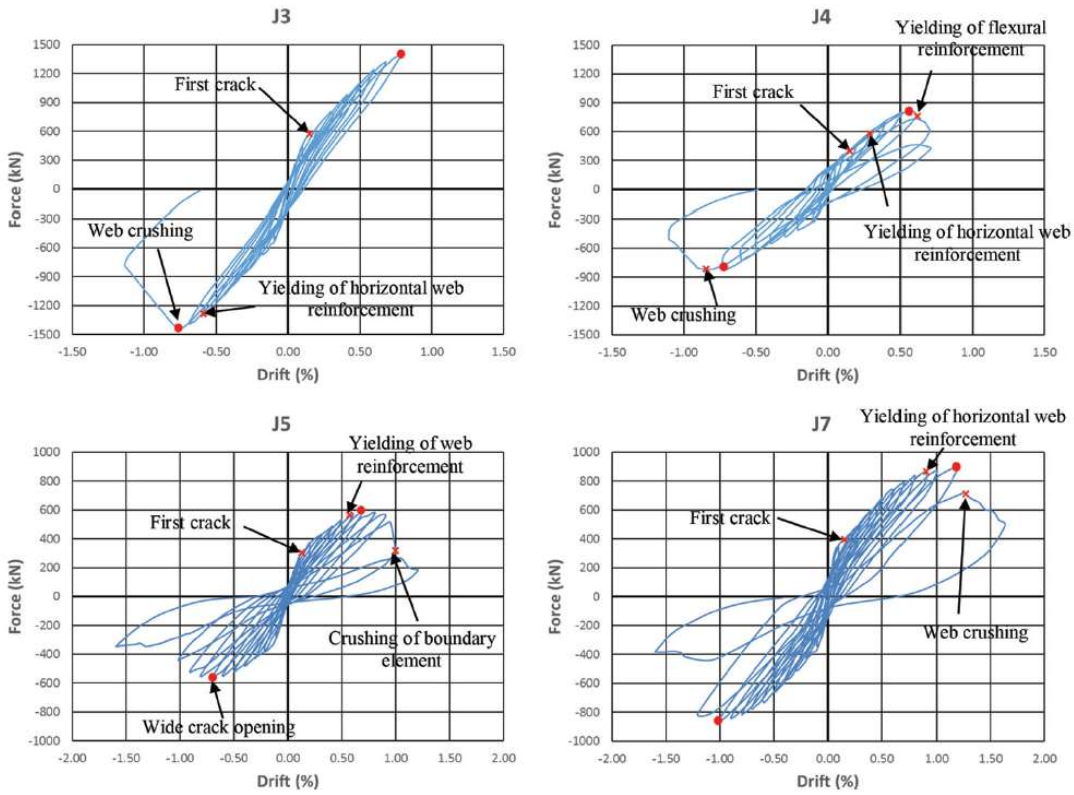

Figure 2.21 – Lateral load-deflection diagrams for walls tested by Teng and Chandra [Adapted from Teng and Chandra, 2016]

2.3.6 Park et al (2015)

Park et al (2015) tested eight reinforced concrete specimens reinforced with Grade 550 MPa [80 ksi] reinforcing bars to investigate the effect of high-strength reinforcement on shear capacity and deformation capacity under cyclic loading. Tested specimens represented walls used in nuclear power plants designed as per ACI 349, Code Requirements for Nuclear Safety-Related Concrete Structures. The main objective of this experimental program was to substantiate evidence for the applicability of Grade 550 MPa [80 ksi] steel reinforcement in the shear design of low-rise walls. The walls in this study had an aspect ratio of 1.2, and test parameters consisted of the grade of horizontal reinforcement, concrete strength, web reinforcement ratios, use of hoops in the boundary regions, shape of cross-section, and expected failure mode (shear vs. flexure). Details of the tested wall specimens are shown in Figure 2.22.

The lateral loading protocol followed the criteria proposed by Hawkins and Ghosh (2004). Instrumentation of the specimens consisted of LVDTs installed to measure the lateral

displacement, sliding at the base, and shear deformations. Strain in the boundary element longitudinal bars, and web vertical and horizontal bars were also recorded using strain gauges.

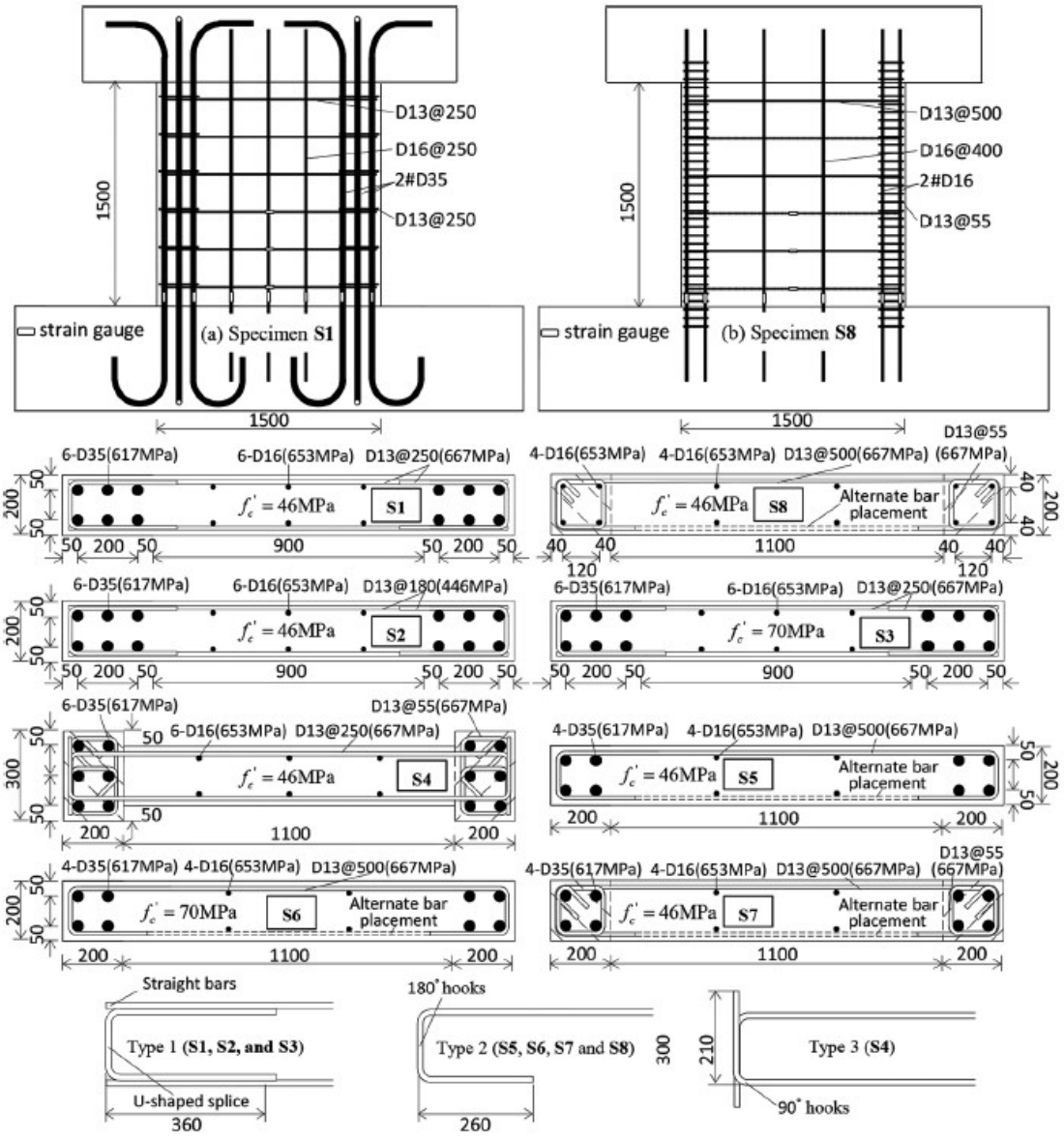

Figure 2.22 - Dimensions and reinforcement details of walls tested by Park et al (2015) [Adapted from Park et al, 2015]

Figure *2.23* resents the experimental hysteresis curves for the walls test by Park et al. (2018). Five of the shear-dominant specimens with confined boundary elements failed due to sliding of the wall panel, while two of the walls that had boundary confinement failed due to web crushing. The wall that was designed to be flexure-dominant failed due to web-crushing following large inelastic

flexural deformations. It was noted that in all shear-dominant walls, at least one horizontal bar yielded before the failure of the walls. The shear strengths of walls obtained experimentally were 30% to 99% higher than the values predicted by the ACI 349 code.

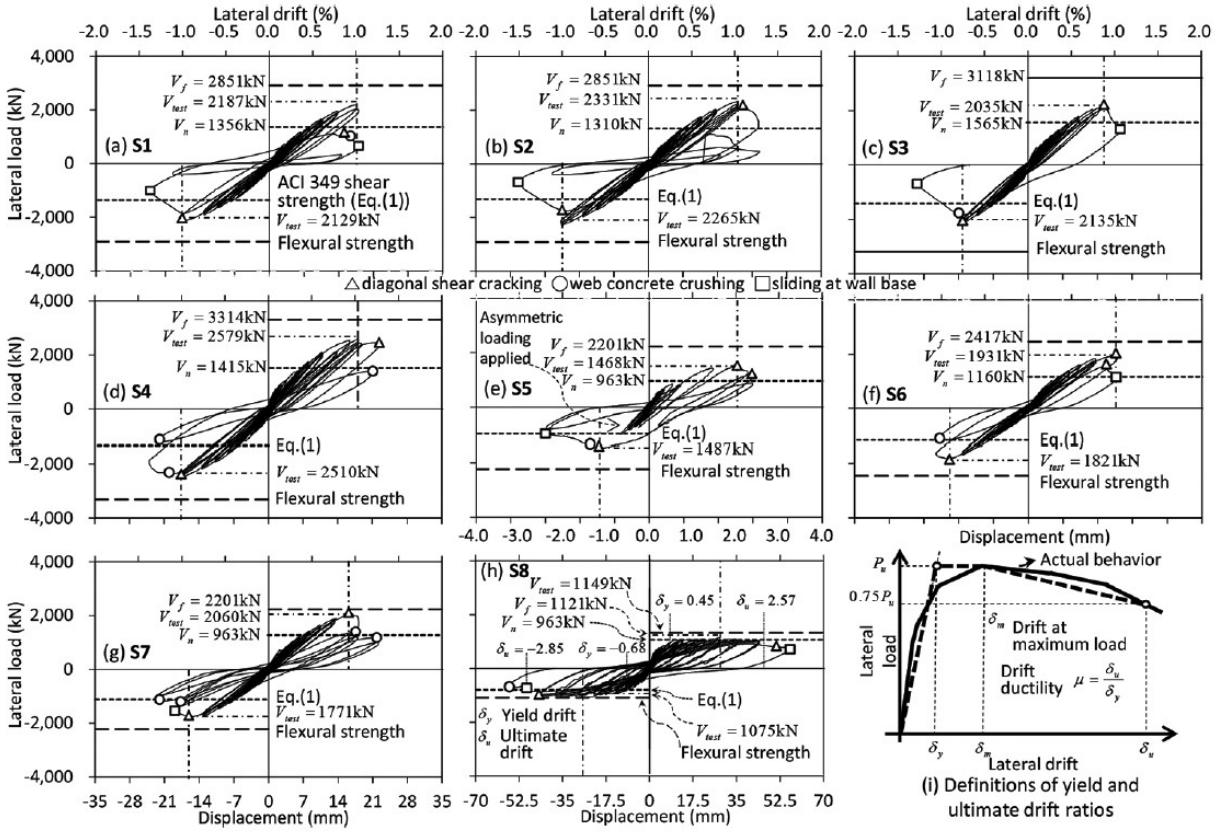

Figure 2.23 - Lateral Load-Displacement Relationships of Tested Specimens
[Adapted from Park et al, 2015]

The main observation in this research is that the behaviour and failure mechanisms of the specimens with high-strength and regular reinforcement were identical except that the wall with high-strength reinforcement had 6% less shear strength. The reduced strength was attributed to the larger spacing of the high-strength horizontal bars that resulted in larger diagonal cracks. Moreover, the flexure-dominant wall reinforced with high-strength bars and boundary confinement showed ductile behaviour, although the response showed premature strength and stiffness decay. It was also observed that boundary hoops increase the shear strength of walls by preventing diagonal cracks from propagating into the boundary elements. In addition, a study of present and past experimental results for walls reinforced with high-strength reinforcement showed

that that the safety margin of the ACI method in predicting the shear strength of walls decreases as $\rho_h f_{yh}$ increases.

2.3.7 Dazio et al (2009)

Dazio et al. tested six (6) reinforced concrete walls to investigate the effects of longitudinal reinforcement properties including ductility of steel reinforcement and longitudinal reinforcement ratio on the cyclic behaviour of concrete shear walls. The main focus of this research program was to investigate the effects of reinforcement ratio and ductility properties of the longitudinal reinforcement on ductility of slender walls designed for moderate seismicity.

Figure *2.24* presents typical details of the tested walls. The tested walls were ½-scale models of the lower part of a shear wall in a representative 6-storey building. All walls had identical dimensions and shear reinforcement that satisfied capacity design requirements but were governed by the longitudinal reinforcement ratio. It was reported that none of the reinforcing bars used in the test specimens exhibited a pronounced yield point or plateau. The 0.2% offset method was used to determine the yield point (f_y = 500 MPa). Figure 2.25 shows the stress-strain relationship for D12 reinforcement used in the tested walls.

The walls in this study had an aspect ratio of 2.3 and the main test parameters included reinforcement ration and ductility properties of the reinforcing steel bars. Wall specimens were tested under reversed cyclic loading and constant axial loads. The effect of the axial load on the behaviour of the wall was investigated by applying different magnitudes of axial loads on different walls (5.1% to 12.8% of $\%A_g f'_c$). The cyclic loading history proposed by Park (1988) was used for testing all specimens which comprised of two displacement cycles for each drift increment.

Data collected during testing included shear deformations, lateral deformations of the walls and strains in the longitudinal reinforcement in boundary elements. Linear Variable Differential Transducers (LDVT) were used to capture the displacements. In addition, Demec measurement sensors were used to record average strains in longitudinal and horizontal reinforcement, as well as concrete strain distribution over the surface of the walls.

The instrumentation used for testing allowed for determining the contribution of flexural and shear deformations on the overall deformation of the test specimens. Shear displacements were determined using a method proposed by Hirashi (1984). Flexural deformations were computed

assuming that plane sections before bending remain plane after bending and by calculating curvatures based on the information supplied by the LVDTs. Total flexural deformation included the 'fixed-end' deformation which was the contribution from the base crack just above the foundation, and the actual flexural deformation from above the base crack.

Figure 2.26 present the load-deflection diagrams for the walls tested in this study. All tested specimens failed in flexure with flexural deformations being considerably higher than shear deformations, which is expected in slender walls. An important observation was the effect of reinforcement ratio on the spread of plasticity along the height of the wall (i.e., plastic hinge length). It was observed that reinforcement with higher post-yield tension hardening resulted in a larger plastic hinge length. In other words, the larger the increase in the flexural tensile force of the cross-section following the onset of yielding, the larger is the inelastic deformations (plastic hinging length) over the height of the wall. The author suggests that the post-yield tension hardening affects the spread of plasticity in the same manner as it affects the moment gradient over the height of the wall and that the impact should be considered in plastic hinge formulations.

Three of the wall specimens experienced premature fracture of the vertical web reinforcement. The author explained that this was due to four main reasons: 1) the smaller spread of plasticity due to smaller reinforcement ratios in the web, 2) local crack patterns which consisted of a single wide crack in the web region which formed due to smaller vertical reinforcement ratios in the web and larger spacing of transverse reinforcement (the single crack did not propagate into the boundary elements due to higher reinforcement ratio in the boundary elements and smaller spacings of the confining steel), 3) smaller diameter bars used in the web region and lack of spalling facilitated a better bond when compared to the longitudinal reinforcement in the boundary regions, which resulted in larger strain concentrations at the cracks within the web region, 4) small tension hardening of the reinforcement which resulted in even higher strain concentrations at the cracks, resulting in premature rupture of bars.

The authors concluded that reinforcement ductility and ratio significantly affected the post-yield behaviour of concrete shear walls. Walls with smaller longitudinal reinforcement ratios experienced pre-mature fracture of the vertical web reinforcement which was deemed to be due to the small reinforcement ratio in the web and limited ductility of the high-strength reinforcement.

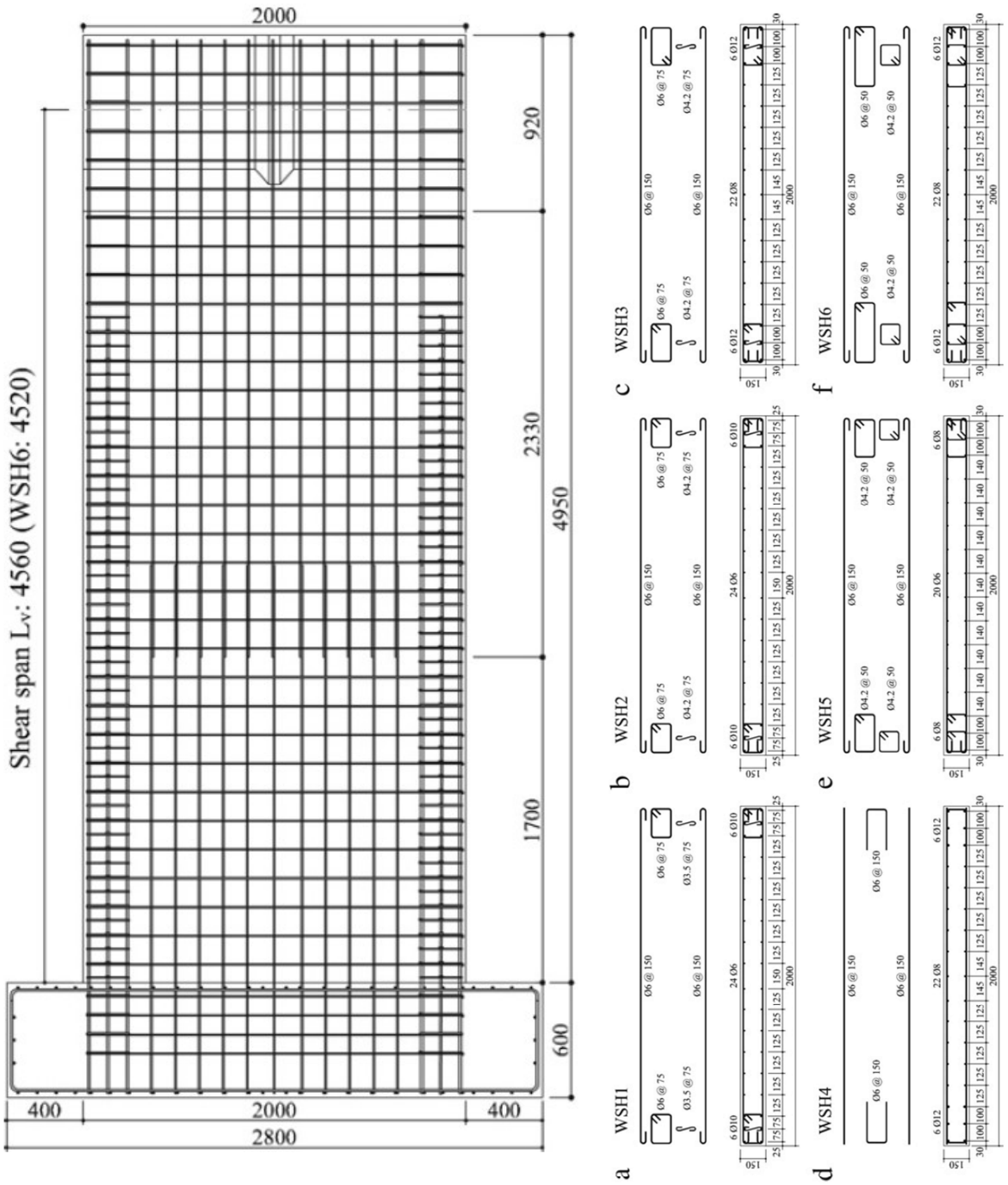

Figure 2.24 - Details of tested wall specimens
[Adapted from Dazio et al, 2009]

The smaller tension hardening gradient led to reduced spread of plasticity, which in turn led to additional strain concentrations at the base crack and contributed to premature fracture of the high-strength reinforcement. The author emphasized the importance of the ductility of the web reinforcement and asserted that it should be as crucial as the ductility of the longitudinal

reinforcement in boundary elements to prevent premature wall failure. Another conclusion from this study is that the base cracks that form due to lack of adequate longitudinal and transverse reinforcement in the web lead to concentrations of strains at the height of the crack following the rupture of the first reinforcing bar, which subsequently leads to the failure of the walls.

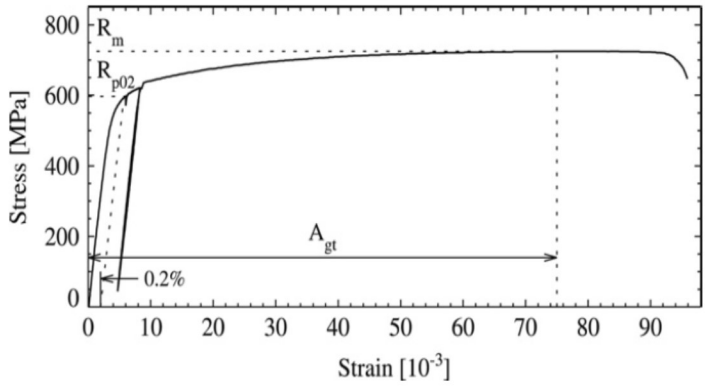

Figure 2.25 - Typical stress-strain diagram for D12 (12mm dia.) bars used by Dazio et al (2009) [Adapted from Dazio et al, 2009]

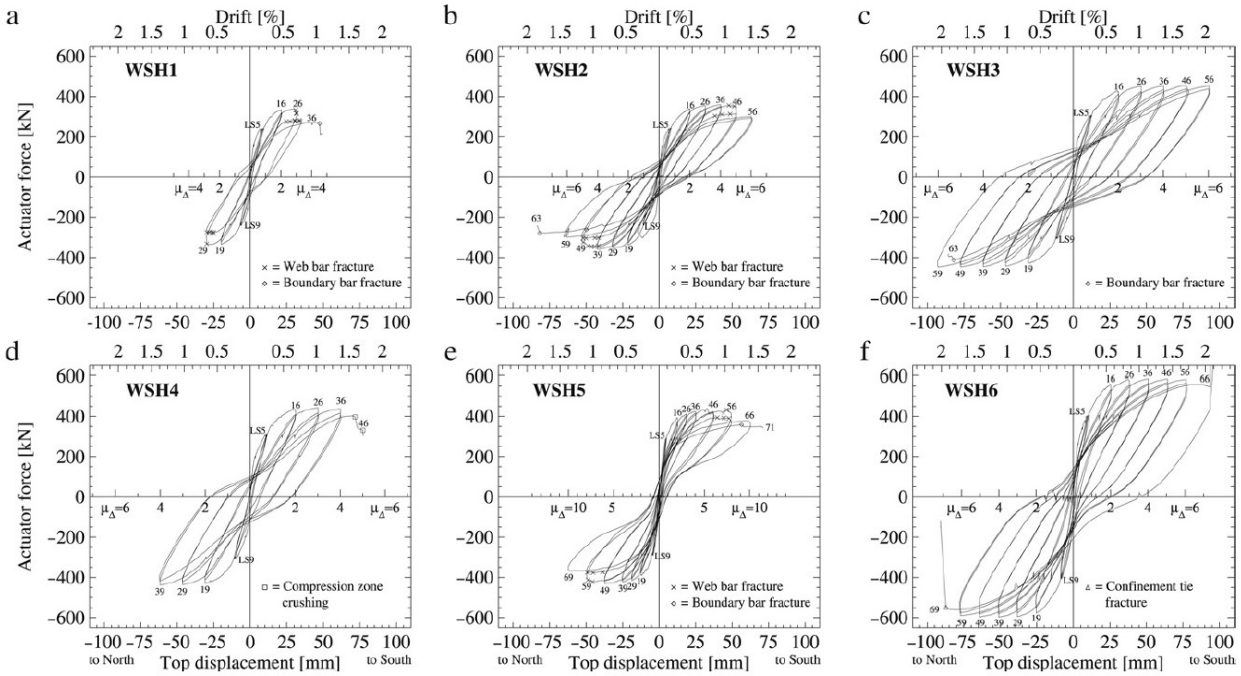

Figure 2.26 - Load-deformation diagrams of the walls tested by Dazio et al. (2009) [Adapted from Dazio et al, 2009]

2.3.8 **Kimura and Sugano (1996)**

Kimura and Sugano (1996) tested five (5) high-strength reinforced concrete walls under reversed cyclic loading and high axial loads to investigate the effects of high-strength concrete, axial load ratios and reinforcement strengths (see Appendix B for details) on the behaviour of the walls. Typical details of the test specimens are illustrated in Figure 2.27. Despite the research title proposed by the author, all specimens had characteristics of squat walls with aspect ratios of 1.7. It is commonly understood that walls with aspect ratios below 2.0 are generally prone to exhibit shear-dominant behavior. Aspect ratio of 2.0 is also used by the ACI code and the CSA standard as the threshold for flexural behaviour.

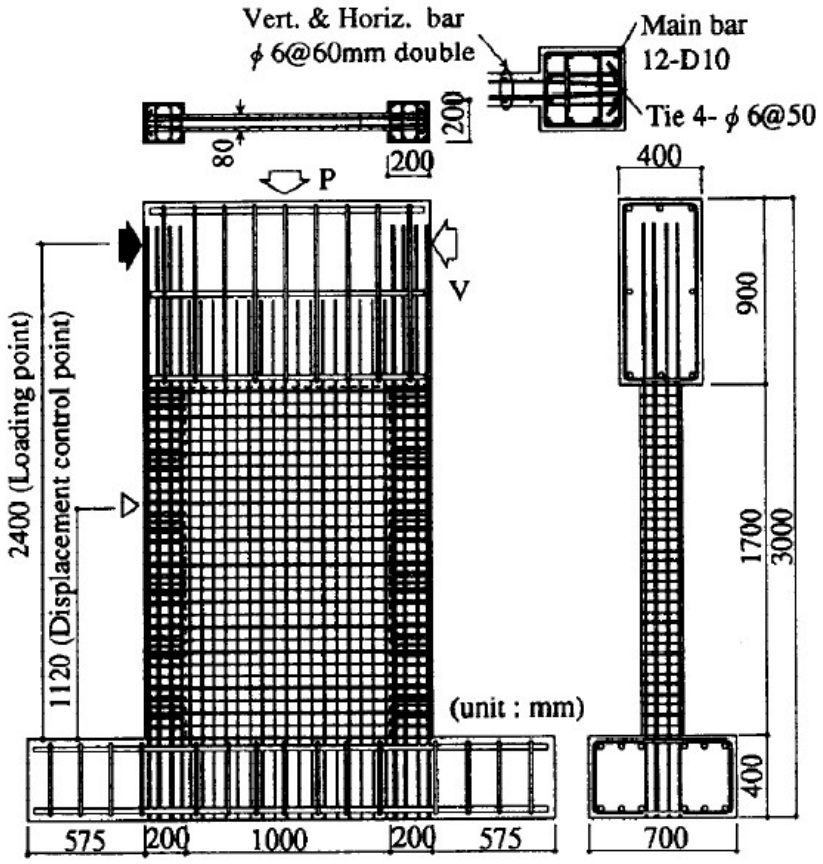

Figure 2.27 – Typical details of walls tested by Kimura and Sugano (1996)
[Adapted from Kimura and Sugano, 1996]

The loading protocol consisted of gradually increasing displacement angles consisting of one reversed cycle of ± 0.002, 0.0033, 0.005, and 0.0075, followed by two reversed cycles of ± 0.01, 0.015, 0.02 and 0.03, where the units of the displacement angles are in radians. The ultimate

displacement angle (R_u) was defined as the displacement angle at which the strength dropped to 80% of the maximum strength. The displacement angle included the contribution of P-Δ effects.

It was generally observed that the ultimate displacement angles of the tested specimens increased as axial loads decreased. This was true for all specimens except W8N08H in which high-strength reinforcement was used in the boundary elements. The authors discussed that the reduced displacement angle for specimen W8N08H was due to rupture of the high-strength longitudinal boundary element reinforcement. It was noted in this study that the elongation capacity of the high-strength reinforcement was smaller than that of normal-strength reinforcement bars used in other specimens, and this caused the rupture of the boundary element reinforcement at an earlier stage of loading.

All specimens except specimen W8N09H failed due to the crushing of concrete at the base of the wall, which, according to the authors, was caused due to shear-compression. The location of the neutral axis was examined for various specimens. It was found that the compression zone in specimens built with 80 MPa [11.6 ksi] concrete was smaller when compared to specimens with normal-strength concrete; in other words, the neutral axis was closer to the compression side in walls with higher concrete compressive strength. This is considered by the authors to be due to delayed crushing and spalling of high-strength concrete which also results in increased ductility. Specimen W8N08H, which was reinforced with high-strength longitudinal bars failed due to the rupture of longitudinal reinforcement at a drift ratio of 2.4%. At the ultimate lateral load, the drift ratio was 1.8% for this wall.

The authors investigated the effect of concrete strength and tie spacing on energy dissipation capacity of the specimens by measuring the equivalent viscous damping factor for each wall. It was observed that the viscous damping factor for all specimens was approximately 0.1 up to a displacement angle of 0.01, and gradually increased thereafter; however, tie spacing and concrete strength did not have a significant impact on the energy dissipation capacity of the specimens.

All longitudinal bars in the boundary elements reached yielding strains during testing. The vertical web reinforcement exhibited yielding for specimens with 80 MPa [11.6 ksi] concrete but not for the wall constructed with 40 MPa [5.8 ksi] concrete. The web transverse reinforcement did not reach yielding for any of the tested walls. The boundary element ties also did not reach yield levels.

The highest strain that the boundary element ties experienced was 0.002 at the base of the walls (height of 0 to 150mm from the base).

The following conclusion can be drawn from the results of this experimental program: 1) High-strength concrete increases the deformation capacity of concrete shear walls under the same axial loads; 2) Shear walls in high-rise buildings, which are typically subjected to high axial loads, can be safely designed using high-strength concrete; 3) Flexural capacity of walls constructed with high-strength concrete can be estimated with good accuracy using conventional equations even under high levels of axial load; 4) Walls with well-confined boundary elements are able to undergo larger deformations after the yielding of the longitudinal reinforcement in the boundary elements. It was also observed that these walls were able to sustain the axial loads after failure due to the crushing of web concrete; 5) Pre-mature rupture of high-strength reinforcement in boundary elements can reduce the deformation capacity of walls.

2.3.9 Japanese New RC Project (1988-1993)

A five-year national research project was conducted in Japan between 1988 and 1993 titled "Development of Advanced Concrete Buildings using High-Strength Concrete and Reinforcement," also referred to as "the New RC" project. Many research organizations were involved in undertaking the large-scale program which included experimental and theoretical investigations of concrete structural members constructed with high-strength concrete and steel reinforcement. The purpose of this project was to promote construction of high-rise reinforced concrete buildings and to provide new methods for use of high-strength materials in such construction.

The results of the New RC project were published in a book titled "Design of Modern High-Rise Reinforced Concrete Structures" in 2001 by Hiroyuki Aoyama which included project scope, results, conclusions and design recommendations broken into 9 chapters (Aoyama, 2001). Various aspects of the study were also summarized by Otani et al (1996). The mechanical properties of the high-strength materials used in the New RC project were discussed in detail in Chapter 3 of the book. It was noted in this chapter that the high-strength reinforcement used in the experimental program did not have a well-defined yield plateau which resulted in loss of ductility in flexural members. The high-strength reinforcement steel that was used for testing included USD685A, USD685B, USD980, USD785, USD1275 as well as SD345.

The experimental program involving shear wall tests was presented in Section 4.3 of the book. Flexural capacity of 'shear-compression failure' type walls were investigated by testing four (4) quarter-scale single-span walls with dumbbell-shaped cross-sections and aspect ratios of 1.9.

Load-deflection hysteretic curves are shown in Figure 2.28. Yielding of longitudinal reinforcement was observed in all walls at drift stages of 0.75% to 1.0%. Wall NW-3 which had the smallest longitudinal reinforcement ratio started to lose strength in the second cycle at 1% wall drift and failed due to the crushing of web section, which was followed by rupturing of the horizontal web reinforcement. All other specimens failed in a similar manner but at a higher drift without rupturing of the horizontal web reinforcement. Walls NW-4 and NW-5 had 16-10mm dia. longitudinal bars in the boundary elements with different web reinforcement ratios. Wall 5 had twice the web horizontal and vertical reinforcement ratio compared to wall NW-4. Test results show that wall NW-5 failed at a drift ratio of 1.5% whereas wall NW-4 failed at about 1%. Wall NW-5 also outperformed wall NW-6 which had higher longitudinal reinforcement ratio and the same web reinforcement as wall NW-5. Wall NW-6 failed at a drift of approximately 1.3% exhibiting the same failure mechanism as the other walls.

The author drew three main conclusions from this experimental investigation: 1) all specimens reinforced with high-strength reinforcement failed in a relatively brittle manner at drifts of 1.0% to 1.5% either by wall crushing or rupture of horizontal web reinforcement; however, the boundary elements, despite being damaged, were capable of carrying the applied axial loads; 2) shear strength of concrete walls reinforced with high-strength reinforcement can be evaluated using the Architectural Institute of Japan (AIJ) guidelines with slight modifications to the model used for concrete members reinforced with normal-strength reinforcement; 3) cumulative deformation capacity of walls increased as shear stresses decreased.

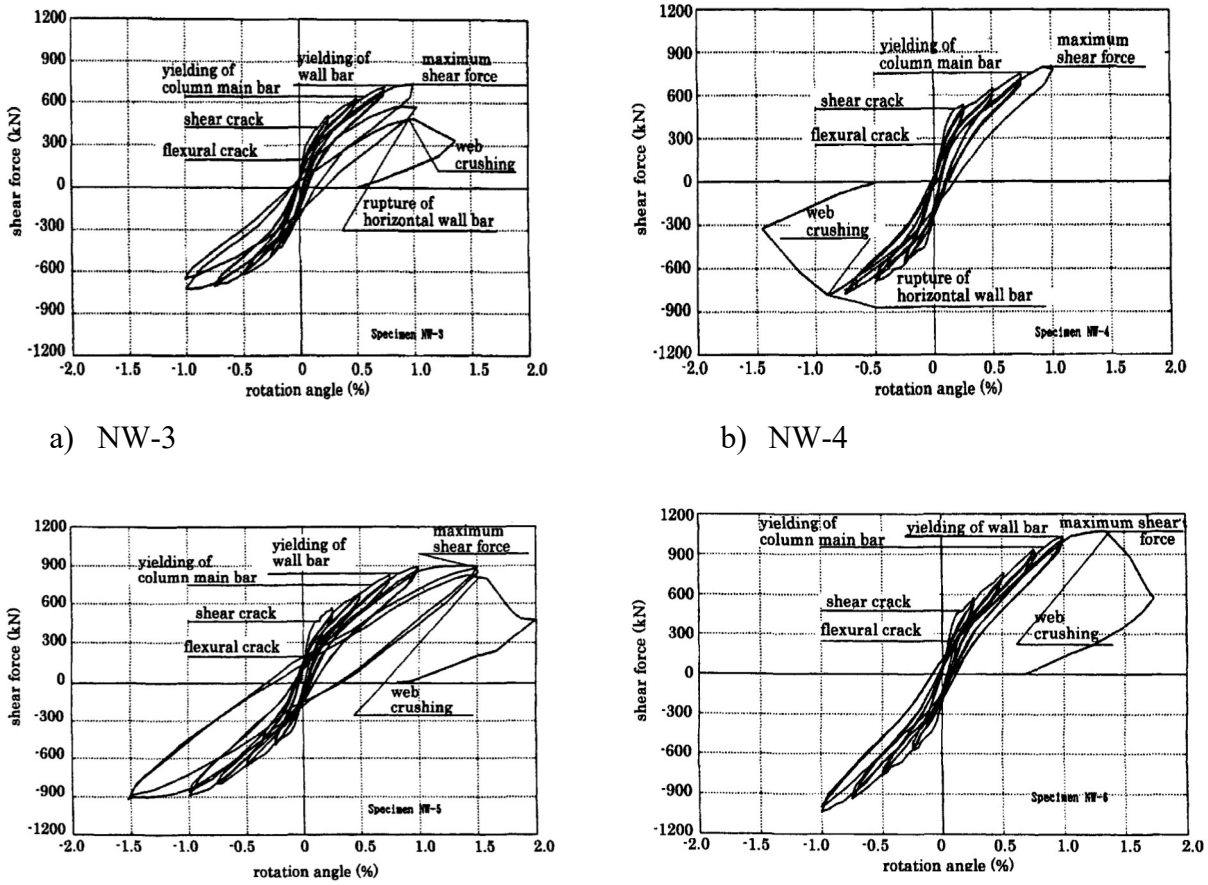

a) NW-3

b) NW-4

c) NW-5

d) NW-6

Figure 2.28 Load-deflection curves for tested shear walls
[Adapted from Otani et. el., 1996]

2.4 Finite Element Modelling (FEM) and Analysis of Reinforced Concrete Shear Walls using VecTo2 Software

The following sections summarize recent studies on reinforced concrete shear walls using Finite Element Analysis methods.

2.4.1 Cortes-Puentes & Palermo (2010)

This paper presents results of an analytical investigation using VecTor2 Finite Element Modelling (FEM) software. Five walls that were previously retrofitted and tested were modelled using the FEM software and the predictions were compared with the experimental results.

Figure *2.29* shows details of the walls modelled in this study. The retrofitted walls were modelled using rectangular mesh elements with smeared reinforcing steel and an average aspect ratio of 3.0 to 2.0. Lateral and axial loads were applied to element nodes, if needed, for each modelled wall.

Recommendations by earlier studies (Palermo & Vecchio, 2007; Cortes-Puentes, 2009) were used to determine the most suitable compression models for concrete. Popovic's Normal Strength Concrete (NSC) model was used for walls with compressive strengths less of than 45 MPa. Popovics High-Strength Concrete (HSC) model was used for walls with concrete compressive strengths of more than 45 MPa. The post-peak modified Park-Kent model was found to provide more accurate results. In addition, the Smith-Young model was found to provide more accurate predictions for a wall with concrete compressive strength of 29 MPa.

Based on the findings of a parametric study conducted by Cortes-Puentes (2009), the Palermo and Vecchio (2003) nonlinear hysteretic model with cyclic decay was used to model the walls. VecTor2 default models were used for secondary effects including compression softening (Vecchio 1992-A), tension softening (Vecchio 2000b), Poisson's ratio (Kupfer 1969), confined concrete enhancement (Kupfer/Richart 1969), cracking strength (Mohr-Coulomb stress criterion), crack width (Vecchio 2000a), and crack shear-slip deformation (Vecchio and Lai 2004).

Individual reinforcing bars were modelled as two-node truss elements using a 'ductile steel reinforcement' model which defined the stress-strain diagram of a typical steel material based on yield strength, ultimate strength, strain hardening strain and ultimate strain. This model was also used for modelling external retrofitting steel plates. External retrofitting material were modelled using 'externally bonded FRP reinforcement', or 'tension only reinforcement'. The hysteretic response of the steel reinforcement was modelled using the Seckin Model (Seckin 1981, Vecchio 1999). Buckling of internal reinforcement was not considered to simplify the models.

The bond between the concrete and the external retrofitting material (e.g., FRP Sheets) was modelled using two-node non-dimensional link elements. The properties of the link elements were defined for each retrofitting material. For example, the link elements for FRP were modelled using a linear elastic ascending response followed by a linear post-peak descending branch (Sato and Vecchio 2003). The ability of VecTor2 in modelling various retrofitting techniques was investigated in this study. These techniques included concrete replacement, externally bonded steel

plates, external bolting of steel plates, and external bonding of FRP sheets. The results indicated the following for the modelled retrofitting techniques:

Concrete Replacement: Two retrofitted walls that were previously tested by Fiorato et al (1983), and Antoniades et al (2003) were modelled in VecTor2. The retrofitting technique involved replacement of the web section up to about mid-height, and replacement of a damaged concrete at the base of the wall. The analytical response of the first wall was in good agreement with the experimental results with the exception a slight underestimation of the lateral load capacity. The model for the second wall overestimates the lateral load capacity, ductility, stiffness, and strength degradation in the post-peak range. External bonding of steel plates: a retrofitted wall previously tested by Elnashai and Pinho (1998) was modelled in VecTor2 using externally bonded steel plates. The analytical response was fond to overestimate the ultimate displacement and underestimate the peak strength of the wall. The stiffness and strength degradation in the post-peak range of the wall was not effectively captured.

External bolting of steel plates: A squat wall previously retrofitted and tested by Taghdi et al (2000b) was modelled in VecTor2 using externally bolted steel plates. Two vertical steel plates were bolted to the ends of the wall. Damaged concrete was not removed or replaced. Each steel plate was modelled using 18 ductile truss bar elements perfectly bonded to the concrete. The VecTor2 model was able to accurately predict the initial stiffness and yield point of the retrofitted wall. The peak strength of the wall was slightly underestimated; however, the maximum displacement (ductility) of the wall was predicted accurately.

External bonding of FRP sheets: A retrofitted wall previously tested by Antoniades et al (2005) was modelled using externally bonded GFRP sheets. The predicted response of the retrofitted wall showed very good agreement with the experimental results.

In general, this study demonstrates the ability of VecTor2 FEM software in predicting the response of reinforced concrete shear walls and different retrofitting techniques. Some discrepancies between the analytical and experimental results were observed that are generally attributed to the lack of detailed information about the process and extent of the repairs and material properties. It was reported in this study that it was more difficult to predict the response of walls with smaller aspect ratios (H/L). It was concluded that FEM software can be used to accurately model retrofitted reinforced concrete walls.

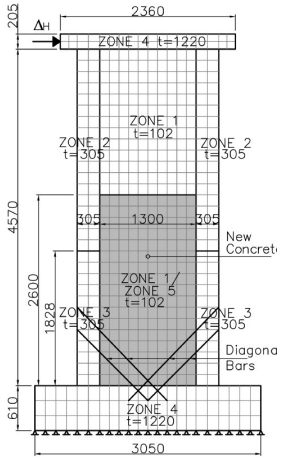

a) Concrete replacement

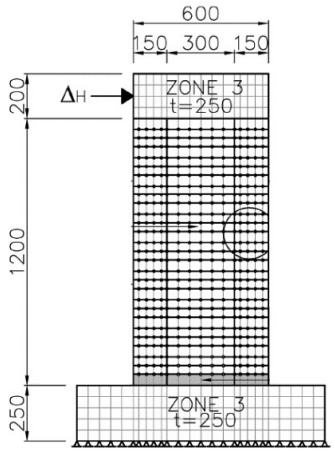

b) External bonding of steel plates

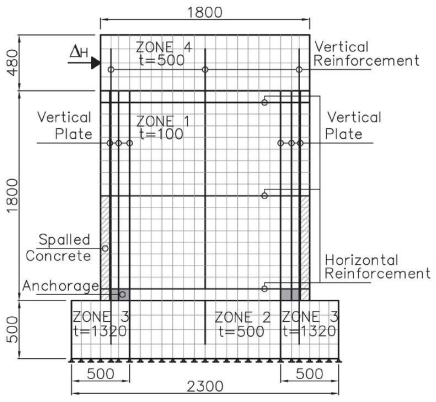

c) External bolting of steel plates

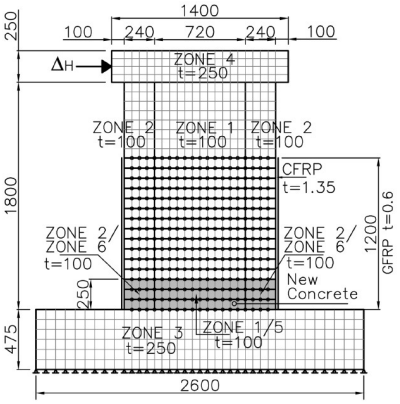

d) Externally-bonded GFRP Sheet

Figure 2.29 VecTor2 FEM models of retrofitted walls investigated by Cortes-Puentes & Palermo (2010) [Adapted from Cortes-Puentes, 2010]

2.4.2 Cortes-Puentes & Palermo (2012)

The objective of this study was to develop a guideline for modelling retrofitted walls using Finite Element Modelling method. Four retrofitted walls were modelled using VecTor2 and the predictions were compared to the experimental results. The retrofitting techniques modelled in this study include bolting of steel plates, externally bonded steel plates and fiber-reinforced polymer (FRP) sheets, as well as external plates with delay mechanisms. Figure *2.30* shows the modelling of retrofitted walls by the researchers.

The walls were modelled using three-node triangular elements and four-node rectangular elements. The triangular elements were used for areas with geometrical constraints. VecTor2's default material models were used for modelling the concrete except for the pre-peak and post-peak

compression response. The Popovics (1973) model for normal-strength concrete, and the Park-Kent model (Park et al, 1982) were used for the pre-peak and post-peak compression responses of the concrete. The hysteretic response of the concrete was modelled using Palermo 2002, a decay model proposed by Palermo and Vecchio (2003). The Smith-Young model (Smith and Young, 1955) was used for the wall with a lower concrete strength. The secondary effects were modelled using VecTor2's default models: Vecchio's 1992-A (compression softening), Vecchio 2000b (tension softening), Kupfer et al (Poisson's ratio), Mohr-Coulomb Criterion (cracking strength), Vecchio 2000a (crack width).

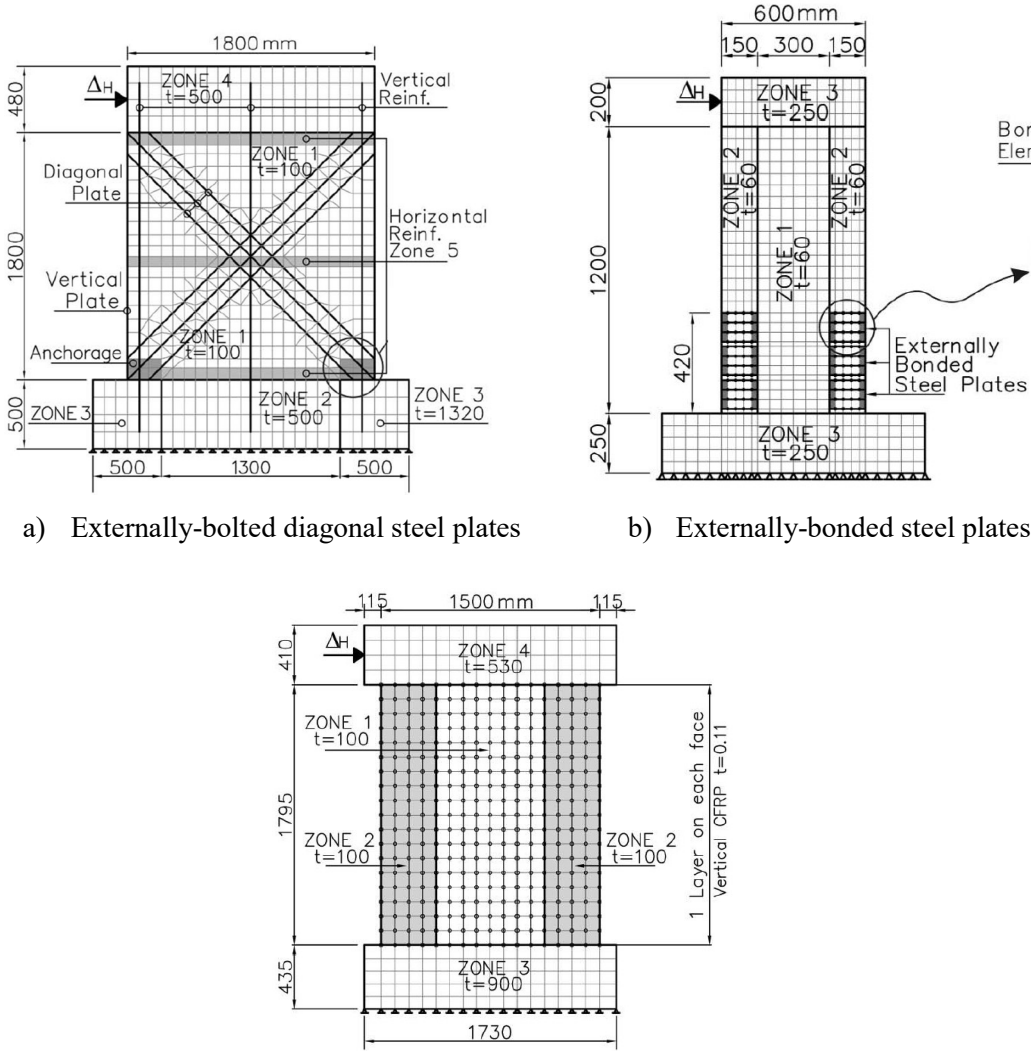

a) Externally-bolted diagonal steel plates

b) Externally-bonded steel plates

c) Externally-bonded FRP sheets

Figure 2.30 VecTor2 FEM models of retrofitted walls investigated by Cortes-Puentes & Palermo (2012) [Adapted from Cortes-Puentes, 2012]

Reinforcement materials included steel reinforcing bars, externally-bonded steel plates, and FRP sheets which were modelled using ductile reinforcement material, tension only reinforcement and externally bonded FRP reinforcement, respectively. Internal distributed reinforcement was modelled as smeared reinforcement. Individual reinforcing bars were modelled as two-node truss elements. The hysteretic response of the steel reinforcement was modelled using the Seckin Model (Seckin 1981, Vecchio 1999). Buckling of the externally bonded steel plates and FRP was considered using the Asazu model (Asazu et al, 2001). Buckling of the internal steel reinforcement or externally bolted steel plates were not considered in the models to simplify the models.

Bolting of steel plates: Taghdi et al (2000b) retrofitted a squat wall with aspect ratio of 1.0 using externally bolted steel plates. The retrofit consisted of two diagonal steel plates as well as steel plates install vertically along the ends of the wall. Both the diagonal and vertical steel plates were anchored to the foundation and the top loading beam. In addition, the diagonal plates were welded together at the center. The steel plates were modelled using tension-only reinforcement which consisted of three truss elements with an equivalent cross-sectional area. The anchored ends of the steel plates were defined using highly reinforced concrete segments with smeared reinforcement that were meshed using rectangular elements. The analytical response was found to be in close agreement with the experimental results. The yield strength was slightly overestimated; however, the initial stiffness of the wall was well predicted. The wall failed due to rupture of the steel plates between the bolts which was captured accurately by the FEM model.

External bonding of steel plates: Elnashai and Pinho (1998) tested a wall with aspect ratio of 2.0 and retrofitted using u-shaped external confinement steel plates in the boundary elements. The externally bonded U-shaped plates were modelled using tension-only truss elements bonded to the concrete using link elements that were defined to simulate the effect of bond slip. The model predicted the overall flexural behaviour of the wall; however, it was not able to accurately predict the ductility and the failure mode of the wall. The discrepancy was attributed to the assumed material properties used in the FE model as well as lack of detailed information.

External bonding of fiber-reinforced polymer (FRP): a wall retrofitted using GFRP sheets and tested by Lombard et al (2000) was modelled using VecTor2. The externally-bonded FRP sheet was modelled using 18 vertical FRP truss elements with an overall equivalent cross-sectional area. Bond-link elements were used to define the bond between the FRP truss bars and the concrete

elements. A bilinear bond stress-slip model was used to simulate the anchorage of the FRP to the foundation using adhesive materials. The resulting analytical prediction was satisfactory considering that it was able to capture the initial stiffness, stiffness degradation, unloading and relocating branches, pinching effect and energy dissipation capacity of the wall. However, the lateral strength of the walls was generally overestimated. Failure of the FRP truss elements were predicted accurately, however, rupture of the steel reinforcement was not captured in the analytical prediction.

The authors conclude that this study demonstrate a strong correlation between the analytical and experimental results. It was shown that simple FE elements can be used to produce highly accurate predictions of retrofitted reinforced concrete walls. In addition, bond-link elements were shown to successfully model the bond between different types of retrofitting materials.

2.4.3 Palermo and Vecchio (2007)

In this study, non-linear finite elements analyses of previously tested walls with different aspect ratios and cross-sectional geometries were conducted using VecTor2 FEM software. The objective of this study was to demonstrate the ability of FE model with low-powered elements and smeared material properties in producing accurate predictions for the seismic performance of reinforced concrete shear walls.

VecTor2's default constitutive models were used in the modelled walls with the exception of the base curve for concrete in compression and the hysteretic response model for concrete. The default models included compression softening by Vecchio 1992-A, tension stiffening by the modified Bentz model (Vecchio 2000), tension softening using a linear descending branch after cracking, concrete dilation by Kupfer (1969) which is based on a variable Poisson's ratio (Vecchio 1992), strength enhancement in concrete due to compression by Kupfer-Richart (Vecchio 1992), and cracking strength by the Mohr-Coulomb stress model. A model proposed by Palermo and Vecchio (2003) was used for the hysteretic behaviour of concrete. Dowel action and bar buckling were not considered in the analyses.

The results of the analyses presented in this study consisted of comparisons of analytical predictions for 5 walls with different aspect ratios corresponding to slender walls ($H/L > 2.0$), slender/squat walls ($H/L = 2.0$), and squat walls ($H/L < 2.0$). Walls with rectangular and barbell-

shaped / flanged cross-sections were modelled. In addition, one wall with an opening was modelled. The presented results included two slender walls previously tested by the Portland Cement Association (Oesterle et al. 1976), once wall with aspect ratio of 2.0 and rectangular cross-section previously tested by Plakoutass and Elnashai (1995), one wall with aspect ratio of 0.5 and a rectangular cross-section previously test by Wiradinata and Saatcioglu (2002), one squat wall with aspect ratio of 0.7 and a flanged cross-section previously tested by Palermo and Vecchio (2002b), and a slender wall with an opening previously tested by Cote and Wallce (1998).

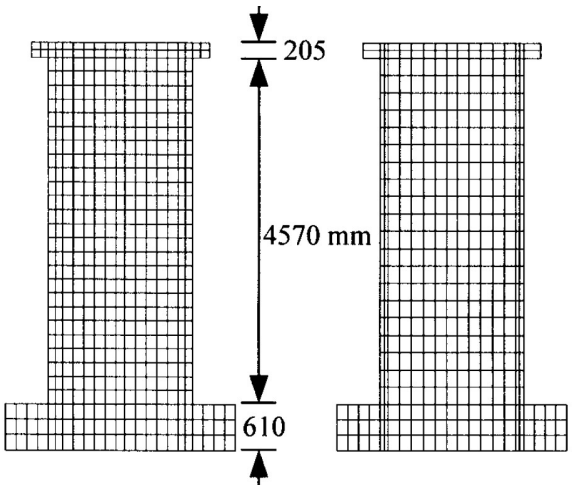

a) Slender walls tested by PCA (Oesterle et al., 1976)

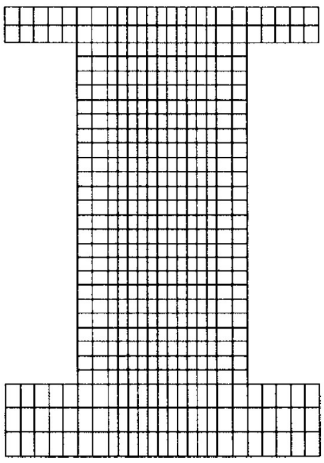

b) Slender / squat wall tested by Plakoutass and Elnashai (1995)

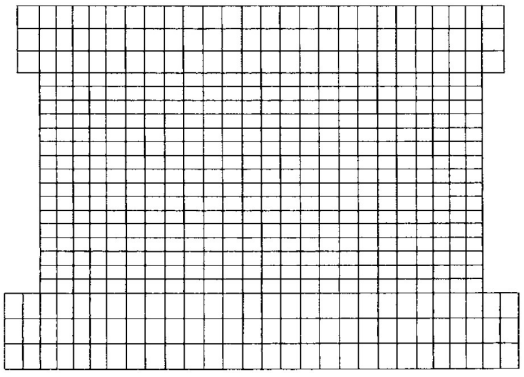

c) Squat wall tested by Wiradinata & Saatcioglu (2002)

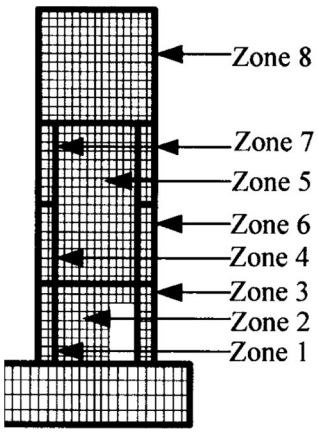

d) Slender wall with opening tested by Cote & Wallace (1998)

Figure 2.31 VecTor2 FEM models of retrofitted walls investigated by Palermo & Vecchio (2007) [Adapted from Palermo & Vecchio, 2007]

The analytical prediction presented in this study demonstrate substantial agreement with the experimental results. In general, the VecTor2 models were able to predict the peak strength, post-peak response, ductility, energy dissipation capacity and failure mechanism of the walls with satisfactory accuracy. Some discrepancies related to the predictions of the displacements at peak lateral loads were reported which were found to be minor following further investigations. The authors conclude that this study demonstrates the practicality, reliability and simplicity of the finite element method in producing accurate predictions for structural behaviour of reinforced concrete shear walls with different geometrical properties. Figure 2.31 illustrates the VecTor 2 models for the above walls.

2.4.4 Summary of the Past Experimental Result

In general, the existing literature suggests that the ductility of walls reinforced with high-strength reinforcement increases or remains unchanged for walls with aspect ratios closer to 1.0 (Cheng et al, 2016; Park et al, 2015; Kimura and Sugano, 1996). As aspect ratios increase, the deformation capacity of such walls decreases and is often accompanied by pre-mature rupture of longitudinal reinforcement in the boundary elements, or the vertical or horizontal web reinforcement (Dazio et al, 2009; Japan's New RC Project, 1988-1993). The literature review presented in the previous sections reveals that that there has been limited tests on slender walls reinforced with high-strength bars in general, with no previous studies on slender shear walls reinforced with Grade 690 MPa ASTM A1035 steel. A summary of the wall details as well their failure modes and deformation capacities are presented in Appendix B.

In addition, a review of previous analytical studies using VecTor2 Finite element Modelling demonstrated that it can be used to reliably and accurately predict the cyclic behaviour of concrete shear walls with different geometrical and material properties. It was shown that selecting the proper models for the specific materials used in the modelled walls can impact the accuracy of the predictions.

Chapter 3

3 Material Properties

This Chapter presents detailed information related to the properties of high-strength materials considered in the experimental phase of current research, especially with regards to the specifics of the ASTM A1035 reinforcing steel produced by MMFX®. The properties of other types of high-strength reinforcing steel considered in the analytical parametric study are presented in Chapter 6. Similarly, the properties of concrete used in the experimental phase are described in this Chapter, whereas those considered in the analytical parametric study are presented in Chapter 6.

3.1 Steel Reinforcement

The steel reinforcement used in the construction of the two large-scale shear wall specimens designed, constructed, and tested consisted of deformed ChromX® 9100 high-strength steel reinforcing bars manufactured by MMFX®, a US-based commercial metals company. ChormX 9100 has a nominal yield strength of 690 MPa [100 ksi] that conforms to the ASTM A1035 standard. It is advertised to have high corrosion resistance with a life span of over 100 years.

US reinforcing bar sizes 3 and 4 (9.525mm dia. and 12.7mm dia., respectively) were used in the construction of walls W1HS and W2HS. No. 4 bars were used as the main flexural reinforcement in the boundary elements. No. 3 bars were used as vertical and transverse reinforcement in the web, as well as for confinement reinforcement in the boundary elements.

Material testing was first performed on the reinforcing steel used. The tests consisted of a series of tensile coupon tests that were conducted in conformance with *ASTM A370 19 - Standard Test Methods and Definition for Mechanical Testing of Steel Products*. The tests were conducted at the Structures Laboratory of the University of Ottawa using a Galdabini® Universal Testing Machine (UTM). The strains were measured using an extensometer with a 50mm grip span (gauge length) and the data was recorded using a data acquisition system. Table 3.1 and Table 3.2 provide results of the steel coupon tests for No. 3 and No. 4 reinforcing bars, respectively. Figure 3.3 shows typical stress-strain curves for No.3 and No. 4 ChromX® bars used in the test specimens. The yield

strengths shown in Table 3.1, Table 3.2, Table 3.3, and Table 3.4 were determined according to the 0.2% offset method as described in the ASTM A370-19 standard. It should be noted that this method is generally developed for conventional steel reinforcement which exhibits a defined yield point. In the case of the ChromX® bars, the yield point is not well-defined as shown in Figure 3.3 and Figure 3.4. Hence, the offset method may not represent the true yield point of the reinforcing bars and may be regarded as an average yield or mid-yield point.

Figure 3.1 - Typical steel bar coupon test setup

Figure 3.2 - Ruptured No. 4 MMFX® steel bar

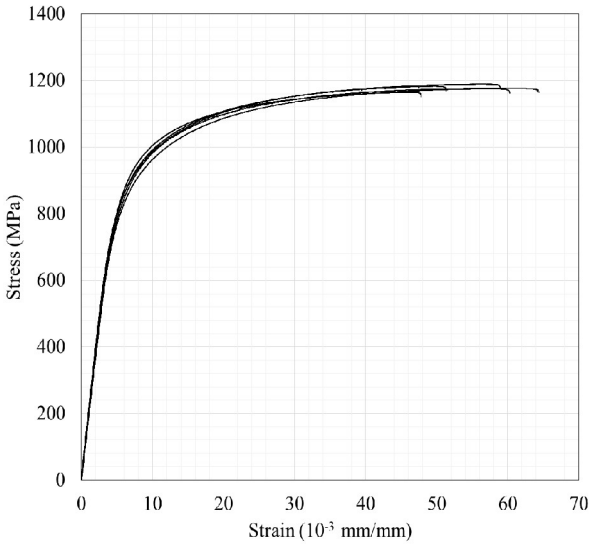

a) Stress-strain curves for No. 3 bars

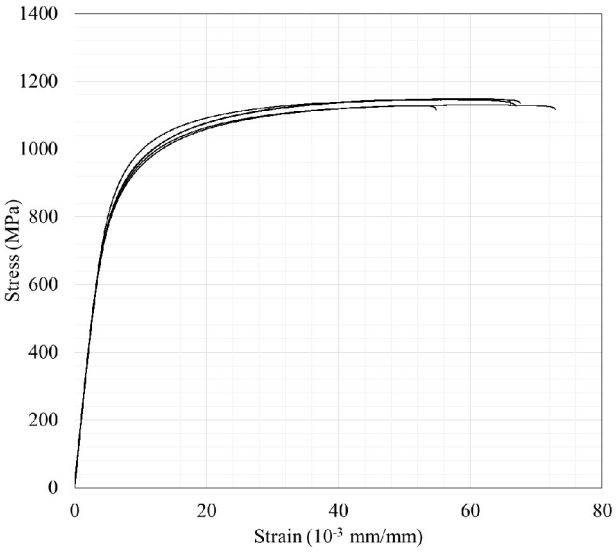

b) Stress-strain curves for No. 4 bars

Figure 3.3 - Stress-strains curves for No.3 and No. 4 reinforcement bars used in wall W1HS

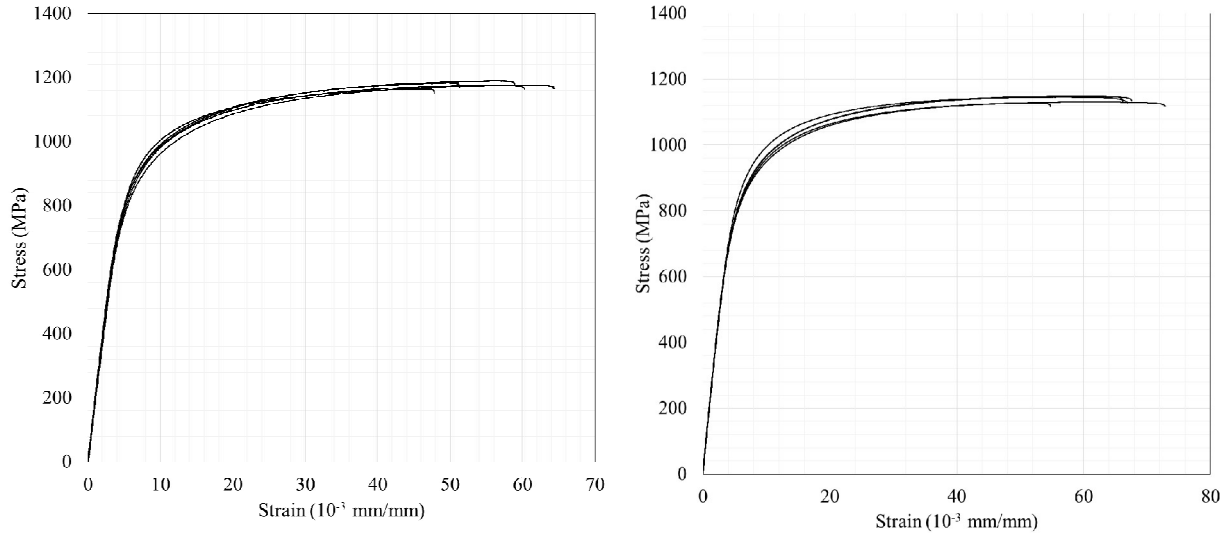

a) Stress-strain curves for No. 3 bars b) Stress-strain curves for No. 4 bars

Figure 3.4 - Stress-strains curves for No.3 and No. 4 reinforcement bars used in wall W2HS

Table 3.1 - Stress-Strain data for No. 3 steel bars used in Wall W1HS

Label	f_y (MPa)	ε_y (10^{-3} mm/mm)	f_u (MPa)	ε_u (10^{-3} mm/mm)	$\varepsilon_{rupture}$ (10^{-3} mm/mm)	E_s (MPa)
W2-R3-1	990	7.2	1189	57	59.0	187010
W2-R3-2	876	7.1	1175	58	60.3	180790
W2-R3-3	921	7.1	1164	47	48.0	187070
W2-R3-4	901	6.9	1182	50	51.3	187700
W2-R3-5	910	7.1	1278	46	46.2	192040
W2-R3-6	887	6.6	1176	5.9	64.4	197020
Average	914	7.0	1194	43.9	54.9	188605

Table 3.2 - Stress-Strain data for No. 4 steel bars used in Wall W1HS

Label	fy (MPa)	εy (10^{-3} mm/mm)	f_u (MPa)	ε_u (10^{-3} mm/mm)	$\varepsilon_{rupture}$ (10^{-3} mm/mm)	E_s (MPa)
W2-R4-1*	-	-	-	-	-	-
W2-R4-2	851	6.6	1130	61	72.9	198200
W2-R4-3	894	6.6	1145	58	66.9	200450
W2-R4-4	854	6.6	1127	52	55.0	187660
W2-R4-5	861	6.5	1147	58	67.6	193670
W2-R4-6	851	6.6	1148	64	66.2	189030
Average	862	6.6	1139	58.6	65.7	193802

*Unsuccessful coupon test.

Table 3.3 - Stress-Strain data for No. 3 steel bars used in Wall W2HS

Label	f_y (MPa)	ε_y (10^{-3} mm/mm)	f_u (MPa)	ε_u (10^{-3} mm/mm)	$\varepsilon_{rupture}$ (10^{-3} mm/mm)	E_s (MPa)
W2-R3-1	910	7.1	1180	61	61.8	182850
W2-R3-2	972	6.8	1263	55	58	200970
W2-R3-3	989	7.1	1271	51	52.5	191040
W2-R3-4	899	6.9	1180	61	61.8	182850
W2-R3-5	908	6.8	1165	51	54	191920
W2-R3-6*	-	-	-	-	-	-
Average	936	6.94	1211.8	55.8	57.62	189926

*Unsuccessful coupon test.

Table 3.4 - Stress-Strain data for No. 3 steel bars used in Wall W2HS

Label	f_y (MPa)	ε_y (10^{-3} mm/mm)	f_u (MPa)	ε_u (10^{-3} mm/mm)	$\varepsilon_{rupture}$ (10^{-3} mm/mm)	E_s (MPa)
W2-R3-1	849	6.6	1129	46.5	46.6	182850
W2-R3-2	-	-	-	-	-	-
W2-R3-3	853	6.5	1129	56	89	180230
W2-R3-4	865	6.5	1138	57	75.5	196350
W2-R3-5	-	-	-	-	-	-
W2-R3-6	860	6.5	1130	56	74	190845
Average	857	6.5	1132	53.9	71.2	186477

*Unsuccessful coupon test.

3.2 Concrete

High-strength concrete with a target 28-day compressive strength of 80 MPa was used in the construction wall W1HS and W-2HS. The concrete was designed and mixed in-house at the Structures Laboratory of the University of Ottawa. Table 3.5 and Table 3.6 provide details of the mix designs used in the walls. Special additives were used in order to achieve the intended density and strength. MasterGlenium® 7500 superplasticizer was used to compensate for the low water-to-cement ratio and enhance the workability of the mix. Master R100 Retarder was used to slow the process of hydration and reduce the heat produced during the curing period. In addition, silica fume and slag were added to the mix to increase the density and achieve a higher-strength concrete. The coarse and fine aggregates used in the concrete mix consisted of ½-inch crushed stone and structural grade clay-free sand.

The concrete was mixed in a pan mixer at the University of Ottawa's structures laboratory. The mixer had a maximum capacity of $0.2m^3$. However, the batch sizes were limited to a maximum of $0.18m^3$ to prevent loss of material during mixing. Hence, 8 batches of concrete were mixed to cast Wall W1HS, and 6 batches were used to cast Wall W2HS.

Table 3.5 - Concrete mix design and actual quantities used in wall W1HS

		Layer 1		**Layer 2**		**Layer 3**		**Layer 4**	
		(July 18, 2018)		**(July 26, 2018)**		**(July 30, 2018)**		**(August 2, 2018)**	
Material	Design Qty.	Batch 1	Batch 2	Batch 1	Batch 2	Batch 1	Batch 2	Batch 1	Batch 2
	(Kg/m3)	(Kg)	(Kg)	(Kg)	(Kg)	(Kg)	(Kg)	(Kg)	(Kg)
Cement	373	67.1	55.9	67.1	55.9	55.9	55.9	55.9	37.3
Slag	164	29.5	24.6	29.5	24.6	24.6	24.6	24.6	16.4
Silica Fume	48	8.6	7.2	8.6	7.2	7.2	7.2	7.2	4.8
Sand	740	133.2	111	133.2	111	111	111	111	74
Aggregate	1120	201.6	168	201.6	168	168	168	168	112
Plasticizer	5850	1450	1200	1450	1300	1300	1300	1300	800
Retarder	1931	350	350	350	300	300	300	300	190
Water	146.3	27	22	26.5	22	22	22	22	14.5
w/c	**0.25**	**0.26**	**0.25**	**0.25**	**0.25**	**0.25**	**0.25**	**0.25**	**0.25**

Table 3.6 - Concrete mix design and actual quantities used in wall W2HS

		Layer 1		**Layer 2**		**Layer 3**	
		(March 5, 2019)		**(May 22, 2019)**		**(June 11, 2019)**	
Material	Design Qty.	Batch 1	Batch 2	Batch 1	Batch 2	Batch 1	Batch 2
	(Kg/m3)	(Kg)	(Kg)	(Kg)	(Kg)	(Kg)	(Kg)
Cement	373	67.1	67.1	67.1	67.1	55.9	55.9
Slag	164	29.5	29.5	29.5	29.5	24.6	24.6
Silica Fume	48	8.64	8.6	8.6	8.6	7.2	7.2
Sand	740	133.2	133.2	133.2	133.2	111	111
Aggregate	1120	201.6	201.6	201.6	201.6	168	168
Plasticizer	5850	1200	1000	1450	1100	1400	1100
Retarder	1930.5	340	335	340	345	345	345
Water	175.5	32	31	31.5	30.5	29	28.0
w/c	**0.30**	**0.30**	**0.29**	**0.30**	**0.29**	**0.33**	**0.31**

Compressive strength of the walls was determined by 100mmx200mm cylinder tests conforming to *ASTM C39 - Standard Test Method for Compressive Strength of Cylindrical Concrete Specimens*. Four concrete cylinder samples were taken from every batch during wall casting. Wall W1HS was cast in 4 layers which required a total of 8 batches of concrete. Wall W2HS was cast in 3 layers using a total of 6 batches of concrete. Representative cylinders were tested 28 days after casting and on the day of testing. Table 3.7 shows the compressive strengths of the tested cylinders at 28 days from casting, as well as the day of testing. The average compressive strength for each layer is shown in Table 3.7 and Table 3.8. The overall average compressive strength for the concrete mixes used in walls W1HS and W2HS were 83 MPa and 74 MPa, respectively. Some of the tested cylinders had compressive strengths that were 30% or more less than the average compressive strength of the concrete for the walls. The lower strength of these specimens was attributed to the poor quality of the samples due to excessive voids, improper consolidation or unbalanced compressive loading that sometimes occurs due to improper grinding of the cylinder ends. These cylinders were considered to be outliers and were not included in the calculation of the average values shown in Table 3.7 and Table 3.8.

a) Concrete testing cylinder test equipment

b) Typical concrete cylinder at the end of testing

Figure 3.5 – Typical concrete compressive cylinder test

Table 3.7 Compressive strength cylinder test results for wall W1HS

No.	Label	Layer No.	Batch No.	Days Cured	f'_c (MPa)
1	L1-B1-1	1	1	28	93
2	L1-B1-2	1	1	28	87
3	L1-B1-3	1	1	72	91
4	L1-B1-4	1	1	72	96
5	L1-B2-1	1	2	28	78
6	L1-B2-2	1	2	28	86
7	L1-B2-3	1	2	72	75
8	L1-B2-4	1	2	72	89
Layer 1 Average =					**87**
9	L2-B1-1	2	1	28	62*
10	L2-B1-2	2	1	28	48*
11	L2-B1-3	2	1	64	74
12	L2-B1-4	2	1	64	70
13	L2-B2-1	2	2	28	85
14	L2-B2-2	2	2	28	88
15	L2-B2-3	2	2	64	80
16	L2-B2-4	2	2	64	79
Layer 2 Average =					**79**
17	L3-B1-1	3	1	28	56*
18	L3-B1-2	3	1	28	81
19	L3-B1-3	3	1	60	78
20	L3-B1-4	3	1	60	85
21	L3-B2-1	3	2	28	94
22	L3-B2-2	3	2	28	85
23	L3-B2-3	3	2	60	81
24	L3-B2-4	3	2	60	79
Layer 3 Average =					**83**
25	L4-B1-1	4	1	28	68
26	L4-B1-2	4	1	28	72
27	L4-B1-3	4	1	57	72
28	L4-B1-4	4	1	57	70
29	L4-B2-1	4	2	28	90
30	L4-B2-2	4	2	28	94
31	L4-B2-3	4	2	57	86
32	L4-B2-4	4	2	57	87
Layer 4 Average =					**80**
Total Average =					**83**
Standard Deviation =					**8**
Median =					**85**

*Outlier data points not considered in calculating the average f'_c

Table 3.8 Compressive strength cylinder test results for wall W2HS

No.	Label	Layer No.	Batch No.	Days Cured	f'_c (MPa)
1	L1-B1-1	1	1	28	79
2	L1-B1-2	1	1	28	76
3	L1-B1-3	1	1	304	73
4	L1-B1-4	1	1	304	81
5	L1-B2-1	1	2	28	77
6	L1-B2-2	1	2	28	78
7	L1-B2-3	1	2	308	78
8	L1-B2-4	1	2	308	77
Layer 1 Average =					**77**
9	L2-B1-1	2	1	28	73
10	L2-B1-2	2	1	28	69
11	L2-B1-3	2	1	308	72
12	L2-B1-4	2	1	308	76
13	L2-B2-1	2	2	28	54*
14	L2-B2-2	2	2	28	71
15	L2-B2-3	2	2	308	76
16	L2-B2-4	2	2	308	74
Layer 2 Average =					**73**
17	L3-B1-1	3	1	28	69
18	L3-B1-2	3	1	28	64
19	L3-B1-3	3	1	310	72
20	L3-B1-4	3	1	310	76
21	L3-B2-1	3	2	28	68
22	L3-B2-2	3	2	28	78
23	L3-B2-3	3	2	304	75
24	L3-B2-4	3	2	304	77
Layer 3 Average =					**72**
Total Average =					**74**
Standard Deviation =					**4.1**
Median =					**76**

*Outlier data points not considered in calculating the average f'_c

Chapter 4

4 Experimental Program

The experimental program consisted of testing two large-scale reinforced concrete shear walls with aspect ratios of H/L = 2.0 and 3.0 under reversed cyclic loading and constant axial compression. The walls were labeled W1HS and W2HS and represented shears walls in a 6-storey building at ¼-scale. The cross-sectional geometry and dimensions of the walls were selected to be identical to the walls previously tested at the university of Ottawa by Navidpour (2018), referred to as the 'control walls' hereafter. This was to facilitate a direct comparison of results. The control walls were constructed using conventional Grade 400 MPa reinforcement conforming to ASTM A615 standard. In addition, the reinforcement details of walls W1HS and W2HS were designed to provide a similar moment capacity to those of their respective control walls. The following sections provide further details related to the design of the tested walls.

4.1 Design Notes

The design of the walls was first performed according to the 2014 version of the ACI 318 design code (ACI 318-14) and was later modified to conform to the requirements of the CSA A23.3-14 (2014). The walls were designed prior to the latest revisions to the ACI 318 and CSA A23.3 codes in 2019. A review of a most recent editions of these codes revealed that the design of ductile concrete shear walls has generally remained the same with some exceptions. Some of the recent additions to the ACI 318-19 is the additional requirements for the design of development length for closely spaced hooked bars. In addition, a factor is added for calculation of the basic reinforcement development length to account for high-strength reinforcement (f_y > 400 MPa).

The reinforcement details of the walls were designed to provide a similar moment capacity to that of their associated control walls. As higher strength reinforcement was used in the construction of the walls compared to the control walls, reinforcement design parameters were modified to provide a similar moment capacity. These parameters included the size and reinforcement ratio of the flexural reinforcement in the boundary elements as well as the web sections. The arrangement of the vertical bars in the boundary elements as well as the web sections of wall W1HS and W2HS

were kept the same as their control walls. The purpose of the design presented in this section was to ensure that the shear and flexural strengths of the designed walls matched closely those of the control walls. Hence, steel and concrete material strength factors of ϕ_s=1.25 and ϕ_c=1.0 were used to obtain the probable moment capacity of each wall. In addition, shear and flexure reduction factors specified by the ACI 318-14 were not incorporated in the design of the wall. These reduction factors are specified in the code to increase the safety margin which was not the intent of the design presented herein.

The following sections provide design details for the wall foundation, boundary element longitudinal and transverse reinforcement, and the distributed vertical and horizontal web reinforcement for walls W1HS and W2HS. Additional design details, including development lengths, tension and compression lap splices, and hooks are provided in Appendix A.

4.1.1 Foundation Units

Heavily reinforced rectangular concrete foundations were used for both walls W1HS and W2HS. The foundation units were 3550 mm long and 1735 mm wide. The selected depths for the foundation units were 600 mm and 500 mm for walls W1HS and W2HS, respectively. The depth of the foundation was reduced for wall W2HS to minimize the weight of the test specimen to meet the capacity of the overhead crane in the Structures Laboratory. The dimensions of the foundation units were selected based on the size and capacity of the walls as well as the spacing of the openings in the strong floor of the laboratory. They were anchored to the floor at four points along each side of the walls using 64 mm dia. high-strength bolts. The reinforcement consisted of two layers of 30M and 25M Grade 400 MPa bars in the longitudinal and transverse directions, respectively. Figure 4.1 presents typical details of the foundation reinforcement. Special hooks made with 25M bars were installed around the openings of the bolts, as well as the footprint of the walls to prevent punching shear failure and minimize vertical deformation of the foundation during testing.

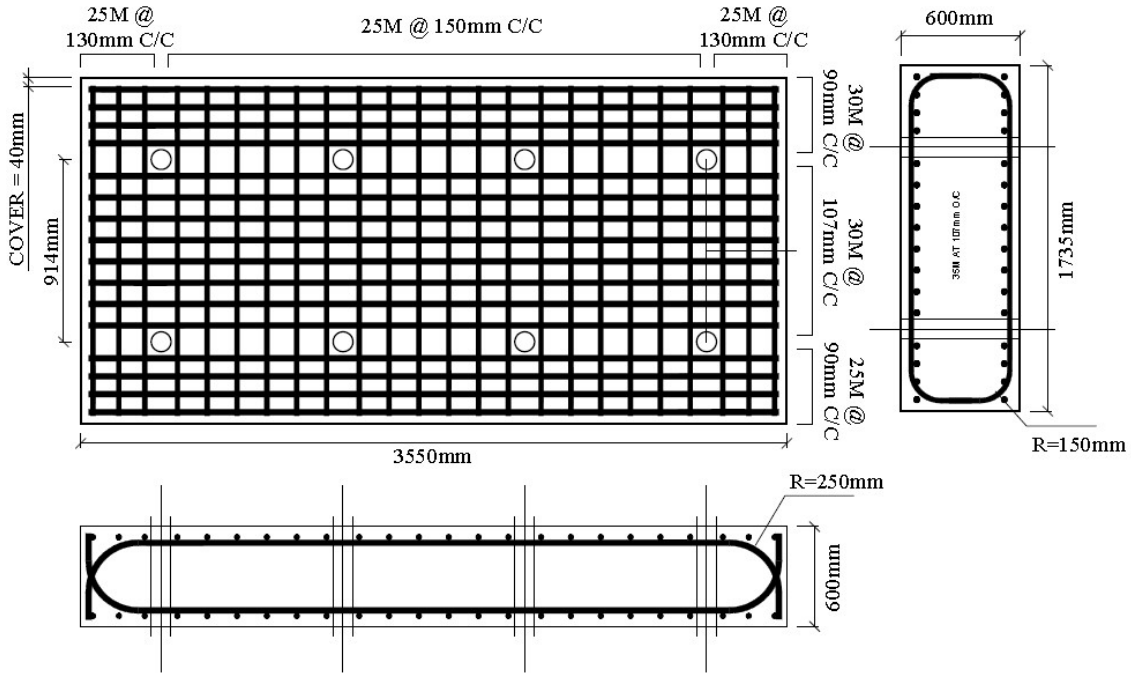

Figure 4.1 - Foundation Design Details

4.1.2 Wall W1HS Design Details

Wall W1HS had a barbell-shaped cross-section; it was 4330 mm high and 1450 mm long. The boundary elements consisted of 250 mm x 250 mm square columns linked by a 100 mm thick web section. A 400 mm deep strip at the top of the wall, where the lateral load was directly applied, was reinforced with twice the transverse reinforcement to enhance the shear capacity of the wall at the point of loading. In addition, this loading section was responsible for transferring the axial loads from the prestressing beams to the rest of the wall; hence, it was designed to be 250 mm thick to increase its bearing capacity.

The wall was constructed using high-strength concrete with a design compressive strength of 80 MPa. The average compressive strength of the concrete was found to be 83 MPa on the day of the test. Grade 690 ASTM A1035 steel bars were used in the construction of Wall W1HS. The longitudinal reinforcement in the boundary elements consisted of US size No. 4 (12.7mm dia.) bars placed in an 8-bar arrangement. Compared to the control wall, which used 20M bar as the longitudinal reinforcement in its boundary elements, 36% less reinforcement was used in the boundary elements of Wall W1HS. The calculated probable moment resistance of the wall was approximately the same as the control wall.

The distributed horizontal and vertical web reinforcement consisted of two curtains of US size No. 3 (9.525mm dia.) bars spaced at 280mm ($\rho_{sh} = 0.51\%$) and 300mm ($\rho_{sv} = 0.45\%$) respectively. The transverse reinforcement in the boundary elements consisted of No. 3 square ties with single crossties in both horizontal and out-of-plane directions, placed at 75mm center-to-center spacing, resulting in a reinforcement ratio of $\rho_{st} = 1.14\%$ in both directions. Figure 4.2 provides a 3D representation of the test wall. Figure 4.3 and Figure 4.4 show the dimensions and reinforcement details of wall W1HS.

The specified provisions for seismic design of structural walls are similar in both the ACI318-14 and the CSA A23.3-14 design standards with a few exceptions that were considered in the design of wall W1HS. One such major difference is that the ACI 318-14 allows for lap-splicing of 100% of the longitudinal reinforcement in the same segment within the high tensile region provided that Type B (Clause 25.5.2.1, ACI 318-14) splices are used. The overlapping length of Type B splices is 30% longer compared to Type A splices. In the CSA A23.3-14 design code, it is required that lap splices be staggered. Clause 21.5.6.5 of the CSA A23.3-14 states that "When (ductility-based force reduction factor) $R_d \geq 3.5$, not more than 50% of the reinforcement at each end of the walls in plastic hinge regions shall be spliced at the same location and a total of at least one-half of the height of each storey shall be completely clear of lap splices in the concentrated reinforcement". Hence, only 50% of the boundary element reinforcement was spliced within the plastic hinge region of the wall.

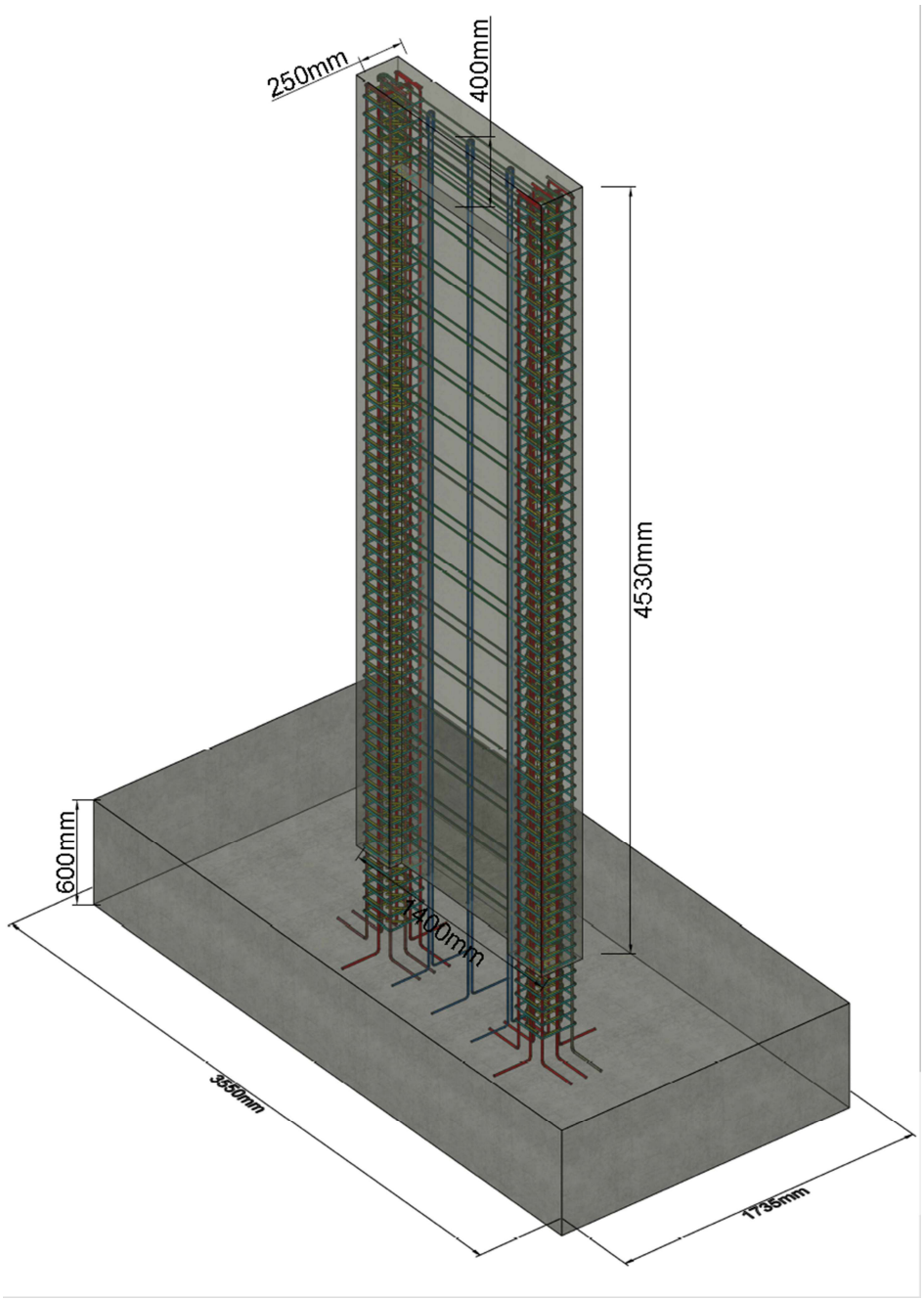

Figure 4.2 - 3D representation of wall W1HS

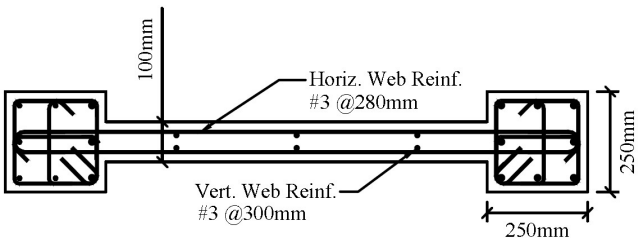

Figure 4.3 - Wall W1HS cross-section

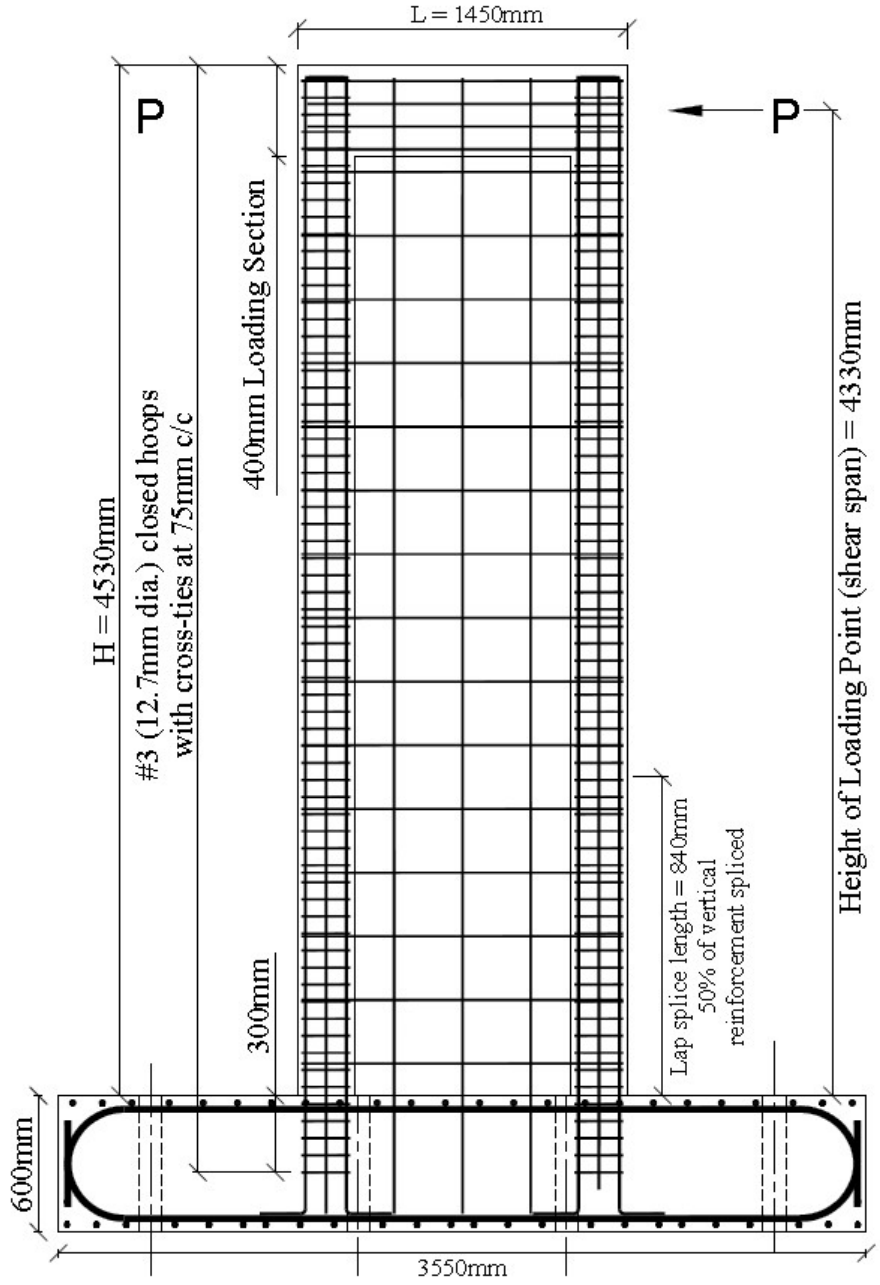

Figure 4.4 – Wall W1HS reinforcement details

4.1.2.1 Boundary Element Longitudinal Reinforcement

The arrangement of the boundary element longitudinal reinforcement was selected to match that of the control wall. Since high-strength reinforcement was used, smaller US size No. 4 and No. 3 bars were used instead of the 20M and 10M bars used in the control wall, respectively. Figure *4.5* shows the arrangement of the vertical flexural reinforcement used in the RC-Section models for wall W1HS and the control wall. Table 4.1 presents the geometric and material specifications of the control wall as well as its sectional properties calculated using the RC-Section software.

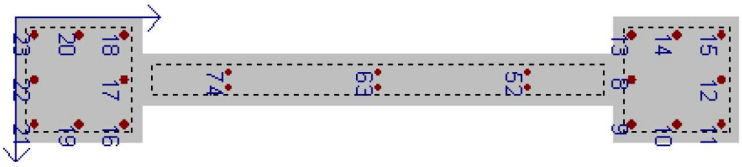

Figure 4.5 - Vertical reinforcement arrangement used RC-Section Model

Table 4.1 – Control wall properties (Navidpour, 2018)

H (m) [in]	**L (m) [in]**	**t (m) [in]**	**f_{yl} (MPa) [ksi]**	**f_{yt} (MPa) [ksi]**	**f'_c (MPa) [psi]**	**P (KN) [kip]**	**M_{exp}, (KN.m) [Kip-ft]**	**M_n (KN.m) [Kip-ft]**	**M_{pr} (KN.m) [Kip-ft]**
4330	1450	100	471	710	82	1500	2650	2245	2521
[118]	[57]	[3.9]	[65]	[73]	[11603]	[296]	[1955]	[1656]	[1860]

In Table 4.1, H denotes wall height, L is wall length, t is wall thickness, f_{yl} is the yield strength of the longitudinal and distributed reinforcement, f_{yt} is the yield strength of the boundary element ties, f'_c is the 28-day compressive strength of concrete, P is the applied axial compression, M_{exp} is the experimental moment resistance obtained from the wall test by Navidpour (2018), M_n is the nominal moment resistance, and M_{pr} is the analytical probable moment resistance.

As previously mentioned, an 8-bar layout consisting of No. 4 bars was selected for the longitudinal reinforcement in the boundary elements. The bars were spaced at 90 mm c/c in both horizontal and vertical directions. The resulting longitudinal reinforcement ratio was 1.65%. In addition, the vertical web reinforcement used in the design consisted of the same arrangement as the control wall with Grade 690 MPa No. 3 bars. The resulting probable moment of the proposed wall was calculated using RC-Section and was further verified using VecTor2 FEM software. Table *4.2* compares the analytical results of wall W1HS to the experimental results of the control wall.

Table 4.2 – Sectional properties of wall W1HS and the control wall

	Wall W1HS		Control Wall		
	RC Section, kN.m [kip.ft]	**VecTor2, kN.m [kip-ft]**	**RC Section, kN.m [kip.ft]**	**VecTor2, kN.m [kip-ft]**	**Experimental kN.m [kip.ft]**
$\mathbf{M_{pr}}$	2913 [2148]	2528 [1862]	2521 [1859]	2532 [1867]	2600 [1917]
$\mathbf{M_r}$	2544 [1876]	-	2245 [1656]	-	-

The probable moment resistance (M_{pr}) of wall W1HS was found to be 15% higher than that of the control wall according to the RC-Section prediction. Using VecTor2, the ultimate moment capacities of wall W1HS was found be almost exactly the same as the control wall. The experimental moment capacity of the control wall was 3% more than the probable moment capacity predicted by VecTor2. Considering design restrictions in terms of availability of bar sizes and steel strengths, the proposed design was deemed to be satisfactory in producing the same probable moment resistance as the control wall.

4.1.2.2 Transverse Web Reinforcement

The design shear force, V_u, corresponding to the probable moment capacity, M_{pr} of wall W1HS was calculated by dividing the probable moment by the shear span or height of the wall. The probable moment of the wall was found to be 2538 kN.m using VecTor2 and 2913 kN.m using RC Section. Since the wall was designed to be flexure-dominant, shear failure had to be prevented; hence, probable moment used to calculate the shear demand of the wall was taken slightly higher than the VecTor2 prediction, at M_{pr} = 2700 kN.m.

$M_{pr} = 1991\ kip.ft$ (2700 $KN.m$)
$V_u = \frac{M_{pr}}{h_w} = \frac{1991}{14.1} = 141\ kip$ (628 KN)

Alternatively, using the shear and moment reduction factors with the nominal moment, M_n (calculated using RC-Section), the ultimate moment was calculated by as follows:

$M_n = M_r = 1876\ kip.ft$ (2544 $KN.m$)
$M_u = V_u h_w$
$V_u \leq \emptyset_{shear} V_n$
$M_u = M_n \emptyset_{flexure}$

where

$\emptyset_{shear} = 0.75$
$\emptyset_{flexure} = 0.9$

$$V_u = \frac{1.2M_n}{h_w} = \frac{1.2 \text{ x } 1876}{14.1} = 160\ kip\ (712\ KN)$$

Using the shear design expressions given in Cl 22.5.1.1 and Cl 22.5.6.1 of the ACI 318-14, the shear reinforcement was calculated as follows:

$$V_n = V_c + V_s \geq V_u \qquad \textit{[Eq. 4.1]}$$

Where

$$V_c = 2\left(1 + \frac{N_u}{2000\ _g}\right)\lambda\sqrt{f_c'}b_w d \qquad \textit{[Eq. 4.2]}$$

$$V_c = 2\left(1 + \frac{292000}{2000 * 225}\right) * 1 * \sqrt{11603} * 3.9 * 57.1 = 79.1\ kip\ (352\ KN)$$

$$V_s = V_u - V_c = 160 - 79.1 = 80.9\ kip\ (360\ KN)$$

where V_c and V_s are concrete and steel contributions to total shear strength, and V_n is the design shear strength, in kips; N_u is the axial force applied normal to the cross-section (taken as 8% of the nominal compressive capacity of the wall), in lbs; λ is the concrete density factor (1.0 for normal-density concrete in imperial units); f_c' is the concrete compressive strength, in psi; b_w is the thickness of the wall section and d is the effective depth of the section that is measured from the extreme compression fiber to the centroid of the tensions steel, in inches; A_g is the gross cross-sectional area of the wall, in in^2.

$$V_s = \frac{A_v f_{yt} d}{s} \qquad \textit{[Eq. 4.3]}$$

where A_v is the area of horizontal reinforcement layer, in in^2, f_{yt} is the yield strength of the horizontal steel, in psi, and s is the spacing of the horizontal reinforcement layer, in inches. Using two curtains of No. 3 (9.525mm dia.) - Grade 690 MPa bars (ACI 318-14, Cl. 18.10.2.2) for horizontal web reinforcement, we obtain the spacing of the horizontal shear reinforcement for wall W1HS as follows (ACI 318-14, Cl. 22.5.1.1):

$$s = \frac{A_v f_{yt} d}{V_s} = \frac{2 * 0.11 * 100{,}000 * 52}{80900} = 14.1\ in\ (358\ mm)$$

Clause 18.10.2.1 limits the minimum distributed web reinforcement to $0.0025A_g$. This Clause also limits the maximum spacing of distributed reinforcement to 18 in (457 mm). Using two curtains of No. 3 bars at 200mm, the horizontal web reinforcement ratio is calculated as follows:

$$s_t = \frac{A_v}{b\rho_t} \qquad \textit{[Eq. 4.4]}$$

$$s_t = \frac{A_v}{b\rho_t} = \frac{0.22}{3.9 * 0.0025} = \boldsymbol{22.6\ in\ (574\ mm)} > 14.1\ in\ (358\ mm)$$

Spacing of the transverse reinforcement shall also meet the requirements of **Clause 11.8.3** as follows:

$$s_t = 8.16\ in \leq \begin{cases} 3h = 3 * 3.9 = 11.7 \text{ in (297 mm)} \\ 18\ in \text{ (457 mm)} \\ \frac{l_w}{5} = \frac{57}{5} = 11.4\ in \text{ (290 mm)} \end{cases} \qquad \textit{[Eq. 4.5]}$$

Two curtains of No. 3 bars were used in the horizontal direction at $\mathbf{s_L}$ **= 280mm (11 in)** center-to-center spacing. The resulting shear capacity of the wall was calculated using equation 4.1 as follows:

$$V_c = 79.1\ kip\ (352\ KN)$$

$$V_s = \frac{A_v f_{yt} d}{s} = \frac{0.22 * 100{,}000 * 52}{11} = 104\ kip\ (463\ KN)$$

$$V_n = 79.1 + 104 = 183.1\ kip\ (814\ KN) \geq V_u = 160\ kip\ (712\ KN)$$

Other code requirements with respect to the spacing of the transverse shear reinforcement were checked to ensure compliance. Additional calculation details are presented in Appendix A.

4.1.2.3 Vertical Web Reinforcement

Two curtains of reinforcement were used in the web vertical direction as per Cl. 18.10.2.2. Clause 18.10.2.1 dictates the minimum distributed web reinforcement:

$$\rho_v = 00025A_g \qquad \textit{[Eq. 4.6]}$$

Where ρ_v is the distributed web vertical reinforcement ratio, and A_g is the gross cross-sectional area of the web section.

$$s_{v-maximum} = \frac{A_v}{b\rho_t} = \frac{0.22}{3.9 * 0.0025} = 22.5\ in\ (572\ mm)$$

In addition, the spacing of the web vertical reinforcement shall meet the requirements of Clause 11.7.2 *[Eq. 4.5]* as follows:

$$s_t \leq \begin{cases} 3h = 3 * 3.9 = 11.7\ in\ (297\ mm) \\ 18\ in\ (457\ mm) \\ \frac{l_w}{3} = \frac{57}{3} = 19\ in\ (483\ mm) \end{cases}$$

Hence, two curtains of No. 3 Grade 690 MPa bars were used at **s_v = 300mm (11.7in)** spacing as the vertical web reinforcement.

4.1.2.4 Boundary Element Transverse Reinforcement (Ties)

Square ties were selected for the boundary elements as permitted by Cl. 18.7.5.2. Crossties of the same bar size were provided in both horizontal and out-of-plane directions according to Cl. 25.7.2.3 a) to enclose all alternate bars by the corner of a tie. The maximum spacing of the boundary element ties was governed by Cl. 18.7.5.3 b). Clause 18.7.5.3 states that the spacing of the transverse reinforcement shall not exceed six times the diameter of the smallest longitudinal bar:

$$s_{ties} = 6 * d_b = 6 * 0.5 = 3.0\ in\ (76.2\ mm)$$

Hence, No. 3 ties with single crossties in both horizontal and out-of-plane directions were used at a spacing of **S_{ties} = 75mm**.

4.1.3 Wall W2HS Design Details

Wall W12HS had a rectangular cross-section and was 2900 high x 1625mm long x 200mm thick. The overall height of the wall was 3250mm which included a 500mm deep strip at the top of the wall where the lateral load was directly applied at a height of 2900mm. This loading section was reinforced with twice the transverse reinforcement to enhance the shear capacity of the wall at the point of loading. In addition, this loading section was responsible for transferring the axial loads from the pre-stressing beams to the rest of the wall.

The wall was constructed using high-strength concrete with a target compressive strength of 80 MPa. The average compressive strength of the concrete was found to be 74 MPa on the day of the test (308 days after the last cast). Grade 690 MPa ASTM A1035 steel bars were used in the construction of wall W-2HS. The longitudinal reinforcement in the boundary elements consisted of US size No. 4 (12.7mm dia.) bars placed in a 10-bar arrangement. Compared to the control wall which used 20M bar as the longitudinal reinforcement in its boundary elements, 57% less longitudinal reinforcement was used in the boundary elements of wall W-2HS. The calculated probable moment of the test wall was approximately the same as the control wall.

The distributed horizontal and vertical web reinforcement consisted of two curtains of US size No. 3 (9.525mm dia.) bars spaced at 175mm ($\rho_{sh} = 0.41\%$) and 200mm ($\rho_{sv} = 0.36\%$) respectively. The transverse reinforcement in the boundary elements consisted of No. 3 square ties with a single crosstie in both horizontal direction and a hoop crosstie in the out-of-plane direction, placed at 65mm center-to-center spacing resulting in a reinforcement ratio of $\rho_{st} = 1.64\%$ in the horizontal direction and $\rho_{st} = 1.46\%$ in the out-of-plane direction. Figure 4.6 provides a 3D representation of the test wall. Figure 4.7 and Figure 4.8 show the dimensions and reinforcement details of wall W2HS.

Similar to the design of wall W1HS, only 50% of the boundary element reinforcement was spliced within the plastic hinge region of wall W2HS.

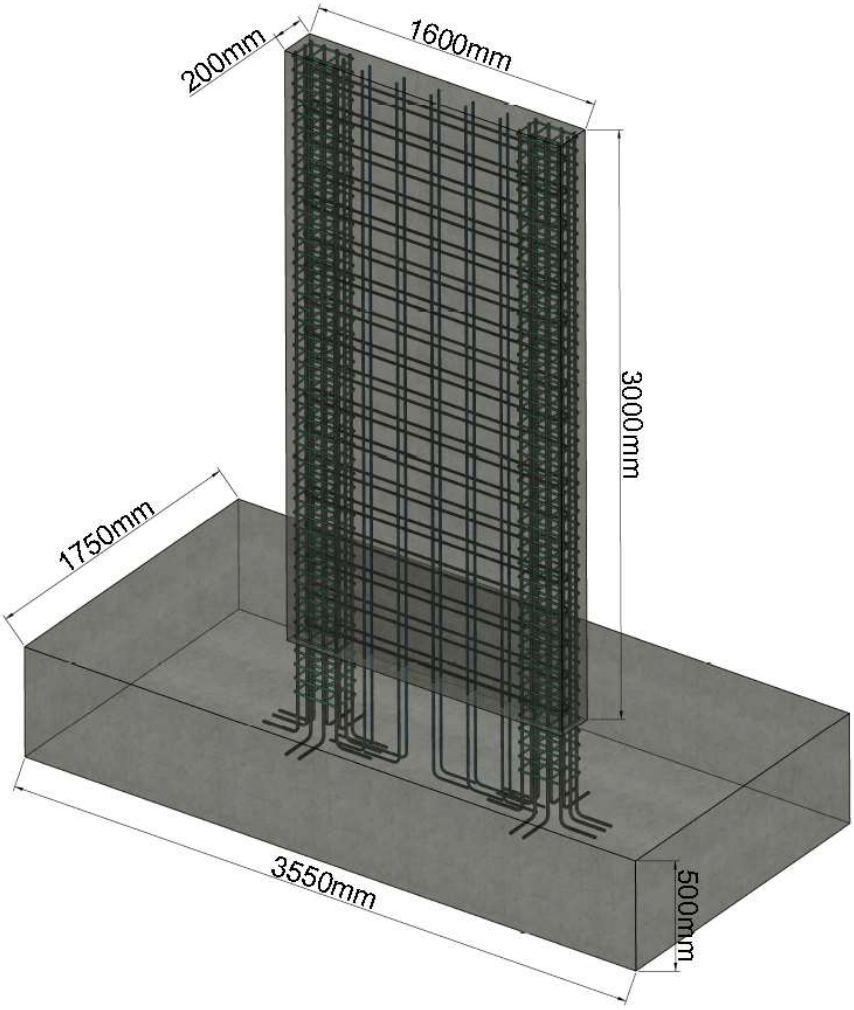

Figure 4.6 - 3D representation of wall W2HS

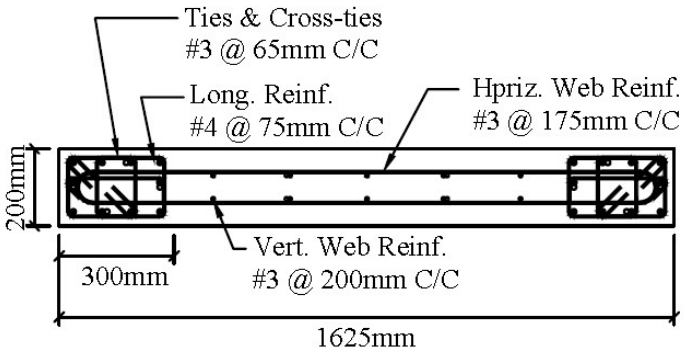

Figure 4.7 - Wall W2HS cross-section

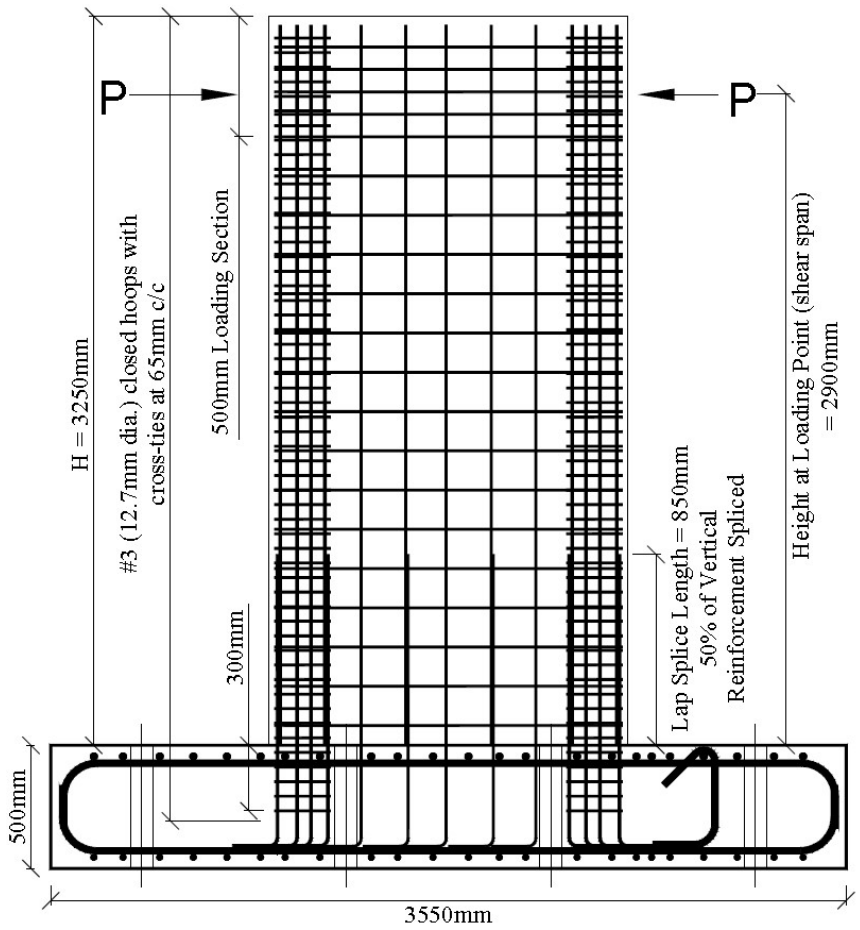

Figure 4.8 – Wall W1HS reinforcement details

4.1.3.1 Boundary Element Longitudinal Reinforcement

The arrangement of the boundary element longitudinal reinforcement was selected to match that of the control wall. Since high-strength reinforcement was used, smaller US size No. 4 and No.3 bars were used instead of the 20M and 10M bars used in the control wall, respectively. Figure 4.9 shows the arrangement of the vertical flexural reinforcement used in the RC-Section models for wall W2HS and the control wall. Table 4.3 presents the geometric and material specifications of the control wall as well as its sectional properties calculated using the RC-Section software.

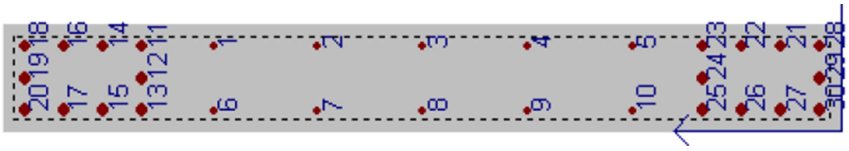

Figure 4.9 - Vertical reinforcement arrangement used in RC-Section Model

Table 4.3 – Control wall properties (Navidpour, 2018)

H (m) [in]	L (m) [in]	t (m) [in]	f_{yl} (MPa) [ksi]	f_{yt} (MPa) [ksi]	f'_c (MPa) [psi]	P (kN) [kip]	M_{exp}, (kN.m) [Kip-ft]	M_n (kN.m) [Kip-ft]	M_{pr} (kN.m) [Kip-ft]
2900 [118]	1625 [57]	200 [3.9]	471 [65]	710 [73]	82 [11893]	1600 [360]	3330 [2456]	3160 [2331]	3660 [2699]

In Table 4.3, H denotes wall height, L is wall length, t is wall thickness, f_{yl} is the yield strength of the longitudinal and distributed reinforcement, f_{yt} is the yield strength of the boundary element ties, f'_c is the 28-day compressive strength of concrete, P is the applied axial compression, M_{exp} is the experimental moment resistance obtained from the wall test by Navidpour (2018), M_n is the nominal moment resistance, and M_{pr} is the analytical probable moment resistance.

As previously mentioned, an 8-bar layout consisting of No. 4 bars was selected for the longitudinal reinforcement in the boundary elements. The bars were spaced at 75mm c/c in the horizontal direction and at 65mm in the out-of-plane direction. The resulting longitudinal reinforcement ratio was 2.2%. In addition, the vertical web reinforcement used in the design consisted of the same arrangement as the control wall with Grade 690 No. 3 bars. The resulting probable moment of wall W2HS was calculated using RC-Section and was further verified using VecTor2 FEM software. Table 4.4 compares the analytical results of wall W2HS to the control wall.

Table 4.4 – Sectional properties of wall W1HS and the control wall

	Wall W-2HS		Control Wall		
	RC Section, kN.m [kip.ft]	VecTor2, kN.m [kip-ft]	RC Section, kN.m [kip.ft]	VecTor2, kN.m [kip-ft]	Experimental kN.m [kip.ft]
M_{pr}	3630 [2677]	3335 [2460]	3660 [2699]	3780 [2788]	3330 [2456]
M_r	3213 [2370]	-	3160 [2331]	-	-

The probable moment resistance (M_{pr}) of wall W2HS was found to be approximately the same as that of the control wall according to the RC-Section prediction. Using VecTor2, the ultimate moment capacity of wall W2HS was found to be 12% less than the control wall. The capacity of wall W2HS was found to be almost exactly the same as the experimental moment resistance of the control wall. The analysis results of the proposed test wall were deemed to be acceptable for the purpose of this experiment.

4.1.3.2 Transverse Web Reinforcement

The design shear force, V_u, corresponding to the probable moment resistance, M_{pr} of wall W2HS was calculated by dividing the probable moment by the shear span or height of the wall. The probable moment of the wall was found to be 3335 kN.m using VecTor2 and 3630 kN.m using RC Section. Since the wall was designed to be flexure-dominant, shear failure had to be prevented; hence, probable moment M_{pr} = 2699 kip.ft (3660 KN.m) obtained using RC-Section was used for the shear force calculation.

$M_{pr} = 2699\ kip.ft\ (3660\ KN.m)$
$V_u = \frac{M_{pr}}{h_w} = \frac{2699}{9.5} = 284\ kip$ (1263 KN)

Alternatively, using the shear and moment reduction factors with the nominal moment, M_n (calculated using RC-Section), the ultimate moment was calculated by as follows:

$M_n = M_r = 2331\ kip.ft\ (3160\ KN.m)$
$M_u = V_u h_w$
$V_u \leq \emptyset_{shear} V_n$
$M_u = M_n \emptyset_{flexure}$

where

$\emptyset_{shea} = 0.75$
$\emptyset_{flexure} = 0.9$

$V_u = \frac{1.2M_n}{h_w} = \frac{1.2 \text{ x } 2331}{9.5} = 294\ kip\ (1307\ KN)$

Using the shear design expressions given in Cl 22.5.1.1 and Cl 22.5.6.1 of the ACI 318-14, the shear reinforcement was calculated using Eq. 4.1, 4.2, and 4.3 as follows:

$V_c = 2\left(1 + \frac{300{,}000}{2000 * 495.5}\right) * 1 * \sqrt{11600} * 7.87 * 57.1 = 126\ kip\ (560\ KN)$

$V_s = V_u - V_c = 294 - 126 = 168\ kip\ (747\ KN)$

Using two curtains of No. 3 (9.525mm dia.) - Grade 690 MPa bars (ACI 318-14, Cl. 18.10.2.2) for horizontal web reinforcement, we obtain the spacing of the horizontal shear reinforcement for wall W2HS as follows (ACI 318-14, Cl. 22.5.1.1):

$$s = \frac{A_v f_{yt} d}{V_s} = \frac{2 * 0.11 * 100{,}000 * 57.1}{168000} = 6.80\ in\ (173mm)$$

Clause 18.10.2.1 limits the minimum distributed web reinforcement to $0.0025A_g$. This Clause also limits the maximum spacing of distributed reinforcement to 18 in (457 mm). Using two curtains of No. 3 bars, the horizontal web reinforcement ratio is calculated using Eq. 4.4 as follows:

$$s_t = \frac{A_v}{b\rho_t} = \frac{0.22}{7.87 * 0.0025} = \mathbf{11.2\ \boldsymbol{in}\ (284\ \boldsymbol{mm})}$$

Spacing of the transverse reinforcement shall also meet the requirements of Clause 11.8.3 [Eq. 4.5] as follows:

$$s_t = 8.16\ in \leq \begin{cases} 3h = 3 * 7.87 = 23.6 \text{ in } (600 \text{ mm}) \\ 18\ in\ (457 \text{ mm}) \\ \frac{l_w}{5} = \frac{64}{5} = 12.8\ in\ (325 \text{ mm}) \end{cases}$$

Two curtains of No. 3 bars were used in the horizontal direction at $\mathbf{s_L}$ **= 175mm (6.9 in)** center-to-center spacing. The resulting shear capacity of the wall was calculated using Eq. 4.1 as follows:

$$V_c = 126\ kip\ (560\ KN)$$

$$V_s = \frac{A_v f_{yt} d}{s} = \frac{0.22 * 100{,}000 * 57.1}{6.9} = 182\ kip\ (810\ KN)$$

$$V_n = 126 + 182 = 308\ kip\ (1370KN) \geq V_u = 294\ kip\ (1307\ KN)$$

Other code requirements with respect to the spacing of the transverse shear reinforcement were checked to ensure compliance. Additional calculation details are presented in Appendix A.

4.1.3.3 Vertical Web Reinforcement

Two curtains of reinforcement were used in the web vertical direction as per Cl. 18.10.2.2. Clause 18.10.2.1 dictates the minimum distributed web reinforcement:

$$s_{v-maximum} = \frac{A_v}{b\rho_t} = \frac{0.22}{7.87 * 0.0025} = 11.2\ in\ (284\ mm)$$

In addition, the spacing of the web vertical reinforcement shall meet the requirements of Clause 11.7.2 [Eq. 4.5] as follows:

$$s_t \leq \begin{cases} 3h = 3 * 7.87 = 23.6\ in\ (599\ mm) \\ 18\ in\ (457\ mm) \\ \frac{l_w}{3} = \frac{64}{3} = 21.3\ in\ (542\ mm) \end{cases}$$

Hence, two curtains of No. 3 Grade 690 MPa bars were used at $\mathbf{s_v}$ = **200mm (7.87 in)** spacing as the vertical web reinforcement. This spacing was selected to be consistent with the design of the control wall.

4.1.3.4 Boundary Element Transverse Reinforcement (Ties)

Rectilinear hoops with crossties were selected for the boundary elements as permitted by Cl. 18.7.5.2. Crossties of the same bar size were provided in both horizontal and out-of-plane directions according to Cl. 25.7.2.3 a) to enclose all alternate bars by the corner of a tie. The maximum spacing of the boundary element ties was governed by Cl. 18.7.5.3 a). Clause 18.7.5.3 a) states that the spacing of the transverse reinforcement shall not exceed ¼ of the minimum column dimension:

$$s_{ties} = \frac{1}{4} * 7.87 = 1.96\ in\ (50\text{mm})$$

Clause 18.10.6.4 e) requires that this limit should be changed to 1/3 of the least dimension of the boundary element:

$$S_{ties} = \tfrac{1}{3} * 7.87 = 2.62\ in\ (66.7\text{mm})$$

Hence, No. 3 ties with crossties in both horizontal and out-of-plane directions were used at a spacing of $\mathbf{S_{ties}}$ = **65mm**.

4.1.4 Construction

The construction of the walls started with the fabrication of the steel reinforcement cages. The reinforcement used in the foundation unit consisted of 25M and 30M Grade 400 ASTM A615 steel bars and were readily available at local steel suppliers. The No. 3 and No. 4 Grade 690 ASTM A1035 steel bars used in the construction of the walls were supplied by MMFX®, a commercial metals company located in US. The reinforcing bars were cut and bent to specified shapes in a local steel fabrication plant.

Figure 4.10 presents construction photos of wall W1HS and W2HS foundation units. Concrete forms were constructed using plywood and construction lumber. The reinforcement cages were then assembled inside the formwork. Dowels were placed in the foundation during the assembly of the steel reinforcement cage and were secured from movement using templates made with plywood. As presented in the design section, only 50% of the flexural reinforcement were spliced at the base of the walls.

The axial compression was applied using prestressing cables that were anchored to the foundation units. The anchors consisted of 1" (25.4mm) diameter high-strength threaded rods. Steel plates were welded to the embedded ends of the rods to improve their anchorage. The threaded rods were secured in place using plywood templates and covered with masking tapes to prevent damage to the threads during casting. Figure 4.10 c) shows an embedded rod before casting.

Ready-mix concrete with 28-day compressive strength of 40 MPa was used to cast the foundation. The footprint area of the wall was roughened to provide a better connection at the cold joint between the wall and the foundation.

The boundary elements were assembled individually due to the congestion of the reinforcement. Once the foundations were cast, the boundary elements as well as the web vertical and transverse reinforcement were installed. The reinforcement cages of the boundary elements were secured using tie wires that provided a convenient way of adjusting the position and plumpness of the wall reinforcement cages before casting. The concrete forms used for the wall sections were constructed using ¾-in plywood and 4in by 4in construction lumber. Special attention was paid to the design of the forms to prevent blowouts. The forms were secured using threaded rods, encased in ½-in copper tubes that passed through the walls. Due to the height of the walls and in order to ensure

proper concrete placement, casting was completed in multiple stages. Small portable vibrators were used to consolidate the concrete during casting. A 0.2m^2 pan mixer was used to mix the concrete. Each formwork layer required 2 batches of concrete. Wall W1HS and W2HS required 8 and 6 batches of concrete in total, respectively. Figure 4.11 shows the walls during construction.

a) Wall W1HS foundation before casting

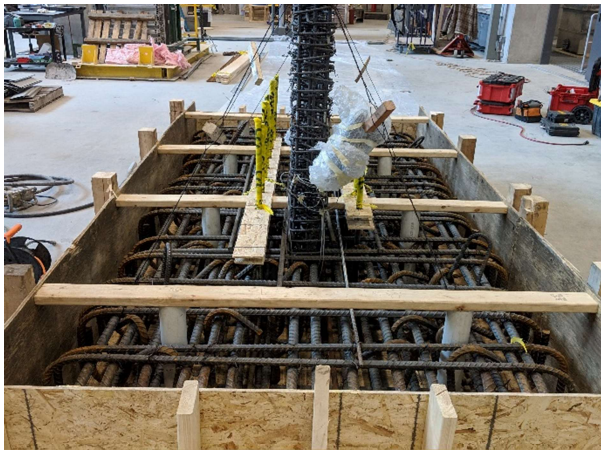

b) Wall W2HS foundation before casting

c) Typical anchored threaded rod (used for applying axial load)

d) Wall W1HS foundation during casting

Figure 4.10 – Construction of the foundation units

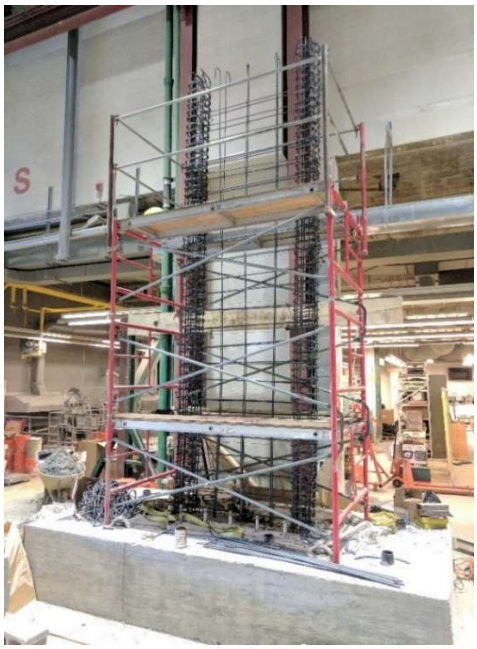

a) Wall W1HS prior to casting

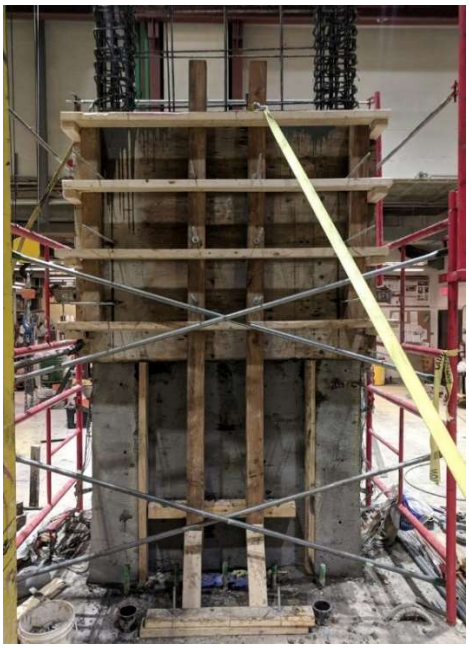

b) Wall W1HS – during casting

c) Wall W2HS prior to casting

d) Wall W2HS – during casting

Figure 4.11 – Construction of the test walls W1HS and W2HS

One of the challenges of constructing large-scale concrete walls was working at heights which required prior training and certified fall prevention and fall arrest equipment. Due to the scale of the project and the fact that many of the methods and tools employed in the construction of the walls were non-conventional and at times state-of-the-art, special attention had to be paid to safety

during the construction. In addition, the size of the walls created challenges with respect to moving or adjusting their location after casting as their weight were close to the maximum capacity of the overhead bridge cranes at the structural laboratory. After casting, each wall weighed approximately 12 tonnes, which meant that once cast, the walls could not be moved using the 10-tonne overhead bridge crane. Furthermore, disposal of the tested walls required specialised equipment and experienced staff to remove the pre-stressing cables and to cut the walls into smaller pieces. Hence, construction and disposal of the walls required careful planning and coordination before and after the tests.

4.1.5 Instrumentation

In order to obtain the necessary test data, cable transducers were installed at strategic locations on the walls and the foundation units. In addition, strain gauges were installed at critical locations of the reinforcing bars to measure and record strains during the test. The collected data included applied load, in-plane wall displacements and reinforcing steel strains. Based on a review of instrumentation techniques used in previous experimental programs available in the literature, the following data were selected to be collected during the tests:

- Lateral force: Applied lateral force was measured via a built-in load cell in the MTS hydraulic actuator. Data obtained by these load cells were communicated through the data acquisition system and were stored in the test file.
- Axial compression during the tests: As discussed, axial compression was applied by means of tensioned pre-stressing 7-wire strands that were previously calibrated. In order to monitor axial load levels during the tests, strain gauges were attached to the cables at their mid-height. Cable strain data were recorded during the tests and were later converted to kilo-Newtons.
- Lateral displacement: Lateral displacement measurements of the walls were recorded at the height of the application of the lateral load as well as critical locations along the heights of the walls. Figure 4.12 presents details of the proposed instrumentation plan for measuring deformations for wall W1HS and W2HS. The collected data were used to generate the lateral load-deformation history of the walls.
- Shear deformation: Shear deformations were recorded using cable transducers installed within the plastic hinge regions of the walls as shown in Figure 4.12. The diagonal readings

from the cable transducers were converted to shear strains. The recorded data were then used to quantify shear deformations and to determine the contribution of shear to the overall rotation of the walls.

- Reinforcement Strains: Reinforcement strains were collected via 120Ω foil strain gauges installed on the reinforcing bars at critical locations. These locations included the outermost longitudinal flexural reinforcement within the boundary elements as well as selected transverse web reinforcement. Figure 4.13 and Figure 4.14 show locations of strain gauges installed within wall W1HS and W2HS. The strain data were used to determine the stresses in the reinforcement at various loading stages.

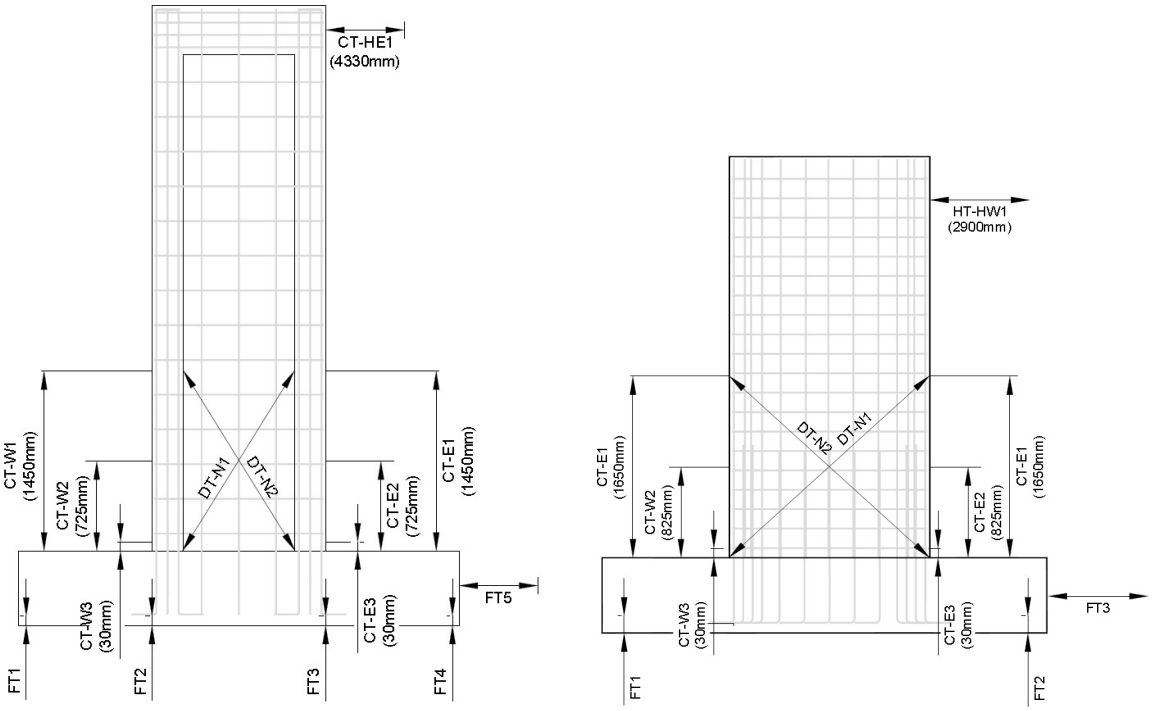

a) Wall W1HS Cable Transducers b) Wall W2HS Cable Transducers

Figure 4.12 – Displacement transducers

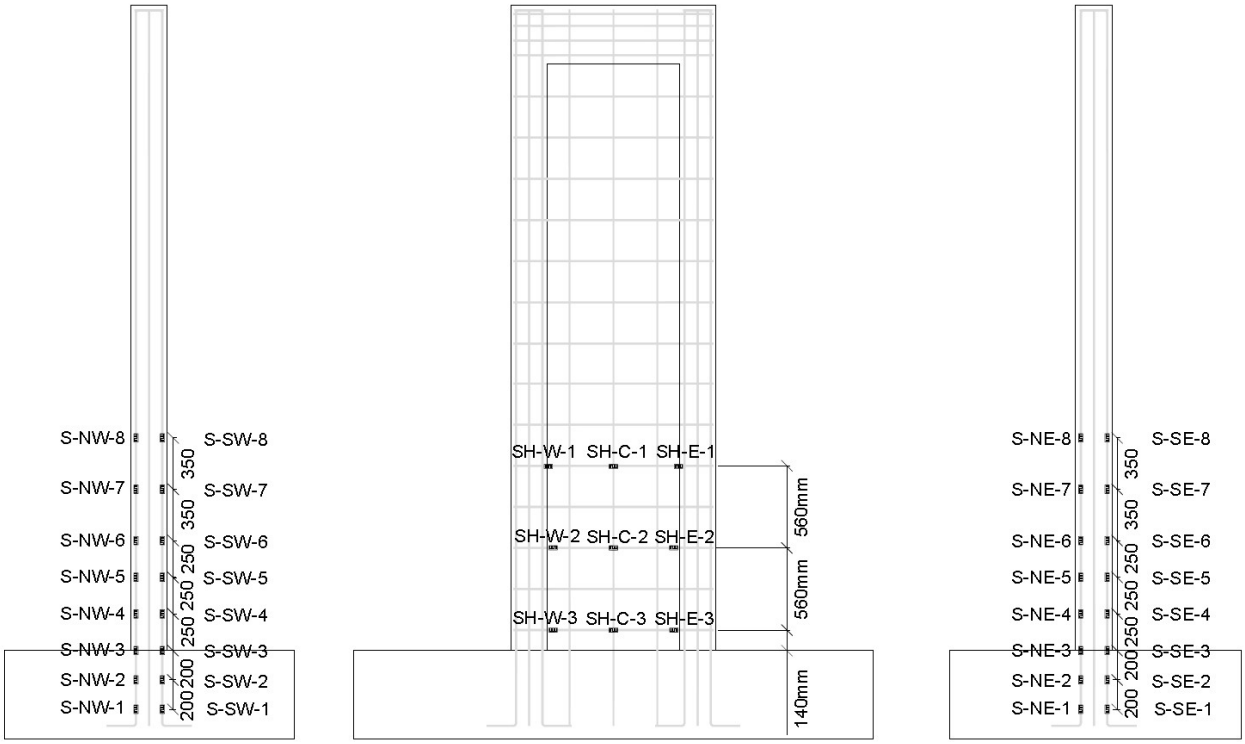

Figure 4.13 – Wall W1HS strain gauge instrumentation plan

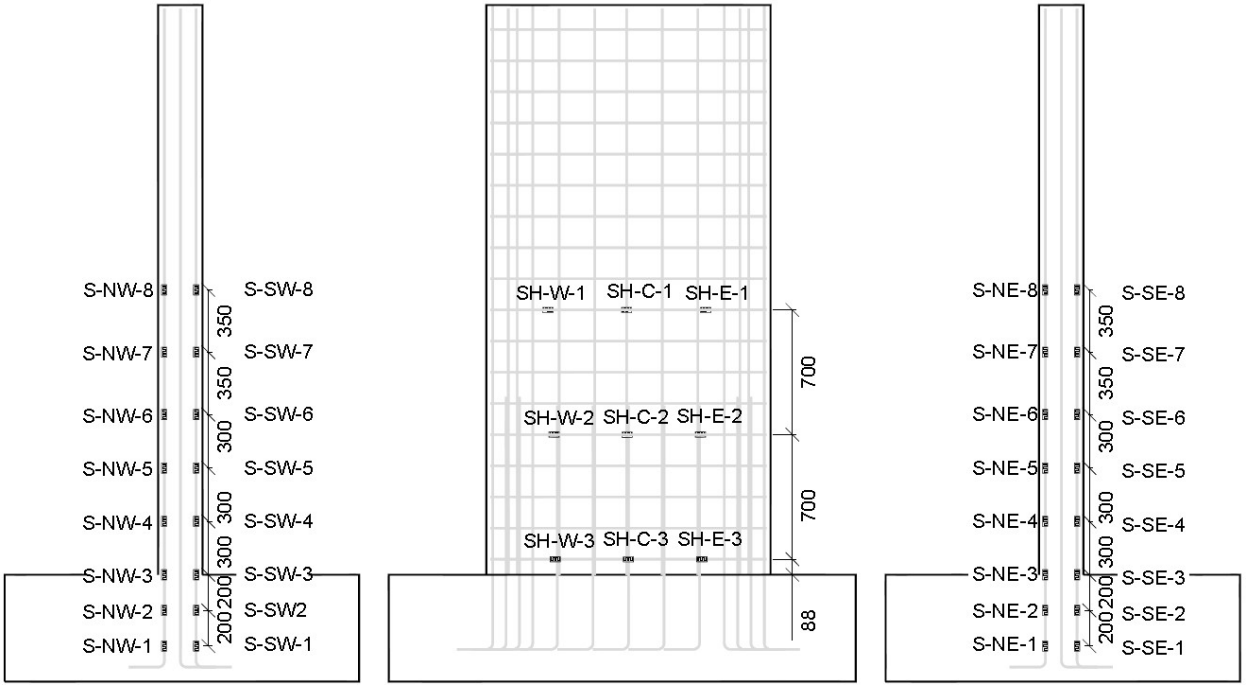

Figure 4.14 – Wall W2HS strain gauge instrumentation plan

- Foundation Uplift and sliding: Uplift of the foundation units during the tested were measured using LVDTs installed along the length of the foundation. Figure 4.15 shows photos of typical LVDT installation on wall W1HS foundation. Sliding of the foundations were measured using cable transducers installed at the ends of the foundation units, measuring sliding with respect to a stationary concrete block resting on laboratory's strong floor.
- Crack Monitoring: The walls were inspected after each loading stage and cracks were marked and photographed. The number of cracks, propagation patterns, and their approximate widths were recorded for later analysis.
- General observations: The wall was closely monitored during the test and their general behaviour during the test including major events, damage, failure mode and rupture of reinforcing bars were recorded. A summary of these observations can be found in Chapter 5.

Figure 4.15 - LVDTs installed along the length of the foundation to monitor uplift

4.1.6 Loading

Wall W1HS was tested in the Structures Laboratory of the University of Ottawa. The loading setup consisted of a 1000 kN MTS hydraulic actuator attached to a rigid steel A-frame that was anchored to the strong floor of the laboratory. The foundation of the wall was bolted to the strong floor to restrict vertical and horizontal movements during the tests. The annulus between the anchoring bolts and the openings in the foundations were filled with sand to minimize sliding. In addition,

the walls were braced to restrict out-of-plane movements during the tests. Figure 4.16 to Figure 4.23 present details of the loading setup for wall W1HS.

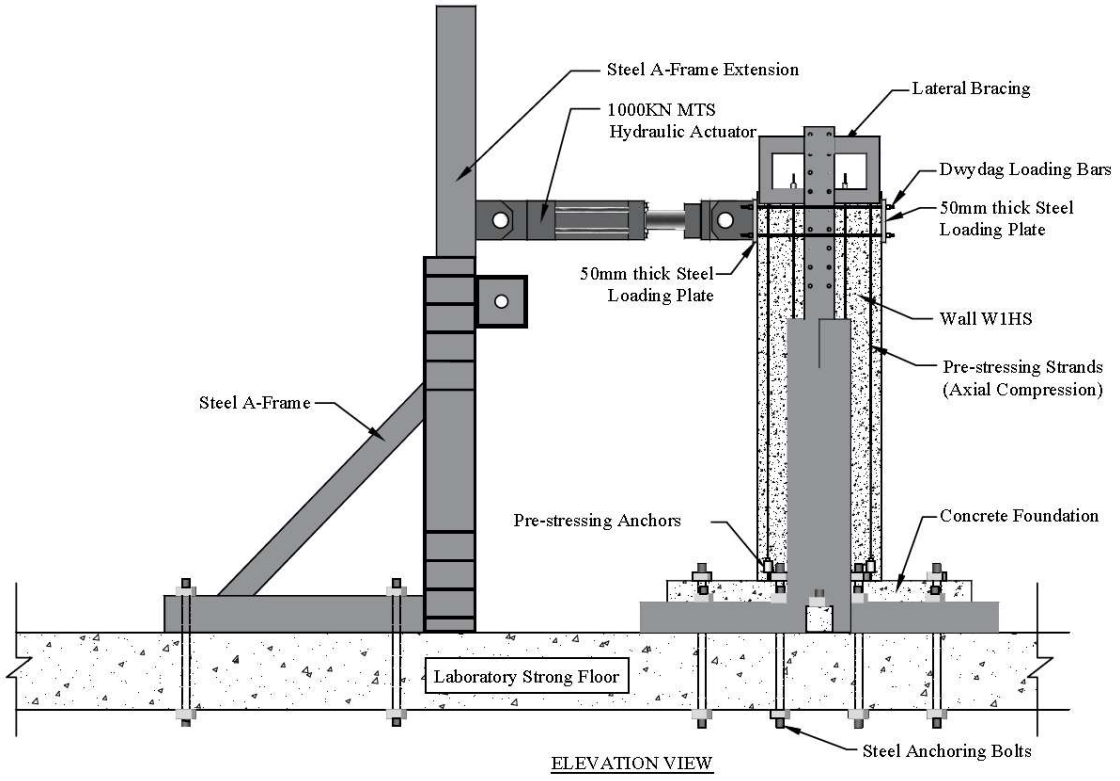

Figure 4.16 - Loading setup for wall W1HS – elevation view

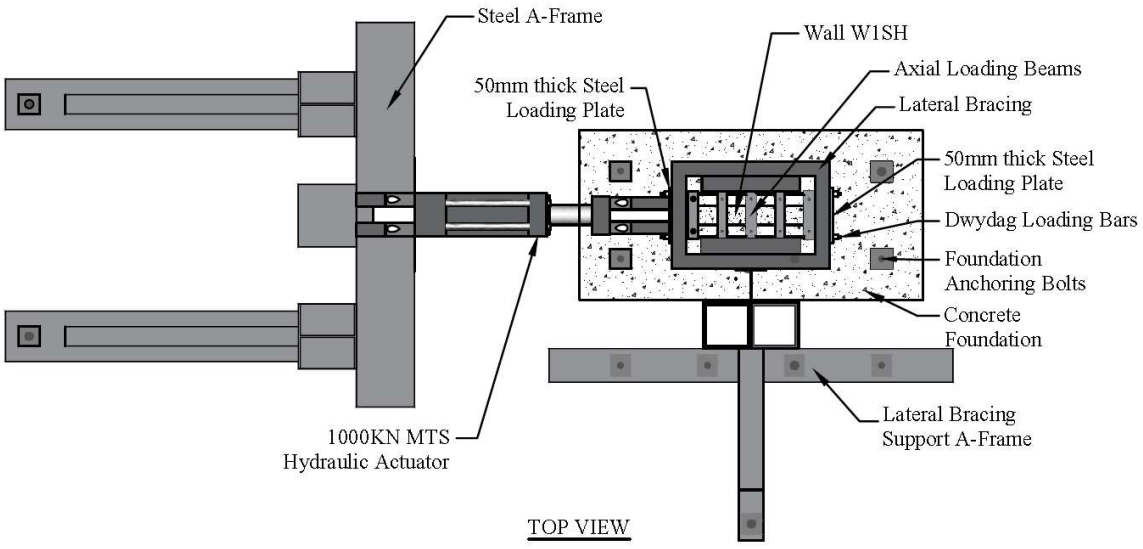

Figure 4.17 - Loading setup for wall W1HS – top view

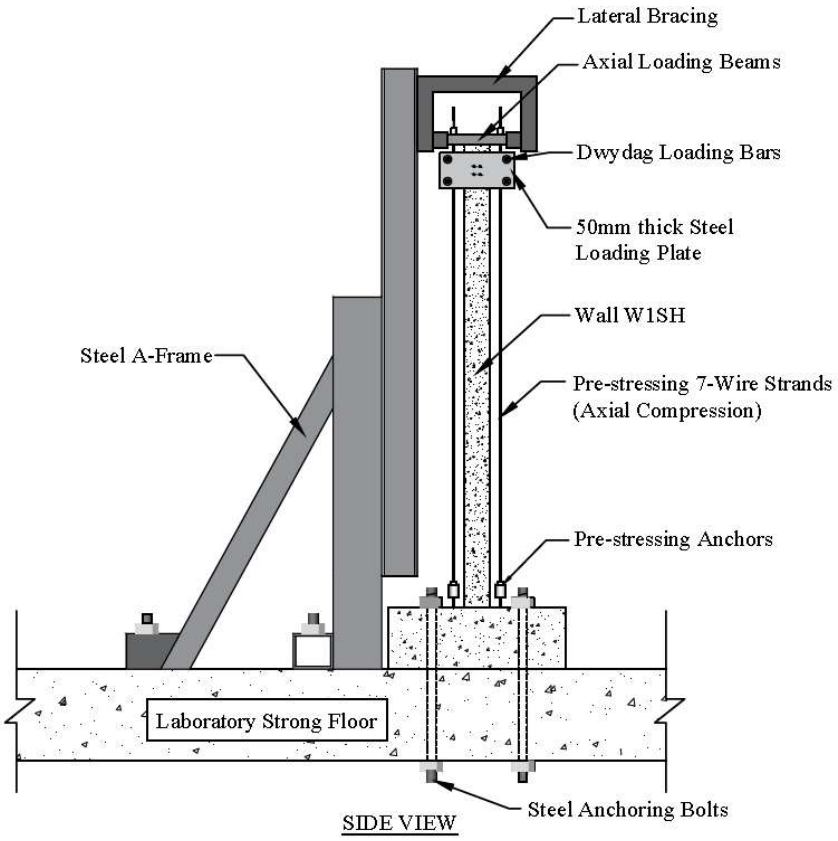

Figure 4.18 - Proposed loading setup for Wall W1HS – side view

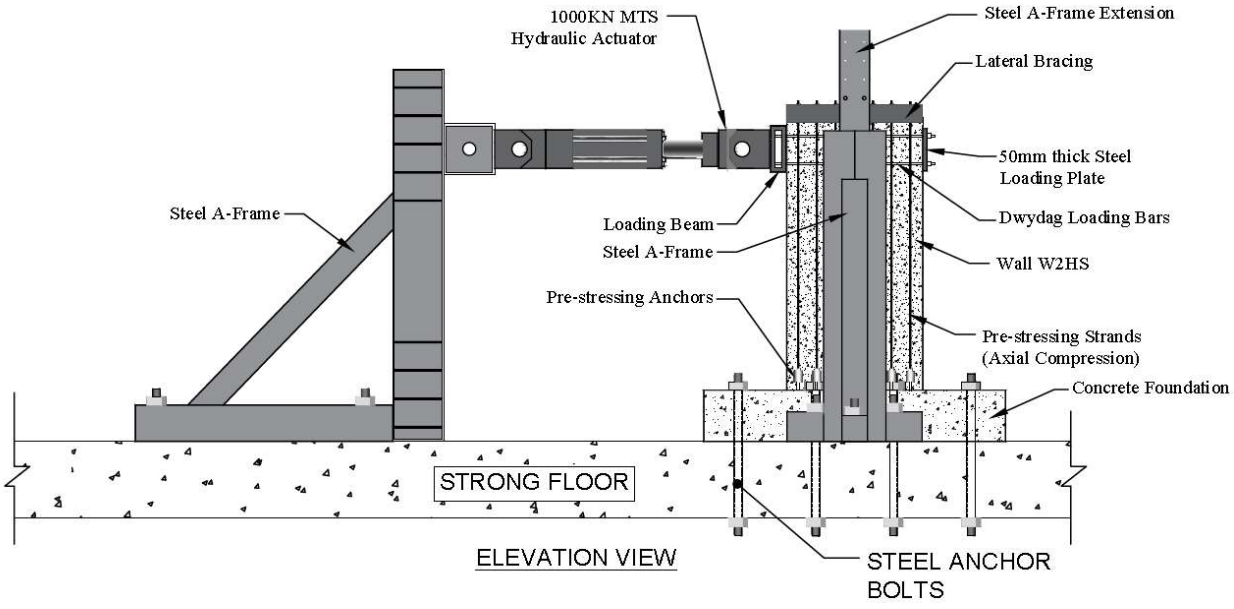

Figure 4.19 - Loading setup for wall W2HS – elevation view

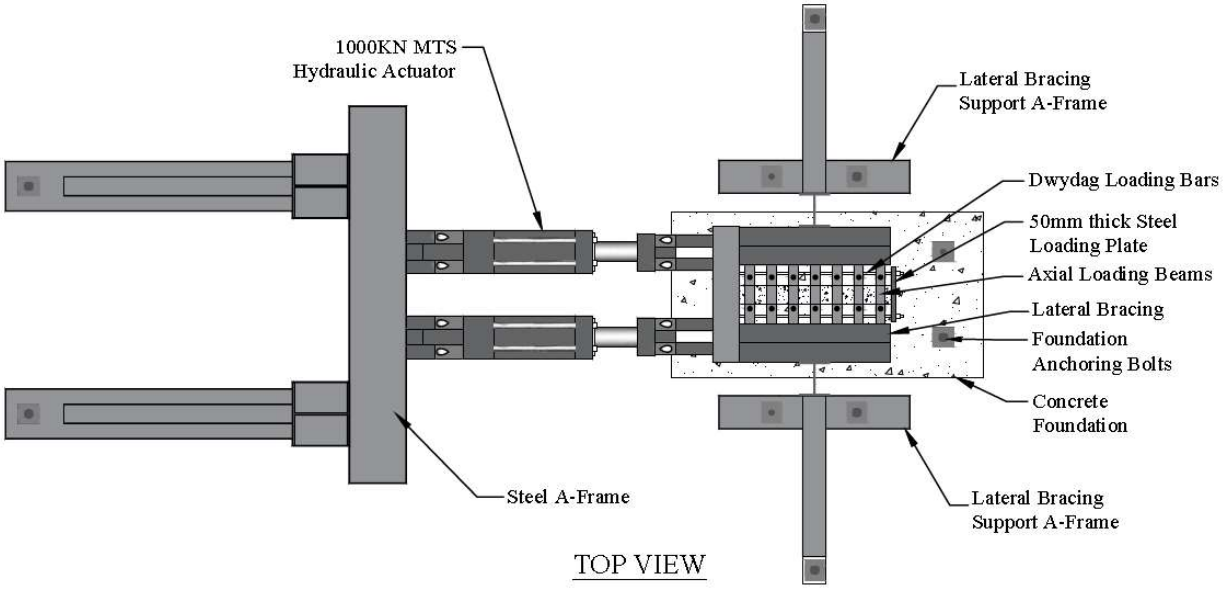

Figure 4.20 - Loading setup for wall W2HS – elevation view

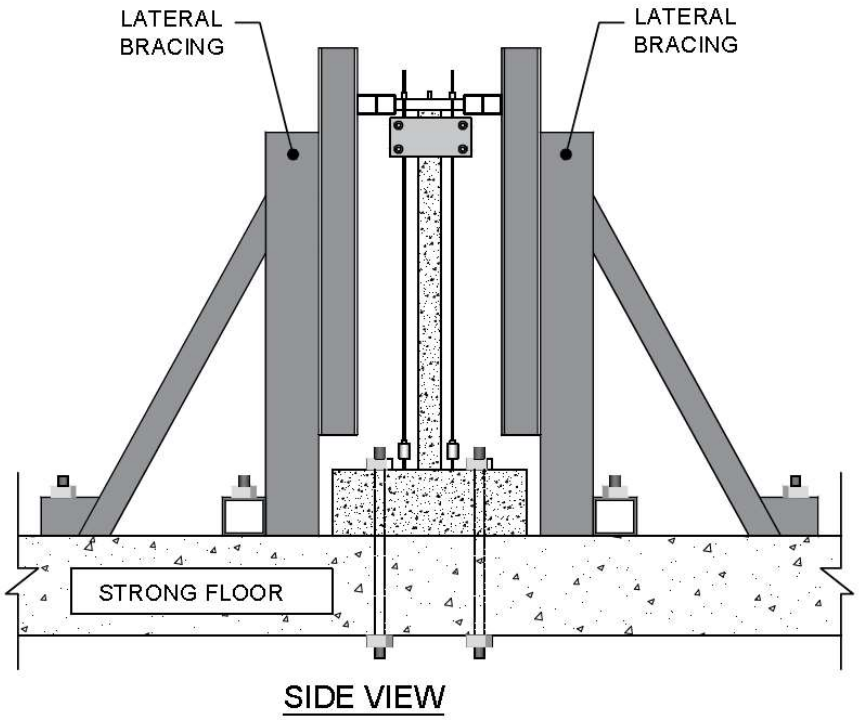

Figure 4.21 - Proposed loading setup for Wall W2HS – side view

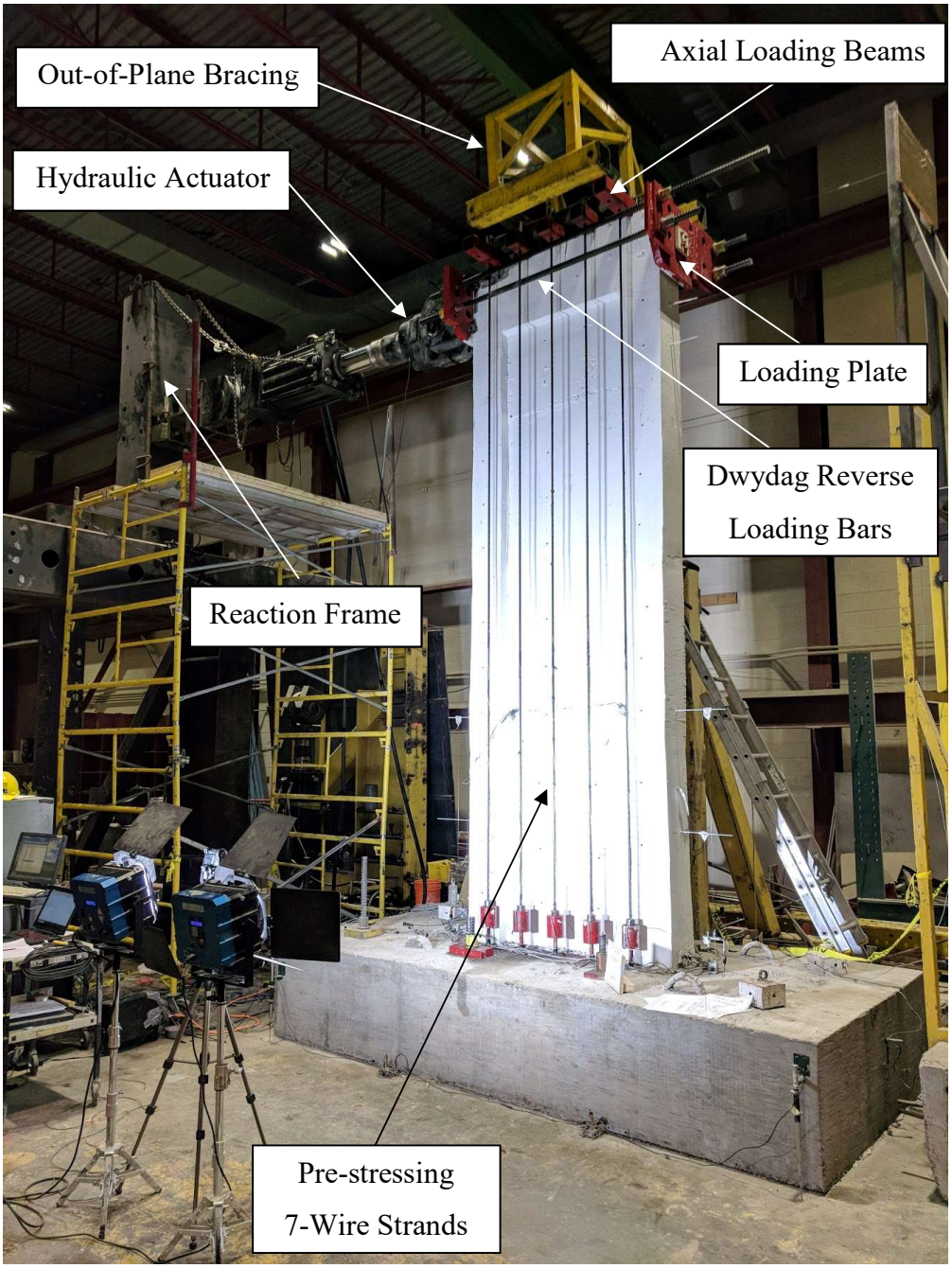

Figure 4.22 – Wall W1HS loading setup

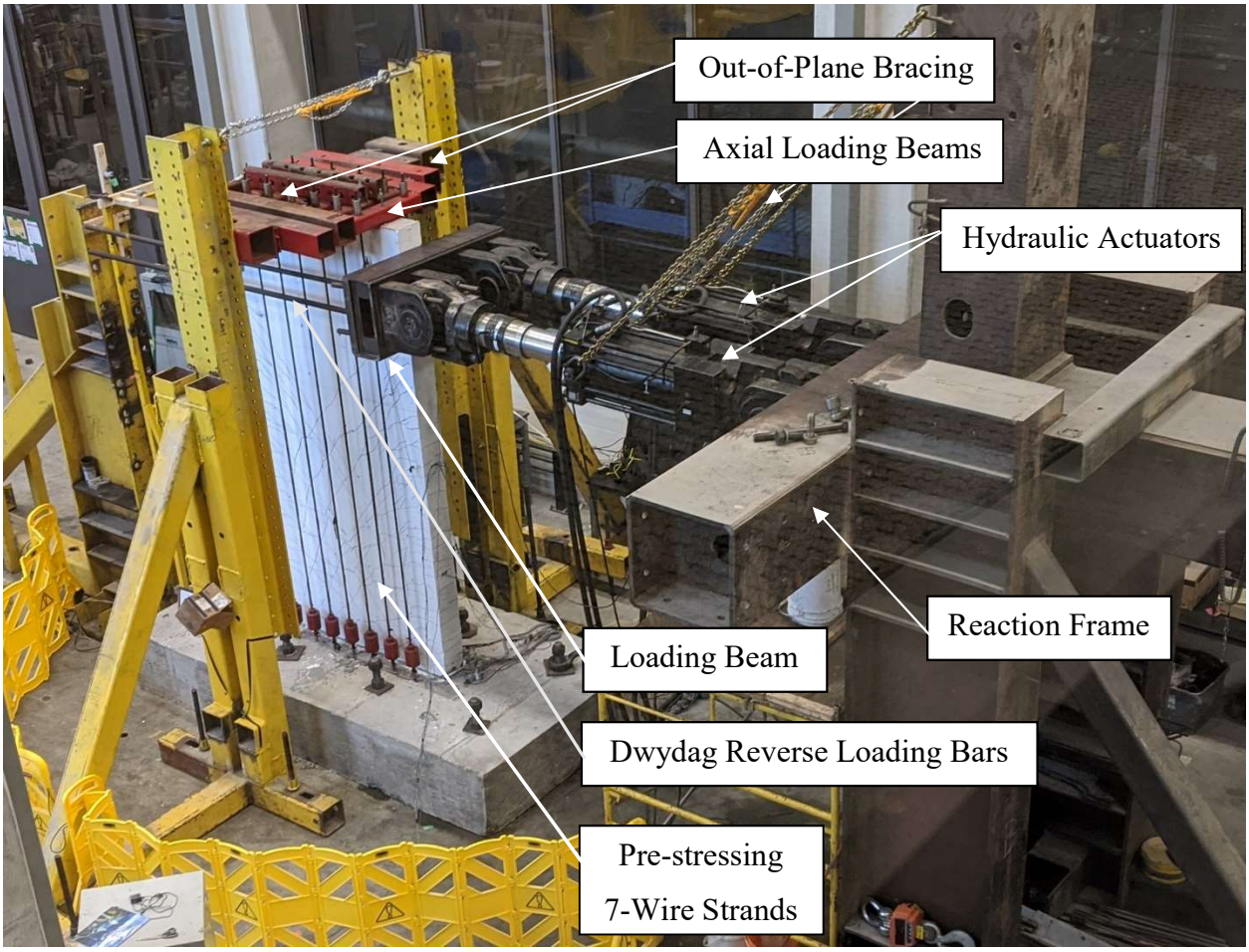

Figure 4.23 – Wall W2HS loading setup

Axial compression was applied using prestressing cables. The strands were anchored to the foundation units using custom-made cylindrical pieces as shown in Figure 4.24 a). The strands passed through hollow structural steel sections installed at the top of the wall that transmitted the axial compressive loading to the over-reinforced loading section of the wall at the top. A 1200 KN hollow cylindrical hydraulic jack with custom-made pre-stressing steel tubes was used to load the cables as shown in Figure 4.24 c).

A smaller hollow cylindrical jack was used to lock the pre-stressing wedges after loading each cable. The level of tension in the cables was controlled manually using the hydraulic pump's throttle valves. Strains in the pre-stressing cables were monitored using strain gauges that attached to the cables at their mid-height. Tensile forces in the cables were obtained by correlating the strain to force using the stress-strain relationship for the pre-stressing cables.

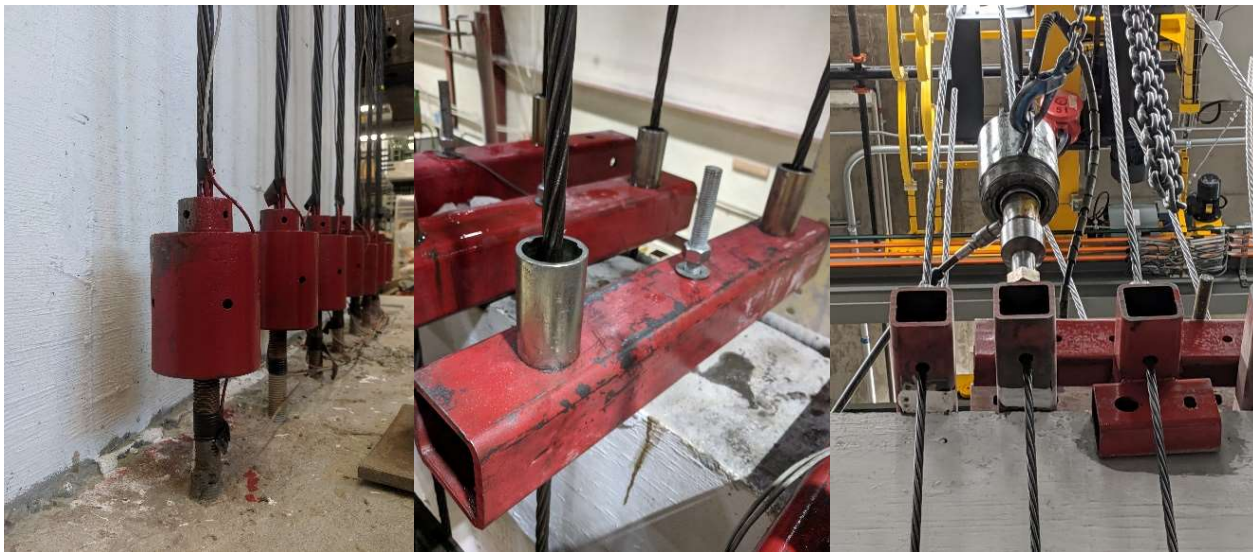

a) Anchoring mechanism b) Tensioning beams at the top of the wall c) Custom-made tensioning system

Figure 4.24 – Wall W1HS axial loading applied using pre-stressing cables

4.1.7 Loading protocol

The loading protocol for the walls consisted of a displacement-controlled loading scheme as shown in Figure 4.25 and Figure 4.26. As ASTM A1035 reinforcing bars do not have a defined yield point, it is difficult to pinpoint a specific yield displacement that is typically used in developing cyclic loading protocols. In order to ensure that the yield point of the wall was effectively captured during testing, small initial drift increments of 0.2% were applied up to a lateral drift of 1.0%. The size of the increments was selected based on the predicted yield 'region' of the wall that was obtained analytically using VeTor2 Finite Element Modelling software.

Following yield, lateral cyclic displacements continued at increments of 0.5% up to failure. Each loading stage was cycled three times to simulate the loading reversals that would occur during an earthquake event.

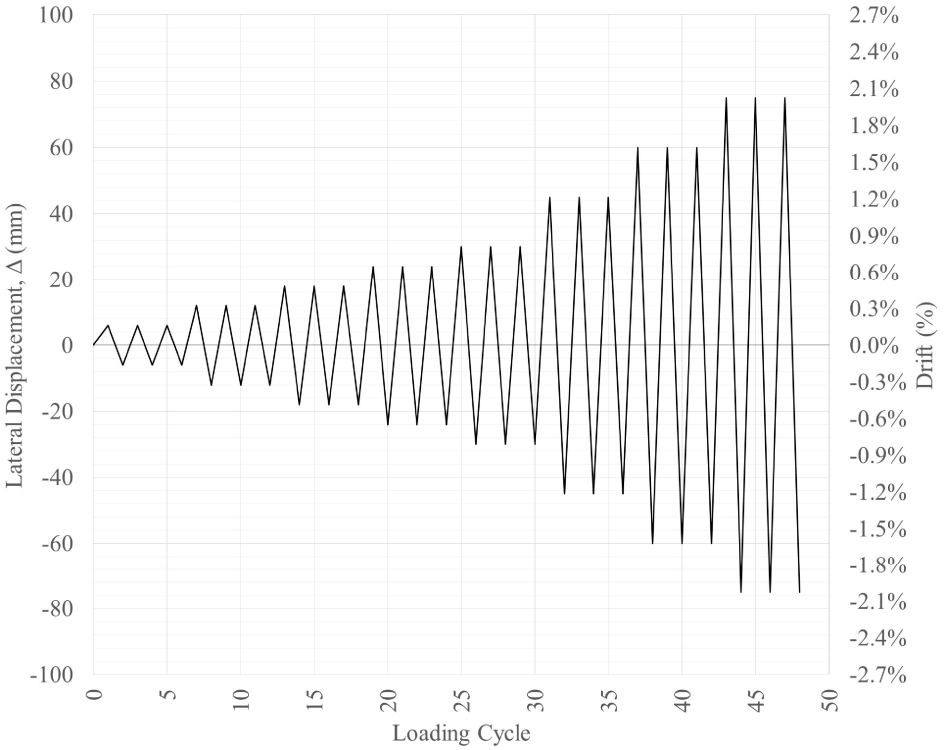

Figure 4.25 – Reversed cyclic loading pattern for wall W1HS

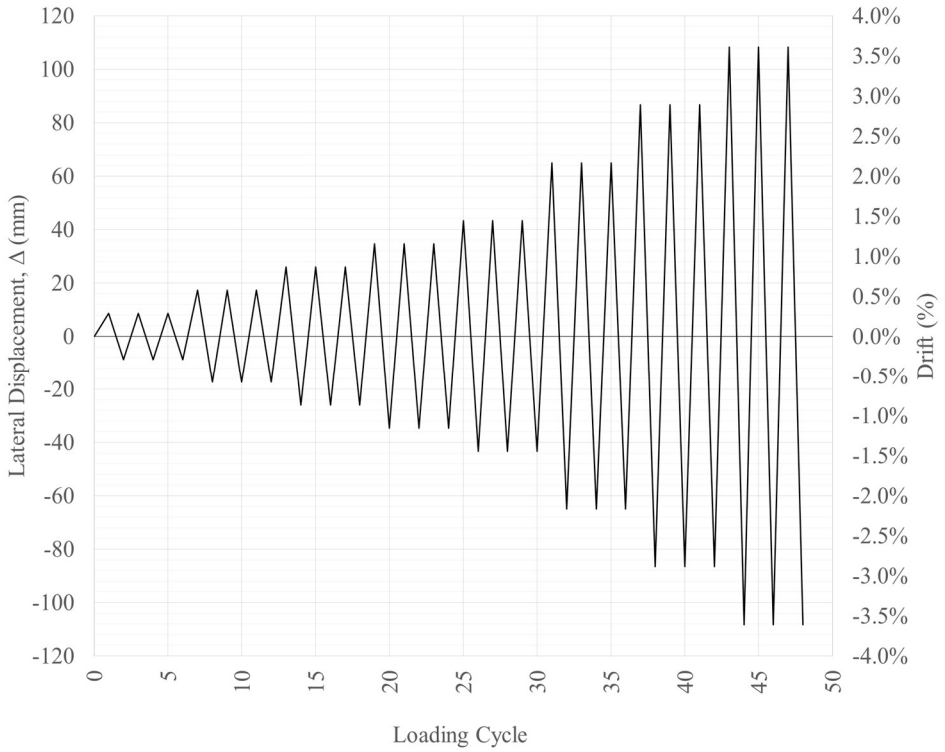

Figure 4.26 – Reversed cyclic loading pattern for wall W2HS

Chapter 5

5 Experimental Results and Discussion

5.1 Test Observations

The walls were closely monitored during the tests. Loading was stopped at the end of each drift cycle to conduct a visual inspection, mark the cracks and photograph the walls. The overall state of the walls, including concrete damage, widening and propagation of the cracks and changes to the cracking patterns, were monitored and recorded.

5.1.1 Wall W1HS

Hairline cracks appeared in the first cycle of the 0.2% drift stage. Horizontal cracks started at the boundary elements mostly within the plastic hinge region of the wall and propagated diagonally through the web section at an inclination of approximately 45 degrees. More cracks continued to appear in the following drift cycles. However, it was observed that the number of individual cracks remained almost the same after the 0.8% drift stage. Some cracks continued to propagate slightly further after this drift stage but very few new cracks were formed. The cracks from the positive and negative loading stages were found to be symmetrical. This indicated symmetrical and consistent loading in the positive and negative directions.

The width of the cracks generally remained the same. Crack widths were not measured during the tests; however, they were visually inspected during the test and were photographed for later analysis. Later review of the photographs confirmed that the width of almost all cracks remained approximately the same throughout the test with the exception of a large crack at the base of the wall. As the lateral displacements increased, the horizontal crack at the interface between the wall and the foundation continued to widen until wall failure. As the wall had to be cut for disposal after the test, there was an opportunity to inspect the cross-section of the wall near its base. The wall was cut horizontally at approximately 100mm from the base of the wall. As shown in Figure 5.1, spalling in the wall limited to the outer boundaries of the longitudinal reinforcement and the confined core concrete within the boundary elements of the wall was entirely intact.

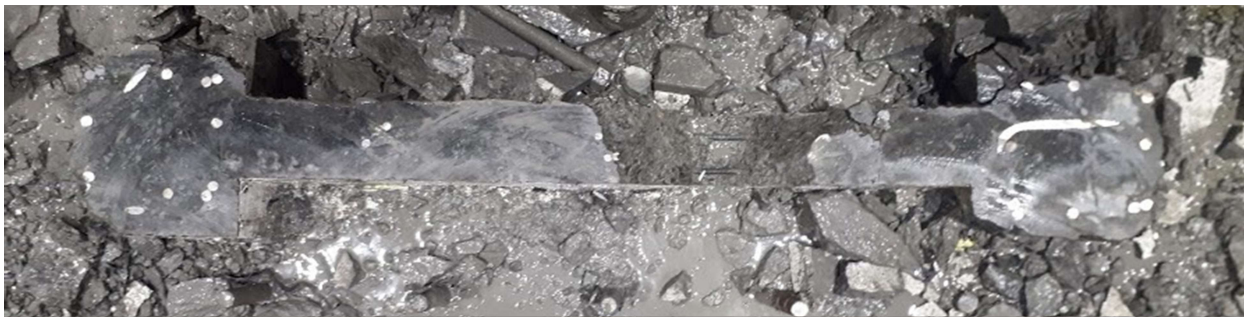

a) Wall W1HS cross-section

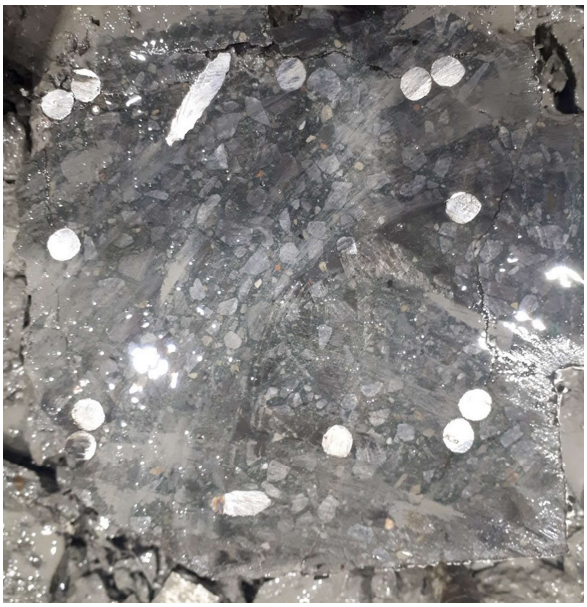

b) East side boundary element

c) West side boundary element

Figure 5.1 - Cross-section of wall W1HS at the end of the test

Figure 5.2 a) and b) shows wall W1HS after the third cycles of the 0.8% and 2.0% drift stages. In addition to the cracks, concrete damage consisted of minor spalling of the concrete cover in the boundary elements. Spalling was visible after the first cycle of the 1.5% drift stage and was limited to approximately 150mm of the wall base, as shown in Figure 5.2 c) and d).

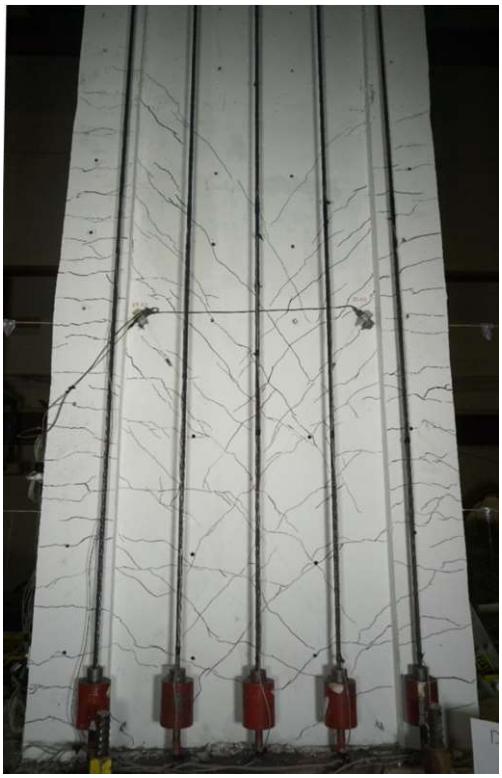

a) Wall W1HS after the 3rd cycle of the 0.8% drift stage

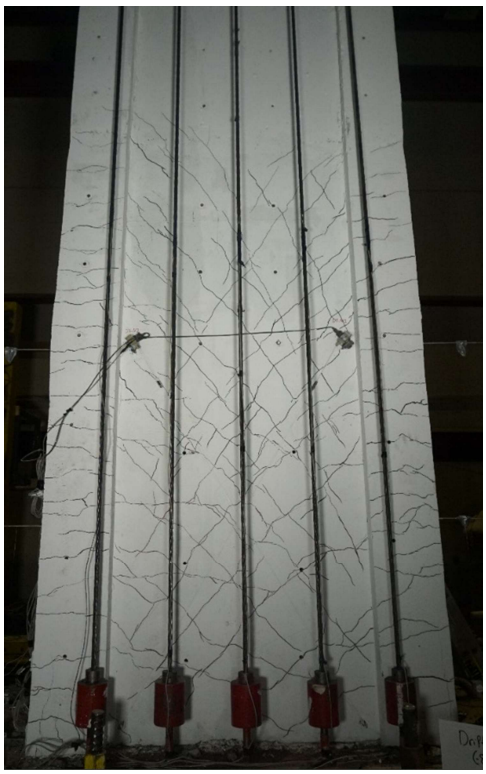

b) Wall W1HS at the end of the 2.0% drift stage

c) West side boundary element at test end

d) East side boundary element at test end

Figure 5.2 Wall W1HS cracking and concrete damage

Further visual inspection of the reinforcement in the boundary elements was conducted after the test was completed. Loose concrete was removed and the reinforcing bars were exposed for a closer look (Figure 5.3). No sign of buckling in the longitudinal reinforcement was observed. Boundary element ties appeared to be intact. The three outer bars that had ruptured, possibly during the first bar rupture event in the first cycle of the 2.0% drift cycle, were visible at the end of the

test after removing the spalled concrete. Figure *5.3* a) shows a ruptured longitudinal reinforcement in the west side boundary element.

a) Ruptured longitudinal reinforcing bar in the west side boundary element

b) Intact confined core concrete at the end of the test

Figure 5.3 – Wall W1HS at the end of testing

The foundation unit was effectively anchored to the strong floor; however, a review of the LVDT readings indicated that slight sliding and lifting of the foundation unit had occurred during the test. The maximum lifting and sliding were recorded at the 2.0% drift stage and were approximately 4 mm and 6 mm, respectively, at the ends of the foundation (1050mm from the wall ends). The recorded displacement data were corrected to account for these movements.

5.1.2 Wall W2HS

Figure 5.4 and Figure *5.5* show the cracking patterns of wall W2HS at different drift stages. Horizontal cracks appeared in the boundary elements during the first cycle of the 0.2% drift stage. Only a few cracks propagated horizontally into the web section at this stage. The initial cracks at the 0.2% drift stage were found only within a height of approximately 1000mm from the base of the wall. More cracks appeared at the 0.4% drift stage, most of the cracks in this stage propagated

diagonally into the web section. No major cracks were found in the foundation or the base of the wall at this stage. Very few new cracks were observed in the 0.5% drift stage. Some flexural cracks appeared in the foundation unit in this stage. In the 0.7% drift stage, more diagonal crack appeared up to a height of approximately 2000mm above the base of the wall. The number of cracks within the lower 1000mm of the wall remained approximately the same and some cracks only extended slightly within the web section. The number of diagonal cracks increased at the 1.1% and 1.4% drift stages.

a) Wall W2HS at the end of 0.7% drift stage b) Wall W2HS at the end of 1.4% drift stage

Figure 5.4 - Wall W2HS cracking pattern up to drift ratio of 1.4%

c) Wall W2HS at the end of 2.3% drift stage

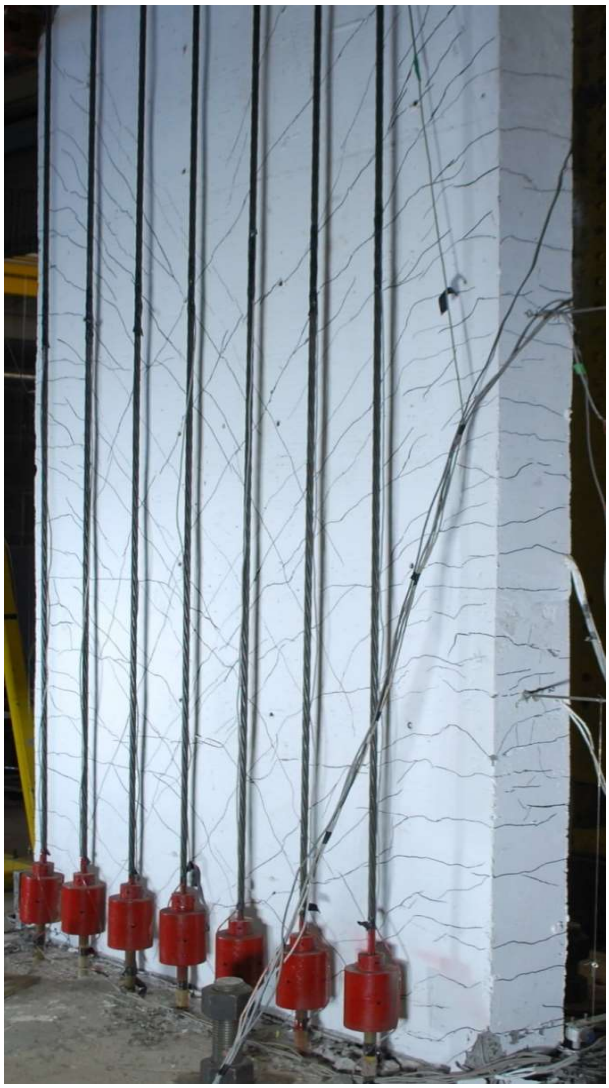

d) Wall W2HS at failure (drift ratio = 2.5%)

Figure 5.5 - Wall W2HS cracking pattern between drift ratio of 1.4% and failure (2.5%)

At the 0.6% drift stage, small cracks appeared in the foundation around the base of the boundary elements as shown in Figure *5.6*. It was noted that these cracks widened noticeably at the 1.1% drift stage as shown in Figure 5.6 and appeared to remain unchanged until the end of the test with the exception of slight widening in the final drift stages.

A large crack appeared at the interface of the wall and the foundation at a drift stage of 1.9% and widened in the following drift stages up to wall failure, as shown in Figure 5.7. This crack was similar to the horizontal crack observed at the base of wall W1HS. The east side boundary element longitudinal reinforcement ruptured at a drift ratio of approximately 2.5% in the positive loading

direction. The longitudinal bars in the west side boundary element also ruptured at a drift ratio of approximately 2.5% in the negative loading direction.

a) Cracks in the foundation at drift stage = 1.1% (West)

b) Cracks in the foundation at drift stage = 1.1% (East)

c) Cracks in the foundation at drift stage = 2.3% (West)

d) Cracks in the foundation at drift stage = 2.3% (East)

Figure 5.6 - Crack in the foundation around the base of wall W2HS

a) Crack at wall base at drift stage = 1.9%

b) Crack at wall base at the end of testing

Figure 5.7 – Horizontal crack at the base of wall W2HS

The extent of damage in the wall was closely inspected after the test. Loose and spalled concrete were removed to expose ruptured reinforcing bars. It was found that the spalling of concrete cover was limited to the lower 150mm of boundary elements. The confined core concrete within the boundary elements were found to be intact with no visible sign of crushing. The boundary element ties within the lower 200mm of the wall were also inspected and were found to be in good condition. The hooks were still embedded inside the confined core concrete and they did not appear to have undergone any noticeable deformation. Figure 5.8 (a) and (b) show the extent of concrete damage in the boundary elements at the end of the test.

All boundary element longitudinal bars were found to have ruptured at the end of the test at 30 mm to 50 mm below the top surface of the foundation. Figure 5.8 (c) and (d) show the ruptured longitudinal bars in the boundary elements and the web section.

No major shear cracks were noted during the test. Diagonal cracks appeared during the early stages of loading (drift ratio = 0.4%) and were found to widen slightly towards the end of testing. However, they did not appear to contribute significantly to the overall top displacement of the wall. This observation was verified using the cable transducers installed diagonally within the prescribed plastic hinge region of the wall. As described further in the following sections, the contribution of shear to the top displacement of the wall was found to be negligible.

It was noted that the foundation sliding and uplift measured during the test were found to be negligible. The top displacement of Wall W2HS was measured with respect to the foundation as

well as the laboratory's strong floor. The displacement data obtained from both transducers were compared at the end of the test and were found to match closely.

a) West side boundary element at test end

b) East side boundary element at test end

c) Rupture of boundary element longitudinal reinforcement at wall base

d) Rupture of vertical web reinforcement at wall base

Figure 5.8 – Extent of damage in Wall W2HS at the end of the test

5.2 Discussion of Results

Calculating the ductility of concrete members reinforced with different types of reinforcement can be a challenge because of the variation in yield displacement calculations. Depending on the stress-strain behaviour of the reinforcement, pinpointing the displacement at which yielding of the steel reinforcement occurs may require alternative established methods to maintain consistency. Based on experimental observations, Park (1989) outlined four alternative methods for determining the yield displacement of reinforced concrete members. The point of first yielding of the reinforcing steel, shown in Figure 5.9, (a), is often used as the yield point of a reinforced concrete member. In the case of steel reinforcement with a well-defined yield point, such as the conventional Grade 400 MPa ASTM A614, the yield strain of reinforcement can be calculated using f_y/E_s or using the stress-strain curves. However, for steel types without a defined yield point, such as the Grade 690MPa ASTM A1035, the yield strain cannot be readily obtained for the stress-strain curves and is often calculated using the 0.2% offset method. In the following sections, the yield point of the wall was assumed to be the point where the longitudinal reinforcement strain first reached the yield strain obtained by the 0.2% offset method. For comparison, the nominal yield point of the tested wall is also reported in the following sections. This is the displacement at which the reinforcing steel reaches the end of its fully elastic range but remains partially elastic ($\varepsilon_y = f_y/E_s$). Steel coupon test data were used to identify the yield strain of the reinforcement.

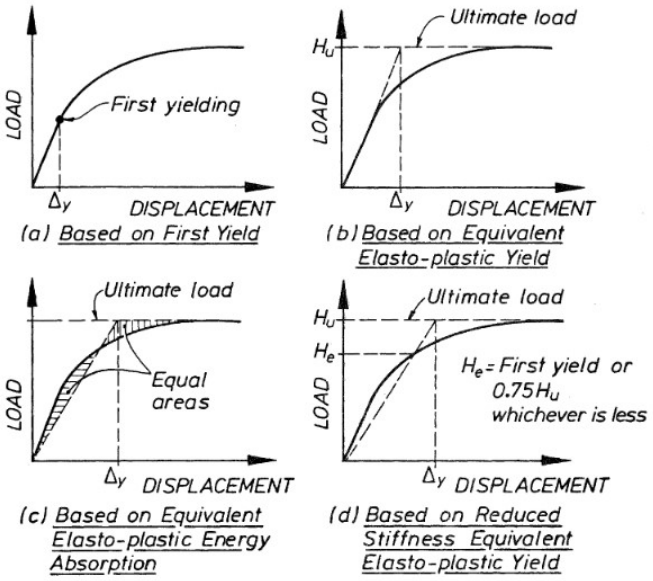

Figure 5.9 – Alternatives proposed by Park (1989) for determining yield displacement [Adapted from Park, 1989]

5.2.1 Wall W1HS

5.2.1.1 Load-Deflection Relationship

Figure 5.10 shows the load-deflection diagram for wall W1HS. In general, the wall exhibited the characteristics of a flexural slender shear wall, as expected, and failed in a brittle flexural mode due to 'pre-mature' rupture of the longitudinal reinforcement in the boundary elements. The term 'pre-mature' is employed to emphasize the fact that the bars ruptured before any significant concrete crushing in the boundary elements.

The first longitudinal reinforcing bar ruptured in the positive direction at a lateral displacement of 77mm (drift = 1.8%) and applied lateral load of 592 KN (M_u = 2563 KN.m). This occurred during the second cycle of the 2.0% drift stage. More bars ruptured in the third cycle of the same loading stage in the positive direction. It was difficult to visually determine the exact number of ruptured bars during the test; however, FEM analysis of the tested wall suggested that two outer longitudinal bars were likely ruptured in the second cycle of the 2.0% drift stage. Following the third cycle of the 2.0% drift stage, loading was reversed and cyclic load reversals were continued in the negative direction. Three bars ruptured in the negative direction in the third cycle of the 2.5% drift stage. The lateral load capacity of the wall reduced to approximately 50% of the ultimate at this stage at which point loading was stopped. Table 5.1 shows measured test parameters at different loading stages up to rupture of flexural reinforcement.

In the early loading stages, 'pinching' of the hysteretic curves was observed. This behaviour is typically observed when shear sliding occurs in the wall or if specialized steel reinforcement such as Shape-Memory Alloys (SMA) are used; however, in the case of wall W1HS, this behaviour is attributed to the stress-strain behaviour of the high-strength reinforcing bars used in the wall. Conventional ASTM A615 steel has a defined yield point beyond which the reinforcing steel becomes fully plastic while the ASTM A11035 steel has a 'yielding region' within which it exhibits partially elastic behaviour in a larger tensile strain range. In other words, the full yielding of the bars is delayed compared to conventional reinforcement. This leads to a self-centering action by the reinforcement, which pulls the wall back to its original position as it restores its elastic deformation within the partial yielding region of the reinforcement.

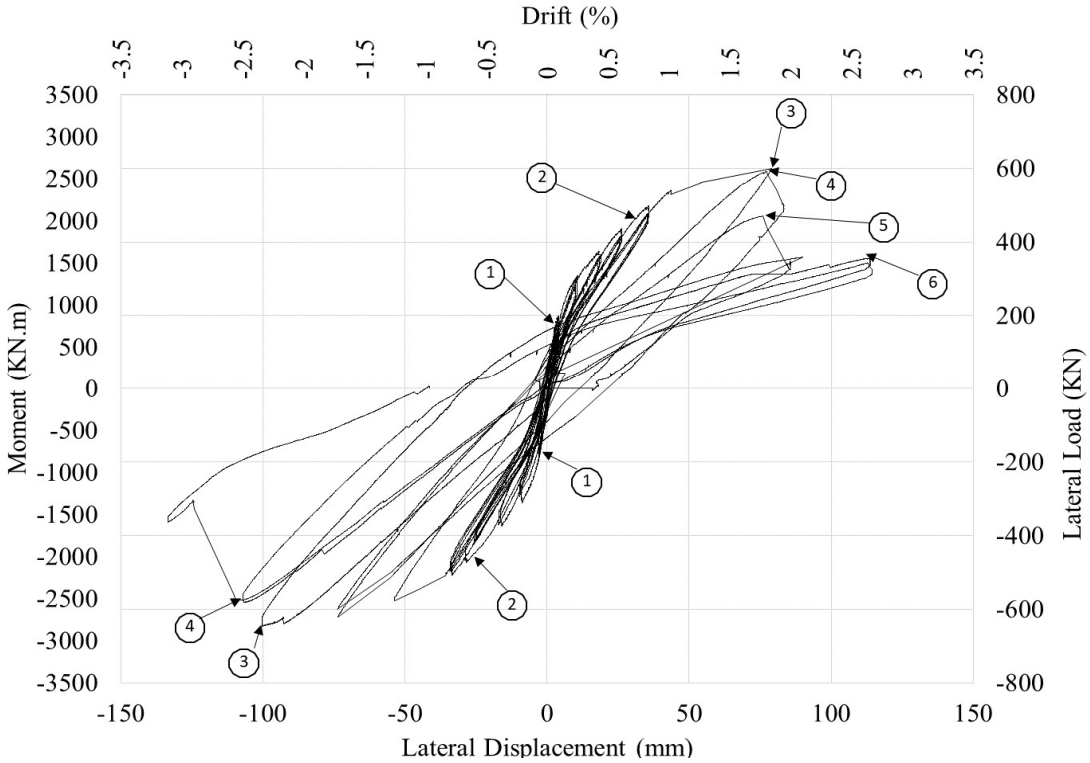

(1) first crack; (2) yield; (3) maximum load; (4) first bar rupture; (5) second bar rupture; (6) additional cycles in the positive loading direction following bar ruptures

Figure 5.10 - Wall W1HS experimental load-deflection diagram.

Table 5.1 - Wall W1HS Experimental Results

Positive Loading					Negative Loading				
Drift (%)	**F (KN)**	**Δ_{top} (mm)**	**M_r (KN.m)**	**Ductility Ratio ($\Delta/\Delta y$)**	**Drift (%)**	**F (KN)**	**Δ_{top} (mm)**	**M_r (KN.m)**	**Ductility Ratio* ($\Delta/\Delta y$)**
0.1	189	4.2	818.4	0.1	**-0.1**	203.1	-3.3	879.4	-0.1
0.3	307	11.3	1329.5	0.3	**-0.2**	309.2	-8.9	1339	-0.2
0.4	363.3	16.9	1573.2	0.5	**-0.3**	350.2	-14	1516.2	-0.4
0.5	411.9	23.3	1783.6	0.6	**-0.4**	370.7	-17.9	1604.9	-0.5
0.7	451.4	28.3	1954.6	0.8	**-0.5**	429	-23.1	1857.5	-0.6
0.8	480.7	33.2	2081.6	0.9	**-0.7**	464	-28.3	2009.2	-0.8
0.9	517.6	40.2	2241.1	1.1	**-0.8**	494.3	-33.4	2140.2	-0.9
1.0	536.2	43.1	2321.9	1.2	**-0.9**	510.1	-37	2208.7	-1.0
1.2	559.5	53.9	2422.6	1.5	**-1.0**	545	-44.9	2359.9	-1.2
1.3	569	54	2463.8	1.5	**-1.1**	565	-48	2446.5	-1.3
1.8	599	79.1	2593.6	2.1	**-2.3**	645.9	-100.2	2796.7	-2.7
1.8	587.4	79.1	2543.5	2.1	**-2.5**	574.7	-106.8	2488.5	-2.9
2.0	469.9	84.6	2034.6	2.3	**-2.5**	573	-109.1	2481.1	-2.9

F=top lateral force; M_r = moment; Δ_{top} = total top displacement; Drift = H/L. *Normalized displacement at different loading stages shown as ductility ratio.

Using the data recorded by the cable transducers, rotations of the wall at different elevations along the height of the wall were calculated and translated to top lateral deflections. Figure 5.11 and Figure 5.12 show backbone force-displacement curves resulting from the rotations recorded at different elevations along the height of the wall for positive and negative load directions, respectively. Recorded shear displacements as well as total top lateral deflection of the wall are also shown. These figures suggest that a large proportion of the rotation within the plastic hinge region occurs within about 30mm of the base of the wall. Approximately 70% of the plastic hinge rotation at the onset of the first flexural bar rupture in the positive direction is due to the rotation of the wall within the 30mm wall segment at the base. Similarly, this ratio is 65% in the negative direction.

Furthermore, the ratio of the contribution of rotation within the plastic hinge region to the total top displacement is only 22% prior to cracking. This contribution increases to 59% at yield and 74% at maximum load for both positive and negative loading directions. This assessment is in agreement with the cracking behavior observed during testing. Most cracks above the base of the wall maintained small widths throughout the test where one major crack at the wall-foundation interface continued to widen until the wall failure due to the rupture of the boundary element longitudinal reinforcement.

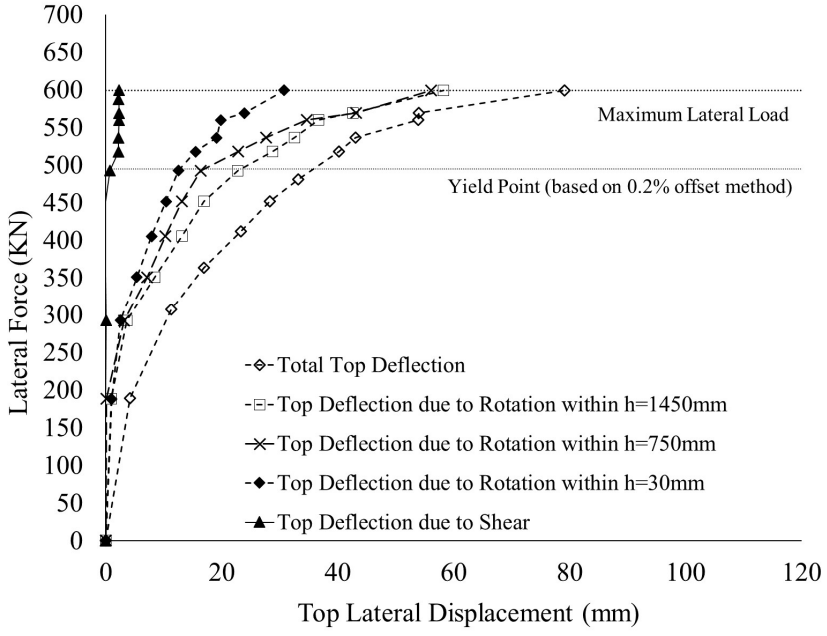

Figure 5.11 - Force-Displacement Diagrams for Loading in Positive Direction

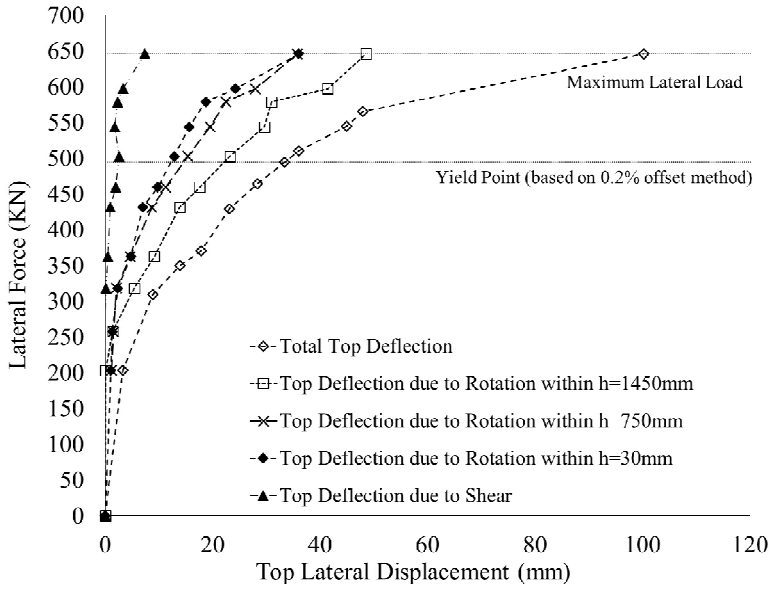

Figure 5.12 - Force-Displacement diagrams for loading in negative direction

5.2.2 Reinforcement Strains

Strains in the steel reinforcement were measured using strain gauges attached to the reinforcing bars at selected critical locations (refer to the instrumentation plan presented in Chapter 4). These locations included two outer longitudinal bars at each end of the wall, as well as selected transverse shear reinforcement in the web. Strain gauges were installed within a height of 1450mm from the base of the wall at intervals shown in the instrumentation plan presented in Chapter 4.

Using tensile coupon tests, the average yield strains of No. 3 and No. 4 reinforcement used in the construction of wall W1HS were found to be 7.0 and 6.6 (10^{-3} mm/mm), respectively. The 0.2% offset method was used to determine the actual yield strain of the reinforcing bars. The nominal yield strain (i.e., strain at f_y = 690 MPa) of No. 3 and No. 4 bars were found to be approximately 4.08 and 3.80 (10^{-3} mm/mm). The nominal yield strain was used to determine the onset of yielding, and the actual yield strain was used to determine whether the bar has fully yielded. Figure 5.13 shows representative strain diagrams for the transverse reinforcement at a height of 140mm from the base of the wall where strains in the shear reinforcement were found to be the highest. It is shown that the strain variation in the web transverse reinforcement was small and that shear stresses were not significant enough to yield the transverse reinforcement. This was expected as the wall had a height-to-length aspect ratio of 3.0 and was expected to have a flexure-dominant

response. The highest recorded strains recorded at the east and the west ends of the web (strain gauges SH-W-3, and SH-E-3) were 2.9 (10^{-3} mm/mm) and 2.7 (10^{-3} mm/mm). These strains corresponded to stresses of 535 MPa and 501 MPa. Strain data for the other transverse reinforcement is provided in Appendix C.

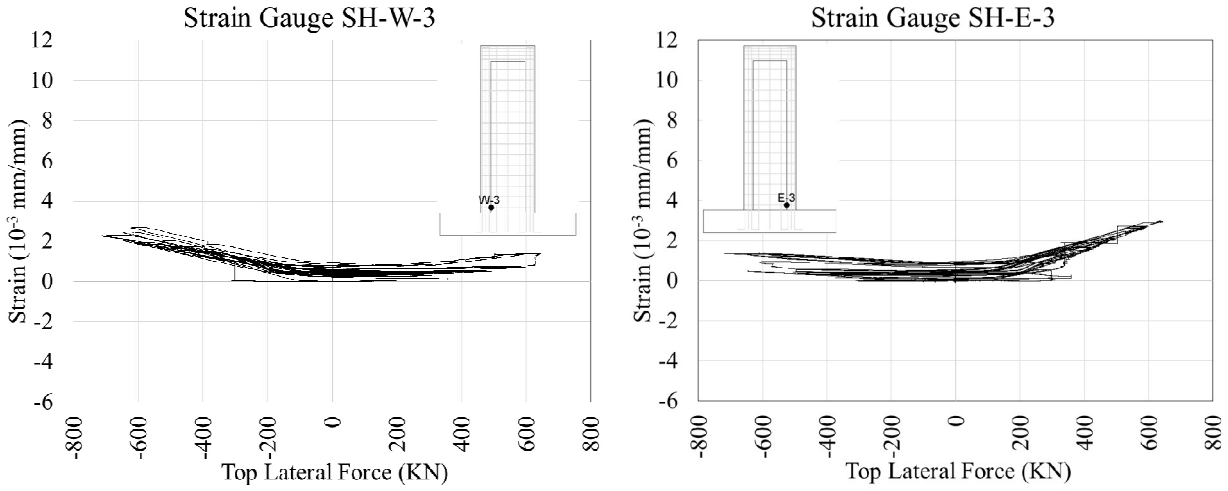

Figure 5.13 – Typical strain data for transverse web reinforcement

Figure 5.14 and Figure 5.15 show the strains in the outermost boundary element longitudinal reinforcing bars in positive and negative loading directions respectively. It can be observed that steel strains increase rapidly at the base of the wall closer to the ultimate load, which suggests that plastic hinging is mostly limited to the base of the wall. Figure 5.16 and Figure 5.17 show strains in the outermost longitudinal reinforcement plotted against lateral forces in the positive and negative loading directions. It can be observed that the longitudinal bars become plastic and continue to strain until bar rupture only at the base of the wall (strain gauges SW-3 and SE-3). Recorded strains at levels above were found to be significantly lower.

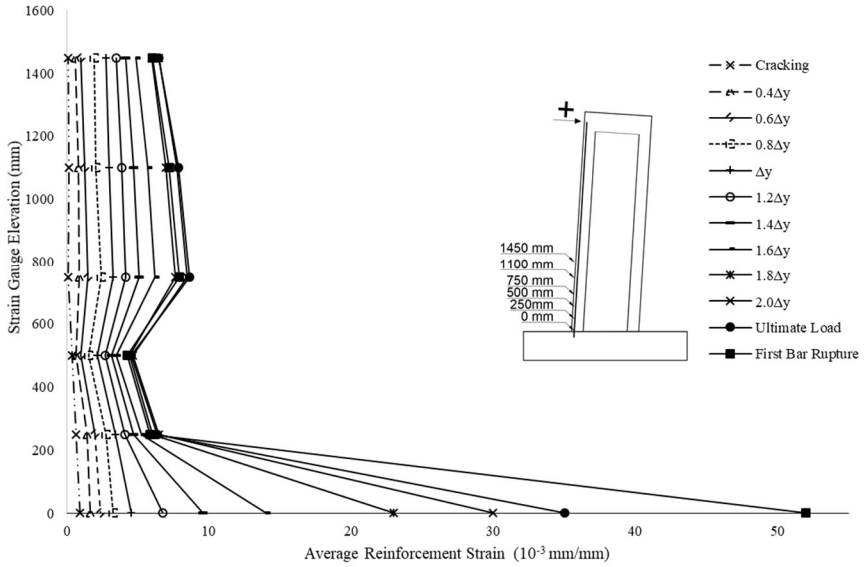

Figure 5.14 - Steel Strains vs wall height in the positive loading direction

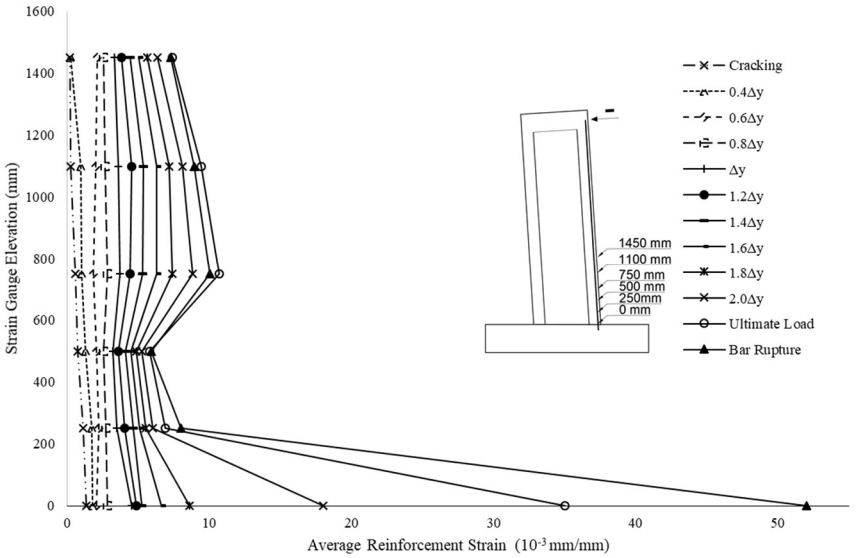

Figure 5.15 - Steel Strains vs wall height in Negative Loading Direction

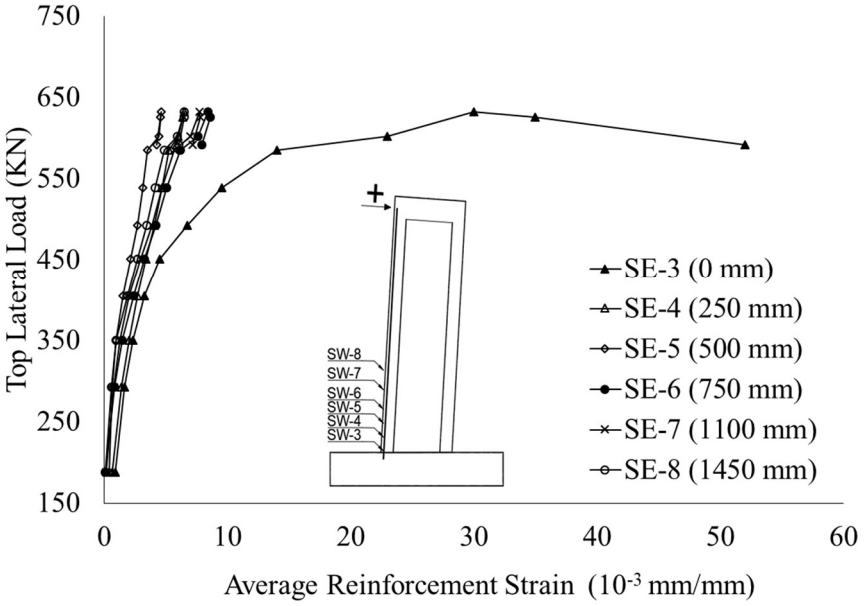

Figure 5.16 - Steel strains vs lateral force in the positive loading direction

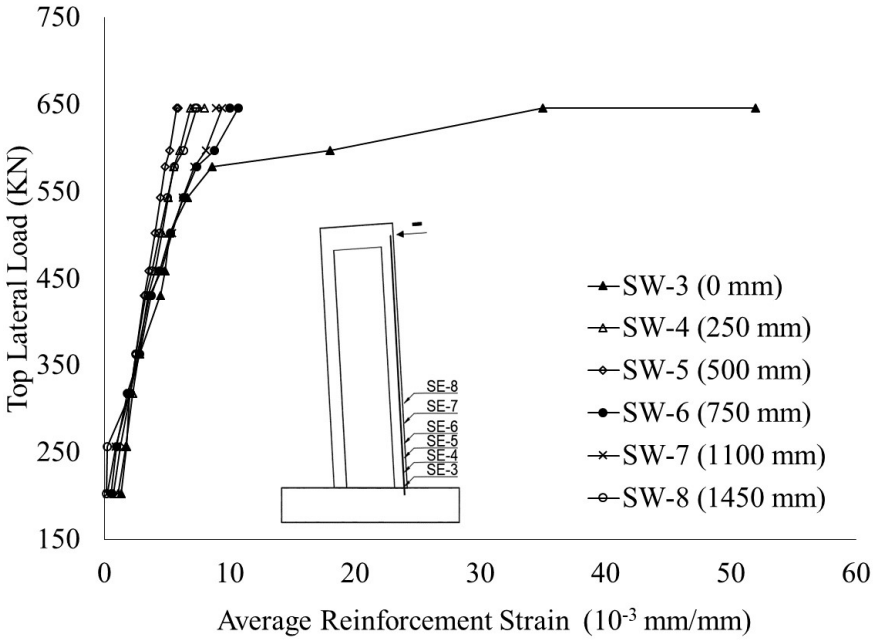

Figure 5.17 - Steel strains vs lateral force in the negative loading direction

5.2.3 Effect of HSR on Wall Stiffness

Figure 5.18 compares the experimental load-deflection diagrams for wall W1HS and the control wall. Both walls had similar flexural load capacities as intended by the design of the wall. The initial stiffness of the walls was found to be very close up to the cracking point; however, wall W1HS had smaller stiffness between the cracking and the yield points. The secant stiffness of wall W1HS matches that of the control wall following the yield point. It should be noted that two yield points were considered for wall W1HS in this comparison: the nominal yield point of the wall which is based on the nominal yield point of the reinforcement, and the yield point determined based on the reinforcement strain obtained using 0.2% offset method.

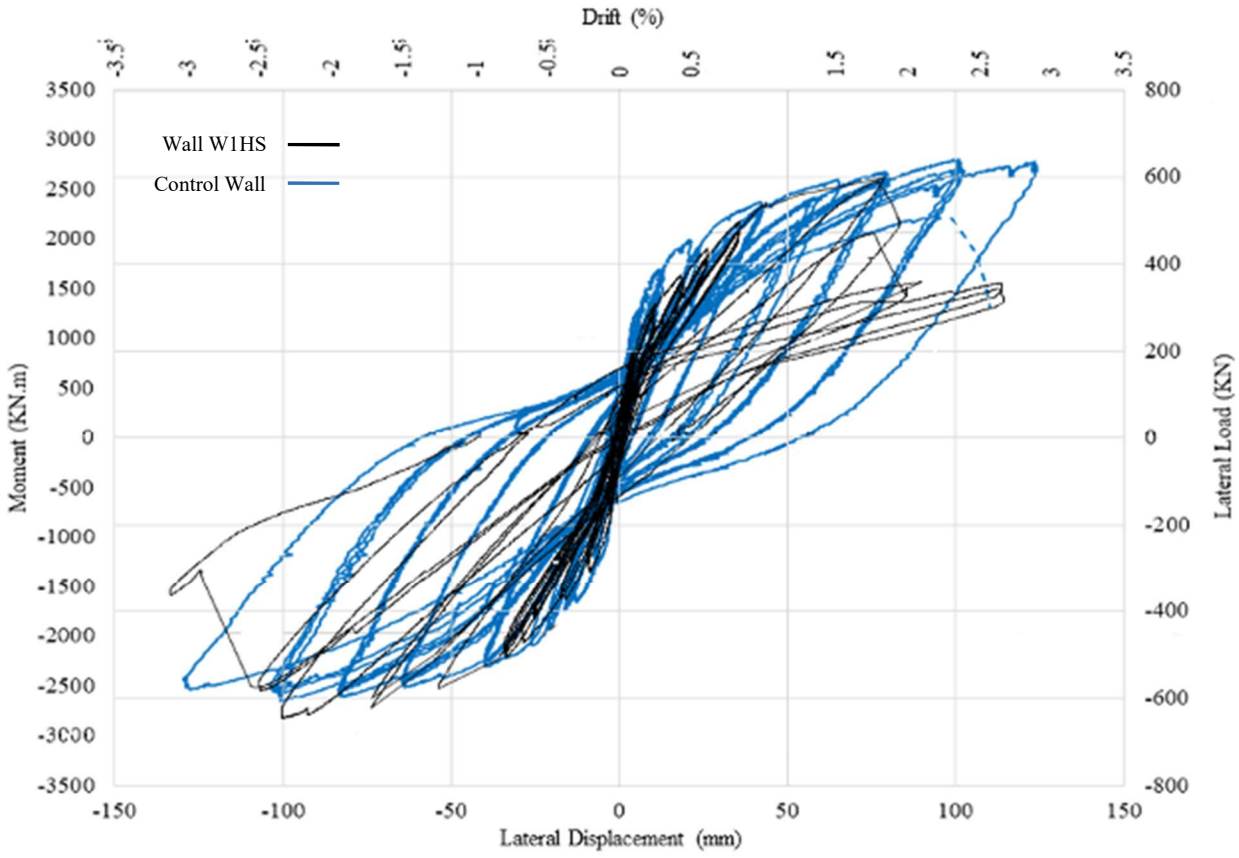

Figure 5.18 - Comparison of results for wall W1HS and the Control Wall (Navidpour, 2018)

As discussed earlier, the ASTM A1035 steel reinforcement used in the construction of wall W1HS did not have defined yield point. Instead, yielding occurred over a region. The yielding region starts at approximately the nominal yield point of the reinforcement (i.e., strain at which $f_y = 690$ MPa). The nominal and actual (0.2% offset method) yield points of the wall were found to be

approximately 23mm and 37mm which corresponded to lateral drift ratios of 0.53% and 0.85%. The yield point of the control wall was found to be approximately 18mm (drift ratio =0.46%). Hence, considering its actual yield point, it can be stated that the yield point of wall W1HS was delayed. Chung-Chan Hung et al. (2017) reported a similar behaviour when high-strength reinforcement (Taiwanese Grade 785 – SD785) lacking a yield point was used as flexural reinforcement in squat walls.

The stiffness of wall W1HS and the control wall in the loading and unloading branches were calculated for both positive and negative loading directions. Table 5.2 and Table 5.3 present the calculated loading stiffness values in the positive and negative directions. Table 5.4 and Table 5.5 present the unloading stiffness in the positive and negative loading directions. Figure 5.19 provides a comparison of the calculated stiffness values for wall W1HS and the control wall. The loading stiffness of the walls was calculated as the slope of the loading branches starting at the point of zero load to the maximum drift of the selected cycle. The unloading stiffness was calculated as the slope of the unloading branches between the maximum drift point at a selected loading stage and the point of zero load.

Table 5.2 – Loading stiffness in the positive loading direction

Wall W1HS					
Drift Ratio (%)	0.10%	0.65%	0.87%	1.83%	1.79%
Stiffness (KN/mm)	45.1	15.9	13.2	6.8	6.7
Control Wall					
Drift Ratio (%)	0.10%	0.42%	0.87%	2.36%	2.86%
Stiffness (KN/mm)	57.9	22.9	13.8	5.4	4.2

Table 5.3 – Loading stiffness in the negative loading direction

Wall W1HS					
Drift Ratio (%)	0.10%	0.53%	0.83%	2.10%	2.43%
Stiffness (KN/mm)	46.9	18.6	14.2	6.7	5.4
Control Wall					
Drift Ratio (%)	0.10%	0.43%	0.87%	2.40%	2.93%
Stiffness (KN/mm)	55.3	23.1	14.2	5.4	3.6

Table 5.4 – Unloading stiffness in the positive loading direction

Wall W1HS					
Drift Ratio (%)	0.10%	0.65%	0.87%	1.83%	1.79%
Stiffness (KN/mm)	45.1	20.8	14.4	8.8	7.6
Control Wall					
Drift Ratio (%)	0.10%	0.42%	0.87%	2.36%	2.86%
Stiffness (KN/mm)	57.9	27.5	19.5	10.9	8.8

Table 5.5 – Unloading stiffness in the negative loading direction

Wall W1HS					
Drift Ratio (%)	0.10%	0.53%	0.83%	2.10%	2.43%
Stiffness (KN/mm)	46.9	22.0	15.2	9.2	7.1
Control Wall					
Drift Ratio (%)	0.10%	0.43%	0.87%	2.40%	2.93%
Stiffness (KN/mm)	55.3	29.4	15.3	11.1	7.9

The calculated stiffness data presented in Figure 5.19 indicates that the stiffness of wall W1HS was lower during the initial stages of loading compared to the control wall. Compared to the control wall, the stiffness of wall W1HS is the lowest between cracking and the yield point of wall W1HS. At cracking, the stiffness of wall W1HS was approximately 22% in the positive loading direction and 15% lower in the negative loading direction. This difference increases to 30% and 20% respectively between cracking and the yield point of wall W1HS and decreases to less than 1% at the yield point of wall W1HS. A similar pattern is observed for the stiffness of the unloading branches in the negative direction. For unloading in the positive loading direction, stiffness of the wall was found to be generally lower compared to the control wall throughout the test as shown in Figure 5.19 (c).

The smaller initial stiffness of wall W1HS is attributed to the yield behaviour of the ASTM A1035 reinforcement. Yielding of this type of reinforcement occurs at a larger steel strain. Hence, compared to the control wall, wall W1HS needs to undergo a larger lateral displacement to reach yield, or in this case the onset of strain hardening. Even though the initial elastic modulus of ASTM A1035 is approximately 200,000, the scant modulus, considering the delayed yielding, is

approximately 132,000 MPa; therefore, the stiffness of the wall is lower on average prior to the yield point.

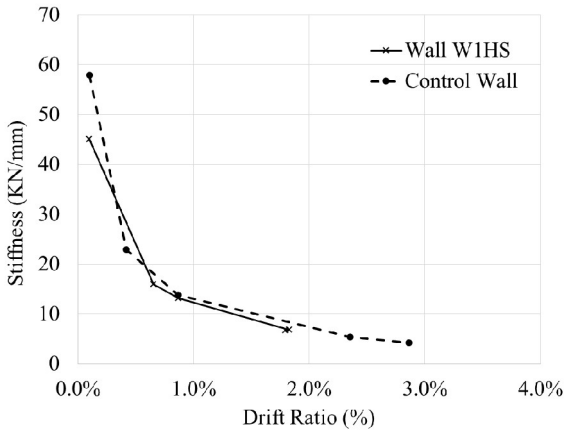

a) Loading stiffness - Positive loading direction

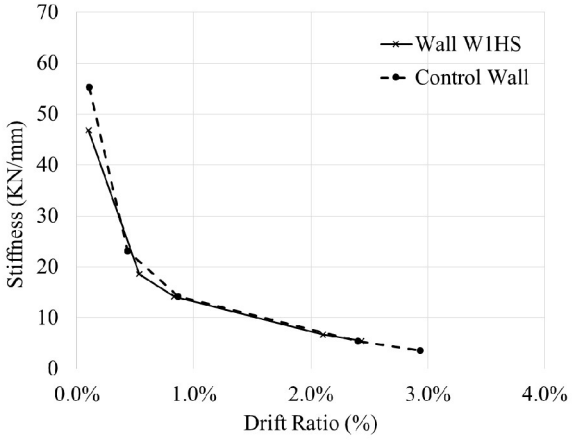

b) Loading stiffness - Negative loading direction

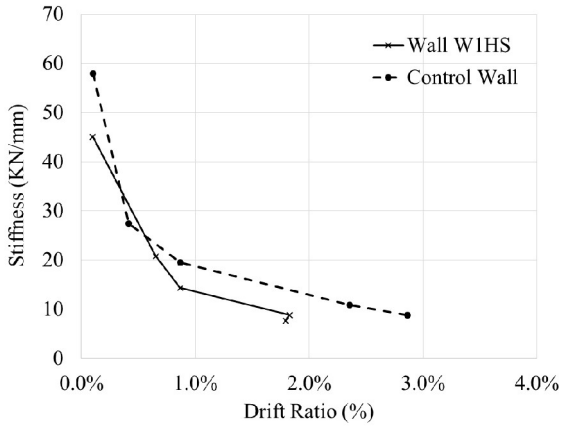

c) Unloading stiffness – Positive loading direction

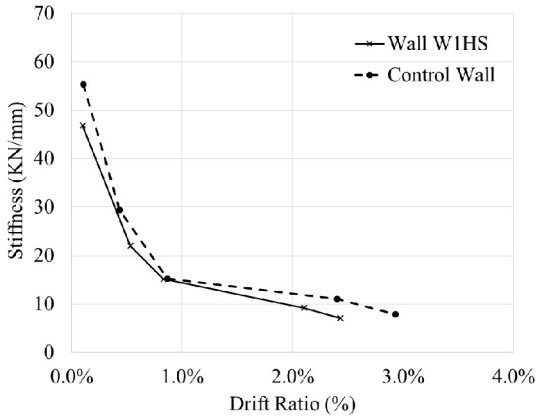

d) Unloading stiffness – Negative loading direction

Figure 5.19 – Comparison of loading and unloading stiffness for wall W1HS and the control wall

In addition, the longitudinal reinforcement ratio of wall W1HS was 36% less compared to the control wall. This is deemed to be another contributing factor to the reduced stiffness observed in the hysteretic behaviour of the wall.

5.2.4 Effect of HSR on Ductility and Energy Dissipation Capacity

As shown in Figure 5.10, wall W1HS fails due to the rupture of reinforcement at a drift level of approximately 1.8% (corresponding to top lateral displacement of 77mm) whereas the control wall continues for another 0.8% drift before failure. This is a 36% reduction in ductility which can be attributed to the use of less ductile high-strength reinforcement (i.e., its lower strain capacity). The

ductility of the wall in the negative loading direction was slightly higher considering the loading cycles applied after the wall failure in the positive direction. This is deemed to be due to the fact that the stiffness of the wall in the negative loading direction decreased after the compression reinforcement had ruptured in the positive direction. Construction defects and loading or instrumentation errors could also have contributed to this difference.

The ductility ratio of wall W1HS was calculated using both nominal and actual yield displacements to be $\mu_{nominal} = 3.3$ and $\mu_{actual} = 2.11$ in the positive loading direction and $\mu_{nominal} = 4.7$ and $\mu_{actual} = 2.9$ in the negative loading direction. The ductility ratio of the control wall was $\mu = 6.9$ and $\mu = 7.1$ in the positive and negative loading directions, respectively. The ductility ratios of the control wall were calculated assuming ultimate displacements of 125mm and 128mm in the positive and negative directions as well as a yield displacement of 18mm in both directions.

Figure 5.20 shows the areas enclosed by the load-deflection diagram of the tested wall that were used to calculate the dissipated energy (strain energy). Table 5.6 presents the ductility and energy dissipation capacity of wall W1HS compared to the control wall. The energy dissipated after wall failure in the positive direction was 22.1 KN.m. This is approximately 60% less compared to the control wall which dissipated 54.6 KN.m of energy at wall failure. Figure 5.21 compares the areas enclosed by the load-deflection diagrams for wall W1HS and the control wall. The total dissipated energy of wall W1HS was 44.3 KN.m at the end of the test. In reality, the wall is considered failed after failure occurs in one direction and thus any further dissipated energy is not considered to be part of the wall's energy dissipation capacity. However, the total dissipated capacity of the tested wall is presented herein for comparison.

Table 5.6 - Ductility and energy dissipation capacity for wall W1HS and the control wall

Wall ID	**Ductility, μ**				**Energy Dissipated (KN.m)**	
	Positive Loading		**Negative Loading**			
	μ-Nominal	μ-Actual	μ-Nominal	μ-Actual	First bar rupture	End of testing
Wall W1HS	3.3	2.1	4.7	2.9	22	44
Control Wall	6.9	7.1	6.9	7.1	-	55

The reduced energy dissipation capacity of the wall is attributed to smaller ductility of the high-strength reinforcement used in the wall. Reduced ductility and increased pinching due to the self-centering action by the reinforcement are considered to be the main factors contributing to the

recued energy dissipation capacity of the wall. In addition, the reduced stiffness of the wall between the cracking and the yield point also contributes slightly to the reduced energy dissipation capacity of the wall.

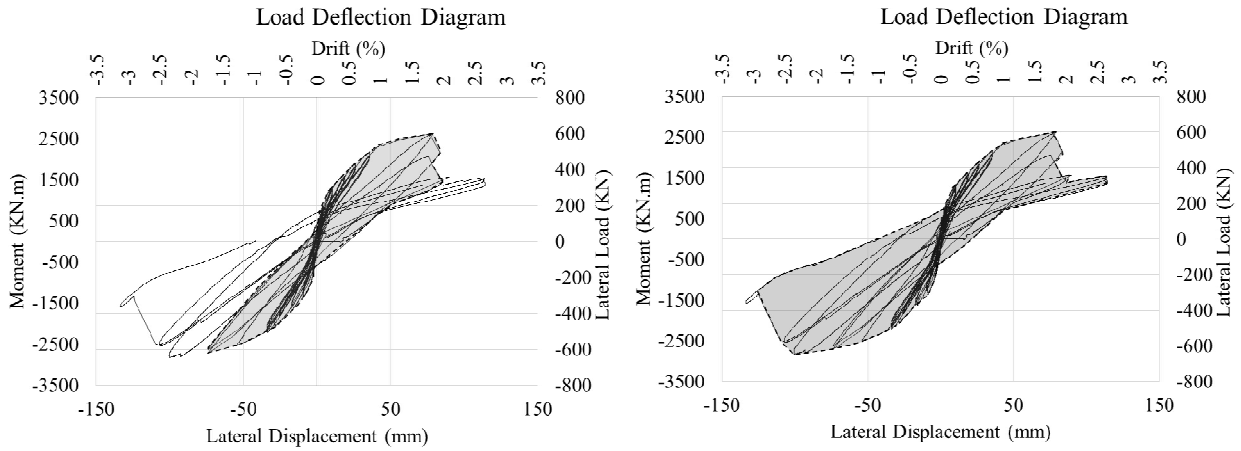

a) Energy dissipated up to first bar rupture b) Energy dissipated at the end of testing

Figure 5.20 - Areas used to calculate energy dissipation by wall W1HS

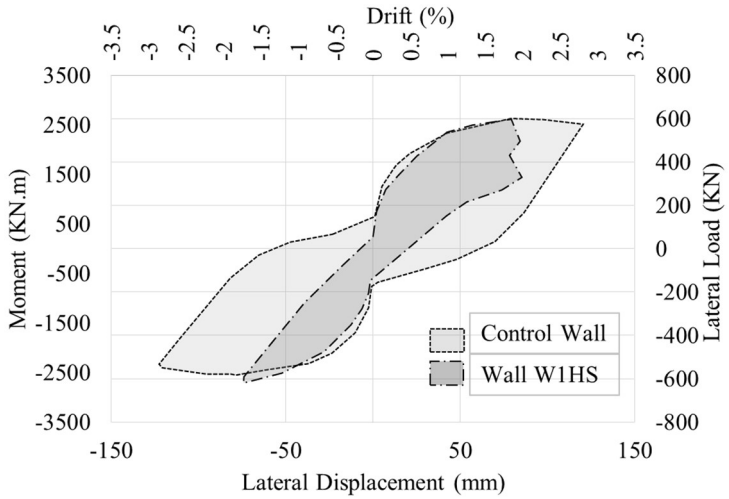

Figure 5.21 – Comparison of the areas enclosed by load-deflection diagrams for wall W1HS and the control wall at failure

5.2.5 Wall W2HS

5.2.5.1 Load-Deflection Relationship

Figure 5.22 shows the load-deflection diagram for wall W2HS. The wall exhibited flexural response and failed due to the rupture of boundary element longitudinal reinforcement. The

backbone curve data for the hysteresis curves is presented in Table 5.7. The yield point, as shown in Figure 5.22, was determined using the reinforcing steel strain data recorded during the test. As described in previous chapters, the Grade 690 MPa - ASTM A1035 bars used in the walls did not have a defined yield point; hence, the yield point of the wall was assumed to be the point where the longitudinal reinforcement strain reached the yield strain obtained by the 0.2% offset method. Using this definition, the outermost boundary element longitudinal reinforcement reached yield strains at top lateral displacements of 27mm and 29mm in the positive and negative loading directions, respectively, which corresponded to drift ratios of 0.9% and 1.0%.

The wall was able to sustain three cycles of loading up to a lateral displacement of 67mm (2.3% drift ratio); however, the boundary element longitudinal reinforcement ruptured at a lateral displacement of 72mm (2.5% drift ratio) in the positive and negative loading directions. Based on the reinforcement yield point obtained using the 0.2% offset method, this drift ratio is equal to ductility ratios (Δ/Δ_y) of 2.7 in both loading directions. All longitudinal bars within the boundary elements were found to have ruptured at failure; hence, the lateral capacity of the wall decreased significantly following the bar ruptures and the loading was stopped.

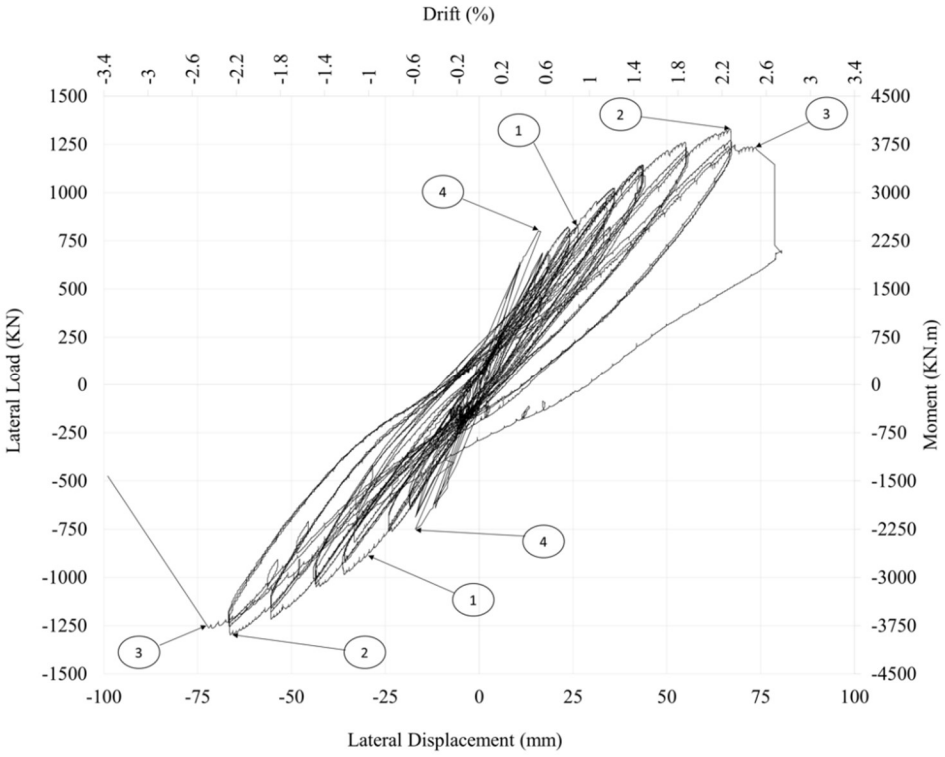

(1) Yield (0.2% offset method) (2) maximum load; (3) bar rupture (4) reinforcement slip;

Figure 5.22 - Wall W2HS experimental load-deflection diagram.

Table 5.7 - Wall W2HS Experimental Results

Drift (%)	Positive Loading				Negative Loading			
	F (KN)	Δ_{top} (mm)	M_r (KN.m)	Ductility Ratio ($\Delta/\Delta y$)	F_u (KN)	Δ_{top} (mm)	M_r (KN.m)	Ductility Ratio ($\Delta/\Delta y$)
0.2	416	5.7	1206	0.2	-420	-6	-1218	0.2
0.4	667	11.7	1934	0.4	-640	-11.7	-1856	0.4
0.6	798	16.4	2314	0.6	-755	-17	-2190	0.6
0.8	802	23.7	2326	0.9	-756	-23.8	-2193	0.9
0.9	850	27	2465	1.0	-827	-27	-2398	1.0
1.0	898	29	2604	1.1	880	29.7	2552	1.1
1.2	1018	36.1	2952	1.3	-984	-35.9	-2854	1.3
1.5	1142	43.7	3312	1.6	-1039	-43	-3013	1.6
1.9	1261	54.9	3657	2.0	-1216	-55.3	-3526	2.0
2.3	1328	66.9	3851	2.5	-1297	-66.3	-3761	2.5
2.5	1233	73.7	3575	2.7	-1262	-72.1	-3660	2.7

F=top lateral force; M = moment; Δ_{top} = total top displacement; Drift = H/L.

Certain test parameters including the overall stiffness and ductility of the wall were monitored closely during the test. The response of the wall was compared to the response predicted using VecTor2 FEM software as well as the hysteresis data from the control wall test. It was noticed in the early stages of loading that the overall stiffness of the wall was less than the stiffness predicted by the VecTor2 model as well as that observed in the control wall test. In addition, the wall was expected to fail at a drift ratio of around 1.5% but it was able to undergo an additional 1.0% of lateral drift before failing at a drift ratio of 2.5%. Later analysis of the results indicated that local slippage of the anchored longitudinal bars within the foundation contributed to the increase in the drift capacity of the wall.

Figure 5.23 shows the recorded strains in four corner boundary element longitudinal bars at the base of the wall, as well as 150mm inside the foundation. The recorded strain data shows that the strains in the boundary element longitudinal reinforcement experienced a sudden decrease in tensile strains. The sudden drop first occurred at a drift ratio of approximately 0.6% in the negative loading directions at around 150mm below the surface of the foundation. The bars at the base of the wall also experienced this sudden drop in tensile strain between 1.3% and 1.9% drift ratio. It is believed that this sudden slip contributed to a large rotation at the base of the wall resulting in a major initial increase (slip) in the top lateral displacement as shown by point #4 in Figure 5.22.

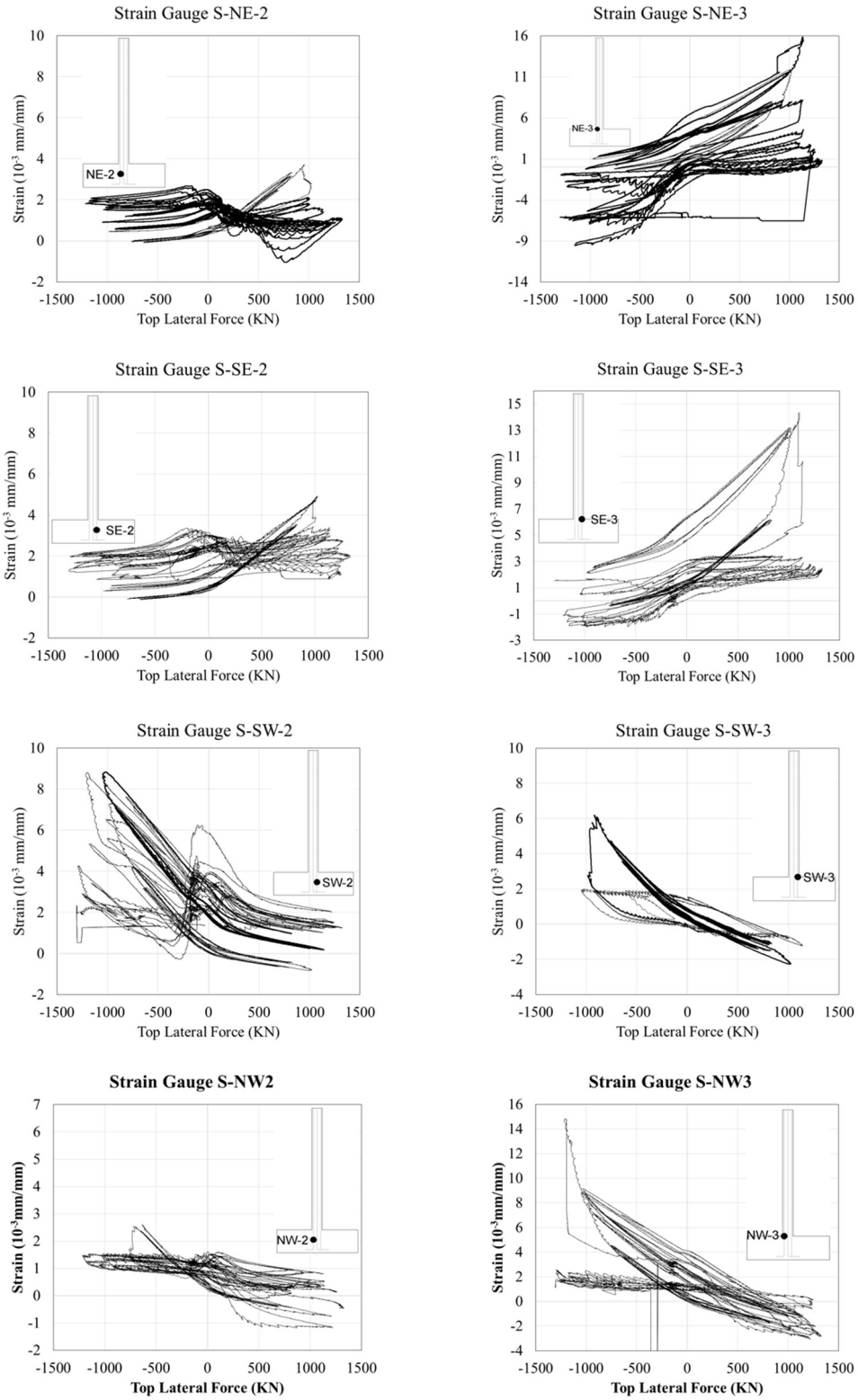

Figure 5.23 - Recorded strains at the base of the wall (0mm and, -150mm)

The corresponding lateral forces at which this displacement slip occurred matched those obtained from the recorded strain data. Based on these observations, it is believed that the increased ductility of the wall was due to the anchorage slip of the boundary element longitudinal bars within the foundation. It is to note that the recorded strain data suggests that the observed slippage was limited to the anchored length between the wall base and a location above the 300mm depth below the wall base as the longitudinal bars did not exhibit any slippage at 300mm below the wall base (130mm above the embedded hooked ends). Hence, it is assumed that the hooks inside the foundation remained intact throughout the test and maintained anchorage strength as intended. In addition, none of the anchored bars pulled out. All bars ruptured near the base of the wall at failure.

A series of tests were conducted on the anchorage of high-strength reinforcing bars with standard hooks at the University of Kansas (Searle et. al, 2018; Sperry et. al, 2017; Ajaam et al, 2018) which investigated various parameters contributing to the anchorage strength of bars. Several parameters including lateral and vertical spacing of bars, bar diameter, steel strength, and concrete cover were investigated. A study by Sperry et al (2017a) found that closely spaced hooked bars result in a lower anchorage strength compared to hooked bars that are widely spaced. In a similar study, Ajaam et al. (2018) conducted an experimental investigation on the effect of bar spacing on the anchorage strength of ASTM A1035 bars. It was noted by Ajaam (2018) that the provisions in the ACI 318-14 code were developed for the development of hooks based on tests involving two hooked bars. The effect of closely spaced bars on the anchorage strength of bars, specifically high-strength bars, was not taken into account in the ACI 318-14 code. Ajaam (2018) reported that the failure of anchored hooked bars with center-to-center spacing of less than $6d_b$ was due to two primary mechanisms: concrete break-out which was defined as a block of concrete pulling out with the hooked bars in the direction of the tensile force; and side splitting which was considered to be when the side of the concrete specimen split off as a result of the hook's wedging action. Figure 5.24 shows the cracking pattern around the anchored bars just before the break-out failure as reported by Ajaam (2018). One of the conclusions from this investigation was that hooked bars with center-to-center spacing of less than $6d_b$ exhibit lower anchorage strengths. This conclusion was adopted by ACI 318-19 (2019) which requires a modification factor $\psi_Y = 1.6$ to be applied to the hooked bar development lengths with spacings of less than $6d_b$. The spacing of the boundary

element longitudinal bars in wall W2HS was 65mm c/c in the out-of-plane direction which is equal to $5.1d_b$.

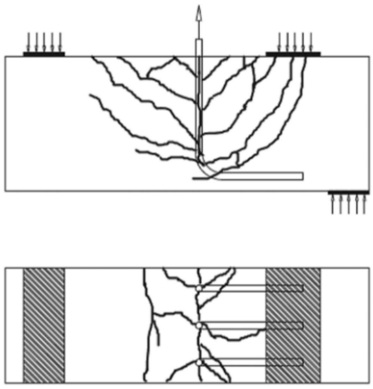

Figure 5.24 - Cracking pattern near anchorage failure reported by Ajaam et al. (2018) [Adapted from Ajam et al., 2018]

Although the results of Wall W2HS warrants further research on the effect of high-strength reinforcement on closely spaced anchored bars, it is deemed that the small spacing of the boundary element longitudinal reinforcement combined with the higher stresses induced in the high-strength longitudinal reinforcement contributed to the anchorage slip observed in the test.

Using the data recorded by the cable transducers, rotations of the wall at different elevations along the height of the wall were calculated and translated to top lateral deflections. Figure 5.25 and Figure 5.26 show backbone force-displacement curves resulting from the rotations recorded at different elevations along the height of the wall for positive and negative load directions. Recorded shear displacements as well as total top lateral deflection of the wall are also shown. These figures suggest that a large proportion of the rotation within the plastic hinge region occurs within about 30mm of the base of the wall. Approximately 65% of the plastic hinge rotation at the onset of the first flexural bar rupture in the positive direction is due to the rotation of the wall within the 30mm wall segment at the base. Similarly, this ratio is 49% in the negative direction.

Furthermore, the ratio of the contribution of rotation within the prescribed plastic hinge region (h=1650mm) to the total top displacement is 73% at the drift ratio of 1.5% and increases to 91% at maximum load in the positive loading direction. These ratios were found to be 64% and 77% in the negative loading direction.

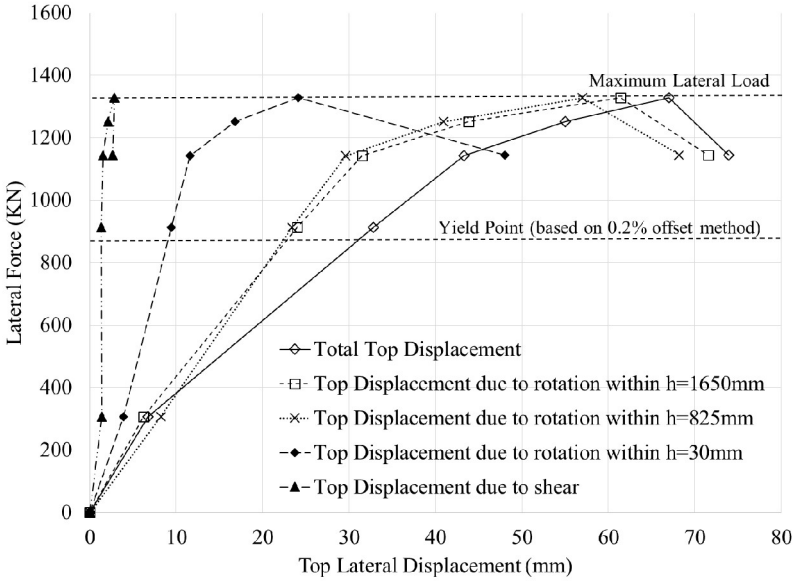

Figure 5.25 – Wall W2HS force-displacement backbone curves for loading in positive direction

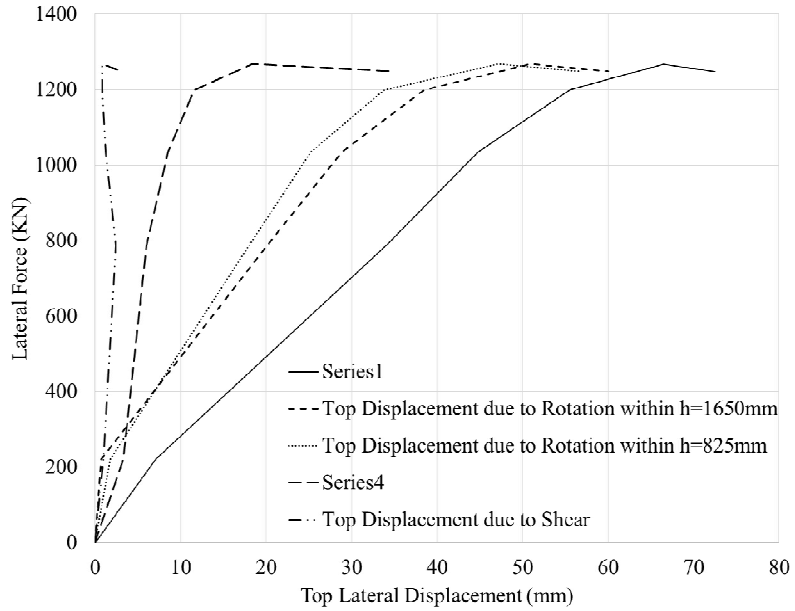

Figure 5.26 – Wall W2HS force-displacement backbone curves for loading in negative direction

5.2.5.2 Approximation of the Wall response without Anchorage Slip

As discussed earlier, the observed longitudinal reinforcement anchorage slip first occurred between 0.6% drift and 1.0% drift resulting in a distinct gap or slip in the load-deflection diagram

as shown by point 4 in Figure 5.22. Further investigation of the load-deflection data revealed that the wall experienced a sudden displacement slip of approximately 9 mm at the top of the wall in the cycles following 0.6% drift ratio. The slip likely continued at smaller increments until the end of the test as the strains in the longitudinal reinforcement in the boundary elements indicate.

To provide a better understanding of the effect of high-strength reinforcement on the wall behaviour, an attempt was made to approximate the hysteretic response of the wall without the effect of the anchorage slip by correcting the displacement values in the drift stages following the anchorage slip. In order to do this, the peak points of the curves following the 0.6% drift stage were pulled back by 9mm. The curves between the zero-load point and the peak points at each drift stage were corrected using a linear reduction factor.

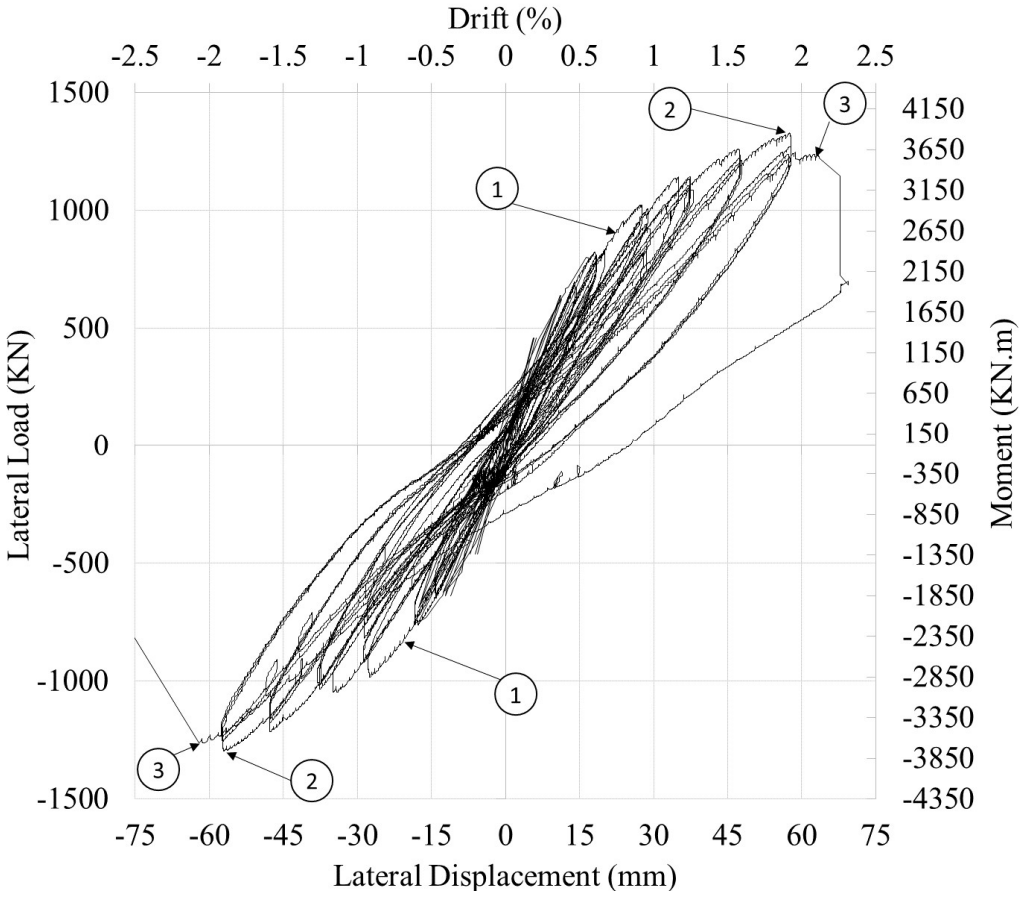

(1) Yield (0.2% offset method) (2) maximum load; (3) bar rupture;

Figure 5.27 - Wall W2HS experimental load-deflection diagram (adjusted for anchorage slip)

Table 5.8 - Wall W2HS Experimental Results (adjusted for anchorage slip)

Drift (%)	Positive Loading				Negative Loading			
	F (KN)	Δ_{top} (mm)	M_r (KN.m)	Ductility Ratio ($\Delta/\Delta y$)	F_u (KN)	Δ_{top} (mm)	M_r (KN.m)	Ductility Ratio ($\Delta/\Delta y$)
0.2	460	6.1	1206	0.3	-460	-5.5	-1218	-0.3
0.4	623	10.9	2314	0.5	-640	-10.7	-2190	-0.6
0.6	787	18.3	2326	0.9	-750	-16.8	-2193	-1.0
0.9	995	26.7	2465	1.3	-981	-26.4	-2398	-1.5
1.2	1132	33.9	2604	1.6	-1046	-33.6	2552	-1.9
1.6	1231	45.8	2952	2.2	-1214	-46.1	-2854	-2.6
1.9	1299	56.0	3312	2.7	-1294	-54.8	-3013	-3.1
2.1	1225	61.5	3657	2.9	-1262	-60.9	-3526	-3.5

F=top lateral force; M = moment; Δ_{top} = total top displacement; Drift = H/L.

It should be noted that the data presented above is an approximation based on available information and may not accurately represent the behaviour of wall W2HS, should the anchorage slip had not occurred. However, considering the response parameters such as ductility and stiffness of the wall, the hysteresis curves presented above may provide a closer representation of the actual wall behaviour without the effect of the anchorage slip. In addition, as presented in Chapter 6, the analytical results obtained from the FEM analysis show a reasonably good agreement with the adjusted hysteresis curves presented above.

Figure 5.28 shows a comparison between the adjusted hysteresis curves for wall W2HS and the control wall (Wall 2) tested by Navidpour (2018). It is shown that the high-strength ASTM A1035 steel reinforcement significantly reduces the overall ductility of the wall. It is shown that the control wall 'Wall 2' was able to reach a lateral drift capacity of 3.0% while the capacity of wall W2HS was approximately 1.9%. This is a significant reduction in ductility which is attributed to the ductility and stress-strain behaviour of the ASTM A1035 flexural reinforcement in wall W2HS. In addition, the flexural capacities of the two walls are very similar. This demonstrates one of potential advantages of high-strength reinforcement considering that 57% less flexural reinforcement in the construction of wall W2HS. However, it was noted that the initial stiffness of wall W2HS was found to be smaller compared to the control wall. This finding is consistent with the results of wall W1HS for which a smaller initial stiffness was also observed. The reduced stiffness is deemed to be due to the stress-strain behaviour of the reinforcing longitudinal bars as well as the smaller longitudinal reinforcement ratio in the boundary elements.

Furthermore, the slope of wall W2HS unloading curves were found to be smaller compared to the control wall. This behaviour was also observed in wall W1HS and is attributed to the partial elasticity of the ASTM A1035 reinforcement in later stages of loading. In other words, the reinforcement does not have a defined yield point and yielding occurs over a 'yielding region', the residual elasticity in the reinforcing bars tend to self-center the wall. This behaviour is more pronounced during the early stages of loading, which diminishes as the wall undergoes larger deformations. In comparison, once the control wall reaches the yield point, deformations become fully plastic with nearly zero recovery.

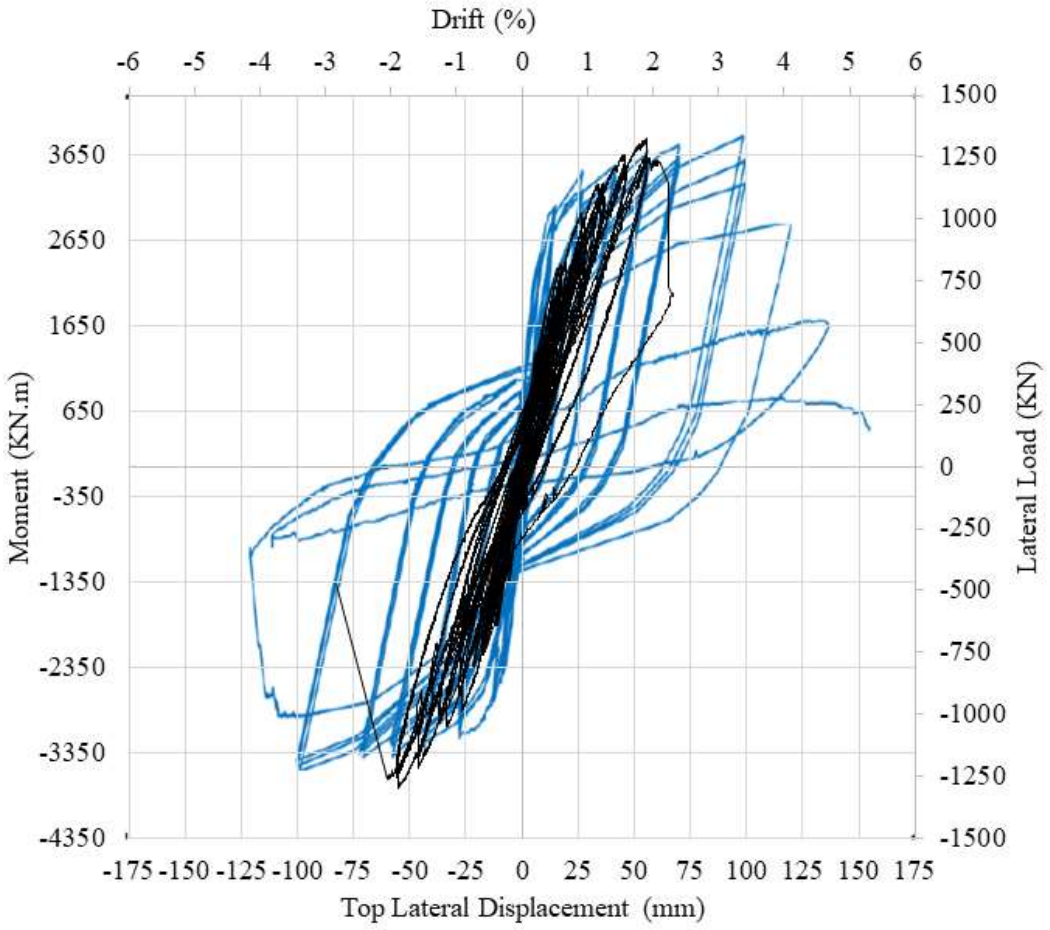

Figure 5.28 - Comparison of results for wall W2HS and the Control Wall (Navidpour, 2018)

An alternate method was used to correct the hysteresis diagram of wall W2HS based on the recorded strains in the boundary element longitudinal reinforcement along the height of the wall. The strains in the outermost longitudinal reinforcement were used to calculate the local curvature of the wall at the location of the strain gauges. The depth of the concrete compression zone at the

base of the wall was obtained from RC-Section analysis and extrapolated linearly for different heights. The top displacement of the wall was then calculated by computing the area under the curvature diagram. In addition to the displacement of the wall, the contribution of anchorage slip was calculated using a method developed by Alsiwat and Saatcioglu (1992). This anchorage slip model uses a bond stress model developed by Pochanard and Harmon (1989) to estimate the total extension of the embedded reinforcement. The hysteresis diagram calculated using this method is presented in Figure 5.29. Based on this approximation, wall W2HS fails at a lateral drift capacity of 1.5% which is 50% smaller compared the drift capacity of the control wall. It should be noted that this approximation does not consider the observed 'break-out' of the boundary element longitudinal reinforcement. It is assumed that the longitudinal reinforcement that are anchored within the foundation undergo anchorage slip defined by the model developed by Alsiwat and Saaticoglu (1992) and that no 'break-out' occurs.

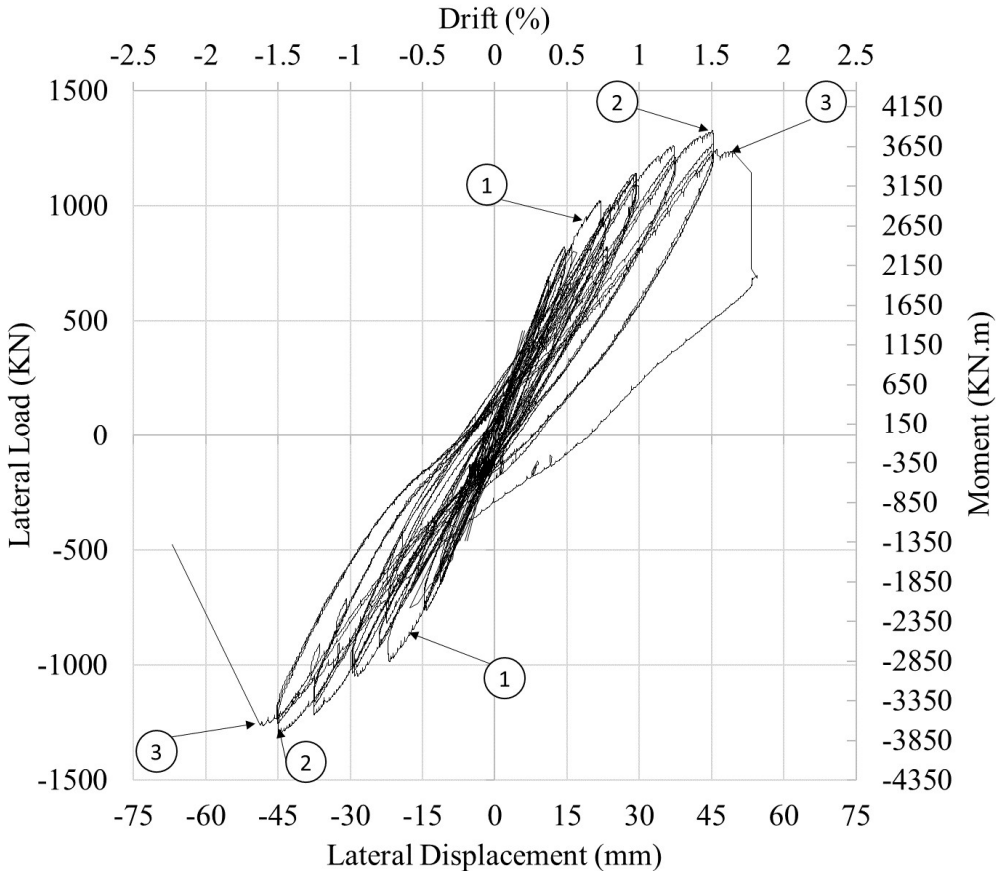

(1) Yield (0.2% offset method) (2) maximum load; (3) bar rupture;

Figure 5.29 - Wall W2HS experimental load-deflection diagram adjusted for anchorage slip using recorded strains and anchorage slip model (Alsiwat & Saatciogu, 1992)

5.2.5.3 Reinforcement Strains

Strains in the steel reinforcement were measured using strain gauges attached to the reinforcing bars at selected critical locations (refer to the instrumentation plan presented in Chapter 4). These locations included two outer longitudinal bars in at each end of the wall as well as selected transverse shear reinforcement in the web section of the wall. Strain gauges were installed within a height of 1650mm from the base of the wall at intervals shown in the instrumentation plan presented in Chapter 4.

Using tensile coupon tests, the average yield strains of the No. 3 and No. 4 reinforcement used in the construction of wall W2HS were found to be 6.9 and 6.5 (10^{-3} mm/mm), respectively. The 0.2% offset method was used to determine the yield strain of the reinforcing bars. The nominal yield strain (i.e., strain at f_y = 690 MPa) of the No. 3 and No. 4 bars were found to be approximately 4.08 and 3.80 (10^{-3} mm/mm). The yield strain obtained from the 0.2% offset method was used to determine the yield point of the wall.

Figure 5.30 shows recorded strains at the center of the transverse reinforcement at heights of 790 mm and 1490mm from the base of the wall where strains in the shear reinforcement were found to be the highest. It is shown that the strain variation in the web transverse reinforcement was relatively small and that the transverse shear reinforcement did not reach the yield strain. The highest recorded strains were 4.7 (10^{-3} mm/mm) and 4.6 (10^{-3} mm/mm) in the positive and negative loading directions, respectively. These strains corresponded a tensile stress of approximately 750MPa. Strain data for the other transverse reinforcement is provided in Appendix C.

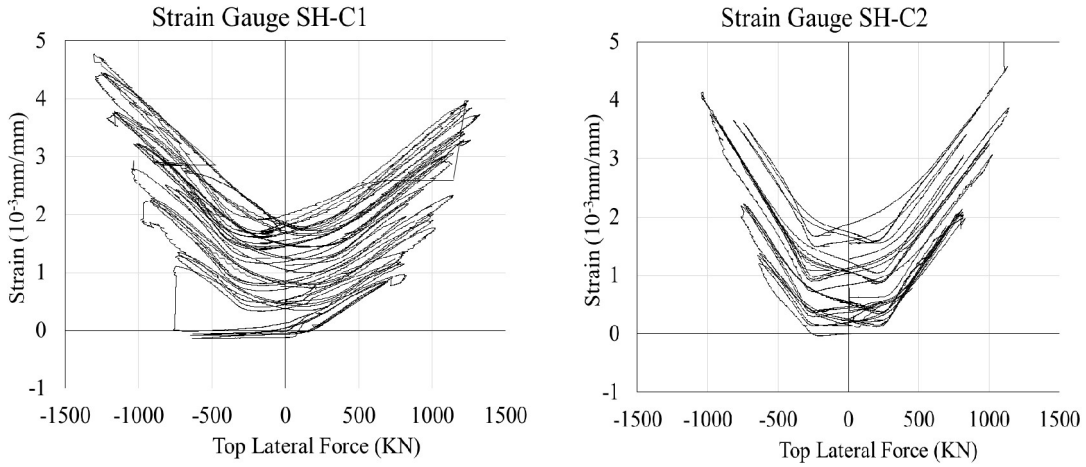

Figure 5.30 – Typical strain data for transverse web reinforcement

Figure 5.31 and Figure 5.32 present the recorded strains in the outer boundary element longitudinal reinforcement along the height of the wall at various loading stages. As described earlier, the anchored section of the bars was found to undergo a sudden slip starting at a drift ratio of 0.6% at 150mm below the wall base and at drift ratios between 1.3% and 1.9% at the base of the wall. It is shown in Figure 5.31 and Figure 5.32 that at the drift ratio of approximately 1.4%, the strains in the longitudinal reinforcement were well within the plastic range and were approaching rupturing strains. Based on this observation, it is believed that the slippage of the anchored reinforcement has contributed to additional top lateral displacement; and the actual drift capacity of the wall, had the anchored reinforcement not experienced slippage, would have been higher than 1.4%.

Figure 5.33 and Figure 5.34 show strains in the outermost longitudinal reinforcement plotted against lateral forces in the positive and negative loading directions. The same reinforcement slippage effect can be observed at the wall base and 150mm inside the foundation. It is observed that, as the anchored portion of the longitudinal bars slip and the strain levels decrease, the remaining strain demand is transferred higher along the wall. This effect can also be seen in Figure 5.31 and Figure 5.32.

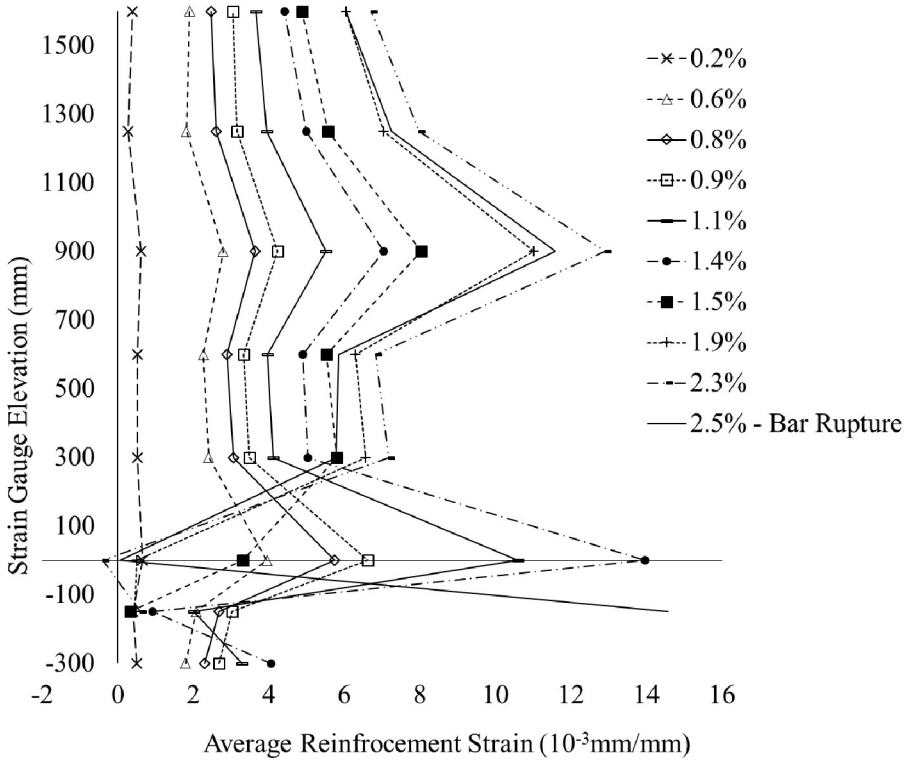

Figure 5.31 – Wall W2HS steel Strains vs wall height in the positive loading direction

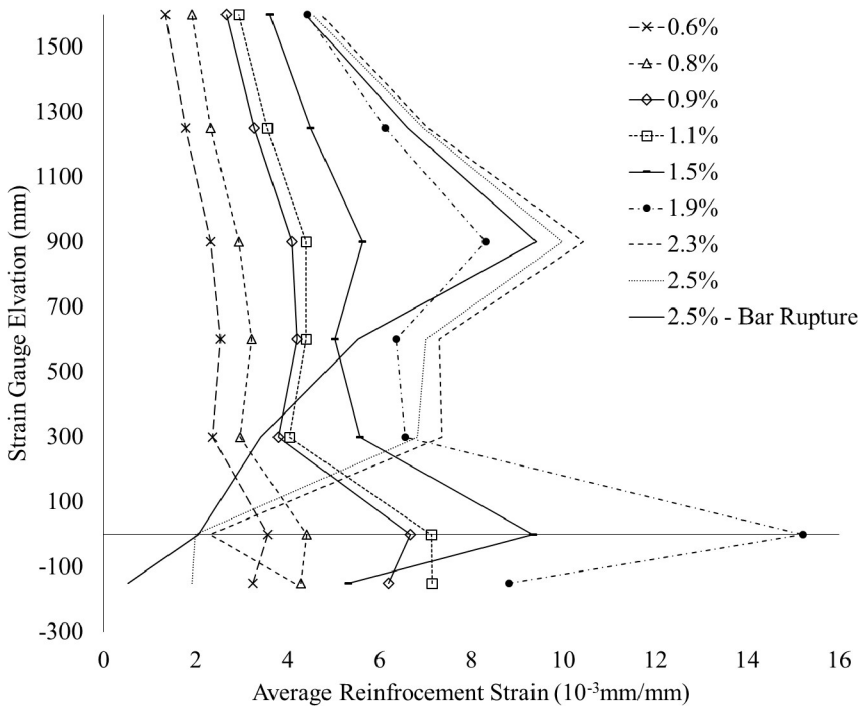

Figure 5.32 – Wall W2HS steel Strains vs wall height in Negative Loading Direction

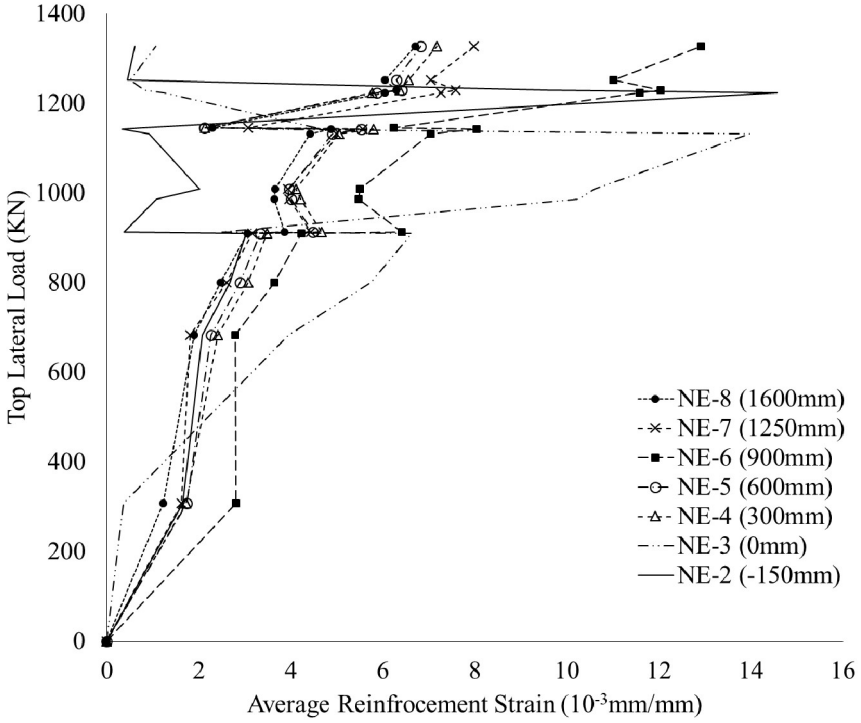

Figure 5.33 – Wall W2HS steel strains vs lateral force in the positive loading direction

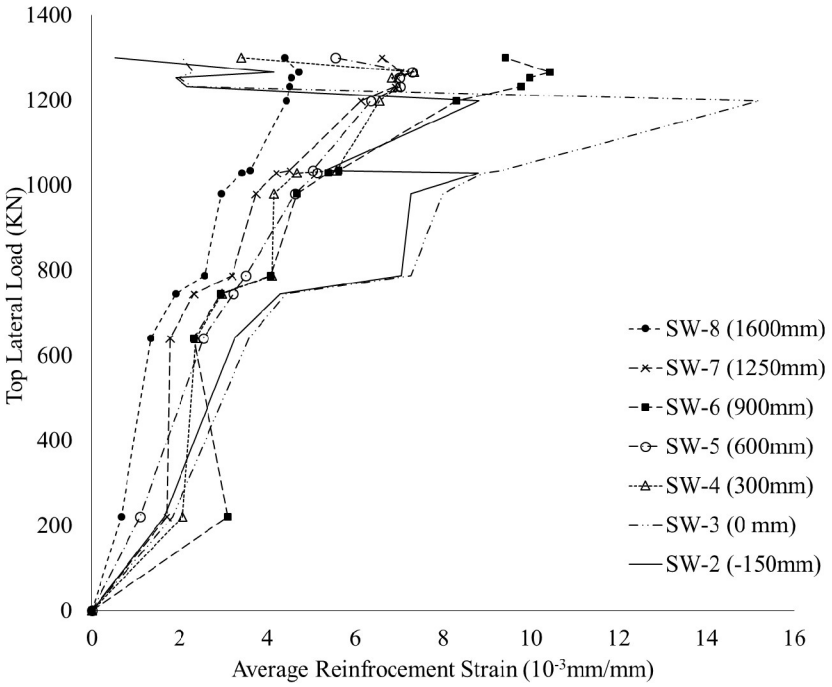

Figure 5.34 – Wall W2HS steel strains vs lateral force in the negative loading direction

5.2.6 Variation of the Compressive Axial Load during the Tests

It was assumed the net axial compressive forces applied using the pre-stressing cables remained constant during the tests. Strains in the cables were recorded during the tests and were later analyzed to verify this assumption. The recorded strains indicated that the net tensile stress in the pre-stressing cables increase the rotation of the walls increase. The strain data suggested that, at the maximum lateral load level, the net compressive axial load increased by approximately 28% in the positive loading direction and 18% in the negative loading direction for wall W1HS. This increase was found to be 38% in the positive loading direction and 30% in the negative loading direction for wall W2HS. This was due to the fact that, as the wall rotated, the inclination of the top surface of the wall increased which resulted in increased stresses in the cables closer to the tension side of the walls. Similarly, the cables in the compression side of the wall were relaxed. This effect was more pronounced in wall W2HS as the width of the wall was larger compared to wall W1HS.

Figure 5.35 shows the recorded strains in the outermost pre-stressing cables. It should be noted that the strains in the pre-stressing cables were zeroed at the start of the test; hence, the strains

shown in figures below, are in reference to the zeroed strains and do not represent total strains in the cables. It should also be noted that, the cables were found to be within their elastic region throughout the test. Figure 5.36 presents the recorded strains in the pre-stressing cables at the maximum lateral load level. It is shown that that the variation of strains in the pre-stressing cables along the width of the wall follows a linear trend. Negative values indicate a decrease in the strain.

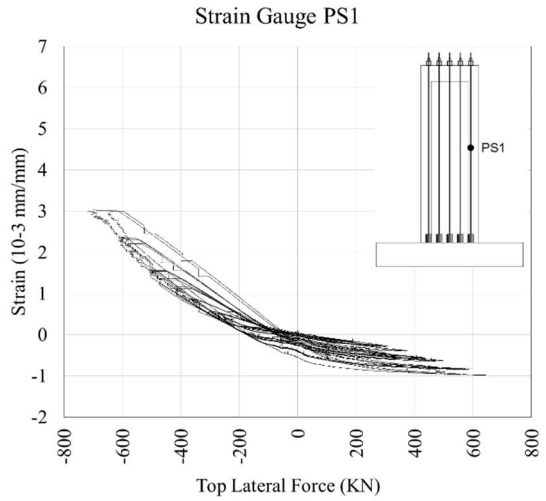

a) Wall W1HS – Strain Gauge #PS1

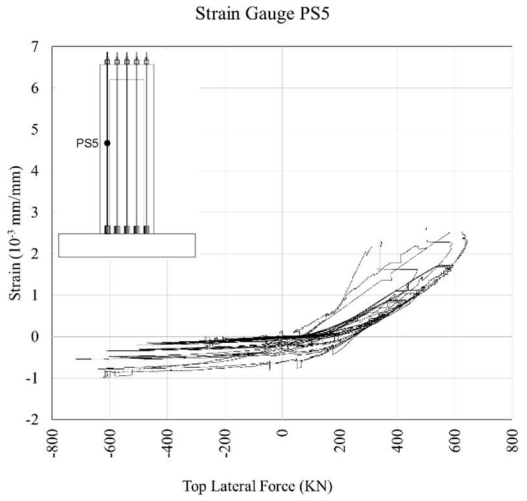

b) Wall W1HS – Strain Gauge #PS5

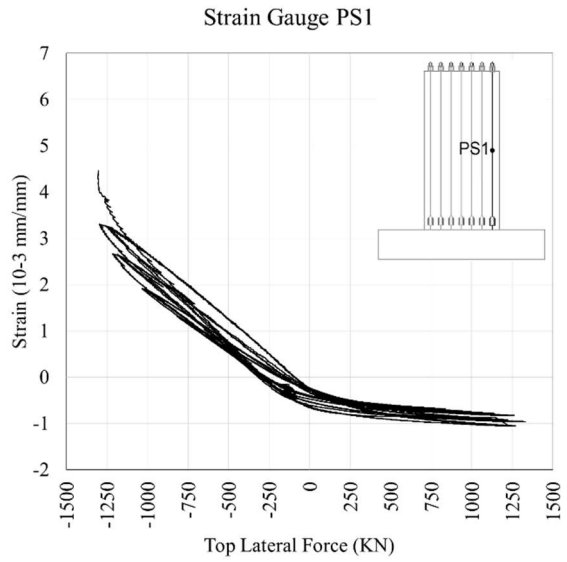

c) Wall W2HS – Strain Gauge #PS1

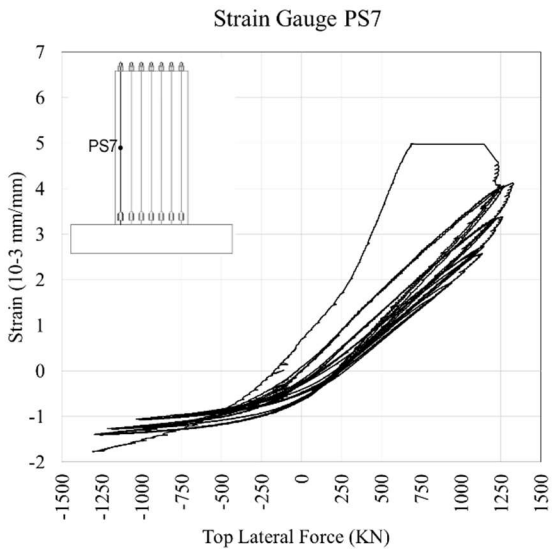

d) Wall W2HS – Strain Gauge #PS7

Figure 5.35 Recorded strains in the pre-stressing cables during the test in the outermost cables

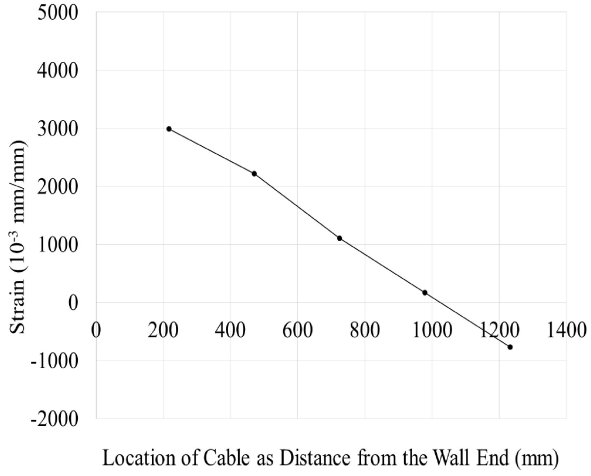

a) Wall W1HS – Positive Loading Direction

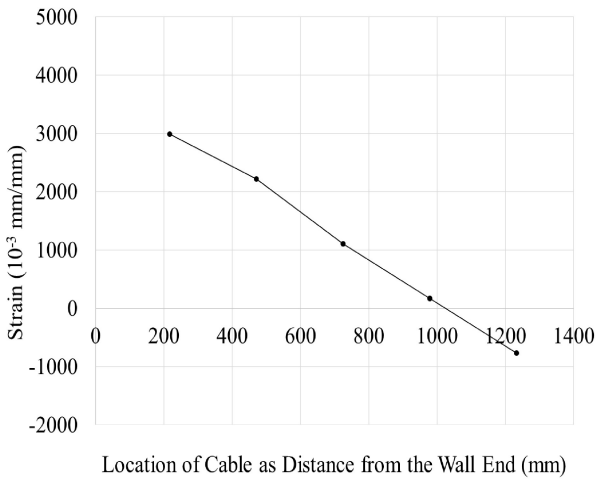

b) Wall W1HS – Negative Loading Direction

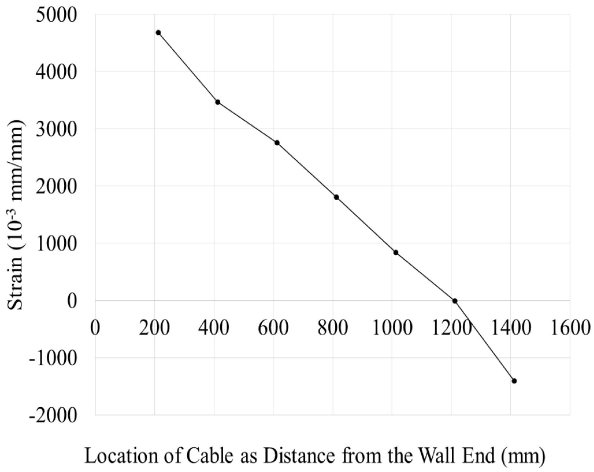

c) Wall W2HS – Positive Loading Direction

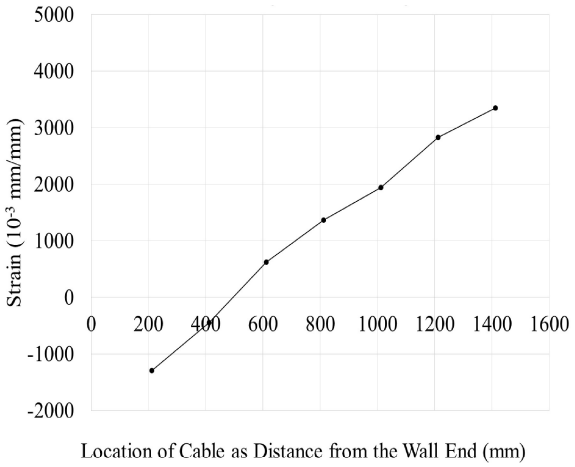

d) Wall W2HS – Negative Loading Direction

Figure 5.36 - Recorded strains in pre-stressing cables at maximum load

Chapter 6

6 Analytical Program

This chapter presents the analytical phase of current research project. The chapter begins by providing an overview of the Finite Element (FE) software used in this study and a description of the constitutive models that are used in numerical analyses. The FE modelling approach is then validated against structural response of various walls tested in the literature. The FE modelling of Wall W1HS is then presented. The model is used to conduct a parametric study to assess the effects of high-strength steel reinforcement on shear wall response. The parameters include wall aspect-ratio, concrete strength, grade and stress-strain characteristics of high-strength reinforcing steel.

6.1 Finite Element Modeling Software

Numerical analyses of Wall W1HS were performed using VecTor2, a two-dimensional Finite Element Modeling (FEM) software which can be used to predict the structural response of reinforced concrete membranes subjected to in-plane static, cyclic and dynamic loading. The theoretical basis of VecTor2 consists of the Modified Compression Field Theory (MCFT; Vecchio & Collins, 1986) and the Disturbed Stress Field Model (DSFM; Vecchio, 2000). The MCFT can be used to predict the load-deformation response of reinforced concrete membranes subjected to in-plane normal and shear stresses. The DSFM extends the relationships in the MCFT by updating the compatibility relationships for the effects of cracked shear-slip deformations. The software includes a large library of realistic nonlinear constitutive models for reinforced concrete with powerful analytical finite element analysis capabilities that facilitates more accurate assessment of structural performance of reinforced concrete members subjected to a variety of loading conditions. The program allows for in-depth investigation of stresses and strains at every step of the analysis. In the context of the current research, this allows for an assessment of the effects of HS reinforcement on member behaviour and plastic hinge formation in shear walls reinforced with high-strength steel.

The capabilities of VecTor2 have been demonstrated in several recent analytical studies of reinforced concrete members subjected to cyclic loading (Lu & Henry, 2018; Cortes-Puentes & Palermo, 2011; Palermo & Vecchio, 2001). This research indicates that VecTor2 can reliably and

accurately predict the behaviour of reinforced concrete shear walls. In this section, the ability of VecTor2 in predicting behaviour of walls with different parameters, including walls with varying aspect ratios, concrete strengths and steel types, as well as failure modes will be further validated. The numerical approach is then used to model the response of wall W1HS from the current study and to conduct a parametric study which aims at further understanding the effect of high-strength reinforcement and various design parameters on the structural response of HS reinforced concrete shear walls.

6.2 Description of Constitutive Models

The default VecTor2 constitutive models were used to model the selected walls for consistency. With regards to the concrete models, the only exception was the pre-peak compression model. The program specifies Hognestad's Parabolic function as the default model for the pre-peak compression relationship of concrete. This model was found to yield acceptable results for normal strength concrete walls; however, during the preliminary analyses it was found that Popovic's High-Strength Concrete (HSC) model was able to generate more reliable results, especially for HSC walls. Popovic's (1973) initial concrete model was developed for normal-strength concrete. Collins and Porasz (1989) later modified the models proposed by Thorenfeldt, Tomaszewicz, and Jensen (1987) and Popovics (1973) to better predict the behaviour of high-strength concrete in compression. A parametric study by Cortes-Puentes (2009) has shown that Popovic's models for normal-strength and high-strength concrete generally result in better predictions of the response of reinforced concrete shear walls.

The following material models were used in the Vector2 analyses that are presented in this chapter:

1) **Compression Pre-Peak:** As discussed above the pre-peak stress-strain behaviour of concrete in compression was modelled using the Popovic's (1973) formulations.
2) **Compression Post-Peak:** The post-peak stress-strain behaviour of concrete was modelled using the Modified Park-Kent (1982) which takes into account the increased strength and ductility of confined concrete. The model assumed a linear decay in post-peak concrete strength and a residual concrete strength of $0.2f'_c$.
3) **Compression softening:** Defined as "the reduction of compressive strength and stiffness relative to the uniaxial compressive strength due to the coexisting transverse cracking and tensile straining" in concrete (VecTor2 User Manual, 2002), the compression softening is

modelled using Vecchio 1992-B (e1/e2-Form), which considers both strength and strain softening mechanisms in concrete.

4) **Tension Stiffening:** This phenomenon accounts for the increase in stiffness of a reinforced concrete section due to the transmission of stresses from the reinforcing steel to concrete and the ability of concrete to carry residual tensile stresses between cracks. These stresses are generally smaller than the cracking stress of concrete, f_{cr} and decay towards zero as straining continues. This effect is modelled using Modified Bentz (2003), which takes into account the combined contribution of reinforcement ratio and bond characteristics. The Modified Bentz model wall slightly modified to better accommodate the ASTM A1035 reinforcement used in the experimental program. In this modified version, the f_{c1} response was sent to approach zero as the stress in steel approached the ultimate stress of the reinforcement. The default Modified Bentz (2003) model was used for all other reinforcement types.
5) **Tension Softening:** This effect is related to the presence of tensile stresses in plain concrete after cracking due to the fact that it is not a perfectly brittle material. A nonlinear model by Hordijk et al (1986) is used to account for this effect.
6) **Confined Strength:** This accounts for the enhancement in strength and ductility of confined concrete subjected to bi-axial or tri-axial compressive stresses. This effect is modelled using a relationship proposed by Kupfer et al. (1969), which calculates the strength of concrete subjected to bi-axial compression. An expression developed by Richart et al. (1928) is combined with Kupfer's model for the case of columns with spiral reinforcement.
7) **Dilation:** This represents the post-peak expansion of concrete under compressive stresses in a direction perpendicular to the direction of the applied compressive force. This was incorporated using a variable Poisson's ratio which was developed based on strain data from earlier works by Kupfer et al. (1969).
8) **Cracking Criterion:** The Mohr-Coulomb criterion is used to determine the shear stress at which concrete fails. Provided that the orientation of the normal stresses is known, the plane of failure (cracking) is determined.

9) **Crack Stress Check:** Shear stress in a crack is calculated using the Modified Compression Field Theory (MCFT) and Disturbed Stress Field Model (DSFM) based on a model by Vecchio-Collins (1986).
10) **Crack Width Check:** The purpose of the crack width check is to reduce the average compressive stress in concrete when crack widths exceed a specified limit. It is computed based on the work done by Vecchio (2000). The limit of crack-width check used in the models is 40% of the nominal aggregate size.
11) **Crack Slip Calculation:** This accounts for the element slip distortion in concrete that enables VecTor2 to calculate strains along the cracks. The Walraven (1981) model was used to define the concrete shear-slip relationship.
12) **Concrete Hysteretic Response:** a nonlinear response model with plastic offsets proposed by Vecchio (1999) was used to model the hysteretic response of concrete.
13) **Steel Stress-Strain Relationship:** The stress-strain relationship of the steel reinforcement is modelled using a model that is composed of three main parts. An initial linear-elastic section between $\varepsilon_s=0$ and $\varepsilon_s=\varepsilon_y$, a yield plateau between $\varepsilon_s=\varepsilon_y$ and $\varepsilon_s=\varepsilon_{sh}$ and a non-linear strain hardening stage between $\varepsilon_s=\varepsilon_{sh}$ and $\varepsilon_s=\varepsilon_{u.}$ The non-linear strain hardening stage is modelled using a curvilinear relationship with exponent P as described in Chapter 3. The VecTor2 default is P=4.
14) **Steel Hysteretic Reponses:** The hysteretic response of the steel reinforcement was computed using a model proposed by Seckin (1981). This model incorporates the Bauschinger effect that accounts for premature yielding of reinforcement as a result of load reversal.
15) **Dowel Action:** Dowel action is the contribution of reinforcing bars to shear strength as they cross cracks that slip transversely with respect to the longitudinal axis of the reinforcement. The Tassios Crack Slip model (Vintzeleou and Tassios, 1987) was used for the models presented herein. The Crack Slip model assumes that the transverse dowel force of the reinforcement offsets the stress of concrete at a crack.
16) **Buckling:** A model proposed by Akkaya (2013) was used to account for the buckling of reinforcement. This model is based on a model original proposed by Dhakal-Maekawa (2002). This model assumes that buckling starts when the ratio of the unsupported length to diameter of the reinforcing bar exceeds 5.0 and that the reinforcement has yielded.

17) **Concrete Bond:** This model defines boned characteristics between confined and unconfined concrete and steel reinforcement. A model proposed by Eligehausen et al. (1983) was used to model the walls. It should be noted the Eligehausen model was used in conjunction with the Modified Bentz (2003) model. Any overlapping effects in the calculation of the anchorage slip was assumed to be negligible.

Table 6.1 presents a list of models used in the analysis of the wall using VecTor2. The VecTor2 basic default analysis models were used for the wall models as shown.

Table 6.1 - Models used in the analysis using VecTor2

Concrete Models		**Reinforcement Models**	
Compression Pre-Peak	Popovics High-Strength Concrete	Hysteretic Response	Bauschinger Effect (Seckin)
Compression Post-Peak	Modified Park-Kent	Dowel Action	Tassios (Crack Slip)
Compression Softening	Vecchio 1992-A	Buckling	Akkaya 2012 (Modified Dhakal-Maekawa)
Tension Stiffening	Modified Bentz 2003		
Tension Softening	Nonlinear (Hordijk)	**Bond Models**	
FRC Tension	SDEM - Monotonic	Concrete Bond	Eligehaousen
Confined Strength	Kupfer / Richart		
Dilation	Variable - Isotropic	**Analysis Models**	
Cracking Criterion	Mohr-Coulomb (Stress)	Strain History	Previous Loading Considered
Crack Stress Calculation	Basic (DSFM / MCFT)	Strain Rate Effects	Not Considered
Crack Width Check	Agg/2.5 Max Crack Width	Structural Damping	Not Considered
Crack Slip Calculation	Walraven	Geometric Nonlinearity	Considered
Creep and Relaxation	Not Considered	Cracking Spacing	CEB-FIP 1978 - Deformed
Hysteretic Response	Nonlinear w/ Plastic Offsets		

6.3 Validation of FE modelling approach

Extensive research data is available in the literature demonstrating the ability of VecTor2 software to provide reliable analyses of reinforced concrete members subjected to static and cyclic loading. Several studies have verified the ability of the program to predict the reversed cyclic behaviour of reinforced concrete shear walls. In the current study, experimental data from previous reinforced concrete shear wall tests in the literature were used to validate the numerical FE approach, which is used in Sections 6.4 and 6.5. Reinforced concrete shear walls with different designs and performance characterises were selected for this validation study, as shown in Table 6.2.

The selected walls consisted of walls with rectangular, barbell-shaped, and flanged cross-sections having geometrical dimensions similar to those of Wall W1HS. In addition, the selected walls were reinforced with different steel Grades with yield strengths ranging between 470 MP and 630 MPa. Furthermore, the range of aspect ratios and reinforcement details in the selected

walls allowed for the evaluation of VecTor2 in predicting different failure mechanisms (e.g., shear and flexure) that are expected in reinforced concrete shear walls.

Table 6.2 - Details of previously tested wall used for validation of VecTor2 results

Wall name	Author (Year)	Cross-Section Shape	Aspect Ratio (H/L)	Axial Load Ratio (% $N/A_g f'_c$)	Concrete strength f'_c (MPa)	Steel yield strength f_y (MPa)	Failure Mode
WSH3	Dazio (2009)	Rectangular	2.3	5.8	57	601	Rupture of Flexural Reinforcement
WSH5	Dazio (2009)	Rectangular	2.3	12.8	56	576	Rupture of Flexural Reinforcement
WSH6	Dazio (2009)	Rectangular	2.3	10.8	59	576	Buckling / Concrete Crushing
S38*	Tran & Wallace (2012)	Rectangular	2	10	48	475	Flexure
S63**	Tran & Wallace (2012)	Rectangular	2	10	48	475	Flexure
J5	Chandra (2017)	Flanged	2	5	103	630	Shear
Wall 3	Navidpour (2018)	Barbell	3	8	82	470	Buckling of Flexural Reinforcement

*RW-A20-P10-S38, ** RW-A20-P10-S63

6.3.1 Walls Tested by Dazio (2009)

Three representative walls with high-strength bars from a research study by Dazio et. al. (2009) were modelled using VecTor2. Six reinforced concrete walls were tested in this study to investigate the effects of longitudinal reinforcement properties including ductility of steel reinforcement and longitudinal reinforcement ratio on the cyclic behaviour of concrete shear walls. The walls had height-to-length aspect ratios of 2.3 and were 4950mm high x 2000mm wide x 150mm thick. The shear span of the walls varied slightly, but all walls had approximately the same aspect ratio. All walls were constructed using high-strength flexural reinforcement with yield strengths ranging from 550MPa to 600 MPa. Walls WSH3, WSH5 and WSH6 were modelled using VecTor2.

The FE models for the selected walls consisted of three concrete regions and three types of steel truss elements, as shown in Figure 6.1. Table 6.3 and Table 6.4 present details for individual truss reinforcement as well as the smeared reinforcement in meshed concrete regions. The meshed concrete regions had maximum element size of 100mm in both the X and Y directions. Hybrid and rectangular elements were selected to model the walls. Hybrid elements were used to mesh the area with geometrical constraints such as rebar crossings. The elements in the wall section were not uniformly sized across the width of the wall due to the reinforcing bars located at unequal spacings. The boundary elements consist of 5 elements (each) and the web section consisted of 22

rectangular elements in the horizontal direction. The height of the wall consisted of 46 equally sized rectangular elements. The reinforcement truss elements were assumed to be perfectly bonded over their entire length and were discretized with the meshed elements. The compressive strengths of concrete used in the models were 39.2 MPa 38.3 MPa, and 45.6 MPa for walls WSH3, WSH5 and WSH6, respectively.

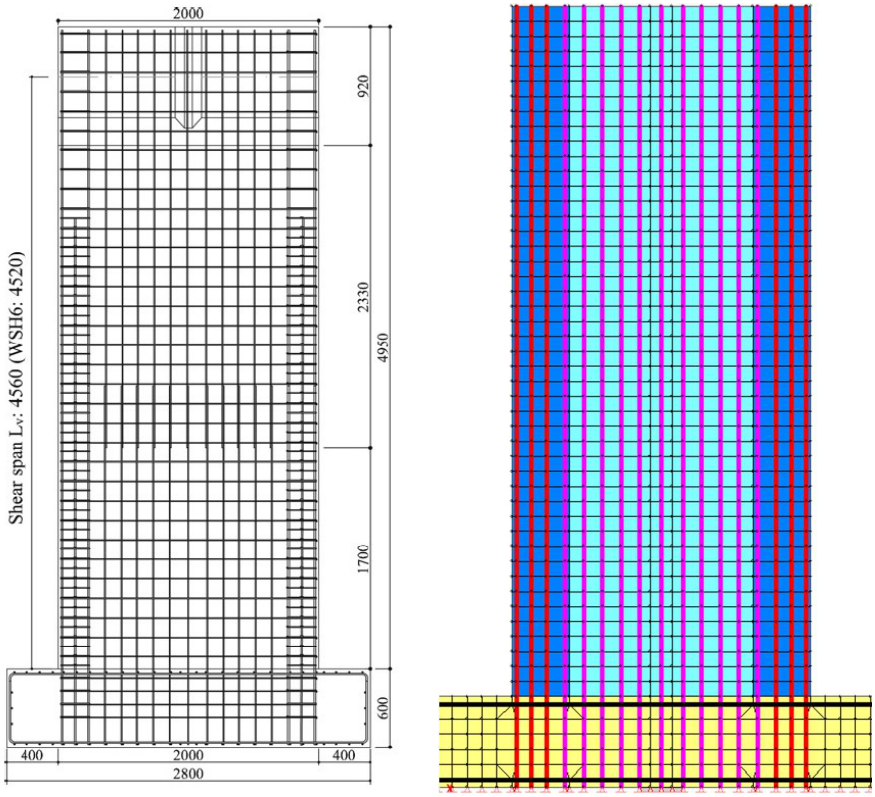

a) Typical reinforcement layout b) Meshed FE model

Figure 6.1 –Typical wall details (Dazio, 2009)

The lateral reversed cyclic loading was applied as a function of support displacement and was distributed among the nodes along the top of the wall. Axial load was defined as monotonically-applied downward point loads acting on selected nodes on top of the wall. The nodal loads were constant during the analysis. The foundation of the wall was fixed against translation in the X and Y direction along its base.

Table 6.3 - Steel truss element details for modelled walls previously tested by Dazio (2009)

No.	Element	Area (mm2)	d_b (mm)	f_y (MPa)	f_u (MPa)	E_s (MPa)	ε_{sh} (10^{-3} mm/mm)	ε_u (10^{-3} mm/mm)
WSH3	Boundary Vert.	233	12	560	706	198200	2.83	68
	Web Vertical	104	8	526	678	213600	2.47	65
	Foundation Long.	10500	30	576	675	200000	2.88	75
WSH5	Boundary Vert.	101	8	584	714	200000	2.93	75
	Web Vert.	57	6	519	559	200000	2.60	75
	Foundation Long.	10500	30	576	675	200000	2.88	75
WSH6	Boundary Vert.	226	12	576	675	200000	2.88	75
	Web Vert.	101	8	576	675	200000	2.88	75
	Foundation Long.	10500	30	576	675	200000	2.88	75

Table 6.4 - Smeared reinforcement details for modelled walls previously tested by Dazio (2009)

No.	Meshed Region	Direction (Degrees)	ρ (%)	d_b (mm)	f_y (MPa)	f_u (MPa)	E_s (MPa)	ε_{sh} (10^{-3} mm/mm)	ε_u (10^{-3} mm/mm)
WSH3	**Boundary Elements**								
	Smeared Reinf. 1	0	0.5	6	478	558	206900	2.31	56
	Smeared Reinf. 2	361	0.29	6	478	558	20900	2.31	56
	Smeared Reinf. 3	361	0.07	4.2	543	623	195100	2.79	52
	Web Section								
	Smeared Reinf. 1	0	0.25	6	478	558	206900	2.31	56
	Foundation								
	Smeared Reinf. 1	90	1	15	519	558	200000	2.6	75
WSH5	**Boundary Elements**								
	Smeared Reinf. 1	0	0.37	4.2	562	615	200000	2.82	75
	Smeared Reinf. 2	361	0.32	4.2	562	615	200000	2.82	75
	Smeared Reinf. 3	0	0.25	6	519	558	200000	2.6	75
	Web Section								
	Smeared Reinf. 1	0	0.25	6	519	558	200000	2.6	75
	Foundation								
	Smeared Reinf. 1	90	1	15	519	558	200000	2.6	75
WSH6	**Boundary Elements**								
	Smeared Reinf. 1	0	1.03	6	519	558	200000	2.6	75
	Smeared Reinf. 2	361	0.44	6	550	600	200000	2.75	75
	Web Section								
	Smeared Reinf. 1	0	0.26	6	519	558	200000	2.6	75
	Foundation								
	Smeared Reinf. 1	90	1	15	519	558	200000	2.6	75

Figure 6.2, Figure 6.3, and Figure 6.4 compare the predicted and experimental load-deformation diagrams for the representative walls tested by Dazio et al (2009). In general, the FEM results obtained from VecTor2 analysis show very good agreement with the experimental results. The analytical and experimental backbone curves match almost exactly, and the cracking and yield points are effectively captured in the analytical hysteresis curves. In addition, the slope of the unloading curves matches very closely the experimental results. It is observed that pinching patterns are slightly different for walls WSH5 and WSH6. The analytical models predict less pinching, which result in the underestimation of the energy dissipation capacity by approximately 5% and 20% for walls WSH5 and WSH6, respectively. The underestimation of pinching by VecTor2 has been reported in the previous research conducted by Cortez & Palermo (2017).

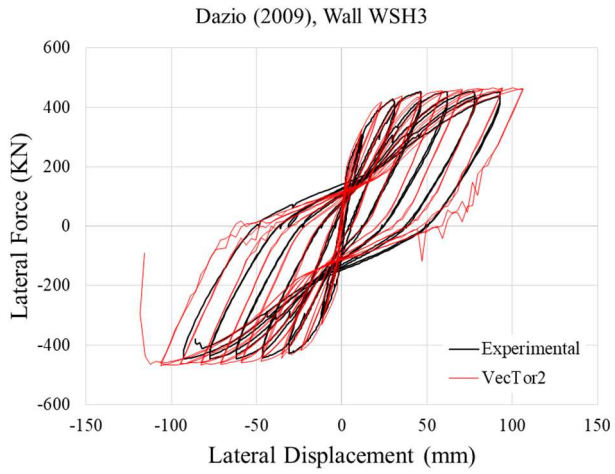

Figure 6.2 - VecTor2 results vs. experimental results for Wall WSH3 by Dazio et al (2009)

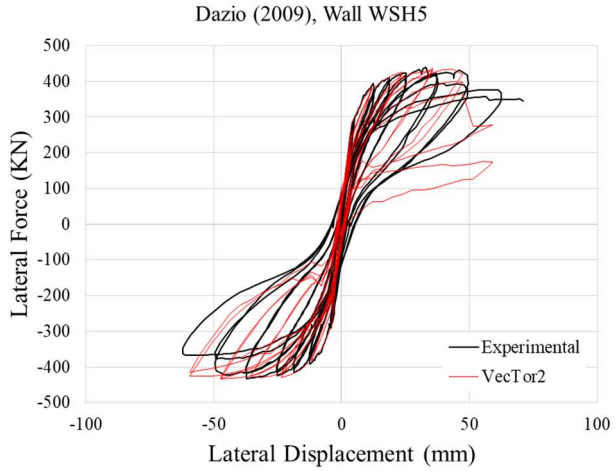

Figure 6.3 - VecTor2 results vs. experimental results for Wall WSH5 by Dazio et al (2009)

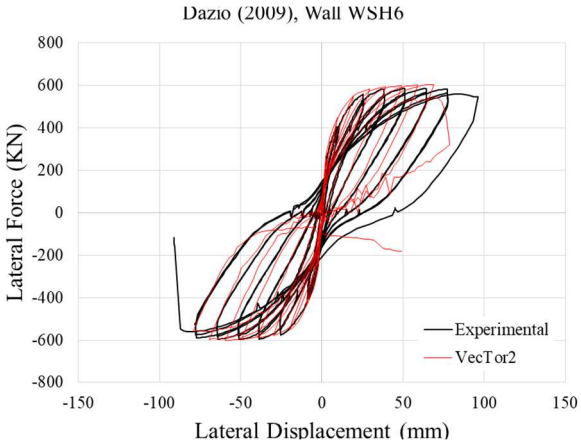

Figure 6.4 - VecTor2 results vs. experimental results for Wall WSH5 by Dazio et al (2009)

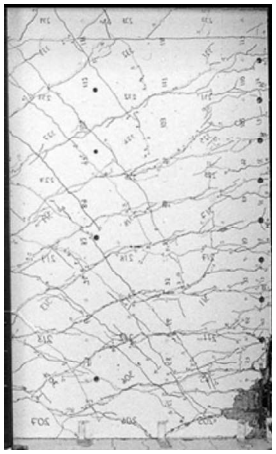

a) Wall WSH3 - Experimental

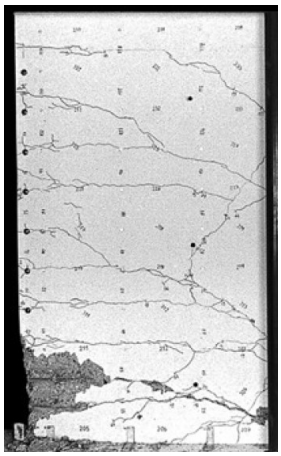

a) Wall WSH5 - Experimental

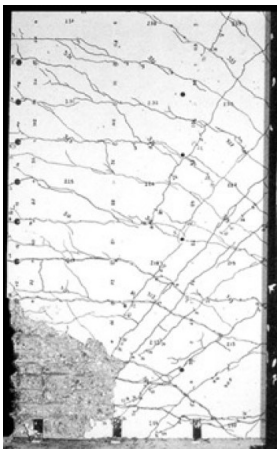

b) Wall WSH6 - Experimental

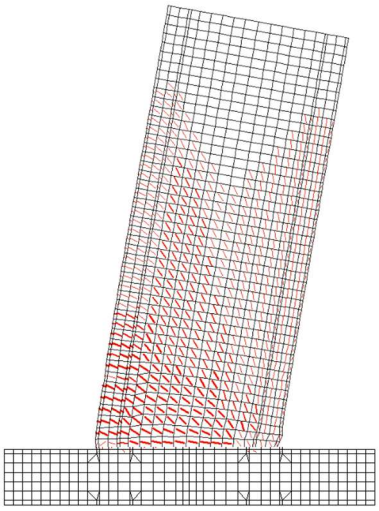

c) Wall WSH3 – VecTor2

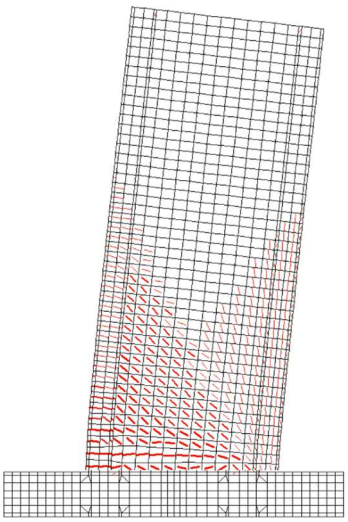

d) Wall WSH5 – VecTor2

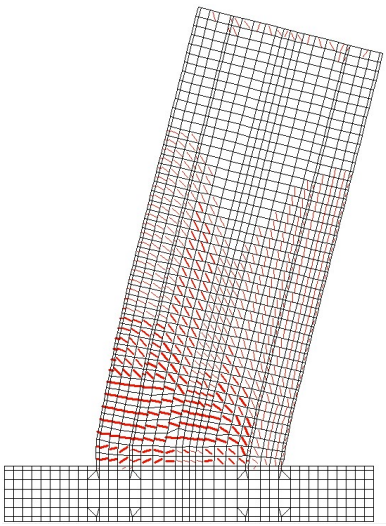

e) Wall WSH6 – VecTor2

Figure 6.5 - Cracking patterns and failure modes for walls tested by Dazio (2009)

Failure modes of the modelled walls were also predicted accurately by VecTor2. Dazio (2009) reports that walls WSH3 failed due to the buckling of flexural reinforcement. In addition, it is reported that walls WSH5 and WSH6 failed due to the rupture of flexural reinforcement in the boundary elements. VecTor2 was able to accurately predict the failure modes for all three walls as shown in Figure 6.5 . In addition, formation of a large horizontal crack at a height of 110mm from the base of wall WSH5 was reported by Dazio (2009). As shown in Figure 6.5 (b), VecTor2 was able to accurately predict the formation of this crack at an elevation of about 100mm from the base. Table 6.5 presents the critical test parameters including the ductility of the walls obtained from both experimental and analytical test results. It is shown that the ductility of walls WSH3, WSH5 and WSH6 were predicted with reasonable accuracy.

Table 6.5 Analytical vs. Experimental results for wall tested by Dazio (2009)

	Analytical					Experimental					$\mu_{Analytical}/\mu_{Exp.}$
Wall Name	F_{yield} (MPa)	Δ_{yield} (mm)	$F_{ultimate}$ (MPa)	$\Delta_{ultimate}$ (mm)	μ	F_{yield} (MPa)	Δ_{yield} (mm)	$F_{ultimate}$ (MPa)	$\Delta_{ultimate}$ (mm)	μ	
WSH 3	328	12.0	465	112.0	9.3	300	11.3	437	92.4	8.2	1.13
WSH 5	343	7.9	425	59.3	7.5	341	7.9	362	62.0	7.8	0.96
WSH 6	443	9.8	558	79.0	8.1	404	9.9	545	93.7	9.5	0.85
										Average	0.98

6.3.2 Walls Tested by Tran and Wallace (2012)

Tran & Wallace (2012) tested 5 large-scale concrete shear walls reinforced with Grade 400MPa steel bars. Walls S38 and S63 were selected for this validation study. The walls were tested under constant axial load and reversed cyclic loading. These walls had an aspect ratio of 2.0 and were subjected to a constant axial of 10% of the concentric axial capacity of the walls. The walls had different reinforcement ratios in both longitudinal and transverse directions. The wall tests showed that walls S38 and S63 failed in different modes. The purpose of conducting the FE analyses was to demonstrate the ability of VecTor2 in capturing failure modes for walls with different reinforcement ratios.

Figure 6.6 presents the reinforcement details and meshed FE models of walls S38 and S63. The FE models consisted of 4 and 5 concrete regions, respectively. All regions had a thickness of 152mm and were modelled using concrete with compressive strengths of 47 MPa and 49 MPa for walls S38 and S63, respectively. The walls were divided into two segments based on their horizontal reinforcement rations including a lower wall section and a top loading section. The

loading section consisted of higher horizontal reinforcement ratio to prevent pre-mature shear failure near the loading point. Hence, different concrete regions were defined for modelling the boundary elements and the web section within the loading region of the walls.

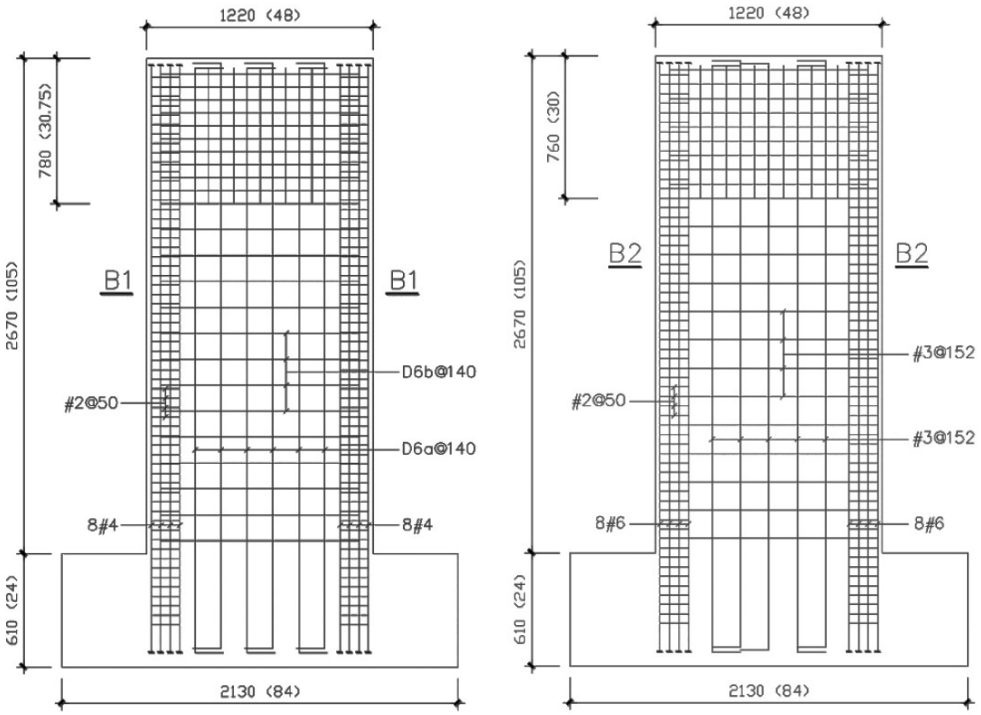

a) Wall S38 reinforcement layout

b) Wall S63 reinforcement layout

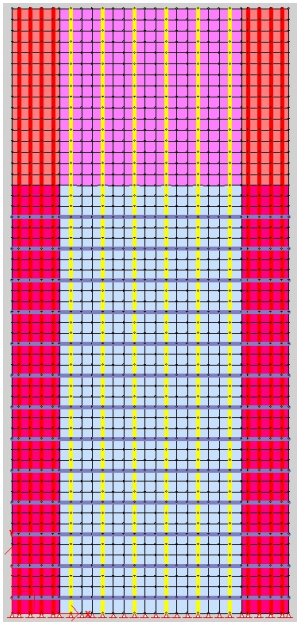

c) Wall S38 meshed FE model

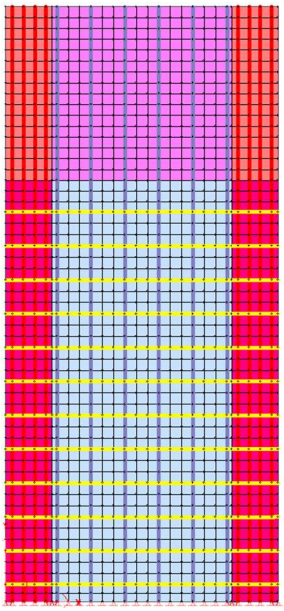

d) Wall S63 meshed FE model

Figure 6.6 - Details of walls tested by Tran & Wallace (2012)

The walls were meshed using rectangular elements with a maximum size of 50mm in both the X and Y directions. Smaller mesh sizes were selected following several iterations that yielded better results for these walls. It is assumed that the smaller mesh sizes were better suited to capture shear stresses in the elements. However, as the number of meshed elements increased, the processing speed was reduced drastically. Hence, the walls were modelled without the foundation units to enhance the speed of analysis. The results of the analysis with and without the foundation units were compared and found to be very similar. The boundary elements consisted of 5 elements (each) and the web section consisted of 17 rectangular elements in the horizontal direction. The height of the wall consisted of 56 equally sized rectangular elements. The reinforcement truss elements were assumed to be perfectly bonded over their entire length and were discretized with the meshed elements. Table 6.6 and Table 6.7 present the details for individual truss reinforcement, as well as the smeared reinforcement in meshed concrete regions. The lateral reversed cyclic loading was applied as the support displacement and was distributed among the nodes along the top of the wall. Axial load was equal to 820 kN and was defined as monotonically-applied downward point loads acting on selected nodes on top of the wall. The nodal loads remained constant during the analysis.

Table 6.6 - Steel truss element details for the modelled walls (Tran & Wallace, 2012)

No.	Element	Area (mm2)	d_b (mm)	f_y (MPa)	f_u (MPa)	E_s (MPa)	ε_{sh} (10^{-3} mm/mm)	ε_u (10^{-3} mm/mm)
S38	Boundary Vert.	254	12.7	472	613	200000	9	110
	Web Vert.	56.6	6	450	661	200000	2.6	110
	Web Horiz.	56.6	6	516	580	200000	2.6	55
S63	Boundary Vert.	570	19.1	477	637	200000	20	140
	Web Vert.	142	9.5	443	707	200000	9	133
	Web Horiz.	142	9.5	550	750	200000	9	133

Figure 6.7 and Figure 6.8 compare the experimental results with the analytical predictions obtained by VecTor2 for walls S38 and S63. It is shown that, in general, the analytical models produce an accurate prediction of the reversed cyclic behaviour of the modelled walls. The maximum lateral force, as well as the ascending and descending branches of the hysteresis curves are predicted with excellent accuracy. However, the initial stiffness of the walls is slightly overestimated between the zero-load point and the yield point for both walls.

Table 6.7 - Smeared reinforcement details for the modelled walls (Tran & Wallace, 2012)

No.	Meshed Region	Direction (Degrees)	ρ (%)	d_b (mm)	f_y (MPa)	f_u (MPa)	E_s (MPa)	ε_{sh} (10^{-3} mm/mm)	ε_u (10^{-3} mm/mm)
S38	**Lower Boundary Elements**								
	Smeared Reinf. 1	0	0.83	6.4	423	492	200000	36	152
	Smeared Reinf. 2	361	0.4	6.4	423	492	200000	36	152
	Upper Boundary Elements								
	Smeared Reinf. 1	0	0.83	6.4	423	492	200000	36	152
	Smeared Reinf. 2	361	1.25	6.4	423	492	200000	36	152
	Upper Web Section								
	Smeared Reinf. 1	0	0.53	6.4	516	580	200000	7.5	55
	Smeared Reinf. 1	90	0.22	6.4	516	580	200000	7.5	125
S63	**Lower Boundary Elements**								
	Smeared Reinf. 1	0	0.84	6.4	423	492	200000	36	152
	Smeared Reinf. 2	361	1.25	6.4	423	492	200000	36	152
	Upper Boundary Elements								
	Smeared Reinf. 1	0	0.83	6.4	423	492	200000	36	152
	Smeared Reinf. 2	361	1.25	6.4	423	492	200000	36	152
	Upper Web Section								
	Smeared Reinf. 1	0	0.53	6.4	516	580	200000	7.5	55
	Smeared Reinf. 1	90	0.53	6.4	516	580	200000	7.5	55

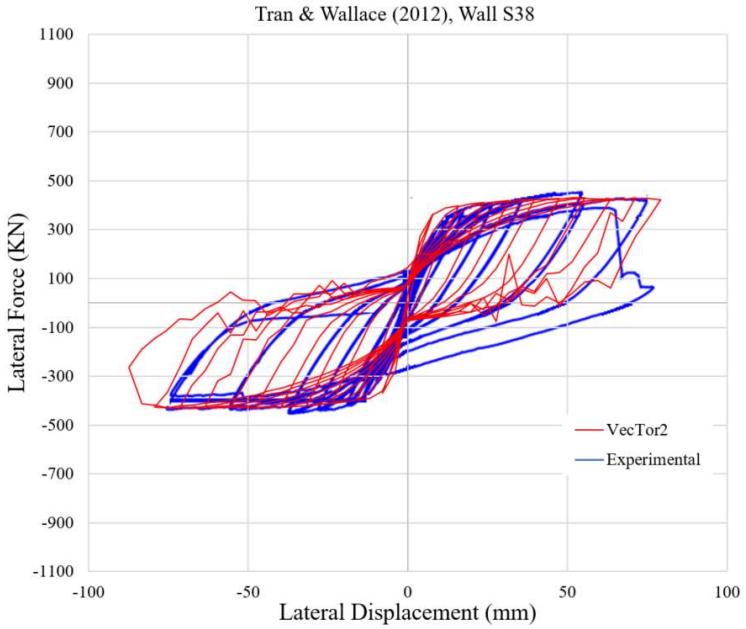

Figure 6.7 - VecTor2 results vs. experimental results for wall S38 (Tran & Wallace, 2012)

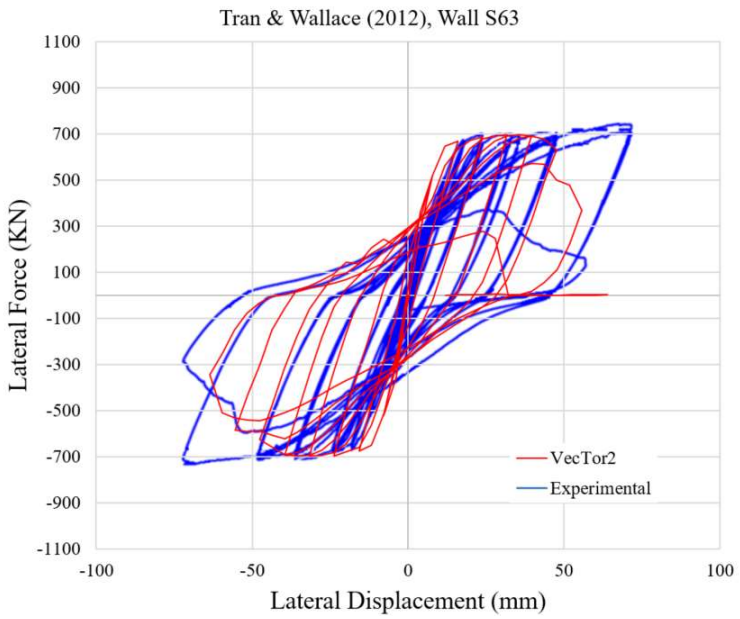

Figure 6.8 - VecTor2 results vs. experimental results for wall S63 (Tran & Wallace, 2012)

Table 6.8 presents the critical test parameters obtained from experimental and analytical results. The analytically predicted ultimate displacement of wall S38 is very close to that of the experimental result; however, the ductility ratio obtained from VecTor2 is approximately 40% higher compared to the ductility ratio obtained from the experiments. The predicted ultimate displacement for wall S63 is underestimated by about 10%, however, the analytical ductility ratio matches almost exactly with the experimental result. This is deemed to be due to the fact that the initial stiffness of the walls is slightly underestimated; therefore, the calculated ductility ratio ($\Delta_{ultimate}/\Delta_{Yield}$) may match that of the experiments, while the ultimate displacements are different.

Table 6.8 Analytical vs Experimental results for the modelled walls (Tran & Wallace, 2012)

	Analytical					**Experimental**					
Wall Name	**F_{yield} (MPa)**	**Δ_{yield} (mm)**	**$F_{ultimate}$ (MPa)**	**$\Delta_{ultimate}$ (mm)**	**μ**	**F_{yield} (MPa)**	**Δ_{yield} (mm)**	**$F_{ultimate}$ (MPa)**	**$\Delta_{ultimate}$ (mm)**	**μ**	**$\mu_{Analytical}/\mu_{Exp.}$**
S38	364	9	411	82	9.1	380	12	420	78	6.5	1.40
S63	646	11.8	585	56	4.7	620	15	720	68	4.5	1.04
										Average	1.22

Figure 6.9 presents the walls at failure with photos of the walls at the end of the test and the crack patterns obtained analytically. It can be observed that the analytical models provide a good representation of the actual failure modes and crack patterns for both walls. Walls S38 failed as a result of diagonal tension failure, initiated by concrete crushing and buckling of wall boundary

longitudinal reinforcement (Tran & Wallace, 2014). Wall S63 failed due to the buckling of the longitudinal reinforcement in the boundary elements, caused by the crushing of the core concrete (Tran & Wallace, 2014). Both failure modes are effectively captured in the results of the FE analyses. The finite element model for wall S38 showed large distortions of the meshed elements in the web, which caused abrupt changes in analytical predictions near wall failure, as shown in Figure 6.9 (a).

a) Wall S38 - Experimental

b) Wall S63 – Experimental

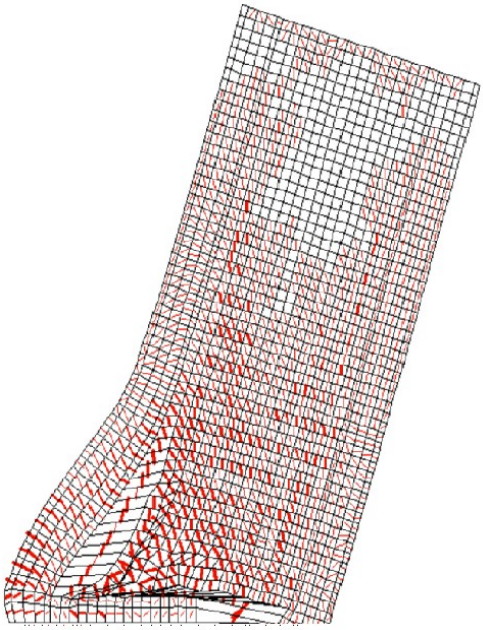

c) Wall S38 – VecTor2

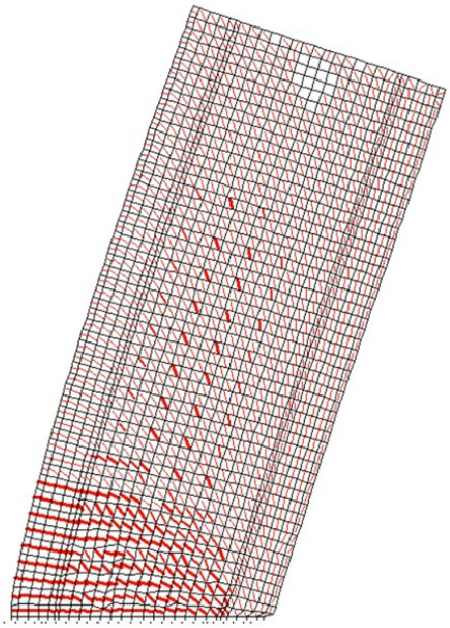

d) Wall S63 – VecTor2

Figure 6.9 - Cracking patterns and failure modes for walls tested by Tran & Wallace (2012)

6.3.3 Wall J5 Tested by Chandra (2017)

Chandra (2017) tested seven large-scale concrete shear walls with aspect ratios of 1.0 and 2.0 with flanged and barbell-shaped cross-sections. The walls were built with high-strength concrete and high-strength steel reinforcement (f_y = 630 MPa). They were tested under reversed cyclic loading and constant axial compression equal to 5% of the wall concentric axial capacity. For the purpose of this validation study, a flanged wall tested by Chandra (2017) was modelled using VecTor2. This analysis was conducted to test the ability of VecTor2 to predict the behaviour of walls with out-of-plane components. Since VecTor2 is a two-dimensional analysis software, the flanged wall was modelled as a 2D membrane. Hence, the vertical reinforcement in the flange section were modelled as longitudinal reinforcement in the boundary elements of the wall.

Figure 6.10 shows the meshed FE model of Wall J5. The model consisted of two concrete regions and two types of steel truss elements. Table 6.9 and Table 6.10 present details of the reinforcement used in the FE model. The wall was meshed using rectangular elements with a maximum size of 100 mm in both X and Y directions. The flange sections of the wall were modelled as boundary elements with the same thickness as the width of the flange section and the same longitudinal reinforcement ratio. The boundary elements consisted of 3 rectangular elements with different aspect ratios in the horizontal direction. The web section was modelled using 8 equally sized rectangular elements with 100 mm thickness in the horizontal direction, as well as 22 equally sized rectangular elements in the vertical direction. Concrete with 28-day compressive strength of 103 MPa was used to construct the model.

The lateral reversed cyclic loading was applied as a function of the support displacement and was distributed among the nodes along the top of the wall. Axial load was equal to 1000 kN (equal to approximately 5% of the concentric axial capacity of the wall) and was defined as monotonically applied downward point loads acting on selected nodes on top of the wall. The nodal loads were constant during the analysis.

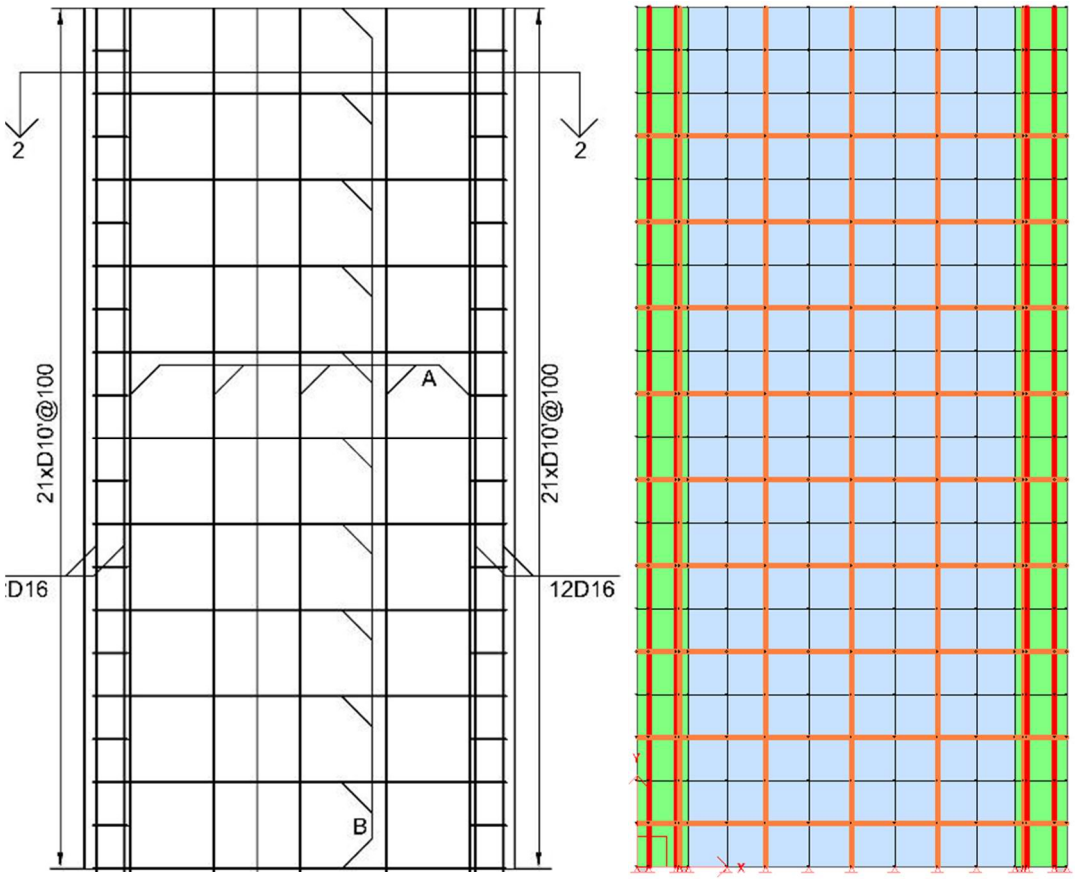

a) Wall J5 reinforcement layout b) Meshed FE model

Figure 6.10 – Details of wall J5 (Chandra, 2017)

Table 6.9 - Steel truss element details for wall J5 (Chandra, 2017)

No.	Element	Area (mm2)	d_b (mm)	f_y (MPa)	f_u (MPa)	E_s (MPa)	ε_{sh} (10^{-3} mm/mm)	ε_u (10^{-3} mm/mm)
J5	Boundary Vert.	1206	15.7	630	715	186000	20	95.2
	Web Vert.	55	6	610	637	197500	3.2	99
	Web Horiz.	55	6	610	637	197500	3.2	99

Table 6.10 - Smeared reinforcement details for modelled wall J5 (Chandra, 2017)

No.	Element	Direction (Degrees)	ρ (%)	d_b (mm)	f_y (MPa)	f_u (MPa)	E_s (MPa)	ε_{sh} (10^{-3} mm/mm)	ε_u (10^{-3} mm/mm)
J5	**Lower Boundary Elements**								
	Smeared Reinf. 1	0	0.3	10	617	709	193000	20	79
	Smeared Reinf. 2	361	1.22	10	617	709	193000	20	79

Figure 6.11 shows the comparisons of experimental and analytical hysteretic relationships. Table 6.11 summarizes the critical data obtained from experimental and analytical results. The analytical results were found to generally agree with the experimental results with some key differences. In the experiments, the maximum flexural capacity of the test wall was reached at a

drift ratio of approximately 0.4%, and this was followed by strength decay which started mainly due to the yielding of the web transverse reinforcement, which in turn led to large splitting cracks (Chandra, 2017). Crushing of the boundary elements at the base and along the height were also observed. The wall was able to undergo slightly higher displacements until the wall failure at a drift ratio of approximately 0.9%. In the FE model, the strength decay started at a drift ratio of 0.2% due to the yielding of the transverse reinforcement with the formation of large diagonal cracks in the web, as well as vertical cracks at the interface of the web and the wall flanges. As the lateral displacements continued increasing, the flexural strength of the wall increased and reached the maximum point at a drift ratio of 0.6%. This was believed to be due to the fact that the transverse reinforcing bars were undergoing strain hardening.

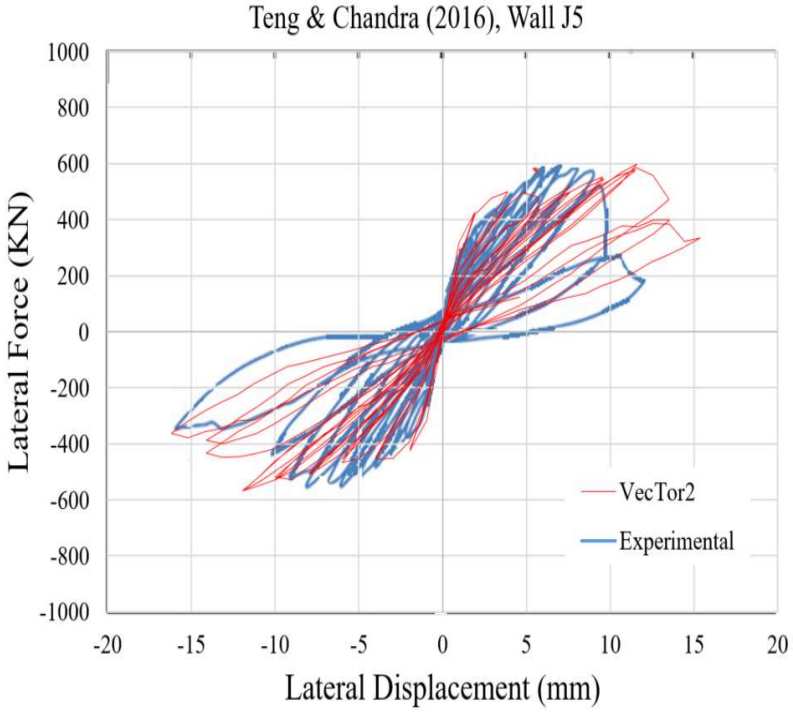

Figure 6.11 - VecTor2 results vs. experimental results for wall J5 tested by Teng & Chandra (2016)

Table 6.11 Analytical vs Experimental results for wall J5 (Teng & Chandra, 2016)

	Analytical					Experimental					
Wall Name	**F_{yield} (MPa)**	**Δ_{yield} (mm)**	**$F_{ultimate}$ (MPa)**	**$\Delta_{ultimate}$ (mm)**	**μ**	**F_{yield} (MPa)**	**Δ_{yield} (mm)**	**$F_{ultimate}$ (MPa)**	**$\Delta_{ultimate}$ (mm)**	**μ**	**$\mu_{Analytical}/\mu_{Exp.}$**
J5	495	6*	614	13	2.2*	460**	7**	596	9**	1.28	1.7

*Based on yield displacement at the initial yielding of the horizontal web reinforcement.
**Estimated from load-deflection curves and experimental yield point reported by Teng (2012)

Figure 6.12 presents a photo of the walls at the end of the test and the crack pattern observed in the FE analysis. It is shown that the general state of the wall at the end of the test was predicted with reasonable accuracy. The location of diagonal shear cracks, as well as the horizontal flexural cracks were captured effectively. It was reported that none of the vertical reinforcement yielded throughout the test, which was predicted accurately by the FE model. The yielding of horizontal web reinforcement was predicted by the FE model to at a lateral displacement of 6 mm (drift ratio = 0.3%), initiated at a height of approximately 700 mm (h/H = 0.35) from the base of the wall. Teng (2012) reported that the yielding of the horizontal reinforcement started between drift ratios of 0.2% and 0.5%.

A comparison of the experimental and analytical load-deflection diagrams indicates that the FE model was able to predict the flexural capacity of the wall with an error of 5%. In addition, the point of ultimate displacement of the wall was predicted with acceptable accuracy. Furthermore, the pinching behaviour of the wall was captured effectively. The unloading branches of the FE model had smaller slope and the wall was predicted to have smaller stiffness following the first onset of strength decay. In general, the VecTor2 FE model was found to provide a good prediction of the ultimate strength and displacements, as well the general failure mechanism of the modelled wall; however, the stiffness and strength decay were not captured accurately.

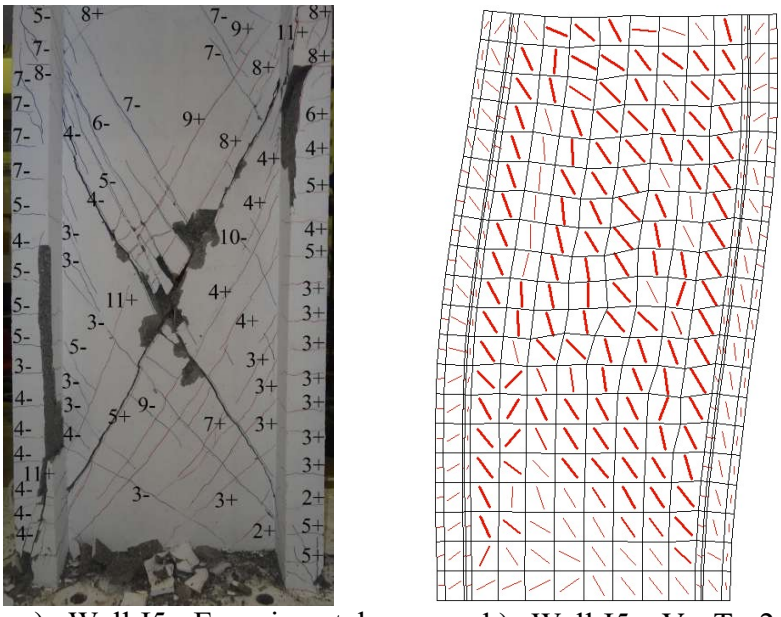

a) Wall J5 - Experimental b) Wall J5 – VecTor2

Figure 6.12 - Cracking patterns and failure modes for walls tested by Teng & Chandra (2016)

6.3.4 Navidpour (2018)

Navidpour (2018) tested three large-scale reinforced concrete shear walls under reversed cyclic loading and constant axial compression. The walls had aspect ratios of 1.5, 1.9 and 3.0, and were reinforced with conventional Grade 400 steel as flexural reinforcement. The boundary elements had Grade 500 MPa welded reinforcement grids as confinement and buckling retraining ties. Concrete with a compressive strength of 80 MPa was used in the construction of the walls. Navidpour's Wall 3 had a barbell-shaped cross-section with 250mm x 250mm boundary elements and a 100mm thick web section. This wall was tested under constant axial load and reversed cyclic loading and was used as the control specimen for Wall 1HS tested in the current investigation. This wall was modelled as part of the preliminary design and analysis that was conducted to develop the design of wall W1HS. This section presents an evaluation of the analytical results obtained from VecTor2 model in comparison to the experimental results obtained by Navidpour (2018).

The FE model consisted of 4 concrete regions that were used to define the boundary elements, web section, foundation and a stiff loading section at the top of the wall as shown in Figure 6.13. Table 6.12 and Table 6.13 provide details of the truss elements and the smeared reinforcement used in the FE model. The reinforcement properties, including the stress-strain relationship for 10M bars and the reinforcement details for the foundation unit were assumed as indicated in Table 6.13, because this information was not available. Concrete with compressive strength of 82 MPa was used to model the wall. The wall mesh consisted of rectangular and hybrid elements with a maximum size of 100 mm in both X and Y directions. The hybrid elements were only used in modelling the foundation where rectangular elements could not be used due to the space constraints. The boundary elements consisted of 4 elements in the horizontal direction. The web section was meshed using 10 elements in the horizontal direction. The size of the elements in the horizontal direction was not uniform due to the irregular spacings of the steel truss elements. The height of the wall consisted of 42 elements with approximately the same size.

The lateral reversed cyclic loading was applied as support displacement and was distributed among the nodes along the top of the wall. Axial load was equal to 1500 kN (equal to approximately 10% of the concentric axial load capacity of the wall) and was defined as monotonically-applied downward point loads acting on selected nodes at the top of the wall. The nodal loads were constant

during the analysis. The foundation of the wall was fixed against translation in X and Y directions along its base, as shown in Figure 6.13. Figure 6.14 compares the analytical prediction obtained from the VecTor2 analysis with the experimental results obtained by Navidpour (2018). The prediction appears to agree very well with the experimental results with only minor discrepancies. The flexural strength of the wall is predicted with high accuracy and the loading and unloading branches appear to match very closely to those of the experimental curves. Pinching of the hysteretic curves is slightly overestimated but it is effectively captured for the purpose of this analysis. The strength decay in the final cycles of loading in both the negative and positive directions is predicted accurately. This is deemed to be due to the crushing of the web section as shown in Figure 6.15 (b).

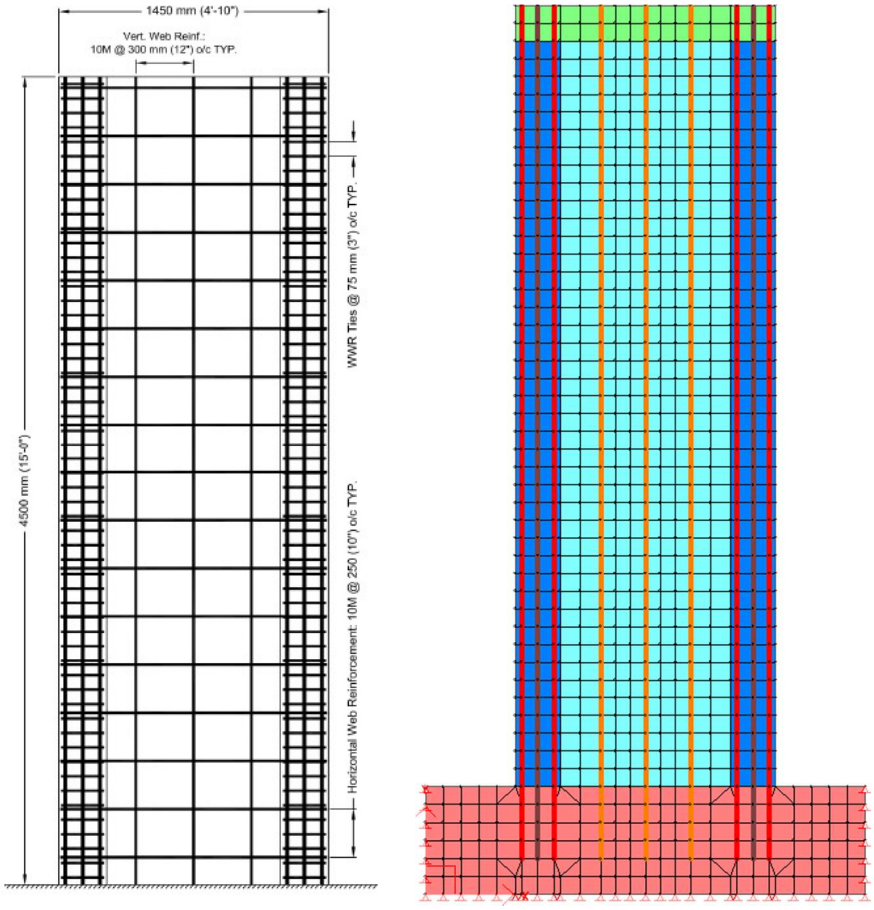

a) Reinforcement layout b) Meshed FE model

Figure 6.13 - Details of Wall 3 (Navidpour, 2018)

Table 6.12 - Steel truss element details for Wall 3 (Navidpour, 2018)

No.	Element	Area (mm^2)	d_b (mm)	f_y (MPa)	f_u (MPa)	E_s (MPa)	ε_{sh} (10^{-3} mm/mm)	ε_u (10^{-3} mm/mm)
Wall 3	Boundary Vert. (Corner)	600	16	471	710	200000	16	115
	Boundary Vert. (center)	400	16	471	710	200000	16	115
	Web Vert.	200	11.3	471	710	200000	16	115

Table 6.13- Steel truss element details for Wall 3 (Navidpour, 2018)

No.	Element	Direction (Degrees)	ρ (%)	d_b (mm)	f_y (MPa)	f_u (MPa)	E_s (MPa)	ε_{sh} (10^{-3} mm/mm)	ε_u (10^{-3} mm/mm)
Wall 3	**Boundary Elements**								
	Smeared Reinf. 1	0	1.136	9.5	550	640	200000	2.8	55
	Smeared Reinf. 2	361	1.136	9.5	550	640	200000	2.8	55
	Smeared Reinf. 2	0	0.8	11.3	436	588	200000	16.4	145*
	Web Section								
	Smeared Reinf. 1	0	0.8	11.3	436	588	200000	16.4	145*
	Loading Section								
	Smeared Reinf. 1	0	1.6	11.3	436	588	200000	16.4	145*
	Foundation								
	Smeared Reinf. 1	0	1.2	35	450	650	200000	15	140*
	Smeared Reinf. 2	361	1.5	25	450	650	200000	15	140*
	Smeared Reinf. 2	90	0.5	25	450	650	200000	15	140*

*Assumed values.

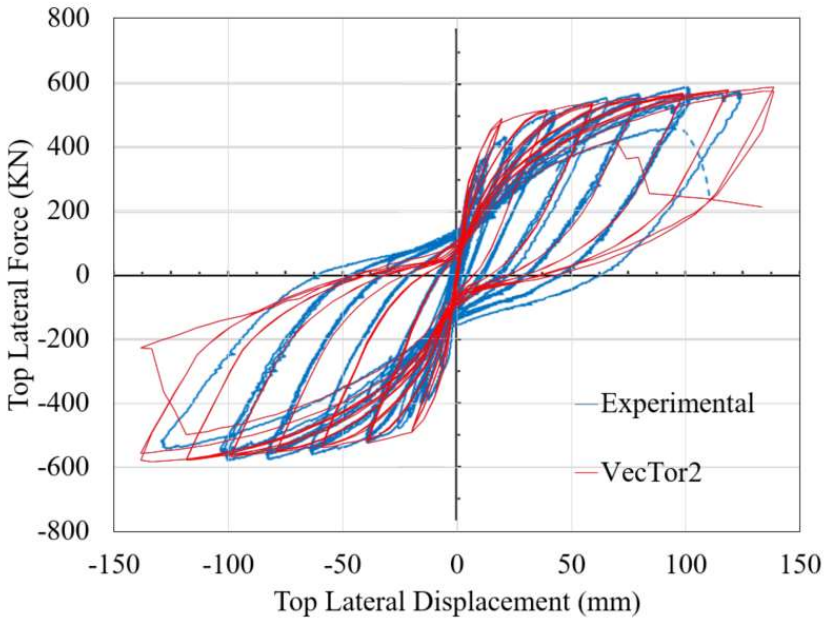

Figure 6.14 - VecTor2 results vs. experimental results for Wall 3 (Navidpour, 2018)

It is observed that the predicted initial stiffness of the wall matches the experimental results up to the cracking point of the wall; however, the stiffness of the wall is slightly overestimated between

the cracking and yield points. The analytical stiffness of the wall appears to match the experimental results between the yield pint and wall failure. This was also observed for the walls tested by Tran & Wallace (2012). The predicted displacement ductility of the wall was overestimated by approximately 11% and 8% in the positive and negative loading directions. In addition, the ductility ratios of the wall in positive and negative loading directions were predicted with 3% and -1.5% difference. Table 6.14 presents a comparison of the analytical and experimental ductility ratios for Wall 3.

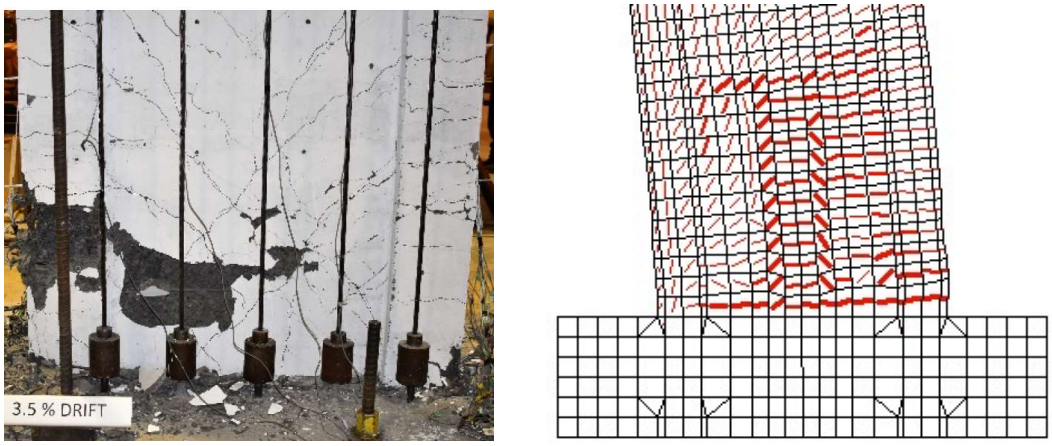

a) Wall 3 - Experimental b) Wall 3 – VecTor2 prediction

Figure 6.15 – Cracking, damage, and failure modes for Wall 3 (Navidpour, 2018)

Table 6.14 Analytical vs Experimental results for Wall 3 (Navidpour, 2018)

	Analytical					Experimental					
Wall Name	F_{yield}	Δ_{yield}	$F_{ultimate}$	$\Delta_{ultimate}$	μ	F_{yield}	Δ_{yield}	$F_{ultimate}$	$\Delta_{ultimate}$	μ	$\mu_{Analytical}/\mu_{Exp.}$
Wall 3 (+ve)	487	16.9	577	138	7	400	18	574	124	6.8	1.03
Wall 3 (-ve)	489	16.9	577	138	7	405	18	545	128	7.1	0.99
										Average	1.01

The analytical predictions presented above are within the acceptable range for the purpose of model validations. However, the failure mechanism of the wall was predicted to be via rupturing of the longitudinal reinforcement. The tested wall failed due to the buckling of the boundary element longitudinal reinforcements. This discrepancy may be explained by the fact that 100% of the vertical reinforcement of Wall 3 was spliced at the base of the wall. Although this is permitted by the ACI 318-94 design code (ACI 318 1994), it results in higher stiffness within the spliced region of the wall, which shifts the plastic hinge upwards, similar to what was observed in Wall 3

by Navidpour (2018). As a result, the compressive stresses in the longitudinal reinforcement at the new plastic hinge region of the wall exceeded the buckling threshold and the wall failed due to the buckling of boundary element longitudinal reinforcement. However, the wall was modelled without the reinforcement lap splices to maintain simplicity.

As a summary, the FE numerical validation study presented in this section consisted of modeling 7 walls previously tested by other researchers to evaluate the ability of the VecTor2 modelling approach to predict the structural response of reinforced concrete walls with varying design parameters. The modelled walls were selected based on their aspect ratio (H/L), cross-sectional shape, steel type, and failure mode. Walls with rectangular, barbell-shaped and flanged cross-sections were modelled. The reinforcement types consisted of conventional Grade 400 MPa reinforcement as well as high-strength reinforcement lacking a defined yield plateau. Concrete strengths varied between 30 MPa and 103 MPa. The default constitutive material models were used to model the walls with the exception of the concrete pre-peak stress-strain response. To better capture concrete response in compression, the Popovic Normal Strength Concrete (NSC) and High-Strength Concrete (HSC) models were used in wall analyses. In addition, the response of steel reinforcement having varying grades was modelled using a simplified tri-linear stress-strain relationship.

The following conclusions are drawn from the validation study presented above:

1) VecTor2 FE models generally provide very accurate predictions for the hysteretic behaviour of reinforced concrete walls;
2) The initial stiffness of walls is generally slightly over-estimated between cracking and yielding points. The secant stiffness of the predicted results was found to match closely for displacements between the yield and ultimate points;
3) VecTor2 generates more accurate results when shear stresses are low. Shear stress is higher for walls with smaller aspect ratios for which shear demand is higher. It is found that the accuracy of VecTor2, despite being generally acceptable, is lower for walls with smaller aspect ratios or higher shear stresses;
4) VecTor2 may not be the best tool for predicting the behaviour of flanged walls. VecTor2 is a two-dimensional analysis software. Walls are modelled using 2D membrane elements which may not be suitable for out-of-plane components (i.e., wall flanges);

5) VecTor2 was found to generate accurate predictions for the loading and unloading branches of flexure-dominant walls;
6) VecTor2 was found to predict the flexural strength, stiffness, and ductility of flexure-dominant walls with high accuracy;
7) VecTor2 was found to predict the behaviour of rectangular and barbell-shaped walls with similar accuracy;
8) Concrete strength and steel type and grade did not appear to impact the accuracy of the analytical results obtained from VecTor2 analysis;
9) Failure modes were predicted accurately in the VecTor2 analysis of walls.

6.4 Finite Element Models of Wall W1HS and W2HS

The walls were modelled using VecTor2 software using as-built details and material properties obtained from the laboratory tests. The material models presented in Section 6.2 were used to model the walls. Popovic's HSC model with f'_c = 80 MPa was used for the concrete. The Grade 690 MPa ASTM A1035 steel was modelled using the Ramberg-Osgoode (1943) stress-strain model as described in Chapter 3. This customized model (designated as the MMFX steel model) was added to the software's material library by VecTor's developers for the purpose of a previous research project at the University Ottawa.

The FE model consisted of 4 concrete regions as shown in Figure 6.16 that were used to define (1) the boundary elements, (2) the web section, (3) the stiff loading section at the top of the wall, and (4) the foundation. In addition, structural steel properties were used in modelling the loading setup for Wall W2HS. The FE mesh consisted of rectangular and hybrid elements with a maximum size of 100 mm in both X and Y directions for both walls. The hybrid elements were only used in the foundation where rectangular elements could not be used due to the space constraints.

The lateral reversed cyclic loading was applied as a function of support displacement and was distributed among the nodes along the top of the walls. The lateral load increments were selected to match the experimental loading protocol as close as possible. The walls were cycled three times at each displacement stage, which was equal to 0.2% drift ratio up 1.0% drift ratio and 0.5% up to the wall failure (refer to the loading protocol diagram in Chapter 4).

The foundation units of both walls were restrained against movement in both horizontal and vertical directions at locations that corresponded to the locations of the bolts that anchored the foundations to the strong floor.

6.4.1 Wall W1HS Finite Element Model

Figure 6.16 (b) shows details of the meshed FE model used for wall W2HS. The boundary elements consisted of 4 elements in the horizontal direction. The web section was meshed using 10 elements in the horizontal direction. The size of the elements in the horizontal direction was not uniform due to the irregular spacings of the steel truss elements. The height of the wall consisted of 42 elements having approximately the same size. The foundation of the wall was fixed against translation in X and Y directions along its base.

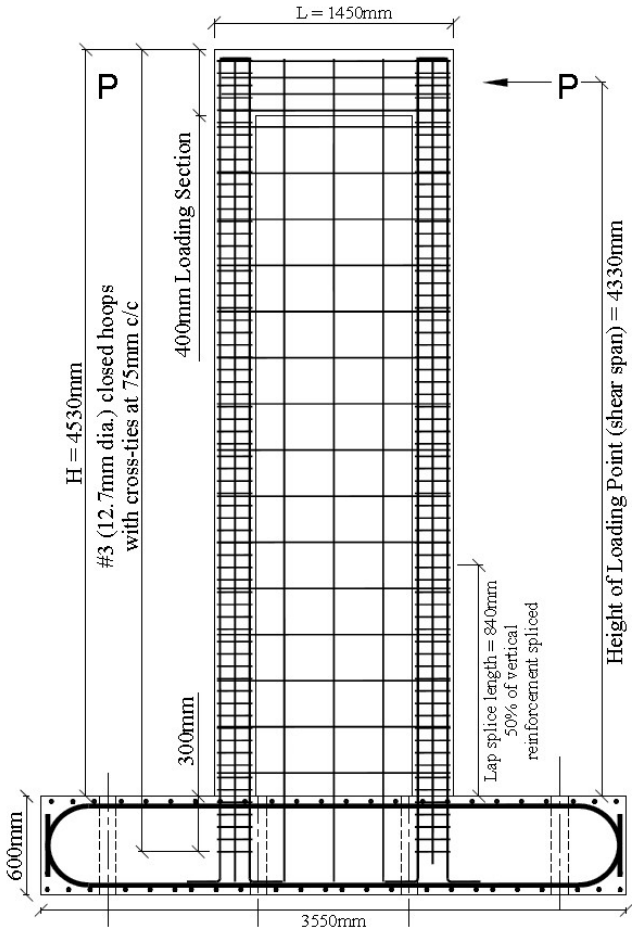

a) Wall W1HS as-built reinforcement layout

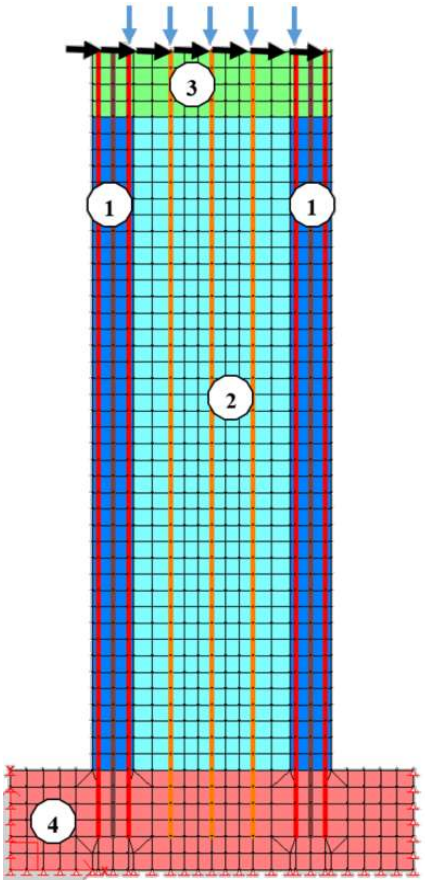

(1) Boundary Elements, (2) Web Section,
(3) Loading Section, (4) Foundation

b) Wall W1HS meshed FE model

Figure 6.16 – Wall W1HS details

Axial load was equal to 1300 kN (equal to approximately 8% of the concentric load capacity of the wall) and was defined as monotonically applied downward point loads acting on selected nodes on top of the wall, as illustrated in Figure 6.16. The selected nodes represented the locations of the actual axial loading applied on the beam along the top of the wall. The nodal loads were constant during the analysis. A separate analysis was conducted with the axial loads modelled as prestressing cables to simulate the exact axial loading mechanism. This resulted in a complex model with a large number of independent nodes. The results were found to be very similar to the FE model presented in this section for Wall W1HS. Hence, to maintain simplicity and in order to enhance the speed of analysis, nodal loads were used for modelling the compressive axial loads for Wall W1HS. Steel truss element details used for modelling Wall W1HS are shown in Table 6.15 and Table 6.16.

Table 6.15 - Steel truss element details for wall W1HS

No.	Element	Area (mm^2)	d_b (mm)	f_y (MPa)	f_u (MPa)	E_s (MPa)	ε_{sh} (10^{-3} mm/mm)	ε_u (10^{-3} mm/mm)
W1HS	Boundary Vert. (Corner)	387	12.7	860	1135	190000	10	66
	Boundary Vert. (center)	254	12.7	860	1135	190000	10	66
	Web Vert.	142	9.5	925	1202	190000	11	56

Table 6.16 - Steel truss element details for wall W1HS

No.	Element	Direction (Degrees)	ρ (%)	d_b (mm)	f_y (MPa)	f_u (MPa)	E_s (MPa)	ε_{sh} (10^{-3} mm/mm)	ε_u (10^{-3} mm/mm)
W1HS	**Bounadry Elements**								
	Smeared Reinf. 1	0	1.136	9.5	925	1202	190000	11	56
	Smeared Reinf. 2	361	1.136	9.5	925	1202	190000	11	56
	Smeared Reinf. 2	0	0.5	9.5	925	1202	190000	11	56
	Web Section								
	Smeared Reinf. 1	0	0.51	9.5	925	1202	190000	11	56
	Loading Section								
	Smeared Reinf. 1	0	1.5	9.5	925	1202	190000	11	56
	Foundation								
	Smeared Reinf. 1	0	1.2	35	450	650	200000	15	140
	Smeared Reinf. 2	361	2	25	450	650	200000	15	140
	Smeared Reinf. 2	90	0.5	25	450	650	200000	15	140

Figure 6.17 presents the analytical hysteretic curves obtained from the VecTor2 FE model for Wall W1HS. The analytical hysteretic curves are compared with the experimental results in Figure 6.18 and Figure 6.19 after the failure in the positive loading direction and at the end of the test, respectively. The analytical response predicted by Vecor2 FE analysis was found to agree very

well with the experimental results. Almost all the comparison parameters, including the initial stiffness, secant stiffness at cracking, yield and ultimate load stages, flexural strength, slopes of the loading and unloading branches, and displacement ductility of the analytical hysteretic curves matched, almost perfectly, those of the experimental results. Pinching of the wall was also captured accurately in general, with minor discrepancies at the end of 1.5% and 2.0% drift stages. The unloading branches were 'pinched' abruptly as the load returned to near zero. Analysis of the wall strain data indicates that some of the web vertical reinforcement were still within their 'yielding region'; therefore, as the wall was unloaded and the lateral resistance was small enough, the partially elastic vertical reinforcing bars tried to re-center the wall.

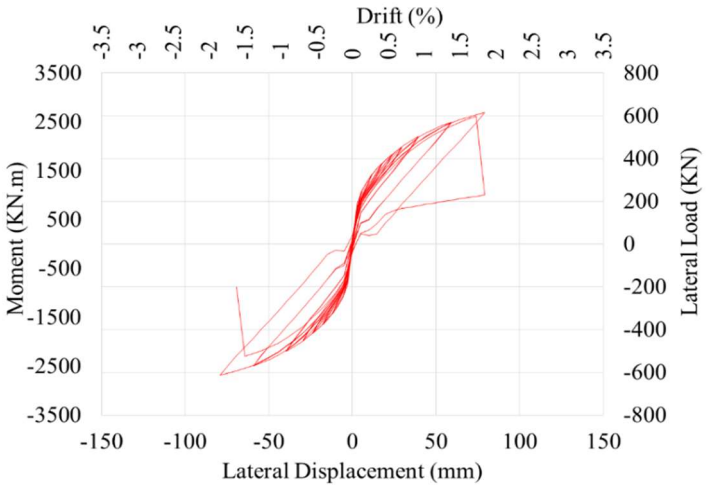

Figure 6.17 – Wall W1HS analytical hysteretic curves predicted by VecTor2

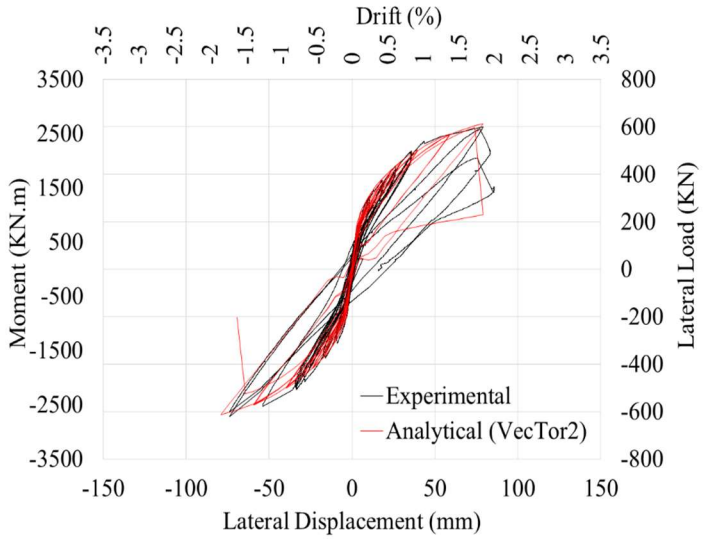

Figure 6.18 – Comparison of analytical and experimental hysteretic curves for wall W1HS after failure in the positive loading direction

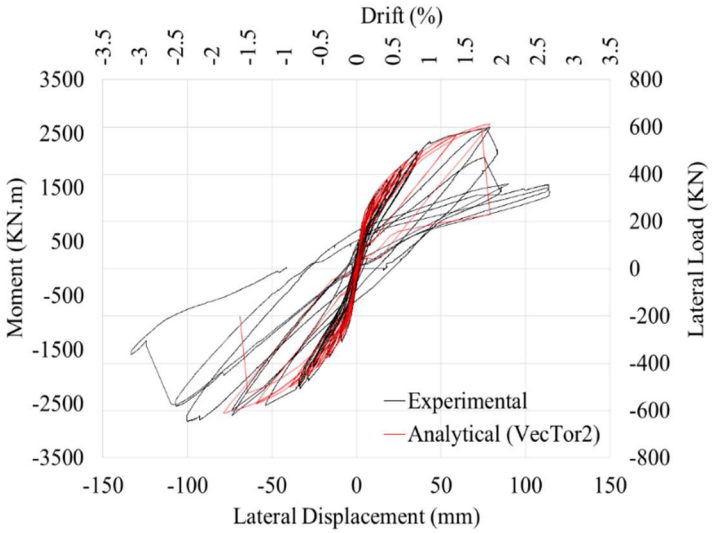

Figure 6.19 – Comparison of analytical and experimental hysteretic curves for wall W1HS after failure in the negative loading direction (end of testing)

The FE model uses a perfectly symmetrical representation of Wall W1HS. As a result, the response of the wall is symmetrical in both the positive and negative loading directions. However, in the experiments, the response of the wall in the negative loading direction was found to be different from the positive loading direction. The wall experienced further displacements and failed at a displacement of 108 mm corresponding to a drift ratio of 2.5%. This behaviour was likely due to the reduction in the stiffness of the wall following the rupture of the flexural bars in the positive direction. In addition, non-symmetric construction and/or loading conditions could have contributed to the additional displacement ductility in the negative direction.

Table 6.17 provides a further comparison of the key analytical and experimental results for Wall W1HS. The yield points presented in this table are based on actual yield points of the wall, which were calculated based on the reinforcement yield strains obtained from the 0.2% offset method, as described in Chapter 3. The analytical and experimental ductility levels of the wall match almost perfectly in the positive direction. In the negative direction, the ductility of the wall is underestimated by approximately 27%.

Figure 6.20 presents a comparison between the analytical and experimental reinforcement strains at cracking, onset of yielding (nominal yield point), and the first bar rupture for positive and negative loading directions. As shown, the analytical strains are in very good agreement with the experimental results. The assumption that VecTor2 can provide accurate verification of

experimental results for Wall W1HS and the accurate prediction of reinforcement strains, form the basis for the parametric study presented in the following sections.

Table 6.17 Analytical vs Experimental results for wall W1HS

	Analytical					Experimental					$\mu_{Analytical}/\mu_{Exp.}$
Wall Name	F_{yield}	Δ_{yield}	$F_{ultimate}$	$\Delta_{ultimate}$	μ	F_{yield}	Δ_{yield}	$F_{ultimate}$	$\Delta_{ultimate}$	μ	
W1HS (+ve)	489	37.1	614	79	2.1	492	37.3	592	78	2.1	1.00
W1HS (-ve)	489	37.1	613	79	2.1	510	36.3	575	108	2.9	0.72

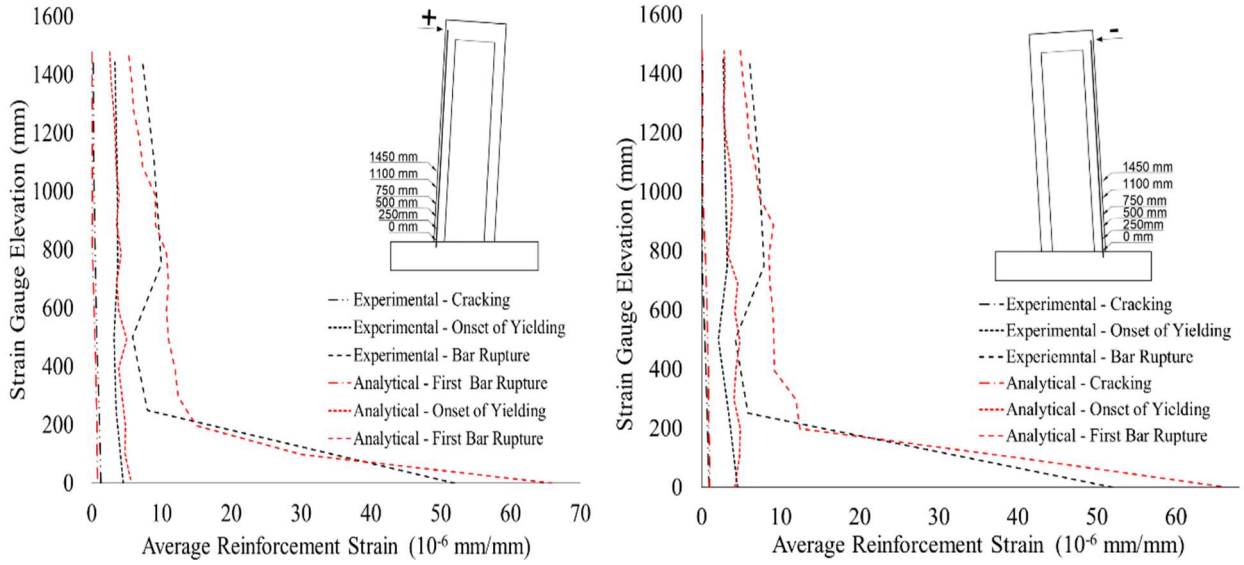

a) Positive loading direction b) Negative loading direction

Figure 6.20 - Comparison of analytical and experimental reinforcement strains

6.4.2 Wall W2HS Finite Element Model

Figure 6.21 (b) shows details of the meshed FE model used for wall W2HS. The boundary elements consisted of 5 elements in the horizontal direction. The web section was meshed using 10 elements in the horizontal direction. The size of the elements in the horizontal direction was not uniform due to the irregular spacings of the steel truss elements. The height of the wall consisted of 33 elements with similar sizes, which included the loading setup and the over-reinforced top loading section of the wall. The foundation of the wall was fixed against translation in the X and Y direction along its base.

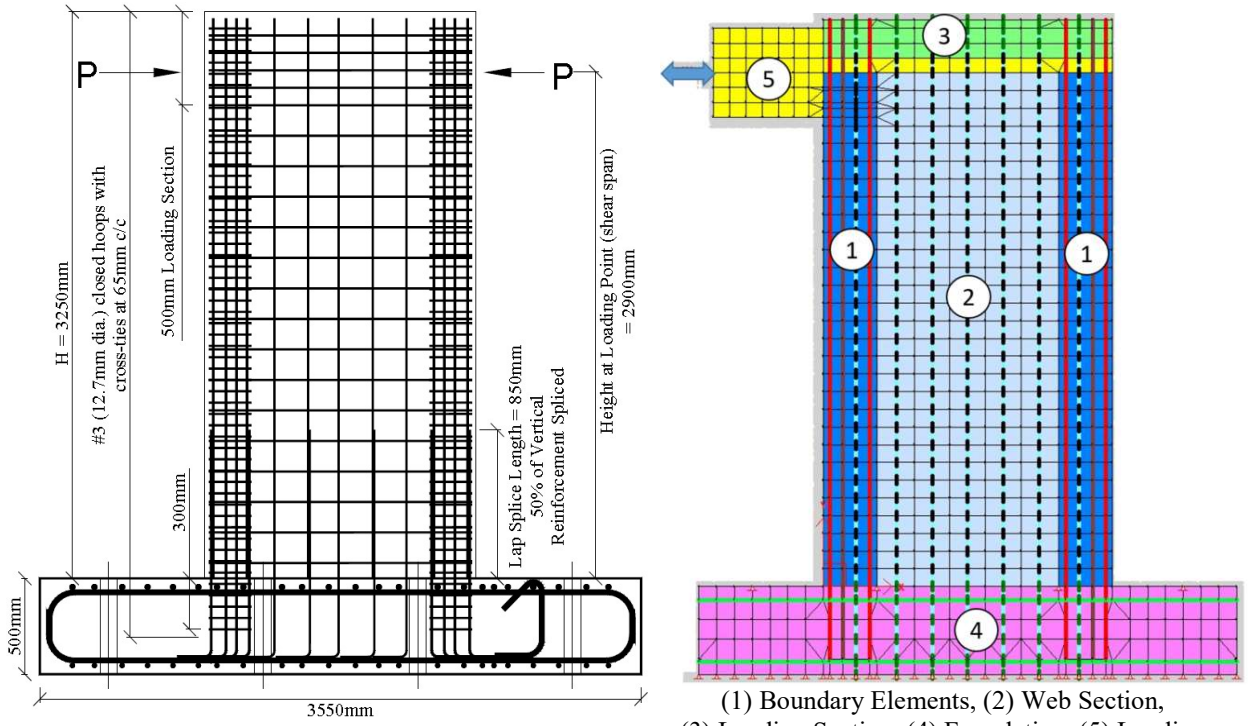

a) Wall W2HS as-built reinforcement layout

(1) Boundary Elements, (2) Web Section, (3) Loading Section, (4) Foundation, (5) Loading Setup

b) Wall W2HS meshed FE model

Figure 6.21 – Wall W2HS details

Axial load was equal to 1500 kN (equal to approximately 7% of the concentric axial capacity of the wall). Wall W2HS was modelled with and without the pre-stressing cables and the results were compared. It was found that, as the wall was longer compared to wall W1HS, the effect of the pre-stressing cables on the analytical results were higher. Hence, instead of applying point loads, the axial load was applied using pre-stressed cables. The cables were stressed to a tensile strain of approximately 3.7 mm/mm, which resulted in an axial load of approximately 1500 kN. A pre-defined pre-stressing material model was used for modelling the stress-strain behaviour of the 7-wire strand pre-stressing cables. In addition, in order to obtain more accurate results, the loading setup used for applying the lateral load at the top of the wall was also modelled. This consisted of a 250 mm wide loading beam as well as a 350 mm wide actuator head. This was done to ensure that the effect of the vertical component of the actuator on wall response wall captured. Steel truss element details used for modelling Wall W2HS are shown in Table 6.18 and Table 6.19.

Table 6.18 - Steel truss element details for wall W2HS

No.	Element	Area (mm^2)	d_b (mm)	f_y (MPa)	f_u (MPa)	E_s (MPa)	ε_{sh} (10^{-3} mm/mm)	ε_u (10^{-3} mm/mm)
W2HS	Boundary Vert. (Corner)	387	12.7	857	1132	190000	10	71
	Boundary Vert. (center)	258	12.7	857	1132	190000	10	71
	Web Vert.	142	9.5	936	1212	190000	11	58
	Pre-stressing	133	13	1300	1860	205000	6.5	140
	Foundation – Longitudinal	9800	35.7	450	650	200000	10	150

Table 6.19 - Steel truss element details for wall W2HS

No.	Element	Direction (Degrees)	ρ (%)	d_b (mm)	f_y (MPa)	f_u (MPa)	E_s (MPa)	ε_{sh} (10^{-3} mm/mm)	ε_u (10^{-3} mm/mm)
W2HS	**Bounadry Elements**								
	Smeared Reinf. 1	0	1.09	9.5	936	1212	190000	11	58
	Smeared Reinf. 2	361	1.46	9.5	936	1212	190000	11	58
	Smeared Reinf. 2	0	0.46	9.5	936	1212	190000	11	58
	Web Section								
	Smeared Reinf. 1	0	0.46	9.5	936	1212	190000	11	58
	Loading Section								
	Smeared Reinf. 1	0	0.8	9.5	936	1212	190000	11	58
	Foundation								
	Smeared Reinf. 2	361	1.2	25	450	650	200000	15	140
	Smeared Reinf. 2	90	0.5	25	450	650	200000	15	140

Figure 6.22 presents the analytical hysteretic curves obtained from the VecTor2 FE model for Wall W2HS. Figure 6.23 compares the analytically produced hysteresis curves with experimental results adjusted for anchorage slip, as described in Chapter 5. The results were found to be in a reasonably good agreement in general. The overall stiffness of the wall, the slopes of the loading and unloading curves and the overall pinching behaviour were captured effectively.

Despite the flexural strength of the wall was predicted well in general, it was slightly underestimated between the lateral drift ratio of 0.6% and the bar rupture point (at 1.4% drift ratio). The flexural strength of the wall was underestimated by approximately 8% in the positive loading direction and 12% in the negative loading direction. This is generally considered to be acceptable; however, it is believed that this inaccuracy is likely caused by the additional displacement that Wall W2HS had to undergo as a result of the anchorage slip described in Chapter 5. In addition, lateral drift capacity of the wall was underestimated by approximately 20%.

Figure 6.24 compares the analytical results to the hysteretic curves that were corrected using the recorded strains in the longitudinal reinforcement and an anchorage slip model developed by Alsiwat and Saatcioglu (1992). This correction method was described in Section 5.2.5.4. The analytically predicted displacement and the drift capacity of the wall matches more closely using this approximation.

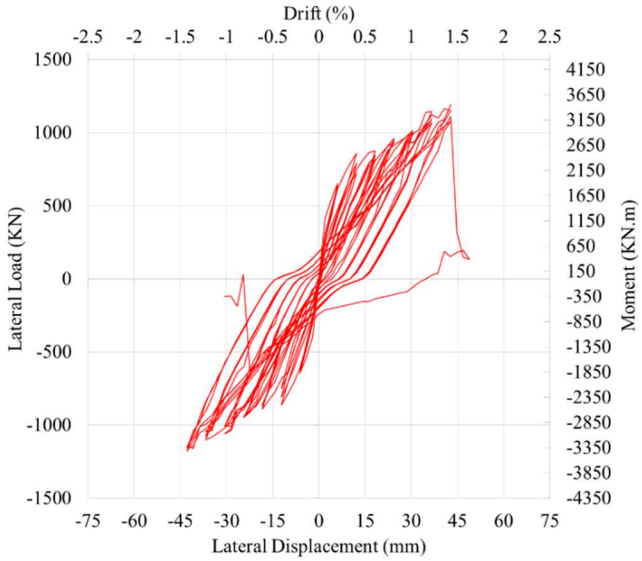

Figure 6.22 – Wall W1HS analytical hysteretic curves predicted by VecTor2

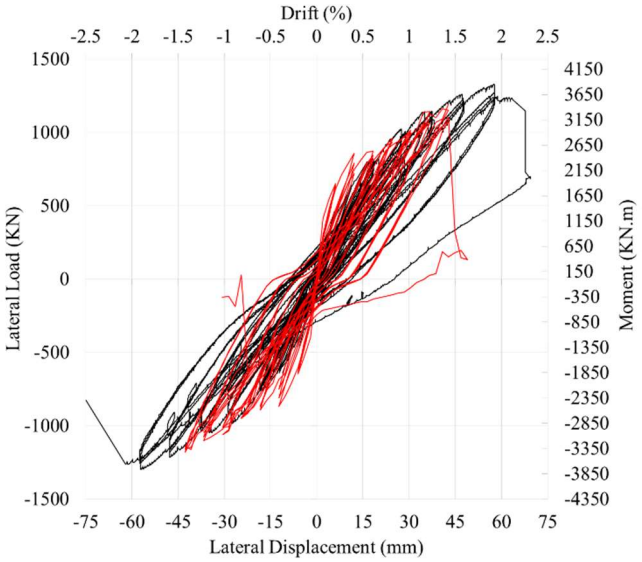

Figure 6.23 – Comparison of analytical and experimental hysteretic curves for wall W1HS after failure in the positive loading direction

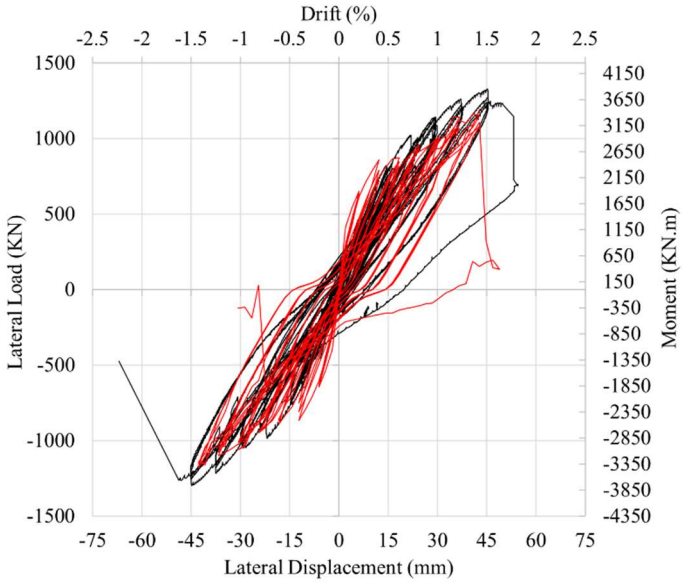

Figure 6.24 – Comparison of analytical and experimental hysteretic curves for wall W1HS after failure in the positive loading direction (corrected using recorded steel strains and anchorage model developed by Alsiwat and Saatcioglu, 1992)

Table 6.20 provides a further comparison of the key analytical and experimental results for Wall W2HS. The yield points presented in this table are based on actual yield points of the wall which were calculated based on the reinforcement yield strains obtained from the 0.2% offset method, as described in Chapter 3. It is shown that the analytical and experimental ultimate displacements match almost perfectly. The yield displacements were slightly overestimated. The ratio of the analytical ductility ratio to experimental ductility ratio ($\mu_{Analytical}$ /$\mu_{Exp.}$) was found to be 0.91 and 0.88 in the positive and negative loading directions, respectively.

Table 6.20 Analytical vs. Experimental results for Wall W2HS

	Analytical					Experimental					
Wall Name	**F_{yield}**	**Δ_{yield}**	**$F_{ultimate}$**	**$\Delta_{ultimate}$**	**μ**	**F_{yield}**	**Δ_{yield}**	**$F_{ultimate}$**	**$\Delta_{ultimate}$**	**μ**	**$\mu_{Analytical}$ /$\mu_{Exp.}$**
W2HS (+ve)	867	20	1122	41.4	2.1	872	21	1224	61.5	2.9	0.72
W2HS (-ve)	872	20	1098	41.4	2.1	834	20	1253	61	3.1	0.68

6.5 Analytical Parametric Investigation

6.5.1 Objectives and Scope

An analytical parametric study was conducted using Finite Element modelling to investigate the effect of different parameters, including; wall aspect ratio, steel type/grade, and concrete strength

using the analytical model for Wall W1HS. Other wall parameters and properties were kept the same as those for Wall W1HS. Steel reinforcement ratios were modified for different types of steel to obtain an equivalent flexural strength as described in Section 6.5.3. Table 6.21 provides a list of walls modelled as part of this parametric study. The FE model described in Section 6.4 was used to model and analyse Wall W1HS with varying parameters. The *aspect ratio* parametric study consisted of modifying the height of Wall W1HS to obtain aspect ratios of 1.0, 2.0 and 4.0. The model presented in Section 6.4 was used for the case of aspect ratio of 3.0. The properties of the steel reinforcement used in the *steel type* parametric study are provided in Section 6.5.3. The stress-strain data for the different types of steel used were obtained from the existing literature. The steel materials were selected to cover a wide range of reinforcing steel properties in terms of ductility, strength, and the ratio of ultimate tensile strength to yield strength of reinforcement. In addition, the steel materials included stress-strain curves with and without a well-defined yield point and a yield plateau.

Table 6.21 – Details of FE models analyses

Analysis Type	Wall No.	Aspect Ratio	Steel Type	Steel Grade	Concrete Strength
Aspect Ratio	W1HS-AR1	1	ASTM A1035	690	80
	W1HS-AR2	2	ASTM A1035	690	80
	W1HS-AR3	3	ASTM A1035	690	80
	W1HS-AR4	4	ASTM A1035	690	80
Steel Type	W1HS-A1035	3	ASTM A1035	690	80
	W1HS-A615	3	ASTM A615	400	80
	W1HS-A706	3	ASTM A706	550	80
	W1HS-A955	3	ASTM A955	550	80
	W1HS-500E	3	AS/NZD 500E	500	80
	W1HS-USD685	3	USD685	685	80
Concrete Strength	W1HS-fc35	3	ASTM A1035	690	35
	W1HS-fc60	3	ASTM A1035	690	60
	W1HS-fc80	3	ASTM A1035	690	80
	W1HS-fc120	3	ASTM A1035	690	120
	W1HS-fc150	3	ASTM A1035	690	150

In order to investigate the impact of the selected parameters on plastic hinge length of the modelled walls, the local curvature of the walls was obtained from the FE analyses and used to calculate the plastic hinge length, l_p, using conventional idealized plastic hinge analysis method, illustrated in Figure 6.25. The base curvatures at yield (ϕ_y) and ultimate loads (ϕ_u) were calculated by assuming

that plane sections before bending remain plane after bending, and by dividing the difference in the steel strains in the tension (ε_{yt} and ε_{ut}) and compression reinforcement (ε_{yc} and ε_{uc}) by distance between them (d_s). This is shown in Equation 6.1 and Equation 6.2. The plastic hinge length, l_p, was then calculated by equating the ultimate displacement obtained from the FE analysis to Equation 6.3. The plastic rotation of the wall was calculated using Equation 6.4. The resulting plastic hinge lengths are presented and discussed in the following sections.

$$\phi_y = \frac{\varepsilon_{yt} - \varepsilon_{yc}}{d_s} \qquad \text{Equation 6.1}$$

$$\phi_u = \frac{\varepsilon_{ut} - \varepsilon_{uc}}{d_s} \qquad \text{Equation 6.2}$$

$$\Delta_u = \frac{\phi_y l^2}{3} + \theta_p \left(l - \frac{l_p}{2}\right) \qquad \text{Equation 6.3}$$

$$\theta_p = (\phi_u - \phi_y) l_p \qquad \text{Equation 6.4}$$

where ε_{yt} is the yield strain of steel on the tension side of the wall, ε_{yc} is the yield strain of steel on the compression side of the wall, d_s is the horizontal distance between the reinforcing bars considered, ε_{ut} is the ultimate strain of steel at the onset of bar rupture in the tension side of the wall, ε_{uc} is the ultimate strain of steel at the onset of bar rupture in the compression side of the wall, ϕ_y is the base curvature at the lateral displacement corresponding to the onset of yielding in the boundary element longitudinal reinforcement, ϕ_u is the base curvature at the onset of the boundary element longitudinal reinforcement rupture, and θ_p is the plastic rotation of the wall.

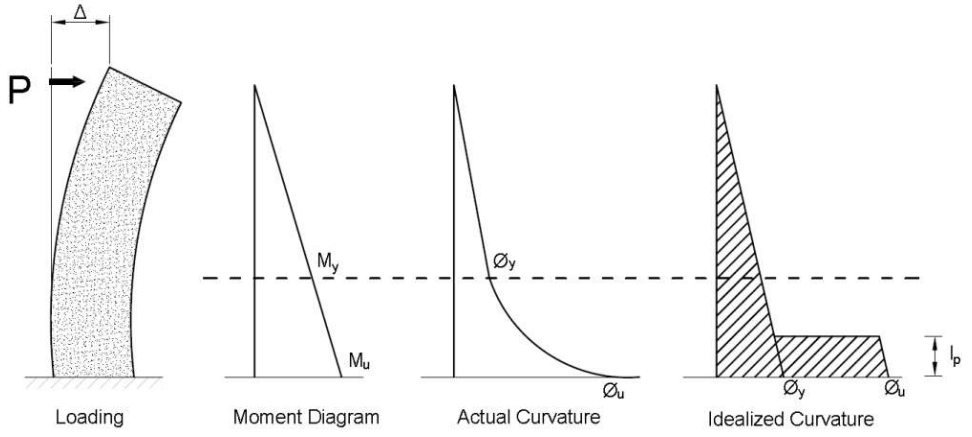

Figure 6.25 - Conventional idealized plastic hinge analysis

6.5.2 Effect of Aspect Ratio on Wall W1HS

Figure 6.26 shows the hysteretic curves for Wall W1HS modelled with different aspect ratios (AR = H/L). As expected, the wall with AR = 1.0 exhibited a shear–dominant response. The cracking pattern indicates that the wall sustained damage due to large diagonal cracks in the web and eventually failed as a result of strength decay due to web crushing. Walls with aspect ratios of 2.0, 3.0, and 4.0 exhibited a flexure-dominant response and failed due to the rupture of the boundary element longitudinal reinforcement.

Table 6.22 presents the ductility ratios ($\mu = \Delta_u/\Delta_y$) for the walls modelled with different aspect ratios. The ultimate drift ratio and the ductility ratio of the walls are plotted with respect to the aspect ratio of the walls in Figure 6.27. It is shown that increasing the aspect ratio of wall W1HS increases its drift capacity. A similar trend is observed for the ductility ratio of the walls.

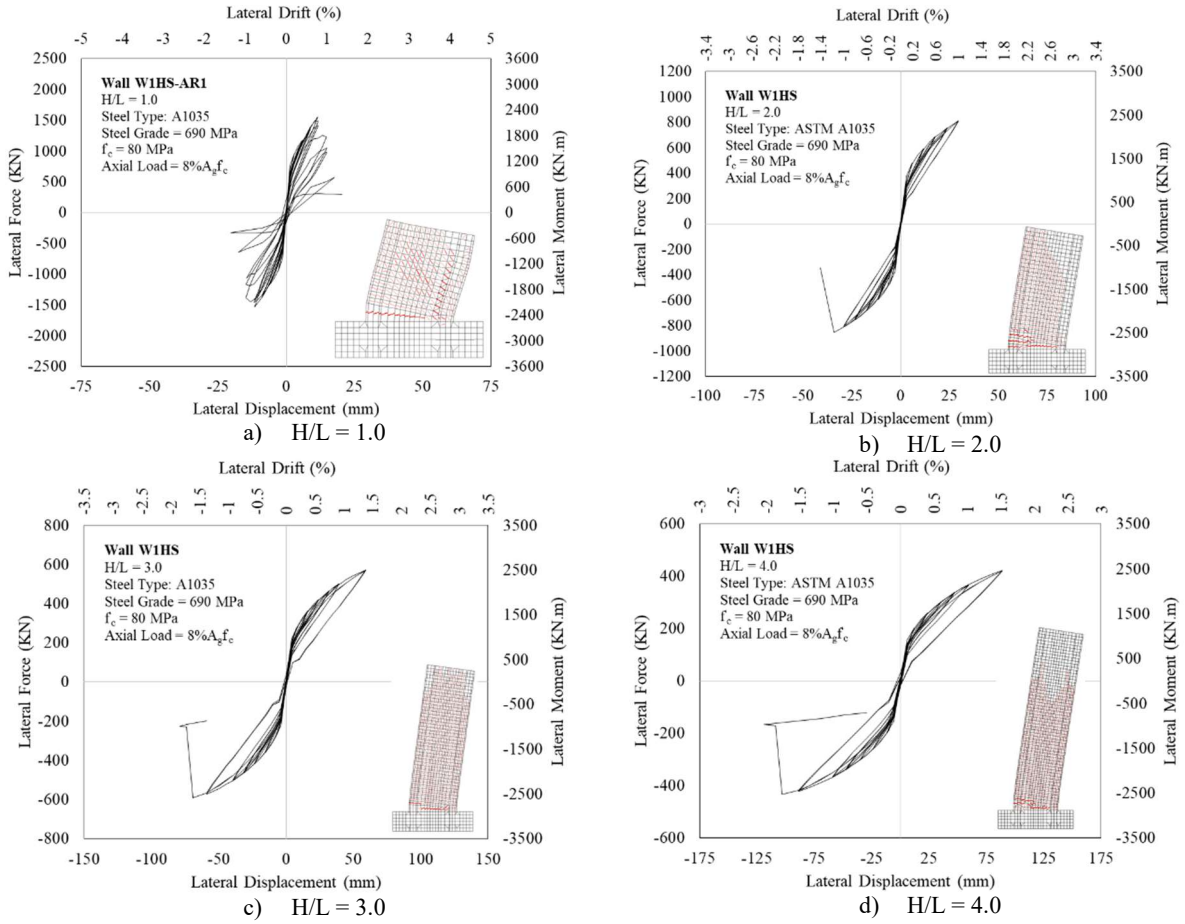

Figure 6.26 – Analytical hysteretic curves for Aspect Ratio (H/L) parametric study

Table 6.22 - Analytical results for walls reinforced with different aspect ratios (H/L)

Wall ID	H/L	Δ_y (mm)	F_y (KN)	Δ_u (mm)	F_u (KN)	μ (Δ_u/Δ_y)	Yield Drift (%)	Ultimate Drift (%)	Maximum Load (KN)
AR1	1	9.7	1396	12	1311	1.24	0.21	0.83	1563
AR2	2	25	755	37	856	1.48	0.55	1.28	856
AR3	3	39.5	503	68	598	1.72	0.91	1.57	598
AR4	4	58	369	103	433	1.78	1.00	1.78	433

In Table 6.22, H/L is the height-to-length aspect ratio of the walls, Δ_y is top lateral displacement at yield taken as the displacement at which the longitudinal reinforcement first reaches the yield strain obtained using the 0.2% offset method, F_y is the top lateral force at yield, Δ_u is the top lateral displacement at wall failure, F_u is the top lateral force at wall failure, and μ is the ductility ratio of the walls.

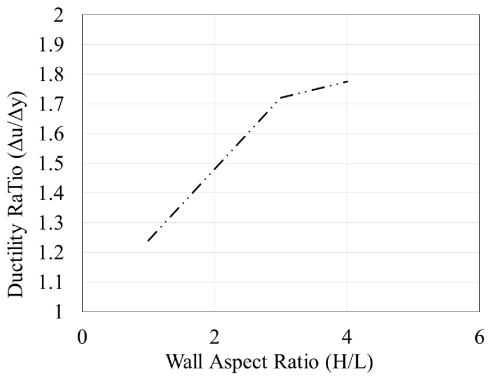

a) Aspect ratio (H/L) vs. ductility ratio (μ)

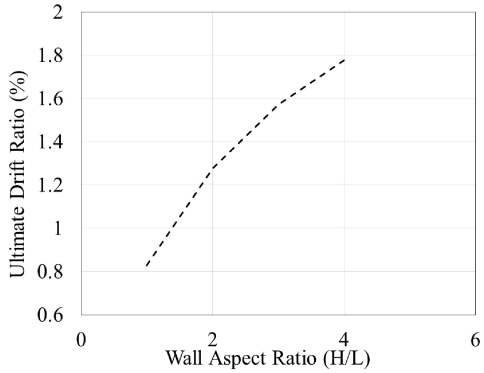

b) Aspect ratio (H/L) vs. drift capacity

Figure 6.27 - Effect of wall aspect ratio (H/L) on ductility ratio and ultimate drift ratio

Figure 6.28 presents the strains in the outermost boundary element longitudinal reinforcement plotted against the normalized height of the walls (h/H). Figure 6.29 presents the combined plots for the strain profiles for a better comparison. It is shown that the elastic strain penetration along the height of the wall is the highest for the wall with AR = 1.0 and decreases as the aspect ratio increases. In addition, the spread of plastic strains along the height of the wall is the lowest for the wall with AR = 4.0. The plastic hinge analysis described in Section 6.5.1 was used to calculate the plastic hinge length for the walls modelled with different aspect ratios. Table 6.23 provides the calculated plastic hinge value for walls with H/L $\geq$ 2.0. Wall AR1 was not expected to develop a plastic hinge region and hence is omitted from this analysis. The minimum plastic hinge length specified by Clause 21.5.2.1.2 of the CSA A23.3-14 ($l_p = 0.5l_w + 0.1h_w$) was also calculated for the modelled walls and is presented in Table 6.23 for comparison.

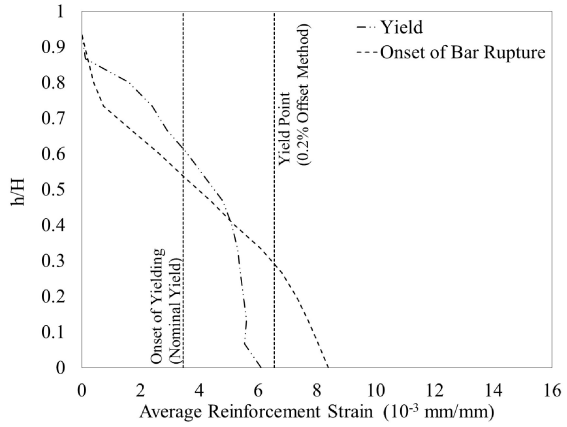

a) H/L = 1.0

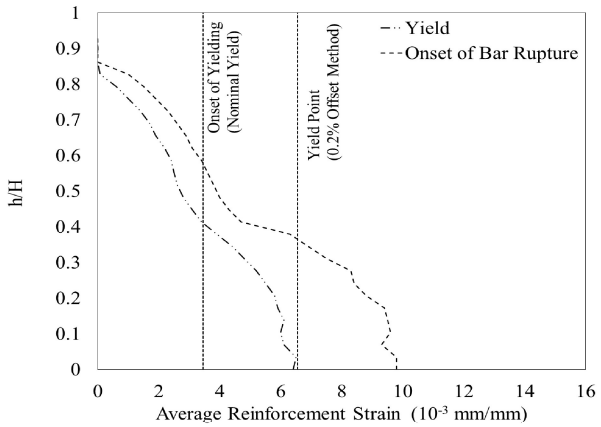

b) H/L = 2.0

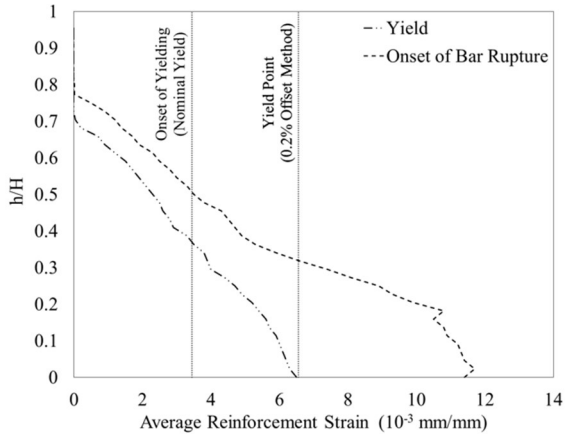

c) H/L = 3.0

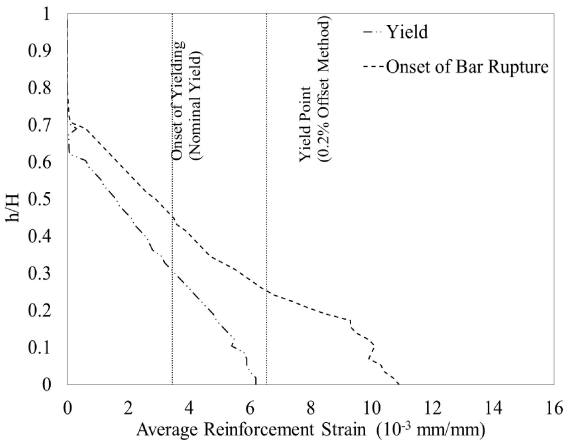

d) H/L = 4.0

Figure 6.28 - Wall W1HS longitudinal reinforcement strain profiles for different aspect ratios

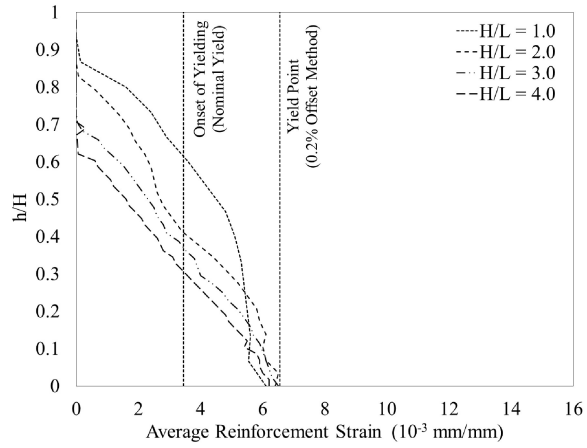

a) Yield

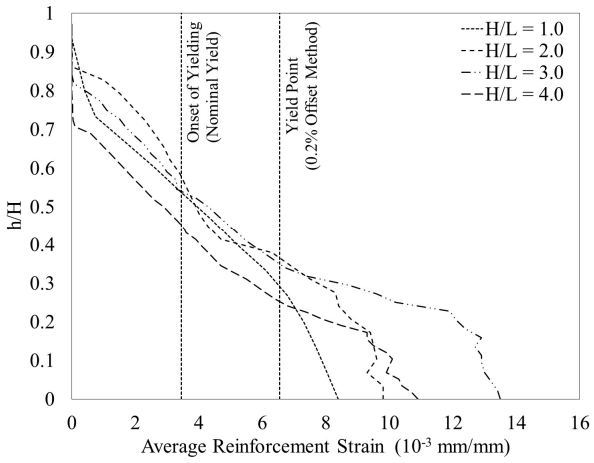

b) Onset of bar rupture

Figure 6.29 – Boundary element reinforcement strain profiles at yield and onset of bar rupture for wall W1HS modelled with different aspect ratios

Table 6.23 - Plasticity spread and plastic hinge length for walls with different aspect ratios

Wall ID	Aspect Ratio (H/L)	l_p/H	l_p/H CSA A23.3-14	l_{ps}
AR1	1	-	-	0.29
AR2	2	1.00	0.35	0.36
AR3	3	0.68	0.27	0.32
AR4	4	0.45	0.23	0.25

In Table 6.23, l_p/H is the normalized plastic hinge length calculated using the idealized curvature method and the CSA A23.3-14 expression for minimum plastic hinge length, and l_{ps} is the spread of plasticity along the height of the wall measured from the wall base. It is shown in Figure 6.30 that the plastic hinge length calculated using the conventional idealized plastic hinge analysis method decreases as the wall aspect ratio increases. A similar trend is observed for the spread of plasticity obtained from plots presented in Figure 6.28.

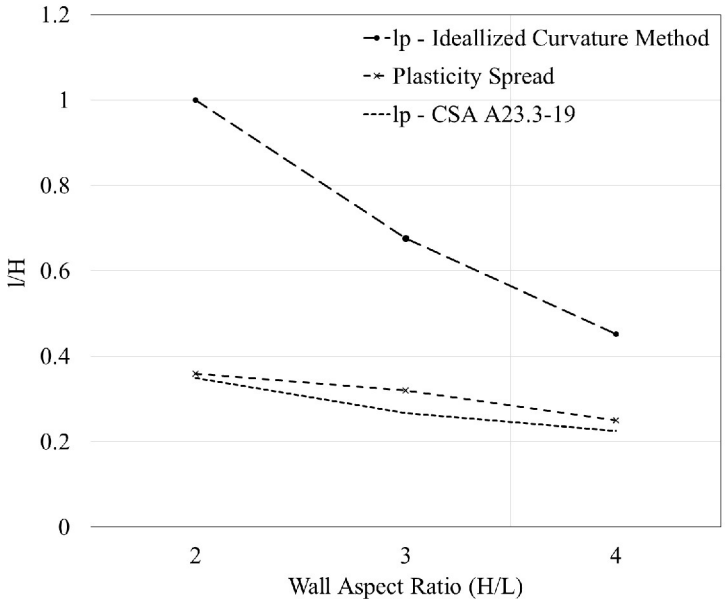

Figure 6.30 – Wall aspect ratio (H/L) vs. plastic hinge length and plasticity spread

The ultimate strain values used for the plastic hinge analysis presented above were obtained from the FE models at the onset of the bar rupture. For ASTM A1035 steel, the highest strain value captured by the FE model prior to the bar rupture was approximately 16% of the ultimate strain of steel bars. This is due to the fact that bar rupture is very localized and occurs over a small length of longitudinal reinforcement as verified in the experimental program. Hence, the plastic hinge

length calculated using the idealized method may be either 1) exaggerated if the ultimate curvature is calculated using the steel strain at a point right before bar rupture (as shown above), or 2) very underestimated if the ultimate curvature is calculated using the ultimate strain of the ASTM A1035 steel reinforcement (ε_u). Hence, even though the analytical results presented in Table 6.23 and Figure 6.30 demonstrate the effect of the aspect ratio on the plastic hinge length of Wall W1HS, they may not provide a realistic approximation for the plastic hinge lengths of the modelled walls.

6.5.3 Effect of Steel Type on Wall W1HS

Wall W1HS was modelled using 6 different steel types to investigate the impact of steel type and strength on its behaviour. Details of the steel reinforcement used in the FE analyses are presented in Table 6.24 and Figure 6.31.

Table 6.24 – Properties of steel material used in the steel type parametric study

Steel Type - Grade	f_y (MPa)	f_u (MPa)	E_s (MPa)	ε_{sh} (10^{-3} mm/mm)	ε_u (10^{-3} mm/mm)	ρ_l (%)	ρ_v (%)
ASTM A1035 – 690 MPa	860	1135	119000	6.6	66	1.64	0.68
ASTM A615 – 400 MPa	471	710	200000	16	135	2.56	0.96
ASTM A706 – 400 MPa	493	685	188992	2.7	146	2.88	0.74
ASTM A955 – 550 MPa	557	710	162000	3.45	219	2.53	1.13
AS/NZD 500E – 500MPa	556	669	200000	20	138	2.50	0.74
USD685 – 685 MPa	738	999	200000	11	120	2.64	0.85

In Table 6.24, f_y and f_u are the yield and ultimate strengths, E_s is the elastic modulus, ε_{sh} is the strain at the onset of strain-hardening, ε_u is the ultimate strain, and ρ_l and ρ_v are the vertical reinforcement ratios in the boundary elements (each) and the web section, respectively, for the FE models presented in the following sections.

The stress-strain behaviour of different steel materials was modelled using a Nonlinear Strain Hardening (NSH) model in VecTor2 (refer to Equation 3.2). As discussed in Section 3.2, the strain hardening branch of the stress-strain model is represented by a curve with exponent P which defines the curve's fit or curvature. The default NSH model in VecTor2 uses P=4, which provides very accurate stress-strain curves for most types of steel. However, this model does not predict the strain-hardening phase of the stress-strain curve for Grade 690 MPa ASTM A1035 reinforcement used in the experimental program. Hence, the Ramberg-Osgoode (1943) model was used to model the ASTM A1035 reinforcement as described in Chapter 3. Figure 6.32 presents a comparison

between the stress-strain curves predicted by the NSH model and the experimental results. As shown, the predicted curves are generally in very good agreement with the experimental results.

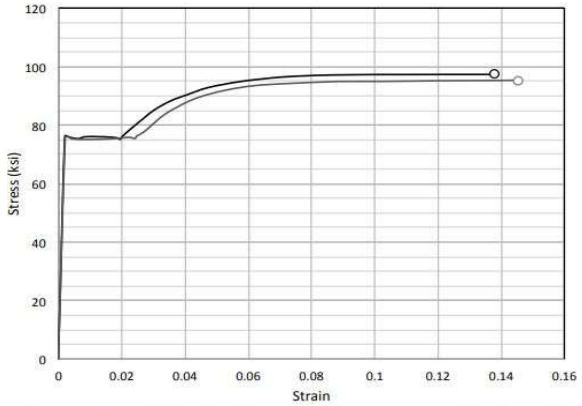

a) AS/NZD 500E 0 Grade 500 MPa
[Lin et al., 2000; Adapted from NIST GCE 14-917-30, 2014]

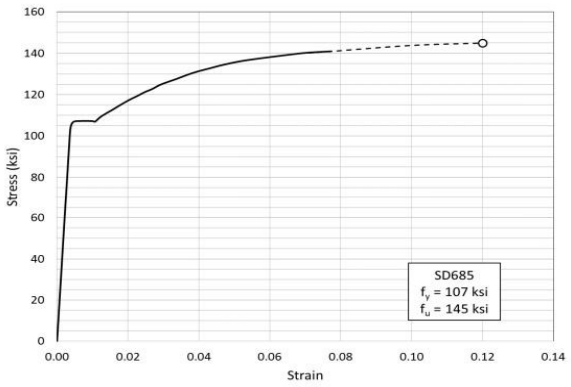

b) USD685 – Grade 685 MPa
[Ousalem et al., 2009; Adapted from NIST GCE 14-917-30, 2014]

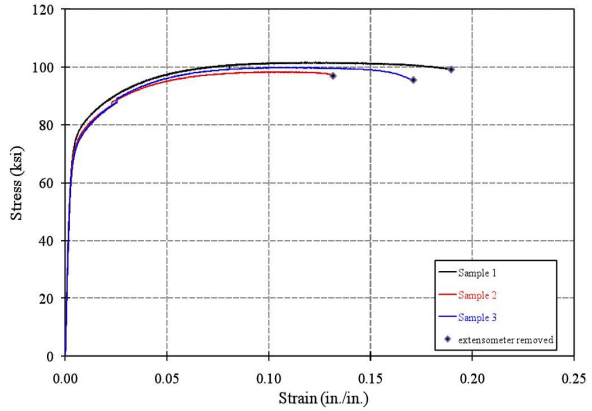

c) ASTM A706 – Grade 400 MPa
[Adapted from NCHRP Report 679, March 2011]

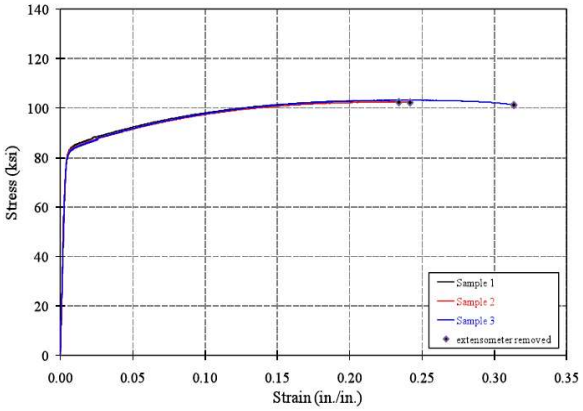

d) ASTM A955 (316) – Grade 550 MPa
[Adapted from NCHRP Report 679, March 2011]

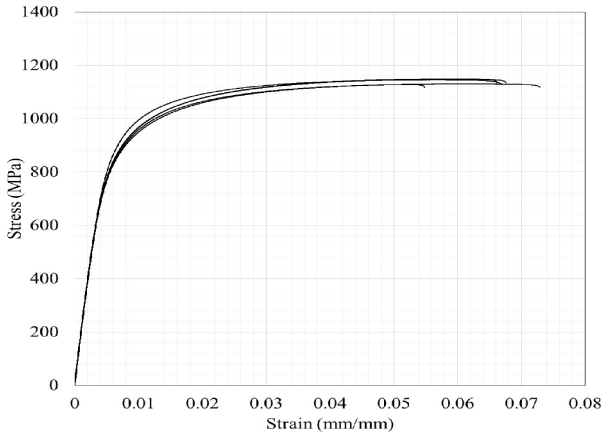

e) ASTM A1035 – Grade 690 MPa

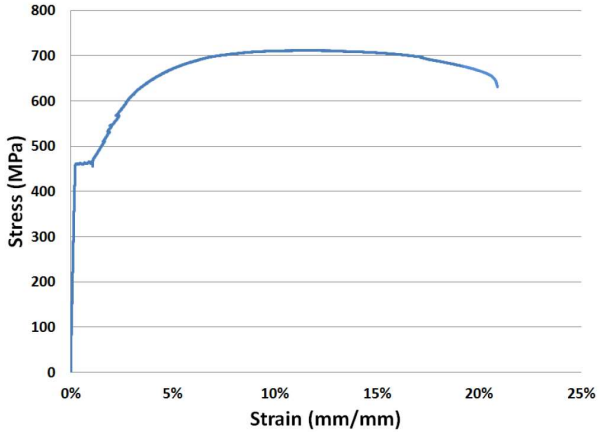

f) ASTM A615 – Grade 400 MPa
[Adapted from Navidpour, 2018]

Figure 6.31 - Stress-strain curves for steel material used in the parametric study

Similar to the design of wall W1HS in the experimental program, the modelled walls needed to have similar probable moment capacities to facilitate a direct comparison. To be able to change the reinforcement properties while keeping the probable moment of the walls in the parametric study the same as wall W1HS, the flexural reinforcement ratios were adjusted to provide the same probable moment capacity. This was achieved by simply proportioning the flexural reinforcement ratio based on the yield strength of the steel reinforcement. For example, the longitudinal reinforcement ratio in the boundary elements of wall W1HS was ρ_l=1.6%. For Grade 400 ASTM A615 steel type, with an actual yield strength of f_y = 471 MPa, ρ_l was modified as follows:

$$\rho_{l-A615} = \frac{\rho_{l-A1035} * f_{y-A1035}}{f_{y-A615}} = \frac{1.6\% * 860}{471} = 2.92\% \qquad \text{Equation 6.5}$$

where $\rho_{l\text{-}A615}$ and $\rho_{l\text{-}A1035}$ are the boundary element longitudinal reinforcement ratios and $f_{y\text{-}A615}$ and $f_{y\text{-}A1035}$ are the yield strengths for ASTM A615 and ASTM A1035 steel types, respectively. Reinforcement ratios for the other wall models were calculated using the same method.

Figure 6.33 presents the analytical hysteretic curves for wall W1HS modelled using different steel types. Figure 6.34 provides the outer boundary element longitudinal reinforcement strains along the height of the modelled walls.

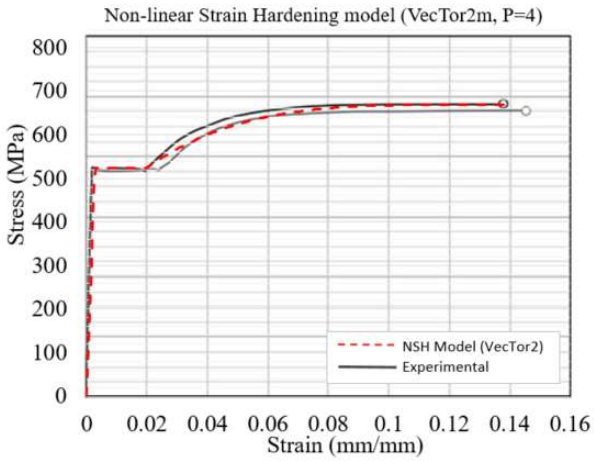

a) AS/NZD 500E 0 Grade 500 MPa
[Adapted from NCHRP Report 679, March 2011]

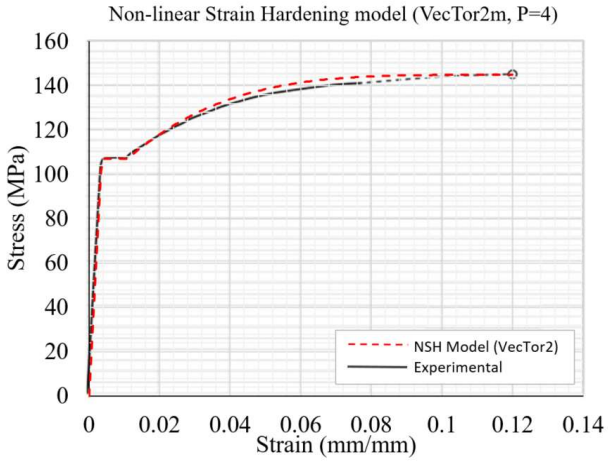

b) USD685 – Grade 685 MPa
[Adapted from NCHRP Report 679, March 2011]

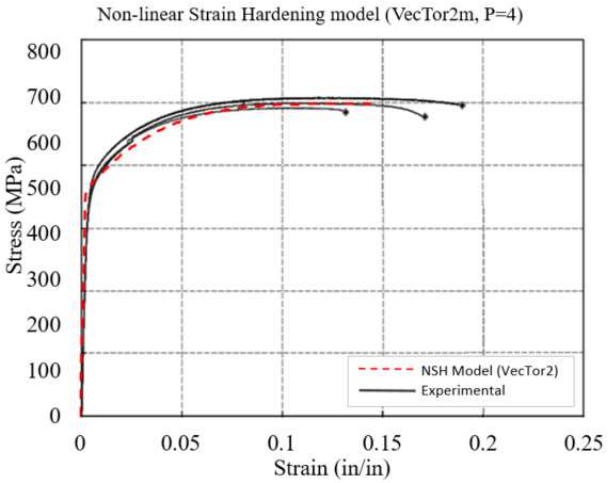

c) ASTM A706 – Grade 400 MPa
[Adapted from NCHRP Report 679, March 2011]

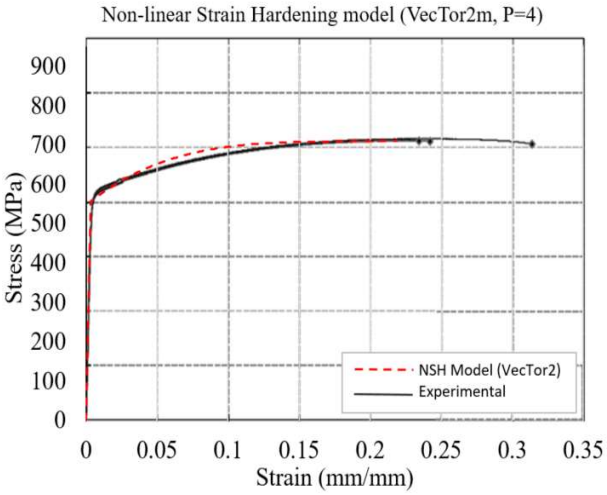

d) ASTM A955 (316) – Grade 550 MPa
[Adapted from NCHRP Report 679, March 2011]

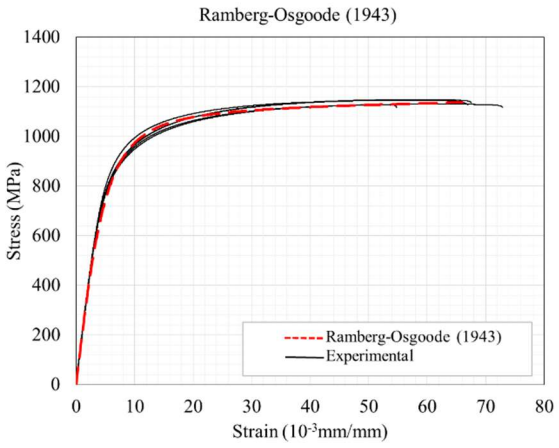

e) ASTM A1035 – Grade 690 MPa

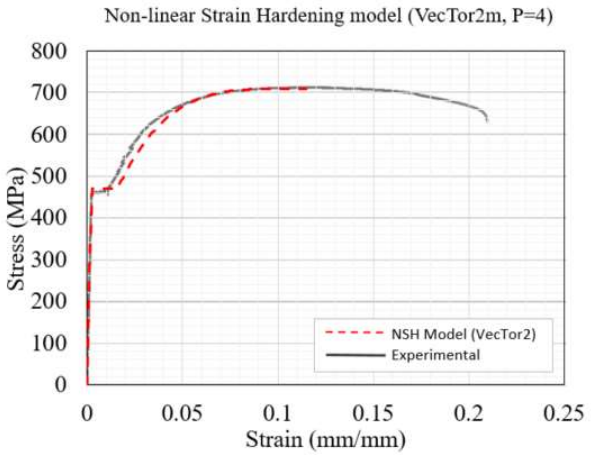

f) ASTM A615 – Grade 400 MPa
[Adapted from Navidpour, 2018]

Figure 6.32 – Comparison of the stress-strain curves predicted by the VecTor2 NSH model to the experimental results

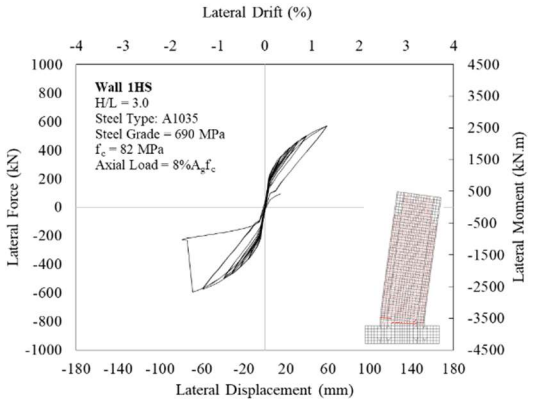

a) ASTM A1035, Grade 690 MPa

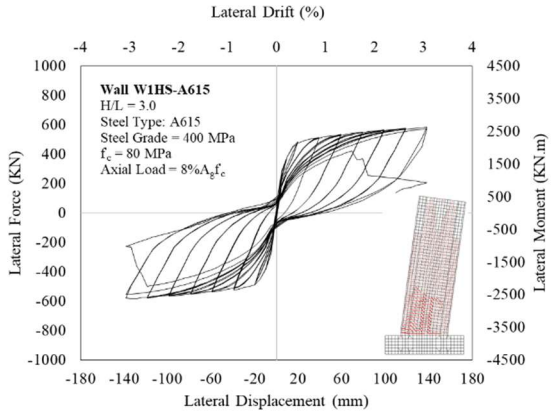

b) ASTM A615, Grade 400 MPa

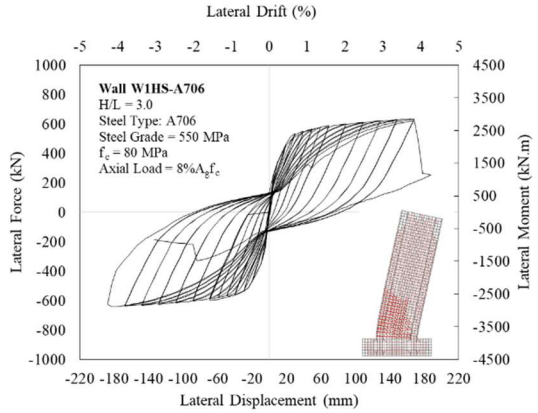

c) ASTM A706, Grade 400 MPa

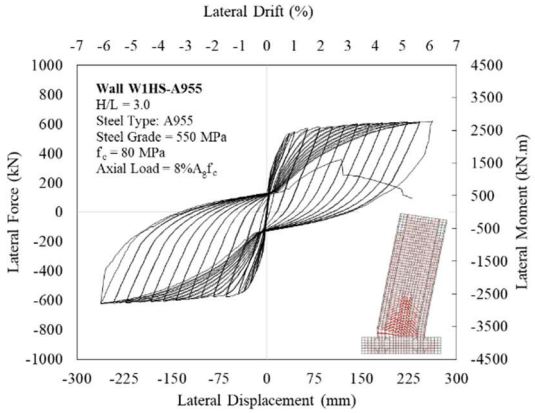

d) ASTM A955, Grade 550 MPa

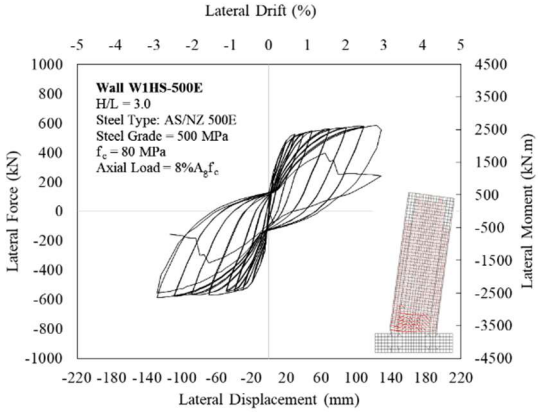

e) AS/NZD 500E, Grade 500 MPa

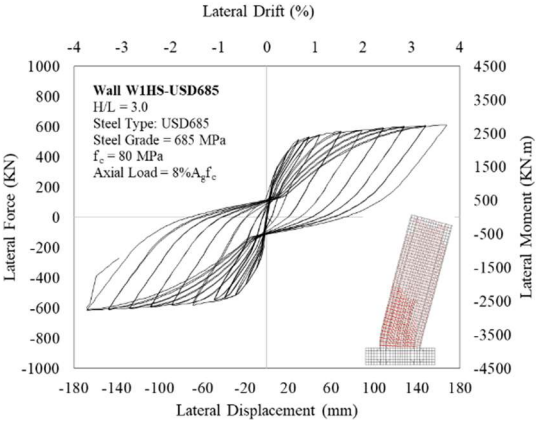

f) USD685, Grade 685 MPa

Figure 6.33 - Analytical hysteretic curves for Steel Type parametric study

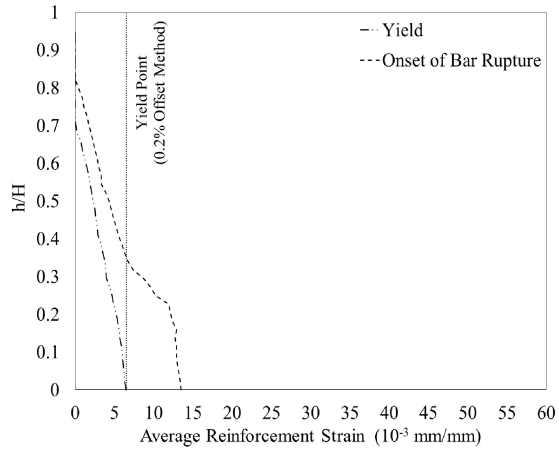

a) ASTM A1035 – Grade 690 MPa

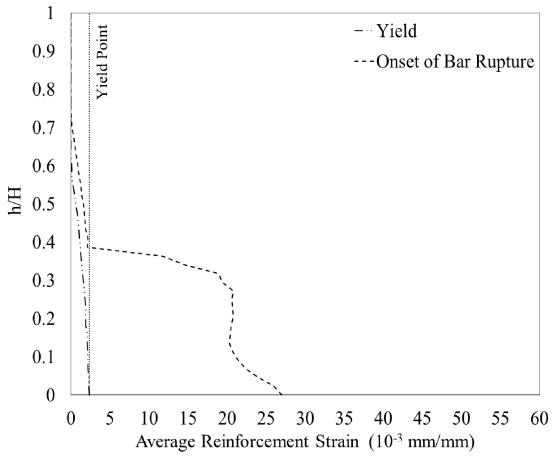

b) ASTM A615 – Grade 400 MPa

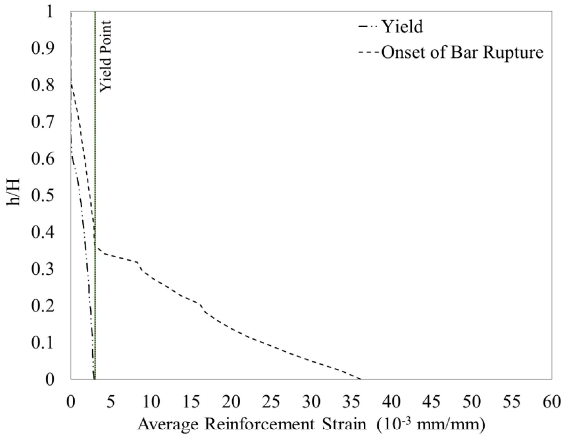

c) ASTM A706 – Grade 400 MPa

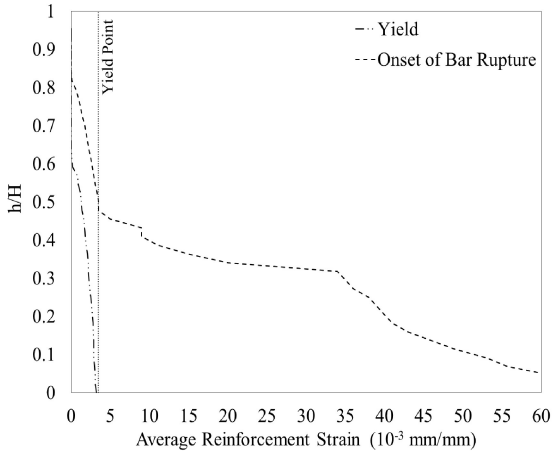

d) ASTM A955 – Grade 550 MPa

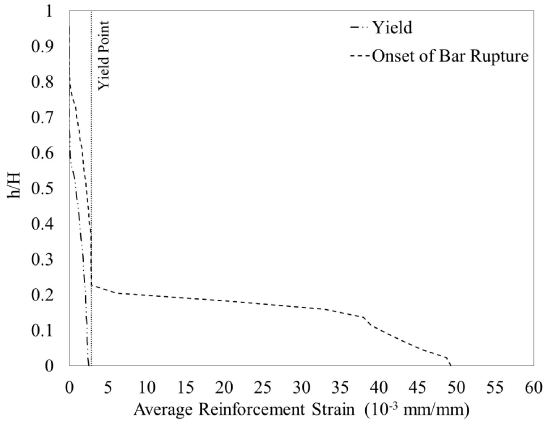

e) AS/NZD 500E – 500 MPa

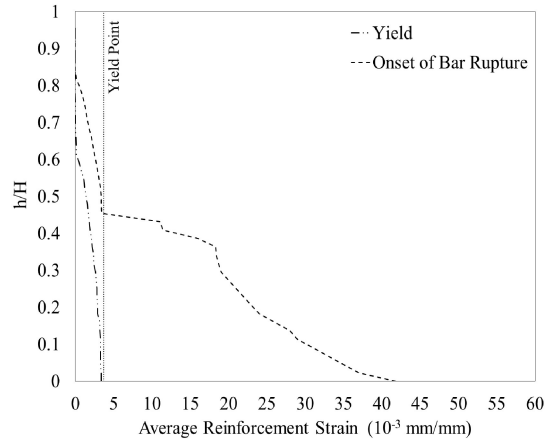

f) USD685 – 685 MPA

Figure 6.34 - Wall W1HS longitudinal reinforcement strain profiles for different steel types

The strain profiles are combined in Figure 6.35 and Figure 6.36 for a better comparison. All walls were found to undergo flexural responses as expected and failed due to the rupture of the boundary element longitudinal reinforcement. The cracking patterns and graphical representations of the walls at failure are shown in Figure 6.33.

All walls had very similar flexural capacities to Wall W1HS as intended. The results indicate that the wall with Grade 690 ASTM A1035 reinforcement was found to have the smallest ductility ratio. The wall reinforced with Grade 500 ASTM A955 (stainless steel) was found to have the largest ductility ratio owing to its much higher ultimate strain capacity. Table 6.25 provides a summary of the analysis results for walls with different type steel reinforcement.

Table 6.25 – Analytical results for walls reinforced with different steel types

Steel Type	f_y (MPa)	f_u (MPa)	ε_u (10^{-3} mm/mm)	f_u/f_y	$\varepsilon_u(f_t/f_y)$	l_p/H	Δ_{yield} (mm)	$\Delta_{ultimate}$ (mm)	μ (Δ_u/Δ_y)
ASTM A1035	860	1135	66	1.32	0.09	0.34	39.5	68	1.7
USD685	738	999	120	1.35	0.16	0.45	21.0	169	8.0
AS/NZD 500E	566	669	138	1.18	0.16	0.23	16.0	130	8.1
ASTM A615	471	710	120	1.51	0.18	0.40	16.5	138	8.4
ASTM A706	493	685	146	1.39	0.20	0.36	18.5	170	9.2
ASTM A955	557	710	219	1.27	0.28	0.48	23.0	262	11.4

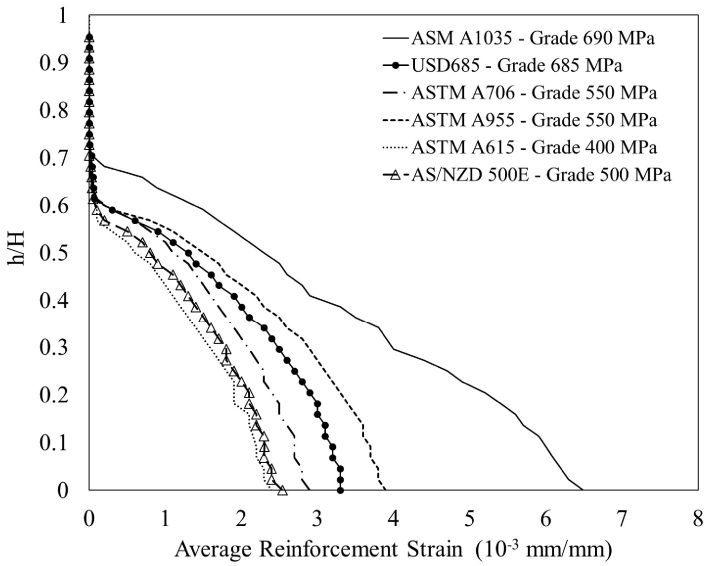

Figure 6.35 – Strain profiles at yield point of wall W1HS for different steel types

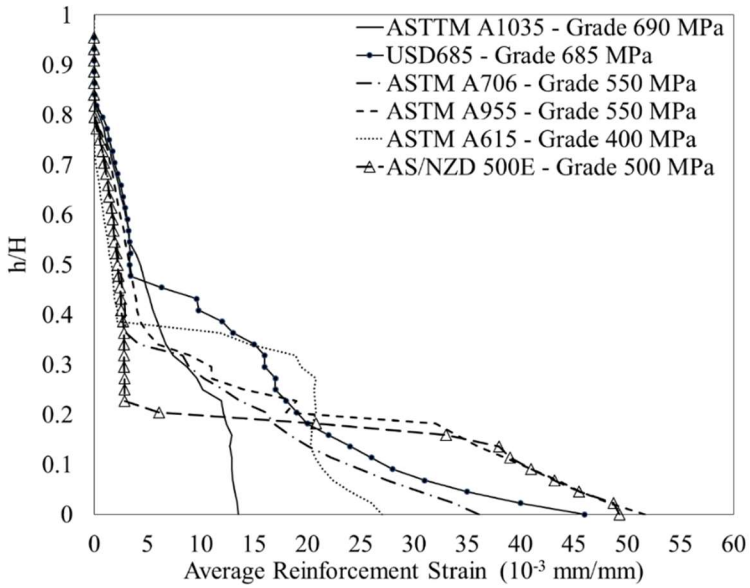

Figure 6.36 - Strain profiles at the onset of bar rupture of wall W1HS for different steel types

The steel types used in this part of the analysis had a wide range of properties, which included the ratio of the ultimate strength to yield strength (f_u/f_y), ultimate strain (ε_u), strain hardening strain (ε_{sh}) and the general shape of the stress-strain curve. In the analysis of the results, it was attempted to understand the relationship between these properties and the seismic characteristics of the walls such as ductility and plastic hinge length. Sokoli et al. (2020) reported that using reinforcing bars with a higher f_u/f_y results in a larger spread of inelastic strains along the height of reinforced concrete columns. A similar effect was observed by To & Moehle (2020) who reported that a higher f_u/f_y results in a larger plasticity spread along the height of reinforced concrete beams and increases the plastic hinge length obtained from the conventional idealized plastic hinge analysis method. This effect was investigated by plotting f_u/f_y against the plasticity spread along the height of the walls, the ductility ratio of the walls (μ), as well as the idealized plastic hinge length, l_p as shown in Figure 6.37. It is shown that, despite a general increasing trend, there is not a strong correlation between f_u/f_y and the selected parameters in the current wall study.

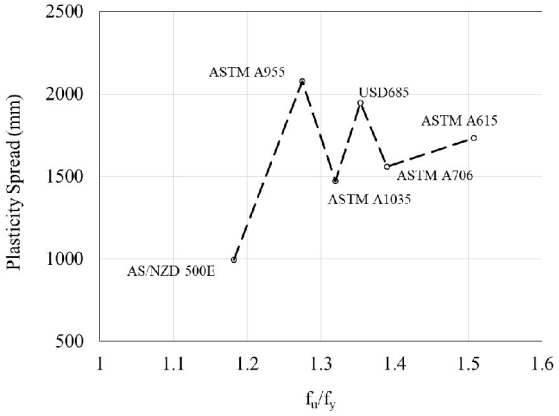

a) f_t/f_y vs. plasticity spread along wall height

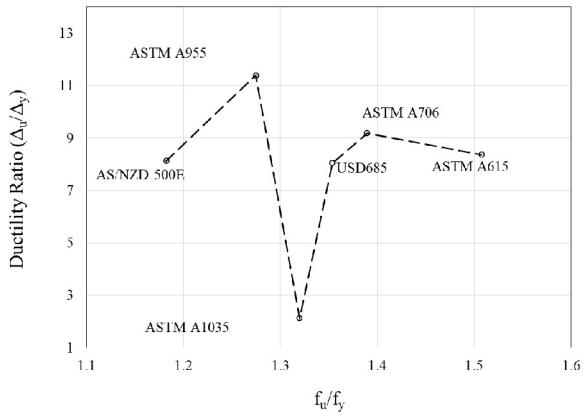

b) f_t/f_y vs. ductility ratio, μ

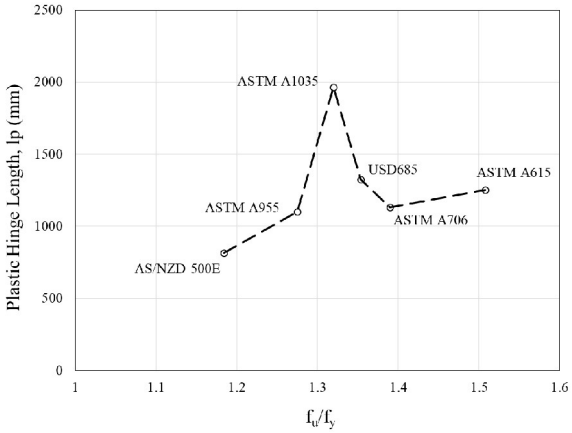

c) f_t/f_y vs. plastic hinge length (l_p)

Figure 6.37 – Effect of f_t/f_y on plasticity spread, plastic hinge length and ductility ratio

Ductility of steel reinforcement plays an important role on the lateral displacement capacity of concrete members. A larger reinforcement elongation results in a more ductile response in flexure-dominant walls provided that other properties remain the same. However, when combined with other properties, such as the ratio f_u/f_y and the strain hardening behaviour, the effect of ultimate steel strain on seismic performance of walls becomes more convoluted. Figure 6.38 (a) presents a plot of the ultimate strain (ε_u) of each reinforcement type against the ductility ratio (μ) of the walls. It is shown that the wall ductility ratio generally increases as the ultimate elongation of the reinforcement increases. However, the trend does not apply to the ASTM A615 and AS/NZD 500E steel types. The noticeable difference between these two steel types and others used in this parametric study is the shape of the stress-strain curves. The amount of ultimate elongation, as well as the ratio of the ultimate strength to the yield strength (f_t/f_y) are different for these two types of reinforcement. AS/NZD 500E has a smaller f_u/f_y ratio (1.18) but a larger ultimate strain (138 x

10^{-3} mm/mm); while ASTM A615, has a larger f_u/f_y ratio (1.51) and smaller ultimate strain (120 x 10^{-3} mm/mm). Although further research is required to fully understand this correlation, it appears that the ductility ratio of the modelled walls is affected by a combination of the parameters f_u/f_y and ε_u. Figure 6.38 (b) presents a plot of the ductility ratio (μ) vs. the product of f_u/f_y and ε_u. It is shown that all steel types investigated in this study follow the same increasing trend with respect to the dimensionless quantity $\varepsilon_u.f_t/f_y$

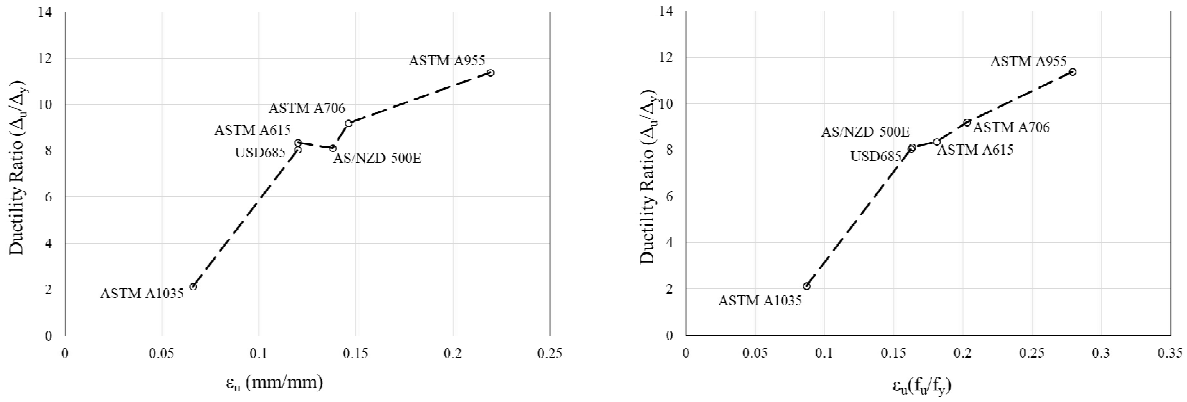

a) ε_u vs. ductility ratio, μ b) $\varepsilon_u.(f_u/f_y)$ vs. ductility ratio, μ

Figure 6.38 - Effect of steel ultimate strain on ductility ratio

The impact of the shape of the reinforcing stress-strain curve on wall response was further investigated by evaluating the relationship between the secant slopes of the strain hardening curves. This was calculated by dividing the difference between the ultimate stress (f_u) and the yield stress (f_y) by the difference between the ultimate strain (ε_u) and the strain at the onset of strain hardening (ε_{sh}). Figure 6.39 shows the plots of the slope of the strain hardening curve against the idealized plastic hinge length and ductility ratio of the wall. As shown, there is a strong correlation between the strain hardening slope and these parameters, with the exception of the Grade 500 AS/NZD 500E steel type, which appears to be an anomaly. It is to note that this steel type has the smallest f_u/f_y ratio and the largest yield plateau compared to the other steel types considered in this study.

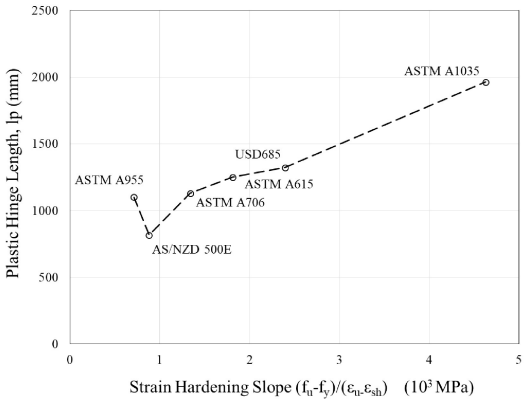

a) Steel strain hardening Slope vs. Plastic Hinge Length (l_p)

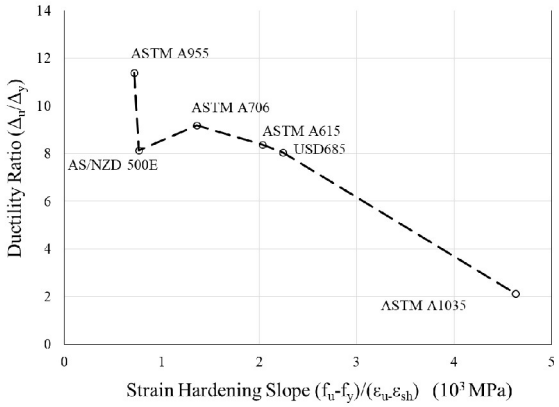

b) Steel strain hardening slope vs. ductility ratio, (μ)

Figure 6.39 – Effect of steel strain hardening slope on plastic hinge length and ductility

6.5.4 Effect of Concrete Strength on Wall W1HS

In this part of the parametric investigation, Wall W1HS was modelled using different concrete strengths as listed in Table 6.21 to investigate the effect of concrete strength on the seismic response of Wall W1HS. The analysis consisted of modelling the wall described in Section 6.4 with different concrete strengths ranging from 35 MPa to 150 MPa. All other wall parameters were kept the same. Figure 6.40 presents the hysteretic curves for the walls modelled with different concrete strengths. Figure 6.41 provides the outer boundary element longitudinal reinforcement strains along the height of the walls. The strain profiles are combined in Figure 6.42 and Figure 6.43 for a better comparison.

Table 6.26 - Analytical results for walls reinforced with different concrete strengths (f'c)

Wall ID	f'c (MPa)	Δ_y (mm)	F_y (KN)	Δ_u (mm)	F_u (KN)	μ (Δ_u/ Δ_y)	Yield Drift (%)	Ultimate Drift (%)	Maximum Load (KN)
FC35	35	441	474	79	567	1.80	1.02	1.82	567
FC60	60	43	507	69	579	1.60	0.99	1.59	579
FC80	80	39.5	503	68	598	1.72	0.91	1.57	598
FC120	120	35	498	64	609	1.83	0.80	1.48	609
FC150	150	34.5	512	59	608	1.71	0.80	1.36	608

All walls exhibited a flexure-dominant behaviour and failed due to the rupture of the boundary element longitudinal reinforcement at slightly different drift ratios. Figure 6.40 shows the cracking

patterns and failure modes for all walls. The cracking pattern at the ultimate displacement of the wall indicates that as the concrete strength (f'_c) increases, the spread of cracking becomes smaller.

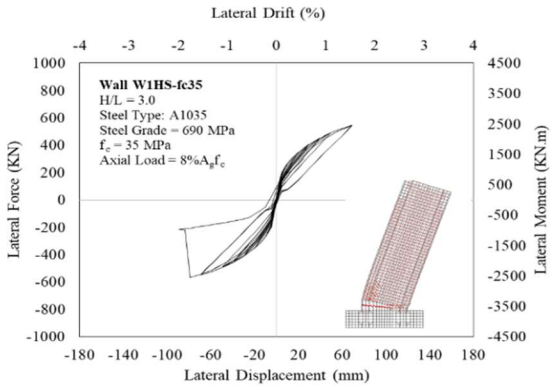

a) $f'_c = 35$ MPa

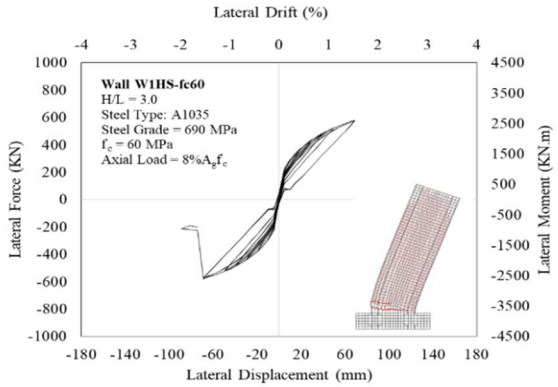

b) $f'_c = 60$ MPa

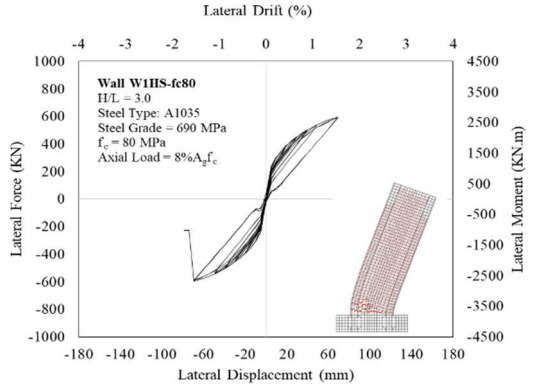

c) $f'_c = 80$ MPa

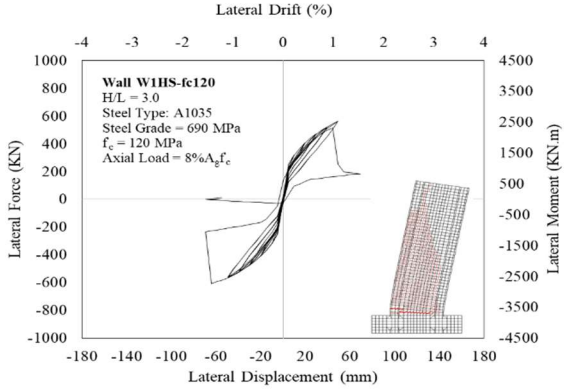

d) $f'_c = 120$ MPa

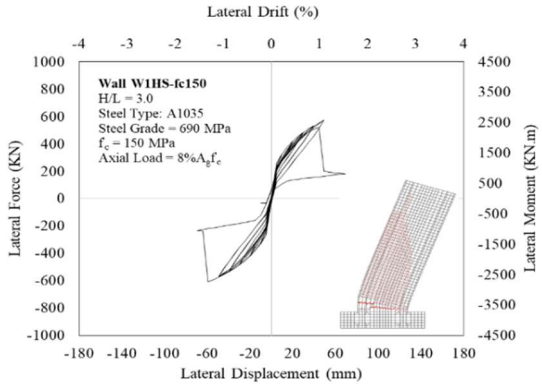

e) $f'_c = 150$ MPa

Figure 6.40 - Analytical hysteretic curves for Concrete Strength (f'_c) parametric study

Considering the strain profiles shown in Figure 6.43, this cracking pattern is explained by a smaller plasticity spread. Figure 6.43 also shows that that the spread of reinforcement strains (including elastic strains) along the height of the wall decreases as the concrete strength increases. One of the implications of this phenomenon is that a wall with a higher concrete strength undergoes smaller lateral (elastic) displacements before reaching the yield point of the wall since the height of the elastic penetration along the height of the wall is smaller. This is believed to be related to the higher tension stiffening and compression softening effects in concrete with a higher compressive strength, f'_c. This observation is confirmed by the lateral displacements obtained from the FE analysis provided in Table 6.26.

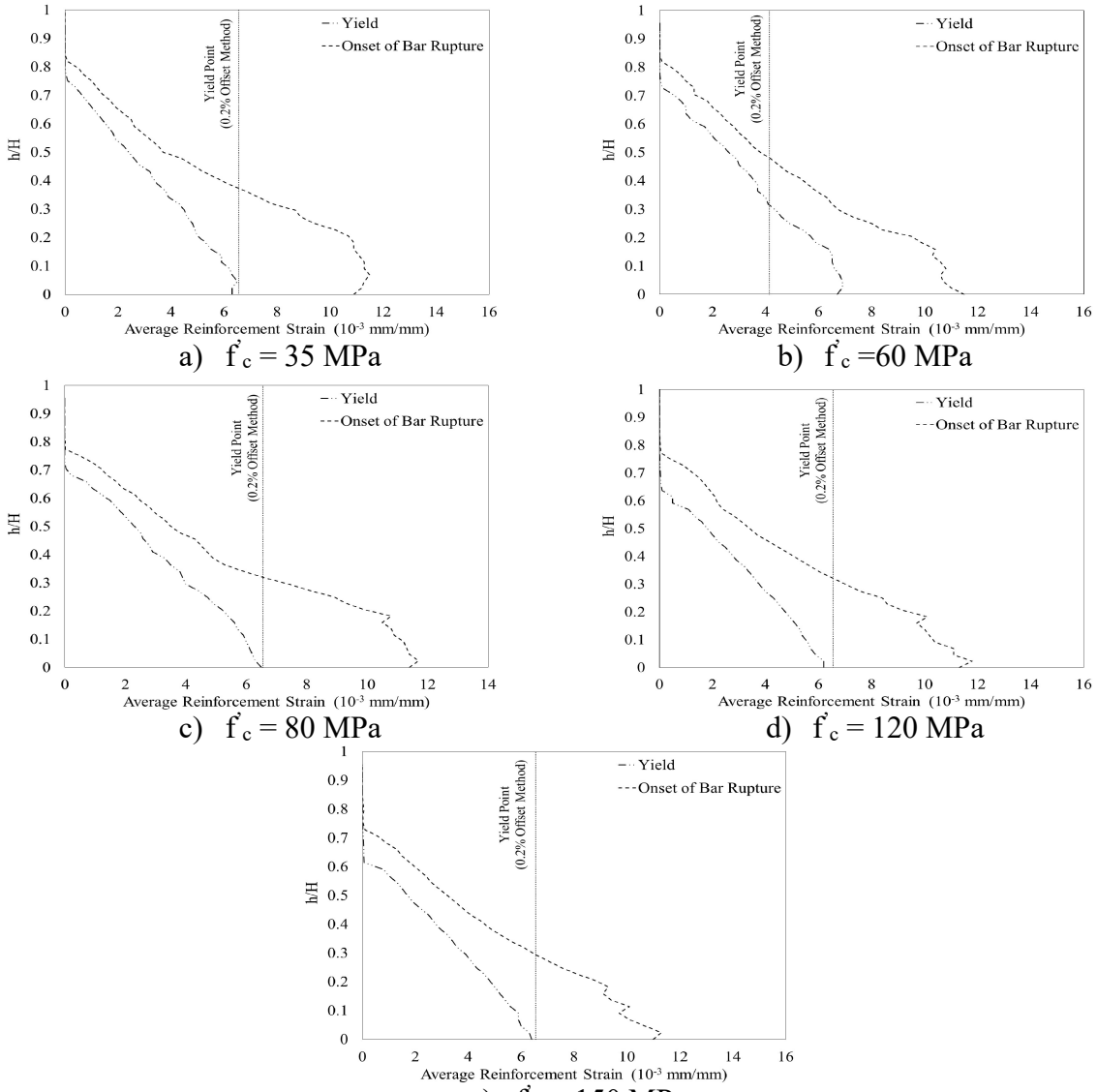

a) f'_c = 35 MPa

b) f'_c =60 MPa

c) f'_c = 80 MPa

d) f'_c = 120 MPa

e) f'_c = 150 MPa

Figure 6.41 - Wall W1HS longitudinal reinforcement strain profiles for different concrete strengths

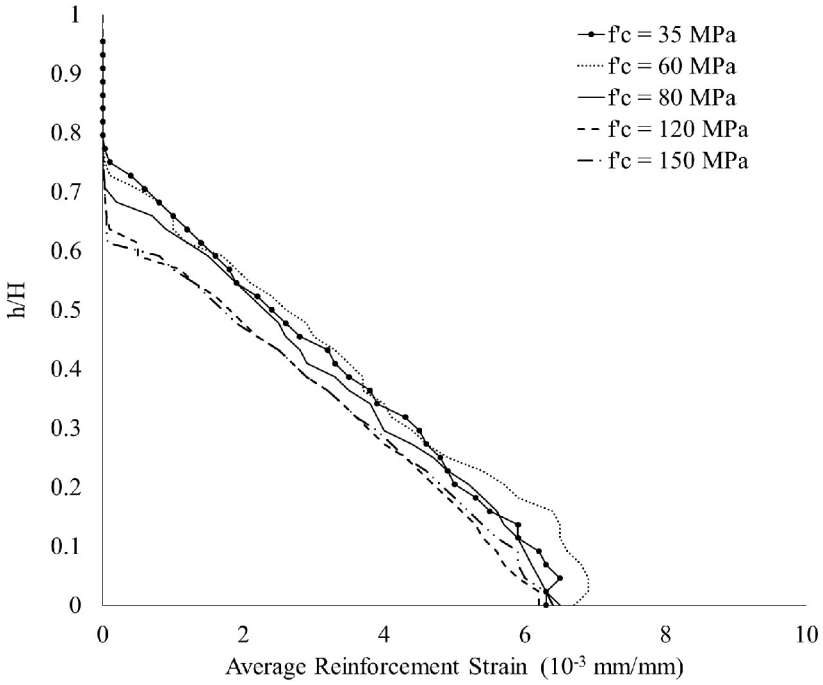

Figure 6.42 - Strain profiles at yield point of wall W1HS for different Concrete Strengths

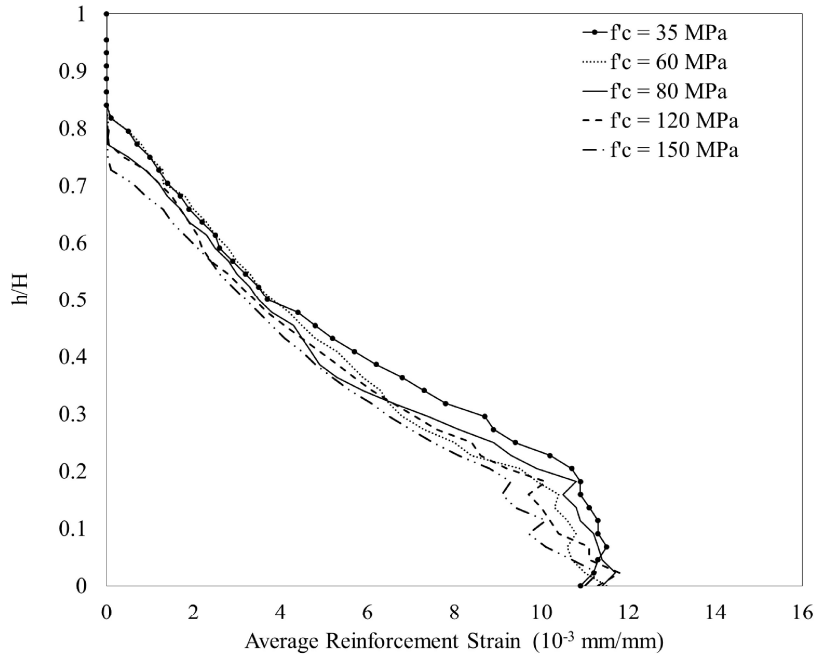

Figure 6.43 - Strain profiles at the onset of bar rupture of wall W1HS for different steel types

Figure 6.44 presents plots of concrete strength (f'_c) vs. ductility ratio and drift capacity for the walls modelled with different concrete strengths. It is shown that as the concrete strength increases, the drift capacity of the wall decreases. No discernable relationship was found between concrete

strength and the ductility ratio of the walls. The idealized plastic hinge analysis method described in Section 6.5.1 was used to calculate the idealized plastic hinge lengths using the local curvatures of the walls obtained from the FE analyses. Figure 6.45 (a) presents a plot of concrete strength (f'_c) with respect to the calculated idealized plastic hinge lengths for the modelled walls. As expected from the above discussions, the plastic hinge length of the walls decreases as the concrete strength (f'_c) increases. Figure 6.45 (b) shows the plasticity spread along the height of the walls. The plasticity spread also decreases as concrete strength (f'_c) increases, as discussed above.

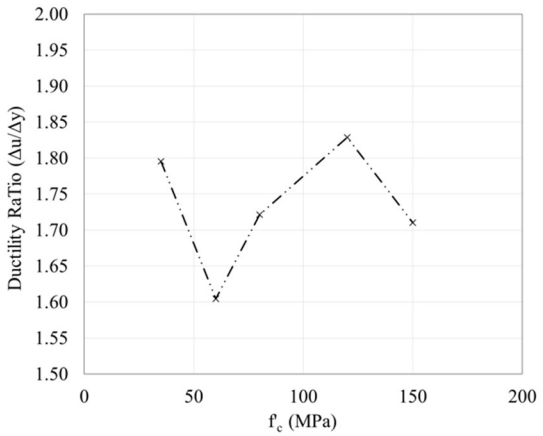

a) Concrete strength (f'_c) vs. ductility ratio (μ)

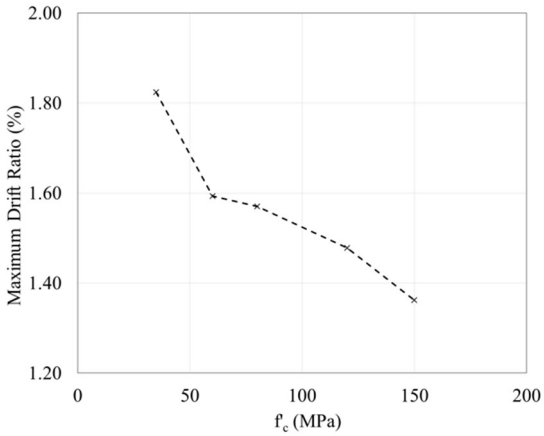

b) Concrete strength (f'_c) vs. maximum lateral drift capacity (%)

Figure 6.44 - Effect of concrete strength of ductility ratio and drift capacity

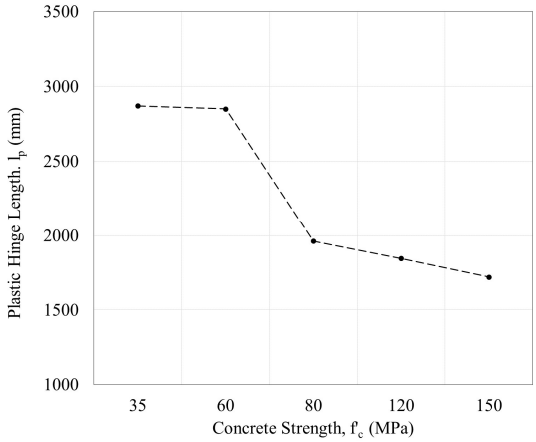

a) Concrete Strength (f'_c) vs. idealized plastic hinge length (l_p)

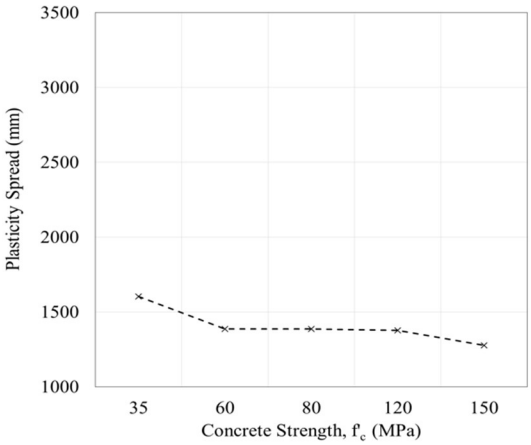

b) Concrete strength (f'_c) vs. plasticity spread

Figure 6.45 - Effect of concrete strength (f'_c) on plasticity spread and idealized plastic hinge length, l_p

Chapter 7

7 Conclusions

This Chapter presents summary and conclusions on experimental and analytical phases of the research project reported in the preceding Chapters. Recommendations for use of Grade 690 MPa ASTM A1035 reinforcement for earthquake-resistant concrete shear walls and future research on the topic are made at the end of the Chapter.

7.1 Experimental Program

Two large-scale concrete shear walls reinforced with Grade 690 MPa ASTM A1035 steel bars were tested under reversed cyclic loading and constant axial compression to investigate the effects of high-strength reinforcement lacking a well-defined yield point and a yield plateau on seismic behaviour of reinforced concrete shear walls. The walls were labelled as W1HS and W2HS. They were designed to be geometrically identical to the walls tested previously by Navidour (2018), called the *control wall* herein. The flexural reinforcement in the control walls consisted of conventional Grade 400 MPa ASTM A615 reinforcement. The reinforcement ratios in the walls presented in this study were modified to achieve the same probable moment capacity as the control walls to facilitate a direct comparison.

The walls represented shear walls in a 6-storey building constructed at ¼-scale. Wall W1HS was 4330mm high x 1450mm long and had a height-to-length aspect ratio of 3.0 and a barbell-shaped cross-section. It had 250mm x 250mm square columns-like boundary elements linked by a 100mm thick web, forming a barbell shape. Wall W2HS was 2900mm high x 1625mm long x 200mm thick and had a height-to-length aspect ratio of 1.8 and a rectangular cross-section.

The walls were constructed monolithically with foundations that were anchored to the strong floor of the structural laboratory. Lateral loading was applied using either one (for Wall W1HS) or two (for Wall W2HS) 1000 kN hydraulic actuators in displacement-controlled mode. The axial loads were applied using uniformly spaced prestressing cables. The walls were instrumented to measure and record the top lateral displacement, wall rotation of the critical region near the base, as well as

shear deformations within the plastic hinge region. Strains in reinforcement and prestressing cables were measured using strain gauges installed at selected strategic locations.

Test results indicate that both walls were flexure-dominant as intended and failed in flexure due to the rupture of boundary element longitudinal reinforcement. The cracking patterns and wall damage were monitored during the tests.

The main findings and observations from the experimental program are summarized as follows:

7.1.1 Wall W1HS

1) Wall W1HS reached its lateral force capacity of 599 kN at 1.8% lateral drift in the positive direction and experienced the first bar rupture during the third cycle of 1.8% drift, having completed two cycles at this deformation level with a 19% strength decay during the second cycle. This marks the deformation capacity of the wall. Beyond the initial bar fracture, the wall experienced a further strength decay of 22% relative to the peak load at 2.0% drift ratio. The displacement ductility ratio at 1.8% lateral drift corresponded to $\mu = \Delta_u/\Delta_y = 2.1$. In contrast, the control wall was able to sustain three cycles at 2.3% drift (μ= 5.6) without any appreciable strength decay and failed due to the buckling of boundary element reinforcement in compression during the second cycle at 2.9% drift (μ= 7.1). The reduced deformability of Wall W1HS is attributed to the stress-strain behaviour of Grade 690 MPa ASTM A1035 reinforcement, which shows a limited elongation capacity of 6.6%, relative to Grade 400 ASTM A615 steel with approximately twice the elongation capacity at rupture. These observations indicate that the inelastic deformability of flexure-dominant shear walls reinforced with Grade 690 MPa steel, conforming to ASTM A1035, has reduced inelastic deformability, but sufficiently high to sustain inelastic deformation cycles during a moderate earthquake with a moderate ductility capacity. The ductility ratio observed corresponds to the design of moderately ductile shear walls using a ductility related force modification factor of $R_d = 2.0$ on the basis of the National Building Code of Canada (NBCC-2015).
2) It was observed that very few cracks formed after the drift ratio of 0.8% (approximately equal to the yield point of the wall). Following this point, the width of all cracks, except for a horizontal crack located at the base of the wall, remained approximately the same

throughout the test. The horizontal crack at the wall-footing interface continued to widen until the boundary element longitudinal reinforcement started to rupture within this crack.

3) It was observed that the majority of the plastic hinge rotation occurred in a crack located within approximately 30mm from the base of the wall. Approximately 70% of the top lateral displacement at the first bar rupture was due to the rotations within this region at the base, which included the horizontal crack at the wall-footing interface.
4) It was observed that the initial stiffness of wall W1HS was lower compared to the control wall. The initial loading stiffness of wall W1HS, calculated as the slope of a loading branch between the point of zero lateral load and maximum drift ratio at the selected loading cycle, was found to be the lowest between the cracking and yield points. Between the cracking and the yield points, the loading stiffness of wall W1HS was found to be approximately 30% lower in the positive loading direction and 20% lower in the negative loading direction. A similar trend was found for the stiffness of the unloading branches. This is deemed to be due to the lack of a well-defined yield point and the roundhouse shape of the yield region in the stress-strain diagram for the ASTM A1035 steel type. In addition, the yield point of the wall is delayed due to the larger yield strain of the steel reinforcement (ε_y = 0.66% obtained via the 0.2% offset method) meaning that the wall had to undergo a larger displacement to reach the yield point compared to the control wall. Considering that the lateral forces at the yield points for both wall W1HS and the control wall were approximately the same as intended by design, the calculated stiffness of wall W1HS was found to be lower before the yield point of the wall.
5) The contribution of shear to the total top lateral displacement was found to be negligible. This was expected as the wall was flexure-dominant and was not expected to undergo large shear stresses. In addition, this was an indication that the wall was effectively controlled against shear.
6) It was found that Wall W1HS dissipated 60% less energy at wall failure in the positive loading direction compared to the control wall. Similar to the ductility of the wall, the smaller energy dissipation capacity of Wall W1HS was deemed to be due to the stress-strain characteristics of the ASTM A1035 reinforcement.

7.1.2 Wall W2HS

1) Wall W2HS was reinforced with Grade 690 MPa reinforcement conforming to ASTM A1035, just like Wall W1HS was, except for two differences; W2HS had a smaller aspect ratio of 1.8 (as opposed to 3.0), and a rectangular cross-section (as opposed to a barbell shaped section). The former increased the effect of shear, though the wall was designed to be a flexure-dominant element and failed through the rupturing of flexural reinforcement, and the latter resulted in closer spacing of main longitudinal reinforcement in the boundary element because of limited wall thickness. The wall suffered from anchorage slip of the exterior most layer of reinforcement within the top 150 mm segment of the foundation at 0.6% drift. The anchorage slip was characterised by "concrete break out" within the top portion of the foundation while the HSR maintained its full anchorage below the 150 mm depth. This is a phenomenon observed in concrete elements reinforced with HSR and resulted in the modification of the development length requirements in ACI 318-2019 Code, which calls for confinement reinforcement within the development length and a minimum spacing between the HSR bars. Wall W2HS was designed based on the requirements of ACI 318-2014 and conformed to the required development length of ACI 318-2014 with a hook at the end of each longitudinal reinforcement. This observation reinforces the importance of the new code requirement for higher grade reinforcement.
2) The anchorage slip of the exterior most layer of boundary element reinforcement resulted in a rigid body movement of the wall, causing an additional 9 mm top deflection. This phenomenon was visually observed by detecting splitting tensile cracks in the foundation near the wall end at the base. However, the reinforcement remained fully anchored below the top 150 mm segment, as measured by the strain gauges placed below this level. An approximate hysteretic relationship was then generated by subtracting the recorded anchorage slip displacement from the total top displacement. The resulting modified curve, though approximate in nature, showed similar inelastic deformability as that shown by Wall W1HS, indicating 1.9% lateral drift prior to failure due to the bar rupturing. The wall performance based on the modified hysteretic relationship showed reasonably good agreement with the analytical hysteretic relationship generated by VecTor2 FE software. The comparison of Wall W1HS (based on the modified hysteretic relationship) with the companion wall with Grade 400 MPa reinforcement indicated approximately 37%

reduction in inelastic deformability. Hence, the performance conclusion obtained from Wall W1HS test also applies to Wall W2HS, i.e., the walls reinforced with Grade 690 MPa reinforcement are not suitable for regions of high seismicity but may be used in regions of moderate seismicity with moderately ductile inelastic deformation capacity.

3) The effect of increased shear stress reversals associated with reduced wall aspect ratio from 3.0 in Wall W1HS to 1.8 was evident in crack patterns. Diagonal cracks consistently increased between 0.4% and 1.4% drift with increased intensity after 1.1% drift. These cracks remained approximately the same beyond 1.4% until flexural failure by bar rupturing at the end of the test. The wall was designed to have a higher shear capacity relative to the shear force associated with flexural failure as per the current seismic design practice. Hence, any shear distress was not expected in the wall, except for intensified diagonal tension cracking, which is what was observed during the test. The contribution of shear to total displacement remained negligible, clearly indicating that walls in the range of an aspect ratio of 1.8 can be designed to performed in flexural mode of response.
4) The majority of wall deformations occurred with the lower 825mm wall segment. In addition, approximately 65% of the plastic hinge rotation at the onset of the first flexural bar rupture in the positive direction was due to the rotation of the wall within the 30mm wall segment at the base. This ratio was 49% in the negative loading direction. These deformations included any anchorage slip that took place within the foundation, both due to the concrete break out associated with local anchorage slippage and yield penetration and the elongation of reinforcement within the foundation under increased tensile forces associated with higher grade reinforcement.
5) The initial stiffness of wall W2HS was found to be smaller compared to the control wall. This finding is consistent with the results of wall W1HS for which a smaller initial stiffness was also observed due to the curved nature of the stress-strain relationship of HSR.

7.2 Analytical Program

The analytical program consisted of Finite Element (FE) analyses of the walls using VecTor2 software. The software consisted of a validation study using previous test results available in the literature, FE modelling and analysis of wall W1HS and wall W2HS, as well as a parametric study to assess the effects of selected design parameters using the analytical model for W1HS.

7.2.1 Finite Element Analysis Validation Study

The validation study consisted of modelling reinforced concrete shear walls previously tested by other researchers, as well as the walls tested in the current investigation. The walls had different geometric and material properties and were modelled to investigate the accuracy and reliability of VecTor2 in predicting the behaviour of reinforced concrete shear walls with different geometric and material properties.

The main findings and observations from the analytical validation study are summarized as follows:

1) VecTor2 FE software was found to provide good correlations with hysteretic behaviour of flexure-dominant reinforced concrete walls. Although the results were generally acceptable for all modelled walls, the hysteretic curves were found to be less accurate for shear-dominant walls with smaller aspect ratios (i.e., H/L = 1.0).
2) Concrete strength (f'_c) and steel type or grade did not impact the accuracy of the analytical results obtained from VecTor2 models.
3) It was found that VecTor2 may not be a suitable tool for the analysis of flanged walls. This was expected as VecTor2 is designed for 2D analysis of concrete elements modelled as planar members; hence, out-of-plane interactions occurring in elements such as wide flange sections are not effectively accounted in VecTor2 analysis.
4) VecTor2 was able to predict failure mechanisms for the modelled walls with high accuracy.
5) The analytical results for Wall W1HS were found to be in very good agreement with the experimental results. The analytically obtained hysteretic curves were found to match almost perfectly the experimental results. The ductility ratio of the wall was predicted with nearly 100% accuracy in the positive loading direction. Some discrepancy was observed in the ductility ratio of the wall in the negative loading direction. The experimental ductility ratio of the wall was approximately 40% higher in the negative loading direction. This is believed to be due to the reduced stiffness of the wall in the negative direction following wall damage in the positive direction. Furthermore, the actual loading during the test was not symmetrical and the displacement cycles meant for 1.8% was accidentally applied at 2.1%, affecting the

deformation capacity and resulting in asymmetry in response. The FE prediction was identical for the positive and negative loading direction.

6) The boundary element longitudinal reinforcement strains obtained from the FE analysis were compared to those recorded during the test within the plastic hinge region. The strains obtained analytically were found to match closely the experimental results.
7) The loading and unloading stiffnesses of the modelled Wall W1HS were found to be in very good agreement with the experimental results.
8) Pinching was effectively captured by the FE analysis. A minor discrepancy was observed in the pinching behaviour near the zero-load point in the unloading branches of 1.5% and 2.0% drift ratios. This was deemed to be due to the abrupt closing of the cracks at smaller loads caused by the vertical reinforcement that was still in its elastic or partially elastic phase. This was captured in the FE analysis due to the idealized nature of the model; however, the small pinching was not observed in the experimental results.
1) The analytical results obtained from VecTor2 FE model were found to be generally in good agreement with the experimental results. The overall stiffness of the wall, the lateral drift capacity, the slopes of the loading and unloading curves and the overall pinching behaviour were captured effectively.
2) The flexural capacity of the wall was underestimated by approximately 8% in the positive loading direction and 12% in the negative loading direction. The inaccuracy is deemed due to the additional displacement that Wall W2HS experienced associated with anchorage slip.

7.2.2 Parametric Investigation

The effects of wall aspect ratio, the characteristics of reinforcement (grade and stress-strain relationship) and concrete strength on seismic performance of shear walls were investigated through an analytical parametric investigation using the analytical model for Wall W1HS. The following summarizes the observations made and the conclusions drawn for the investigation:

1) There is a strong correlation between the wall aspect ratio and the lateral deformation capacity. It was shown that, both the wall drift capacity and the displacement ductility ratio increased with wall aspect ratio.

2) The spread of plastic strains in boundary element longitudinal reinforcement decreases with increasing aspect ratio.
3) VecTor2's default model for strain hardening of steel reinforcement provides good analytical predictions for stress-strain relationships of the steel types considered except for Grade 690 ASTM A1035 reinforcement. The Ramberg-Osgoode (1943) model was found to produce accurate results for this type of reinforcement. In addition, the ACI IG-6R model also provides reasonably good results.
4) Grade 690 MPa ASTM A1035 reinforcement was found to have the smallest inelastic deformability among all the walls modelled with other types of reinforcement considered in the investigation.
5) The increase in the ratio of ultimate steel strength to yield strength (f_u/f_y) of flexural reinforcement increases the plasticity spread and the plastic hinge length of the walls; however, the correlation was not found to be very strong. The ductility ratio of the wall did not have a discernable correlation with f_u/f_y.
6) The plastic hinge length and the ductility ratio of flexure-dominant walls both increase with ultimate elongation capacity of longitudinal reinforcement (ε_u). A stronger correlation exists between the ductility ratio of the walls and the product $\varepsilon_u.(f_u/f_y)$.
7) The plastic hinge length increases with the slope of the strain hardening region of flexural reinforcement (except for Grade 500 ASTM A955 steel).
8) The spread of plasticity decreases with increasing concrete strength. As a result, the lateral displacement of the wall at yield becomes smaller as the concrete strength increases.
9) Inelastic deformability of walls decreases with increasing concrete strength as higher strength concretes show more brittle behaviour. The plastic hinge length as well the spread of plasticity also decreases with increasing concrete strength.
10) High-strength reinforcement does not necessarily perform better with high-strength concrete. The increase in reinforcement strength dominates the wall behaviour relative to the increase in concrete strength in terms of wall deformability.

7.3 Design Recommendations

The following design recommendations can be made for the use of Grade 690 MPa ASTM A1035 reinforcement in earthquake-resistant shear walls, designed to perform predominantly in the flexure mode of deformations:

- The use of Grade 690 MPa steel in concrete shear walls results in limited inelastic deformability, with maximum drift capacities below the level typically expected from fully ductile walls designed and detailed using Grade 400 MPa ASTM A615 reinforcement. The deformability of walls with Grade 690 MPa steel may not reach the minimum displacement ductility ratio associated with the use $R_d = 3.5$ in fully ductile walls designed as per NBCC-2015. However, these walls possess moderate ductility with maximum drift ratios in the range of 1.6% to 1.8%. They may be designed as moderately ductile walls using a ductility-based force modification factor of $R_d = 2.0$ and the related provisions of NBCC-2015 (NRC 2015).
- The plastic hinge length for walls with Grade 690 MPa steel can be shorter than those specified in current codes and standards, which were developed for Grade 400 MPa reinforcement conforming to ASTM A615. The plastic hinge length in walls with higher grade reinforcement should be calculated using the steel stress-strain relationship as established by coupon tests, with due considerations given to the post-yield characteristics of steel, including the ultimate elongation capacity ε_u and the ratio of ultimate to yield strengths (f_u/f_y) in applying the idealized plastic hinge concept with a constant curvature region over the plastic hinge length.
- Grade 690 MPa may have longer development length requirements, especially if they are used with close spacing. Such walls may experience “concrete breakout” and associated anchorage slip. Hence, they should not be designed using the development length expressions developed for ordinary Grade 400 MPa reinforcement. It is recommended that the ACI 318-2019 development length requirements be implemented in design with appropriate confinement reinforcement within the bond length, while respecting the minimum spacing requirement intended for these bars.
- Grade 690 MPa reinforcement may be used as distributed vertical and horizontal web reinforcement, using the current shear design provisions, while ensuring that the capacity in shear is always higher than that corresponding to probable moment resistance in flexure.

7.4 Recommendations for future research

1) The following is recommended for future research:
    a. Perform additional tests of large-scale concrete shear walls reinforced with different types of high-strength steel under simulated seismic loading to enhance the research database. It is recommended that the wall test matrix consist of walls with different steel stress-strain characteristics, percentages of reinforcements, concrete strength, reinforcement distribution and detailing, and wall geometry.
    b. Investigate analytically the effect of steel reinforcement stress-strain characteristics including f_u/f_y, yield plateau, slope or curvature of the strain hardening region, and ultimate elongation of steel reinforcement on the response of reinforced concrete shear walls.
    c. Investigate the premature rupturing mechanism of high-strength reinforcement at the base of the wall. More advanced techniques for recording the reinforcement strains at the base of the wall may be useful for providing more insight into how the high-strength reinforcement transitions from 6% of its ultimate elongation to bar rupture in the last loading cycle (as described in Section 6.5.2).
    d. Investigate the impact of steel reinforcement with different stress-strain characteristics on the conventional idealized plastic hinge analysis method.
    e. Investigate the impact of steel reinforcement with different stress-strain characteristics on the minimum plastic hinge length specified by the CSA A23.3 standard and the ACI 318 code.
    f. Investigate the effect of ASTM A1035 steel reinforcement on anchorage strength in concrete shear walls with different wall aspect ratios, confinement reinforcement in the bond region and the spacing of longitudinal reinforcement.

References

1 ACI Committee 318 (2014). Building Code Requirements for Structural Concrete (ACI 318-14) and Commentary (ACI 318R-14). *American Concrete Institute, Farmington Hills*, MI, 519 pp.

2 ACI Committee 318 (2019). Building Code Requirements for Structural Concrete (ACI 318-19) and Commentary (ACI 318R-19). American Concrete Institute, Farmington Hills, MI, 2019, 623 pp.

3 ACI Innovation Task Group 6 (2010). Design Guide for the Use of ASTM A1035/A1035M Grade 100 (690) Steel Bars for Structural Concrete (ACI ITG-6R-10), *American Concrete Institute, Farmington Hills*, MI.

4 Ajaam, A., Yasso, S., Darwin, D., O'Reilly, M., & Sperry, J. (2018). Anchorage Strength of Closely-Spaced Hooked Bars. ACI Structural Journal, 115(4), 1143–1173

5 Akkaya, Y., Guner, S., & Vecchio, F. J. (2019). Constitutive Model for Inelastic Buckling Behavior of Reinforcing Bars. *ACI Structural Journal*, *116*(2), 195-10.

6 Antoniades, K. K., Salonikios, T. N., & Kappos, A. J. (2003). Cyclic tests on seismically damaged reinforced concrete walls strengthened using fiber-reinforced polymer reinforcement. *ACI Structural Journal*, *100*(4), 510-518.

7 Antoniades, K. K., Salonikios, T. N., & Kappos, A. J. (2005). Tests on seismically damaged reinforced concrete walls repaired and strengthened using fiber-reinforced polymers. *Journal of Composites for Construction*, *9*(3), 236-246.

8 Aoyama, H. (2001). *Design of modern highrise reinforced concrete structures* (Vol. 3). World Scientific.

9 ASAZU, N., UNJOH, S., HOSHIKUMA, J. I., & KONDOH, M. (2001). Plastic hinge length of reinforced concrete columns based on the buckling characteristics of longitudinal reinforcement. *Doboku Gakkai Ronbunshu*, *2001*(682), 177-194.

10 ASTM A1035 / A1035M-19, Standard Specification for Deformed and Plain, Low-Carbon, Chromium, Steel Bars for Concrete Reinforcement, ASTM International, West Conshohocken, PA, 2019, www.astm.org

11 ASTM A370-19e1, Standard Test Methods and Definitions for Mechanical Testing of Steel Products, ASTM International, West Conshohocken, PA, 2019, www.astm.org

12 ASTM A615 / A615M-20, Standard Specification for Deformed and Plain Carbon-Steel Bars for Concrete Reinforcement, ASTM International, West Conshohocken, PA, 2020, www.astm.org

13 ASTM A706 / A706M-16, Standard Specification for Deformed and Plain Low-Alloy Steel Bars for Concrete Reinforcement, ASTM International, West Conshohocken, PA, 2016, www.astm.org

14 ASTM A955 / A955M-20c, Standard Specification for Deformed and Plain Stainless Steel Bars for Concrete Reinforcement, ASTM International, West Conshohocken, PA, 2020, www.astm.org

15 B.M. Shahrooz, Miller, R. A., Harries, K. A., and Russell, H. G. (2011). Design of Concrete Structures Using High-Strength Steel Reinforcement. *NCHRP Report 679*. Transportation Research Board, Washington, DC, 2011, p. 77.

16 Baek, J. W., Park, H. G., Shin, H. M., & Yim, S. J. (2017). Cyclic loading test for reinforced concrete walls (Aspect Ratio 2.0) with grade 550 MPa (80 ksi) shear reinforcing bars. *ACI Structural Journal*, *114*(3), 673.

17 Barda, F.; Hanson, J. M.; and Corley, W. G. (1977). Shear Strength of Low-Rise Walls with Boundary Elements. Reinforced Concrete in Seismic Zones, SP-53, N. M. Hawkins and D. Mitchell, eds., *American Concrete Institute, Farmington Hills*, MI, pp. 149-202.

18 Bars, R., & Splice, M. (2020). *ICC-ES Evaluation Report*. *January*, 1–7.

19 Budek, A., Priestley, M., and Lee, C. (2002). Seismic design of columns with high-strength wire and strand as spiral reinforcement. *ACI Structural Journal*, Vol. 99, No. 5, pp. 660-670.

20 Chandra, J. (2017). *Shear behaviour of high strength concrete walls subjected to cyclic lateral loading* (Doctoral dissertation).

21 Cheng, M.Y.; Giduquio, M..B. (2014). Experimental Study of Corner Slab-Column Connection. *American Concrete Institute Structural Journal,* Vol. 111(5), 2014, pp. 1123-1134.

22 Cheng, M.Y.; Hung, S.C.; Lequesne, R.D.; Lepage, A. (2016). Earthquake-Resistant Squat Walls Reinforced with High-Strength Steel. *American Concrete Institute Structural Journal,* Vol. 113(5), 2016, pp.1065-1076.

23 Cornelissen, H., Hordijk, D., & Reinhardt, H. (1986). Experimental determination of crack softening characteristics of normal weight and lightweight. *Heron*, *31*(2), 45-46.

24 Cortes Puentes, W. L. (2009). *Nonlinear modelling and analysis of repaired and retrofitted shear walls* (Doctoral dissertation, University of Ottawa (Canada)).

25 Cortés-Puentes, W. L., & Palermo, D. (2012). Modeling of RC shear walls retrofitted with steel plates or FRP sheets. *Journal of Structural Engineering*, *138*(5), 602-612.

26 Cortés-Puentes, W. L., & Palermo, D. (2017). SMA tension brace for retrofitting concrete shear walls. *Engineering Structures*, *140*, 177-188.

27 CSA A23.1-14/A23.2-14 (2014). Concrete materials and methods of concrete construction / Test methods and standard practices for concrete. *Canadian Standards Association*, *Mississauga, Canada*.

28 CSA A23.3-14 (2014). Design of Concrete Structures. *Canadian Standards Association, Mississauga, Canada.*

29 CSA-G40.20-13/G40.21-13 (2013). General requirements for rolled or welded structural quality steel / Structural quality steel. *Canadian Standards Association, Mississauga, Canada.*

30 Dazio, A.D.A., Beyer, K., and Bachmann, H. (2009). Quasi-static cyclic tests and plastic hinge analysis of RC structural walls. *Engineering Structures*, Vol. 31, pp. 1556-1571.

31 Dhakal, R. P., & Maekawa, K. (2002). Reinforcement stability and fracture of cover concrete in reinforced concrete members. *Journal of structural engineering*, *128*(10), 1253-1262.

32 Thorenfeldt, E. (1987). Mechanical properties of high-strength concrete and applications in design. In *Symposium Proceedings, Utilization of High-Strength Concrete, Norway, 1987*.

33 Eligehausen, Rolf & Popov, Egor & Bertero, Vitelmo. (1983). Local Bond stress slip relationship of deformed bars under generalized excitations. Report EERC-83/23, Univ. of California, Berkeley.

34 Emamy Farvashany, F., Foster, S.J., Vijaya Rangan, B. (2008). Strength and Deformation of High-Strength Concrete Shear Walls. *ACI Structural Journal*, Vol. 105, No. 1, pp. 21-29.

35 Sharp, S. R., & Moruza, A. K. (2009). *Field comparison of the installation and cost of placement of epoxy-coated and MMFX 2 steel deck reinforcement: establishing a baseline for future deck monitoring* (No. FHWA/VTRC 09-R9). Virginia Transportation Research Council.

36 G30.18-09 (2014). Carbon steel bars for concrete reinforcement. *Canadian Standards Association, Mississauga, Canada.*

37 Gaston, J.R., and Hognestad, E. (1962). High strength bars as concrete reinforcement, Part 3—Tests of full-scale roof girder. *Journal of the PCA Research and Development Laboratories*, Vol. 4, No. 2, pp. 10-23.

38 Gulec, C., and Whittaker, A. (2011). Empirical equations for peak shear strength of low aspect ratio reinforced concrete walls. *ACI Structural Journal*, Vol. 108, No. 1, pp. 80-89.

39 Gulec, C., Whittaker, A., and Stojadinovic, B. (2008). Shear strength of squat rectangular reinforced concrete walls. *ACI Structural Journal*, Vol. 108, No. 4, pp. 488-497.

40 Gupta, A., and Rangan, B. V. (1998). High-Strength Concrete (HSC) Structural Walls. *ACI Structural Journal*, V. 95, No. 2, pp. 194-204.

41 Kupfer, H., Hilsdorf, H. K., & Rusch, H. (1969, August). Behavior of concrete under biaxial stresses. In *Journal Proceedings* (Vol. 66, No. 8, pp. 656-666).

42 Hawkins, N.M., Ghosh, S.K. (2004). Acceptance Criteria for Special Precast Concrete Structural Walls Based on Validation Testing. *PCI Journal*, V. 49, no. 5, pp. 78-92.

43 Hidalgo PA, Ledezma CA, Jordán R.M. (2002). Seismic behavior of squat reinforced concrete shear walls. *Earthquake Spectra*, Vol. 18, No. 2, pp. 187–208.

44 Hiraishi H. Evaluation of shear and flexural deformations of flexural type shear walls (1984). *Bull New Zealand Soc. Earthq. Eng.* Vol. 17, No. 2, pp. 135-44.

45 Hung, C. C., Li, H., & Chen, H. C. (2017). High-strength steel reinforced squat UHPFRC shear walls: cyclic behavior and design implications. *Engineering Structures*, *141*, 59-74.

46 Huq, M. S. (2018). *High-Strength Steel Bars in Earthquake-Resistant T-Shaped Concrete Walls* (Doctoral dissertation, University of Kansas).

47 Kaar, P.H. (1966). High strength bars as concrete reinforcement, Part 8—Similitude in flexural cracking of T-beam flanges. *Journal of the PCA Research and Development Laboratories*, Vol. 8, No. 2, pp. 2-12.

48 Kabeyasawa, T., and Hiraishi, H. (1998). Tests and analyses of high-strength reinforced concrete shear walls in Japan - High-Strength Concrete in Seismic Regions*, ACI Special Publication 176, American Concrete Institute, Farmington Hills, Michigan.*

49 Kent, D. C., & Park, R. (1971). Flexural members with confined concrete. *Journal of the Structural Division*.

50 Kimura, H., & Ishikawa, Y. (2008). Seismic Performance of High-Strength Reinforced Concrete Slender Walls Subjected to High Axial Loading. In *8th International Symposium on Utilization of High-Strength and High-Performance Concrete, Tokyo, Japan, Oct* (pp. 27-29).

51 Kimura, H., Sugano, S., Nagashima, T., & Ichikawa, A. (1993). Seismic loading tests of reinforced concrete beams using high strength concrete and high strength steel bars. In *Proceedings of the 3rd International Symposium on Utilization of High Strength Concrete* (pp. 377-384).

52 Lefas, I. D.; Kotsovos, M. D.; and Ambraseys, N. N. (1990). Behavior of Reinforced Concrete Structural Walls: Strength, Deformation Characteristics, and Failure Mechanism. *ACI Structural Journal*, Vol. 87, No. 1, pp. 23-31.

53 Lombard, J., Lau, D. T., Humar, J. L., Foo, S., & Cheung, M. S. (2000, January). Seismic strengthening and repair of reinforced concrete shear walls. In *Proc., 12th World Conf. on Earthquake Engineering* (pp. 1-8).

54 Lowes, L.N., Lehman, D.E., Birely, A.C., Kuchma, D.A., Marley, K.P., and Hart, C.R. (2012). Earthquake response of slender planar concrete walls with modern detailing. *Engineering Structures*, Vol. 43, pp. 31-47.

55 Lu, Y., & Henry, R. S. (2018). Comparison of Minimum Vertical Reinforcement Requirements for Reinforced Concrete Walls. *ACI Structural Journal*, *115*(3).

56 Collins, M. P., & Porasz, A. (1989). Shear design for high strength concrete. *CEB Bulletin d'Information*, *193*, 77-83.

57 Moehle, J. P., Hooper, J. D., Fields, D. C., & Gedhada, R. (2012). Seismic Design of Cast-in-Place Concrete Special Structural Walls and Coupling Beams A Guide for Practicing Engineers. *NEHRP Seismic Design Technical Brief No. 6, 6, 41.*

58 Muguruma, H., Watanabe, F. (1990). Ductility Improvement of High-Strength Concrete Columns with Lateral Confinement. *ACI Structural Journal*, Vol. 121, pp. 47-60.

59 NIST GCR 14-917-30 (2014). Use of High-Strength Reinforcement in Earthquake-Resistant Concrete Structures. *NEHRP Consultants Joint Venture, Gaithersburg, MD*, 231 pp.

60 Otani, S., Nagai, S., and Aoyama, H. (1996). Load-deformation relationship of high strength reinforced concrete beams. *Mete A. Sozen Symposium – A Tribute From His Students*, ACI SP-162-2, pp. 35-52, *American Concrete Institute, Farmington Hills, Michigan.*

61 Ousalem, H., Takatsu, H., Ishikawa, Y., & Kimura, H. (2009). Use of high-strength bars for the seismic performance of high-strength concrete columns. *Journal of Advanced Concrete Technology*, *7*(1), 123-134.

62 Palermo, D., & Vecchio, F. J. (2001). Behaviour of Cyclically Loaded Shear Walls. *ASCE Special Publication: Modeling of Inelastic Behavior of RC Structures under Seismic Loads*, 562-579.

63 Palermo, D., Vecchio, F. J., & Solanki, H. (2002). Behavior of three-dimensional reinforced concrete shear walls. *ACI Structural Journal*, *99*(1), 81-89.

64 Palermo, D., & Vecchio, F. J. (2003). Compression field modeling of reinforced concrete subjected to reversed loading: formulation. *Structural Journal*, *100*(5), 616-625.

65 Palermo, D., & Vecchio, F. J. (2007). Simulation of cyclically loaded concrete structures based on the finite-element method. *Journal of Structural Engineering*, *133*(5), 728-738.

66 Park, H. G., Baek, J. W., Lee, J. H., & Shin, H. M. (2015). Cyclic Loading Tests for Shear Strength of Low-Rise Reinforced Concrete Walls with Grade 550 MPa Bars. *ACI Structural Journal*, *112*(3).

67 Park, R. (1989). Evaluation of ductility of structures and structural assemblages from laboratory testing. *Bulletin of the new Zealand society for earthquake engineering*, *22*(3), 155-166.

68 Paulay, T., & Priestley, M. N. (1993). Stability of ductile structural walls. *Structural Journal*, *90*(4), 385-392.

69 Paulay, T., Priestley, M. J. N., & Synge, A. J. (1982, July). Ductility in earthquake resisting squat shearwalls. In *Journal Proceedings* (Vol. 79, No. 4, pp. 257-269).

70 Paulson, C., Graham, S. K., & Rautenberg, J. M. (2013). Determination of Yield Strength for Nonprestressed Steel Reinforcement. *Charles Pankow Foundation, Vancouver, WA*.

71 Paulson, C., Rautenberg, J. M., Graham, S. K., & Darwin, D. (2016). Defining yield strength for nonprestressed reinforcing steel. American Concrete Institute.

72 Pfister, J. F., & Mattock, A. H. (1963). *High strength bars as concrete reinforcement, part 5: lapped splices in concentrically loaded columns* (Vol. 63, p. 1963). Portland Cement Association, Research and Development Laboratories.

73 Pfund, S. J. (2012). Cyclic Response of Concrete Beams Reinforced with ASTM A1035 Grade-120 Steel Bars.

74 Pilakoutas, K., & Elnashai, A. S. (1995). Cyclic behavior of reinforced concrete cantilever walls, Part I: Experimental results. *ACI structural journal*, *92*(3), 271-281.

75 Popovics, S. (1973). A numerical approach to the complete stress-strain curve of concrete. *Cement and concrete research*, *3*(5), 583-599.

76 Rautenberg, J. M., Pujol, S., Tavallali, H., & Lepage, A. (2013). Drift capacity of concrete columns reinforced with high-strength steel. *ACI Structural Journal*, *110*(2), 307.

77 Rautenberg, J.M. (2011). Drift Capacity of Concrete Columns Reinforced with High Strength Steel. Ph.D. Thesis, *Purdue University, West Lafayette, Indiana.*

78 Restrepo, J. I., Seible, F., Stephan, B., & Schoettler, M. J. (2006). Seismic testing of bridge columns incorporating high-performance materials. *ACI Materials Journal*, *103*(4), 496.

79 Restrepo, J. I., Seible, F., Stephan, B., & Schoettler, M. J. (2006). Seismic testing of bridge columns incorporating high-performance materials. *ACI Materials Journal*, *103*(4), 496.

80 Richart, F. E., Brandtzaeg, A., & Brown, R. L. (1928). A study of the failure of concrete under combined compressive stresses. *Engineering Experiment Station. University of Illinois at Urbana Champaign, College of Engineering.*

81 Richart, F.E., and Brown, R.L. (1934). An Investigation of Reinforced Concrete Columns. *Engineering Experiment Station, University of Illinois, Urbana, Illinois.* Bulletin No. 267.

82 Saatcioglu, M., & Razvi, S. R. (1992). Strength and ductility of confined concrete. *Journal of Structural engineering*, *118*(6), 1590-1607.

83 Saatcioglu, M., & Razvi, S. R. (2002). Displacement-based design of reinforced concrete columns for confinement. *Structural Journal*, *99*(1), 3-11.

84 Salonikios, T. N., & Kappos, A. J. (1999). Cyclic Load Behavior of Low-Slenderness Reinforced. *ACI Structural Journal*, *96*(4).

85 Searle, N., DeRubeis, M., Darwin, D., Matamoros, A. B., O'Reilly, M., & Feldman, L. (2014). Anchorage of High-Strength Reinforcing Bars with Standard Hooks-Initial Tests. University of Kansas Center for Research, Inc.

86 Seckin, M. (1982). HYSTERETIC BEHAVIOR OF CAST-IN-PLACE EXTERIOR BEAM COLUMN SUB-ASSEMBLIES.

87 Shahrooz, B. M. (2011). Design of concrete structures using high-strength steel reinforcement (Vol. 679). Transportation Research Board. *Transportation Research Board of the National Academies*, *Washington, D.C.*

88 Sokoli, D., Limantono, A., & Ghannoum, W. M. (2020). Special Moment Frames with High-Strength Reinforcement--Part 2: Columns. *ACI Structural Journal*, *117*(2).

89 Sperry, J., Yasso, S., Searle, N., DeRubeis, M., Darwin, D., O'Reilly, M., Matamoros, A., Feldman, L., Lepage, A., Lequesne, R., & Ajaam, A. (2017). Conventional and High-Strength Hooked Bars—Part 1: Anchorage Tests. ACI Structural Journal, 114(1), 255

90 Taghdi, M., Bruneau, M., & Saatcioglu, M. (2000). Seismic retrofitting of low-rise masonry and concrete walls using steel strips. *Journal of Structural Engineering*, *126*(9), 1017-1025.

91 Tavallali, H., Lepage, A., Rautenberg, J., & Pujol, S. (2011). Cyclic response of concrete frame members reinforced with ultrahigh strength steel. In *Structures Congress 2011* (pp. 560-570).

92 Taylor, C. P., Cote, P. A., & Wallace, J. W. (1998). Design of slender reinforced concrete walls with openings. *Structural Journal*, *95*(4), 420-433.

93 Teng, S., & Chandra, J. (2016). *Cyclic Shear Behavior of High Strength Concrete Structural Walls* (Doctoral dissertation, Petra Christian University).

94 Teng, S., Chandra, J. (2016). Cyclic Shear Behaviour of High-Strength Concrete Structural Walls. *ACI Structural Journal*, 113(6), 1335-1345.

95 Thomas, K., & Sozen, M. A. (1965). *A study of the inelastic rotation mechanism of reinforced concrete connections*. University of Ill., Department of Civil Engineering.

96 Thomsen IV, J. H., & Wallace, J. W. (2004). Displacement-based design of slender reinforced concrete structural walls—experimental verification. *Journal of structural engineering*, *130*(4), 618-630.

97 Thomson, J. H., & Wallace, J. W. (1994). Lateral load behavior of reinforced concrete columns constructed using high-strength materials. *Structural Journal*, *91*(5), 605-615.

98 To, D. V., & Moehle, J. P. (2020). Special Moment Frames with High-Strength Reinforcement--Part 1: Beams. *ACI Structural Journal*, *117*(2).

99 Todeschini, C. E., Bianchini, A. C., & Kesler, C. E. (1964, June). Behavior of concrete columns reinforced with high strength steels. In *Journal Proceedings* (Vol. 61, No. 6, pp. 701-716).

100 Tran, T. A. (2012). *Experimental and analytical studies of moderate aspect ratio reinforced concrete structural walls* (Doctoral dissertation, UCLA).

101 Tran, T. A., & Wallace, J. W. (2014, July). Cyclic Behavior of Special Reinforced Concrete Shear Walls. In *Proceedings of the National Conference on Earthquake Engineering*.

102 Tran, T. A., & Wallace, J. W. (2012, September). Experimental study of nonlinear flexural and shear deformations of reinforced concrete structural walls. In *15th World Conference on Earthquake Engineering*.

103 Tran, T. A., & Wallace, J. W. (2015). Cyclic testing of moderate-aspect-ratio reinforced concrete structural walls. *ACI Structural Journal*, *112*(6), 653.

104 Tretiakova, K. (2013). Cyclic Response of Concrete Columns Reinforced with SAS 670 Grade-97 Steel Bars. M.S. Thesis, *Pennsylvania State University, University Park, Pennsylvania.*

105 Vecchio FJ, Wong P. VecTor2 and formworks user's manual (2003). *Toronto (Canada): University of Toronto.*

106 Vecchio, F. J. (1999). Towards cyclic load modeling of reinforced concrete. *ACI Structural Journal*, *96*, 193-202.

107 Vecchio, F. J. (2000). Disturbed stress field model for reinforced concrete: formulation. *Journal of structural engineering*, *126*(9), 1070-1077.

108 Vecchio, F. J. (1992). Finite element modeling of concrete expansion and confinement. *Journal of Structural Engineering*, *118*(9), 2390-2406.

109 Vecchio, F. J., & Collins, M. P. (1986). The modified compression-field theory for reinforced concrete elements subjected to shear. *ACI Structural Journal.*, *83*(2), 219-231.

110 Vecchio, F. J., & Lai, D. (2004). Crack shear-slip in reinforced concrete elements. *Journal of Advanced Concrete Technology*, *2*(3), 289-300.

111 Vintzeleou, E. N., & Tassios, T. P. (1987). Behavior of dowels under cyclic deformations. *Structural Journal*, *84*(1), 18-30.

112 Wallace, J. W. (1994). New methodology for seismic design of RC shear walls. *Journal of Structural Engineering*, *120*(3), 863-884.

113 Walraven, J. C. (1981). Fundamental analysis of aggregate interlock. *Journal of the Structural Division*, *107*(11), 2245-2270.

114 Walraven, J. C., & Reinhardt, H. W. (1981). Concrete mechanics. Part A: Theory and experiments on the mechanical behavior of cracks in plain and reinforced concrete subjected to shear loading. *Nasa Sti/recon Technical Report N*, *82*.

115 Wiradinata, S., & Saatcioglu, M. (1986, August). Tests of squat shear walls under lateral load reversals. In *Proceedings of the Third US National conference on earthquake engineering* (Vol. 2, pp. 1395-1406).

116 Wood, S. L. (1990). Shear strength of low-rise reinforced concrete walls. *Structural Journal*, *87*(1), 99-107.

117 Li, Y. (2016). *Blast Performance of Reinforced Concrete Beams Constructed with High-Strength Concrete and High-Strength Reinforcement* (Doctoral dissertation, University of Ottawa).

118 Zhang, Y., & Wang, Z. (2000). Seismic behavior of reinforced concrete shear walls subjected to high axial loading. *Structural Journal*, *97*(5), 739-750.

Appendix A

Design Details

A.1 WALL W1HS Design Details as per ACI 318 (2014)

A.1.1 Boundary Elements Longitudinal Reinforcement

Wall W1HS was designed to develop the probable moment resistance (M_{pr}) of the control wall. The design shear strength was therefore the shear force corresponding to the probable moment M_{pr} of Control wall.

The longitudinal reinforcement in the boundary elements of the control wall consisted of 8-15M [0.63 in dia.] bars placed in the layout shown in Figure A-1. Distributed reinforcement consisted of 10M [0.44 in dia.] bars. Both the longitudinal and distributed reinforcement were Grade 400 MPa [60 ksi]. Table A-1 presents the material and sectional properties of the control wall.

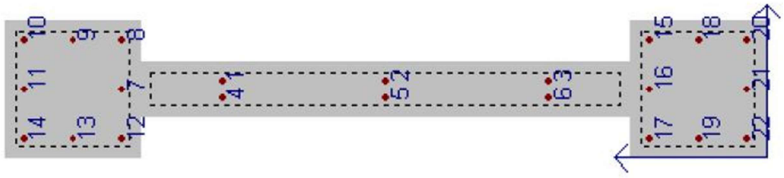

Figure A-1 – Control wall cross-section and reinforcement details modelled using RC-Section Software

Table A-1 – Control wall properties

H	**L**	**t**	**f_{yl}**	**f_{yt}**	**f'_c**	**P**	**M_{exp},**	**M_n**	**M_{pr}**
(m)	**(m)**	**(m)**	**(MPa)**	**(MPa)**	**(MPa)**	**(KN)**	**(KN.m)**	**(KN.m)**	**(KN.m)**
[in]	**[in]**	**[in]**	**[ksi]**	**[ksi]**	**[psi]**	**[kip]**	**[Kip-ft]**	**[Kip-ft]**	**[Kip-ft]**
4330	1450	100	471	710	82	1500	2650	2245	2521
[118]	[57]	[3.9]	[65]	[73]	[11603]	[296]	[1955]	[1656]	[1860]

In Table A-1, H denotes height, L is length, t is thickness, f_{yl} is the actual yield strength of the longitudinal and distributed reinforcement, f_{yt} is the yield strength of the boundary elements transverse reinforcement, f'_c is the 28-day compressive strength of concrete, P_n is the axial load, $M_{r\text{-}exp}$ is the experimental moment resistance, $M_{r\text{-}A}$ is the analytical moment resistance obtained suing RC-Section software, and $M_{pr\text{-}A}$ is the analytical probable moment resistance obtained using RC-Section software.

The longitudinal and distributed vertical reinforcement were selected to match those of the control wall except that smaller No. 4 [12.7mm dia.] and No. 3 [9.525mm dia.] bars were used instead of 15M [16mm dia.] and 10M [11mm dia.] bars respectively. The resulting probable moment of the wall was calculated using RC-Section and was further verified using VecTor2 software. Table A-2 presents these results compared to the experimental data obtained from the control wall test.

Table A-2 - Experimental vs Analytical sectional properties of Wall W1HS and the control wall

	Wall W1HS		**Control Wall**		
	RC Section, KN.m [kip.ft]	**VecTor2, KN.m [kip-ft]**	**RC Section, KN.m [kip.ft]**	**VecTor2, KN.m [kip-ft]**	**Experimental KN.m [kip.ft]**
M_{pr}	2913 [2148]	2528 [1862]	2521 [1859]	2532 [1867]	2600 [1917]
M_r	2544 [1876]	-	2245 [1656]	-	-

In Table A-2, V_n and $V_{n\text{-}pr}$ are the nominal and probable shear resistances of the walls corresponding to the nominal moment resistance M_r and probable moment resistance M_{pr} of the walls.

Figure A-2 shows the reinforcement layout for Wall W1HS. Based on the above, the probable moment considered for the shear design of the wall is taken as M_{pr} = 1991 kip-ft (2700 KN.m) that corresponds to a shear force of V_{pr}= 141 kip (628 KN).

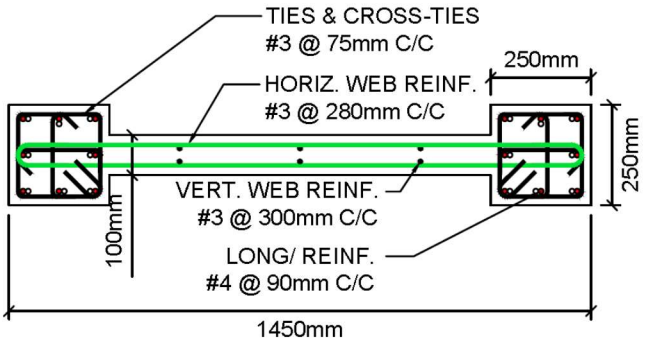

Figure A-2 - Reinforcement details of Wall W1HS

A.1.2 Horizontal Web Reinforcement

A.1.2.1 Design Shear Force, Vu

The V_u corresponding to the probable moment, M_{pr} of Wall W1HS was calculated using RC-Section software with material factors of $\phi_s = 1.25$ and $\phi_c = 1.0$:

$$M_{pr} = 1991\ kip.ft\ (2700\ KN.m)$$
$$V_u = \frac{M_{pr}}{h_w} = \frac{1991}{14.1} = 141\ kip\ (628\ \text{KN})$$

Also, using the shear and moment reduction factors with the nominal moment, M_n (calculated using RC-Section), the ultimate moment can also be calculated by as follows:

$$M_n = M_r = 1876\ kip.ft\ (2544\ KN.m)$$
$$M_u = V_u h_w$$
$$V_u \leq \emptyset_{shear} V_n$$
$$M_u = M_n \emptyset_{flexure}$$

where

$$\emptyset_{shear} = 0.75$$
$$\emptyset_{flexure} = 0.9$$

$$V_u = \frac{1.2M_n}{h_w} = \frac{1.2 \text{ x } 1876}{14.1} = 160\ kip\ (712\ KN)$$

A.1.2.1.1 Spacing of Horizontal Web Reinforcement

Distributed web horizontal reinforcement consisted of No. 3 (9.525mm dia.) Grade 690 MPa [100 ksi] MMFX ™ bars conforming to ASTM A1035 standard. The nominal yield strength of bars, f_y = 690 MPa [100 ksi] was used in shear design as follows.

According to **Clause 18.10.2.2**, at least two curtains of reinforcement shall be used in a wall if

$$V_u > 2\ A_{cv} \lambda \sqrt{f_c'} \text{ or } h_w / \ell_w \geq 2.0$$

in which h_w and ℓ_w refer to height and length of entire wall, respectively.

Since, $V_u = 160\ kip\ (712\ KN) > 2\ A_{cv}\lambda\sqrt{f_c'} = 2 * 3.9 * 57 * 1.0 * \sqrt{11603} = 47.9$ kip (213 KN), and $h_w / \ell_w = 4.3 / 1.45 = 3.0 \geq 2.0$, two curtains of reinforcement shall be used for the vertical and horizontal web reinforcement.

According to **Clause 22.5.1.1**, the nominal one-way shear strength of a section is given by:

$$V_u = V_n = V_c + V_s$$

Where V_c is given by **Clause 22.5.6.1** as follows:

$$V_c = 2\left(1 + \frac{N_u}{2000A_g}\right)\lambda\sqrt{f_c'}b_w d = 2\left(1 + \frac{292000}{2000 * 225}\right) * 1 * \sqrt{11603} * 3.9 * 57.1$$
$$= 79.1\ kip\ (352\ KN)$$

where d is the effective depth of the section is measured from the extreme compression fiber to the centroid of the tension reinforcement (57 – 9.8/2 = 52 in (1322 mm)), A_g is the gross area of the section, and N_u is the factored axial force normal to the cross-section.

$$V_s = V_u - V_c = 160 - 79.1 = 80.9\ kip\ (360\ KN)$$

$$V_s = \frac{A_v f_{yt} d}{s}$$

where A_v is the area of horizontal reinforcement layer, f_{yt} is the yield strength of the horizontal web reinforcement, and s is the spacing of the horizontal reinforcement. Using two curtains of No. 3 [9.525mm dia.] Grade 690MPa [100 ksi] bars for horizontal web reinforcement, the spacing of the transverse reinforcement becomes:

$$s = \frac{A_v f_{yt} d}{V_s} = \frac{2 * 0.11 * 100{,}000 * 52}{80900} = 14.1\ in\ (358\ mm)$$

Clause 18.10.2.1 limits the minimum distributed web reinforcement to $0.0025A_g$. This Clause also limits the maximum spacing of distributed reinforcement to 18 in (457 mm). Using two curtains of No. 3 (9.525 mm dia.) bars at 200mm, the horizontal web reinforcement ratio is calculated as follows:

$$s_t = \frac{A_v}{b\rho_t} = \frac{0.22}{3.9 * 0.0025} = 22.6\ in\ (574\ mm) > 16.8\ in\ (427\ mm)$$

Spacing of the transverse reinforcement shall also meet the requirements of **Clause 11.8.3** as follows:

$$s_t = 8.16\ in \leq \begin{cases} 3h = 3 * 3.9 = 11.7 \text{ in (297 mm)} \\ 18\ in\ (457 \text{ mm}) \\ \frac{l_w}{5} = \frac{57}{5} = 11.4\ in\ (290 \text{ mm}) \end{cases} \quad (\boldsymbol{Cl\ 11.7.3})$$

Based on **Clause 22.5.6.1, Clause 18.10.2.1,** and **Clause 11.8.3,** the spacing of the horizontal web reinforcement shall be limited to a maximum of 290mm.

Use two curtain of No. 3 (ϕ9.525 mm) Grade 690 MPa [100 ksi] ASTM A1035 reinforcement at **11 in (280 mm**) spacing.

Clause 18.10.4.1 states that the nominal shear strength of structural walls shall be smaller than the following:

$$V_n = A_{cv}\left(\alpha_c \lambda \sqrt{f_c'} + \rho_t f_y\right)$$

where the coefficient $\boldsymbol{\alpha_c}$ is 3.0 for hw/ℓw ≤ 1.5, is 2.0 for $h_w/\ell_w \geq 2.0$, and varies linearly between 3.0 and 2.0 for h_w/ℓ_w between 1.5 and 2.0.

$$A_{cv} = 3.9 * 57 = 222\ in^2\ (143{,}226\ mm^2)$$
$$\alpha_c\ = 3.0\ for\ walls\ with\ h_w/l_w\ > 2.0$$
$$f_c' = 11600\ psi\ (80\ MPa)$$
$$f_y = 100{,}076\ psi\ (690\ Mpa)$$
$$\rho_t = \frac{A_v}{bs_t} = \frac{0.22}{3.9 * 11} = 0.0051$$

$$V_n = 160{,}000\ lb <\ 222\ *\ \left(3\ *\ 1.0\ *\sqrt{11600} + 0.0051 * 100{,}076\right) = 185{,}000\ lb$$

Clause18.10.4.4 states that for all vertical wall segments, V_n shall not be taken greater than $\boldsymbol{8\ A_{cv}\sqrt{f_c'}}$ where A_{cv} is the gross area of concrete bounded by web thickness and length of section.

$$V_n = 160\ kip < 8 * 225 * \sqrt{11600} = 193\ kip$$

A.1.3 Vertical Web Reinforcement

Distributed web horizontal reinforcement consisted of No. 3 (9.525mm dia.) Grade 690 MPa [100 ksi] MMFX ™ bars conforming to ASTM A1035 standard. The nominal yield strength of bars, f_y = 690 MPa [100 ksi] was used in the design as follows.

According to **Clause 18.10.2.2**, at least two curtains of reinforcement shall be used in a wall if

$$V_u >\ 2\ A_{cv}\lambda\ \sqrt{f_c'}\ \text{ or }\ h_w/\ell_w \geq 2.0$$

in which h_w and ℓ_w refer to height and length of entire wall, respectively.

Since, $V_u = 160\ kip\ (654\ KN) > 2\ A_{cv}\lambda\sqrt{f_c'} = 2 * 3.9 * 57 * 1.0 * \sqrt{11603} = 47.9$ kip (213 KN), and $h_w / \ell_w = 4.3 / 1.45 = 3.0 \geq 2.0$, two curtains of reinforcement shall be used for the vertical and horizontal web reinforcement.

Clause 18.10.2.1 limits the minimum distributed web reinforcement to $0.0025A_g$. Using two curtains of No. 3 (9.525 mm dia.) bars, the spacing of the web vertical reinforcement at reinforcement ratio of $0.0025A_g$ is:

$$s_{t-maximum} = \frac{A_v}{b\rho_t} = \frac{0.22}{3.9 * 0.0025} = 22.5\ in\ (572\ mm)$$

Two curtains of No. 3 [9.525 mm dia.] Grade 690 MPa [100 ksi] bars were used as web vertical reinforcement. The spacing of the web vertical reinforcement shall meet the requirements of **Clause 11.7.2** as follows:

$$s_t \leq \begin{cases} 3h = 3 * 3.9 = 11.7\ in\ (297\ mm) \\ 18\ in\ (457\ mm) \\ \frac{l_w}{3} = \frac{57}{3} = 19\ in\ (483\ mm) \end{cases} \qquad (\boldsymbol{Cl.11.7.2})$$

According to **Cl 11.7.2**, Spacing of the vertical reinforcement shall be limited to 11.7 in = 297 mm ≈ 300 mm

Two curtains of No. 3 (9.525 mm dia.) Grade 690 MPa [100 ksi] MMFX ™ bars were used at **11.7 in (300 mm)** spacing as the vertical web reinforcement.

A.1.4 Boundary Elements Transverse Reinforcement

Clause 18.10.6.1: The need for special boundary elements at the edges of structural walls was evaluated in accordance with **Cl 18.10.6.2** or **Cl 18.10.6.3**. The requirements of **Cl 18.10.6.4** and Cl **18.10.6.5** were also satisfied as described in the following sections.

Clause 18.10.6.2: Walls or wall piers with $h_w/\ell_w \geq 2.0$ that are effectively continuous from the base of structure to top of wall and are designed to have a single critical section for flexure and axial loads shall satisfy (a) and (b) or shall be designed by **Cl 18.10.6.3**:

According to **Clause 18.10.6.3**, and assuming that the extreme compression fibers in Wall W1HS exceeds 0.2f'c, boundary elements were required in Wall W1HS.

Clause 18.10.6.2: Walls or wall piers with $\boldsymbol{h_w/\ell_w \geq 2.0}$ that are effectively continuous from the base of structure to top of wall and are designed to have a single critical section for flexure and axial loads shall satisfy (a) and (b) or shall be designed by **Cl 18.10.6.3**:

(a) Compression zones shall be reinforced with special boundary elements where

$$c > \frac{l_x}{600(1.5\delta_u/h_w)}$$

and $\boldsymbol{c}$ corresponds to the largest neutral axis depth calculated for the factored axial force and nominal moment strength consistent with the direction of the design displacement $\boldsymbol{\delta_u}$. Ratio $\boldsymbol{\delta_u/h_w}$ shall not be taken less than 0.005.

$$c = 7.5\ in\ (190\ mm) < \frac{57"}{600(1.5 * 0.005)} = 12.66 \text{ in } (322 \text{ mm})$$

NOTE: c is calculated using RC-Section software.

According to the **Cl 18.10.6.2** a) special boundary elements are not required; however, for the purpose of investigating the effect of high-strength reinforcement on the behaviour of walls designed for high seismic loads, special boundary elements were considered for Wall W1HS. This also provided design consistency between wall W1HS and the control wall.

(b) Where special boundary elements are required by (a), the special boundary element transverse reinforcement shall extend vertically above and below the critical section at least the greater of $\boldsymbol{\ell_w}$ and $\boldsymbol{M_u/4V_u}$, except as permitted in 18.10.6.4 (g).

$$l_w = 57\ in\ (1448\ mm)$$

$$M_u/4V_u = \frac{1991}{4*160} = 3.11\ ft = 37.3\ in\ (948\ \text{mm})$$

Boundary elements transverse reinforcements hall extend beyond the critical section at least 57 in (1448). However, in order to be consistent with the control wall, the transverse reinforcement in the boundary elements were not terminated and covered the entire height of the wall.

The following requirements of **Clause 18.10.6.4** must be satisfied where special boundary elements are required by **Clause 18.10.6.2**:

(a) The boundary element shall extend horizontally from the extreme compression fiber a distance at least the greater of ($c - 0.1\ell_w$) and ($c/2$), where c is the largest neutral axis depth calculated for the factored axial force and nominal moment strength consistent with δ_u.

c = 7.5 in (190 mm) (using RC-Section Software)
b = Boundary element width = 9.8 in (250 mm)

$$\text{b} = 9.8\ \text{in} > c - 0.1l_w = 7.5 - 0.1 * 57 = 1.8\ in\ (46\ mm)$$

$$\text{b} = 9.8\ \text{in} > c/2 = \frac{7.5}{2} = 3.75\ in\ (95.3\ mm)$$

Width of the boundary elements are greater both limits above.

(b) Width of the flexural compression zone, b, over the horizontal distance calculated by 18.10.6.4(a), including flange if present, shall be at least $h_u/16$.

$$h_u/16 = 14 \text{ ft} * \frac{12}{16} = 10.5 \text{ in (267 mm)} < 3.9 \text{ in (250 mm)}$$

Width of the boundary elements are slightly less than the above limit, however, since the difference is very small and to be consistent with the geometry of the control wall, this requirement is deemed satisfied for the boundary element dimensions.

(c) For walls or wall piers with $\mathbf{h_w/\ell_w \geq 2.0}$ that are effectively continuous from the base of structure to top of wall, designed to have a single critical section for flexure and axial loads, and with $\boldsymbol{c/\ell_w \geq 3/8}$, width of the flexural compression zone ***b*** over the length calculated in 18.10.6.4(a) shall be greater than or equal to 12 in.

$$c/l_w = \frac{7.5}{57} = 0.13 < \frac{3}{8} = 0.375;$$

Therefore, the width of the compression zone, b, did not need to be greater than or equal to 12 inches.

(d) In flanged sections, the boundary element shall include the effective flange width in compression and shall extend at least 12 in. into the web.

Wall W1HS was not considered to be a flanged wall.

(e) The boundary element transverse reinforcement shall satisfy 18.7.5.2(a) through (e) and 18.7.5.3, except the value h_x in 18.7.5.2 shall not exceed the lesser of 14 in. and two-thirds of the boundary element thickness, and the transverse reinforcement spacing limit of 18.7.5.3(a) shall be one-third of the least dimension of the boundary element.

$$h_x \leq \begin{cases} 14 \text{ in (356 mm)} \\ \frac{2}{3} * \text{b} = \frac{2}{3} * 9.8 = 6.5 \text{ in (165 mm)} \end{cases}$$

By using an 8-bar longitudinal reinforcement layout as shown in Figure A-1, the longitudinal bar spacing h_x were 3.5 in (89 mm) assuming a ¾ in (20 mm) cover.

(f) The amount of transverse reinforcement shall be in accordance with Table 18.10.6.4(f).

Table A-3 - Transverse reinforcement for special boundary elements (ACI 318-14, Table 18.10.6.4(f))

Transverse reinforcement	Applicable expressions		
A_{sh}/sb_c for rectilinear hoop	Greater of	$0.3\left(\frac{A_g}{A_{ch}}-1\right)\frac{f'_c}{f_{yt}}$	(a)
		$0.09\frac{f'_c}{f_{yt}}$	(b)
ρ_s for spiral or circular hoop	Greater of	$0.45\left(\frac{A_g}{A_{ch}}-1\right)\frac{f'_c}{f_{yt}}$	(c)
		$0.12\frac{f'_c}{f_{yt}}$	(d)

[Adapted from ACI 318-14]

$$\frac{A_{sh}}{sb_c} \geq \begin{cases} 0.3\left(\frac{A_g}{A_{ch}}-1\right)\frac{f'_c}{f_{yt}} \\ 0.09\frac{f'_c}{f_{yt}} \end{cases}$$

$$f_{yt} = 690MPa = 100{,}076\ psi$$

$$f'_c = 80MPa = 11{,}600\ psi$$

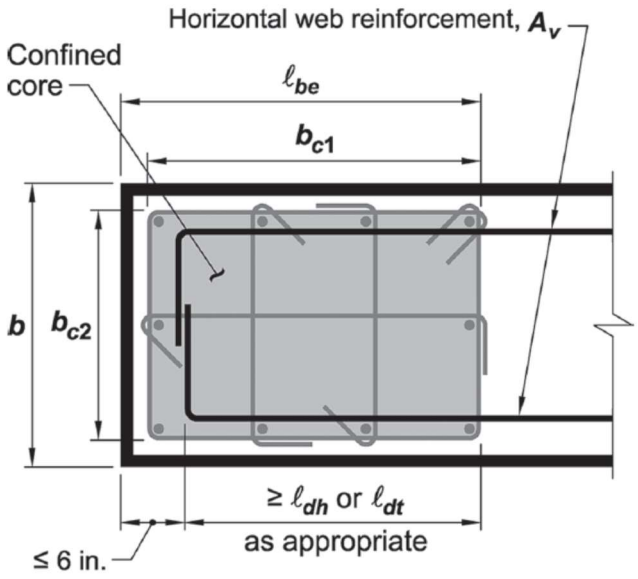

[Adapted from ACI 318-14]

$$A_g = l_{be}b = \left(\frac{250-20}{25.4}\right) * 9.8 \ = \ 88.7\ in.^2 \ (55{,}726\ mm^2)$$

$$A_{ch} = b_{c1}b_{c2} = \left(\frac{250-40}{25.4}\right)^2 = 68.4\ in.^2 \ (44{,}129\ mm^2)$$

$$\frac{A_{sh}}{sb_c} \geq \begin{cases} 0.3\left(\frac{A_g}{A_{ch}} - 1\right)\frac{f_c'}{f_{yt}} = 0.3 * \left(\frac{88.7}{68.4} - 1\right)\frac{11600}{100076} = 0.0103 \\ 0.09\frac{f_c'}{f_{yt}} = 0.09 * \frac{11600}{100076} = 0.0104 \end{cases}$$

with crossties, transverse reinforcement in the longitudinal direction was $A_{sh} = 3 * 0.11 = 0.33\ in.^2$

$$b_c = 9.8\ in.$$

$$\frac{0.33}{(s * 9.8)} \geq 0.0103$$

$$s \leq \frac{0.33}{9.8 * 0.0103} = \mathbf{3.27\ in\ (83\ mm)}$$

(g) Where the critical section occurs at the wall base, the boundary element transverse reinforcement at the wall base shall extend into the support at least ℓ_d, in accordance with

Cl 18.10.2.3, of the largest longitudinal reinforcement in the special boundary element. Where the special boundary element terminates on a footing, mat, or pile cap, special boundary element transverse reinforcement shall extend at least 12 in into the footing, mat, or pile cap, unless a greater extension is required by Cl 18.13.2.3.

Critical section was assumed to be at the base of the wall and the wall was to be supported by a footing. Hence, the transverse reinforcement in the boundary elements needed to extend 12 inches (300 mm) into the footing.

(h) Horizontal reinforcement in the wall web shall extend to within 6 in. of the end of the wall. Reinforcement shall be anchored to develop f_y within the confined core of the boundary element using standard hooks or heads. Where the confined boundary element has sufficient length to develop the horizontal web reinforcement, and A_sf_y/s of the horizontal web reinforcement does not exceed A_sf_{yt}/s of the boundary element transverse reinforcement parallel to the horizontal web reinforcement, it shall be permitted to terminate the horizontal web reinforcement without a standard hook or head.

Note: the spacing of the boundary elements transverse reinforcement was 3.0 in (75 mm) as calculated in the following sections

Horizontal web reinforcement: $\frac{A_sf_y}{s} = 0.22 * \frac{100076}{11} = 2{,}001$

Boundary element transverse reinforcement: $\frac{A_sf_y}{s} = 0.33 * \frac{100076}{3.0} = 11{,}008$

A_sf_y/s of the horizontal web reinforcement did not exceed A_sf_{yt}/s of the boundary element transverse reinforcement; however, boundary elements were not deep enough for the horizontal reinforcement to develop f_y, hence the horizontal transverse reinforcement were hooked inside the boundary elements.

Clause 18.7.5.2: Transverse reinforcement shall be in accordance with:

(a) Transverse reinforcement shall comprise either single or overlapping spirals, circular hoops, or rectilinear hoops with or without crossties.

Rectangular hoops were used in wall W1HS.

(b) Bends of rectilinear hoops and crossties shall engage peripheral longitudinal reinforcing bars.

Bends of the hoops engaged the peripheral longitudinal bars.

(c) Crossties of the same or smaller bar size as the hoop shall be permitted, subject to the limitation of **Cl 25.7.2.2**. Consecutive crossties shall be alternated end for end along the longitudinal reinforcement and around the perimeter of the cross section.

Cross-ties were the same size as the rectangular ties and were in accordance with Clause 25.7.2.2.

(d) Where rectilinear hoops or crossties are used, they shall provide lateral support to longitudinal reinforcement in accordance with **Cl 25.7.2.2** and **Cl 25.7.2.3**.

Clause 25.7.2.2: Diameter of tie bars shall be at least No. 3 (9.525 mm dia.) enclosing No. 10 (32.2 mm dia.) or smaller longitudinal bars.

No. 3 (9.525 mm dia.) bars were used as ties in the boundary elements enclosing No. 4 (12.7 mm dia.) bars were used as the longitudinal reinforcement in the boundary elements which satisfied the requirements of this Clause.

Clause 25.7.2.3: Rectilinear ties shall be arranged to satisfy (a) and (b):

(a) Every corner and alternate longitudinal bar shall have lateral support provided by the corner of a tie with an included angle of not more than 135 degrees.

All corner bars and alternate longitudinal bars were enclosed by the corner of a tie.

(b) No unsupported bar shall be farther than 6 in. clear on each side along the tie from a laterally supported bar

According to this Clause, the middle bars in an 8-bar configuration did not need to be supported by crossties as the longitudinal reinforcement spacing was less than 6 inches. However, to satisfy the requirements of Table 18.10.6.4 (f) and to be as close as possible to the control wall design, cross-ties in the horizontal and out-of-plane directions were provided.

Hence, cross-ties in both horizontal and out-of-plane directions were provided to support all longitudinal bars.

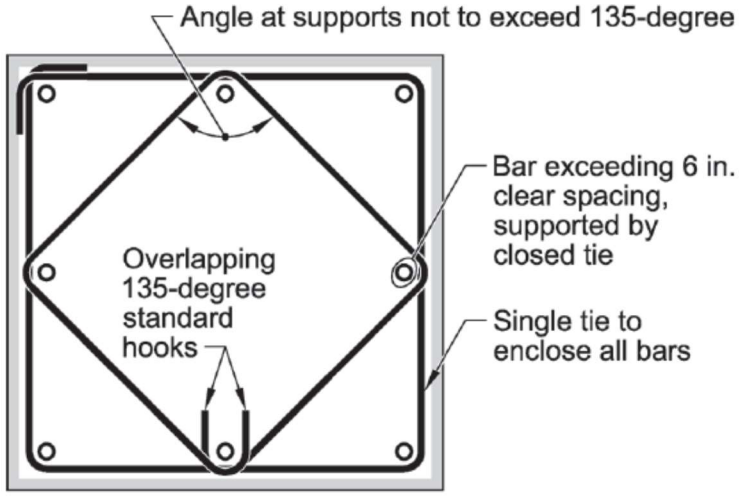

[Adapted from ACI 318-14]

(e) Reinforcement shall be arranged such that the spacing $\mathbf{h_x}$ of longitudinal bars laterally supported by the corner of a crosstie or hoop leg shall not exceed 14 in. around the perimeter of the column.

Clause 18.10.6.4 e) states that h_x in **Clause 18.7.5.2** shall be the lesser of 14 in (356 mm) or two-thirds of the boundary element thickness which in the case of Wall W1HS was 2/3 x 9.8 = 6.6 in (167 mm). All bars were supported by a corner of a crosstie or hoop as shown below.

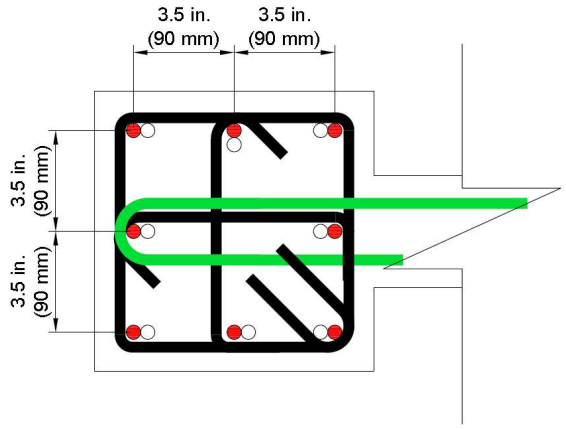

Figure A-3 Wall W1HS boundary element reinforcement details

Maximum spacing between supported bars is 3.5 in (90 mm) which satisfies the above limits.

Clause 18.7.5.3: Spacing of transverse reinforcement shall not exceed the smallest of (a) through (c):

(a) One-fourth of the minimum column dimension:

$$s_{ties} = \frac{1}{4} * 9.8 \text{ in} = \mathbf{2.5\ \textit{in}\ (62\ mm)}$$

Clause 18.10.6.4 e) requires that this limit should be changed to 1/3 of the least dimension of the boundary element:

$$S_{ties} = \frac{1}{3} * 9.8 \text{ in} = \mathbf{3.27\ (83\ mm)}$$

(b) Six times the diameter of the smallest longitudinal bar

$s_{ties} = 6 * d_b = 6 * 0.5 = \mathbf{3.0\ in}\ (\mathbf{76.2\ mm})$ (assuming No.4 longitudinal bars)

(c) s_o, calculated as follows:

Cover = 0.79 in (20 mm)
d_{tie} = 0.33 in (9.5 mm)
$d_{long.}$ = 0.5 in (12.7 mm)

$h_x = 3.5\ in\ (90\ mm)$ (as per definition of Figure R18.7.5.2 for an 8-bar reinforcement layout in the boundary elements)

The smaller of $\begin{cases} s_o = 4 + \left(\frac{14-h_x}{3}\right) = 4 + \left(\frac{14-3.5}{3}\right) = 7.5\ in\ (191\ mm) \\ 4\ in < s_o < 6\ in\ (102\ mm < s_o < 152\ mm) \end{cases}$

$\boldsymbol{s_o = 6\ in\ (152.4\ mm)}$

The value of ***so*** from Eq. (18.7.5.3) shall not exceed 6 in. and need not be taken less than 4 in.

The spacing of transverse reinforcement was limited to $\boldsymbol{S_{ties} = 3.27\ in\ (83\ mm)}$ calculated according to **Clause 18.10.6.4 (f)**.

To be consistent with the control wall, slightly conservative, use No. 3 (9.525 mm dia.) Grade 690 MPa (100 ksi) MMFX™ bars at $\boldsymbol{S_{ties} = 2.95\ in\ (75\ mm)}$.

A.1.5 Reinforcement Details

A.1.5.1 Reinforcement Details for Special Structural Walls

General requirements for reinforcement details including development of reinforcement and lap splices are given in Chapter 25 of ACI 318-14. Specifications for development length in structural walls are covered in section 18.10 of the code. The following sections summarize the design reinforcement details for Wall W1HS.

Clause 18.10.2.3: Reinforcement in structural walls shall be developed or spliced for f_y in tension in accordance with Cl 25.4, Cl 25.5, and (a) through (c):

(a) Longitudinal reinforcement shall extend beyond the point at which it is no longer required to resist flexure by least $0.8\ell w$, except at the top of a wall.

Longitudinal reinforcement extend to the top of the wall.

(b) At locations where yielding of longitudinal reinforcement is likely to occur as a result of lateral displacements, development lengths of longitudinal reinforcement shall be 1.25 times the values calculated for f_y in tension

The development lengths calculated later in this section were multiplied by a factor of 1.25.

(c) Mechanical splices of reinforcement shall conform to 18.2.7 and welded splices of reinforcement shall conform to 18.2.8

Clause 18.2.7 requires mechanical splices to be of Type 1 or Type 2. Type 1 mechanical splices can develop a minimum tensile strength of $1.25f_y$ (Cl 25.5.7.1). Type 2 mechanical splices must be able to develop the specified tensile strength of the spliced bars.

Type 2 Mechanical splices (via couplers) were used in Wall W1HS. The ultimate tensile strength of No. 4 bars that were used in the longitudinal boundary elements was 175 ksi (1206 MPa).

Clause 25.4.1.1: Calculated tension or compression in reinforcement at each section of a member shall be developed on each side of that section by embedment length; hook, headed deformed bar, mechanical device, or a combination thereof.

Clause 25.4.1.4: The values of $\sqrt{f_c'}$ used to calculate development length shall not exceed 100 psi (0.69 MPa).

f_c' of Wall W1HS was 80 MPa (11600 psi), $\sqrt{f_c'} = 107\ psi\ (0.74\ MPa)$; hence, $\sqrt{f_c'} = 100\ psi\ (0.69\ MPa)$ were used for development length design.

Clause 25.4.2 specifies requirements for development of deformed bars and deformed wires in tension

Clause 25.4.2.1 Development length ℓ_d for deformed bars and deformed wires in tension shall be the greater of (a) and (b):

(a) Length calculated in accordance with 25.4.2.2 or 25.4.2.3 using the applicable modification factors of 25.4.2.4;

Development lengths calculated according to Cl 25.4.2.3 were shorter compared to those calculated as per Cl 25.4.2.2 in the case of Wall W1HS. This was due to the fact that Cl 25.4.2.3 considers factors such as the effect of concrete density, bar size, bar coating, and casting position that reduce development length. It also takes into account the effect of concrete confinement. Knowing that the Clause 25.4.2.2 results in a longer development length, a detailed calculation as per Cl 25.4.2.3 was not performed.

(b) 12 in.

Clause 25.4.2.2: For deformed bars or deformed wires, ℓ_d shall be calculated in accordance with Table 25.4.2.2.

Spacing and cover	No. 6 and smaller bars and deformed wires	No. 7 and larger bars
Clear spacing of bars or wires being developed or lap spliced not less than d_b, clear cover at least d_b, and stirrups or ties throughout ℓ_d not less than the Code minimum or Clear spacing of bars or wires being developed or lap spliced at least $2d_b$ and clear cover at least d_b	$\left(\frac{f_y \psi_t \psi_e}{25\lambda\sqrt{f_c'}}\right) d_b$	$\left(\frac{f_y \psi_t \psi_e}{20\lambda\sqrt{f_c'}}\right) d_b$
Other cases	$\left(\frac{3 f_y \psi_t \psi_e}{50\lambda\sqrt{f_c'}}\right) d_b$	$\left(\frac{3 f_y \psi_t \psi_e}{40\lambda\sqrt{f_c'}}\right) d_b$

[Adapted from ACI 318-14]

$f_y = 100{,}000\ psi\ (690\ MPa)$;

$f_c' = 11{,}600\ psi\ (80\ MPa)$;

λ= 1.0 (Normal density concrete);

$\psi_t = 1.0$ Less than 12 in (305 mm) of fresh concrete placed below horizontal reinforcement;

$\psi_e = 1.0$ Uncoated bars to be used;

Clear spacing of bars > $2d_b$;

Clear cover > d_b;

No. 4 (12.7 mm dia.) bars were used as longitudinal reinforcement in boundary elements;

No. 3 (9.525 mm dia.) bars were used as web vertical and horizontal reinforcement;

where d_b is the diameter of the bar being developed.

A.1.5.2 Basic Development Length of Boundary Elements Longitudinal Reinforcement

From Table 25.4.2.2, and assuming that the clear spacing between bars being developed was at least $2d_b$ and the clear cover was at least d_b, the basic development length for boundary element longitudinal reinforcement was calculated as follows:

Smallest clear cover between longitudinal reinforcement = 3.5 in (90 mm) > 2 x d_b =2 x 0.5 in = 1.0 in (25.4 mm)

Clear concrete cover = 0.79 in (20 mm) > d_b = 0.5 in (12.7 mm); therefor the following equation from Table 25.4.2.2 was used:

$$l_d = \left(\frac{f_y \psi_t \psi_e}{25\lambda\sqrt{f_c'}}\right) d_b$$

For No. 4 bars, d_b = 0.5 in (12.7 mm)

$$l_d = \left(\frac{f_y \psi_t \psi_e}{25\lambda\sqrt{f_c'}}\right) d_b = \left(\frac{100000*1.0*1.0}{25*1.0*100}\right) 0.5 = \mathbf{20\ in\ (508\ mm)} > 12in\ (305\ mm) \text{(cl 25.4.2.1 b)}$$

Cl 18.10.2.3 b) requires the development length calculated for f_y to be multiplied by 1.25 for structural walls:

l_d = 20*1.25 = **25 in (635 mm)**; this value is greater than the available vertical space in the foundation; hence, hooks were required.

A.1.5.3 Basic Development Length of Distributed Web Reinforcement

For No. 3 bars, d_b = 0.375 in (9.525 mm)

$$l_d = \left(\frac{f_y \psi_t \psi_e}{25\lambda\sqrt{f_c'}}\right) d_b = \left(\frac{100000*1.0*1.0}{25*1.0*100}\right) 0.375 = \mathbf{15\ in\ (381\ mm)} > 12in\ (305\ mm) \text{(cl 25.4.2.1 b)}$$

Cl 18.10.2.3 b) requires the development length calculated for f_y to be multiplied by 1.25 for structural walls:

l_d = 15*1.25 = **18.75 in (476 mm)**; this value is greater than the available vertical space in the foundation; hence, hooks were required.

NOTE: Clause 25.4.2.3 provides another equation for calculating the basic development length that considers the effect of confinement (e.g. by transverse reinforcement) and results in a slightly shorter development length. In order to be conservative and to ensure that reinforcement is effectively developed without relying on the effect of confinement, the value obtained from **Clause 25.4.2.2** was used.

A.1.5.4 Development Length of standard hooks in tension

Clause 25.4.3 specifies requirements for Development of standard hooks in tension.

Clause 25.4.3.1: Development length ℓ_{dh} for deformed bars in tension terminating in a standard hook shall be the greater of (a) through (c):

a) $\left(\frac{f_y \psi_e \psi_c \psi_r}{50\lambda\sqrt{f_c'}}\right) d_b$ with ψ_e, ψ_c, ψ_r, and λ given in 25.4.3.2.

b) 8d

c) 6 in

$\lambda = 1.0$ $(normal\ density\ concrete)$

$\psi_e = 1.0$ $(Uncoated\ steel)$

$\psi_c = 1.0$ $(cover < 2\ in\ (50\ mm))$

$\psi_r = 1.0$ for development length not enclosed in ties; 0.8 for development length enclosed in ties.

A.1.5.4.1 Boundary Elements Longitudinal Reinforcement Developing into the Foundation with 90-degree Standard Hooks

$$8d_b = 8 * 0.5 = 4\ in\ (102\ mm) < 6\ in\ (152\ mm)$$

$$l_{dh} = \left(\frac{f_y \psi_c \psi_e \psi_r}{50\lambda\sqrt{f_c'}}\right) d_b = \left(\frac{100000*1.0*1.0*1.0}{50*1.0*100}\right) * 0.5 = \mathbf{10\ in\ (254\ mm)}$$

A.1.5.4.2 Vertical Web Reinforcement Developing into the Foundation with 90-degree Standard Hooks

$$8d_b = 8 * 0.375 = 3\ in\ (76\ mm) < 6\ in\ (152\ mm)$$

$$l_{dh} = \left(\frac{f_y \psi_c \psi_e \psi_r}{50\lambda\sqrt{f_c'}}\right) d_b = \left(\frac{100000*1.0*1.0*1.0}{50*1.0*100}\right) * 0.375 = \mathbf{7.5\ in\ (191\ mm)}$$

A.1.5.4.3 Horizontal Web Reinforcement Developing into the Boundary Elements with 180-degree Hooks

$$\psi_r = 0.8\ (180^o\ hooks; also\ enclosed\ in\ ties)$$

$$8d_b = 8 * 0.375 = 3\ in < 6\ in\ (152\ mm)$$

$$l_{dh} = \left(\frac{f_y \psi_c \psi_e \psi_r}{50\lambda\sqrt{f_c'}}\right) d_b = \left(\frac{100000*1.0*1.0*0.8}{50*1.0*100}\right) * 0.375 = \mathbf{6.0\ in\ (152\ mm)}$$

A.1.5.4.4 Details of Standard Hooks Used in Tension

Clause 25.3.1 specifies requirements for standard hooks for the development of deformed bars in tension as follows:

90-degree hooks

Longitudinal reinforcement in boundary elements:

Minimum Inside Bend Diameter = $6d_b$ = 6*0.5 in = **3.0 in (76 mm)**

Straight extension = $12d_b$=12*0.5 in = **6.0 in (152 mm)**\

Web vertical reinforcement:

Minimum Inside Bend Diameter = $6d_b$ = 6*0.375 in = **2.25 in (57 mm)**

Straight extension = $12d_b$=12*0.375 in = **4.5 in (114 mm)**

180-degree hooks

Web horizontal reinforcement:

Minimum Inside Bend Diameter = $6d_b$ = 6*0.375 = **2.25 in (57 mm)**

Minimum Straight extension = **2.5 in (64 mm)**

Rectangular hoops with 135-degree hooks

Minimum Inside Bend Diameter = $4d_b$ = 4*0.375 9.525 = 38.1mm = **1.5 in**

Straight extension = greater of $6d_b$=6*9.525=57.2mm = 2.25 in or **3 in (76.2mm)**

Cross-ties with 135-degree hooks

Minimum Inside Bend Diameter = $4d_b$ = 4*9.525 = 38.1mm = **1.5 in**

Straight extension = greater of $6d_b$=6*9.525=57.2mm = 2.25 in or **3 in (76.2mm)**

Cross-ties with 90-degree hooks

Minimum Inside Bend Diameter = $4d_b$ = 4*9.525 = 38.1mm = **1.5 in**

Straight extension = greater of $6d_b$=6*9.525=57.2mm = 2.25 in or **3 in (76.2mm)**

A.1.5.4.5 Additional Details for Seismic Hooks

Clause 25.3.4: Seismic hooks used to anchor stirrups, ties, hoops, and crossties shall be in accordance with (a) and (b):

(a) Minimum bend of 90 degrees for circular hoops and 135 degrees for all other hoops;

All hoops had 135-degree hooks.

(b) Hook shall engage longitudinal reinforcement and the extension shall project into the interior of the stirrup or hoop

All hoop / cross-tie hooks engaged the peripheral longitudinal reinforcement.

Clause 25.3.5 Crossties shall be in accordance with (a) through (e):

a) Crosstie shall be continuous between ends;
b) There shall be a seismic hook at one end;
c) There shall be a standard hook at other end with minimum bend of 90 degrees;
d) Hooks shall engage peripheral longitudinal bars;
e) 90-degree hooks of two successive crossties engaging the same longitudinal bars shall be alternated end for end unless crossties satisfy **Cl 18.6.4.3** or **Cl 25.7.1.6.1**.

All cross-ties were continuous with a 90-degree hook at one end and a 180-degree hook at the other. Both ends of the cross-ties engaged a peripheral longitudinal bar and alternated between the 90-degree and 180-degree hooks over the height of the wall.

A.1.5.5 Tension lap Splices

Clause 25.5.1.2: For contact lap splices, minimum clear spacing between the contact lap splice and adjacent splices or bars shall be in accordance with the requirements for individual bars in **Cl 25.2.1**:

Clause 25.2.1: For parallel non-pre-stressed reinforcement in a horizontal layer, clear spacing shall be at least the greatest of 1 in., d_b, and **(4/3)** d_{agg}.

$d_{agg} = 0.39\ in\ (10\ mm)$

(a) $\frac{4}{3} * 0.39 = 0.52\ in\ (13.2\ mm)$;
(b) $1\ in$ (25.4 mm);
(c) $d_b = 0.5\ in\ (12.7\ mm)$ for No. 4 bars used as longitudinal reinforcement in the boundary elements;
(d) $d_b = 0.375\ in\ (9.5\ mm)$ for No. 3 bars used as vertical web reinforcement.

Clear spacing of vertical web reinforcement was **300 mm** which was greater than the above limits.

Clause 25.2.3: For longitudinal reinforcement in columns, pedestals, struts, and boundary elements in walls, clear spacing between bars shall be at least the greatest of **1.5 in**., **1.5d_b**, and **(4/3) d_{agg}**.

$d_{agg} = 0.39\ in\ (10\ mm)$;

a) 1.5 in (38.1mm);
b) $\frac{4}{3} * 0.39 = 0.52$ in (13.2 mm);
c) $1.5d_b = 0.75\ in\ (19.1\ mm)$ for No. 4 bars used as longitudinal reinforcement in the boundary elements;
d) $1.5d_b = 0.56\ in\ (14.2\ mm)$ for No. 3 bars used as vertical web reinforcement.

The smallest of the clear spacings of longitudinal reinforcement was **90 mm** which was greater than the above limits.

Clause 25.5.2.1: Tension lap splice length ℓ_{st} for deformed bars and deformed wires in tension shall be in accordance with **Table 25.5.2.1**, where ℓ_d shall be in accordance with 25.4.2.1(a).

Table A-4 Lap splice lengths of deformed bars and deformed wires in tension
(ACI 318-14, Table 25.5.2.1)

$A_{s,provided}/A_{s,required}$[1] over length of splice	Maximum percent of A_s spliced within required lap length	Splice type	ℓ_{st}	
≥ 2.0	50	Class A	Greater of:	$1.0\ell_d$ and 12 in.
	100	Class B	Greater of:	$1.3\ell_d$ and 12 in.
< 2.0	All cases	Class B		

[1]Ratio of area of reinforcement provided to area of reinforcement required by analysis at splice location.

[Adapted from ACI 318-14]

A.1.5.5.1 Lap Spices of Boundary Elements Longitudinal Reinforcement

l_d = 25 in (635 mm) (as per **Cl 25.4.2.1 a)**, and multiplied by 1.25 as per **Cl 18.10.2.3. b)**);

- $A_{s,provided}/A_{s,required} < 2$
- According to **Table 25.5.2.1**, splice type was Class B with splice length equal to the greater of
  - $1.3l_d = 1.3 * 25\ in = \mathbf{32.5\ in}\ (\mathbf{826\ mm}),\ a$nd;
  - $12\ in$ (305 mm)

Longitudinal reinforcement in the boundary elements had a minimum lap splice length of **32.5 in (826 mm)**.

A.1.5.5.2 Tension Lap Splice of Vertical Web Reinforcement:

l_d = 18.75 in (476 mm) (as per **Cl 25.4.2.1 a)**, and multiplied by 1.25 as per **Cl 18.10.2.3. b)**);

- $A_{s,provided}/A_{s,required} < 2$
- According to Table 25.5.2.1, splice type was Class B with splice length equal to the greater of

- $1.3l_d = 1.3 * 18.75\ in = \mathbf{24.4\ in}\ (\mathbf{619\ mm}),\ and$;
- $12\ in$ (305 mm)

Vertical web reinforcement had a minimum lap splice length of **24.4 in (619 mm)**.

A.1.5.5.3 Location of Lap Splices

As shown in Table 10.7.5.2.2, Clause 10.7.5.2.2 of ACI 318-14 allows for lap splicing of all reinforcement at the same section of the wall (over wall height) given that Type B lap splices are specified. However, CSA A23.3 requires that only up to 50% of reinforcement be lap spliced at any section. Therefore, for Wall W1HS to conform to the requirements of CSA A23.3, only 50% of the reinforcement was spliced at the critical section of the wall.

10.7.5.2.2: If the bar force due to factored loads is tensile, tension lap splices shall be in accordance with **Table 10.7.5.2.2**.

Table A-5 – Tension Lap Splices
(ACI 318-14, Table 10.7.5.2.2)

Tensile bar stress	Splice details	Splice type
$\leq 0.5f_y$	$\leq$ 50% bars spliced at any section and lap splices on adjacent bars staggered by at least ℓ_d	Class A
	Other	Class B
$> 0.5f_y$	All cases	Class B

A.1.5.6 Compression lap splices

Clause 25.5.5.1: Compression lap splice length $\boldsymbol{\ell_{sc}}$ of No. 11 or smaller deformed bars in compression shall be calculated in accordance with (a) or (b):

(a) For $\boldsymbol{f_y \leq 60{,}000}$ **psi**: $\boldsymbol{\ell_{sc}}$ is the greater of $\mathbf{0.0005}\boldsymbol{f_y d_b}$ and 12 in.
(b) For $\boldsymbol{f_y > 60{,}000}$ **psi**: $\boldsymbol{\ell_{sc}}$ is the greater of $\mathbf{(0.0009}\boldsymbol{f_y} \mathbf{- 24)}\ \boldsymbol{d_b}$ and 12 in.

Compression Lap Splices of Boundary Elements Longitudinal Reinforcement

$$l_{sc} = (0.0009 * 100000 - 24) * 0.5 = 33\ in = 838.2\ mm$$

Compression Lap Splices of Vertical Web Reinforcement

$$l_{sc} = (0.0009 * 100000 - 24) * 0.375 = 24.75\ in = 829\ mm$$

Note: Compression lap splice lengths calculated according to Cl 25.5.5.1 governed over tension lap splices.

A.2 WALL W2HS Design Details as per ACI 318 (2014)

A.2.1 Boundary Elements Longitudinal Reinforcement

Wall2-HS is designed to develop the probable moment resistance (Mpr) of the companion wall. The design shear strength is thus the shear corresponding to the probable moment Mpr of Wall2. The longitudinal reinforcement in the boundary elements of Wall 2 consisted of 10-20M [ϕ0.77 in] bars placed in the layout shown in Figure A-4. Distributed reinforcement consisted of 10M [ϕ0.44 in] bars. Both the longitudinal and distributed reinforcement were Grade 400 MPa [60 ksi]. Refer to section 4.3.1.1 of the proposal for additional reinforcement details. Table A-6 presents geometric and material properties of Wall2.

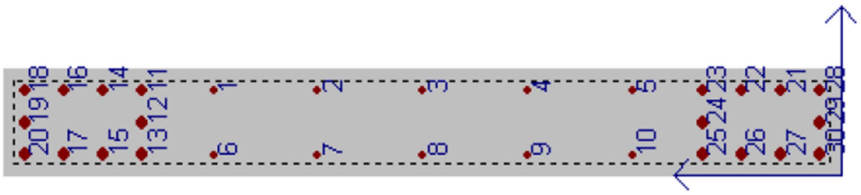

Figure A-4 – Wall 2 (companion) cross-section and reinforcement details

Table A-6 - Wall 2 (companion wall) properties

H, m [in]	**L, m [in]**	**t, m [in]**	**f_{yl}, MPa [ksi]**	**f_{yt}, MPa [ksi]**	**f'_c, MPa [psi]**	**P_n, KN [kip]**	**$M_{r\text{-}exp}$, KN.m [Kip-ft]**	**$M_{r\text{-}A.}$, KN.m [Kip-ft]**	**$M_{pr\text{-}A}$ KN.m [Kip-ft]**
3000 [118]	1600 [63]	200 [7.9]	450 [65]	500 [73]	82 [11893]	1300 [292]	3330 [2456]	3157 [2328]	3660 [2699]

In Table A-6, H denotes height, L is length, t is thickness, f_{yl} is the actual yield strength of the longitudinal and distributed reinforcement, f_{yt} is the yield strength of the boundary elements transverse reinforcement, f'_c is the 28-day compressive strength of concrete, P_n is the axial load, $M_{r\text{-}exp}$ is the experimental moment resistance, $M_{r\text{-}A}$ is the analytical moment resistance obtained suing RC-Section software, and $M_{pr\text{-}A}$ is the analytical probable moment resistance obtained using RC-Section software.

The longitudinal and distributed vertical reinforcement were selected to match those of the companion wall except that smaller No. 4 [12.7mm dia.] and No. 3 [9.525mm dia.] bars were used

instead of 20M [19.5mm dia.] and 10M [11mm dia.] bars respectively. The resulting probable moment of the proposed wall was calculated using RC-Section and were further verified using VecTor2 software. Table A-7 presents these results compared to the experimental data obtained from the companion Wall 2 test.

Table A-7 - Experimental vs Analytical sectional properties of Wall2 and Wall2-HS

	Wall W2HS		**Control Wall**		
	RC Section, KN.m [kip.ft]	**VecTor2, KN.m [kip-ft]**	**RC Section, KN.m [kip.ft]**	**VecTor2, KN.m [kip-ft]**	**Experimental KN.m [kip.ft]**
M_{pr}	3630 [2677]	3550 [2618]	3660 [2699]	3780 [2788]	3500 [2581]
M_r	3213 [2370]	-	3157 [2328]	-	-

In table A-7, V_n and $V_{n\text{-}pr}$ are the nominal and probable shear resistances of the walls corresponding to the nominal moment resistance M_r and probable moment resistance M_{pr} of the walls.

Figure A-5 shows the proposed reinforcement layout of Wall2-HS. Based on the above, the probable moment considered for the shear design of the wall is taken as M_{pr} = 2699 kip-ft (3660 KN.m) that corresponds to a shear force of V_{pr}= 272 kip (1210 KN).

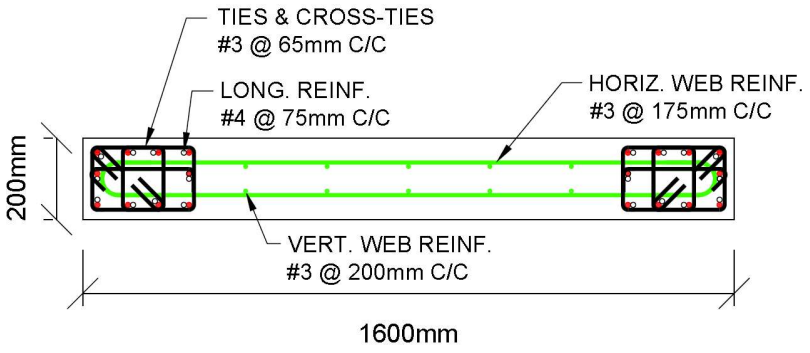

Figure A-5 - Reinforcement details of Wall W2HS

A.2.2 Horizontal Web Reinforcement

A.2.2.1 Design Shear Force, Vu

The V_u corresponding to the probable moment, M_{pr} of the proposed Wall2-HS was calculated using RC-Section software with material factors of ϕ_s = 1.25 and ϕ_c = 1.0:

$$M_{pr} = 2699\ kip.ft\ (3660\ KN.m)$$
$$V_u = \frac{M_{pr}}{h_w} = \frac{2699}{9.84} = 274\ kip\ (1219\ \text{KN})$$

Also, using the shear and moment reduction factors with the nominal moment, M_n (calculated using RC-Section), the ultimate moment can also be calculated by as follows:

$$M_n\ =\ 3157\ KN.m\ (RC - Section) = 2328.4\ kip.ft$$
$$M_u\ = V_u h_w$$
$$V_u\ \leq \emptyset_{shear} V_n$$

$$\emptyset_{shea}\ = 0.75$$

$$M_u\ = M_n \emptyset_{flexure}$$

$$\emptyset_{flexure} = 0.9$$

$$V_u\ = \frac{1.2M_n}{h_w} = \frac{2794}{9.84} =\ 284\ kip\ (1263\ KN)$$

A.2.2.2 Spacing of Horizontal Web Reinforcement

Distributed web horizontal reinforcement consist of #3 (ϕ9.525mm) Grade 690 MPa [100 ksi] MMFX ™ bars conforming to ASTM A1035 standard. The nominal yield strength of bars, f_y = 690 MPa [100 ksi] is used in shear design as follows.

According to **Clause 18.10.2.2**, at least two curtains of reinforcement shall be used in a wall if

$$V_u >\ 2\ A_{cv} \lambda \sqrt{f_c'}\ \text{ or }\ h_w / \ell_w \geq 2.0$$

in which h_w and ℓ_w refer to height and length of entire wall, respectively.

Since, $V_u = 284\ kip\ (1263\ KN) > 2\ A_{cv} \lambda \sqrt{f_c'} = 2 * 7.9 * 63 * 1.0 * \sqrt{11893} =$ 108.6 kip (480 KN), two curtains of reinforcement shall be used for the vertical and horizontal reinforcement.

According to **Clause 22.5.1.1**, the nominal one-way shear strength of a section is given by:

$$V_u = V_n = V_c + V_s$$

Where V_c is given by **Clause 22.5.6.1** as follows:

$$V_c = 2\left(1 + \frac{N_u}{2000A_g}\right)\lambda\sqrt{f_c'}b_w d = 2\left(1 + \frac{300{,}000}{2000 * 495.8}\right) * 1 * \sqrt{11600} * 7.87 * 57.1$$
$$= 126\ kip\ (560\ KN)$$

where d is the effective depth of the section is measured from the extreme compression fiber to the centroid of the tension reinforcement (1600 – 300/2 = 1450 = 57.1 in), A_g is the gross area of the section, and N_u is the factored axial force normal to the cross-section.

$$V_s = V_u - V_c = 284 - 126 = 158\ kip\ (703\ KN)$$

$$V_s = \frac{A_v f_{yt} d}{s}$$

Using two curtains of #3 [ϕ9.525mm] Grade 690MPa [100 ksi] bars for horizontal web reinforcement we obtain:

$$S_t = \frac{A_v f_{yt} d}{V_s} = \frac{2 * 0.11 * 100{,}000 * 57.1}{158000} = 7.95in\ (202\ mm)$$

Use No. 3 bars at 7.9 in (200 mm) spacing.

Clause 18.10.2.1 limits the minimum distributed web reinforcement to $0.0025A_g$. This Clause also limits the maximum spacing of distributed reinforcement to 18 in (457 mm). Using two curtains of #3 (ϕ9.525 mm) bars at 200mm, the horizontal web reinforcement ratio is calculated as follows:

$$s_t = 7.9\ in < s_{t-maximum} = \frac{A_v}{b\rho_t} = \frac{0.22}{7.9 * 0.0025} = 11.14\ in\ (283\ mm)$$

Spacing of the transverse reinforcement shall also meet the requirements of **Clause 11.8.3** as follows:

$$s_t = 8.16\ in \leq \begin{cases} 3h = 3 * 7.9 = 23.7\ in. \\ 18\ in. \\ \frac{l_w}{5} = \frac{63}{5} = 12.6\ in. \end{cases} \quad (\boldsymbol{Cl\ 11.7.3})$$

Clause 18.10.4.1 states that the nominal shear strength of structural walls shall be smaller than the following:

$$V_n = A_{cv}\left(\alpha_c \lambda \sqrt{f_c'} + \rho_t f_y\right)$$

where the coefficient $\boldsymbol{\alpha_c}$ is 3.0 for hw/ℓw ≤ 1.5, is 2.0 for $h_w/\ell_w \geq 2.0$, and varies linearly between 3.0 and 2.0 for h_w/ℓ_w between 1.5 and 2.0.

$$A_{cv} = 7.9" * 63" = 497.7\ in.^2$$
$$\alpha_c = 2.25\ for\ \frac{h_w}{l_w} = 1.875$$
$$f_c' = 80\ MPa = 11893\ psi$$
$$f_y = 690\ Mpa = 100{,}076\ psi$$
$$\rho_t = \frac{A_v}{bs_t} = \frac{0.22}{7.87 * 6.88} = 0.44\%$$

$$V_n = 284{,}000\ lb < 497.7 * \left(2.25 * 1.0 * \sqrt{11893} + 0.0044 * 100{,}076\right) = 324{,}497\ lb$$

Clause18.10.4.4 states that for all vertical wall segments, V_n shall not be taken greater than $\boldsymbol{A_{cv}\sqrt{f_c'}}$. A_{cv} is the gross area of concrete bounded by web thickness and length of section.

$$V_n = 290kip < 8 * 497.7 * \sqrt{11600} = 429\ kip > 290\ kip$$

A.2.3 Vertical Web Reinforcement

Distributed web vertical reinforcement consisted of No. 3 (9.525mm dia.) Grade 690 MPa [100 ksi] MMFX ™ bars conforming to ASTM A1035 standard. The nominal yield strength of bars, f_y = 690 MPa [100 ksi] was used in the design as follows.

According to **Clause 18.10.2.2**, at least two curtains of reinforcement shall be used in a wall if

$$V_u > 2\ A_{cv}\lambda\sqrt{f_c'}$$ or $h_w/\ell_w \geq 2.0$.

$h_w/l_w = 3000/1600 = 1.875 < 2.$

$$V_u = 284\ kip > 2\ A_{cv}\lambda\sqrt{f_c'} = 2 * 7.9 * 63 * 1.0 * \sqrt{11893} = 108.6\ \text{kip}.$$

Two curtains of reinforcement shall be used for the vertical and horizontal reinforcement. (Clause 18.10.2.2)

Clause 18.10.2.1 limits the minimum distributed web reinforcement to $0.0025A_g$. Using two curtains of #3 (ϕ9.525 mm) bars, the spacing of the web vertical reinforcement at reinforcement ratio of $0.0025A_g$ is:

$$s_{t-maximum} = \frac{A_v}{b\rho_t} = \frac{0.22}{7.9 * 0.0025} = 11.14\ in = 283\ mm$$

Two curtains of #3 [ϕ9.525 mm] Grade 690 MPa [100 ksi] bars will be used as web vertical reinforcement. The spacing of the web vertical reinforcement shall meet the requirements of **Clause 11.7.2** as follows:

$$s_t \leq \begin{cases} 3h = 3 * 7.87 = 23.62\ in. \\ 18\ in. \\ \frac{l_w}{3} = \frac{63}{3} = 21\ in. \end{cases} \qquad (\boldsymbol{Cl.11.7.2})$$

According to Cl 11.7.2, Spacing of the vertical reinforcement shall be limited to 18 in = 457 mm.

Two curtains of No.3 (9.525 mm dia.) Grade 690 MPa [100 ksi] MMFX bars were used at 7.9 in (200mm) spacing as the vertical web reinforcement.

A.2.4 Boundary Elements Transverse Reinforcement

Clause 18.10.6.1: The need for special boundary elements at the edges of structural walls was evaluated in accordance with **Cl 18.10.6.2** or **Cl 18.10.6.3**. The requirements of **Cl 18.10.6.4** and Cl **18.10.6.5** were also satisfied as described in the following sections.

Clause 18.10.6.2: Walls or wall piers with $h_w/\ell_w \geq 2.0$ that are effectively continuous from the base of structure to top of wall and are designed to have a single critical section for flexure and axial loads shall satisfy (a) and (b) or shall be designed by **Cl 18.10.6.3**:

According to **Clause 18.10.6.3**, and assuming that the extreme compression fibers in Wall2-HS will exceed 0.2f'c, boundary elements are required in Wall2-HS.

The following requirements of **Clause 18.10.6.4** must be satisfied where special boundary elements are required by **Clause 18.10.6.3**:

(i) The boundary element shall extend horizontally from the extreme compression fiber a distance at least the greater of (c – 0.1ℓ_w) and (c/2), where c is the largest neutral axis depth calculated for the factored axial force and nominal moment strength consistent with δ_u.

$$c > \frac{l_x}{600(1.5\delta_u/h_w)} = \frac{63}{600 * (1.5 * 0.005)} = 14"$$

$$c - 0.1l_w = 14 - 0.1*63 = 7.7\ in\ (196\ mm)$$

$$c/2 = \frac{14}{2} = 7\ in\ (178\ mm)$$

The length of the boundary element is 11.8" (300mm) which is greater than the above limits.

(j) Width of the flexural compression zone, b, over the horizontal distance calculated by 18.10.6.4(a), including flange if present, shall be at least $h_u/16$.

$$h_u/16 = 9.84 \text{ ft} * \frac{12}{16} = 7.4 \text{ in (188 mm)} < 7.9 \text{ in (200 mm)}$$

Width of the wall over its entire length is 7.9 in (200 mm) which is greater than the above limit.

(k) For walls or wall piers with $\boldsymbol{h_w/\ell_w \geq 2.0}$ that are effectively continuous from the base of structure to top of wall, designed to have a single critical section for flexure and axial loads, and with $\boldsymbol{c/\ell_w \geq 3/8}$, width of the flexural compression zone ***b*** over the length calculated in 18.10.6.4(a) shall be greater than or equal to 12 in.

$h_w/\ell_w = 1.875 < 2.0$; hence this requirement does not need to be satisfied for wall 2.

(l) In flanged sections, the boundary element shall include the effective flange width in compression and shall extend at least 12 in. into the web.

Wall 2 is not flanged.

(m) The boundary element transverse reinforcement shall satisfy 18.7.5.2(a) through (e) and 18.7.5.3, except the value h_x in 18.7.5.2 shall not exceed the lesser of 14 in. and two-thirds of the boundary element thickness, and the transverse reinforcement spacing limit of 18.7.5.3(a) shall be one-third of the least dimension of the boundary element.

$$h_x \leq \begin{cases} 14 \text{ in (356 mm)} \\ \frac{2}{3} * 7.87 \text{ in} = 5.25 \text{ in (133 mm)} \end{cases}$$

By using 10-bar longitudinal reinforcement configuration, the longitudinal bar spacing h_x would be 3" (75mm) in the horizontal direction and 2.4" (60mm) in the out-of-plane direction which are both less than above limits.

(n) The amount of transverse reinforcement shall be in accordance with Table 18.10.6.4(f).

Table 18.10.6.4(f)—Transverse reinforcement for special boundary elements

Transverse reinforcement	Applicable expressions		
A_{sh}/sb_c for rectilinear hoop	Greater of	$0.3\left(\frac{A_g}{A_{ch}}-1\right)\frac{f'_c}{f_{yt}}$	(a)
		$0.09\frac{f'_c}{f_{yt}}$	(b)
ρ_s for spiral or circular hoop	Greater of	$0.45\left(\frac{A_g}{A_{ch}}-1\right)\frac{f'_c}{f_{yt}}$	(c)
		$0.12\frac{f'_c}{f_{yt}}$	(d)

[Adapted from ACI 318-14]

$$\frac{A_{sh}}{sb_c} \geq \begin{cases} 0.3\left(\frac{A_g}{A_{ch}}-1\right)\frac{f'_c}{f_{yt}} \\ 0.09\frac{f'_c}{f_{yt}} \end{cases}$$

$$f_{yt} = 100{,}076\ psi\ (690MPa)$$

$$f'_c = 11{,}600\ psi\ (80MPa)$$

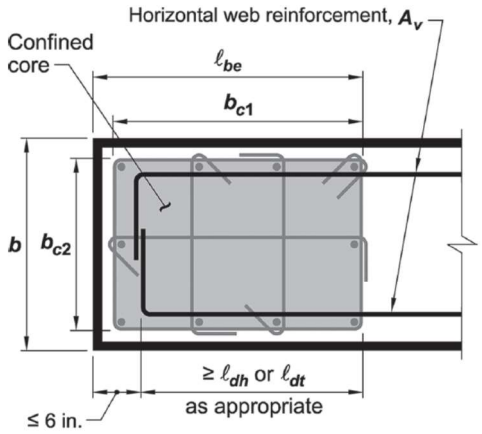

[Adapted from ACI 318-14]

Cover = ¾ in (20 mm)

Tie bar diameter = 0.375 in (9.525 mm)

$$A_g = l_{be}b = \left(\frac{300-20}{25.4}\right) * 7.87" \ = 86.8\ in^2\ (56{,}000\ mm^2)$$

$$A_{ch} = b_{c1}b_{c2} = \frac{(300-40)*(200-40)}{(25.4)^2} = 64.48\ in^2 (41{,}600\ mm^2)$$

$$\frac{A_{sh}}{sb_c} \geq \begin{cases} 0.3\left(\frac{A_g}{A_{ch}}-1\right)\frac{f_c'}{f_{yt}} = 0.3 * \left(\frac{86.8}{64.48}-1\right)\frac{11600}{100076} = 0.01204 \\ 0.09\frac{f_c'}{f_{yt}} = 0.09 * \frac{11600}{100076} = 0.0104 \end{cases}$$

Assuming one crosstie (in the horizontal direction inside the boundary element) resulting in a total of 3x No. 3 (9.525 mm dia.) shear legs in the horizontal direction

$$A_{sh} = 3 * 0.11 = 0.33\ in.^2$$

$$b_c = 7.87\ in.$$

$$\frac{0.33}{(s * 7.87)} \geq 0.01204$$

$$S_{t-maximum} \leq \frac{0.33}{7.87 * 0.01204} = 3.48\ in\ (88.45mm)$$

This clause limits boundary elements tie spacing to a maximum of 3.48 in (88.45mm); however, the requirements of **Cl 17.8.5.3 b)** should also be satisfied.

(o) Where the critical section occurs at the wall base, the boundary element transverse reinforcement at the wall base shall extend into the support at least ℓ_d, in accordance with Cl 18.10.2.3, of the largest longitudinal reinforcement in the special boundary element. Where the special boundary element terminates on a footing, mat, or pile cap, special

boundary element transverse reinforcement shall extend at least 12 in into the footing, mat, or pile cap, unless a greater extension is required by Cl 18.13.2.3.

Critical section occurs at the base of the wall and is to be supported by a footing. Hence, the transverse reinforcement in the boundary elements extended 12 inches (300 mm) into the footing.

(p) Horizontal reinforcement in the wall web shall extend to within 6 in. of the end of the wall. Reinforcement shall be anchored to develop f_y within the confined core of the boundary element using standard hooks or heads. Where the confined boundary element has sufficient length to develop the horizontal web reinforcement, and A_sf_y/s of the horizontal web reinforcement does not exceed A_sf_{yt}/s of the boundary element transverse reinforcement parallel to the horizontal web reinforcement, it shall be permitted to terminate the horizontal web reinforcement without a standard hook or head.

Horizontal web reinforcement: $\frac{A_s f_y}{s} = 0.22 * \frac{100076}{7.87} = 2797$

Boundary element transverse reinforcement: $\frac{A_s f_y}{s} = 0.22 * \frac{100076}{2.56} = 8600$

A_sf_y/s of the horizontal web reinforcement does not exceed A_sf_{yt}/s of the boundary element transverse reinforcement; however, boundary elements are not deep enough for the horizontal reinforcement to develop f_y, hence the horizontal transverse reinforcement were hooked inside the boundary elements.

Clause 18.7.5.2: Transverse reinforcement shall be in accordance with:

(f) Transverse reinforcement shall comprise either single or overlapping spirals, circular hoops, or rectilinear hoops with or without crossties.

Rectangular hoops were used in wall 2.

(g) Bends of rectilinear hoops and crossties shall engage peripheral longitudinal reinforcing bars.

Bends of the proposed hoops engaged the peripheral longitudinal bars.

(h) Crossties of the same or smaller bar size as the hoop shall be permitted, subject to the limitation of **Cl 25.7.2.2**. Consecutive crossties shall be alternated end for end along the longitudinal reinforcement and around the perimeter of the cross section.

Cross-ties will be the same size as the rectangular ties and will be in accordance with Clause 25.7.2.2.

(i) Where rectilinear hoops or crossties are used, they shall provide lateral support to longitudinal reinforcement in accordance with **Cl 25.7.2.2** and **Cl 25.7.2.3**.

Clause 25.7.2.2: Diameter of tie bar shall be at least No. 3 (ϕ9.525 mm) enclosing No. 10 (ϕ32.2 mm) or smaller longitudinal bars.

The longitudinal reinforcement in the boundary elements will be No. 4 (ϕ12.7 mm) hence No. 3 (ϕ9.525 mm) bars will be used as ties in the boundary elements.

Clause 25.7.2.3: Rectilinear ties shall be arranged to satisfy (a) and (b):

(c) Every corner and alternate longitudinal bar shall have lateral support provided by the corner of a tie with an included angle of not more than 135 degrees.

All corner bars and alternate longitudinal bars will be enclosed by the corner of a tie.

(d) No unsupported bar shall be farther than 6 in. clear on each side along the tie from a laterally supported bar

According to this Clause, the middle bars in a 10-bar configuration do not need to be supported by crossties as the longitudinal reinforcement spacing is less than 6". However, to satisfy the requirements of Table 18.10.6.4 (f) and to be as close as possible to the Companion Wall 2 design, cross-ties in the horizontal direction will be provided.

Cross-ties will also be provided in the out-of-plane direction that will support the alternate bars.

Hence, cross-ties in both horizontal and out-of-plane directions will be provided to support all longitudinal bars.

(j) Reinforcement shall be arranged such that the spacing h_x of longitudinal bars laterally supported by the corner of a crosstie or hoop leg shall not exceed 14 in. around the perimeter of the column.

Clause 18.10.6.4 e) states that h_x in **Clause 18.7.5.2** shall be the lesser of 14 in (356 mm) or two-thirds of the boundary element thickness which in the case of wall W2HS is 2/3 x 7.87 = 5.3 in (135 mm). All bars will be supported by a corner of a crosstie or hoop as shown below.

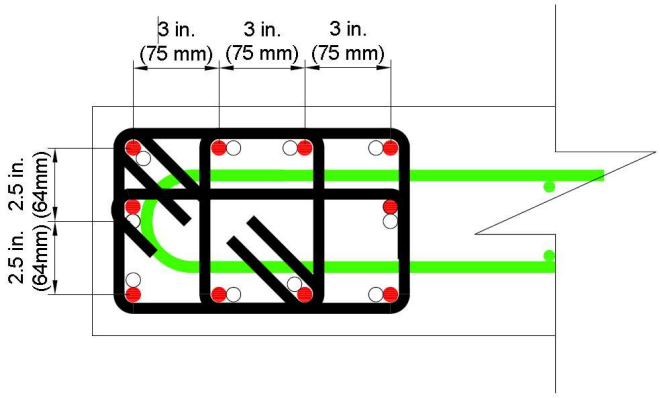

Maximum spacing between supported bars is 3 in (75mm) which is less than the above limits.

Clause 18.7.5.3: Spacing of transverse reinforcement shall not exceed the smallest of (a) through (c):

(a) One-fourth of the minimum column dimension:

$$s_{ties} = \frac{1}{4} * 7.87" = 1.96\ in\ (50\text{mm})$$

Clause 18.10.6.4 e) requires that this limit should be changed to 1/3 of the least dimension of the boundary element:

$$S_{ties} = \frac{1}{3} * 7.87" = 2.62\ in\ (\mathbf{66.7mm})$$

(b) Six times the diameter of the smallest longitudinal bar

$s_{ties} = 6 * d_b = 6 * 0.5 = 3.0\ in\ (76.2\ mm)$ (assuming No.4 (ϕ12.7mm) longitudinal bars)

(c) s_o, calculated as follows:

Cover =0.79 in (20 mm)

d_{tie} = 0.33 in (9.5 mm)

$d_{long.}$ = 0.5 in (12.7 mm)

$h_x = 3\ in\ (75\ mm)$ (as per definition of Figure R18.7.5.2 for a 10-bar reinforcement layout in the boundary elements)

$$\text{The smaller of } \begin{cases} s_o = 4 + \left(\frac{14-h_x}{3}\right) = 4 + \left(\frac{14-3}{3}\right) = 7.67\ in. \\ 4" < s_o < 6" \end{cases}$$

$$\boldsymbol{s_o = 6\ in\ (152.4\ mm)}$$

The value of ***so*** from Eq. (18.7.5.3) shall not exceed 6 in. and need not be taken less than 4 in.

The spacing of transverse reinforcement is limited to $\boldsymbol{S_{ties} = 2.63\ in\ (66.7\ mm)}$ as calculated according to **Clause 18.7.5.2** (and 18.10.6.4 e)).

Use #3 (ϕ9.525 mm) Grade 690 MPa (100 ksi) MMFX™ bars at $\boldsymbol{S_{ties} = 2.56\ in\ (65\ mm)}$

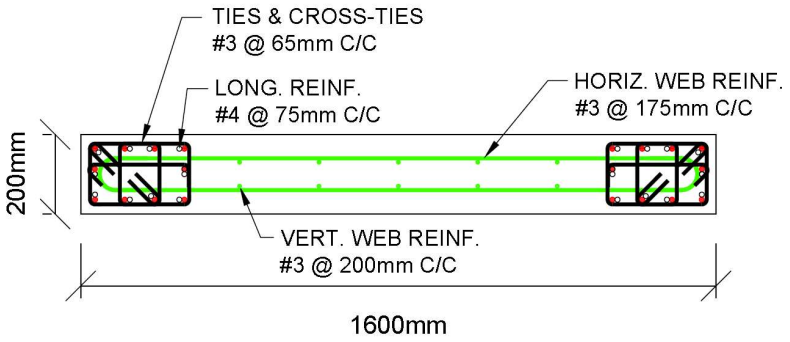

A.2.5 Reinforcement Details

A.2.5.1 Reinforcement Details for Special Structural Walls

General requirements for reinforcement details including development of reinforcement and lap splices are given in Chapter 25 of ACI 318-14. Specifications for development length in structural walls are covered in section 18.10 of the code. The following sections summarize reinforcement details for Wall2-HS.

Clause 18.10.2.3: Reinforcement in structural walls shall be developed or spliced for f_y in tension in accordance with Cl 25.4, Cl 25.5, and (a) through (c):

(a) Longitudinal reinforcement shall extend beyond the point at which it is no longer required to resist flexure by least **0.8ℓ_w**, except at the top of a wall.

Longitudinal reinforcement extend to the top of the wall.

(b) At locations where yielding of longitudinal reinforcement is likely to occur as a result of lateral displacements, development lengths of longitudinal reinforcement shall be 1.25 times the values calculated for f_y in tension

The development lengths calculated later in this section will be multiplied by a factor of 1.25.

(c) Mechanical splices of reinforcement shall conform to **Cl 18.2.7** and welded splices of reinforcement shall conform to 18.2.8

Mechanical or welded splices will not be used in Wall 2.

Clause 25.4.1.1: Calculated tension or compression in reinforcement at each section of a member shall be developed on each side of that section by embedment length; hook, headed deformed bar, mechanical device, or a combination thereof.

Clause 25.4.1.4: The values of $\sqrt{f_c'}$ used to calculate development length shall not exceed 100 psi (0.69 MPa).

Design f_c' of wall W2HS was 80 MPa (11600 psi), $\sqrt{f_c'} = 107\ psi\ (0.74\ MPa)$; hence, $\sqrt{f_c'} = 100\ psi\ (0.69\ MPa)$ will be used for development length design.

Clause 25.4.2 specifies requirements for development of deformed bars and deformed wires in tension

Clause 25.4.2.1 Development length ℓ_d for deformed bars and deformed wires in tension shall be the greater of (a) and (b):

(a) Length calculated in accordance with 25.4.2.2 or 25.4.2.3 using the applicable modification factors of 25.4.2.4

Development lengths calculated according to Cl 25.4.2.3 are shorter compared to those calculated as per Cl 25.4.2.2 in the case of Wall2-HS. This is due to the fact that Cl 25.4.2.3 considers factors such as the effect of concrete density, bar size, bar coating, and casting position that reduce development length if. It also takes into account the effect of confinement concrete confinement. Knowing the Clause 25.4.2.2 results in a longer development length, a detailed calculation as per Cl 25.4.2.3 is not included in this document.

(b) 12 in.

Clause 25.4.2.2: For deformed bars or deformed wires, ℓ_d shall be calculated in accordance with Table 25.4.2.2.

Table 25.4.2.2—Development length for deformed bars and deformed wires in tension

Spacing and cover	No. 6 and smaller bars and deformed wires	No. 7 and larger bars
Clear spacing of bars or wires being developed or lap spliced not less than d_b, clear cover at least d_b, and stirrups or ties throughout ℓ_d not less than the Code minimum or Clear spacing of bars or wires being developed or lap spliced at least $2d_b$ and clear cover at least d_b	$\left(\frac{f_y \psi_t \psi_e}{25\lambda\sqrt{f'_c}}\right) d_b$	$\left(\frac{f_y \psi_t \psi_e}{20\lambda\sqrt{f'_c}}\right) d_b$
Other cases	$\left(\frac{3 f_y \psi_t \psi_e}{50\lambda\sqrt{f'_c}}\right) d_b$	$\left(\frac{3 f_y \psi_t \psi_e}{40\lambda\sqrt{f'_c}}\right) d_b$

[Adapted from ACI 318-14]

$f_y = 100{,}000\ psi\ (690\ MPa)$;

$f_c' = 11{,}600\ psi\ (80\ MPa)$;

λ= 1.0 (Normal density concrete);

$\psi_t = 1.0$ Less than 12 in (305 mm) of fresh concrete placed below horizontal reinforcement;

$\psi_e = 1.0$ Uncoated bars to be used;

Clear spacing of bars > $2d_b$;

Clear cover > d_b;

No. 4 (12.7 mm dia.) bars used as longitudinal reinforcement in boundary elements;

#3 (9.525 mm dia.) bars used as web vertical and horizontal reinforcement;

where d_b is the diameter of the bar being developed.

A.2.5.2 Basic Development Length of Boundary Elements Longitudinal Reinforcement

From Table 25.4.2.2, and assuming that the clear spacing between bars being developed as at least $2d_b$ and the clear cover is at least d_b, the basic development length for boundary element longitudinal reinforcement is calculated as follows:

Smallest clear cover between longitudinal reinforcement = 2.5 in (64 mm) > 2 x d_b =2 x 0.5 in = 1.0 in (25.4 mm)

Clear concrete cover = 0.79 in (20 mm) > d_b = 0.5 in (12.7 mm); therefor use the following equation from Table 25.4.2.2:

$$l_d = \left(\frac{f_y \psi_t \psi_e}{25\lambda\sqrt{f_c'}}\right) d_b$$

For #4 bars, d_b = 0.5 in (12.7 mm)

$$l_d = \left(\frac{f_y \psi_t \psi_e}{25\sqrt{f_c'}}\right) d_b = \left(\frac{100000*1.0*1.0}{25*1.0*100}\right) 0.5 = \mathbf{20\ in\ (508\ mm)} > 12in\ (305\ mm) \text{(cl 25.4.2.1 b)}$$

Cl 18.10.2.3 b) requires the development length calculated for f_y to be multiplied by 1.25 for structural walls:

l_d = 20*1.25 = **25 in (635 mm)**; this value is greater than the available vertical space in the foundation; hence, hooks will be required.

A.2.5.3 Basic Development Length of Distributed Web Reinforcement

For No. 3 bars, d_b = 0.375 in (9.525 mm)

$$l_d = \left(\frac{f_y \psi_t \psi_e}{25\lambda\sqrt{f'_c}}\right) d_b = \left(\frac{100000*1.0*1.0}{25*1.0*100}\right) 0.375 = \mathbf{15\ in\ (381\ mm)} > 12in\ (305\ mm) \text{(cl 25.4.2.1 b)}$$

Cl 18.10.2.3 b) requires the development length calculated for f_y to be multiplied by 1.25 for structural walls:

l_d = 15*1.25 = **18.75 in (476 mm)**; this value is greater than the available vertical space in the foundation; hence, hooks will be required.

NOTE: Clause 25.4.2.3 provides another equation for calculating the basic development length that considers the effect of confinement (e.g. by transverse reinforcement) and results in slightly shorter development length. In order to be conservative and to ensure that reinforcement is effectively developed, the value obtained from **Clause 25.4.2.2** is used.

A.2.5.4 Development Length of standard hooks in tension

Clause 25.4.3 specifies requirements for Development of standard hooks in tension.

Clause 25.4.3.1: Development length ℓ_{dh} for deformed bars in tension terminating in a standard hook shall be the greater of (a) through (c):

a) $\left(\frac{f_y \psi_e \psi_c \psi_r}{50\lambda\sqrt{f_c'}}\right) d_b$ with ψ_e, ψ_c, ψ_r, and λ given in 25.4.3.2.

b) $8d_b$

c) 6 in

$\lambda = 1.0$ $(normal\ density\ concrete)$

$\psi_e = 1.0$ $(Uncoated\ steel)$

$\psi_c = 1.0$ $(cover < 2\ in\ (50\ mm))$

$\psi_r = 1.0$ for development length not enclosed in ties; 0.8 for development length enclosed in ties.

A.2.5.4.1 Boundary Elements Longitudinal Reinforcement Developing into the Foundation with 90-degree Standard Hooks

$$8d_b = 8 * 0.5 = 4\ in\ (102\ mm) < 6\ in\ (152\ mm)$$

$$l_{dh} = \left(\frac{f_y \psi_c \psi_e \psi_r}{50\lambda\sqrt{f_c'}}\right) d_b = \left(\frac{100000*1.0*1.0*1.0}{50*1.0*100}\right) * 0.5 = \mathbf{10\ in\ (254\ mm)}$$

A.2.5.4.2 Vertical Web Reinforcement Developing into the Foundation with 90-degree Standard Hooks

$$8d_b = 8 * 0.375 = 3\ in\ (76\ mm) < 6\ in\ (152\ mm)$$

$$l_{dh} = \left(\frac{f_y \psi_c \psi_e \psi_r}{50\lambda\sqrt{f_c'}}\right) d_b = \left(\frac{100000*1.0*1.0*1.0}{50*1.0*100}\right) * 0.375 = \mathbf{7.5\ in\ (191\ mm)}$$

A.2.5.4.3 Horizontal Web Reinforcement Developing into the Boundary Elements with 180-degree Hooks

$$\psi_r = 0.8\ (180^o\ hooks; also\ enclosed\ in\ ties)$$

$$8d_b = 8 * 0.375 = 3\ in < 6\ in\ (152\ mm)$$

$$l_{dh} = \left(\frac{f_y \psi_c \psi_e \psi_r}{50\lambda\sqrt{f_c'}}\right) d_b = \left(\frac{100000*1.0*1.0*0.8}{50*1.0*100}\right) * 0.375 = \mathbf{6.0\ in\ (152\ mm)}$$

A.2.5.4.4 Details of Standard Hooks Used in Tension

Clause 25.3.1 specifies requirements for standard hooks for the development of deformed bars in tension as follows:

90-degree hooks

Longitudinal reinforcement in boundary elements:

Minimum Inside Bend Diameter = $6d_b$ = 6*0.5 in = **3.0 in (76 mm)**

Straight extension = $12d_b$=12*0.5 in = **6.0 in (152 mm)**

Web vertical reinforcement:

Minimum Inside Bend Diameter = $6d_b$ = 6*0.375 in = **2.25 in (57 mm)**

Straight extension = $12d_b$=12*0.375 in = **4.5 in (114 mm)**

180-degree hooks

Web horizontal reinforcement:

Minimum Inside Bend Diameter = $6d_b$ = 6*0.375 = **2.25 in (57 mm)**

Minimum Straight extension = **2.5 in (64 mm)**

Rectangular hoops with 135-degree hooks

Minimum Inside Bend Diameter = $4d_b$ = 4*0.375 9.525 = 38.1mm = **1.5 in**

Straight extension = greater of $6d_b$=6*9.525=57.2mm = 2.25 in or **3 in (76.2mm)**

Cross-ties with 135-degree hooks

Minimum Inside Bend Diameter = $4d_b$ = 4*9.525 = 38.1mm = **1.5 in**

Straight extension = greater of $6d_b$=6*9.525=57.2mm = 2.25 in or **3 in (76.2mm)**

Cross-ties with 90-degree hooks

Minimum Inside Bend Diameter = $4d_b$ = 4*9.525 = 38.1mm = **1.5 in**

Straight extension = greater of $6d_b$=6*9.525=57.2mm = 2.25 in or **3 in (76.2mm)**

A.2.5.4.5 Additional Details for Seismic Hooks

Clause 25.3.4: Seismic hooks used to anchor stirrups, ties, hoops, and crossties shall be in accordance with (a) and (b):

(c) Minimum bend of 90 degrees for circular hoops and 135 degrees for all other hoops;

All hoops will have 135-degree hooks.

(d) Hook shall engage longitudinal reinforcement and the extension shall project into the interior of the stirrup or hoop

All hoop and cross-tie hooks will engage the longitudinal reinforcement.

Clause 25.3.5 Crossties shall be in accordance with (a) through (e):

f) Crosstie shall be continuous between ends;
g) There shall be a seismic hook at one end;
h) There shall be a standard hook at other end with minimum bend of 90 degrees;
i) Hooks shall engage peripheral longitudinal bars;
j) 90-degree hooks of two successive crossties engaging the same longitudinal bars shall be alternated end for end unless crossties satisfy 18.6.4.3 or 25.7.1.6.1.

As shown in Figure A-5, all cross-ties will be continuous with a 90-degree hook at one end and a 180-degree hook at the other. Both ends of the cross-ties will engage a peripheral longitudinal bar and will alternate between the 90-degree and 180-degree hooks over the height of the wall.

A.2.5.5 Tension lap Splices

Clause 25.5.1.2: For contact lap splices, minimum clear spacing between the contact lap splice and adjacent splices or bars shall be in accordance with the requirements for individual bars in **Cl 25.2.1**:

Clause 25.2.1: For parallel non-pre-stressed reinforcement in a horizontal layer, clear spacing shall be at least the greatest of 1 in., d_b, and **(4/3)** d_{agg}.

$d_{agg} = 0.39\ in\ (10\ mm)$

(e) $\frac{4}{3} * 0.39 = 0.52\ in\ (13.2\ mm)$;

(f) $1\ in$ (25.4 mm);

(g) $d_b = 0.5\ in\ (12.7\ mm)$ for #4 bars used as longitudinal reinforcement in the boundary elements;

(h) $d_b = 0.375\ in\ (9.5\ mm)$ for #3 bars used as vertical web reinforcement.

Clear spacing of vertical web reinforcement will be 200mm which greater than the above limits.

Clause 25.2.3 For longitudinal reinforcement in columns, pedestals, struts, and boundary elements in walls, clear spacing between bars shall be at least the greatest of **1.5 in**., **1.5**d_b, and **(4/3)** d_{agg}.

$d_{agg} = 0.39\ in\ (10\ mm)$;

1.5 in (38.1mm);

$\frac{4}{3} * 0.39 = 0.52\ in\ (13.2\ mm)$;

(a) $1.5d_b = 0.75\ in\ (19.1\ mm)$ for #4 bars used as longitudinal reinforcement in the boundary elements;

(b) $1.5d_b = 0.56\ in\ (14.2\ mm)$ for #3 bars used as vertical web reinforcement.

The smallest of the clear spacings of longitudinal reinforcement will be 64mm which is greater the above limits.

Clause 25.5.2.1: Tension lap splice length ℓ_{st} for deformed bars and deformed wires in tension shall be in accordance with **Table 25.5.2.1**, where ℓ_d shall be in accordance with 25.4.2.1(a).

Table 25.5.2.1—Lap splice lengths of deformed bars and deformed wires in tension

$A_{s,provided}/A_{s,required}$[1] over length of splice	Maximum percent of A_s spliced within required lap length	Splice type	ℓ_{st}	
≥ 2.0	50	Class A	Greater of:	$1.0\ell_d$ and 12 in.
	100	Class B	Greater of:	$1.3\ell_d$ and 12 in.
< 2.0	All cases	Class B		

[1]Ratio of area of reinforcement provided to area of reinforcement required by analysis at splice location.

[Adapted from ACI 318-14]

A.2.5.5.1 Lap Spices of Boundary Elements Longitudinal Reinforcement

l_d = 25 in (635 mm) (as per **Cl 25.4.2.1 a)**, and multiplied by 1.25 as per **Cl 18.10.2.3. b)**);

- $A_{s,provided}/A_{s,required} < 2$
- According to Table 25.5.2.1, splice type is Class B with splice length of the greater of
  - $1.3l_d = 1.3 * 25\ in = \mathbf{32.5\ in\ (826\ mm)},\ a$nd;
  - $12\ in$ (305 mm)

Longitudinal reinforcement in the boundary elements shall have a minimum lap splice length of **32.5 in (826 mm)**.

A.2.5.5.2 Tension Lap Splice of Vertical Web Reinforcement:

l_d = 18.75 in (476 mm) (as per **Cl 25.4.2.1 a)**, and multiplied by 1.25 as per **Cl 18.10.2.3. b)**);

- $A_{s,provided}/A_{s,required} < 2$
- According to Table 25.5.2.1, splice type is Class B with splice length of the greater of
  - $1.3l_d = 1.3 * 18.75\ in = \mathbf{24.4\ in}\ (\mathbf{619\ mm}),\ and$;
  - $12\ in$ (305 mm)

Vertical web reinforcement shall have a minimum lap splice length of **24.4 in (619 mm)**.

A.2.5.5.3 Location of Lap Splices

As shown in Table 10.7.5.2.2, Clause 10.7.5.2.2 of ACI 318-14 allows for lap splicing of all reinforcement at the same section of the wall (over wall height) given that Type B lap splices are specified. However, CSA A23.3 requires that only up to 50% of reinforcement be lap spliced at any section. Therefore, for Wall2-HS to conform to the requirements of CSA A23.3, only 50% of reinforcement will spliced at the critical section of the wall which is located at its base. This requirement of the CSA A23.3 Standard will be verified in detail later in this document.

10.7.5.2.2 If the bar force due to factored loads is tensile, tension lap splices shall be in accordance with Table
10.7.5.2.2.

Table 10.7.5.2.2—Tension lap splice class

Tensile bar stress	Splice details	Splice type
$\leq 0.5f_y$	$\leq$ 50% bars spliced at any section and lap splices on adjacent bars staggered by at least ℓ_d	Class A
	Other	Class B
$> 0.5f_y$	All cases	Class B

[Adapted from ACI 318-14]

A.2.5.5.4 Compression lap splices

Clause 25.5.5.1 Compression lap splice length $\boldsymbol{\ell_{sc}}$ of No. 11 or smaller deformed bars in compression shall be calculated in accordance with (a) or (b):

(c) For $\boldsymbol{f_y \leq 60{,}000}$ **psi**: $\boldsymbol{\ell_{sc}}$ is the greater of $\boldsymbol{0.0005 f_y d_b}$ and 12 in.

(d) For $\boldsymbol{f_y > 60{,}000}$ **psi**: $\boldsymbol{\ell_{sc}}$ is the greater of $\boldsymbol{(0.0009 f_y - 24)\, d_b}$ and 12 in.

Compression Lap Splices of Boundary Elements Longitudinal Reinforcement

$$l_{sc} = (0.0009 * 100000 - 24) * 0.5 = 33\ in = 838.2\ mm$$

Compression Lap Splices of Vertical Web Reinforcement

$$l_{sc} = (0.0009 * 100000 - 24) * 0.375 = 24.75\ in = 829\ mm$$

Note: Compression lap splice lengths calculated according to **Cl 25.5.5.1** govern over tension lap splices.

Appendix B

Details of Previously Tested Walls from the Literature

Table B-1- Details of tested concrete shear walls reinforced with **high-strength** reinforcement

Author	ID	Cross-section Shape	Web Thickness (mm)	Boundary Element Dimensions (mm x mm)	Wall Length (mm)	Shear Span (mm)	Aspect Ratio	Axial Compression (% $N/A_g f'_c$)	f'_c (MPa)	f_y (MPa) Boundary Element Long. Reinf.	f_y (MPa) Vert. Web Reinf.	f_y (MPa) Hori. Web Reinf.	f_y (MPa) Hoops	Drift Capacity (%)	Failure Mode
Baek et al. (2017)	NS2	Rectangular	200	300 x 200	1500	3000	2	0	36.5	617	470	470	-	2.10	WC
	HS2	Rectangular	200	300 x 200	1500	3000	2	0	36.5	617	667	667	-	2.05	WC
	NS2L	Rectangular	200	300 x 200	1500	3000	2	0	36.5	617	470	470	-	1.40	DT
	HS2L	Rectangular	200	300 x 200	1500	3000	2	0	36.5	617	667	667	-	1.25	DT
	NF2	Rectangular	200	150 x 200	1500	3000	2	0	38.1	617/653	470	470	-	1.99	CC/DT
	HF2	Rectangular	200	150 x 200	1500	3000	2	0	36.7	617/653	667	667	-	1.95	CC/DT
	HF2-500	Rectangular	200	150 x 200	1500	3000	2	0	38.2	617/653	563	563	-	1.61	CC/DT
	HF2-600	Rectangular	200	150 x 200	1500	3000	2	0	26.1	617/653	625/642	625/642	-	2..01	CC/DT
Hug et al. (2017)	T1	T-Shaped	254	762 x 254	1450	3000	2	0	55	400	400	400	400	3.73	B / BR
	T2	T-Shaped	254	763 x 254	1450	3000	2	0	55	690	690	690	690	2.05	BR
	T3	T-Shaped	254	764 x 254	1450	3000	2	0	55	690	690	690	690	3.95	B / BR
	T4	T-Shaped	254	765 x 254	1450	3000	2	0	55	690	690	690	690	4.05	B / BR
Cheng et al (2016)	M60	Rectangular	203	254 x 203	2032	2032	1	-	39	450	453	453	453	2.41	WC
	M115	Rectangular	203	254 x 203	2032	2032	1	-	38	770	786	786	453	3.05	BR
	H60	Rectangular	203	254 x 203	2032	2032	1	-	44	450	475	475	453	1.59	*
	H115	Rectangular	203	254 x 203	2032	2032	1	-	44	770	806	806	453	1.87	*
	H60X	Rectangular	203	254 x 203	2032	2032	1	-	42	450	475	475	453	1.56	*
Hung et al (2016)	UHPC-HS-0.5√f'c	Rectangular	160	276 x 160	1500	1320	0.9	0	166	706	849	849	849	1.0	WC
	UHPFRC-NS-0.5√f'c	Rectangular	160	276 x 160	1500	1320	0.9	0	125	706	825	825	849	2.0	HS
	UHPC-HS-0.83√f'c	Rectangular	160	276 x 160	1500	1320	0.9	0	158	706	825	825	849	1.0	WC
	UHPFRC-HS-0.83√f'c	Rectangular	160	276 x 160	1500	1320	0.9	0	115	706	825	825	849	3.0	WC/DT

Failure Modes: WC = Web Crushing, DT = Diagonal Tension, CC = Concrete Crushing, B = Buckling (of the boundary element longitudinal reinforcement), BR = Bar Rupture (boundary element longitudinal reinforcement), *failure characterized by severe deterioration of concrete at the base, HS = Hinge Sliding, VSC = Vertical Splitting Crack within or at the interface of the boundary elements, SC = Shear Compression failure at the corner of wall base, HBR – Horizontal Bar Rupture.

Table B-2 - Details of tested concrete shear walls reinforced with **high-strength** reinforcement

Author	ID	Cross-section Shape	Web Thickness (mm)	Boundary Element Dimensions (mm x mm)	Wall Length (mm)	Shear Span (mm)	Aspect Ratio	Axial Compression (% N/Agf'c)	f'c (MPa)	fy (MPa) Boundary Element Long. Reinf.	fy (MPa) Vert. Web Reinf.	fy (MPa) Hori. Web Reinf.	fy (MPa) Hoops	Drift Capacity (%)	Failure Mode
Chandra (2017)	J1	Barbell	100	120 x 500	1000	1000	1.0	5	103.3	630	610	610	578	0.39	CC / VSC
	J2	Barbell	100	120 x 500	1000	1000	1.0	5	96.8	630	610	610	578	0.68	WC / VSC
	J3	Barbell	100	120 x 500	1000	1000	1.0	5	110.7	630	610	610	578	0.76	WC / VSC
	J4	Rectangular	100	280 x 120	1000	1000	1.0	5	93.5	630	610	610	578	0.54	DT / CC
	J5	Barbell	100	120 x 500	1000	2000	2.0	5	103.3	630	610	610	578	0.70	DT / CC
	J6	Barbell	100	120 x 500	1000	2000	2.0	5	96.8	630	610	610	578	0.71	DT / CC
	J7	Barbell	100	120 x 500	1000	2000	2.0	5	110.7	630	610	610	578	0.99	WC
Park et al (2015)	S1	Rectangular	200	300 x 200	1500	1750	1.2	7	47	617	653	667	-	1.00	WCS
	S2	Rectangular	200	300 x 200	1500	1750	1.2	7	47	617	653	477	-	1.00	WCS
	S3	Rectangular	200	300 x 200	1500	1750	1.2	7	70	617	653	667	-	0.75	WCS
	S4	Barbell	200	200 x 300	1500	1750	1.2	7	47	617	653	667	667	1.00	WC
	S5	Rectangular	200	200 x 200	1500	1750	1.2	7	46	617	653	667	-	1.00	WCS
	S6	Rectangular	200	200 x 200	1500	1750	1.2	7	70	617	653	667	-	0.90	WCS
	S7	Rectangular	200	200 x 200	1500	1750	1.2	7	47	617	653	667	667	0.95	WC
	S8	Rectangular	200	200 x 200	1500	1750	1.2	7	47	653	653	667	667	2.57	WC
Dazio et al (2009)	WSH1	Rectangular	150	200 x 150	2000	4560	2.3	5.1	55	547.3	584	584	656	1.04	BR
	WSH2	Rectangular	150	200 x 150	2000	4560	2.3	5.7	55	583	485	485	526	1.5	BR
	WSH3	Rectangular	150	260 x 150	2000	4560	2.3	5.8	57	601	569	489	562	2.04	BR
	WSH4	Rectangular	150	-	2000	4560	2.3	5.7	59	576	584	519	562	1.4	CC
	WSH5	Rectangular	150	260 x 150	2000	4560	2.3	12.8	56	576	519	519	562	1.35	B / BR
	WSH6	Rectangular	150	260 x 150	2000	4560	2.3	10.8	59	576	584	519	562	1.77	CC

Failure Modes: WC = Web Crushing, DT = Diagonal Tension, CC = Concrete Crushing, B = Buckling (of the boundary element longitudinal reinforcement), BR = Bar Rupture (boundary element longitudinal reinforcement), *failure characterized by severe deterioration of concrete at the base, HS = Hinge Sliding, VSC = Vertical Splitting Crack within or at the interface of the boundary elements, SC = Shear Compression failure at the corner of wall base, HBR – Horizontal Bar Rupture.

Table B-3 - Details of tested concrete shear walls reinforced with **high-strength** reinforcement (continued)

Author	ID	Cross-section Shape	Web Thickness (mm)	Boundary Element Dimensions (mm x mm)	Wall Length (mm)	Shear Span (mm)	Aspect Ratio	Axial Compression (% $N/A_g f'_c$)	f'_c (MPa)	f_y (MPa) Boundary Element Long. Reinf.	f_y (MPa) Vert. Web Reinf.	f_y (MPa) Hori. Web Reinf.	f_y (MPa) Hoops	Drift Capacity (%)	Failure Mode
Kimura & Sugano (2008)	W8N18	Barbell	80	200 x 200	1400	2400	1.7	15.1	73	385	852	849	385	1.5	SC
	W8N13	Barbell	80	200 x 200	1400	2400	1.7	10	79	385	852	849	385	2.0	SC
	W8N08H	Barbell	80	200 x 200	1400	2400	1.7	6.2	79	580	852	849	385	2.0	BR / SC
	W4N18	Barbell	80	200 x 200	1400	2400	1.7	25.7	43	385	852	849	385	1.0	SC
	W4N18C	Barbell	80	200 x 200	1400	2400	1.7	25.7	43	385	852	849	385	1.0	SC
Japanese New RC Project (1988-1993)	NW-3	Barbell	80	200 x 200	1700	3300	1.9	14.5	60	727	768	768	1258	1.0	WC / HBR
	NW-4	Barbell	80	200 x 200	1700	3300	1.9	14.5	60	727	768	768	1258	1.0	WC / BR
	NW-5	Barbell	80	200 x 200	1700	3300	1.9	12.7	60	727	768	768	1258	1.5	CC / WC
	NW-6	Barbell	80	200 x 200	1700	3300	1.9	12.7	60	740	768	768	1258	1.0	CC

Failure Modes: WC = Web Crushing, DT = Diagonal Tension, CC = Concrete Crushing, B = Buckling (of the boundary element longitudinal reinforcement), BR = Bar Rupture (boundary element longitudinal reinforcement), *failure characterized by severe deterioration of concrete at the base, HS = Hinge Sliding, VSC = Vertical Splitting Crack within or at the interface of the boundary elements, SC = Shear Compression failure at the corner of wall base, HBR – Horizontal Bar Rupture.

Table B-4- Details of tested concrete shear walls reinforced with **normal-strength** reinforcement

Author	ID	Cross-section Shape	Web Thickness (mm)	Boundary Element Dimensions (mm x mm)	Wall Length (mm)	Shear Span (mm)	Aspect Ratio	Axial Compression (% $N/A_g f'_c$)	f'_c (MPa)	f_y (MPa) Boundary Element Long. Reinf.	f_y (MPa) Vert. Web Reinf.	f_y (MPa) Hori. Web Reinf.	f_y (MPa) Hoops
Tran and Wallace (2014)	RW-A20-P10-S38	Rectangular	152	210	1220	2440	2	10	48	475	475	475	440
	RW-A20-P10-S63	Rectangular	152	210	1220	2440	2	7.7	48	475	440	440	440
	RW-A15-P10-S51	Rectangular	152	210	1220	1830	1.5	7.7	48	475	475	475	440
	RW-A15-P10-S78	Rectangular	152	210	1220	1830	1.5	7.7	56	475	440	440	440
	RW-A15-P2.5-S64	Rectangular	152	210	1220	1830	1.5	1.6	56	475	440	440	440
Emamy et al (2008)	HSCW1	Barbell	75	375 x 90	980	1100	1.1	4.3	104	400*	400*	400*	400*
	HSCW2	Barbell	75	375 x 90	980	1100	980	8.5	93	400*	400*	400*	400*
	HSCW3	Barbell	75	375 x 90	980	1100	980	9.2	86	400*	400*	400*	400*
	HSCW4	Barbell	75	375 x 90	980	1100	980	21.6	91	400*	400*	400*	400*
	HSCW5	Barbell	75	375 x 90	980	1100	980	9.5	84	400*	400*	400*	400*
	HSCW6	Barbell	75	375 x 90	980	1100	980	5.1	90	400*	400*	400*	400*
	HSCW7	Barbell	75	375 x 90	980	1100	980	7.8	102	400*	400*	400*	400*
Thomsen & Wallace (2004)	RW1	Rectangular	102	102 x 210	1220	3810	3.1	10	31.6	414	414	414	414
	RW2	Rectangular	102	102 x 210	1220	3810	3.1	10	34	414	414	414	414
	TW1	Tee	102	102 x 210	1220	3810	3.1	10	43.6	414	414	414	414
	TW2	Tee	102	102 x 210	1220	3810	3.1	10	41.7	414	414	414	414

* - Nominal yield strength

Table B-5 - Details of tested concrete shear walls reinforced with **normal-strength** reinforcement (continued)

Author	ID	Cross-section Shape	Web Thickness (mm)	Boundary Element Dimensions (mm x mm)	Wall Length (mm)	Shear Span (mm)	Aspect Ratio	Axial Compression (% $N/A_g f'_c$)	f'_c (MPa)	f_y (MPa) Boundary Element Long. Reinf.	f_y (MPa) Vert. Web Reinf.	f_y (MPa) Hori. Web Reinf.	f_y (MPa) Hoops
Hidalgo et al (2002)	1	Rectangular	120	NA	1000	2000	2	0	19.4	392	392	392	392
	3	Rectangular	120	NA	1000	2000	2	0	19.6	402	402	402	402
	4	Rectangular	120	NA	1000	2000	2	0	19.5	402	402	402	402
	6	Rectangular	120	NA	1300	1800	1.4	0	17.6	314	314	314	314
	7	Rectangular	120	NA	1300	1800	1.4	0	18.1	471	471	471	471
	8	Rectangular	120	NA	1300	1800	1.4	0	15.7	471	471	471	471
	9	Rectangular	80	NA	1300	1800	1.4	0	17	366	366	366	366
	10	Rectangular	100	NA	1300	1800	1.4	0	16.4	367	367	367	367
	11	Rectangular	100	NA	1400	1800	1.3	0	16.3	362	362	362	362
	12	Rectangular	100	NA	1400	1800	1.3	0	17	366	366	366	366
	13	Rectangular	80	NA	1400	1800	1.3	0	18.1	370	370	370	370
	14	Rectangular	80	NA	1700	1200	0.7	0	17.1	366	366	366	366
	15	Rectangular	80	NA	1700	1200	0.7	0	19	366	366	366	366
	16	Rectangular	100	NA	1700	1200	0.7	0	18.8	366	366	366	366
	21	Rectangular	100	NA	1300	1800	1.4	0	24.2	-	-	-	-
	22	Rectangular	100	NA	1300	1800	1.4	0	17.2	-	-	-	-
	23	Rectangular	100	NA	1300	1800	1.4	0	24.2	431	431	431	431
	24	Rectangular	100	NA	1300	1800	1.4	0	23.9	431	431	431	431
	25	Rectangular	100	NA	1400	1400	1.3	0	23.9	-	-	-	-

Table B-6 - Details of tested concrete shear walls reinforced with **normal-strength** reinforcement (continued)

Author	ID	Cross-section Shape	Web Thickness (mm)	Boundary Element Dimensions (mm x mm)	Wall Length (mm)	Shear Span (mm)	Aspect Ratio	Axial Compression (% $N/A_g f'_c$)	f'_c (MPa)	f_y (MPa) Boundary Element Long. Reinf.	f_y (MPa) Vert. Web Reinf.	f_y (MPa) Hori. Web Reinf.	f_y (MPa) Hoops
Hidalgo et al (2002)	26	Rectangular	100	NA	1400	1400	1.3	0	17.7	-	-	-	-
	27	Rectangular	100	NA	1400	1400	1.3	0	23.9	431	431	431	431
	28	Rectangular	100	NA	1400	1400	1.3	0	23.3	431	431	431	431
	29	Rectangular	80	NA	1500	1050	0.7	0	23.2	-	-	-	-
	30	Rectangular	80	NA	1500	1050	0.7	0	17.9	-	-	-	-
	31	Rectangular	80	NA	1500	1050	0.7	0	23.1	431	431	431	431
	32	Rectangular	80	NA	1500	1050	0.7	0	23.3	431	431	431	431
Zhang & Wang (2000)	SW7	Rectangular	100	100 x 100	700	2250	3.2	24	30	405	305	305	366
	SW8	Rectangular	100	100 x 100	700	2250	3.2	35	32	432	305	305	366
	SW9	Rectangular	100	100 x 100	700	2250	3.2	24	35	375	305	305/366	366
	SRCW12	Rectangular	100	100 x 100	700	2250	3.2	35	28	432	305	305/366	366
Salonikios et al (1999)	MSW1	Rectangular	100	100 x 240	1200	1800	1.5	7	26	585	585 / 610	585 / 610	585
	MSW2	Rectangular	100	100 x 240	1200	1800	1.5	7	26	585	585	585	585
	MSW3	Rectangular	100	100 x 240	1200	1800	1.5	7	24	585	585	585	585
	MSW4	Rectangular	100	100 x 240	1200	1800	1.5	7	25	585	585	585	585
	MSW5	Rectangular	100	100 x 240	1200	1800	1.5	7	22	585	585	585	585

Table B-7 - Details of tested concrete shear walls reinforced with **normal-strength** reinforcement (continued)

Author	ID	Cross-section Shape	Web Thickness (mm)	Boundary Element Dimensions (mm x mm)	Wall Length (mm)	Shear Span (mm)	Aspect Ratio	Axial Compression (% $N/A_g f'_c$)	f'_c (MPa)	f_y (MPa) Boundary Element Long. Reinf.	f_y (MPa) Vert. Web Reinf.	f_y (MPa) Hori. Web Reinf.	f_y (MPa) Hoops
Salonikios et al (1999)	MSW6	Rectangular	100	100 x 240	1200	1800	1.5	7	28	585	585 / 610	585 / 610	585
	LSW1	Rectangular	100	100 x 240	1200	1200	1	7	22	585	585 / 610	585 / 610	585
	LSW2	Rectangular	100	100 x 240	1200	1200	1	7	22	585	585	585	585
	LSW3	Rectangular	100	100 x 240	1200	1200	1	7	24	585	585	585	585
	LSW4	Rectangular	100	100 x 240	1200	1200	1	7	23	585	585	585	585
	LSW5	Rectangular	100	100 x 240	1200	1200	1	7	25	585	585	585	585
Gupta et al (1998)	S-1	Barbell	75	375 x 100	1000	1000	1	0	79.3	545/529	545	578	250*
	S-2	Barbell	75	375 x 100	1000	1100	1	6.2	65.1	545/531	545	578	250*
	S-3	Barbell	75	375 x 100	1000	1100	1	13.2	69	545/531/529	545	578	250*
	S-4	Barbell	75	375 x 100	1000	1100	1	0	85.2	533/531	533	578	250*
	S-5	Barbell	75	375 x 100	1000	1100	1	6.2	73.1	533/521/529	533	578	250*
	S-6	Barbell	75	375 x 100	1000	1100	1	13.2	70.5	533/531	533	578	250*
	S-7	Barbell	75	375 x 100	1000	1100	1	6.2	71.2	545/531	545	578	250*
	S-F	Barbell	75	375 x 100	1000	1100	1	3.7	60.5	545/578	545	578	250*
Lefas et al (1990)	SW11	Rectangular	70	140 x 70	750	825	1.1	0	52	470	470	520	420
	SW12	Rectangular	70	140 x 70	750	825	1.1	10	54	470	470	520	420
	SW13	Rectangular	70	140 x 70	750	825	1.1	20	41	470	470	520	420
	SW14	Rectangular	70	140 x 70	750	825	1.1	0	42	470	470	520	420
	SW15	Rectangular	70	140 x 70	750	825	1.1	10	43	470	470	520	420
	SW16	Rectangular	70	140 x 70	750	825	1.1	20	52	470	470	520	420

*Nominal yield strength

Table B-8 - Details of tested concrete shear walls reinforced with **normal-strength** reinforcement (continued)

Author	ID	Cross-section Shape	Web Thickness (mm)	Boundary Element Dimensions (mm x mm)	Wall Length (mm)	Shear Span (mm)	Aspect Ratio	Axial Compression (% $N/A_g f'_c$)	f'_c (MPa)	f_y (MPa) Boundary Element Long. Reinf.	f_y (MPa) Vert. Web Reinf.	f_y (MPa) Hori. Web Reinf.	f_y (MPa) Hoops
Lefas et al (1990)	SW17	Rectangular	70	140 x 70	750	825	1.1	0	48	470	470	520	420
	SW21	Rectangular	65	140 x 65	650	1825	2.8	0	43	470	470	520	420
	SW22	Rectangular	65	140 x 65	650	1825	2.8	10	51	470	470	520	420
	SW23	Rectangular	65	140 x 65	650	1825	2.8	20	48	470	470	520	420
	SW24	Rectangular	65	140 x 65	650	1825	2.8	0	48	470	470	520	420
	SW25	Rectangular	65	140 x 65	650	1825	2.8	20	45	470	470	520	420
	SW26	Rectangular	65	140 x 65	650	1825	2.8	0	30	470	470	520	420
Oesterle et al (1976)	R1	Rectangular	102	-	1910	4670	2.5	-	44.7	511.6	400*	400*	400*
	R2	Rectangular	102	-	1910	4670	2.5	-	46.4	450.2	400*	400*	400*
	B1	Barbell	102	305 x 305	1910	4670	2.5	-	53	449.5	400*	400*	400*
	B2	Barbell	102	305 x 305	1910	4670	2.5	-	47.3	437.8	400*	400*	400*
	B3	Barbell	102	305 x 305	1910	4670	2.5	-	45	450.2	400*	400*	400*
	B4	Barbell	102	305 x 305	1910	4670	2.5	-	53.6	410.2	400*	400*	400*
	B5	Barbell	102	305 x 305	1910	4670	2.5	-	45.3	444	400*	400*	400*
	B5R	Barbell	102	305 x 305	1910	4670	2.5	-	42.8	-	400*	400*	400*
	B6	Barbell	102	305 x 305	1910	4670	2.5	2.93	21.8	440.6	400*	400*	400*
	B7	Barbell	102	305 x 305	1910	4670	2.5	3.76	49.3	457.8	400*	400*	400*
	B8	Barbell	102	305 x 305	1910	4670	2.5	3.76	42	447.5	400*	400*	400*
	B9	Barbell	102	305 x 305	1910	4670	2.5	3.76	44.1	429.5	400*	400*	400*
	B9R	Barbell	102	305 x 305	1910	4670	2.5	3.1	51.8	429.5	400*	400*	400*
	B10	Barbell	102	305 x 305	1910	4670	2.5	3.76	45.6	447.5	400*	400*	400*
	F1	Flanged	102	102 x 910	1910	4670	2.5	0	38.4	444.7	400*	400*	400*
	F2	Flanged	102	102 x 910	1910	4670	2.5	3.31	45.6	430.2	400*	400*	400*

*Nominal yield stre

Appendix C

Steel Strain Data

Wall W1HS

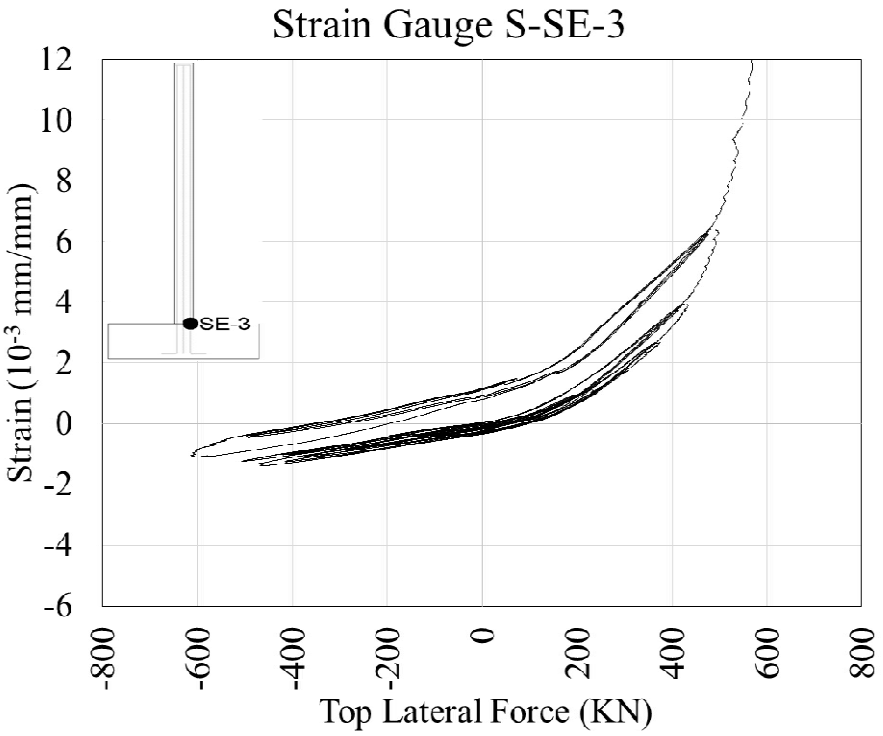
Strain Gauge S-SE-3
Strain (10^{-3} mm/mm)
12
10
8
6
4
2
0
-2
-4
-6
SE 3
-800
-600
-400
-200
0
200
400
600
800
Top Lateral Force (KN)

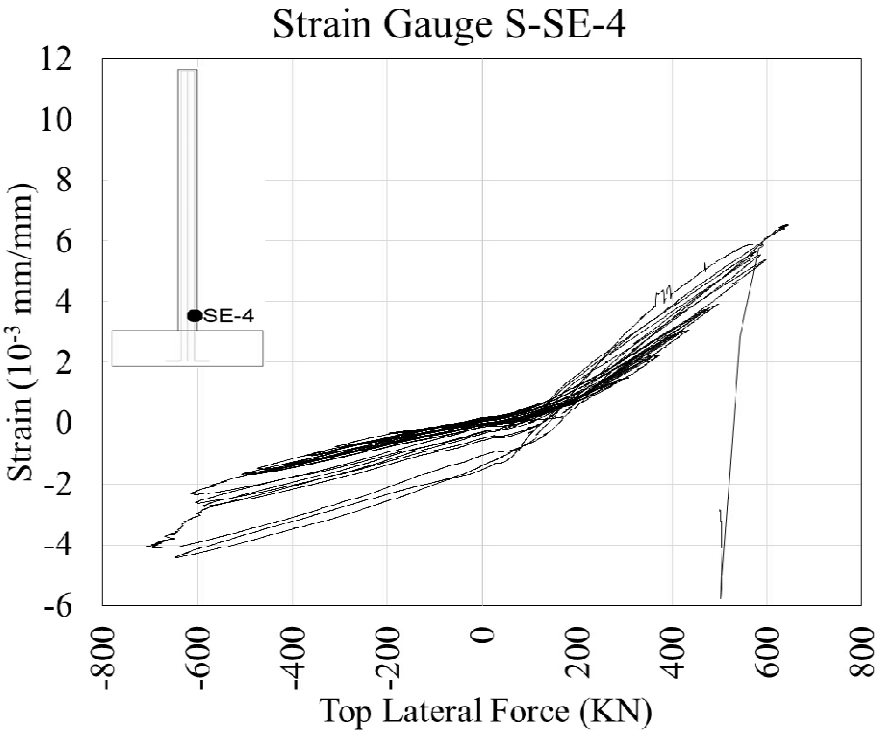
Strain Gauge S-SE-4
Strain (10^{-3} mm/mm)
12
10
8
6
4
2
0
-2
-4
-6
SE-4
-800
-600
-400
-200
0
200
400
600
800
Top Lateral Force (KN)

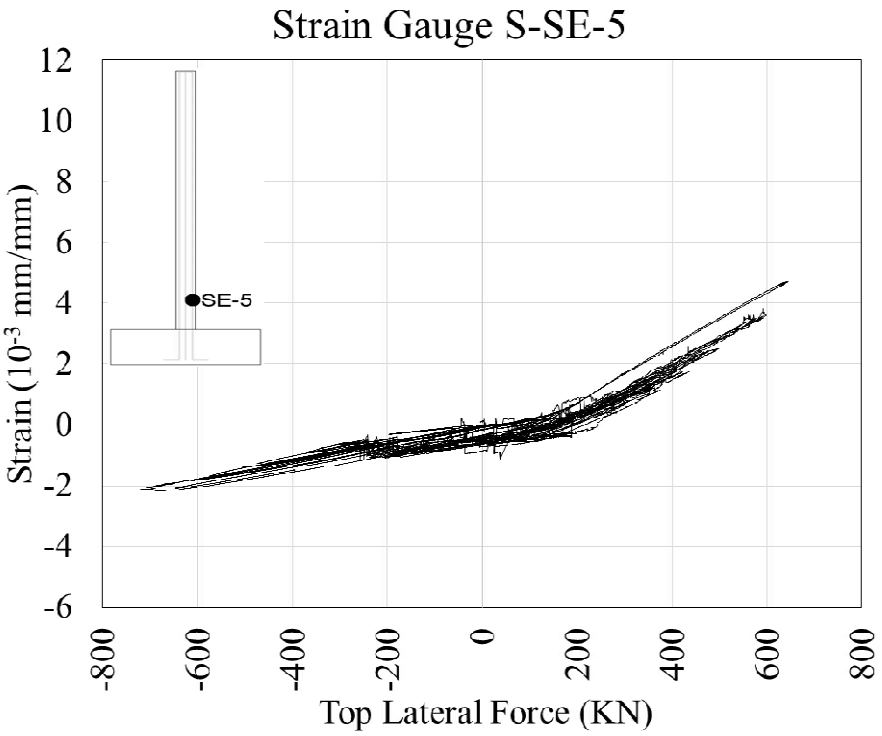
Strain Gauge S-SE-5
SE-5
Strain (10^{-3} mm/mm)
12
10
8
6
4
2
0
-2
-4
-6
-800
-600
-400
-200
0
200
400
600
800
Top Lateral Force (KN)

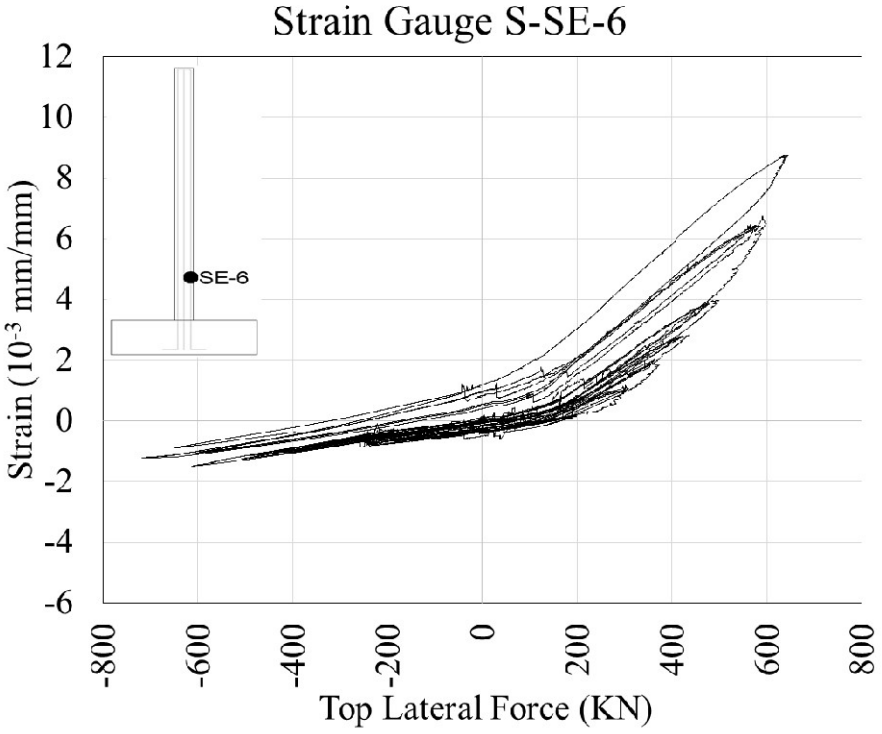
Strain Gauge S-SE-6
SE-6
Strain (10^{-3} mm/mm)
12
10
8
6
4
2
0
-2
-4
-6
-800
-600
-400
-200
0
200
400
600
800
Top Lateral Force (KN)

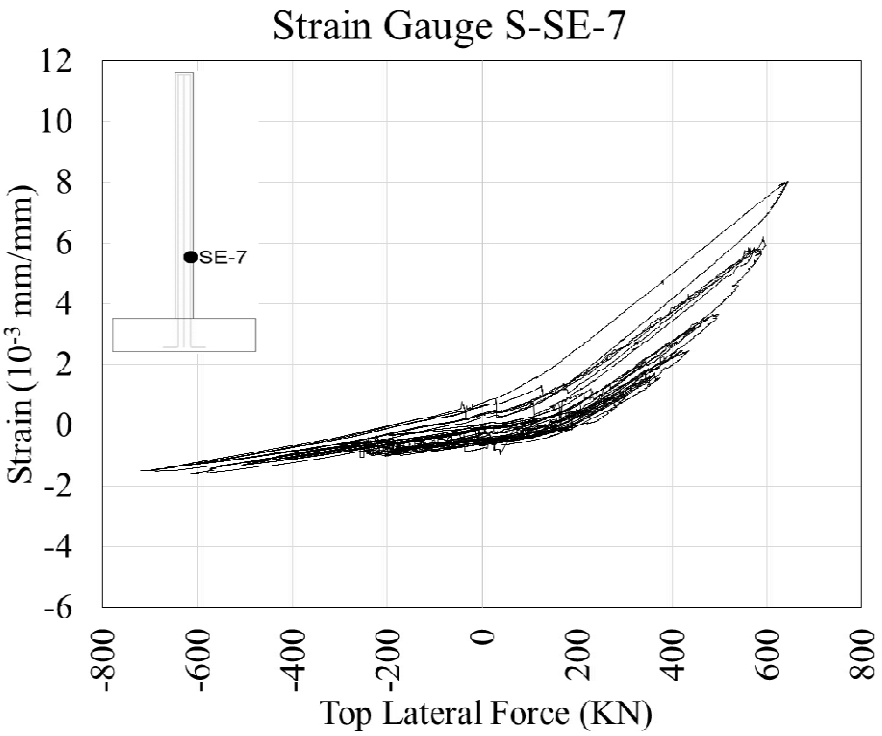
Strain Gauge S-SE-7
SE-7
Strain (10^{-3} mm/mm)
12
10
8
6
4
2
0
-2
-4
-6
-800
-600
-400
-200
0
200
400
600
800
Top Lateral Force (KN)

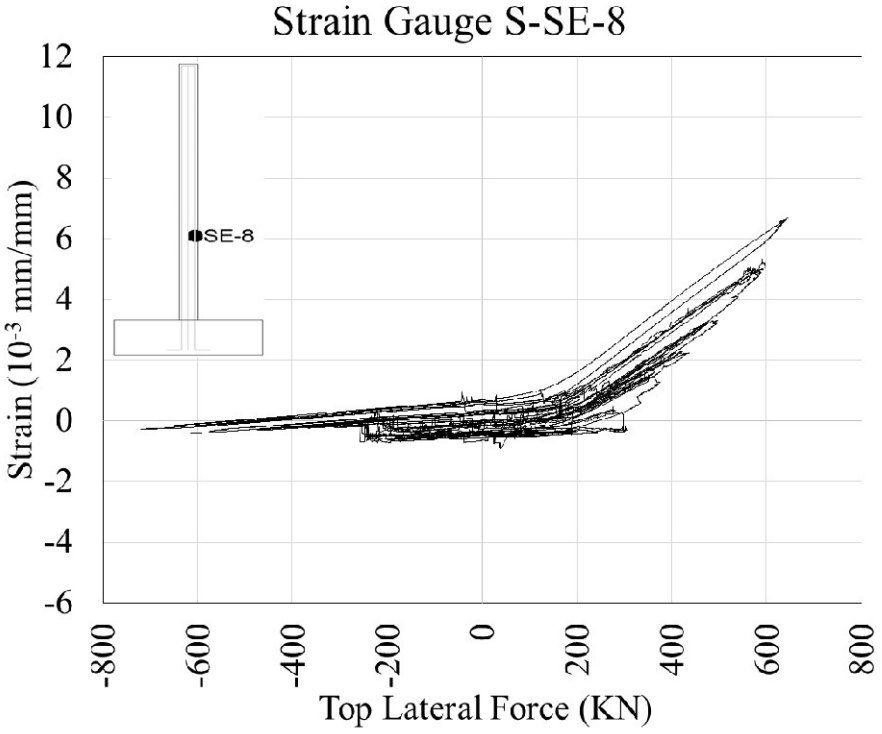
Strain Gauge S-SE-8
SE-8
Strain (10^{-3} mm/mm)
12
10
8
6
4
2
0
-2
-4
-6
-800
-600
-400
-200
0
200
400
600
800
Top Lateral Force (KN)

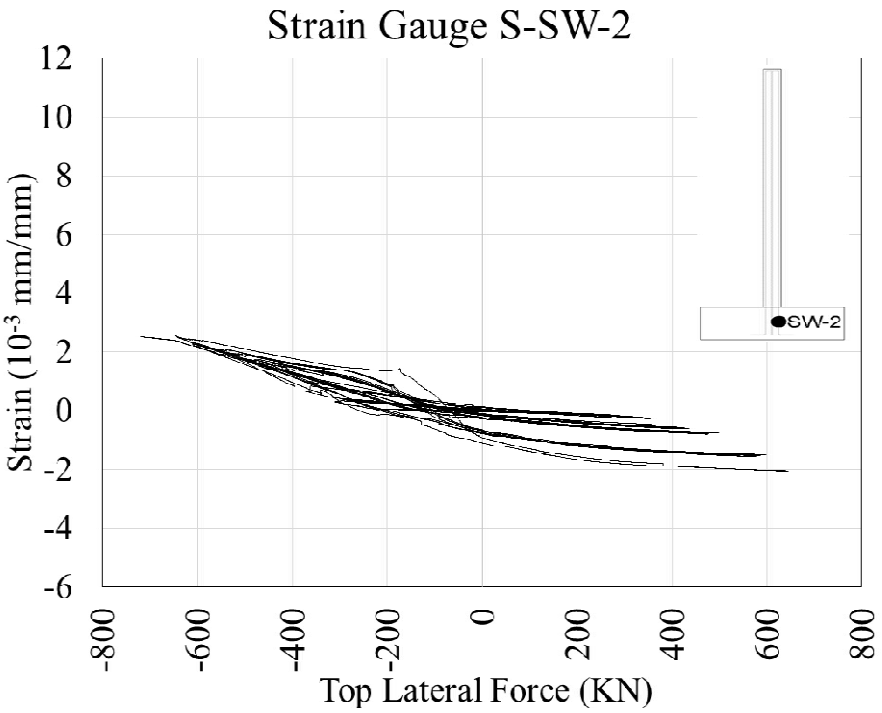
Strain Gauge S-SW-2
Strain (10^{-3} mm/mm)
12
10
8
6
4
2
0
-2
-4
-6
-800
-600
-400
-200
0
200
400
600
800
Top Lateral Force (KN)
SW-2

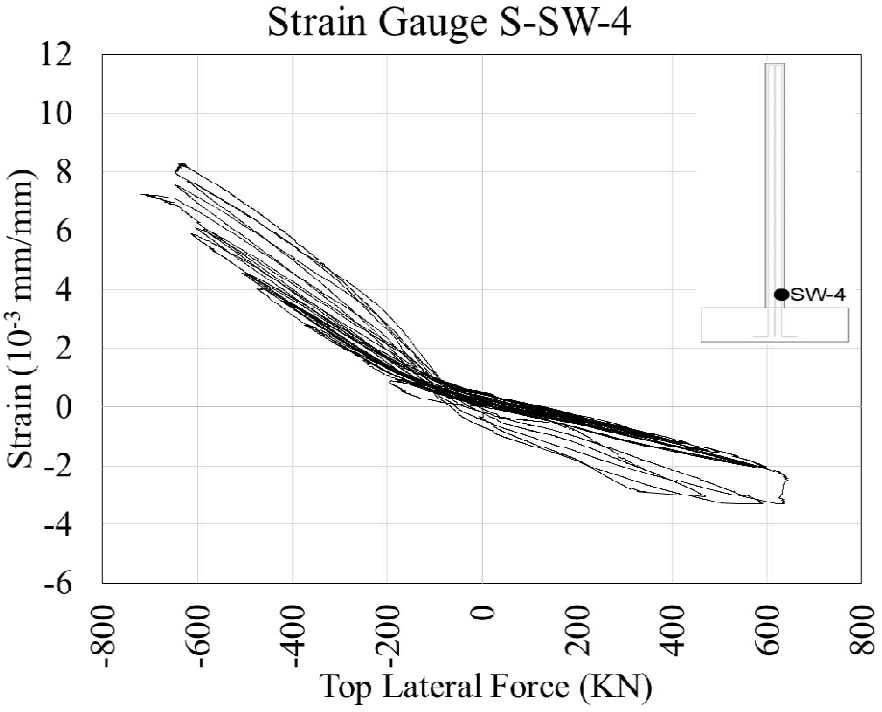
Strain Gauge S-SW-4
Strain (10^{-3} mm/mm)
12
10
8
6
4
2
0
-2
-4
-6
-800
-600
-400
-200
0
200
400
600
800
Top Lateral Force (KN)
SW-4

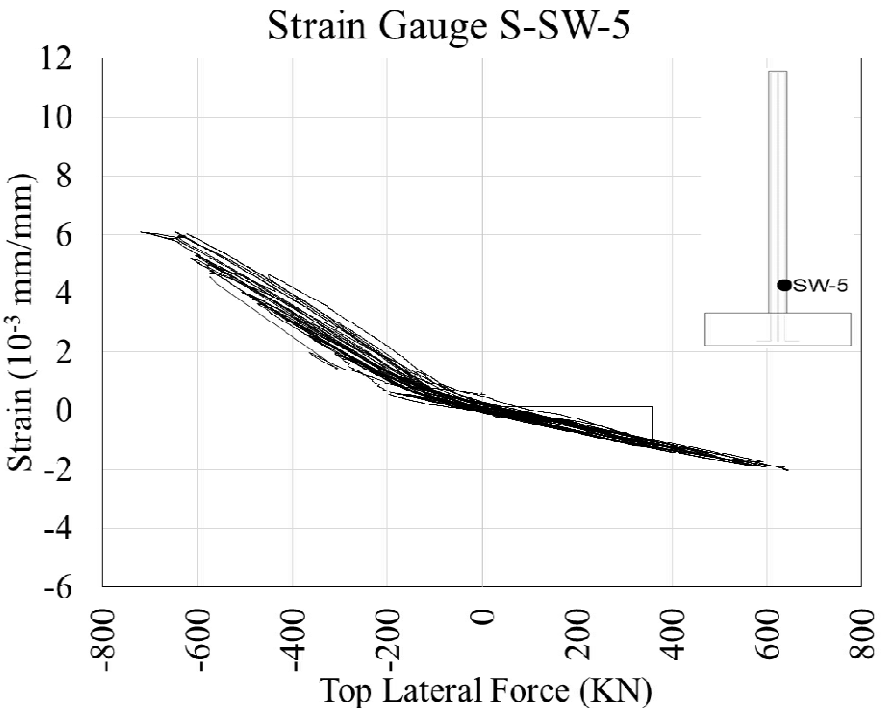
Strain Gauge S-SW-5
Strain (10^{-3} mm/mm)
12
10
8
6
4
2
0
-2
-4
-6
-800
-600
-400
-200
0
200
400
600
800
Top Lateral Force (KN)
SW-5

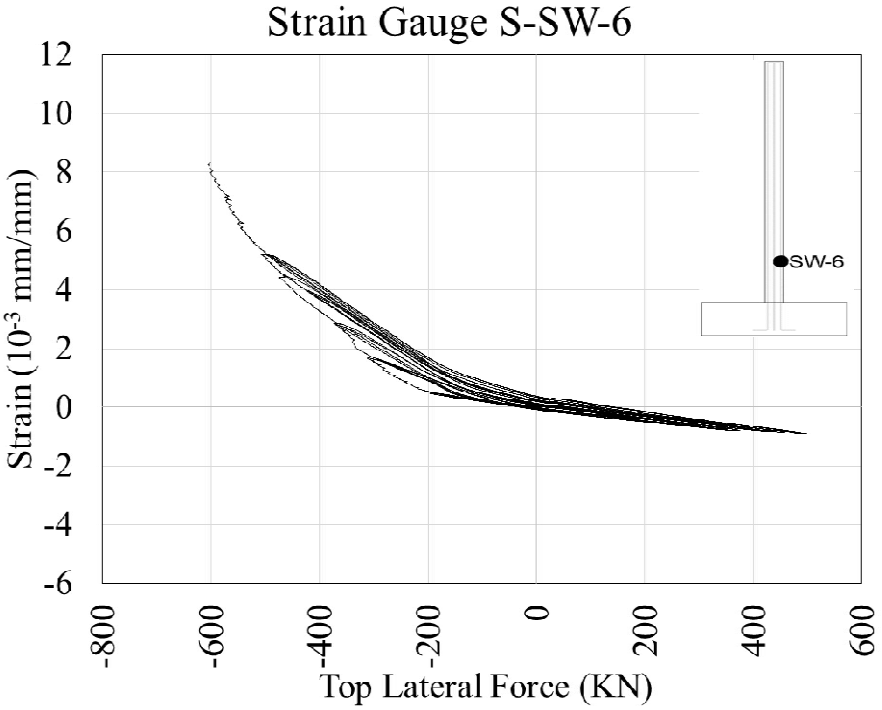
Strain Gauge S-SW-6
Strain (10^{-3} mm/mm)
12
10
8
6
4
2
0
-2
-4
-6
-800
-600
-400
-200
0
200
400
600
Top Lateral Force (KN)
SW-6

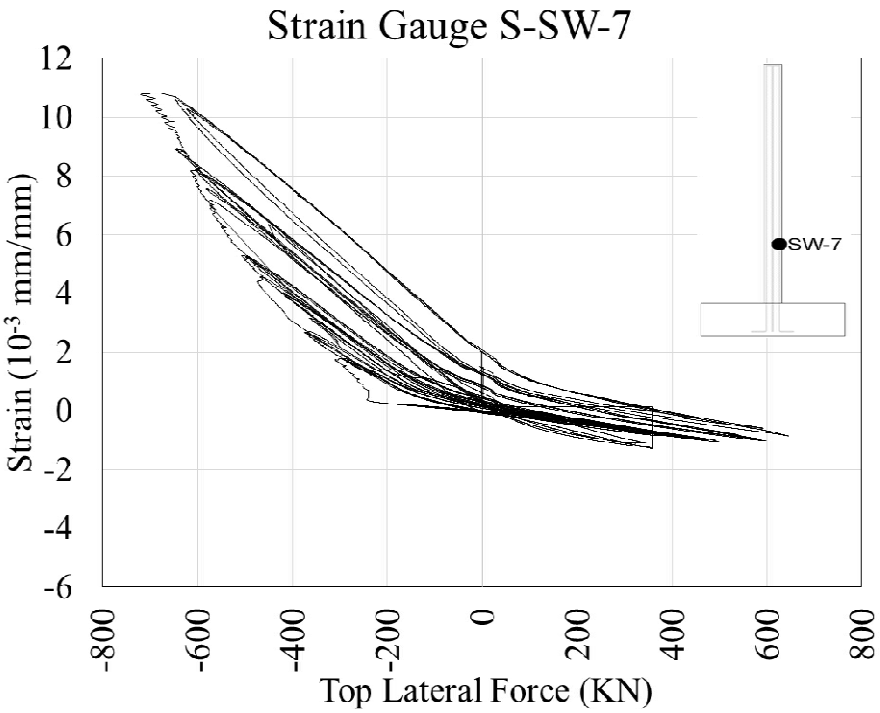
Strain Gauge S-SW-7
Strain (10^{-3} mm/mm)
12
10
8
6
4
2
0
-2
-4
-6
-800
-600
-400
-200
0
200
400
600
800
Top Lateral Force (KN)
SW-7

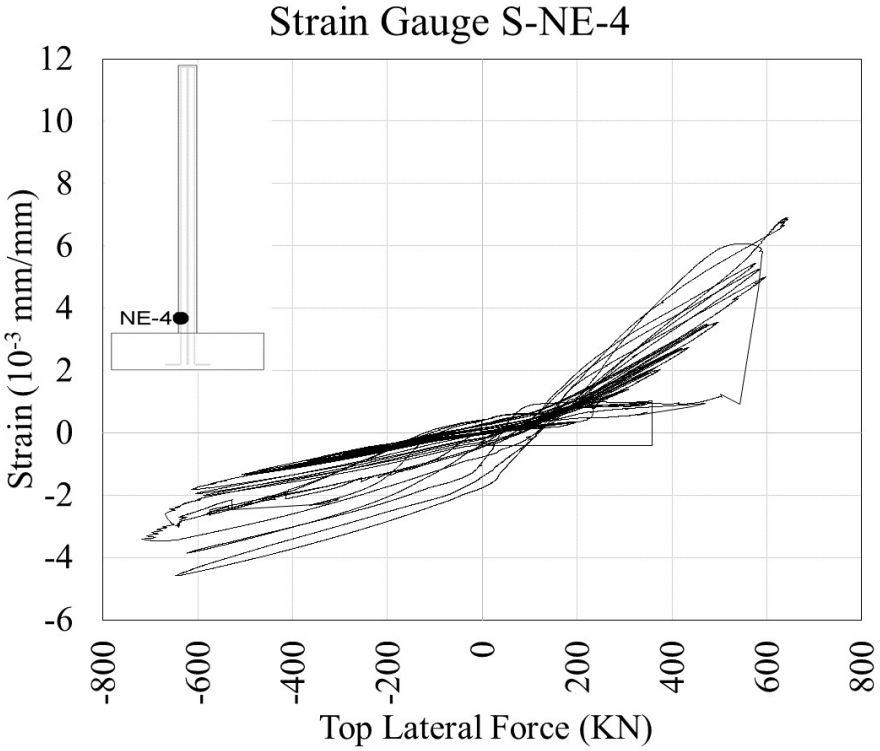
Strain Gauge S-NE-4
Strain (10^{-3} mm/mm)
12
10
8
6
4
2
0
-2
-4
-6
-800
-600
-400
-200
0
200
400
600
800
Top Lateral Force (KN)
NE-4

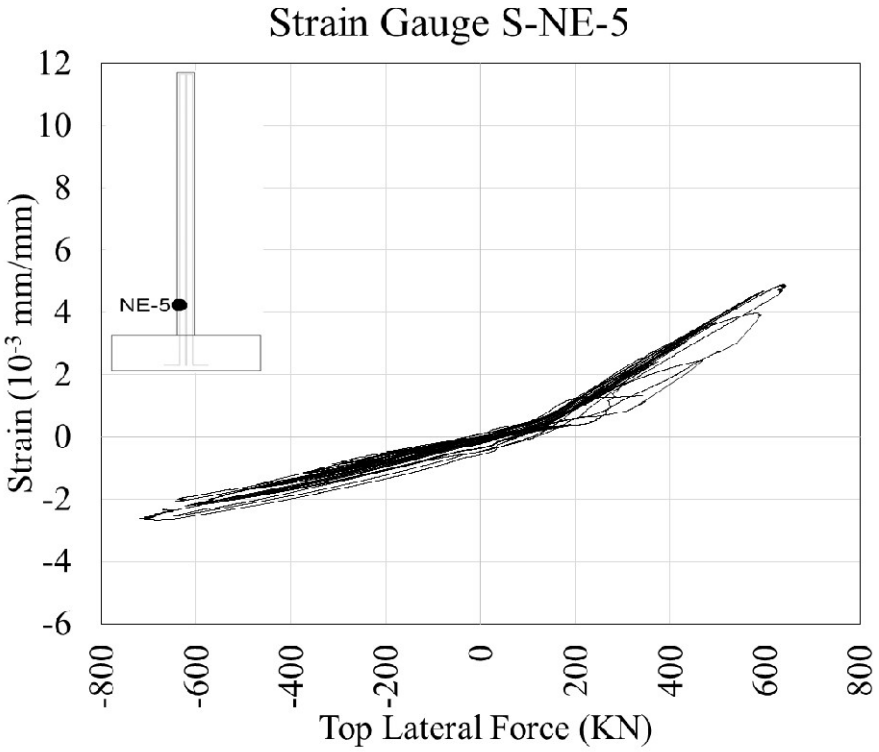
Strain Gauge S-NE-5
NE-5
Strain (10^{-3} mm/mm)
12
10
8
6
4
2
0
-2
-4
-6
-800
-600
-400
-200
0
200
400
600
800
Top Lateral Force (KN)

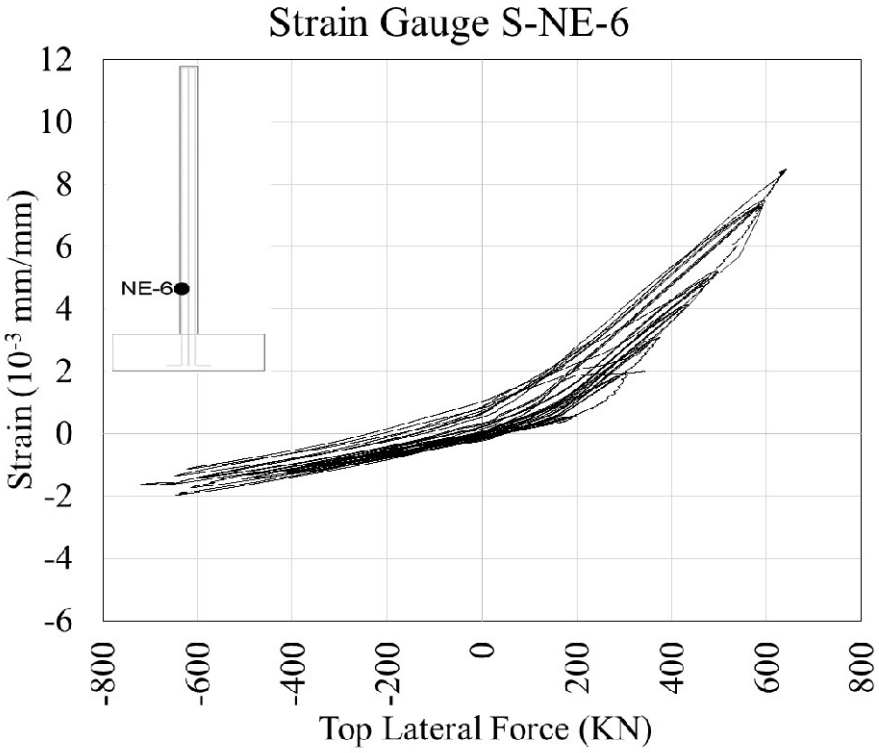
Strain Gauge S-NE-6
NE-6
Strain (10^{-3} mm/mm)
12
10
8
6
4
2
0
-2
-4
-6
-800
-600
-400
-200
0
200
400
600
800
Top Lateral Force (KN)

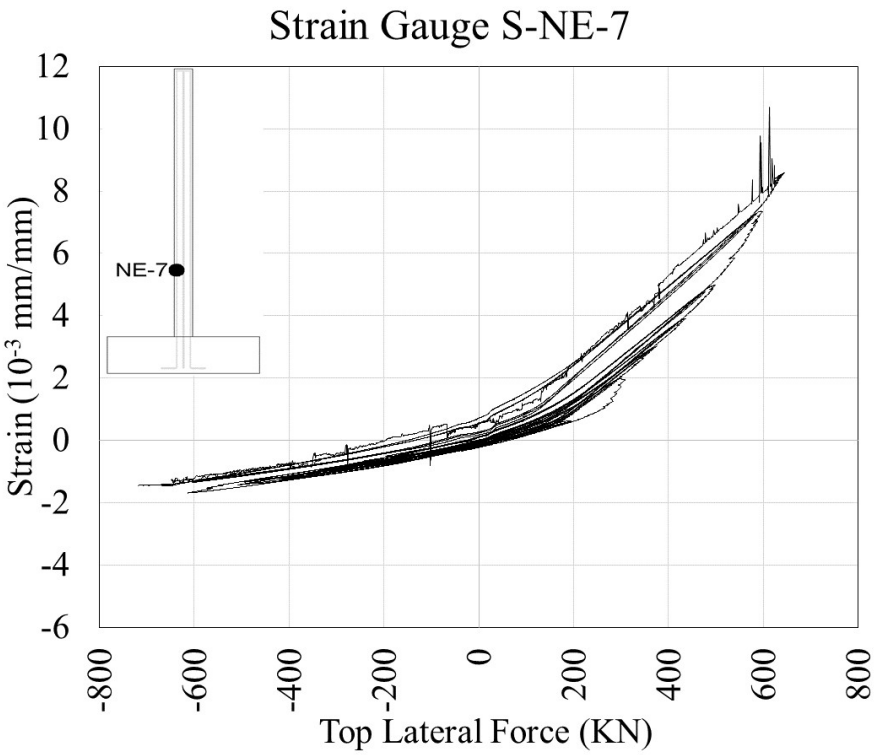
Strain Gauge S-NE-7
NE-7
Strain (10^{-3} mm/mm)
12
10
8
6
4
2
0
-2
-4
-6
-800
-600
-400
-200
0
200
400
600
800
Top Lateral Force (KN)

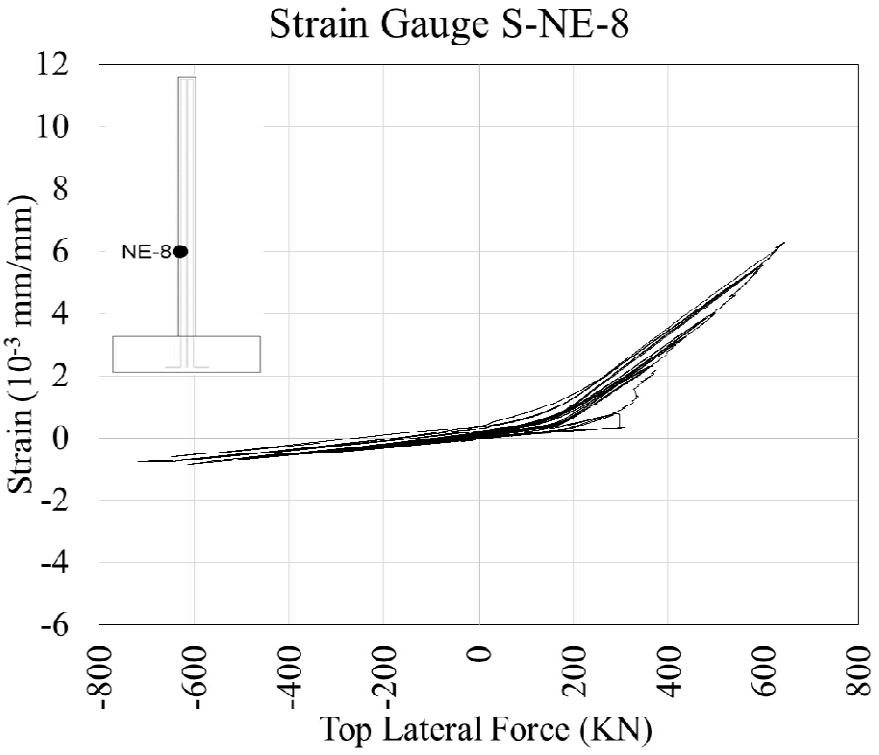
Strain Gauge S-NE-8
NE-8
Strain (10^{-3} mm/mm)
12
10
8
6
4
2
0
-2
-4
-6
-800
-600
-400
-200
0
200
400
600
800
Top Lateral Force (KN)

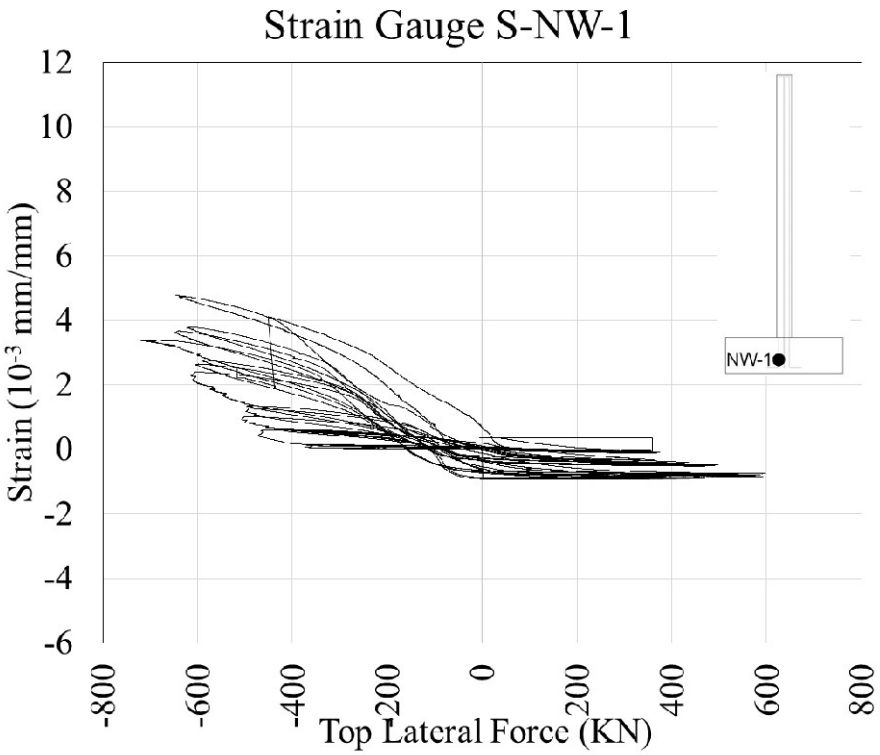
Strain Gauge S-NW-1
Strain (10^{-3} mm/mm)
12
10
8
6
4
2
0
-2
-4
-6
-800
-600
-400
-200
0
200
400
600
800
Top Lateral Force (KN)
NW-1

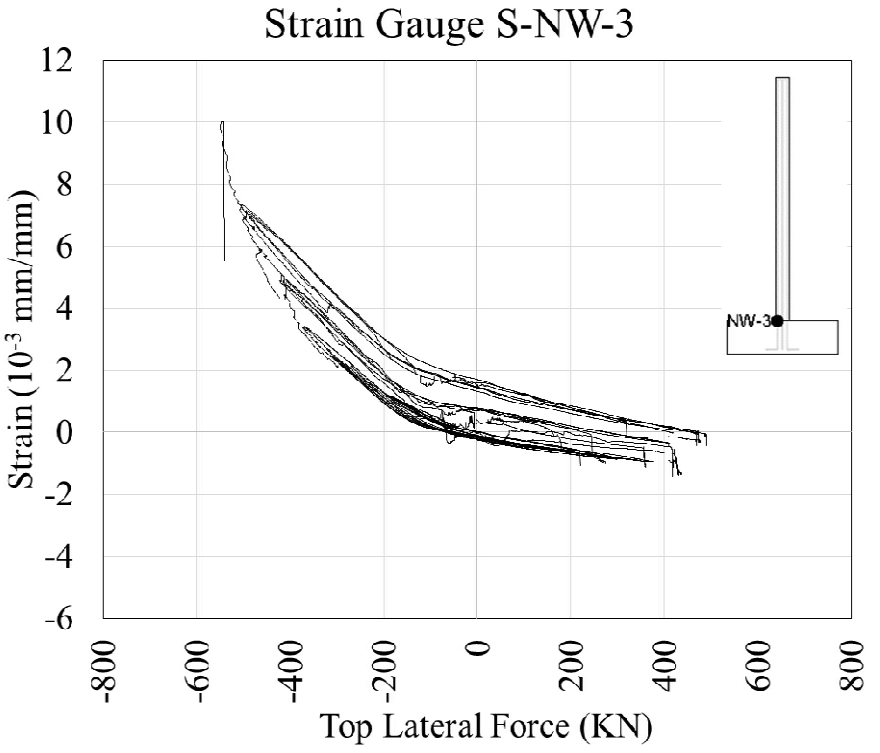
Strain Gauge S-NW-3
Strain (10^{-3} mm/mm)
12
10
8
6
4
2
0
-2
-4
-6
-800
-600
-400
-200
0
200
400
600
800
Top Lateral Force (KN)
NW-3

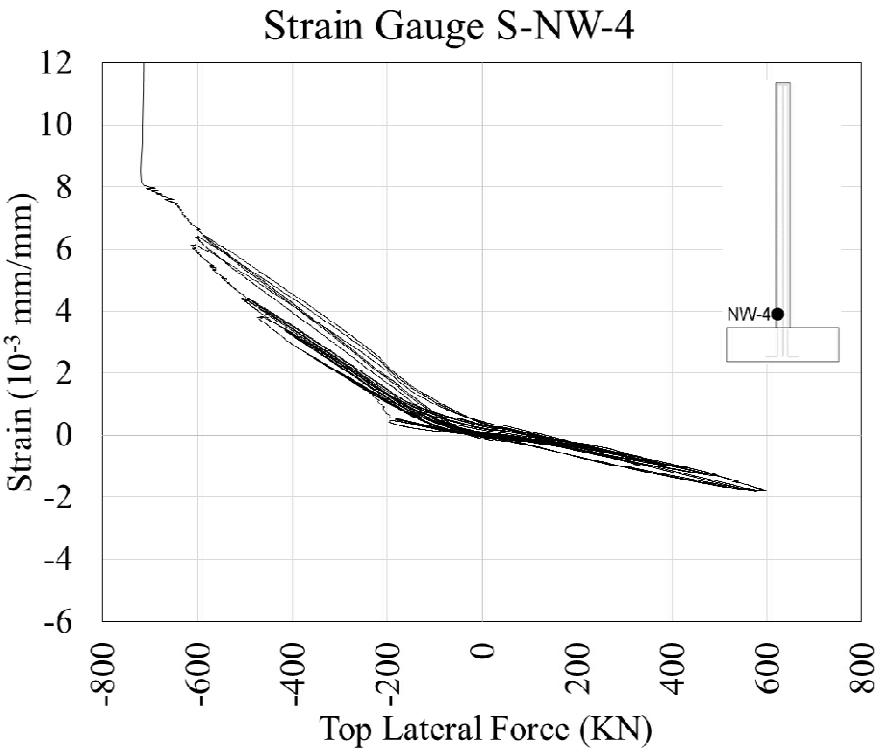
Strain Gauge S-NW-4
Strain (10^{-3} mm/mm)
12
10
8
6
4
2
0
-2
-4
-6
-800
-600
-400
-200
0
200
400
600
800
Top Lateral Force (KN)
NW-4

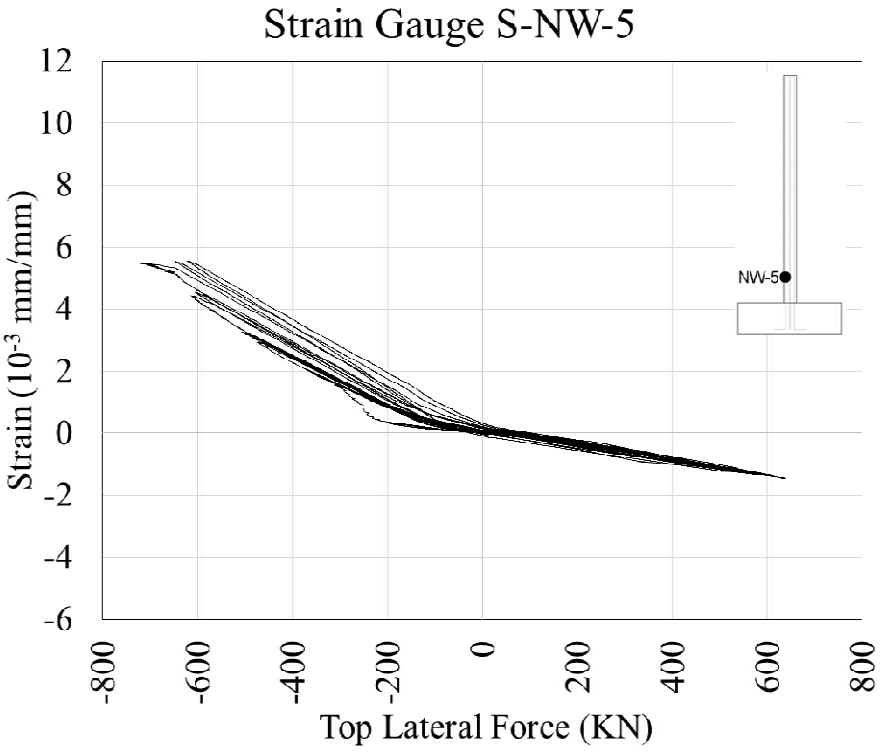
Strain Gauge S-NW-5
Strain (10^{-3} mm/mm)
12
10
8
6
4
2
0
-2
-4
-6
-800
-600
-400
-200
0
200
400
600
800
Top Lateral Force (KN)
NW-5

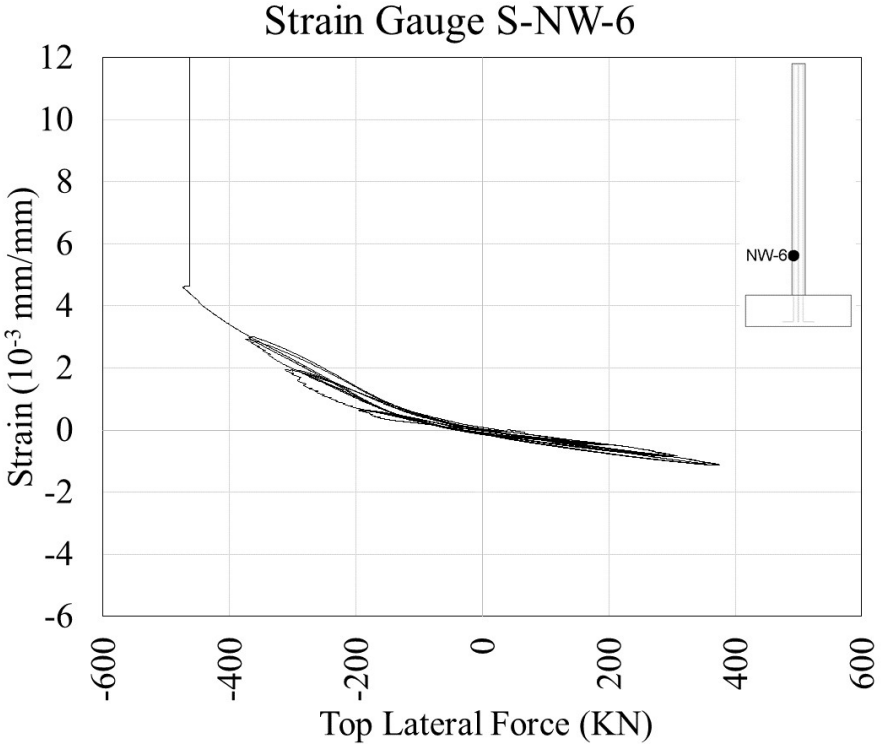
Strain Gauge S-NW-6
Strain (10^{-3} mm/mm)
12
10
8
6
4
2
0
-2
-4
-6
-600
-400
-200
0
200
400
600
Top Lateral Force (KN)
NW-6

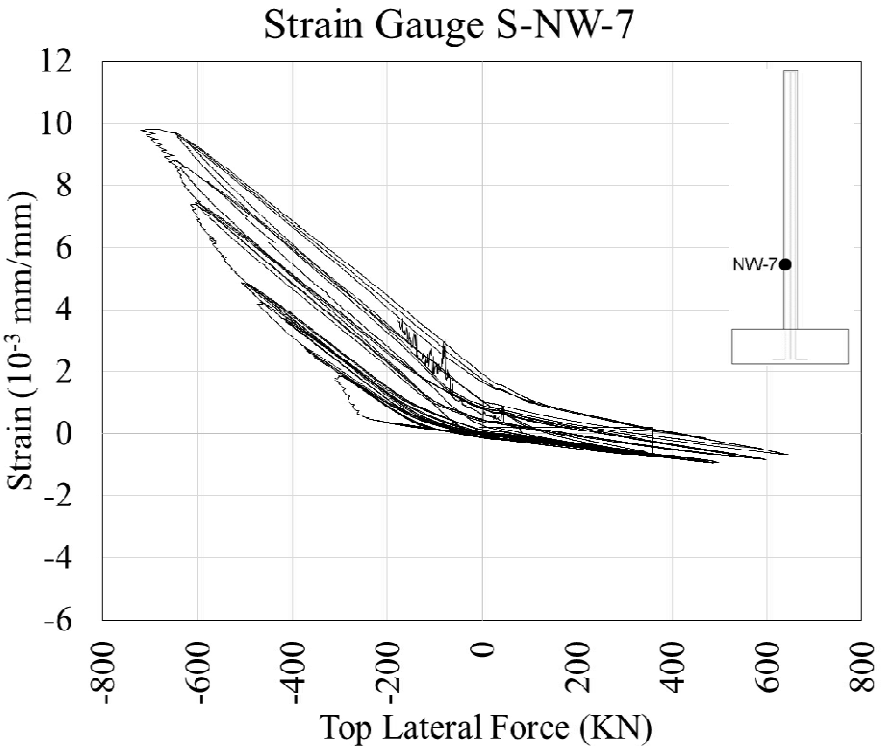
Strain Gauge S-NW-7
Strain (10^{-3} mm/mm)
12
10
8
6
4
2
0
-2
-4
-6
-800
-600
-400
-200
0
200
400
600
800
Top Lateral Force (KN)
NW-7

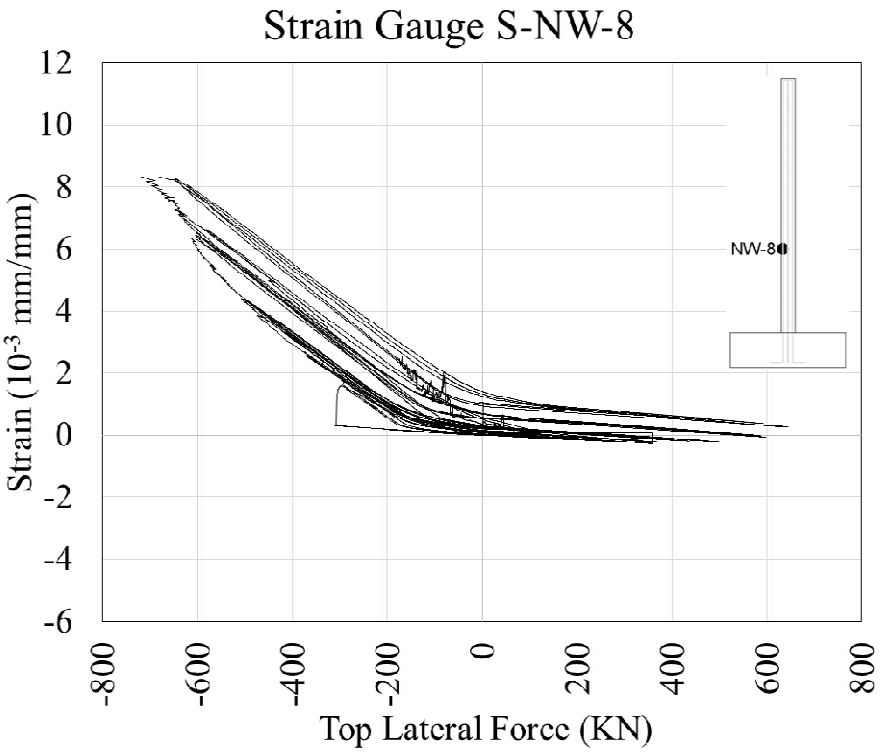
Strain Gauge S-NW-8
12
10
8
6
4
2
0
-2
-4
-6
Strain (10-3 mm/mm)
NW-8
-800
-600
-400
-200
0
200
400
600
800
Top Lateral Force (KN)

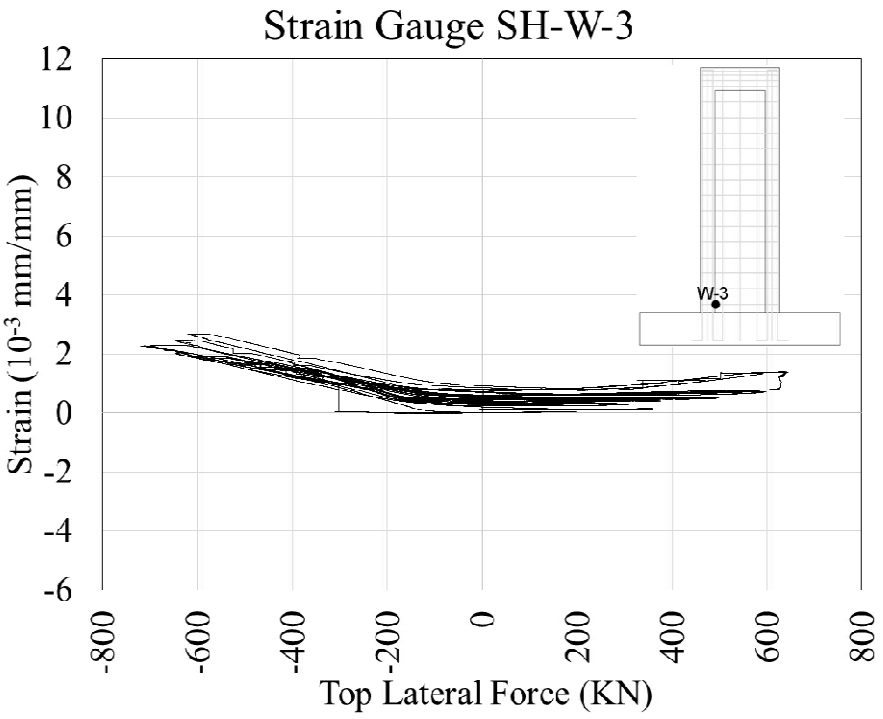
Strain Gauge SH-W-3
12
10
8
6
4
2
0
-2
-4
-6
Strain (10-3 mm/mm)
W-3
-800
-600
-400
-200
0
200
400
600
800
Top Lateral Force (KN)

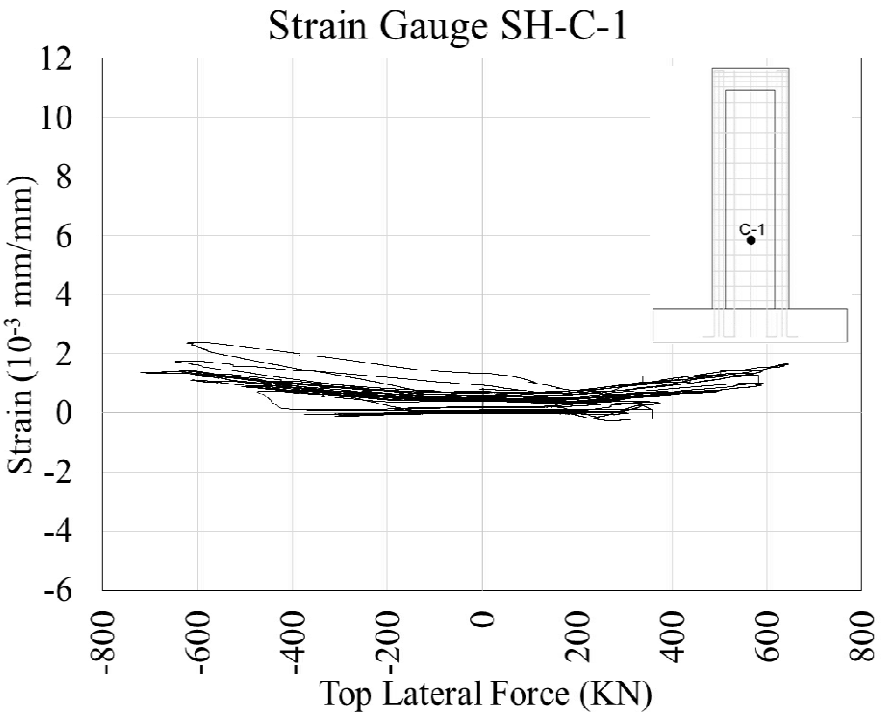
Strain Gauge SH-C-1
Strain (10^{-3} mm/mm)
12
10
8
6
4
2
0
-2
-4
-6
-800
-600
-400
-200
0
200
400
600
800
Top Lateral Force (KN)
C-1

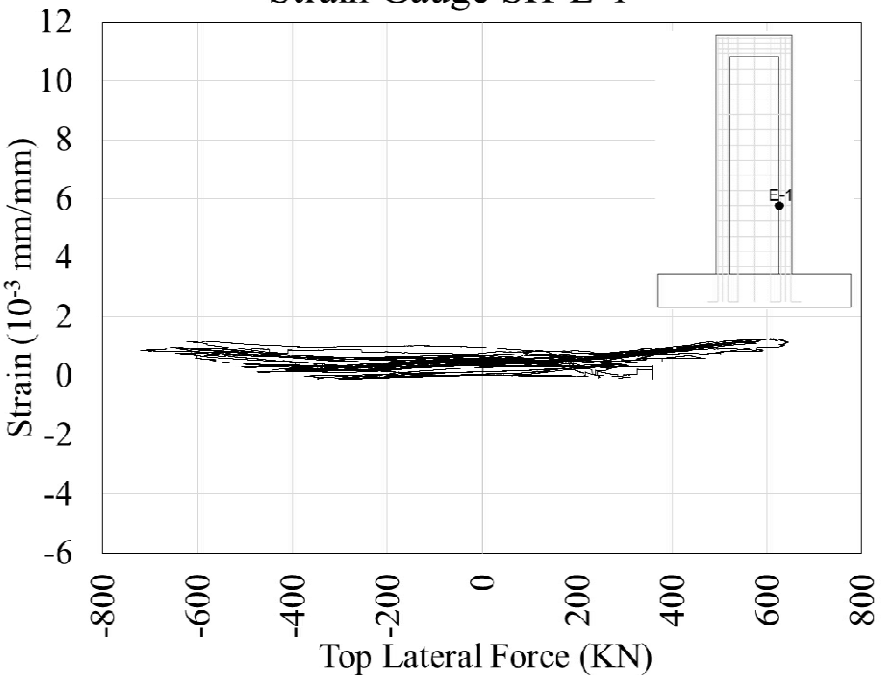
Strain Gauge SH-E-1
Strain (10^{-3} mm/mm)
12
10
8
6
4
2
0
-2
-4
-6
-800
-600
-400
-200
0
200
400
600
800
Top Lateral Force (KN)
E-1

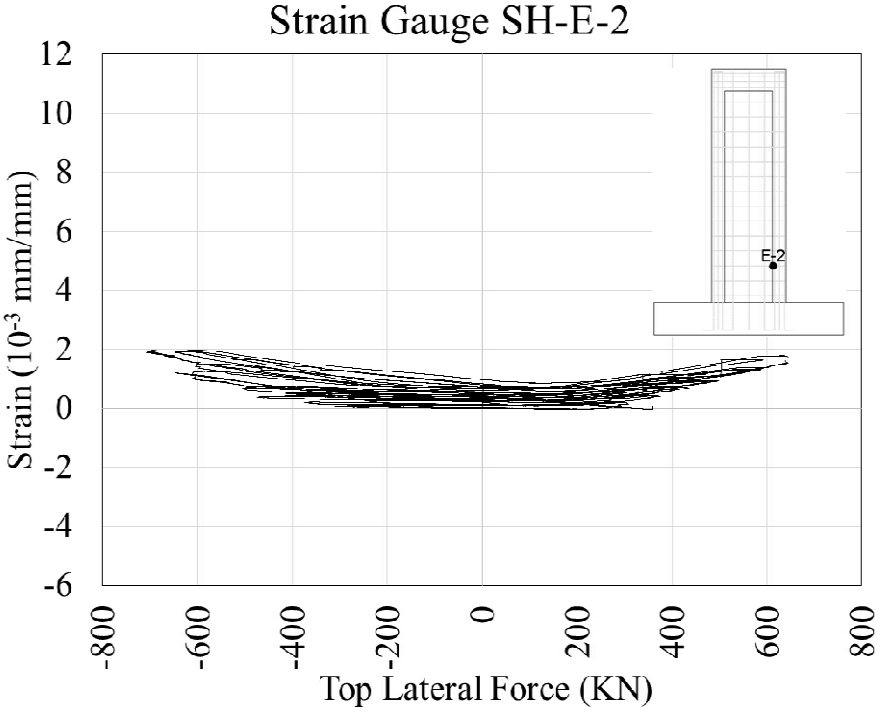
Strain Gauge SH-E-2
Strain (10^{-3} mm/mm)
12
10
8
6
4
2
0
-2
-4
-6
-800
-600
-400
-200
0
200
400
600
800
Top Lateral Force (KN)
E-2

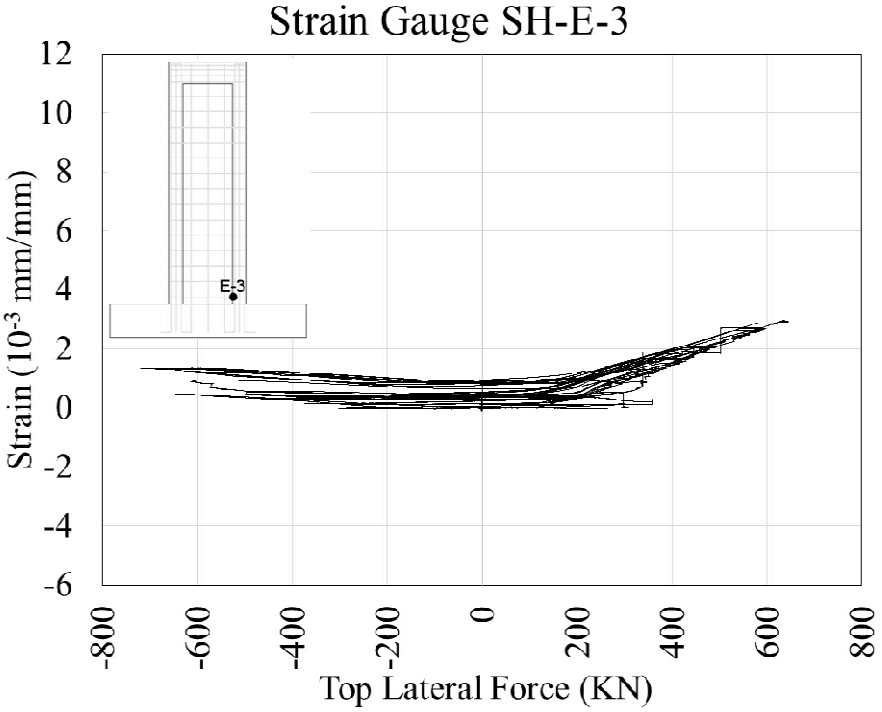
Strain Gauge SH-E-3
Strain (10^{-3} mm/mm)
12
10
8
6
4
2
0
-2
-4
-6
-800
-600
-400
-200
0
200
400
600
800
Top Lateral Force (KN)
E-3

Wall W2HS

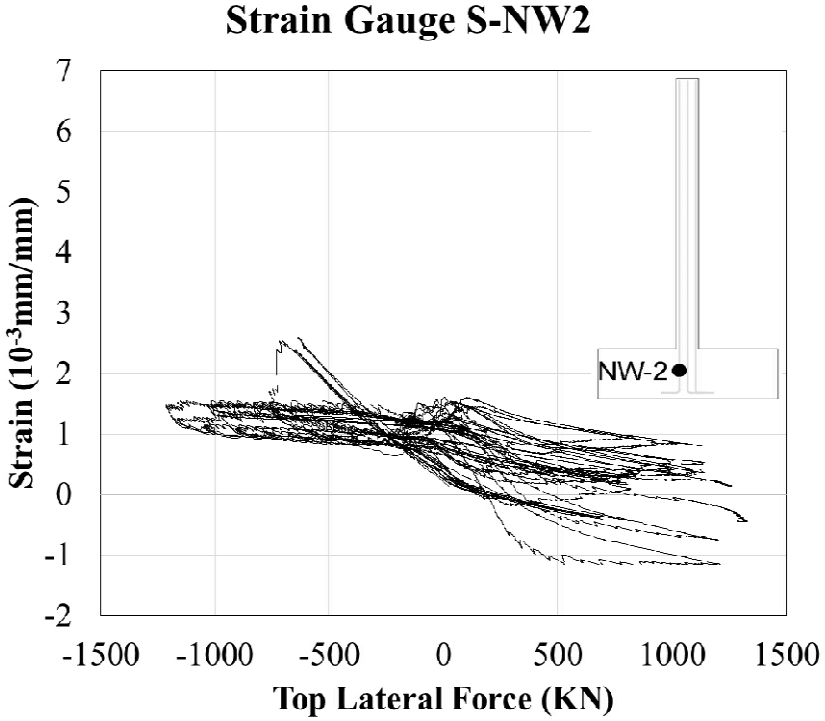
Strain Gauge S-NW2
Strain (10^{-3}mm/mm)
7
6
5
4
3
2
1
0
-1
-2
-1500
-1000
-500
0
500
1000
1500
Top Lateral Force (KN)
NW-2

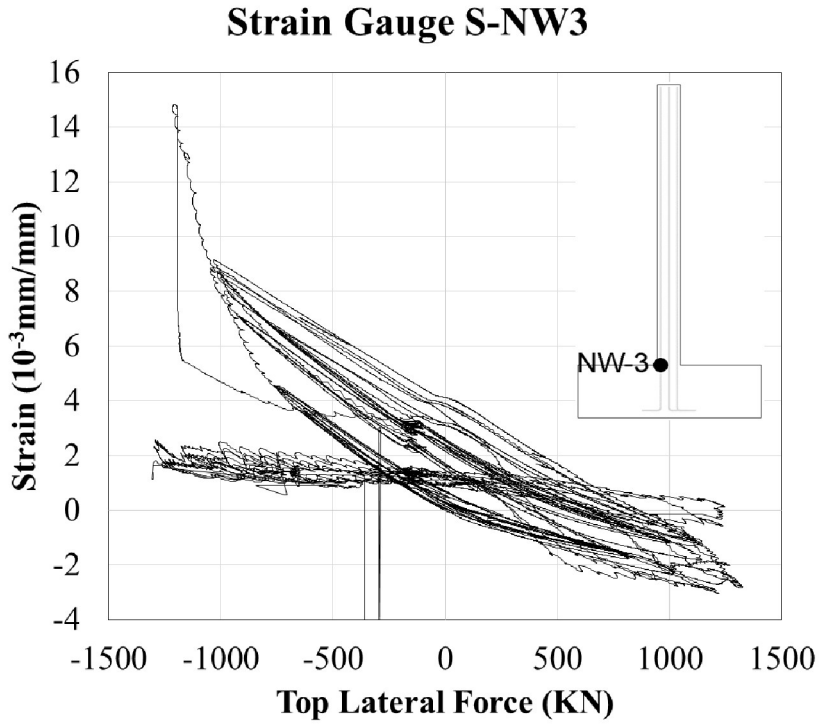
Strain Gauge S-NW3
Strain (10^{-3}mm/mm)
16
14
12
10
8
6
4
2
0
-2
-4
-1500
-1000
-500
0
500
1000
1500
Top Lateral Force (KN)
NW-3

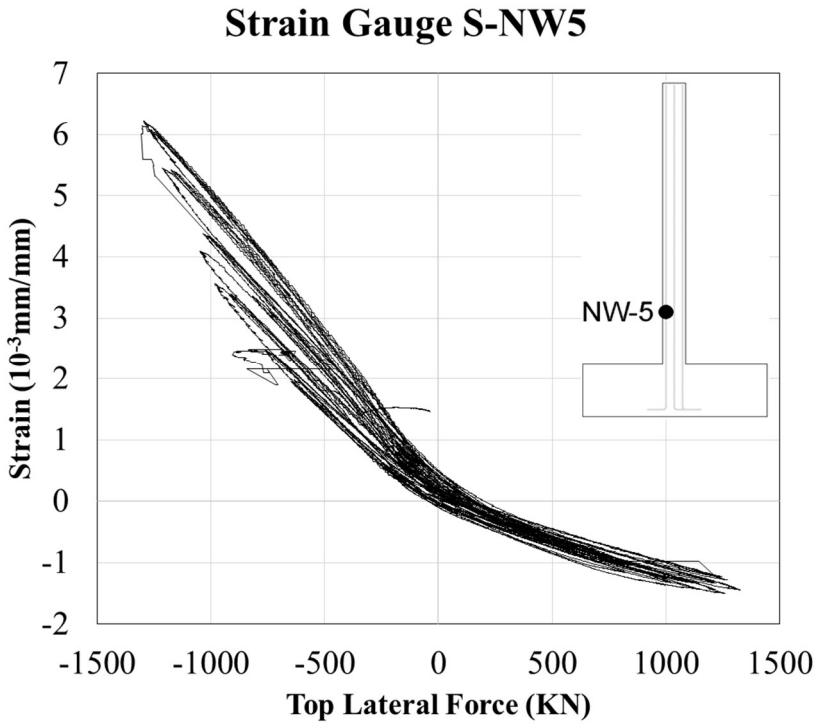
Strain Gauge S-NW5
Strain (10-3mm/mm)
7
6
5
4
3
2
1
0
-1
-2
-1500
-1000
-500
0
500
1000
1500
Top Lateral Force (KN)
NW-5

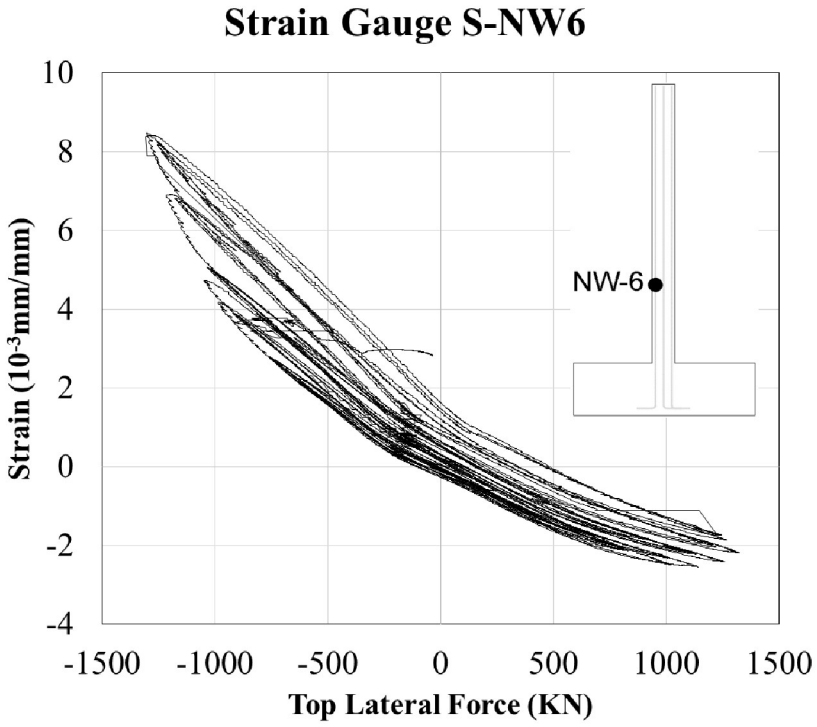
Strain Gauge S-NW6
Strain (10-3mm/mm)
10
8
6
4
2
0
-2
-4
-1500
-1000
-500
0
500
1000
1500
Top Lateral Force (KN)
NW-6

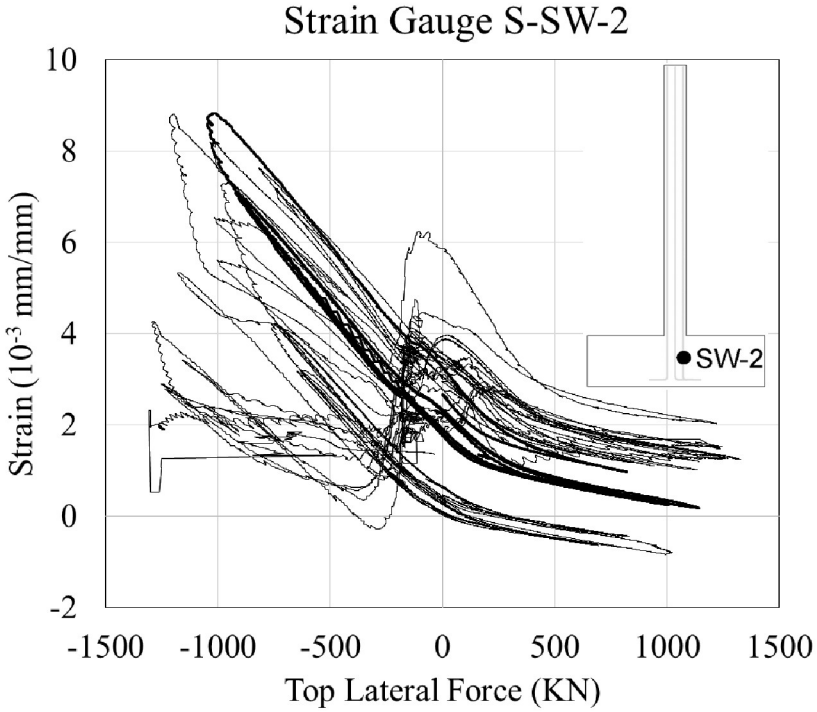
Strain Gauge S-SW-2
10
8
6
4
2
0
-2
Strain (10^{-3} mm/mm)
-1500
-1000
-500
0
500
1000
1500
Top Lateral Force (KN)
SW-2

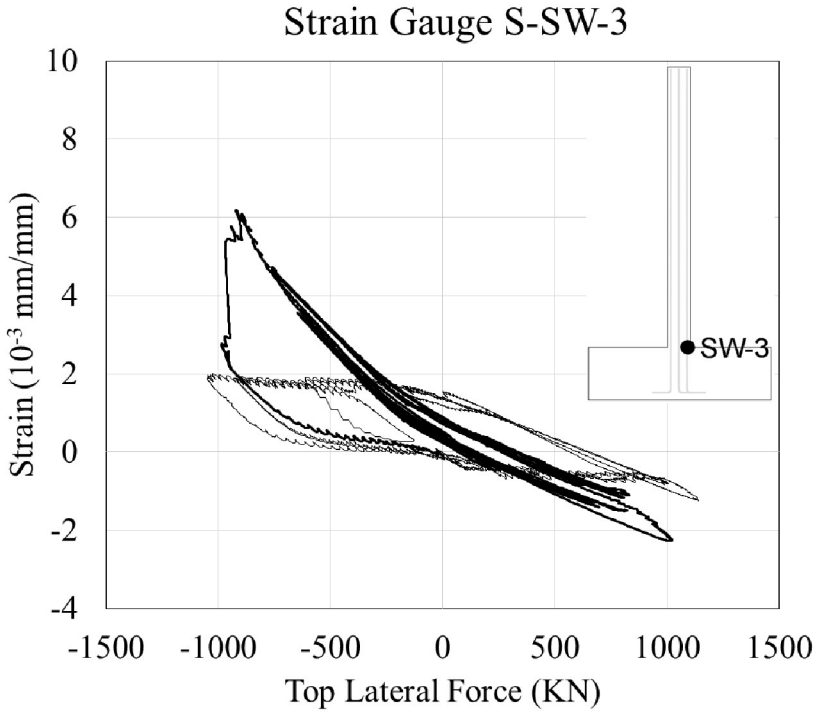
Strain Gauge S-SW-3
10
8
6
4
2
0
-2
-4
Strain (10^{-3} mm/mm)
-1500
-1000
-500
0
500
1000
1500
Top Lateral Force (KN)
SW-3

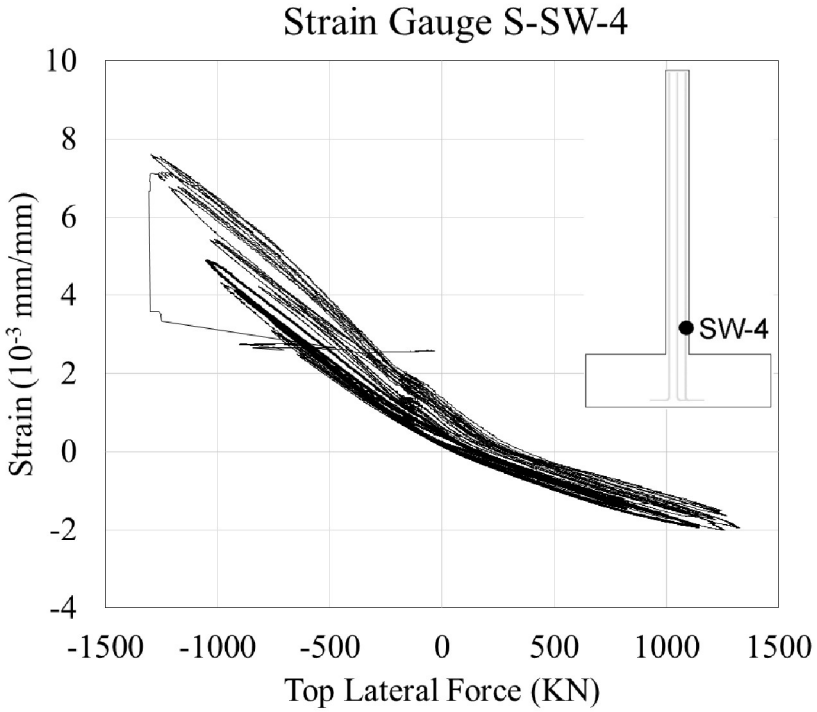
Strain Gauge S-SW-4
10
8
6
4
2
0
-2
-4
Strain (10^{-3} mm/mm)
-1500
-1000
-500
0
500
1000
1500
Top Lateral Force (KN)
SW-4

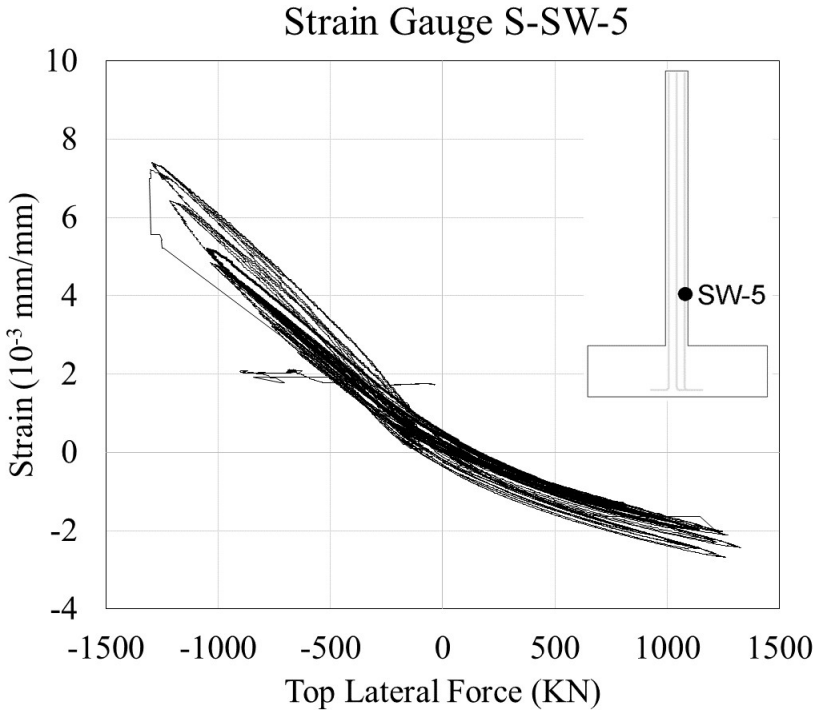
Strain Gauge S-SW-5
10
8
6
4
2
0
-2
-4
Strain (10^{-3} mm/mm)
-1500
-1000
-500
0
500
1000
1500
Top Lateral Force (KN)
SW-5

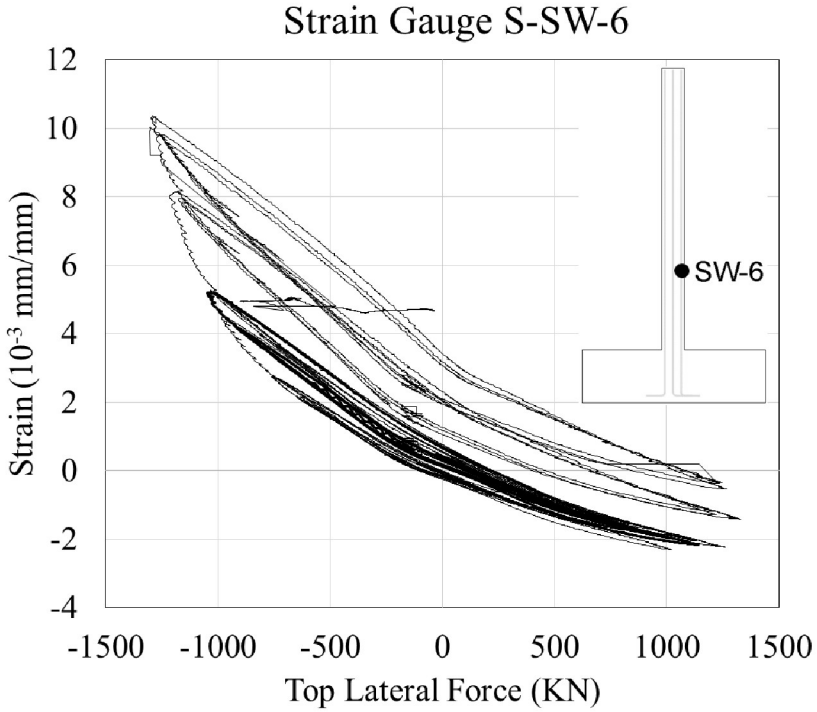
Strain Gauge S-SW-6
12
10
8
6
4
2
0
-2
-4
Strain (10^{-3} mm/mm)
SW-6
-1500
-1000
-500
0
500
1000
1500
Top Lateral Force (KN)

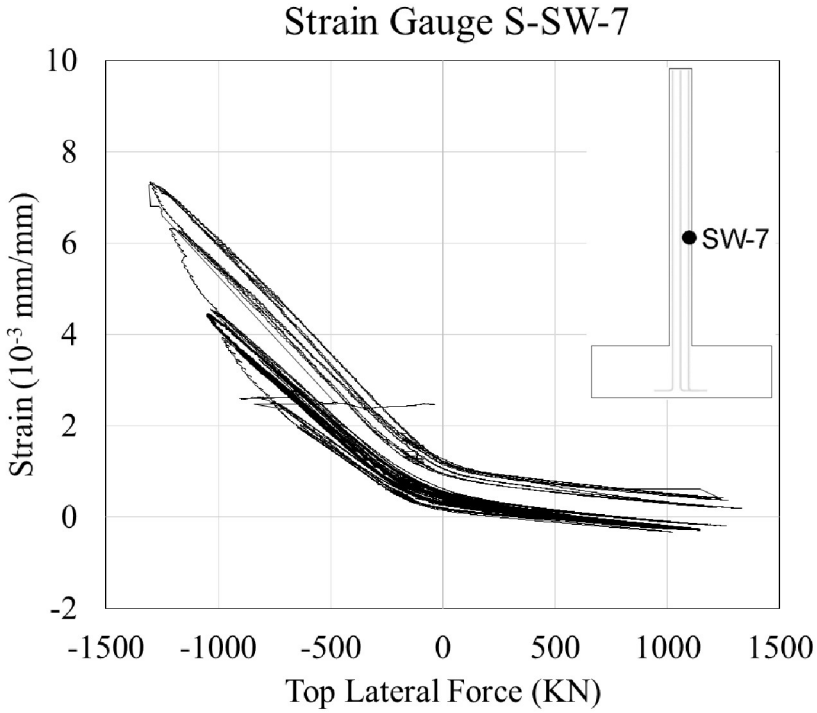
Strain Gauge S-SW-7
10
8
6
4
2
0
-2
Strain (10^{-3} mm/mm)
SW-7
-1500
-1000
-500
0
500
1000
1500
Top Lateral Force (KN)

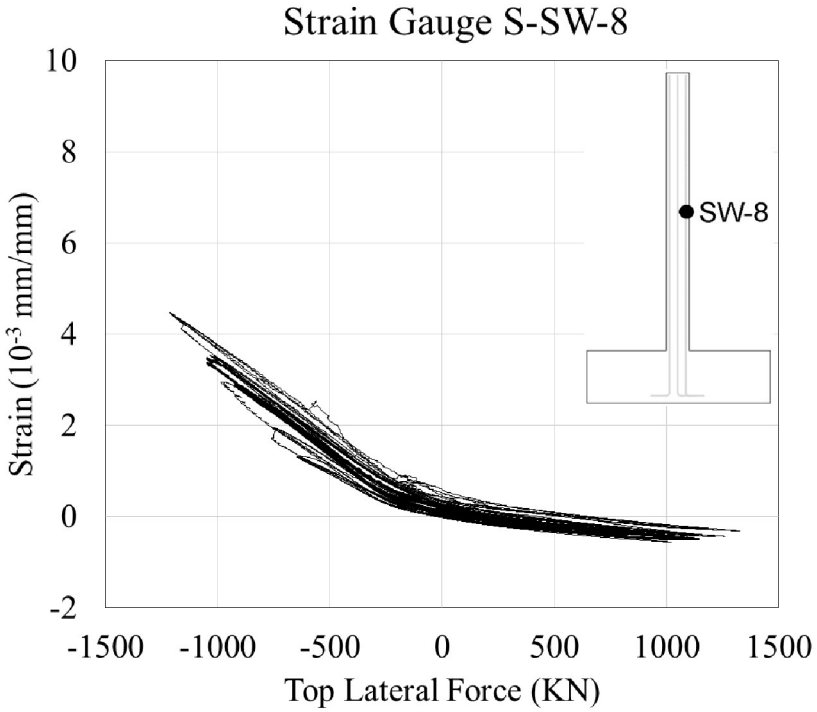
Strain Gauge S-SW-8
10
8
6
4
2
0
-2
Strain (10^{-3} mm/mm)
-1500
-1000
-500
0
500
1000
1500
Top Lateral Force (KN)
SW-8

#17 - NE-1

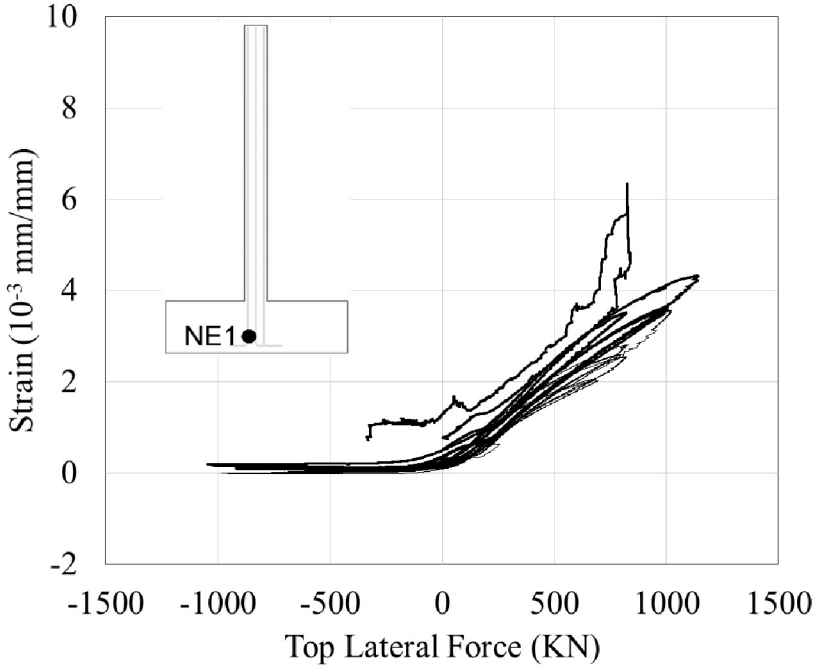

Strain Gauge S-NE-2

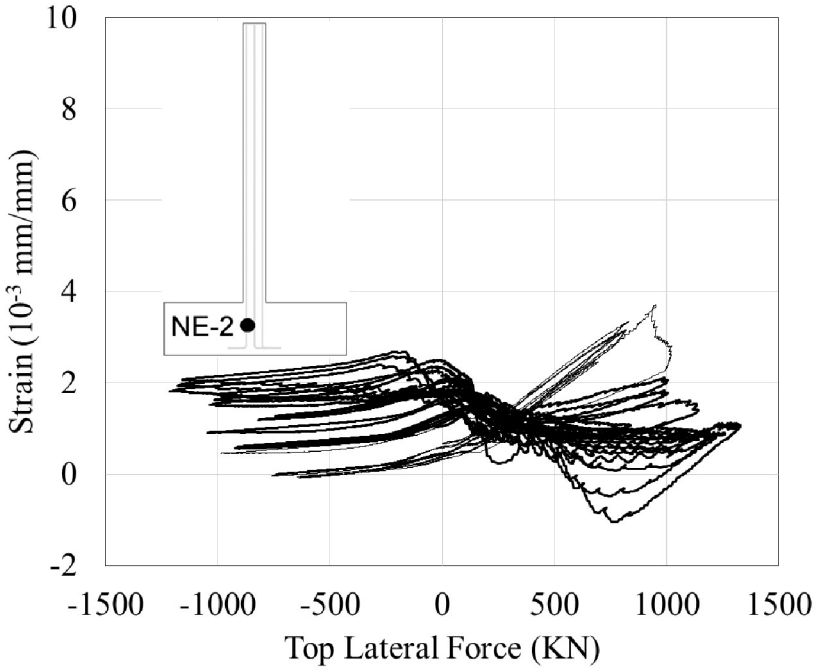

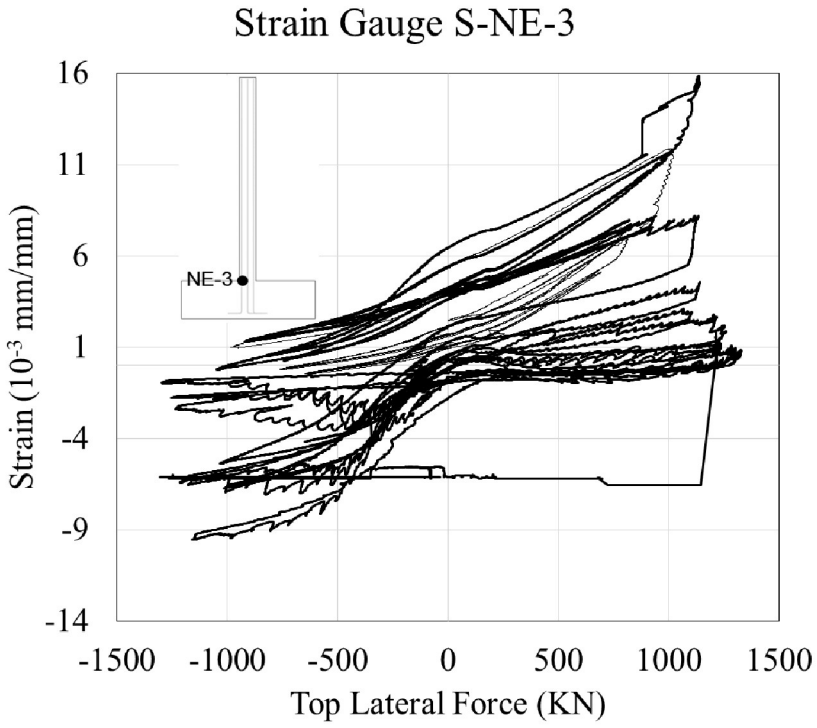
Strain Gauge S-NE-3
16
11
6
1
-4
-9
-14
NE-3
Strain (10-3 mm/mm)
-1500
-1000
-500
0
500
1000
1500
Top Lateral Force (KN)

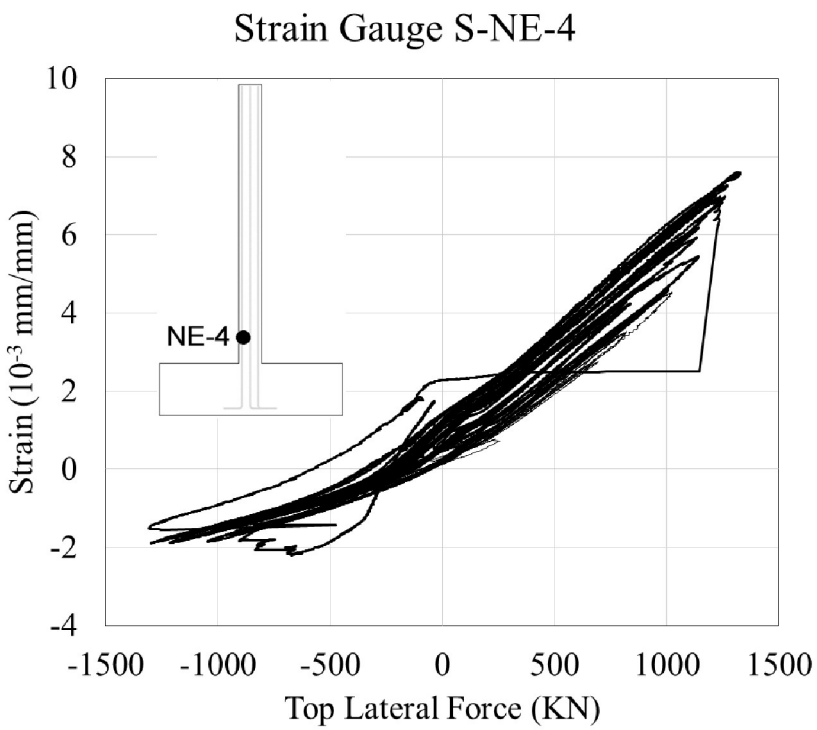
Strain Gauge S-NE-4
10
8
6
4
2
0
-2
-4
NE-4
Strain (10-3 mm/mm)
-1500
-1000
-500
0
500
1000
1500
Top Lateral Force (KN)

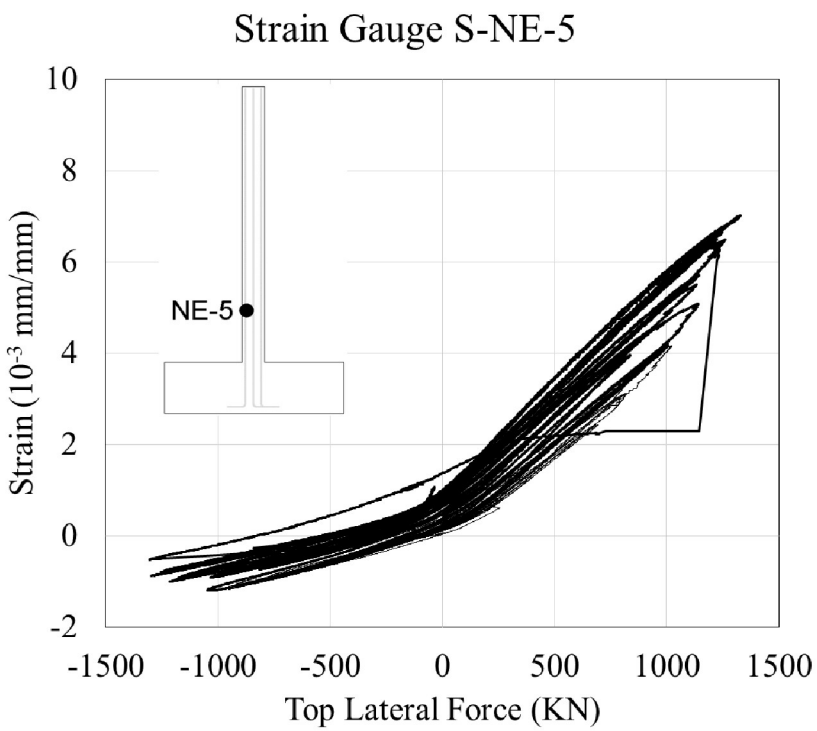
Strain Gauge S-NE-5
NE-5
Strain (10^{-3} mm/mm)
10
8
6
4
2
0
-2
-1500
-1000
-500
0
500
1000
1500
Top Lateral Force (KN)

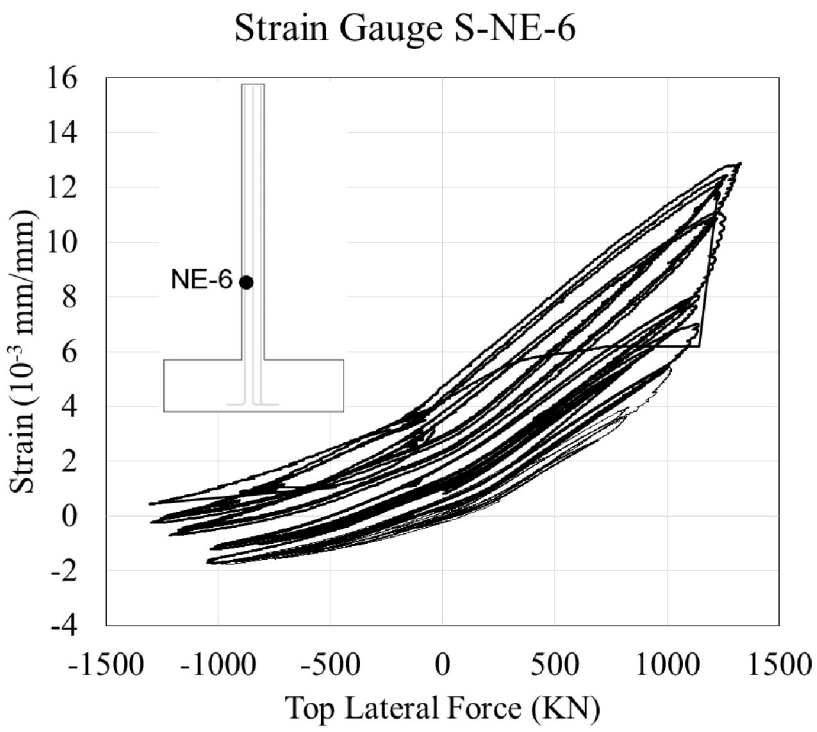
Strain Gauge S-NE-6
NE-6
Strain (10^{-3} mm/mm)
16
14
12
10
8
6
4
2
0
-2
-4
-1500
-1000
-500
0
500
1000
1500
Top Lateral Force (KN)

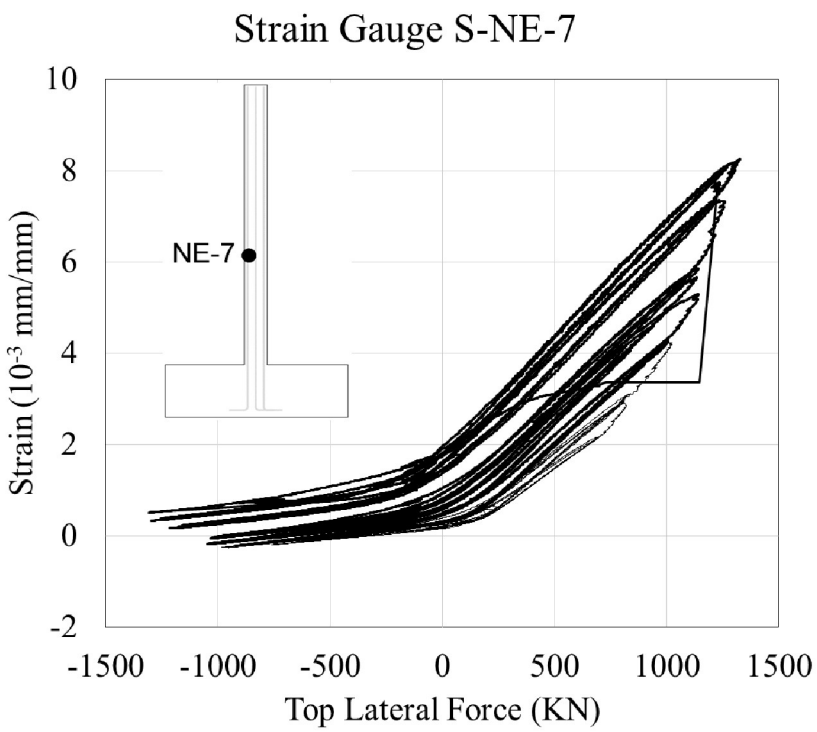
Strain Gauge S-NE-7
NE-7
Strain (10^{-3} mm/mm)
Top Lateral Force (KN)
10
8
6
4
2
0
-2
-1500
-1000
-500
0
500
1000
1500

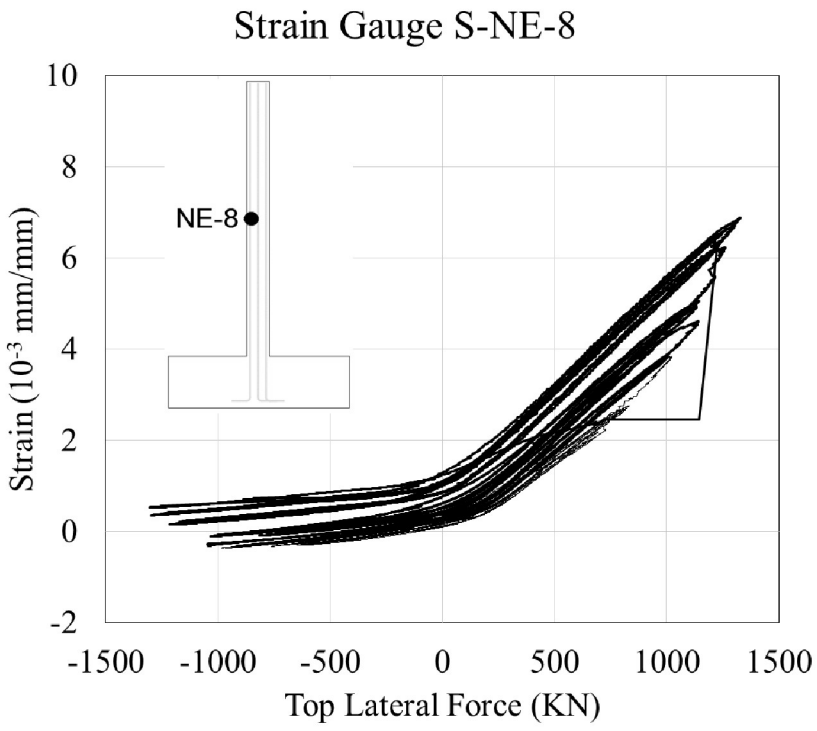
Strain Gauge S-NE-8
NE-8
Strain (10^{-3} mm/mm)
Top Lateral Force (KN)
10
8
6
4
2
0
-2
-1500
-1000
-500
0
500
1000
1500

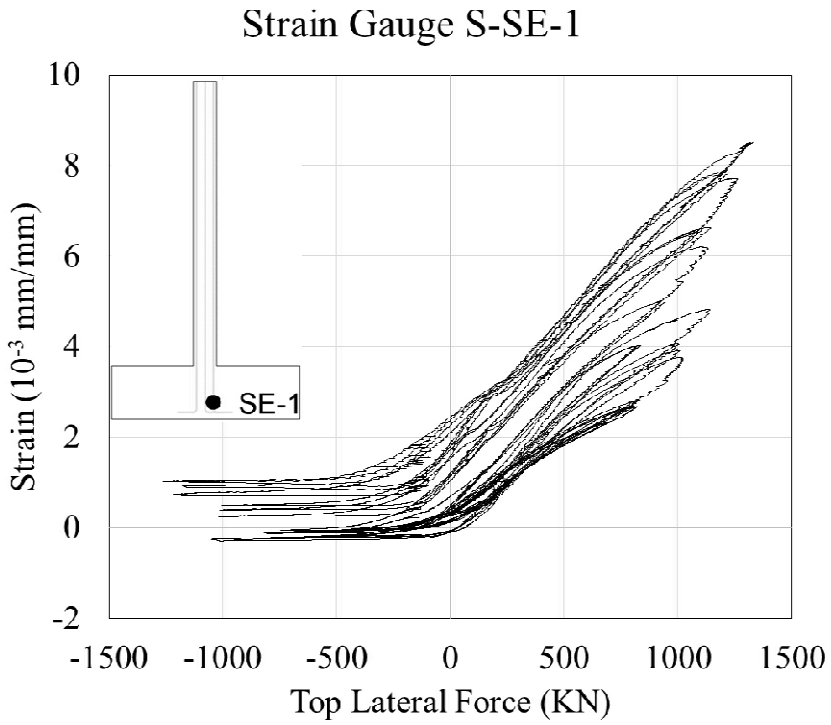
Strain Gauge S-SE-1
10
8
6
4
2
0
-2
Strain (10^{-3} mm/mm)
SE-1
-1500
-1000
-500
0
500
1000
1500
Top Lateral Force (KN)

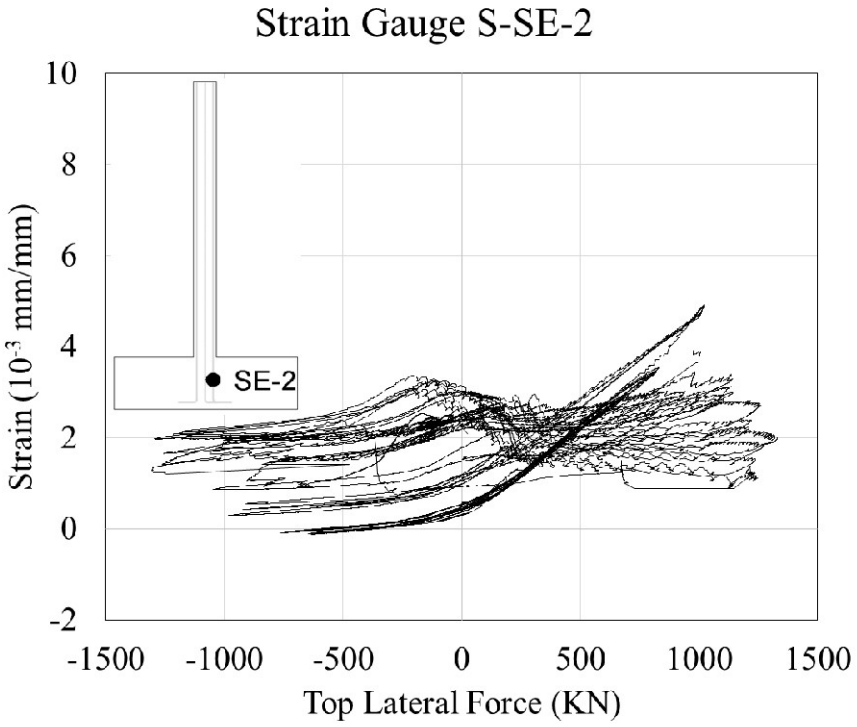
Strain Gauge S-SE-2
10
8
6
4
2
0
-2
Strain (10^{-3} mm/mm)
SE-2
-1500
-1000
-500
0
500
1000
1500
Top Lateral Force (KN)

Strain Gauge S-SE-3

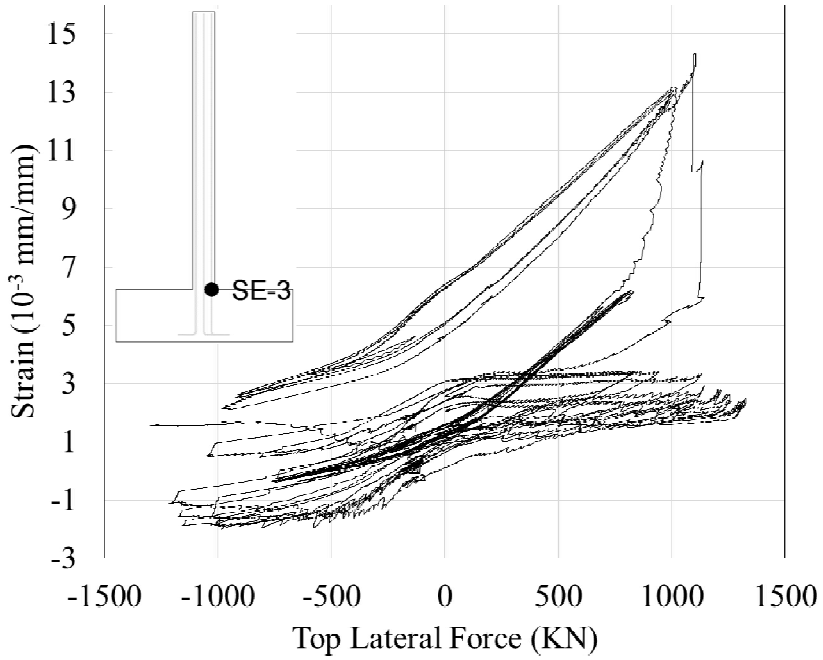

Strain Gauge S-SE-4

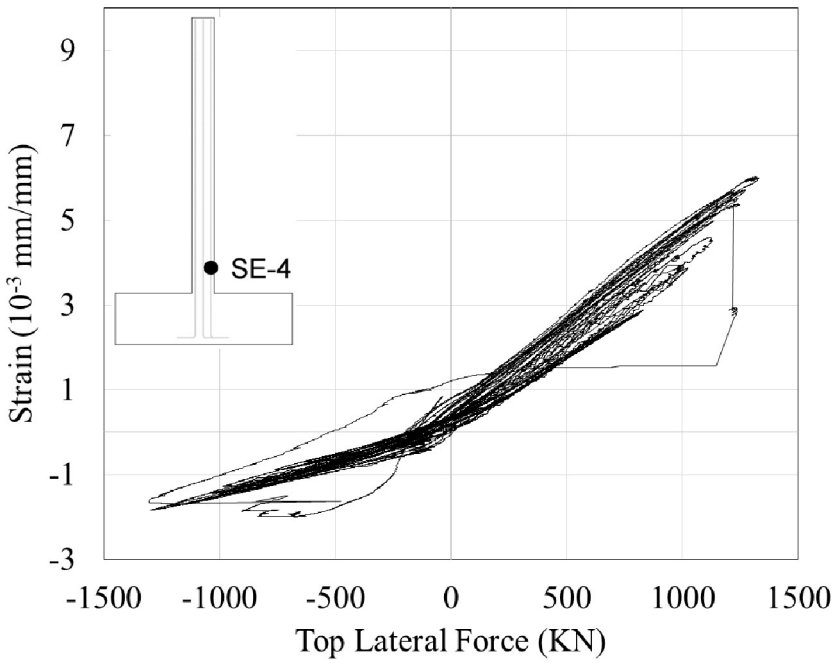

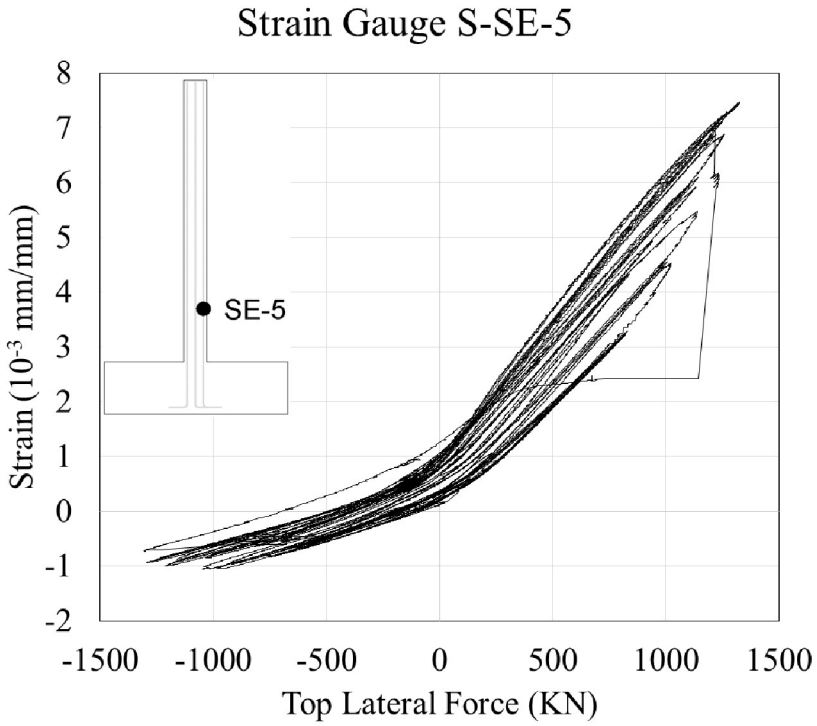
Strain Gauge S-SE-5
SE-5
Strain (10^{-3} mm/mm)
8
7
6
5
4
3
2
1
0
-1
-2
-1500
-1000
-500
0
500
1000
1500
Top Lateral Force (KN)

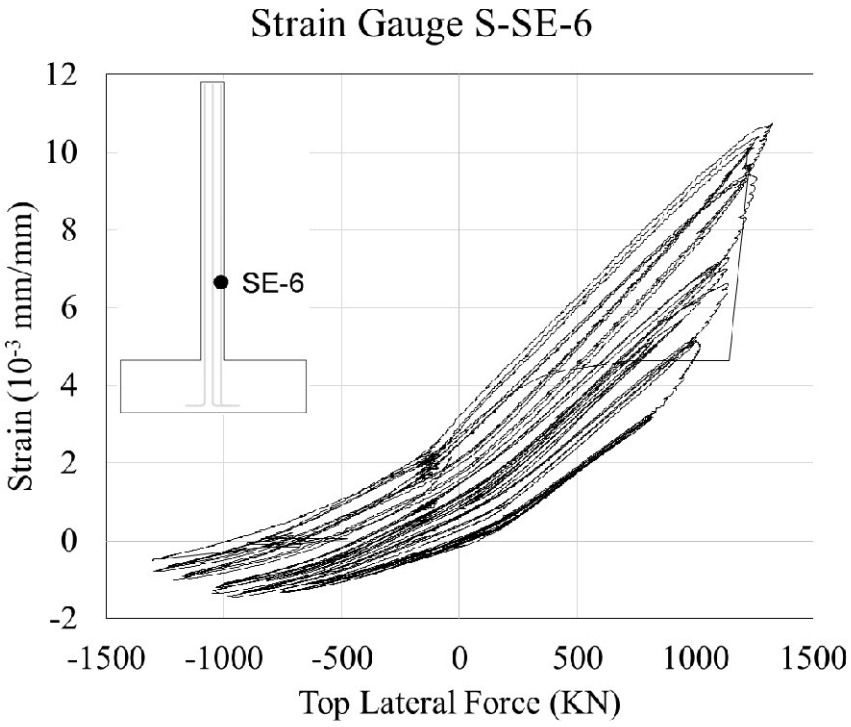
Strain Gauge S-SE-6
SE-6
Strain (10^{-3} mm/mm)
12
10
8
6
4
2
0
-2
-1500
-1000
-500
0
500
1000
1500
Top Lateral Force (KN)

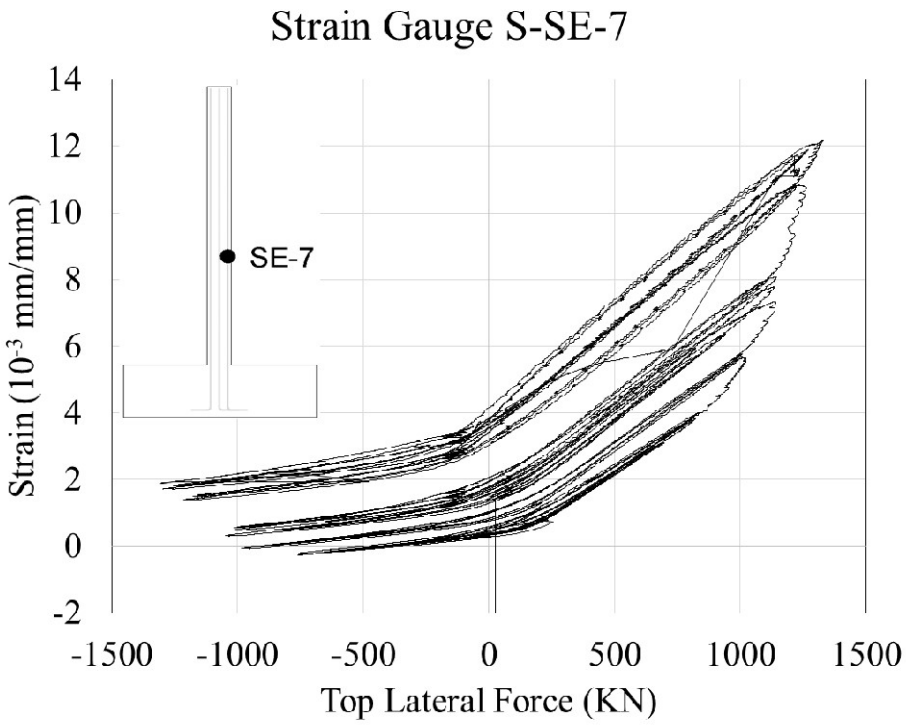
Strain Gauge S-SE-7
SE-7
Strain (10^{-3} mm/mm)
14
12
10
8
6
4
2
0
-2
-1500
-1000
-500
0
500
1000
1500
Top Lateral Force (KN)

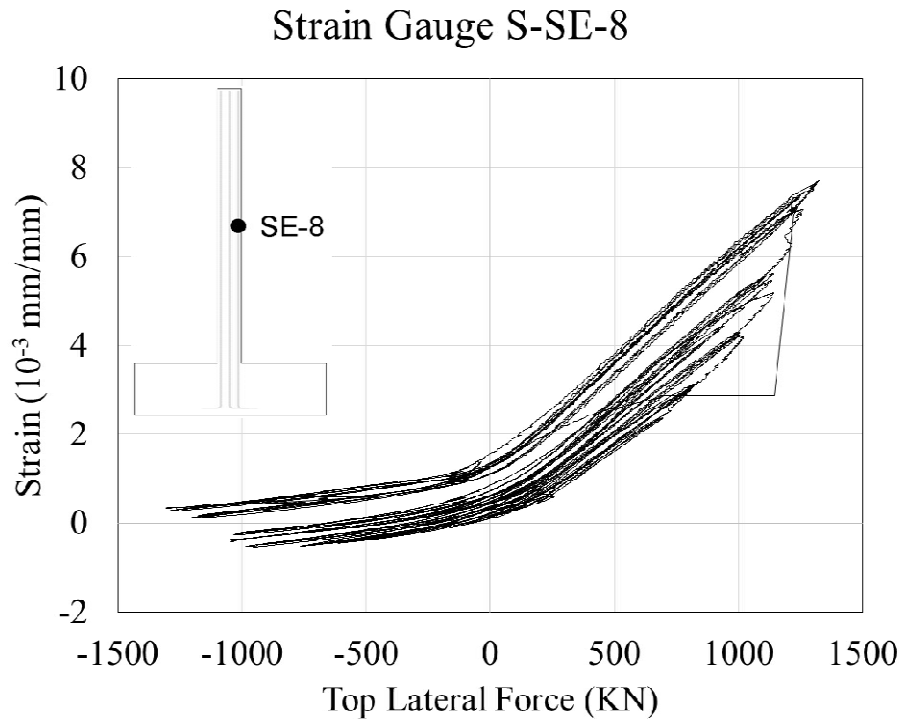
Strain Gauge S-SE-8
SE-8
Strain (10^{-3} mm/mm)
10
8
6
4
2
0
-2
-1500
-1000
-500
0
500
1000
1500
Top Lateral Force (KN)

Strain Gauge PN1

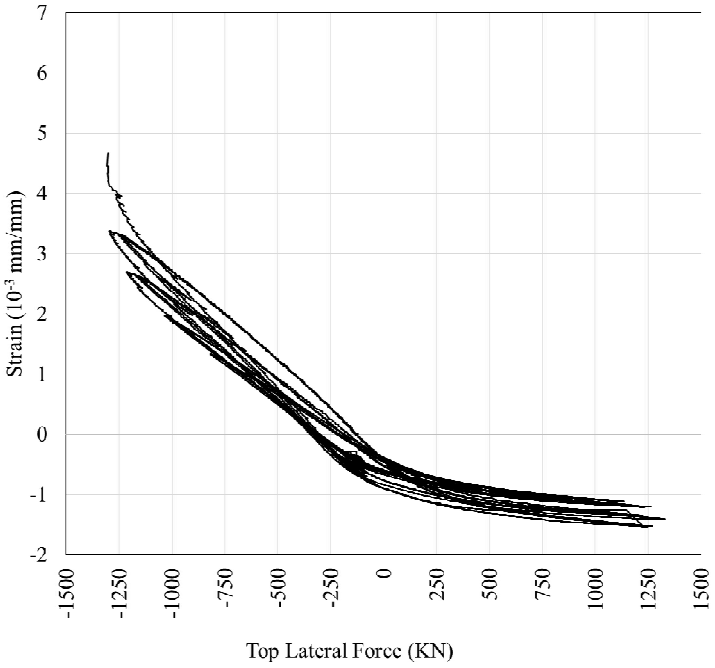

Strain Gauge PN2

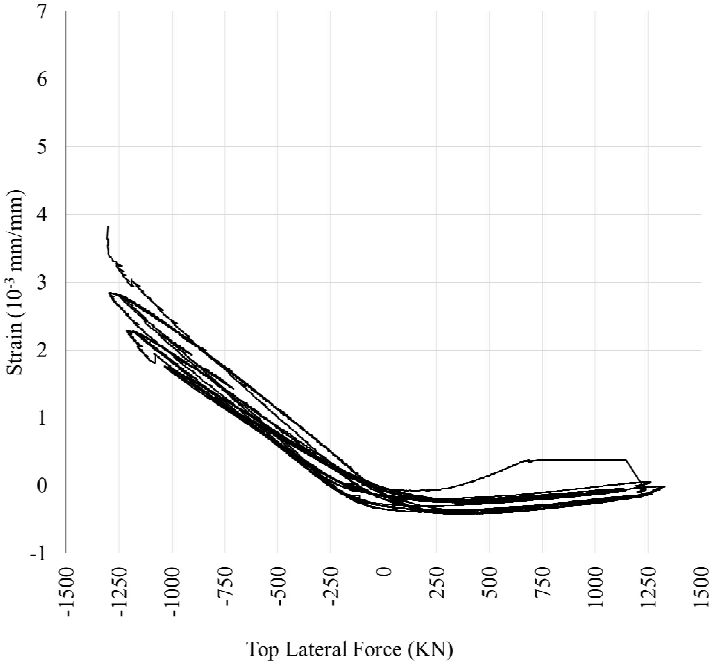

Strain Gauge PN3

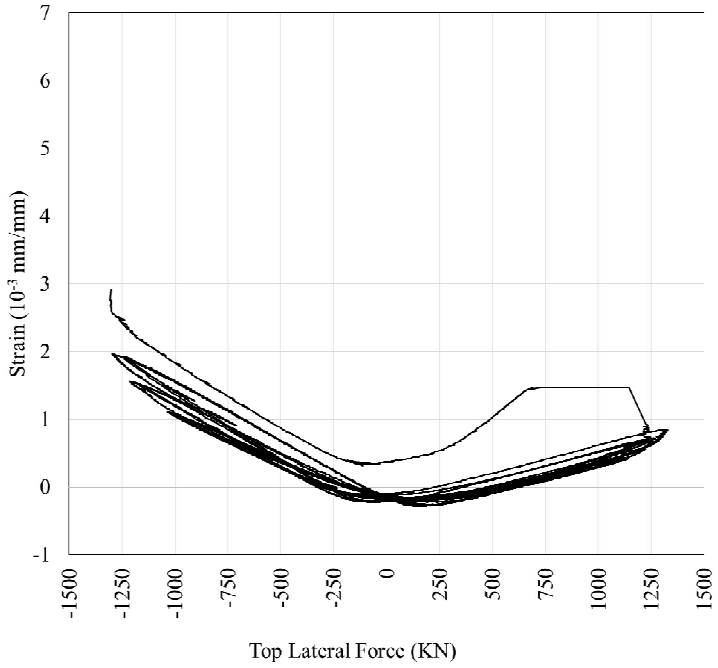

Strain Gauge PN4

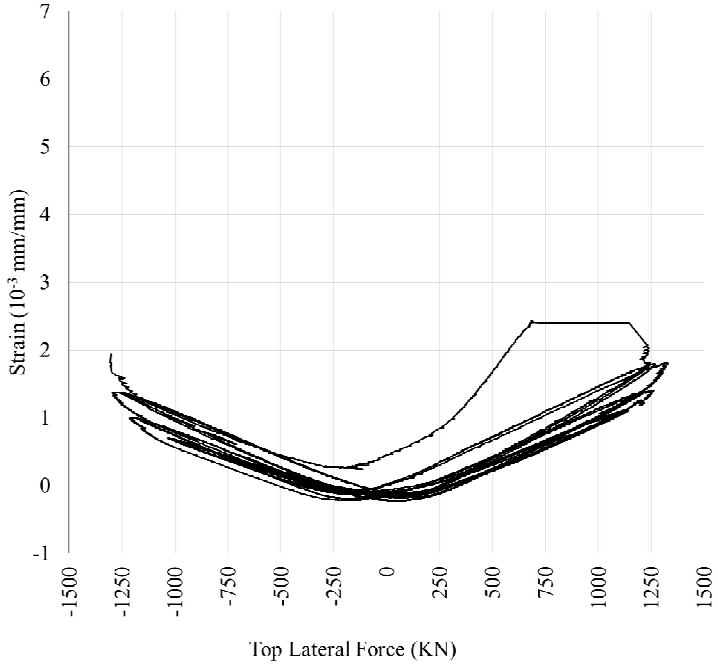

Strain Gauge PN5

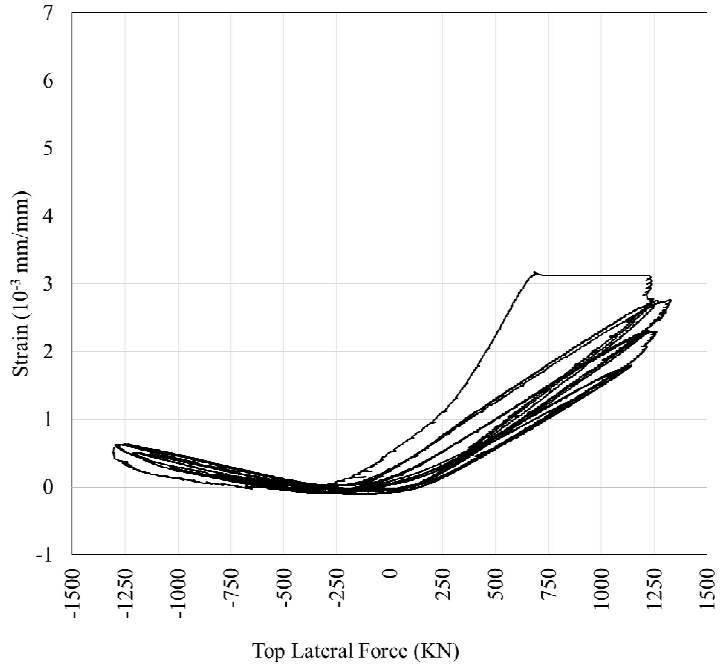

Strain Gauge PN6

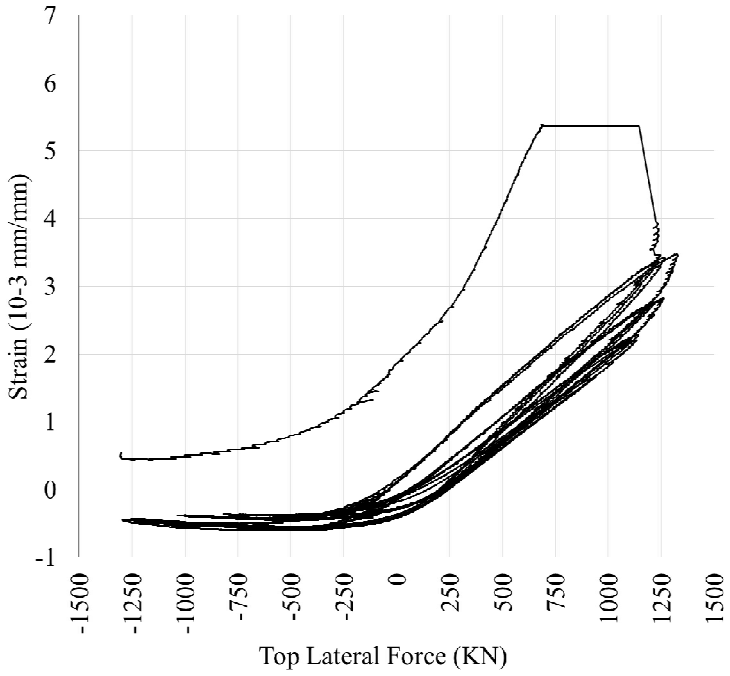

Strain Gauge PN7

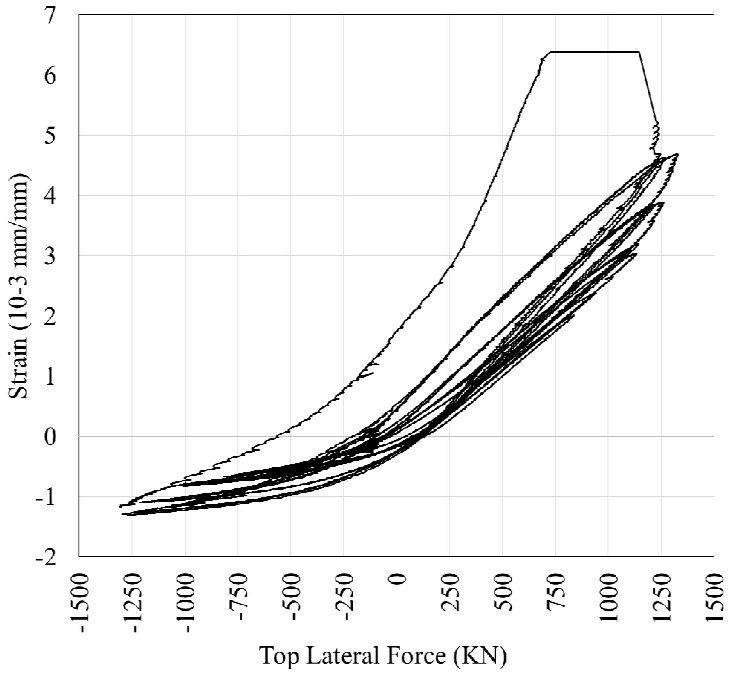

Strain Gauge PS1

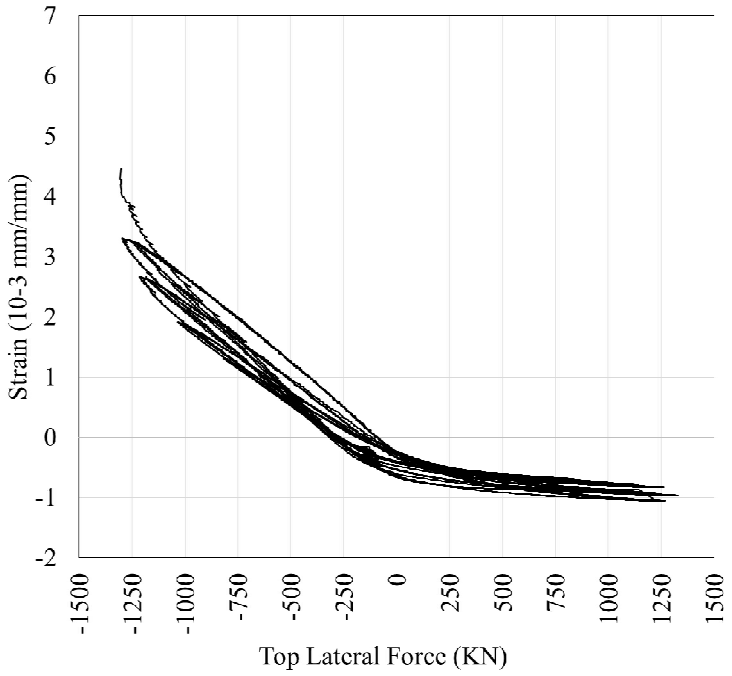

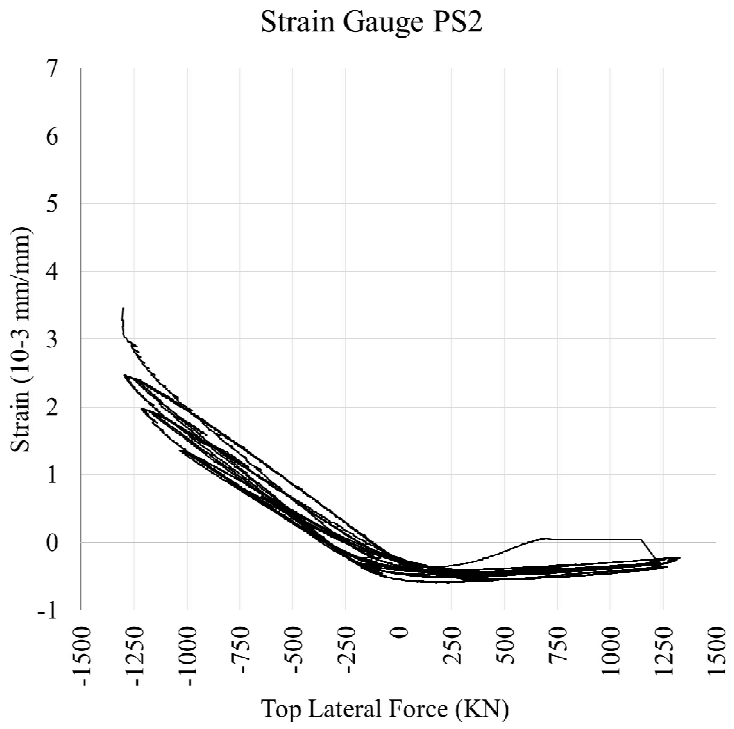
Strain Gauge PS2
Strain (10-3 mm/mm)
7
6
5
4
3
2
1
0
-1
-1500
-1250
-1000
-750
-500
-250
0
250
500
750
1000
1250
1500
Top Lateral Force (KN)

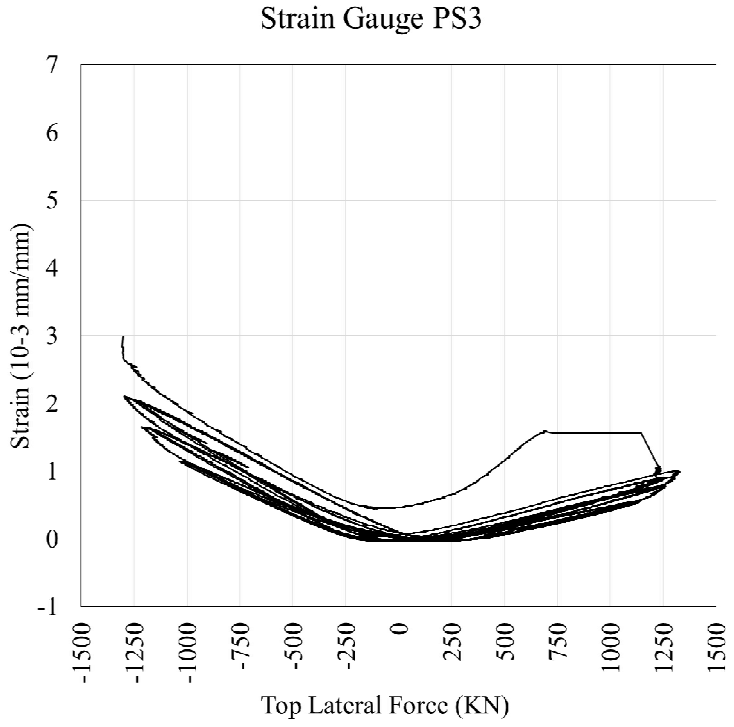
Strain Gauge PS3
Strain (10-3 mm/mm)
7
6
5
4
3
2
1
0
-1
-1500
-1250
-1000
-750
-500
-250
0
250
500
750
1000
1250
1500
Top Lateral Force (KN)

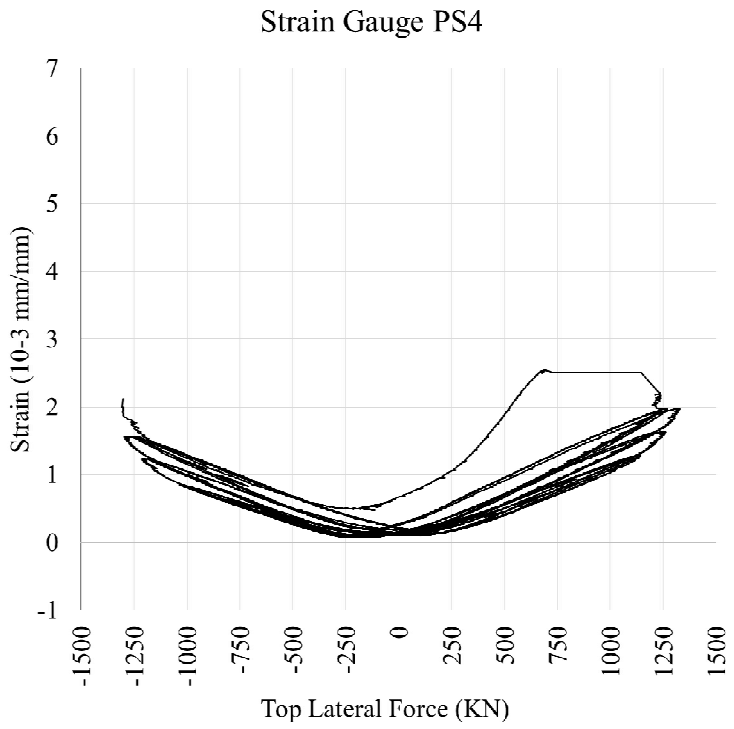
Strain Gauge PS4
Strain (10-3 mm/mm)
7
6
5
4
3
2
1
0
-1
-1500
-1250
-1000
-750
-500
-250
0
250
500
750
1000
1250
1500
Top Lateral Force (KN)

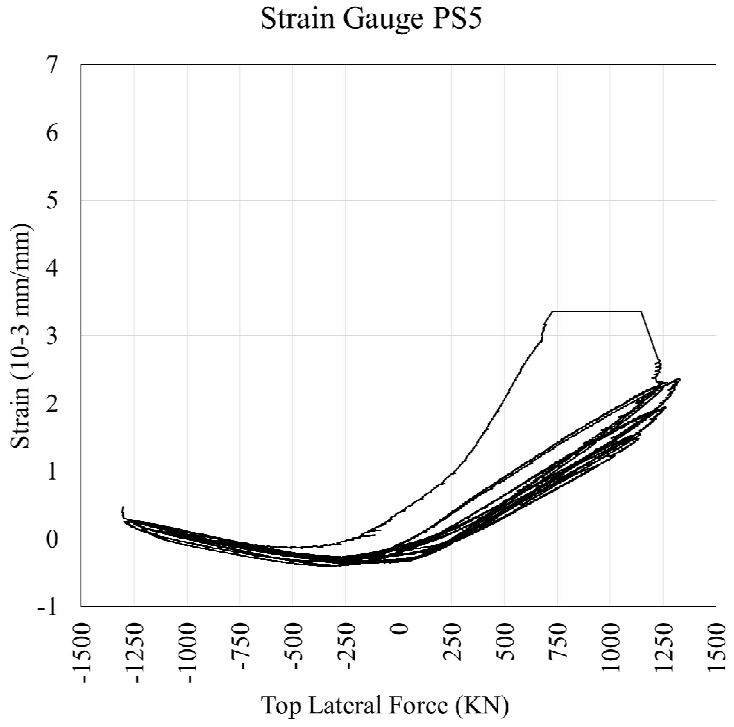
Strain Gauge PS5
Strain (10-3 mm/mm)
7
6
5
4
3
2
1
0
-1
-1500
-1250
-1000
-750
-500
-250
0
250
500
750
1000
1250
1500
Top Lateral Force (KN)

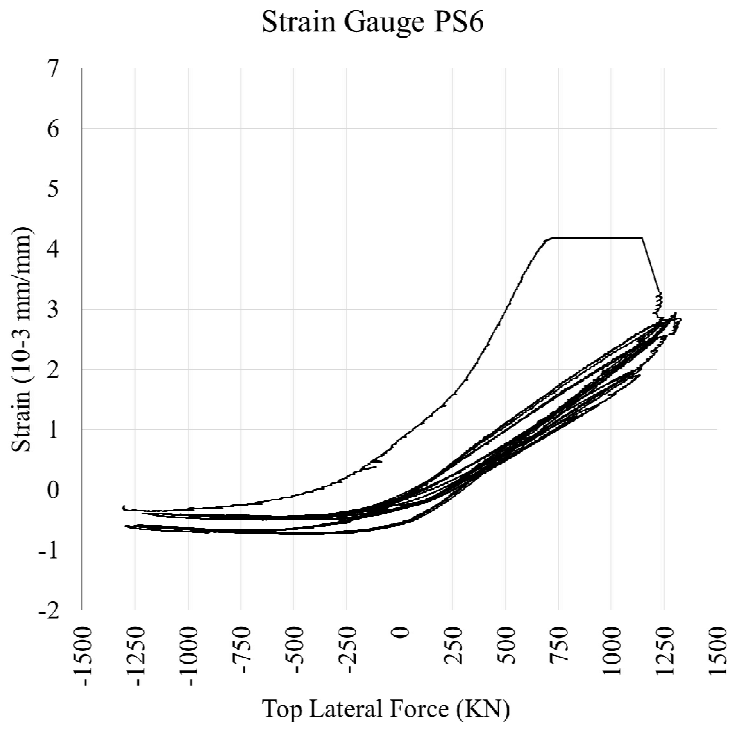
Strain Gauge PS6
Strain (10-3 mm/mm)
7
6
5
4
3
2
1
0
-1
-2
-1500
-1250
-1000
-750
-500
-250
0
250
500
750
1000
1250
1500
Top Lateral Force (KN)

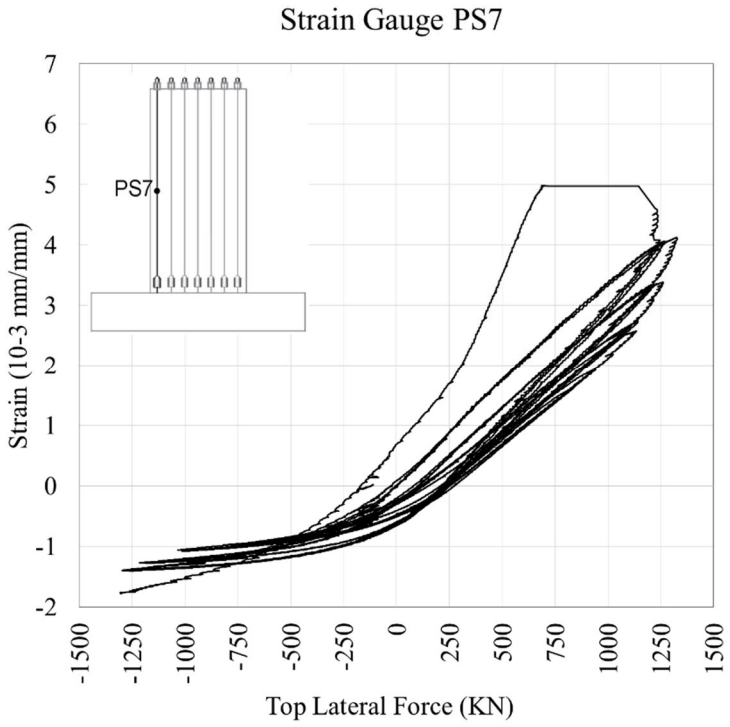
Strain Gauge PS7
PS7
Strain (10-3 mm/mm)
7
6
5
4
3
2
1
0
-1
-2
-1500
-1250
-1000
-750
-500
-250
0
250
500
750
1000
1250
1500
Top Lateral Force (KN)

Appendix D

Recorded Displacement Data

Wall W1HS

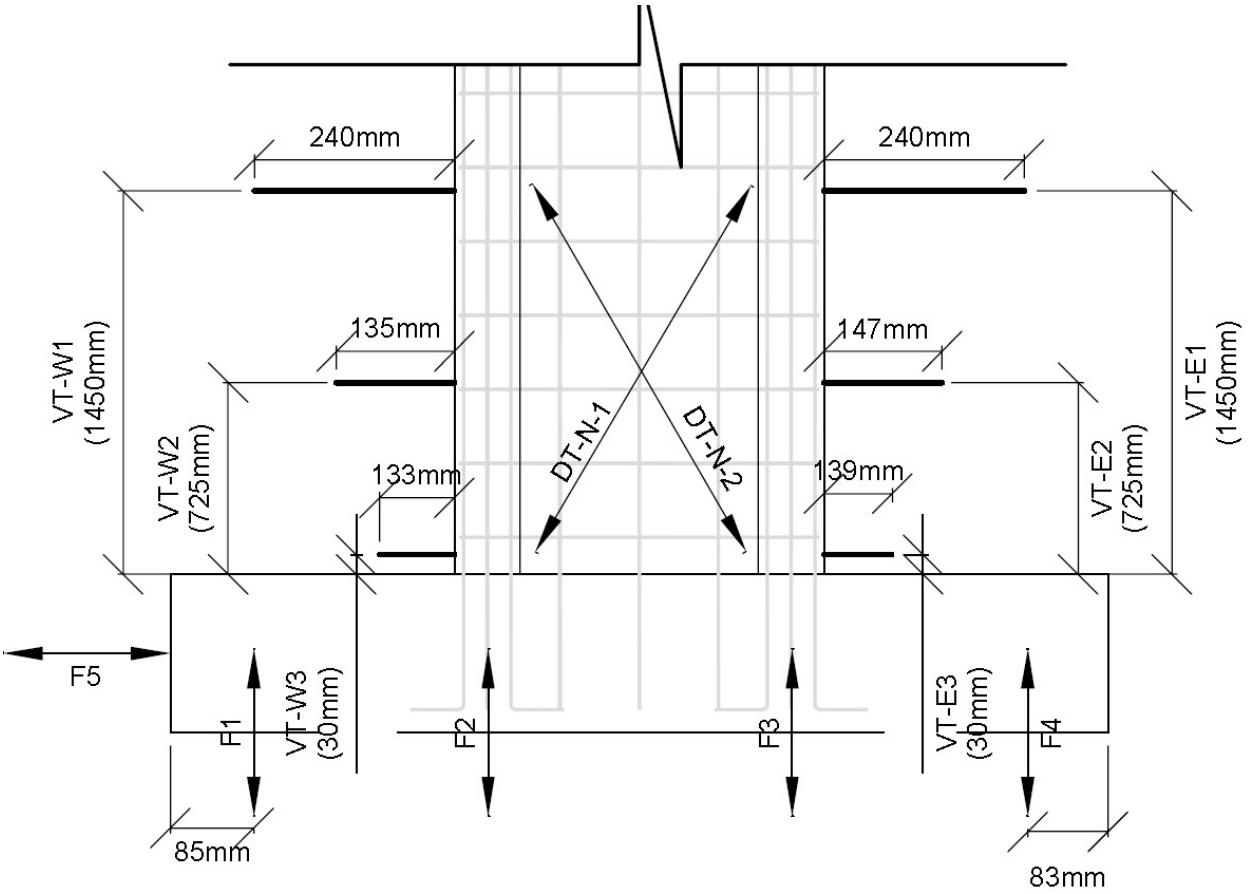

Figure D-1 – As-built measurements of cable transducer and LVDT locations

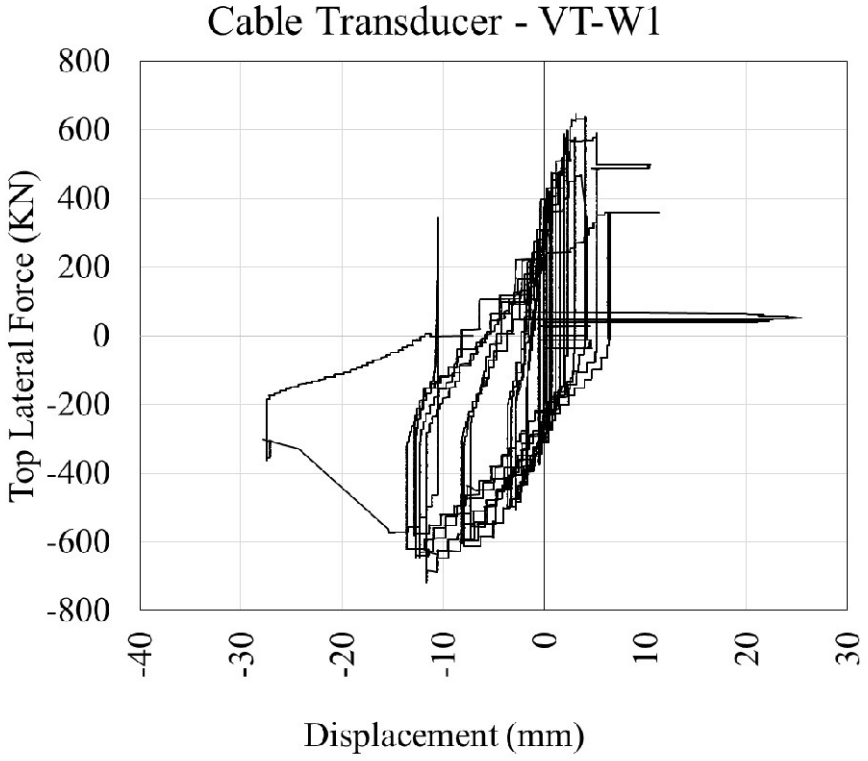
Cable Transducer - VT-W1
Top Lateral Force (KN)
800
600
400
200
0
-200
-400
-600
-800
-40
-30
-20
-10
0
10
20
30
Displacement (mm)

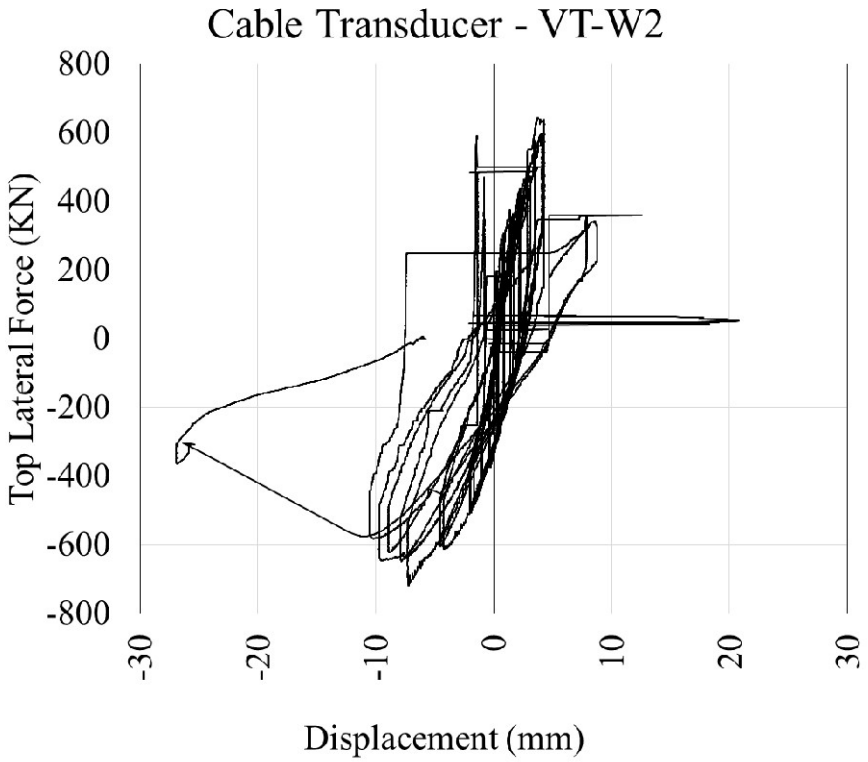
Cable Transducer - VT-W2
Top Lateral Force (KN)
800
600
400
200
0
-200
-400
-600
-800
-30
-20
-10
0
10
20
30
Displacement (mm)

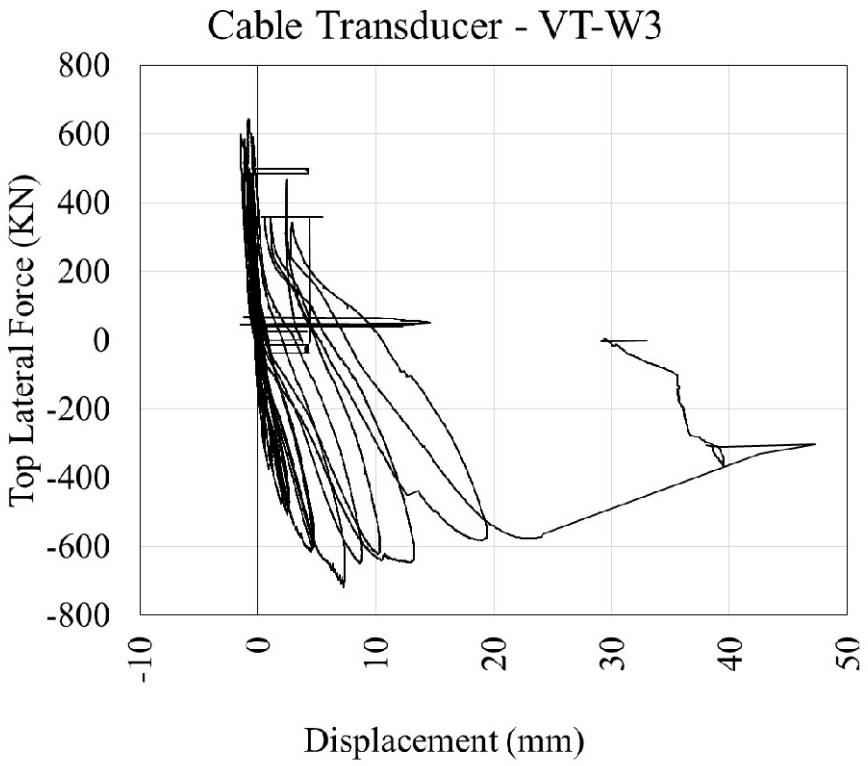
Cable Transducer - VT-W3
Top Lateral Force (KN)
800
600
400
200
0
-200
-400
-600
-800
-10
0
10
20
30
40
50
Displacement (mm)

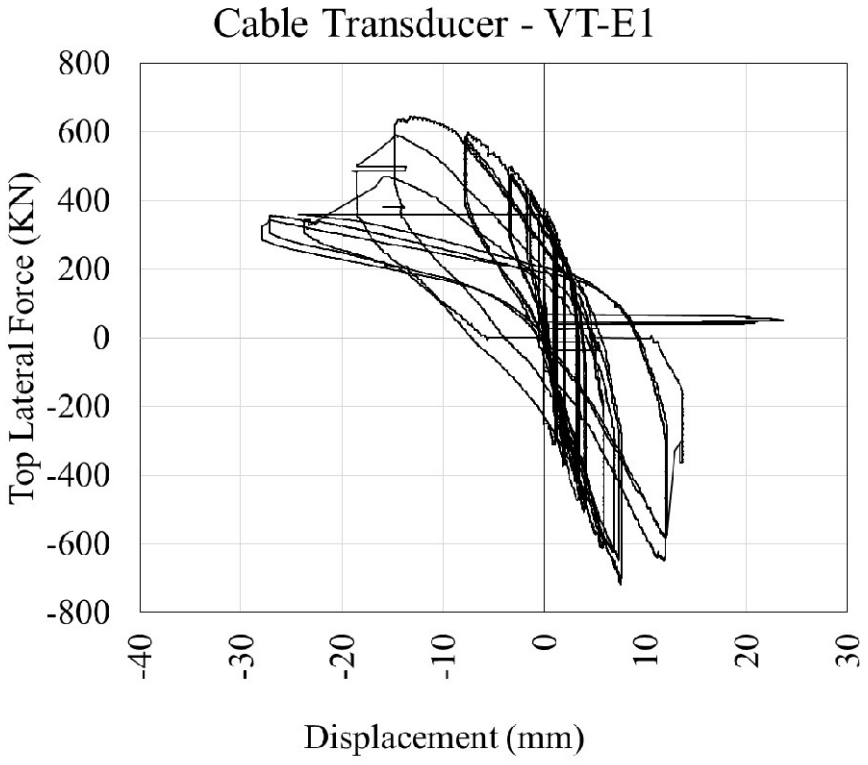
Cable Transducer - VT-E1
Top Lateral Force (KN)
800
600
400
200
0
-200
-400
-600
-800
-40
-30
-20
-10
0
10
20
30
Displacement (mm)

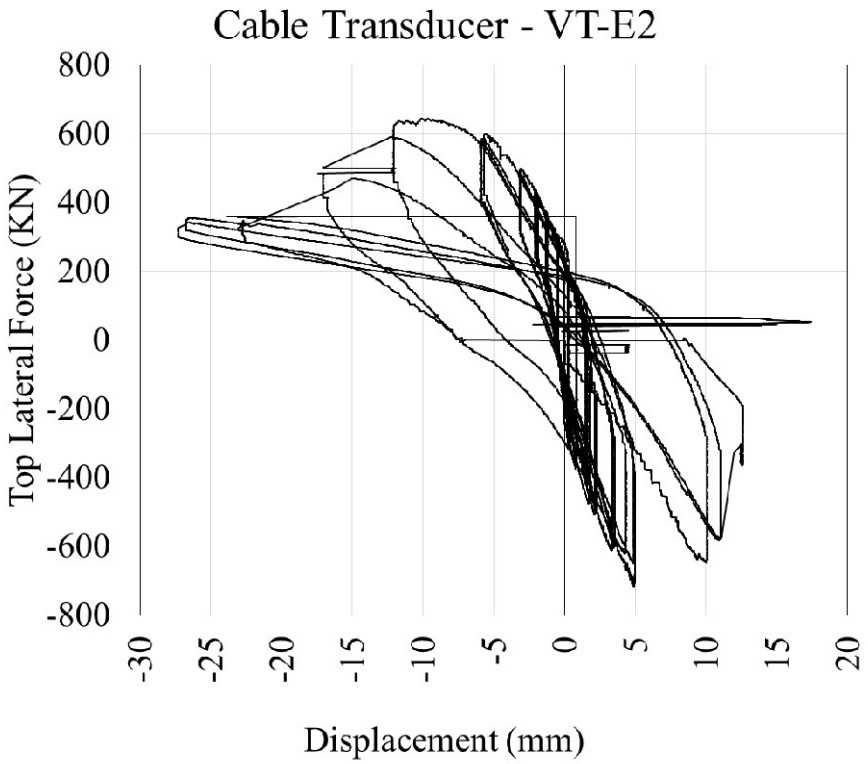
Cable Transducer - VT-E2
Top Lateral Force (KN)
800
600
400
200
0
-200
-400
-600
-800
-30
-25
-20
-15
-10
-5
0
5
10
15
20
Displacement (mm)

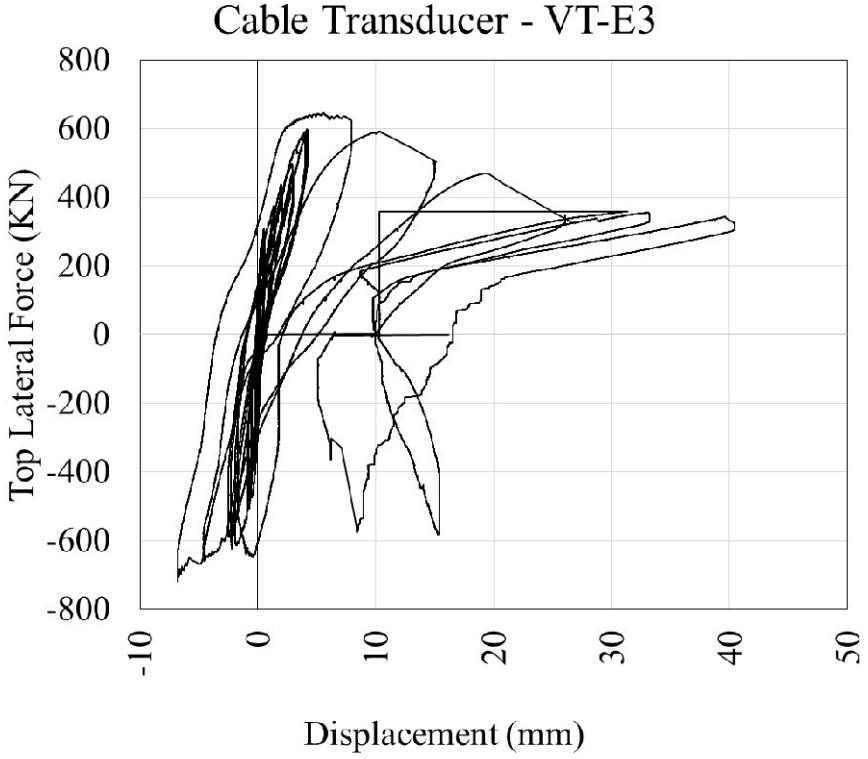
Cable Transducer - VT-E3
Top Lateral Force (KN)
800
600
400
200
0
-200
-400
-600
-800
-10
0
10
20
30
40
50
Displacement (mm)

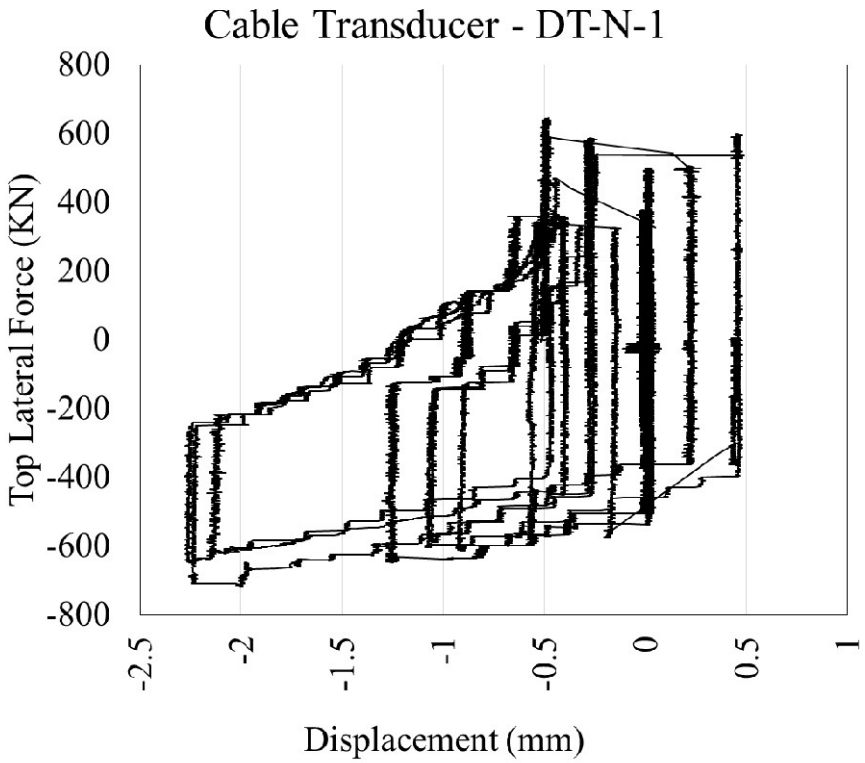
Cable Transducer - DT-N-1
Top Lateral Force (KN)
800
600
400
200
0
-200
-400
-600
-800
-2.5
-2
-1.5
-1
-0.5
0
0.5
1
Displacement (mm)

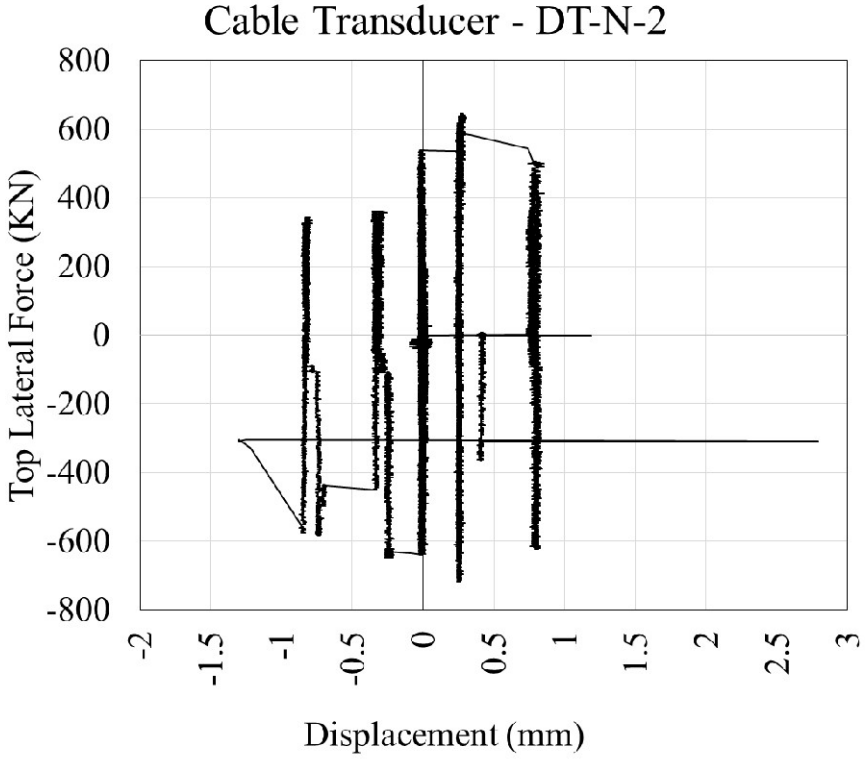
Cable Transducer - DT-N-2
Top Lateral Force (KN)
800
600
400
200
0
-200
-400
-600
-800
-2
-1.5
-1
-0.5
0
0.5
1
1.5
2
2.5
3
Displacement (mm)

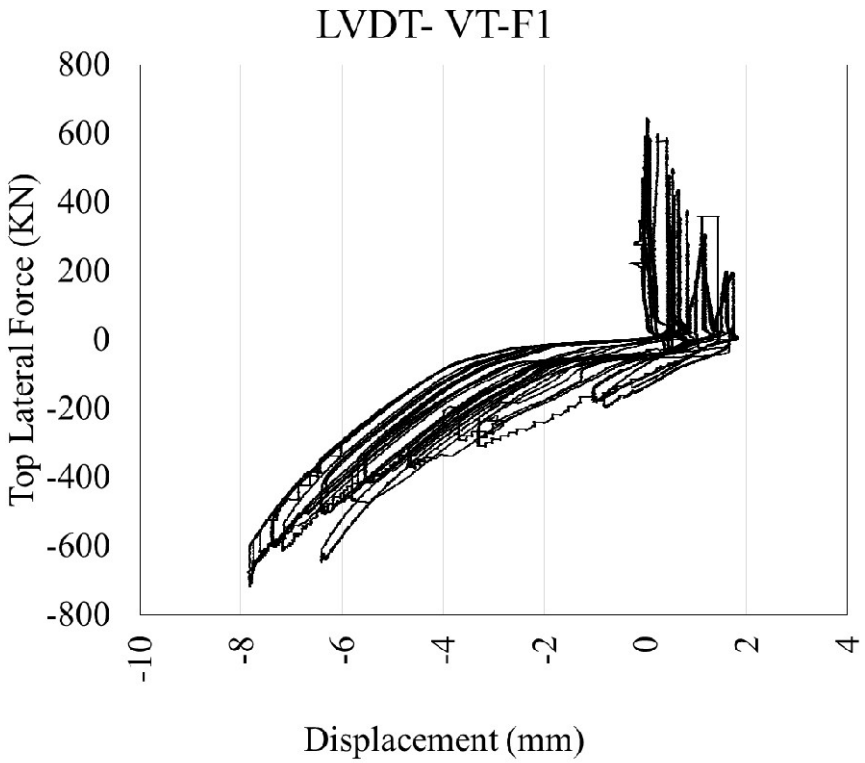
LVDT- VT-F1
Top Lateral Force (KN)
800
600
400
200
0
-200
-400
-600
-800
-10
-8
-6
-4
-2
0
2
4
Displacement (mm)

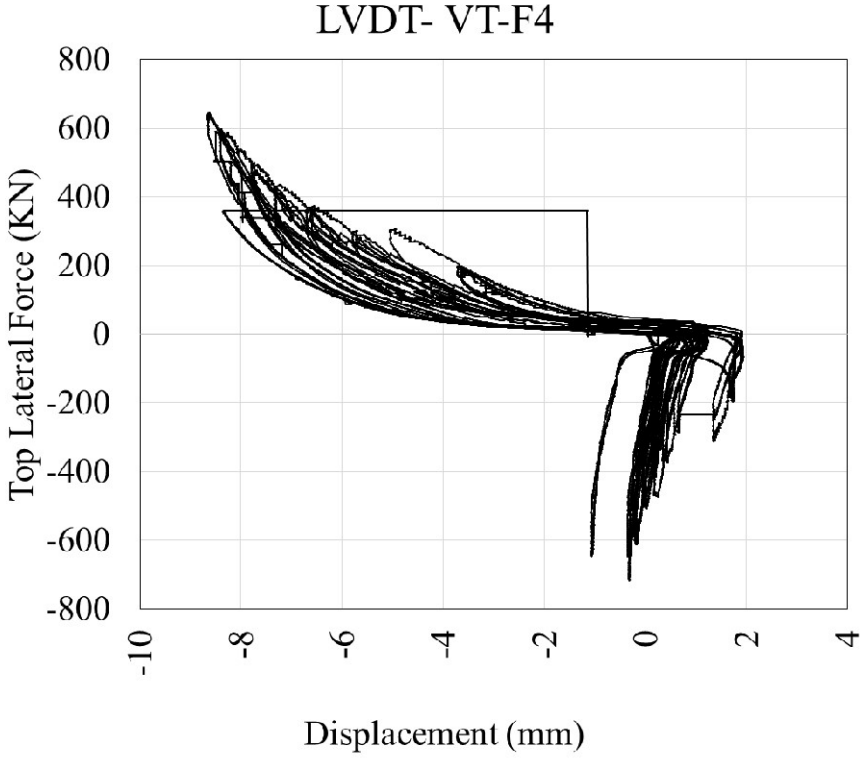
LVDT- VT-F4
Top Lateral Force (KN)
800
600
400
200
0
-200
-400
-600
-800
-10
-8
-6
-4
-2
0
2
4
Displacement (mm)

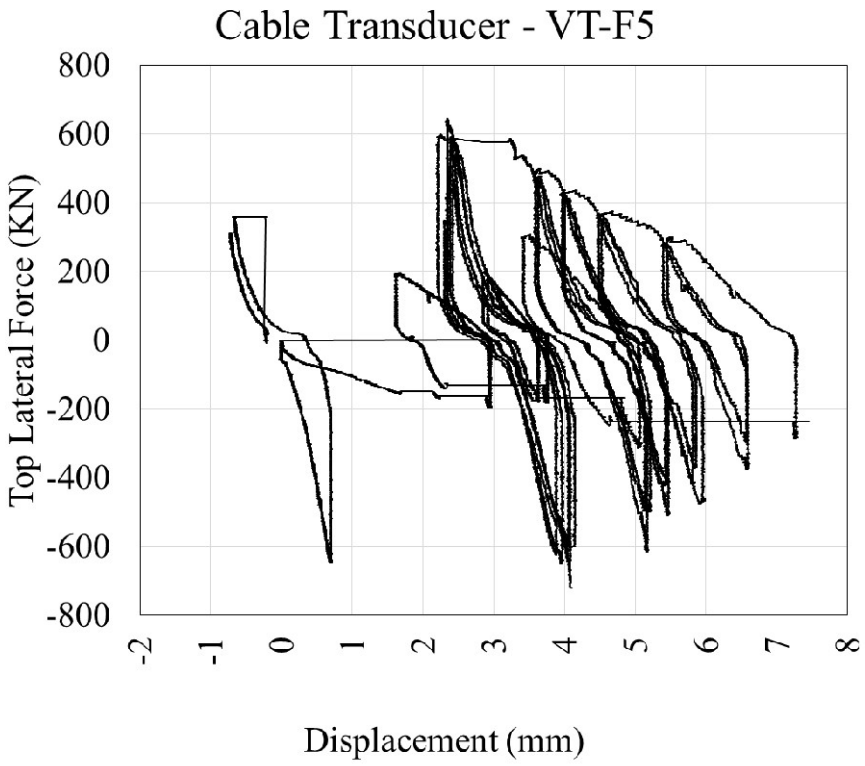
Cable Transducer - VT-F5
800
600
400
200
0
-200
-400
-600
-800
Top Lateral Force (KN)
-2
-1
0
1
2
3
4
5
6
7
8
Displacement (mm)

Wall W2HS

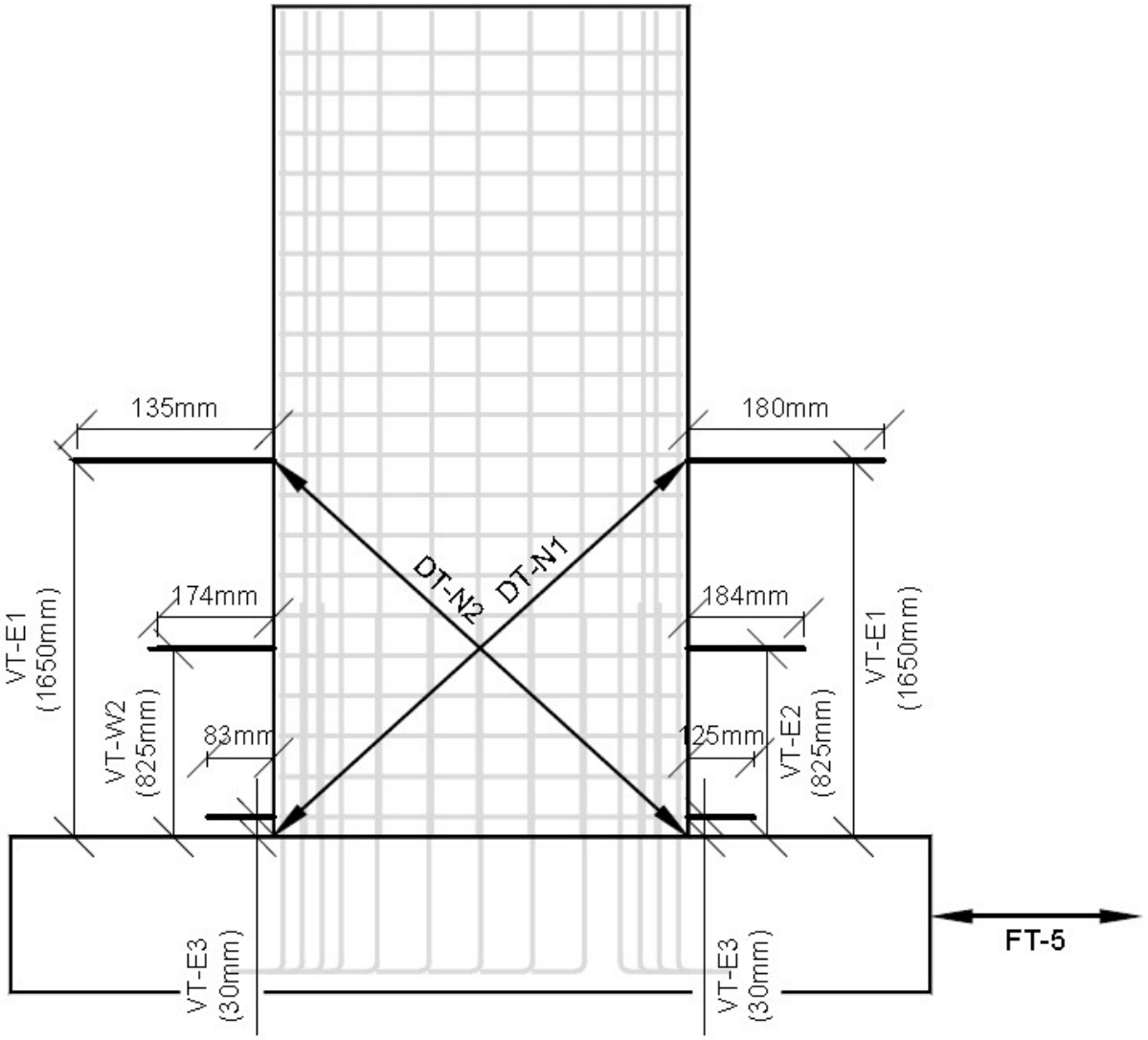

Figure D-2 – As-built measurements of cable transducer locations

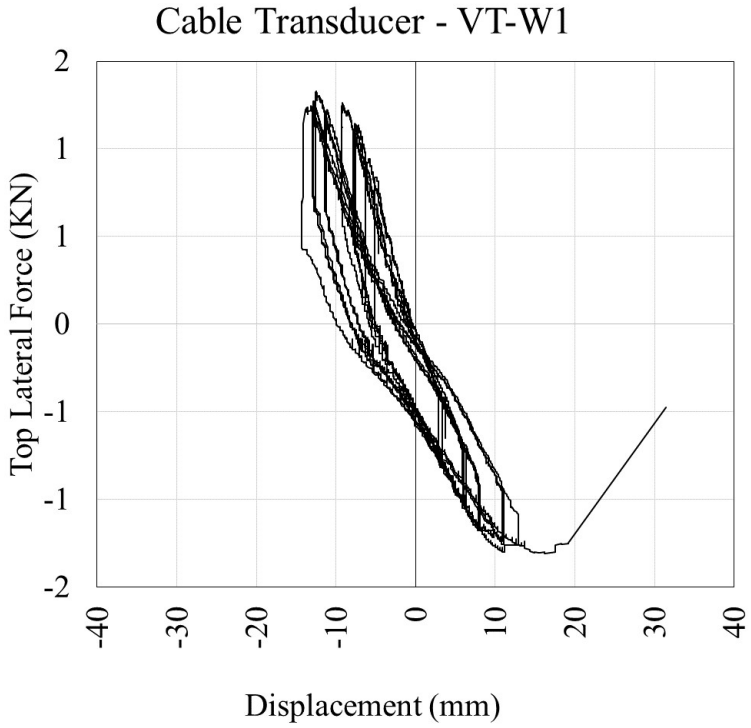
Cable Transducer - VT-W1
Top Lateral Force (KN)
2
1
1
0
-1
-1
-2
-40
-30
-20
-10
0
10
20
30
40
Displacement (mm)

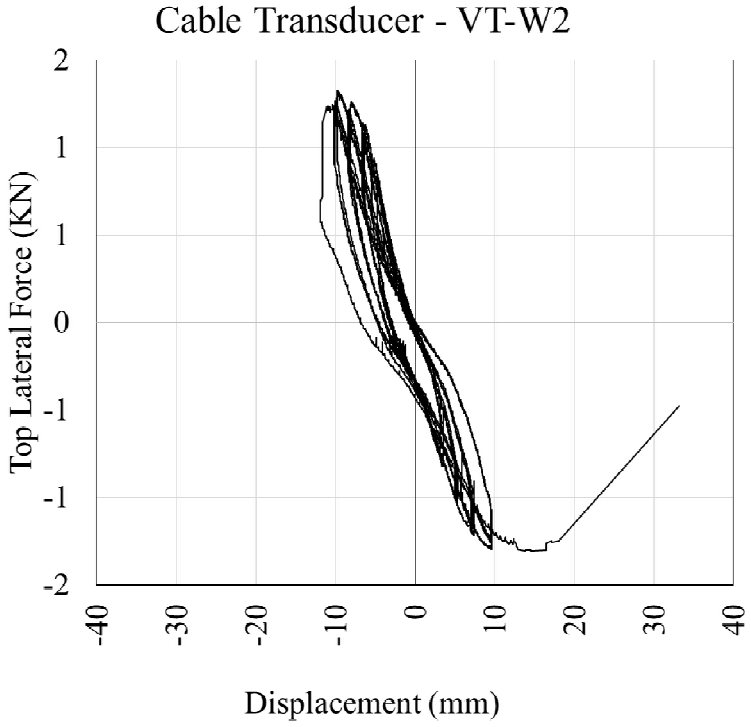
Cable Transducer - VT-W2
Top Lateral Force (KN)
2
1
1
0
-1
-1
-2
-40
-30
-20
-10
0
10
20
30
40
Displacement (mm)

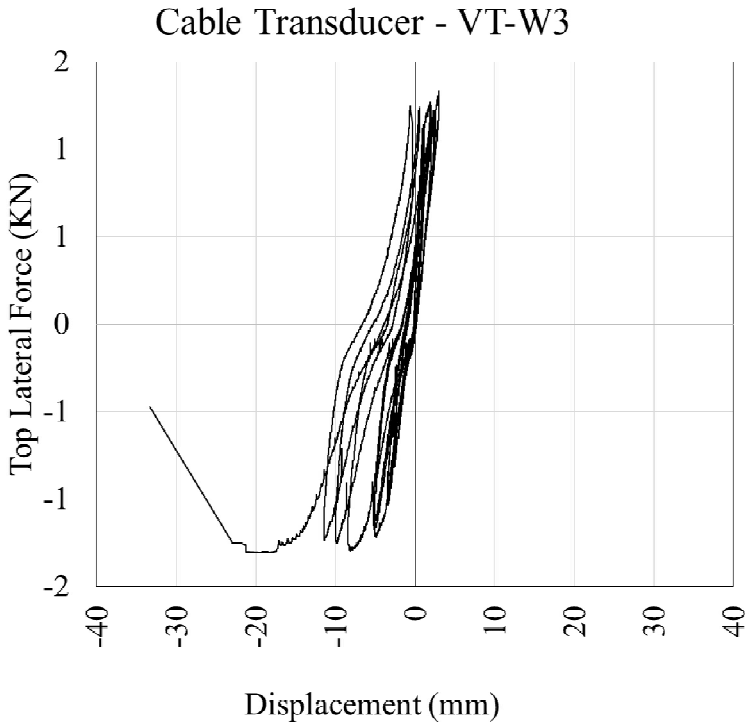
Cable Transducer - VT-W3
Top Lateral Force (KN)
2
1
1
0
-1
-1
-2
-40
-30
-20
-10
0
10
20
30
40
Displacement (mm)

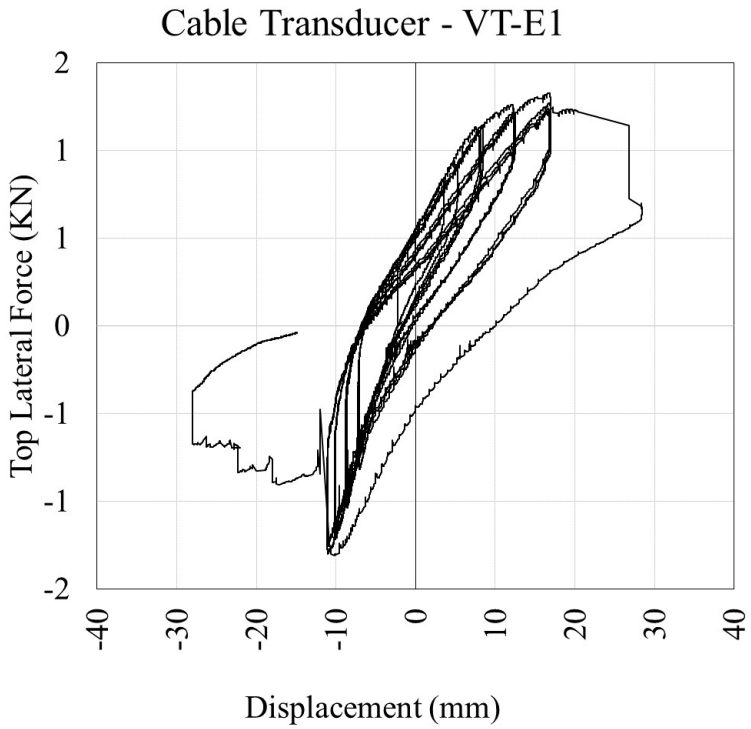
Cable Transducer - VT-E1
Top Lateral Force (KN)
2
1
1
0
-1
-1
-2
-40
-30
-20
-10
0
10
20
30
40
Displacement (mm)

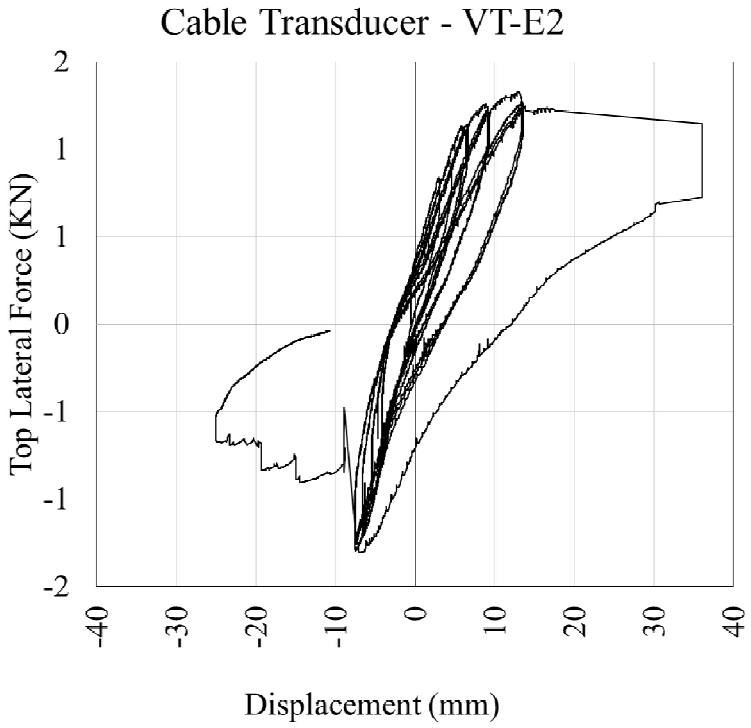
Cable Transducer - VT-E2
Top Lateral Force (KN)
2
1
1
0
-1
-1
-2
-40
-30
-20
-10
0
10
20
30
40
Displacement (mm)

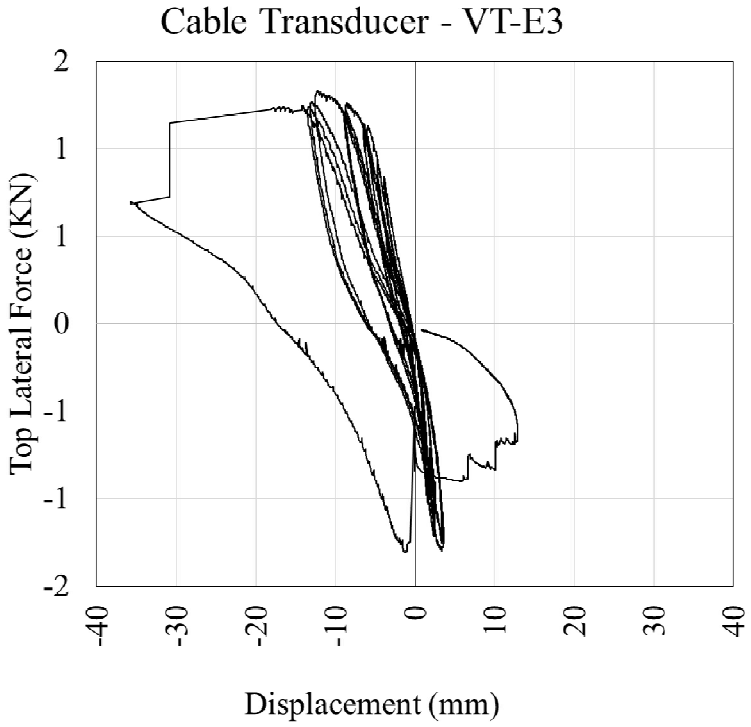
Cable Transducer - VT-E3
Top Lateral Force (KN)
2
1
1
0
-1
-1
-2
-40
-30
-20
-10
0
10
20
30
40
Displacement (mm)

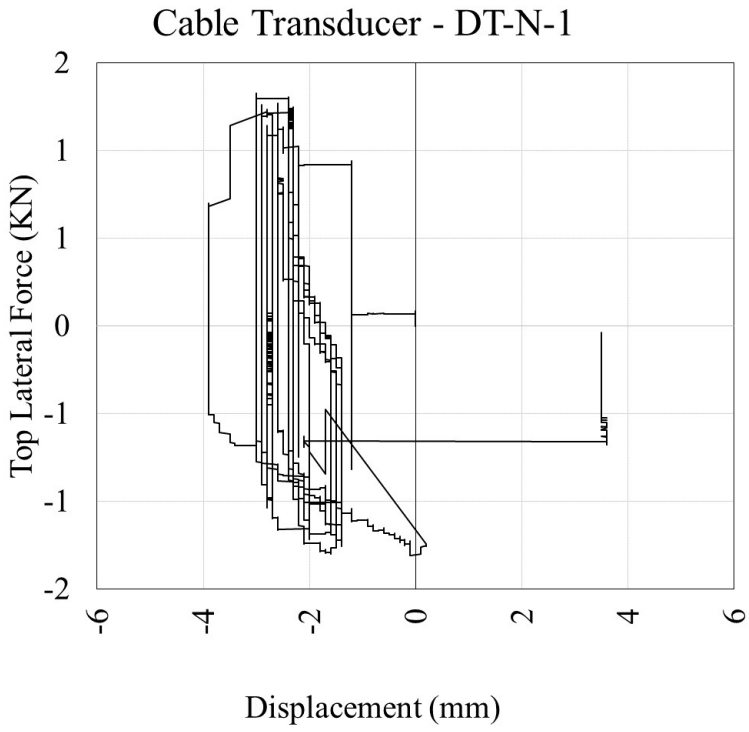
Cable Transducer - DT-N-1
Top Lateral Force (KN)
2
1
1
0
-1
-1
-2
-6
-4
-2
0
2
4
6
Displacement (mm)

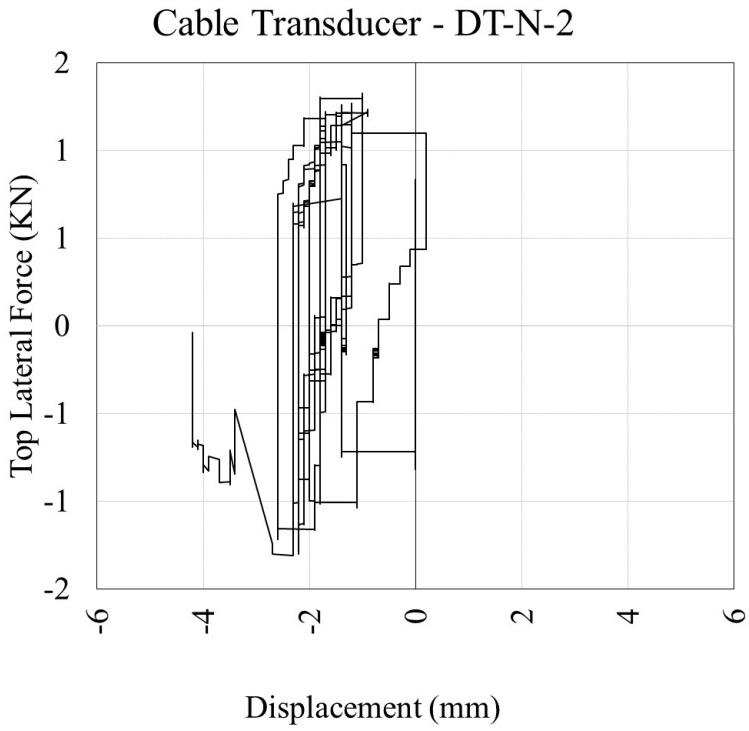
Cable Transducer - DT-N-2
Top Lateral Force (KN)
2
1
1
0
-1
-1
-2
-6
-4
-2
0
2
4
6
Displacement (mm)

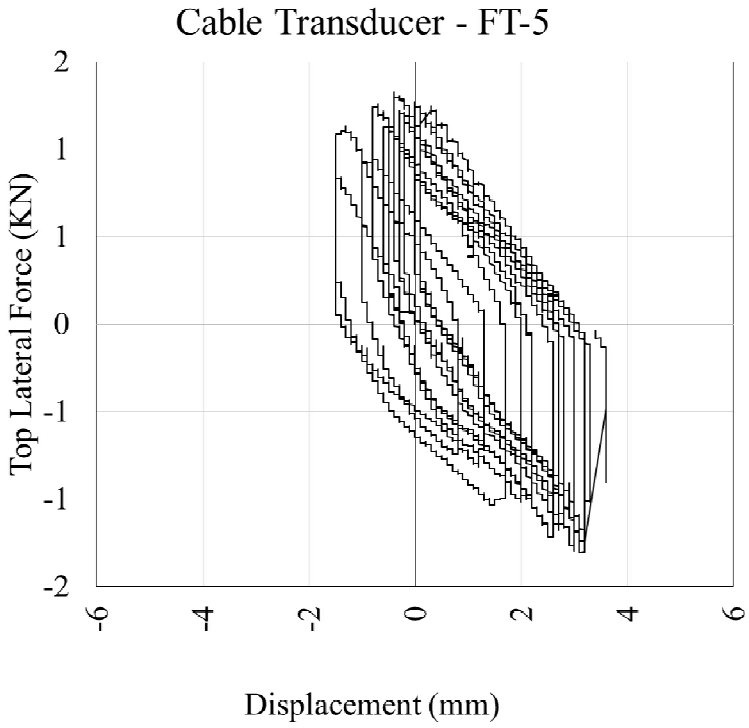
Cable Transducer - FT-5
Top Lateral Force (KN)
2
1
1
0
-1
-1
-2
-6
-4
-2
0
2
4
6
Displacement (mm)

Appendix D

Recorded Displacement Data

Wall W1HS

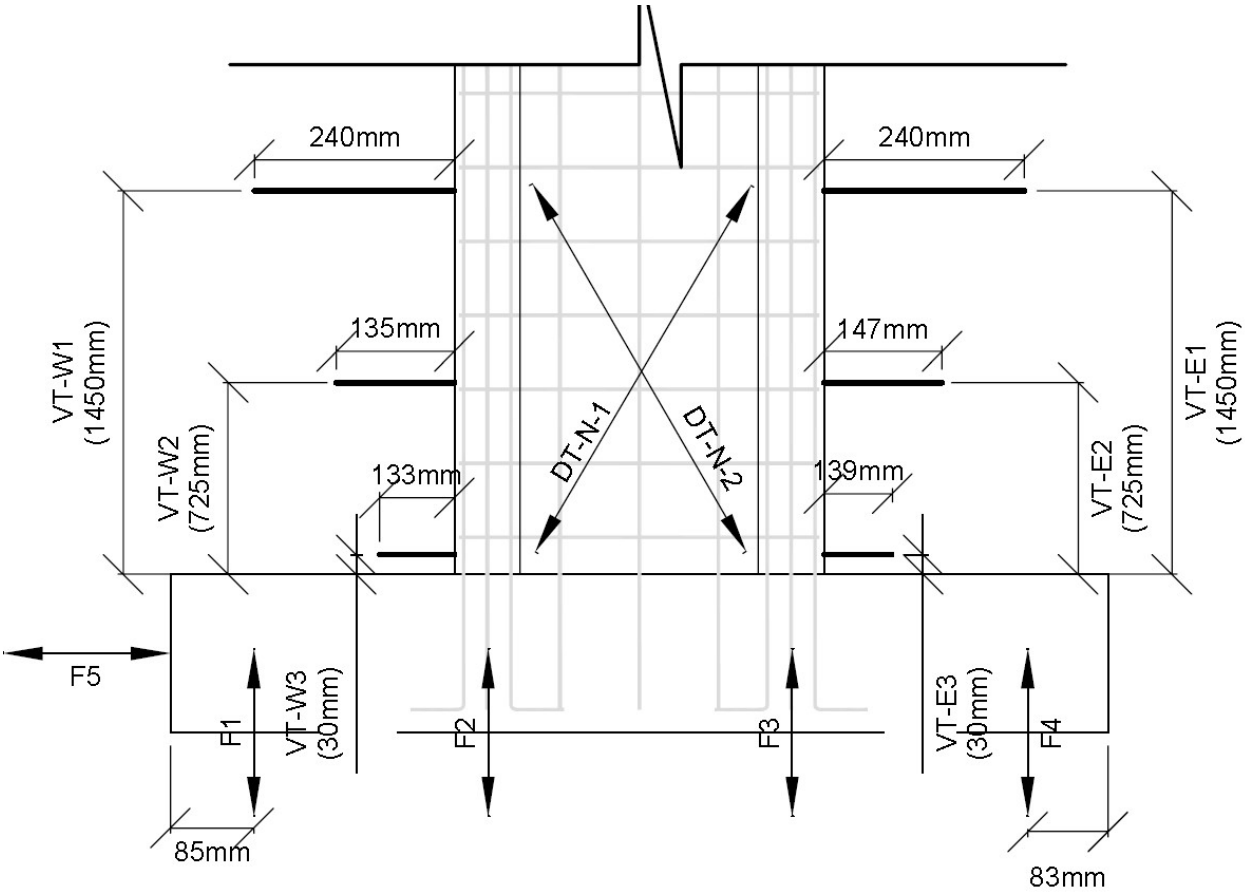

Figure D-1 – As-built measurements of cable transducer and LVDT locations

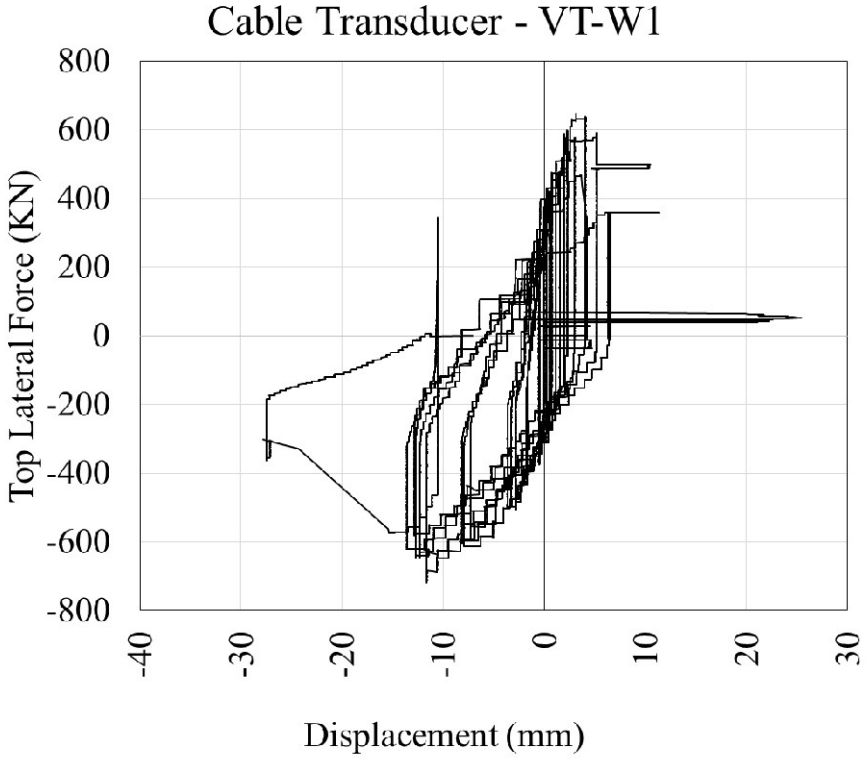
Cable Transducer - VT-W1
Top Lateral Force (KN)
800
600
400
200
0
-200
-400
-600
-800
-40
-30
-20
-10
0
10
20
30
Displacement (mm)

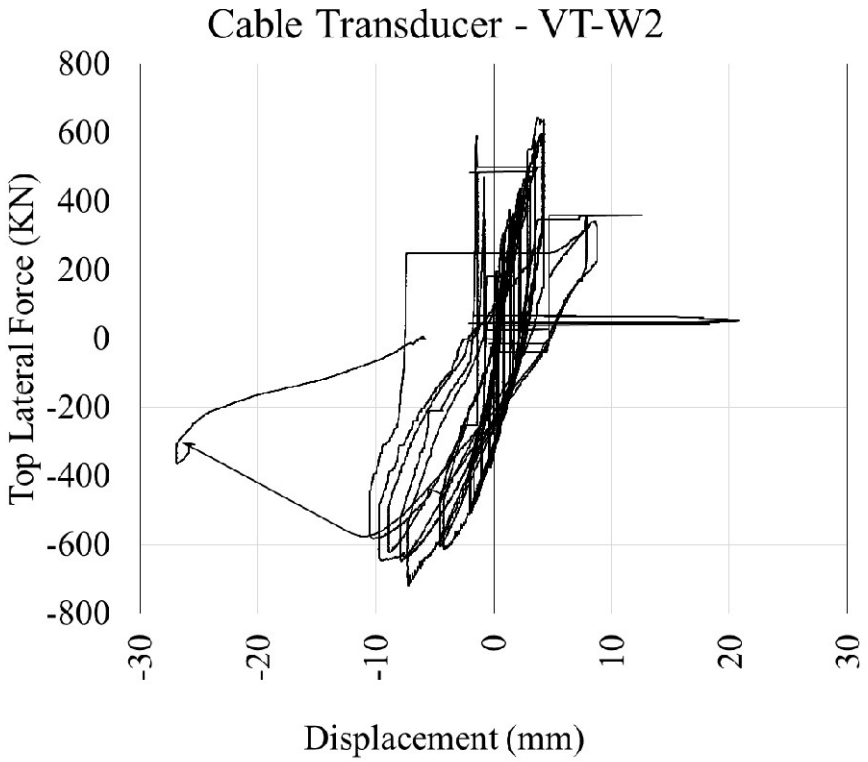
Cable Transducer - VT-W2
Top Lateral Force (KN)
800
600
400
200
0
-200
-400
-600
-800
-30
-20
-10
0
10
20
30
Displacement (mm)

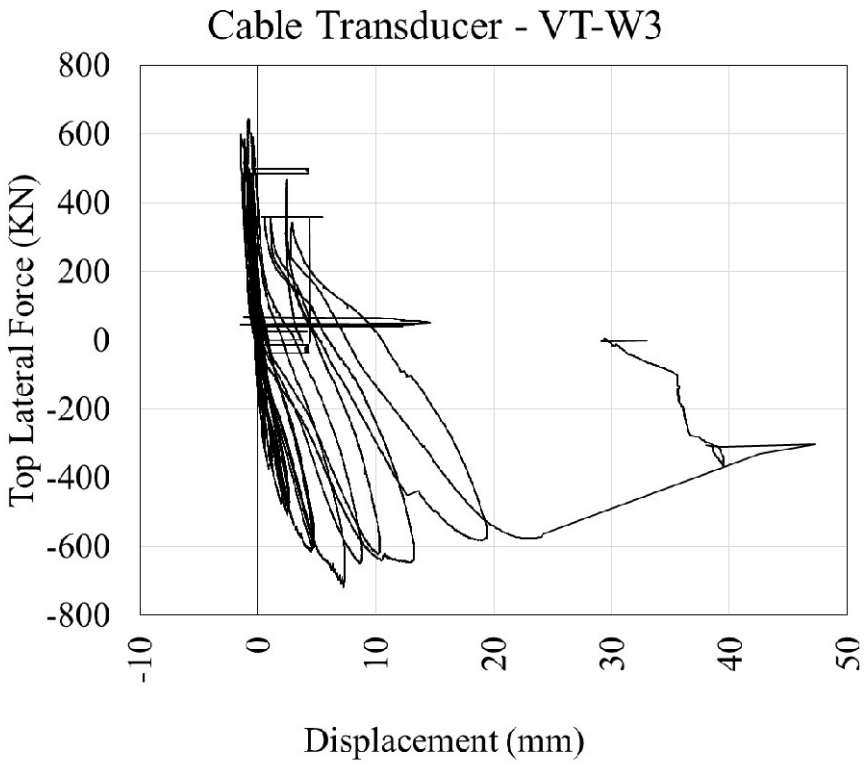
Cable Transducer - VT-W3
Top Lateral Force (KN)
800
600
400
200
0
-200
-400
-600
-800
-10
0
10
20
30
40
50
Displacement (mm)

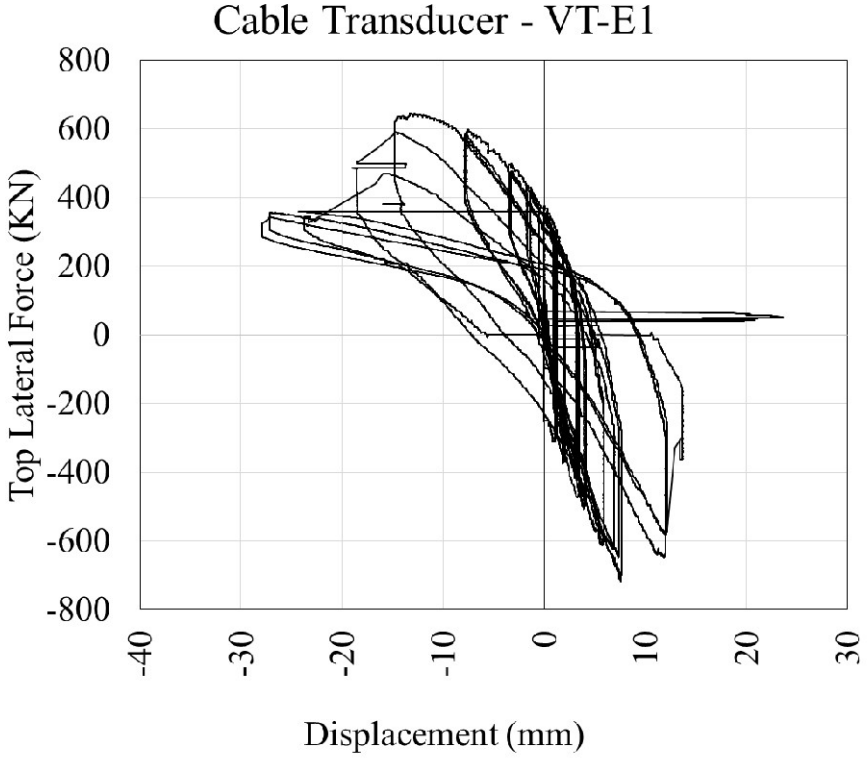
Cable Transducer - VT-E1
Top Lateral Force (KN)
800
600
400
200
0
-200
-400
-600
-800
-40
-30
-20
-10
0
10
20
30
Displacement (mm)

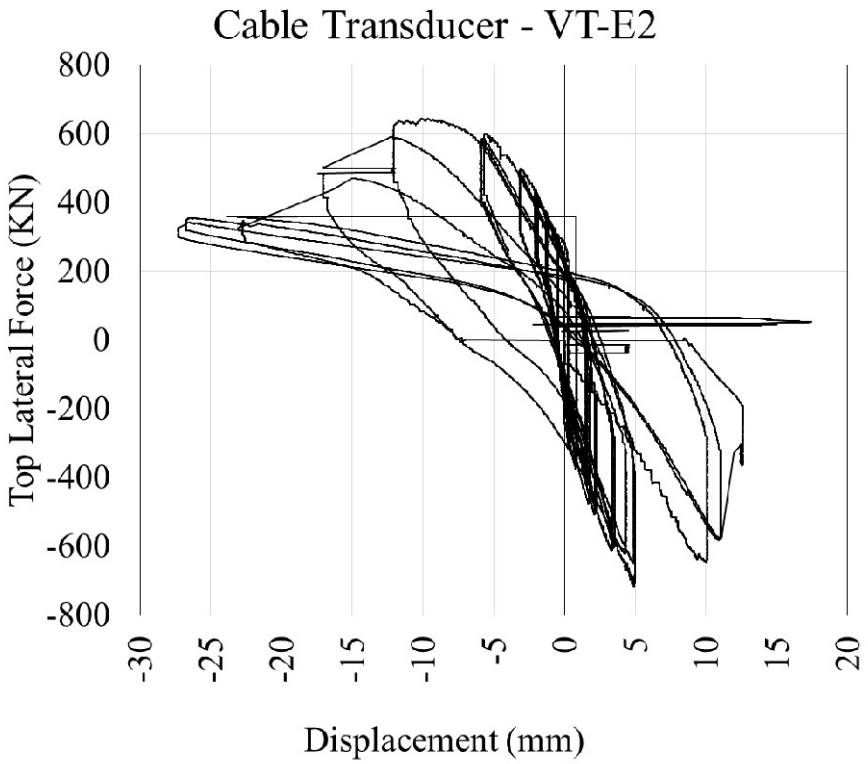
Cable Transducer - VT-E2
Top Lateral Force (KN)
800
600
400
200
0
-200
-400
-600
-800
-30
-25
-20
-15
-10
-5
0
5
10
15
20
Displacement (mm)

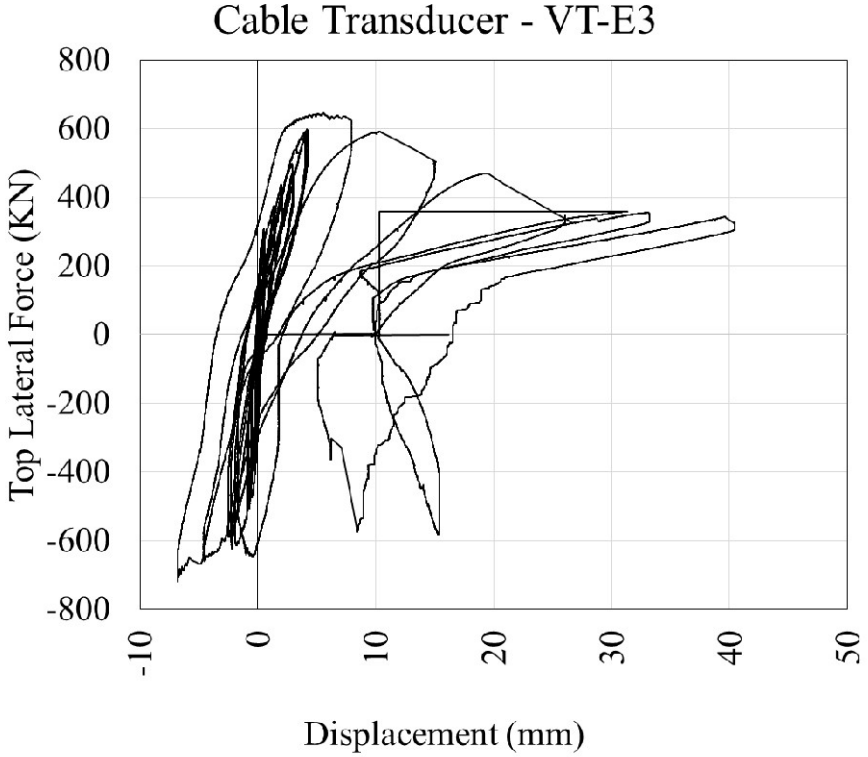
Cable Transducer - VT-E3
Top Lateral Force (KN)
800
600
400
200
0
-200
-400
-600
-800
-10
0
10
20
30
40
50
Displacement (mm)

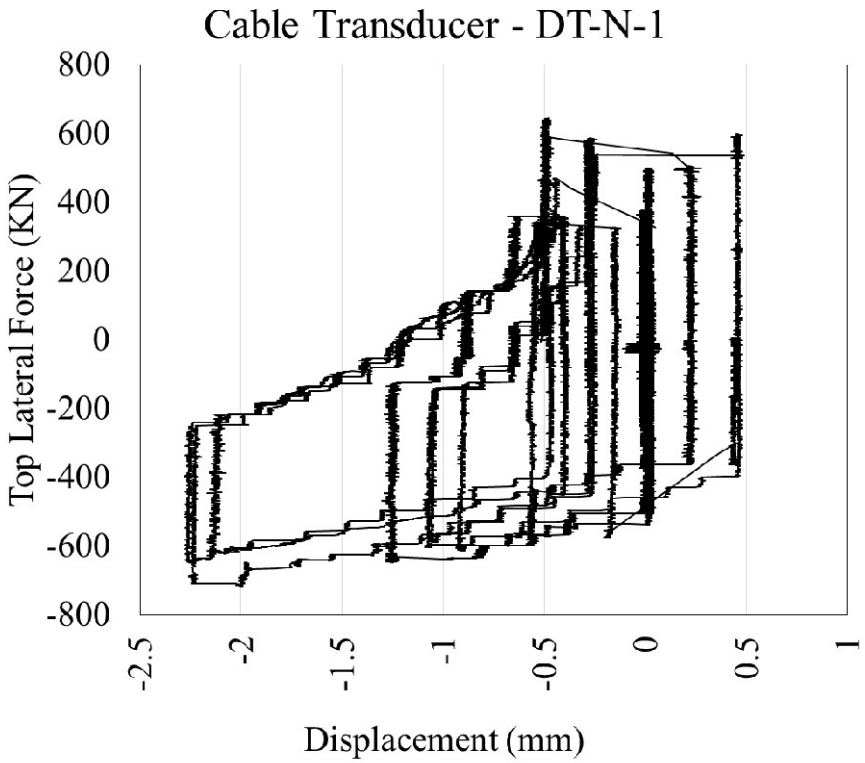
Cable Transducer - DT-N-1
Top Lateral Force (KN)
800
600
400
200
0
-200
-400
-600
-800
-2.5
-2
-1.5
-1
-0.5
0
0.5
1
Displacement (mm)

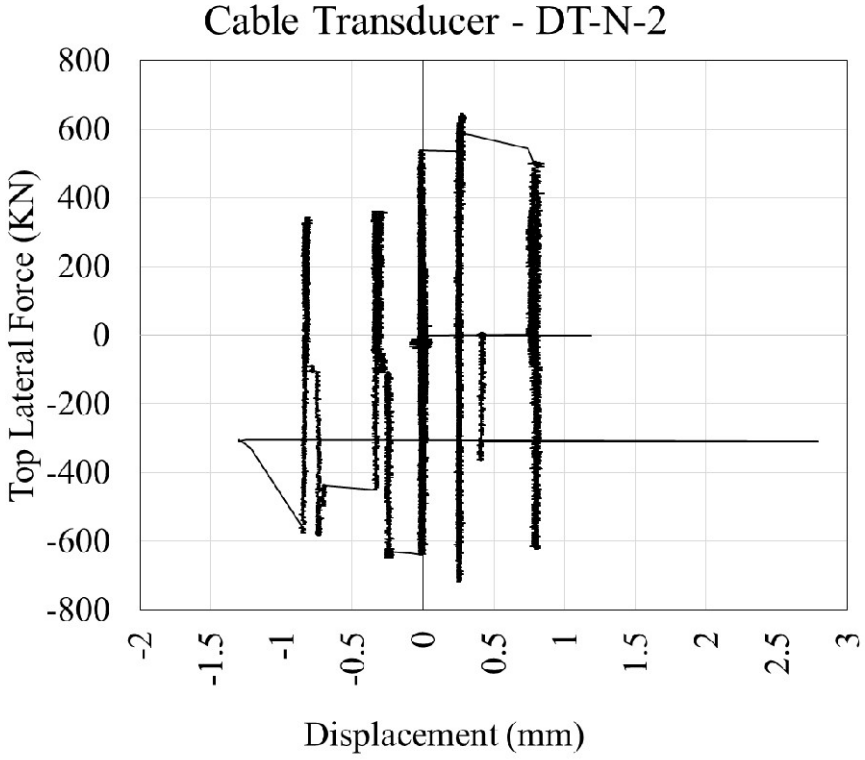
Cable Transducer - DT-N-2
Top Lateral Force (KN)
800
600
400
200
0
-200
-400
-600
-800
-2
-1.5
-1
-0.5
0
0.5
1
1.5
2
2.5
3
Displacement (mm)

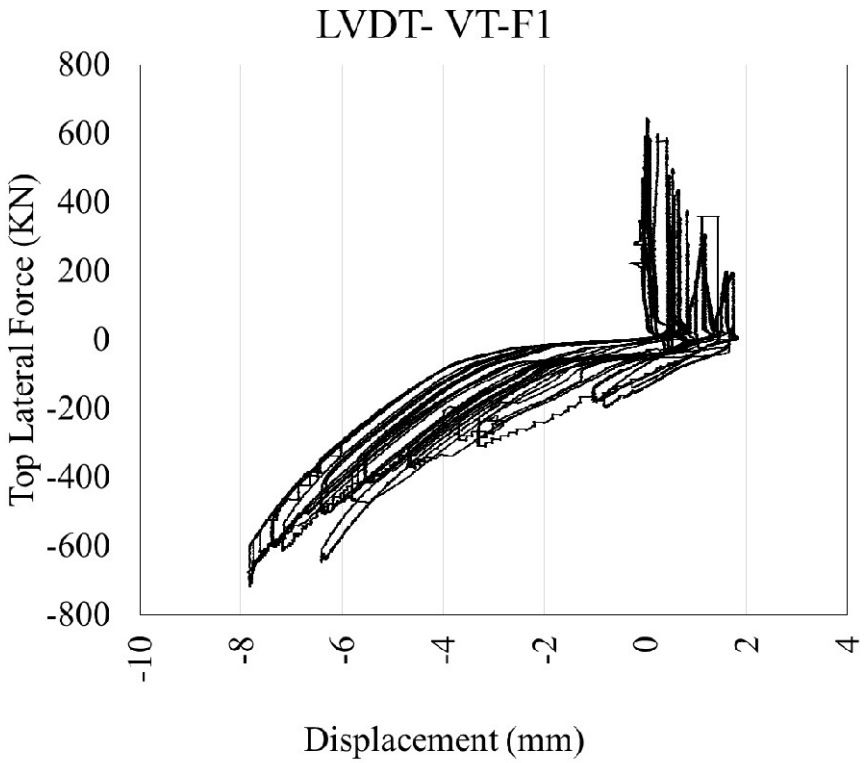
LVDT- VT-F1
800
600
400
200
0
-200
-400
-600
-800
Top Lateral Force (KN)
-10
-8
-6
-4
-2
0
2
4
Displacement (mm)

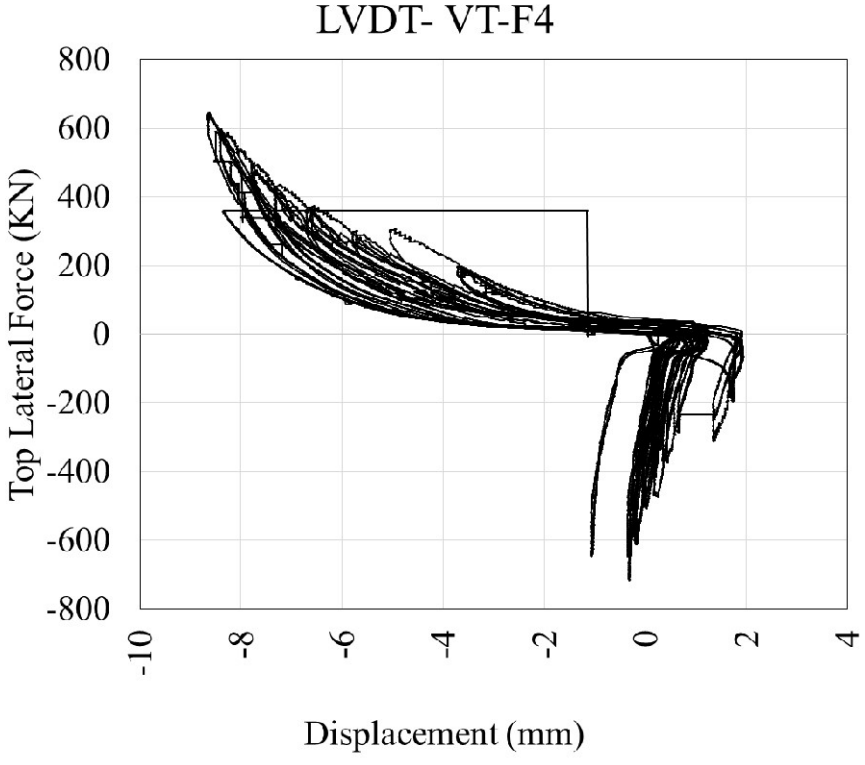
LVDT- VT-F4
800
600
400
200
0
-200
-400
-600
-800
Top Lateral Force (KN)
-10
-8
-6
-4
-2
0
2
4
Displacement (mm)

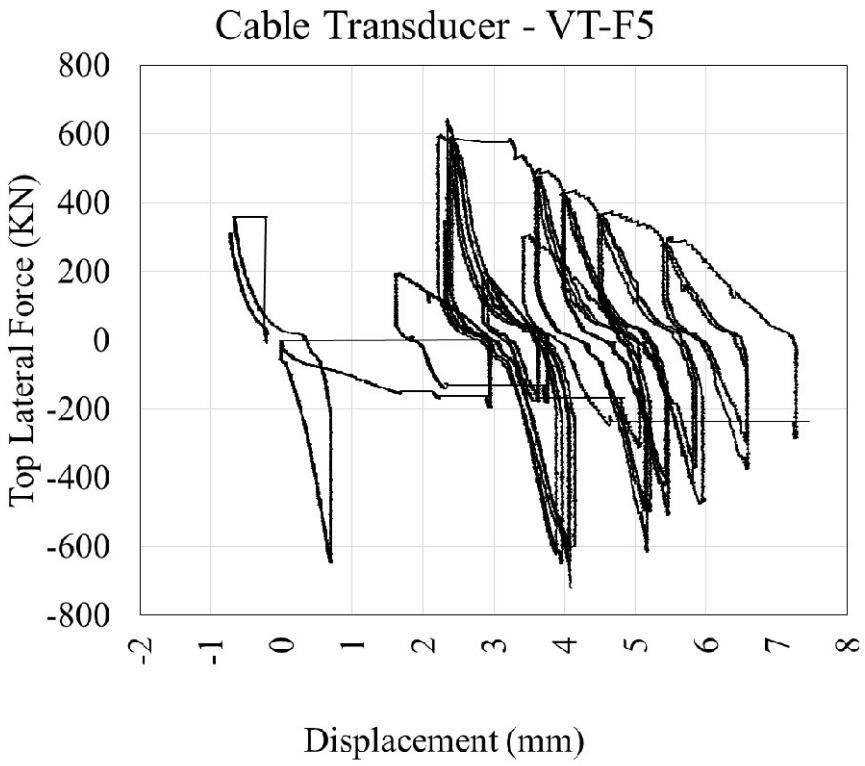
Cable Transducer - VT-F5
800
600
400
200
0
-200
-400
-600
-800
Top Lateral Force (KN)
-2
-1
0
1
2
3
4
5
6
7
8
Displacement (mm)

Wall W2HS

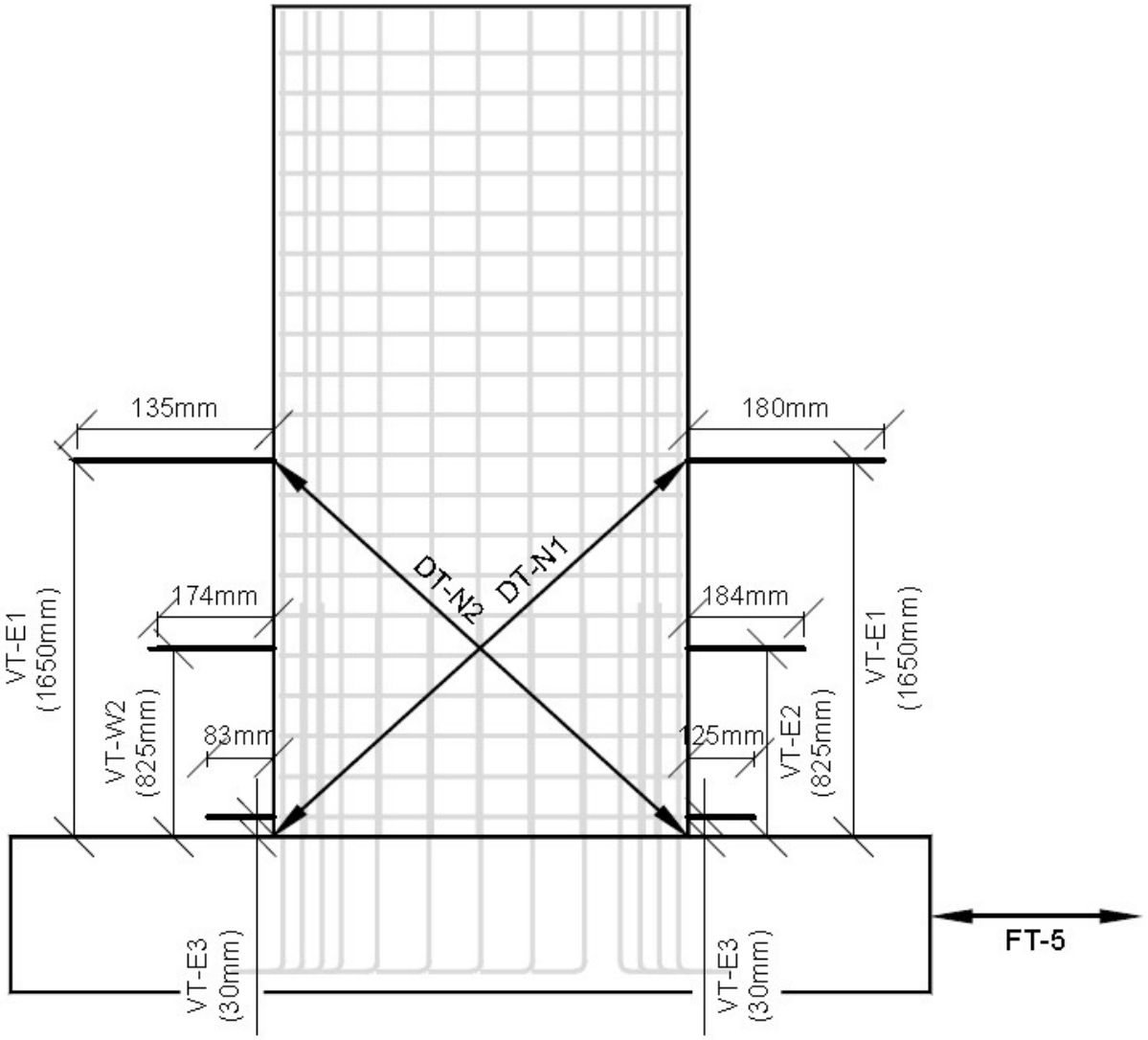

Figure D-2 – As-built measurements of cable transducer locations

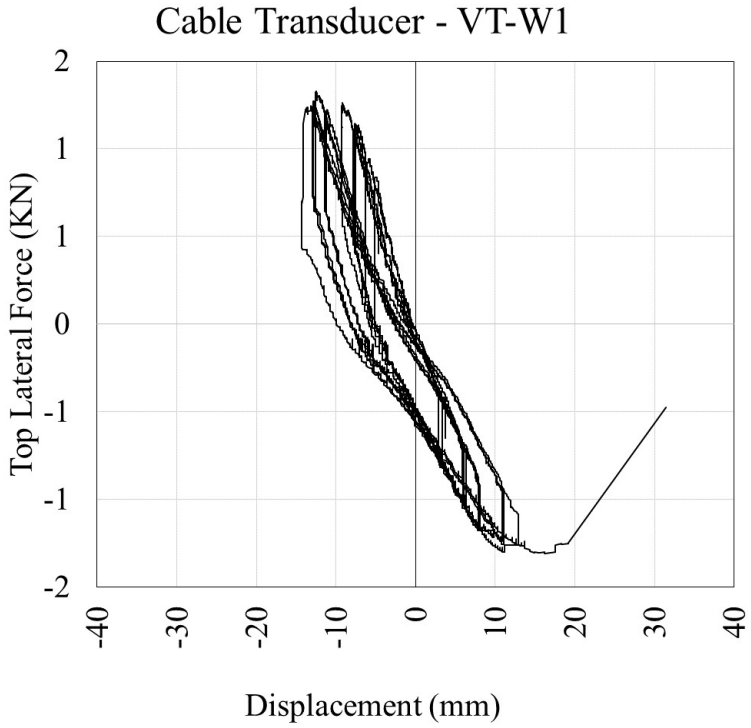
Cable Transducer - VT-W1
Top Lateral Force (KN)
2
1
1
0
-1
-1
-2
-40
-30
-20
-10
0
10
20
30
40
Displacement (mm)

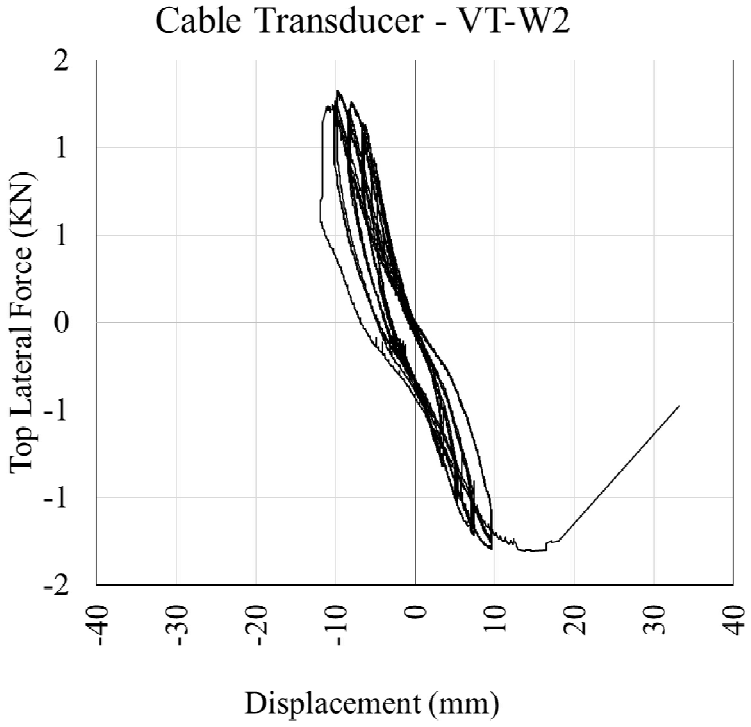
Cable Transducer - VT-W2
Top Lateral Force (KN)
2
1
1
0
-1
-1
-2
-40
-30
-20
-10
0
10
20
30
40
Displacement (mm)

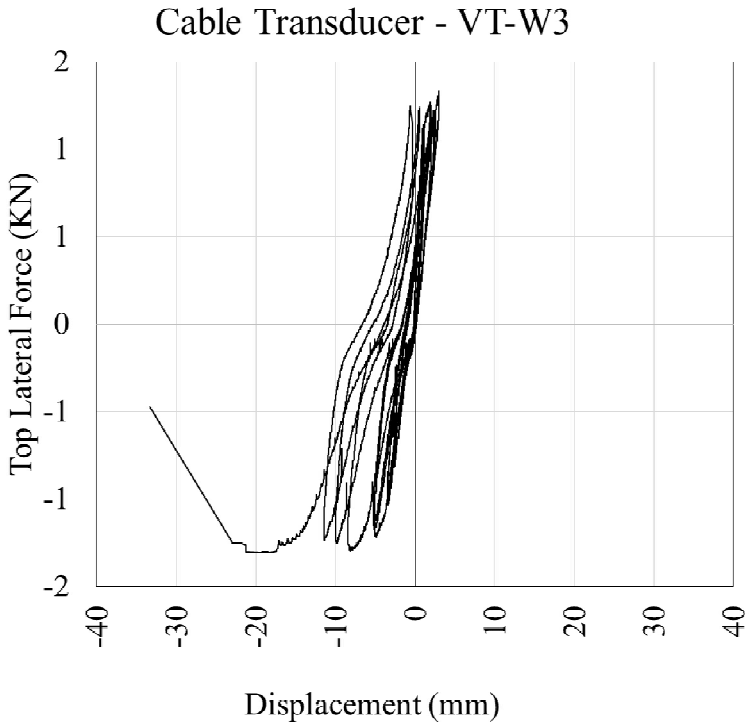
Cable Transducer - VT-W3
Top Lateral Force (KN)
2
1
1
0
-1
-1
-2
-40
-30
-20
-10
0
10
20
30
40
Displacement (mm)

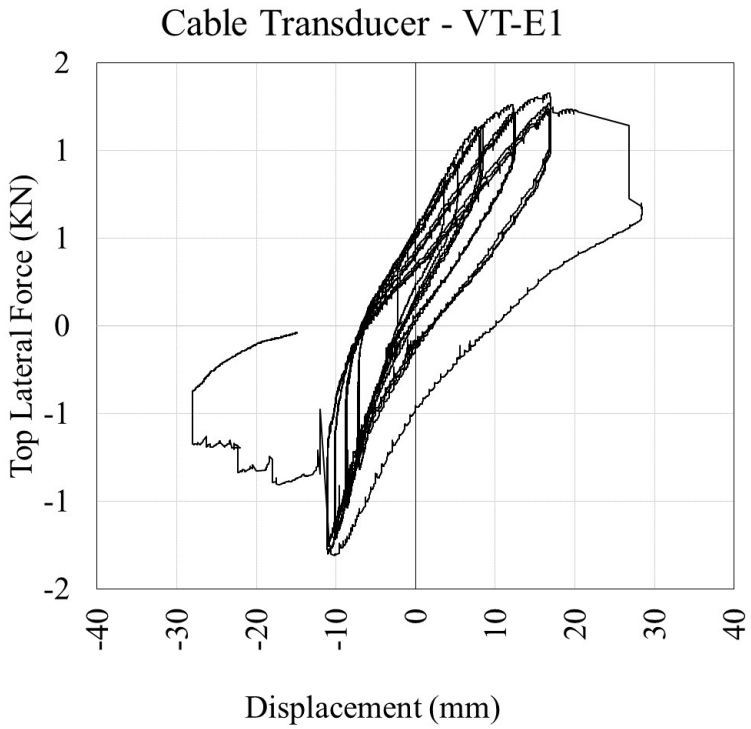
Cable Transducer - VT-E1
Top Lateral Force (KN)
2
1
1
0
-1
-1
-2
-40
-30
-20
-10
0
10
20
30
40
Displacement (mm)

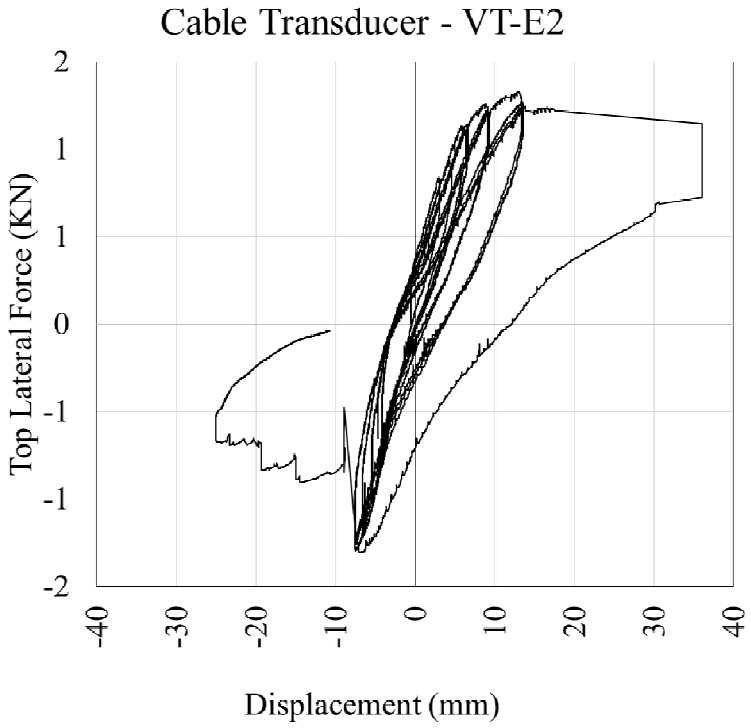
Cable Transducer - VT-E2
Top Lateral Force (KN)
2
1
1
0
-1
-1
-2
-40
-30
-20
-10
0
10
20
30
40
Displacement (mm)

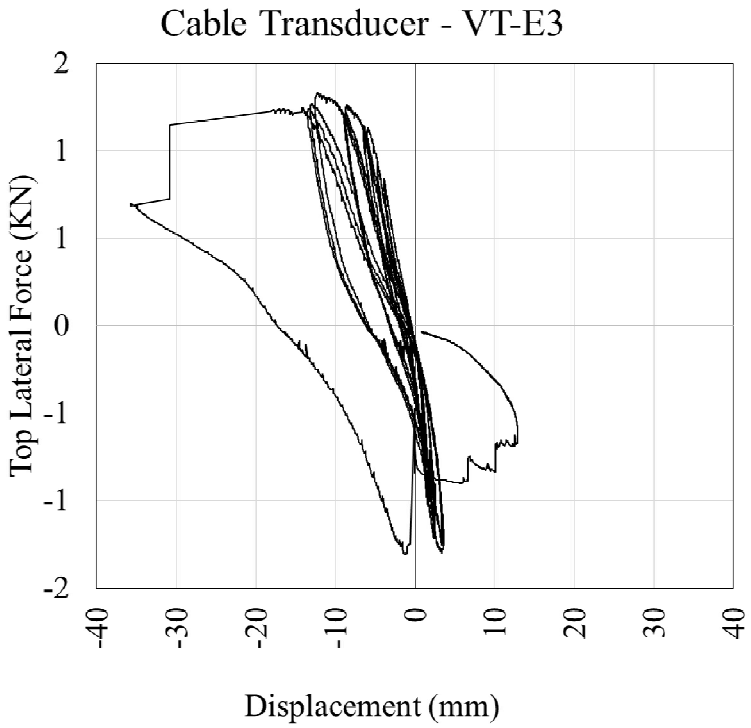
Cable Transducer - VT-E3
Top Lateral Force (KN)
2
1
1
0
-1
-1
-2
-40
-30
-20
-10
0
10
20
30
40
Displacement (mm)

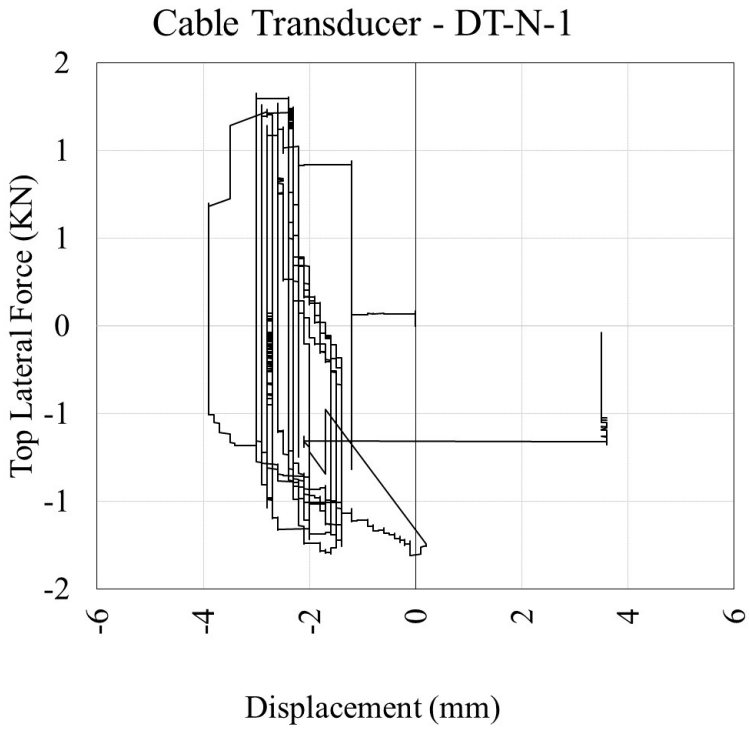
Cable Transducer - DT-N-1
Top Lateral Force (KN)
2
1
1
0
-1
-1
-2
-6
-4
-2
0
2
4
6
Displacement (mm)

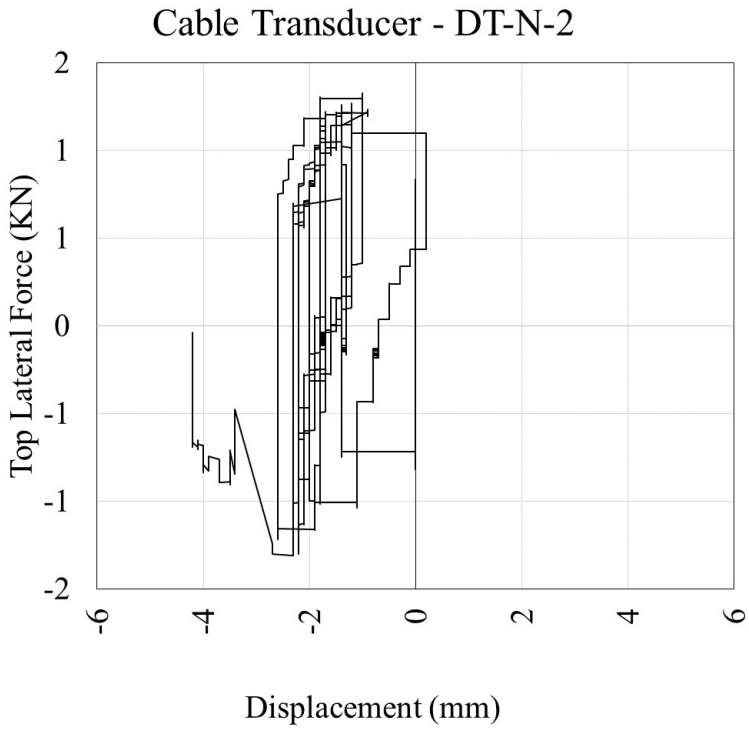
Cable Transducer - DT-N-2
Top Lateral Force (KN)
2
1
1
0
-1
-1
-2
-6
-4
-2
0
2
4
6
Displacement (mm)

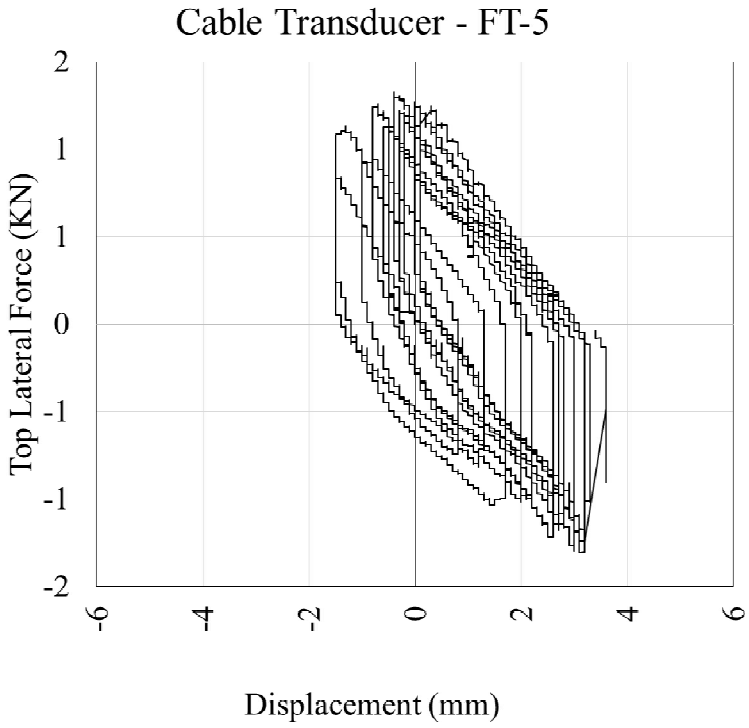
Cable Transducer - FT-5
Top Lateral Force (KN)
2
1
1
0
-1
-1
-2
-6
-4
-2
0
2
4
6
Displacement (mm)